Synthesis and Photophysics of Linear and Star-Shaped Oligomers of Squaraine Dyes

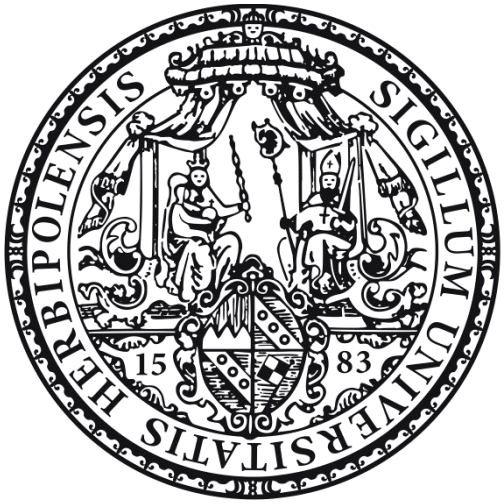

Dissertation zur Erlangung
des naturwissenschaftlichen Doktorgrades der
Julius-Maximilians-Universität Würzburg

vorgelegt von

Maximilian Hubert Schreck

aus Röllbach

Würzburg 2018

Eingereicht bei der Fakultät für Chemie und Pharmazie am

_____

Gutachter der schriftlichen Arbeit

1. Gutachter: Prof. Dr. Christoph Lambert

2. Gutachter: Prof. Dr. Frank Würthner

Prüfer des öffentlichen Promotionskolloquiums

1. Prüfer: Prof. Dr. Christoph Lambert

2. Prüfer: Prof. Dr. Frank Würthner

3. Prüfer: _____

Datum des öffentlichen Promotionskolloquiums

_____

Doktorurkunde ausgehändigt am

_____

Für meine Eltern und Großeltern

Die vorliegende Arbeit wurde in der Zeit von Juni 2014 bis September 2018 am Institut für Organische Chemie der Universität Würzburg angefertigt.

Mein besonderer Dank gilt

Herrn Prof. Dr. Christoph Lambert

für die Vergabe des vielseitigen und interessanten Themas,
den damit verbundenen Diskussionen, dem Vertrauen und
den Freiheiten bei dessen Bearbeitung.

COPYRIGHT

The following theses also contributed to this work:

1. *Synthese und Charakterisierung von polymeren cis-Indolenin Squarain-Farbstoffen*, A. Stoy, Bachelor Thesis, Julius-Maximilians-Universität, Würzburg, **2014**.
2. *Synthese und Charakterisierung von polymeren Benzodipyrrolenin Squarain-Farbstoffen*, L. Wittmann, Bachelor Thesis, Julius-Maximilians-Universität, Würzburg, **2015**.
3. *Synthese und spektroskopische Untersuchung von polymeren cisoiden Indolenin Squarain-Farbstoffen*, L. Breitschwerdt, Bachelor Thesis, Julius-Maximilians-Universität, Würzburg, **2016**.

CONTENTS

ABBREVIATIONS

AFM	atomic force microscopy
CD	circular dichroism
CNC	critical micelle concentration
COD	1,5-cyclooctadiene
COSY	correlation spectroscopy
CV	cyclic voltammetry
DCM	dichloromethane
DFT	density functional theory
DMF	dimethylformamide
DMSO	dimethyl sulfoxide
DOSY	diffusion ordered spectroscopy
dppf	1,1'-bis(diphenylphosphino)ferrocen
EL	electroluminescence
ESI	electrospray ionisation
GPC	gel permeation chromatography
HOMO	highest occupied molecular orbital
HOPG	highly oriented pyrolytic graphite
HRMS	high resolution mass spectrometry
HSQC	heteronuclear single quantum coherence
LUMO	lowest unoccupied molecular orbital
MCH	methylcyclohexane
NIR	near infrared
NMR	nuclear magnetic resonance
NOE	nuclear Overhauser effect
OLED	organic light emitting diode

PEDOT:PSS	poly(3,4-ethylenedioxythiophene):polystyrene sulfonate
PL	photoluminescence
ppm	parts per million
ROESY	rotating-frame nuclear Overhauser enhancement spectroscopy
SDS	sodium dodecyl sulphate
SQ	squaraine
rt	room temperature
TBAHFP	tetrabutylammonium hexafluorophospate
TCE	1,1,2,2-tetrachloroethane
TDDFT	time-dependent density functional theory
THF	tetrahydrofuran
TMS	tetramethylsilane
UV	ultraviolet
Vis	visible

1 Introduction

Squaraines, sometimes also referred to as squarylium dyes, are compounds of the polymethine family, because they comprise an odd number of repeating methine (–CH=) units with alternating single and double bonds, whereas polyenes possess even-numbered methine groups. The classification within the family of polymethine dyes relies on the respective electronic structure and properties, which can be manipulated by changing the length of the π-conjugation chain and by adding various electron acceptor (A) or electron donor (D) terminal moieties, affording the following molecular structures: cationic D–π–D and anionic A–π–A (both cyanine-type), and neutral D–π–A (merocyanine-type). Additional electron acceptor or donor groups may be incorporated in the conjugated π-system, giving rise to neutral quadrupolar structures, such as D–π–A–π–D (squaraine-type) or A–π–D–π–A.[1] The term squaraine established by *Schmidt* in 1980 is a portmanteau word which is made up of "squaric" and "betaine" and reflects the intrinsic structural properties of squaraines, i.e., the central quadratic cyclobutadiene acceptor unit and their zwitterionic structure.[2] The betaine structure can either be expressed as a dipolar cyanine (I) or a cyclobutenediyliumdiolate structure (II). For stabilisation of the D–A–D structure, strong electron donating groups (e.g., heterocycles) or electron rich aromatic units (e.g., aniline or phenol derivatives) denoted as nucleophiles (Nu) in Scheme 1 are typically found embedded in the dye scaffold.

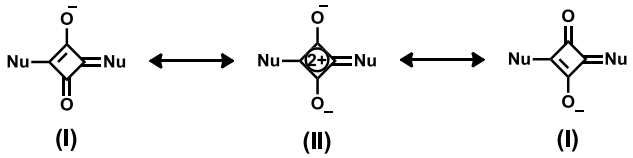

Scheme 1: Mesomeric resonance formulas of squaraine dyes.

Squaraine dyes are structurally similar to zwitterionic merocyanines, their absorption and emission features are, however, more reminiscent of cyanine dyes with their characteristic narrow bandwidths and small Huang-Rhys factor[3-5,I] rather than of merocyanine dyes which typically exhibit broad and diffuse charge-transfer bands as a result of their strong dipolar character.[6] Consequently, squaraine dyes have attracted much attention because of their highly advantageous optical properties, i.e., intense ($\varepsilon_{max} > 10^5\ M^{-1}cm^{-1}$) and narrow absorption in the red to near-infrared (NIR) region, high fluorescence quantum yield and

[I] The electron-phonon coupling strength is characterised by the Huang-Rhys factor $S = d^2m\omega/2\hbar$, where d is the displacement between the potential energy surfaces of the ground and excited states, and m and ω are the reduced mass and harmonic frequency of a vibrational mode, respectively. S yields information about the change in geometry between ground and excited state.

considerable photostability, together with their large structural variety.[2,7-12] These superior optical properties have led to squaraine dyes being used in a large diversity of applications, including as biolabels,[13-24] photoconductors,[25] materials for data storage,[26] ion sensors, [27-33] NIR emitters in thin-film dye-doped organic light-emitting diodes (OLED), [34,35] and in non-linear optics (NLO).[36-43] In the light of their beneficial absorption in the red region of the visible solar spectrum, squaraine dyes also proved suitable for organic photovoltaic applications.[44-66]

1.1 Intramolecular Aggregates of Squaraine Oligo- and Polymers

Because the absorption of squaraine dyes only covers a small portion of the solar spectrum, the narrow absorption may be considered disadvantageous. In order to address this issue, various synthetic strategies were developed in particular by Völker, Lambert et al. to achieve a spectral broadening of their absorption, e.g., by attaching electron donors[67-69] or acceptors,[70] or by coupling multiple squaraine chromophores in squaraine polymers[44,71,72] or other copolymers.[68,70] In classical conjugated low-band gap polymers such as styrene-derived MEH-PPV (poly[2-methoxy-5-(2-ethylhexyloxy)-1,4-phenylenevinylene]) or thiophene-derived P3HT (poly(3-hexylthiophene-2,5-diyl), the polymer properties significantly differ from those of the comparably small monomers. In contrast to these systems, the isolated monomers of squaraine homo- and copolymers already provide a low-bandgap and thus a strong absorption in the red spectral region.[73] Even though the monomers are covalently connected to each other the resulting oligomer/polymer may be rationalised as chains of individual chromophores as their monomeric character is mostly conserved within the dye conjugate. The resulting spectral features of these dye conjugates, i.e., red-shifting of the longest-wavelength absorption band along with a significant broadening of the absorption, can be adequately explained in terms of exciton theory.[74,75] As a matter of fact, excitonically coupled systems take advantage of a more precise prediction and control of the optical properties which is typically not attainable with classical polymers such as MEH-PPV or P3HT because of strongly interacting monomer units. Hence, the coupling of transition moments of squaraine chromophores may be considered as a reliable alternative to other methodologies for designing and fine-tuning the absorption of low-bandgap conjugates.[6,76,77] This approach was also a substantial and integral part of several other reports on polysquaraines in particular by the groups of Ajayaghosh,[78-80] Maeda,[60] Kuster,[81] Hecht,[82,83] and Zhang et al.[84,85]

Furthermore, the synthesis of discrete oligomers with known molecular weight enables the possibility to compare oligomer properties with those of analogous polymers in order to get insights on how to manipulate polysquaraines in order to achieve a desired optical property and to establish valuable structure-property relationships. The fundamental understanding of the underlying exciton interactions in small model oligomers may lead to a more precise prediction of the polymer properties.[86]

Exciton coupling theory is without doubt a key part in this work and is integral to understanding the spectroscopic properties of squaraine oligomers and polymers. Therefore, the subsequent chapter is exclusively devoted to its description.

1.2 Exciton Coupling Theory

In a pioneering work, the Russian physicists Frenkel and Davidov and the American photochemist Kasha developed the fundamental concepts for understanding electronic excitations in molecular aggregates. Particularly the work of Kasha at the beginning of the 1960s had a great influence on the photochemistry community and manifested the terminology of H- and J-aggregates which refer to hypsochromically (H) and bathochromically (J) shifted absorption bands for the aggregated dyes compared to those of their isolated monomers.[6,75]

The exciton model may be described as the mathematical treatment of the resonance interaction between excited states of weakly coupled systems. This formal treatment can be applied to covalently bound intramolecular aggregates as well as to intermolecular aggregates.[74] Please note that the mathematical treatment presented in the following makes no claim to completeness and should therefore be considered rather as a semi-quantitative description of the formation of the exciton eigenstates in various aggregate arrangements (e.g., in dimers, trimers, and polymers) which are of fundamental importance in this work. For a thorough mathematical description the reader is referred to the references quoted in the text as well as to the original works by Kasha et al.[74,75,87]

Considering the simplest exciton system, i.e., a dimer, two exciton states are formed resulting from the coupling between the respective excited states of the monomers due the dipole-dipole coupling J between them:[75,88]

$$J = \frac{1}{4\pi\varepsilon_0 hc}\left(\frac{\vec{\mu}_A\vec{\mu}_B}{r_{AB}^3} - \frac{3(\vec{\mu}_A\vec{r}_{AB})(\vec{\mu}_B\vec{r}_{AB})}{r_{AB}^5}\right), \quad (1)$$

where ε_0, h, c are the vacuum permittivity, the Planck constant and the vacuum speed of light, respectively, $\vec{\mu}_A$ and $\vec{\mu}_B$ represent the transition moments of monomer A and monomer B and $\vec{r}_{AB}$ is the corresponding centre-to-centre distance. From equation (1), it can be appreciated that the coupling strength J crucially depends on the mutual orientation of the monomer transition moment vectors as well as on the distance of the chromophores and can even change sign.

In case of a homodimer, exciton coupling of two identical chromophores causes a splitting (= $2J$) of the excited states if dispersion interactions between the chromophores in the ground state are neglected. In contrast, for two different chromophores in a heterodimer, the energies of the exciton states are further apart and can be calculated according to equation (2) where $\overline{E} = (E_A + E_B)/2$ and $\Delta E = (E_A - E_B)/2$ with $E_A > E_B$:[72]

$$E_{\pm\text{heterodimer}} = \overline{E} \pm \sqrt{\Delta E^2 + J^2} \tag{2}$$

In this equation, $2\Delta E$ equals the energy difference between the diabatic (non-interacting) energy levels of the two chromophores in the heterodimer. The midpoint between these diabatic levels are set to zero energy. The splitting of the exciton levels in homo- and heterodimers is given by equations (3) and (4), respectively:[72,89]

$$\delta E_{\text{heterodimer}} = 2\sqrt{\Delta E^2 + J^2} \tag{3}$$

$$\delta E_{\text{homodimer}} = 2J \tag{4}$$

Whether optical transitions into exciton states are allowed depends on the mutual orientation of the transition moments. The transition moments $\vec{\mu}_\pm$ from the ground state to the exciton states can be approached from the monomer transition moments $\vec{\mu}_A$ and $\vec{\mu}_B$, respectively, according to equations (5) and (6):[75,88,90,91]

$$\vec{\mu}_+ = \vec{\mu}_A \cos\theta + \vec{\mu}_B \sin\theta \tag{5}$$

$$\vec{\mu}_- = \vec{\mu}_A \sin\theta + \vec{\mu}_B \cos\theta, \tag{6}$$

where θ is defined by $\tan 2\theta = J/(E_A - E_B)$. In the case of two identical monomers, equations (5) and (6) transform to:

$$\vec{\mu}_\pm = \frac{1}{\sqrt{2}} \left(\vec{\mu}_A \pm \vec{\mu}_B\right) \tag{7}$$

According to (7), the transition moments are oriented perpendicularly to each other and the transition strength is distributed between them depending on the angle between the monomer transition moments. In a perfect collinear, head-to-tail arrangement, the transition moment $\vec{\mu}_-$ refers to the upper exciton state (termed S_1' in the following) and vanishes, so the full

transition strength is concentrated in the lower exciton state S_1, reflecting a J-dimer in analogy to J-aggregates.[92] In contrast, in a perfect parallel, face-to-face arrangement, the full transition strength is concentrated in the S_1' state and may be termed as H-dimer similar to H-aggregates. Since the transition moments are typically unequal for heterodimers and thus do not cancel for the upper exciton state in the head-to-tail arrangement and for the lower exciton state in the face-to-face arrangement, both states are now allowed, respectively.[72,89] The corresponding exciton coupling diagrams are depicted in Figure 1.

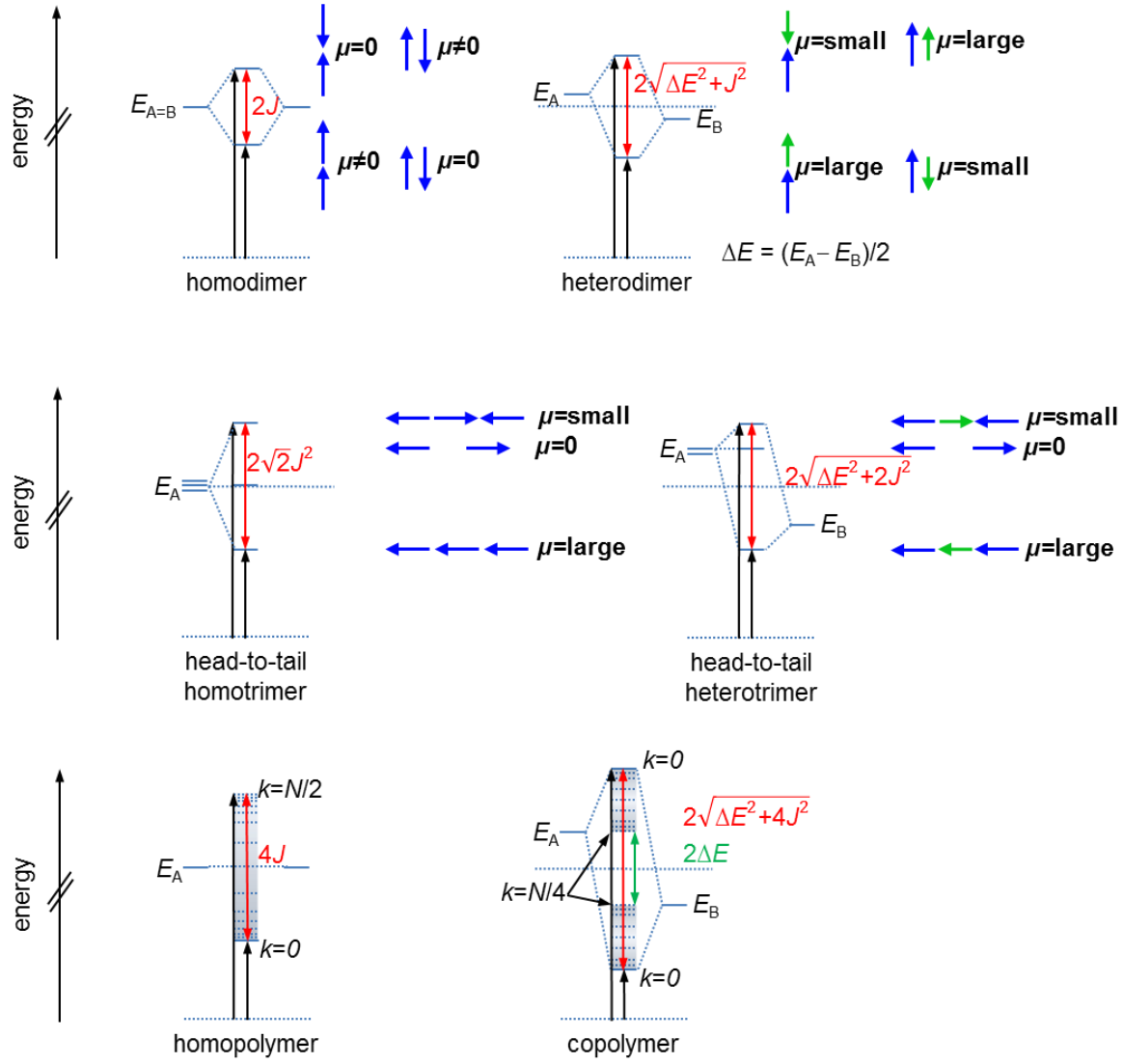

Figure 1: Exciton eigenstates formed by exciton coupling in case of a homodimer (A_2), heterodimer (AB), (head-to-tail) homotrimer (A_3), (head-to-tail) heterotrimer (ABA), and for an infinitely long homopolymer ($[A]_{2N}$) and a copolymer ($[AB]_N$) with $E_A > E_B$. In the dimer and trimer case, blue (A) and green (B) arrows represent the phase relations of the individual localised transition moments. Their length is proportional to their magnitude.[72,93]

In case of a heterotrimer (ABA), the corresponding exciton interaction matrix[93,II] can be formulated according to equation (8) applying the nearest-neighbour approximation and neglecting dispersion between the chromophores in the ground state:[89]

$$\begin{vmatrix} \Delta E - \varepsilon & J & 0 \\ J & -\Delta E - \varepsilon & J \\ 0 & J & \Delta E - \varepsilon \end{vmatrix} = 0 \tag{8}$$

Solving the secular determinant (equation (8)) affords the exciton state diagram in Figure 1 with three exciton eigenstates and the splitting according to equation (9):[89]

$$\delta E_{\text{heterotrimer}} = 2\sqrt{\Delta E^2 + 2J^2} \tag{9}$$

In contrast, considering a homotrimer with three equal chromophores (A = B, $\Delta E = (E_A - E_A)/2 = 0$), equation (9) simplifies to:[93]

$$\delta E_{\text{homotrimer}} = 2\sqrt{2}J \tag{10}$$

The formula for the splitting according to equation (9) also holds true for a BAB-heterotrimer.[89]

In case of the homopolymers the energies of the N eigenstates can be evaluated by equation (11) using $\overline{E} = E_A$ and $\Delta E = 0$, where (±) has to be replaced by (–) for $0 \leq |k/N| \leq 1/4$ and by (+) for $1/4 < |k/N| \leq 1/2$. The quantum number k runs from 0, ±1, ±2, …, $N/2$, where N is the number of chromophores. Again, the nearest-neighbour approximation was applied, i.e., only the coupling (J) between neighbouring chromophores was considered.[72]

$$E_{\pm}(k)_{\text{polymer}} = \overline{E} \pm \sqrt{\Delta E^2 + \left(2J\cos\left(\frac{2\pi k}{N_A}\right)\right)^2} \tag{11}$$

The resulting splitting, also called exciton bandwidth E_{bw} amounts to $\delta E_{\text{homopolymer}} = 4J$ and equals twice the splitting of the homodimer ($2J$) which can be rationalised by twice the number of adjacent chromophores in the polymer compared to the dimer with only one neighbouring chromophore. In terms of the copolymer, equation (11) predicts a gap of energy states of $2\Delta E$ in the exciton manifold. The total splitting can be calculated by the following equation:[72]

$$\delta E_{\text{copolymer}} = 2\sqrt{\Delta E^2 + 4J^2} \tag{12}$$

[II] Exciton coupling of localised states generates a set of exciton eigenstates (exciton manifold) whose eigenvalues ε_i and eigenvectors c_{ij} can be calculated by solving the respective secular determinant. In these determinants, the nearest-neighbour approximation is considered. Consequently, the transition moments of the exciton states can be written as linear combinations of the localised transition moment vectors μ where the coefficients are those of the normalised eigenvectors.

It can be seen from equation (12), that the exciton bandwidth of the copolymer is even larger than that of the homopolymer which should indeed lead to a comparably broader absorption. Regarding the *k* space, the Brillouin zone[94,III] has halved compared to the homopolymer since the unit cell has doubled. Hence, in case of the copolymer, the quantum number *k* runs from $0, \pm1, \pm2, \ldots, N/4$.[72]

As mentioned above, the selection rules for allowed and forbidden transitions depend on the mutual orientation of transition moments, which is shown for selected cases (dimers and trimers) in Figure 1. In analogy to the homodimer, a head-to-tail (collinear) alignment of chromophores in the homopolymer yields a single allowed transition into the lowest exciton state with $k/N = 0$ whereas all other transitions are forbidden. Considering a face-to-face arrangement, the transition is only allowed into the highest exciton state. For the copolymer, both transitions into the lowest and highest exciton states are allowed simultaneously, depending on the spatial arrangement and magnitude of the localised transition moments of the individual chromophores A and B in analogy to a heterodimer. On the other hand, transitions into states with $k/N = 1/4$ are forbidden in all cases.[72]

1.3 Intermolecular Aggregates of Squaraine Dyes

Aside from intramolecular aggregates in oligomers and polymers outlined in the first section, it has widely been reported that squaraines also exhibit a high tendency to form intermolecular H- and J-type aggregates in solution,[19,24,27,29,31,95-115] Langmuir-Blodgett films,[97,98,116-118] and crystalline solids.[11,25,119-122] While the latter two are of minor relevance for this work, the aggregation behaviour will exclusively be discussed in solution. But before literature examples of squaraine aggregates are outlined in detail, three fundamental mathematical models for the self-assembly process are presented which are ubiquitous nowadays in supramolecular chemistry and which are frequently used for a thermodynamic interpretation of the respective underlying aggregation mechanism.

1.3.1 Dimerization Model[123-126]

The most fundamental aggregation model is the dimerization model. Accordingly, the equilibrium between two identical monomers (M) forming one dimer (D) in solution can be formulated as:

[III] The Brillouin zone equals a uniquely defined primitive cell in reciprocal space.

$$M + M \rightleftharpoons D \tag{13}$$

This equilibrium can mathematically be described by the dimerization constant K_{dim} using the mass action law:

$$K_{dim} = \frac{[D]}{[M]^2} = \frac{c_D}{{c_M}^2} \tag{14}$$

where $[M] = c_M$ and $[D] = c_D$ represent the concentration of the monomers and dimers, respectively. With c as the total concentration of all molecules, the molar fraction of aggregated species α_{agg} (equation (16)) can be expressed as follows:

$$\alpha_M = \frac{c_M}{c} \tag{15}$$

$$\alpha_{agg} = 1 - \alpha_M \tag{16}$$

where α_M denotes the molar fraction of monomers. Taking into account the relation $c = 2c_D + c_M$, the following equations for c_M, α_M, and α_{agg} as a function of K_{dim} can be derived:

$$c_M = \frac{\sqrt{8K_{dim}\,c + 1} - 1}{4K_{dim}} \tag{17}$$

$$\alpha_M = \frac{\sqrt{8K_{dim}c + 1} - 1}{4K_{dim}c} \tag{18}$$

$$\alpha_{agg} = \frac{4K_{dim}c + 1 - \sqrt{8K_{dim}c + 1}}{4K_{dim}c} \tag{19}$$

Furthermore, the apparent extinction coefficient $OD(\lambda)/(c \cdot d)$ of the dye in solution can be expressed as:

$$\frac{OD(\lambda)}{c \cdot d} = \varepsilon_M \alpha_M + \varepsilon_{agg} \alpha_{agg} \tag{20}$$

where ε_M and ε_{agg} are the molar absorptivities of a molecular dissolved monomer and the aggregated dimer at a fixed wavelength, respectively. Combining equations (19) and (20), one obtains equation (21):

$$\frac{OD(\lambda)}{c \cdot d} = (\varepsilon_M - \varepsilon_{agg}) \frac{\sqrt{8K_{dim}c + 1} - 1}{4K_{dim}c} + \varepsilon_{agg} \tag{21}$$

Non-linear least-squares analysis of the apparent extinction coefficient of the corresponding dye as a function of concentration according to equation (21) yields the dimerization constant K_{dim} and the molar absorptivities of the monomeric and dimeric species ε_M and ε_{agg} at a fixed wavelength, respectively.

1.3.2 Isodesmic Model[125,127-130]

The simplest and most commonly used method to describe a supramolecular polymerization process yielding extended dye aggregates > 2 constitutes the so-called isodesmic or equal *K* model. It relies on the assumptions that the aggregates are one-dimensional, acyclic, and that the reversible formation of noncovalent bonds is equal for every single binding event. Hence, the equilibrium/binding constant and Gibbs free energy changes are considered identical for each step of the supramolecular aggregation process. In other words, there should be no energy difference between adding a monomer to a polymer or to another monomer. The isodesmic growth of aggregates can be stated as follows:

$$M + M \rightleftharpoons M_2 \qquad c_2 = K_2 c_1^2 \tag{22}$$

$$M_2 + M \rightleftharpoons M_3 \qquad c_3 = K_3 c_2 c_1 = K_2 K_3 c_1^3 \tag{23}$$

$$M_{n\text{-}1} + M \rightleftharpoons M_n \qquad c_n = K_n c_{n-1} c_1 = K_2 K_3 \ldots K_{n-1} K_n c_1^n \tag{24}$$

c_1, c_2, c_3, …, c_n are the respective molar concentrations of monomer, dimer, trimer, and *n*-mer aggregates, and K_2, K_3, …, K_n are the respective equilibrium/binding constants for the aggregation of monomer to monomer, to dimer, and to (*n*–1)-mer with $n = 2$ to infinity. Taking into account that all *K* values are identical, the molar concentration of n-mer species c_n and the total molar concentration of all molecules in solution *c*, respectively, are given by

$$c_n = K^{n-1} c_1^n \tag{25}$$

$$c = c_1 + 2Kc_1^2 + 3K^2 c_1^3 + \ldots + nK^{n-1} c_1^n. \tag{26}$$

Simplifying equation (26) by using the series expansion $1 + 2x + 3x^2 + \ldots + nx^{n-1} = 1/(1-x)^2$ (for $0 < x < 1$) yields

$$c = \frac{c_1}{(1 - Kc_1)^2}. \tag{27}$$

Solving equation (27) for c_1 gives

$$c_1 = \frac{2Kc + 1 - \sqrt{4Kc + 1}}{2K^2 c}. \tag{28}$$

Using equation (15) from above, the mole fraction of aggregated species α_{agg} can be expressed as a function of *K* and *c*:

$$\alpha_{agg} = 1 - \frac{2Kc + 1 - \sqrt{4Kc + 1}}{2K^2 c^2}. \tag{29}$$

Combining equations (29) and (20) yields the following expression for the apparent extinction coefficient $OD(\lambda)/(c \cdot d)$:

$$\frac{OD(\lambda)}{c \cdot d} = (\varepsilon_M - \varepsilon_{agg}) \frac{2Kc + 1 - \sqrt{4Kc + 1}}{2K^2c^2} + \varepsilon_{agg} \,. \tag{30}$$

Applying non-linear least-squares analysis of the apparent extinction coefficient of the corresponding dye as a function of concentration according to equation (30) yields the binding constant K and the molar absorptivities of the monomeric and aggregated species ε_M and ε_{agg} at a fixed wavelength, respectively.

A graphical comparison between the dimer and isodesmic model can be established by plotting the molar fraction α_{agg} vs. the dimensionless expression Kc according to equations (19) and (29), respectively (Figure 2). From the plots it can be seen that in the isodesmic model, α_{agg} approaches faster unity than in the dimerization model. In the latter scenario, high degrees of aggregation ($\alpha_{agg} < 0.90$) are only accessible with comparably high values for Kc.

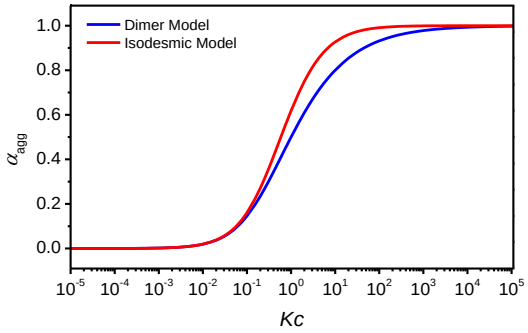

Figure 2: Plot of molar fraction of aggregated species α_{agg} vs. Kc for the dimer and isodesmic according equations (19) and (29), respectively.

1.3.3 Cooperative Nucleation-Growth Model[109,124,129-132]

In many cases, the supramolecular polymerisation process proceeds via a cooperative pathway which entails a two-step mechanism, i.e., nucleation and elongation. Such nucleation-elongation behaviour was first discovered in protein polymerisation many years ago.[130] The nucleation process relies on the initial oligomerisation of monomers which is slow and energetically disfavoured in contrast to the subsequent fast chain elongation into long fibres. Evidently, this scenario is not appropriately described by the isodesmic model which therefore has to be augmented by considering an activation step preceding the chain elongation or growth.

The simplest version of this model constitutes the cooperative K_2/K model which only considers one dimerization step of nucleation described by the equilibrium constant K_2, followed by isodesmic elongation steps described by the equilibrium constant K with $K_2 \neq$

$K_3 = K_4 \ldots = K_n = K$. It is assumed that the formation of dimers (nucleation) faces a different steric and electronic situation than the following growth process (elongation):

$$\mathrm{M} + \mathrm{M} \rightleftharpoons \mathrm{M}_2 \qquad c_2 = K_2 c_1^2 \tag{31}$$

$$\mathrm{M}_2 + \mathrm{M} \rightleftharpoons \mathrm{M}_2\mathrm{M} \qquad c_3 = K c_2 c_1 = K K_2 c_1^3 \tag{32}$$

$$\mathrm{M}_3 + \mathrm{M} \rightleftharpoons \mathrm{M}_3\mathrm{M} \qquad c_4 = K c_3 c_1 = K^2 K_2 c_1^4 \tag{33}$$

$$\mathrm{M}_{n-1} + \mathrm{M} \rightleftharpoons \mathrm{M}_{n-1}\mathrm{M} \quad c_n = K c_{n-1} c_1 = K^{n-2} K_2 c_1^n = \sigma K^{-1} (Kc)^n \qquad (n \geq 2) \tag{34}$$

with the cooperativity factor $\sigma = K_2/K$, which is the main physical parameter describing the cooperative growth. The total molar concentration c can be expressed as follows:

$$c = c_1 + \sum_{n=2}^{\infty} n\sigma K^{-1} (Kc_1)^n = (1-\sigma) c_1 + \frac{\sigma c_1}{(1 - Kc_1)^2} \tag{35}$$

Multiplying equation (35) with K yields equation (36). Hence, Kc can be calculated as a function of Kc_1 for certain σ values from 0.001-1000 in steps of one order of magnitude:

$$Kc = (1-\sigma) Kc_1 + \frac{\sigma K c_1}{(1 - Kc_1)^2} \tag{36}$$

$$\alpha_{\mathrm{agg}} = 1 - \frac{Kc_1}{Kc} \tag{37}$$

The corresponding plot is shown in reverse (Kc_1 vs. Kc) in Figure 3(a). The values obtained for Kc can be used to calculate the degree of aggregation α_{agg} according to equation (37). For an illustrative comparison between different systems, α_{agg} is plotted as a function of the total molar concentration c normalised with the elongation constant K, yielding an expression which is independent of the aggregation constants (Figure 3(b)). The resulting plot can be divided into two sections: The first section refers to values for $\sigma > 1$ and describes anti-cooperative self-assembly processes, while the second section with $\sigma < 1$ reflects cooperative processes. The curve for $\sigma = 1$ corresponds to the isodesmic model which was introduced above. From Figure 3(b), it can be seen that, in a highly cooperative system ($\sigma << 1$), when $Kc < 1$, almost all the molecules are in the monomeric state (i.e., $c_1 \approx c$). With increasing total concentration c, the monomer concentration c_1 rises concomitantly, but to a certain limit. When Kc exceeds unity the monomer concentration c_1 stops rising and stays constant at the value of K^{-1} (Figure 3(a)). The remaining molecules (c–c_1) are transformed into polymers. Hence, K^{-1} is definded as the critical concentration (c_{critical}) above which notable polymerisation occurs. Even though the mathematical models for the cooperative self-assembly processes appear rather intricate, it is yet quite easy to distinguish experimentally

between the cooperative and isodesmic model, as the former is marked by a $c_{critical}$ at which monomers self-associate within a narrow regime fairly sharply into extended polymers. Another interesing finding is that when Kc is around unity, the monomer concentration is considerably higher than that found in an isodesmic system. This goes hand in hand with experimental observations in which a substiantial amount of protein monomer was found to exist along with high polymers at equilibrium.

To design a polymerisation system providing cooperative chain growth, an essential prerequisite has to be fulfilled. The repeating units must be capable to undergo at least two supramolecular interactions with other units in the same chain, e.g., π-π stacking and hydrogen bonding. Well-defined, higher-order structures can thus be achieved which are the results of interactions between non-adjacent units.

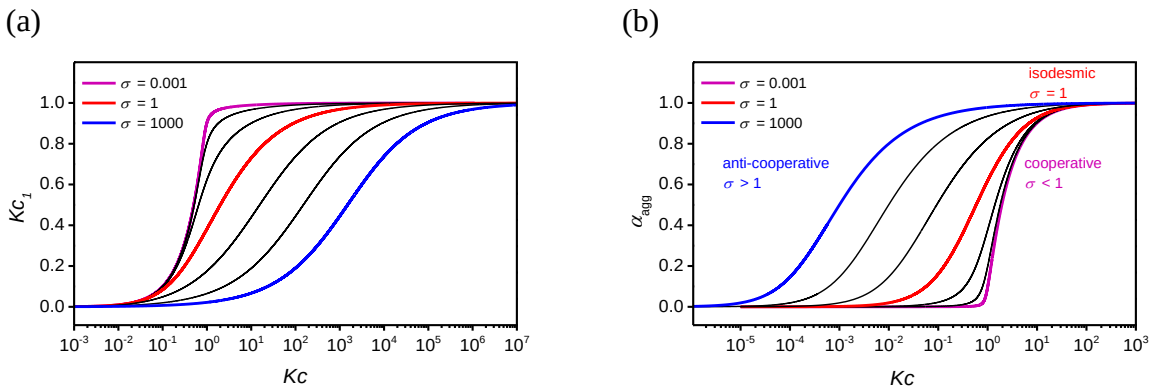

Figure 3: Plots of (a) Kc_1 and (b) α_{agg} vs. Kc using equation (24) and (37), respectively, with σ = 0.001-1 000 in steps of one order of magnitude.

A great variety of systems have hitherto been examined in which the supramolecular polymerisation process was shown to comply with the cooperative model. In contrast, there are only a few studies featuring anti-cooperative behaviour. Recently, Gershberg et al. showed that equation (36) does not properly describe the aggregation behaviour of a newly synthesised chiral perlyene bisimide dye in non-polar solvents.[124] While the dye exclusively forms dimeric aggregates in $CHCl_3$, these dimers self-associate further into larger oligomers in non-polar solvents following an anti-cooperative mechanism in which even numbers of aggregated species are predominant. The initial model evidently does not account for such an anti-cooperative elongation mechanism as it does not differentiate between even and odd numbered aggregates. In the light of this discrepancy, a new K_2/K-model was established.[124] Accordingly, the formation of dimers is described by equation (38) with the dimerization constant K_2:

$$M + M \rightleftharpoons M_2 \qquad c_2 = K_2 c_1^2 \tag{38}$$

Under consideration that elongation is less favoured than dimerization ($K < K_2$), dimers can further assemble with another monomer yielding trimers:

$$M_2 + M \rightleftharpoons M_2M \qquad c_3 = Kc_2c_1 \tag{39}$$

In contrast, the dimers can also assemble with another dimer leading to tetramers:

$$M_2 + M_2 \rightleftharpoons M_4 \qquad c_4 = Kc_2c_2 = Kc_2^2 \tag{40}$$

In general, further association for odd and even numbered aggregate species can be expressed by equation (41) and (42), respectively:

$$c^{\text{odd}} = K_2^{\frac{n-1}{2}} K^{\frac{n-1}{2}} {c_1}^n \tag{41}$$

$$c^{\text{even}} = K_2^{\frac{n}{2}} K^{\frac{n}{2}} {c_1}^n \tag{42}$$

The sum over all odd and even n yields the concentration of all molecules in odd and even numbered aggregates, respectively:[IV]

$$c_{\text{agg}}^{\text{odd}} = \frac{Kc_1c_2(3 - Kc_2)}{(1 - Kc_2)^2} \tag{43}$$

$$c_{\text{agg}}^{\text{even}} = \frac{2c_2}{(1 - Kc_2)^2} \tag{44}$$

In the end, it can be shown that the maximal fraction of molecules in odd numbered aggregates is always smaller than the square root of the aggregation constants according to equation (45):

$$\frac{c_{\text{agg}}^{\text{odd}}}{c_{\text{agg}}^{\text{even}}} < \sqrt{\frac{K}{K_2}} \tag{45}$$

1.3.4 Literature Examples of Intermolecular Squaraine Aggregates

In the early 90s, the aggregation behaviour of squaraine dyes has extensively been studied in particular by the groups of Buncel, Whitten, and Das. The studies were mostly performed in aqueous solutions or mixtures where the hydrophobic effect easily outweighs the non-covalent forces that lead to aggregation.[126]

Buncel and co-workers investigated a series of symmetrical anilino-based squaraines (**SQ1**–**SQ3**) with increasing *N*-alkyl chains (*n*-butyl, *n*-octyl, and *n*-dodceyl) which showed an

[IV] For a detailed derivation of equations (43)–(44), please see supporting information of reference (124) Gershberg, J.; Fennel, F.; Rehm, T. H.; Lochbrunner, S.; Würthner, F. *Chem. Sci.* **2016**, *7*, 1729.

ambivalent aggregation behaviour in dimethyl sulfoxide (DMSO)-water mixtures which is strongly controlled by the composition of the binary solvent system (Figure 4).[95,96]

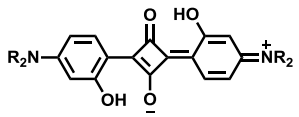

SQ1 R = *n*-butyl
SQ2 R = *n*-octyl
SQ3 R = *n*-dodecyl

Figure 4: Chemical structure of symmetrical anilino-based squaraine dyes **SQ1**–**SQ3**.

While J-aggregate formation was observed in water with low DMSO content, solvent mixtures containing high percentages of DMSO caused H-aggregate behaviour. For the intermediate range, a dynamic conversion from metastable J- to thermodynamically stable H-type aggregates was monitored. Dynamic light scattering (DLS) measurements revealed that the transition between the aggregate forms directly results from an intramolecular reorganisation, since no change in aggregate size was monitored during this process. The main driving force for H-type aggregates at high DMSO contents was ascribed to highly favourable dipole-dipole interactions between solvent and aggregate. In contrast, hydrophobic and charge-transfer interactions were found to be the main operating forces for the stabilization of J-aggregates in solvent mixtures with low DMSO contents. In addition, DLS measurements in 10 % DMSO revealed a strong correlation between the aggregate size and the length of peripheral alkyl-chains. Thus, on traversing the *n*-butyl, *n*-octyl, *n*-dodecyl series, the aggregates were found to consist of 210, 290, and 365 molecules, respectively, clearly demonstrating a relationship between the degree of aggregation and hydrophobicity.
In a further study, Whitten and co-workers reported on a similar squaraine dye (**SQ4**) embedded within an amphiphilic structure (Figure 5).[97]

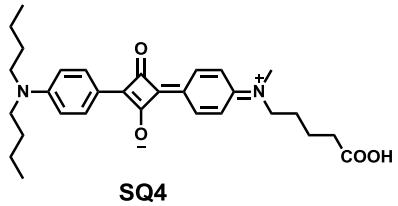

SQ4

Figure 5: Chemical structure of unsymmetrical aniline-derived squaraine dye **SQ4**.

The aggregation behaviour of **SQ4** was studied in a variety of media, including organic solvents and aqueous solutions. The dye was readily soluble in $CHCl_3$, MeOH, and DMSO, giving rise to blue solutions with sharp absorption and fluorescence bands, respectively.

These findings are typical signatures of squaraine dyes in the monomeric state. Furthermore, the dye provided sufficient solubility and stability in water at a pH of 7.5 for spectroscopic evaluations. The aqueous absorption spectrum exhibited a maximum at 650 nm with a shoulder at 594 nm. With increasing concentration of **SQ4** the high energy peak at 594 nm increased relative to that at 650 nm. Diluted aqueous solutions of **SQ4** also showed fluorescence with a peak at 678 nm. The excitation spectrum probed at this wavelength was in good agreement with the absorption band at lower energies. The spectral changes observed upon increasing the concentration of **SQ4** in aqueous solution were ascribed to a thermodynamic equilibrium between two explicit species, i.e., the monomer and the dimer. The blue-shift of the absorption concomitant with dimer formation implies an H-type dimer or card pack assembly. In addition, the dimerization process was quantitatively assessed yielding a binding constant $K_D = 4.0 \times 10^4$ M^{-1}.

Thermodynamic studies were also carried out by Das and co-workers on bis(2,4-dihydroxyphenyl) squaraine (**SQ3**) and bis(2,4,6-trihydroxyphenyl) squaraine (**SQ4**) in the highly polar solvent MeCN (Figure 6).[102]

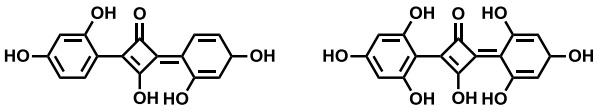

SQ5 **SQ6**

Figure 6: Chemical structures of hydroxyphenyl-squaraine dyes **SQ5** and **SQ6**.

Both dyes possess energetically accessible keto-enol forms which are able to engage intra- and intermolecular hydrogen bonds. The absorption spectra of both dyes in MeCN show a broad band centred around 480 nm. With an increasing concentration of **SQ5** and **SQ6**, a sharp new band at 565 nm arises which was interpreted to be cause by J-type aggregate formation, respectively. Interestingly, for **SQ5**, a very weak band was additionally spotted at 400 nm which was assigned to H-type aggregates rationalised by a sandwich-type orientation. The aggregate size was determined to be 2 for **SQ5** and **SQ6**, indicating a reversible thermodynamic equilibrium between the monomer and dimer species. The dimerization constants K_D were estimated to be 3.1 and 2.2×10^5 M^{-1}, respectively. These high values suggest a high driving force for aggregation even in dilute solutions. Involvement of intermolecular hydrogen bonding in the aggregation process was further confirmed by adding minor amounts of solvents which are capable of hydrogen bonding which led to a decrease of the aggregate band in favour of the absorption in the monomer region.

In a more recent study, Hecht and co-workers reported a L-proline-derived amphiphilic bis(4-dialkylamino-2,6-dihydroxyphenyl) squaraine dye (**SQ7**), which was prepared from a chiral secondary amine with 1,3,5-trihydroxybenzene and subsequent reaction with squaric acid in a one pot reaction (Figure 7).[107] In this study, chirality was used as directing element in an elegant way to bias the self-assembly process of **SQ7**.

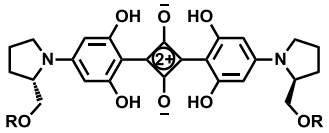

SQ7
R = *n*-decyl

Figure 7: L-Proline-derived squaraine dye **SQ7**.

The dye bearing four hydroxy-functions exhibits much higher fluorescence quantum yields, increased relative stability, and a more pronounced aggregation propensity than their non-hydroxylated congeners due to the rigidifying nature of intramolecular hydrogen bonds. The absorption spectra of the chiral **SQ7** display a prominent and sharp band centred around 640 nm indicating the monomeric state. Negligible red-shifts were observed upon changing the solvent polarity from cyclohexane to $CHCl_3$ and to MeCN. Because of the hydrophobic character of **SQ7** and the property of water to facilitate aggregation as a consequence of the hydrophobic effect, solvent titration studies were carried out in which the water content in MeCN solutions was systematically varied. It was demonstrated that at 18 vol.-% water content aggregate bands start to arise. Upon further increasing the water content the monomer band is drastically reduced in favour of blue and red-shifted bands at 555 and 761 nm, respectively. The aggregation behaviour was also studied by circular dichroism (CD) which yields information about the difference in the absorption of left- and right-handed circularly polarised light and thus detects the presence of enantiomeric or diastereomieric excess.[133]
The CD spectra showed a strong negative Cotton effect[134,V] which corresponds to the low-energy aggregate band. The pronounced effect is highly suggestive of strong exciton coupling of the monomers within the aggregate. In contrast, a rather weak exciton couplet was observed for the blue-shifted band at 555 nm. The marked aggregation behaviour was also studied as a function of temperature in aqueous MeCN solutions with high water content. Upon raising the temperature from 298 to 333 K, the aggregate bands decrease with a concomitant rise of the monomer band. Two clear isosbestic points were observed indicating

[V] The characteristic change in optical rotary dispersion (ORD) and/or CD occurring in the spectral region of an absorption band is called Cotton effect.

a dynamic conversion of only one aggregate species to the non-aggregated squaraine **SQ7**. This was further evidenced by monitoring the deaggregation process by CD spectroscopy, which revealed the loss of ellipticity and the presence of an isodichroic point at 700 nm. The occurrence of two absorptions bands exclusively originating from one aggregate type along with a large exciton splitting (4 880 cm^{-1}) and a strong Cotton effect are indicative of a helical aggregate architecture.

A similar approach towards supramolecular squaraine assemblies was taken by Ramaiah and co-workers in 2007 who synthesised a cholesterol-appended chiral squaraine dye (**SQ8**) (Figure 8).[108]

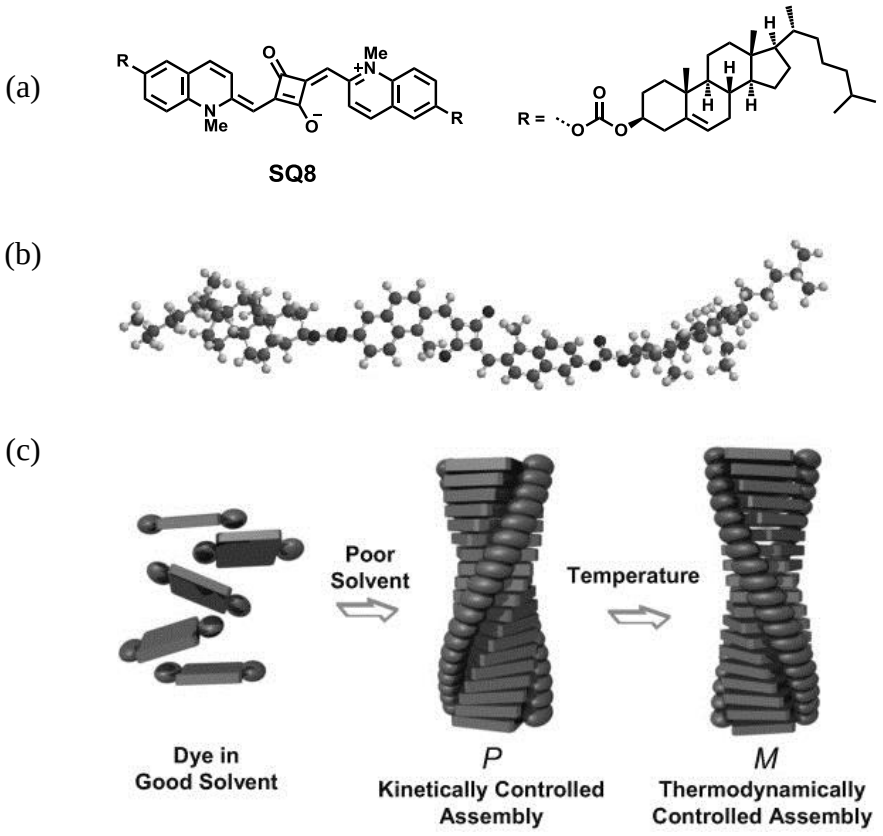

Figure 8: (a) Chemical and (b) geometry-optimised structure of cholesterol-appended squaraine dye **SQ8**. (c) Schematic representation of kinetically and thermodynamically controlled self-assembly of **SQ8**. Reproduced with permission from *Chiral Supramolecular Assemblies of a Squaraine Dye in Solution and Thin Films: Concentration-, Temperature-, and Solvent-Induced Chirality Inversion*, K. Jyothish, M. Hariharan, D. Ramaiah, Copyright © (2007) WILEY-VCH Verlag GmbH & Co. KGaA, Weinheim.

Absorption studies in binary solvent mixtures of $CHCl_3$ and MeCN demonstrated that **SQ8** self-assembles in two H-type chiral supramolecular architectures with opposite chirality at different solvent compositions. The aggregation behaviour was studied by CD spectroscopy in a 1:1 solvent mixture of $CHCl_3$/MeCN and revealed a bisignate CD signal with a negative Cotton effect indicating the presence of a left-handed helical assembly. Upon increasing the

fraction of MeCN the CD spectra changed from a negative to a positive Cotton effect which can be rationalised by a conversion from a left-handed (M) to a right-handed assembly. Joint temperature- and concentration dependent experiments showed that the supramolecular assembly formed at lower fractions of MeCN can be ascribed to the thermodynamically stable form, while the assembly formed at higher fractions of MeCN can be referred to the kinetically controlled form. In the light of the solvent-driven chirality inversion, it was argued that solvent effects such as solvation and solvent polarity surrounding the aggregate mainly direct the handedness of the resulting supramolecular architecture.

In 2012, Würthner et al. presented the first example of a cooperative self-assembly process of a pyrrole-derived squaraine dye (**SQ9**).[109]

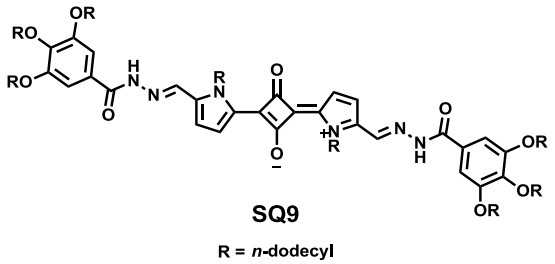

Figure 9: Chemical structure of pyrrole-derived squaraine dye **SQ9**.

The absorption behaviour was studied in solvents of different polarity, including DCM, THF, toluene, and MCH. In DCM and THF, the dye exhibited typical absorption features of squaraine chromophores in the monomeric state, i.e., a sharp and intense absorption band in the low-energy region along with a blue-shifted vibronic progression. In contrast, by switching to the non-polar solvent toluene, the absorption of **SQ9** additionally showed a hypsochromic band aside the low-energy band, which was assigned to H-type aggregates. In the least polar solvent MCH, the absence of monomer band and the sole presence of the aggregate band clearly indicate a high degree of aggregation. The large hypsochromic shift of 3 311 cm^{-1} in MCH compared to DCM points towards the formation of extended H-aggregates of tightly stacked π-systems undergoing pronounced exciton coupling. Interestingly, the spectra in MCH turned out to be time-dependent indicating kinetically trapped states, whose conversion into thermodynamically stable H-aggregates proved to be very slow. On the other hand, thermodynamically stable aggregates of **SQ9** instantaneously formed in toluene. The size of aggregates was investigated in toluene by DLS experiments which revealed an aggregate size distribution in the range of ~ 100 nm to several micrometres, as anticipated for extended columnar assemblies. Concentration- and temperature-dependent absorption studies in toluene showed a gradual transition from

aggregated to monomeric species with a clear isosbestic point, respectively. The thermodynamic interpretation of the self-assembly process was carried out by using the cooperative K_2/K nucleation-elongation model as the alternative isodesmic model clearly failed to describe the supramolecular polymerization of **SQ9** accurately. The data could be fitted with good agreement to the cooperative growth process revealing a cooperativity factor σ (= K_2/K) of 0.1, an equilibrium constant K for the elongation regime of $4.87 \pm 0.13 \times 10^5$ M^{-1}, along with an equilibrium constant K_2 for the nucleation (dimerization) regime of $4.87 \pm 0.13 \times 10^4$ M^{-1}. The structural features of the aggregates were further investigated by AFM studies, revealing the formation of extended fibres with lengths of 3–10 µm. It was argued that concerted dispersion and hydrogen bonding were the main operating forces for the formation of such extended supramolecular architectures.

A somewhat different approach towards squaraine aggregates is the use of organising media, such as anionic surfactants. Accordingly, Pang and co-workers reported a series of charged benzothiazole squaraine dyes (**SQ10** – **SQ12**), whose self-association turned out to be highly susceptible to the polarity of the surrounding media (Figure 10).[112]

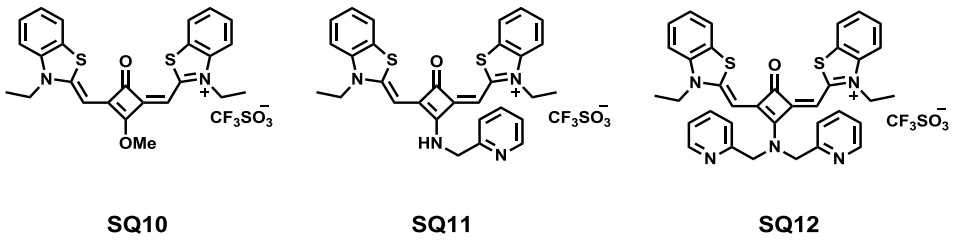

Figure 10: Chemical structures of charged squaraine dyes **SQ10** – **SQ12**.

It could be shown that the dyes provided characteristic absorption profiles of molecularly dissolved species in organic solvents, whereas blue-shifted H-type aggregate bands emerged in aqueous solutions. The relative absorption intensity of these new bands increased from **SQ12**, to **SQ10**, and finally to **SQ11**, indicating their relative propensity for self-assembly in aqueous solutions. The situation significantly changed upon addition of SDS. Using SDS concentrations below the critical micelle concentration (CMC), the absorption spectra of **SQ11** and **SQ12** feature new bands at lower energies indicating J-type aggregates, whereas the H-aggregate band in **SQ11** remains present. In sharp contrast, **SQ10** exhibits a strongly blue-shifted band with a remarkably narrow bandwidth, suggesting a well-defined aggregate structure. Thus, these spectral findings emphasise the structure-directing nature of SDS towards aggregate formation, which is interpreted to rely on the intermolecular interactions of SDS with the positively charged squaraine dyes leading to a disruption of the non-covalent

forces between the dye. In this regard, it was speculated that the anionic ends of the surfactant interact with the cationic sites of the dyes, thereby rendering the dyes less polar and thus enhance aggregation. In addition, regarding the different chemical structures of the dyes, it was found that the increase in steric bulkiness from **SQ10** to **SQ12** considerably influences H- and J-type selectivity. By means of molecular modelling, it could be shown that **SQ10** adopts a parallel H-aggregate form thus allowing for maximum π–π interactions due to the absence of steric constraints at the centre of the chromophore. With increasing steric constraint from **SQ11** to **SQ12**, the chromophores favour a more antiparallel H-type and finally a slipped J-type arrangement, respectively. In summary, the elaborations by Pang et al. could disclose a valuable insight into the possibilities of how to control the supramolecular H- and J-type aggregate formation, which was elegantly achieved by adequately conceived dyes embedded in an organised media.

In a related study, Yefimova and co-workers also investigated the aggregation behaviour of an indolenine squaraine dye (**SQ13**) in the presence of SDS in binary DMSO-water solvent mixtures (Figure 11).[110]

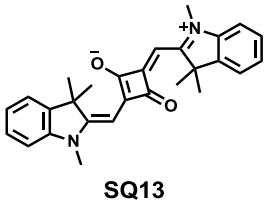

SQ13

Figure 11: Chemical structure of squaraine dye **SQ13**.

In contrast to the previous study, the absorption experiments were conducted above the CMC in order to promote the dye ordered self-assembly. In pure DMF and even in binary mixtures with water contents up 90 %, the dye exhibited typical monomer absorption characteristics. In contrast, upon increasing the water content up to 95 %, the corresponding spectrum became very broad and diffuse, which hints towards structurally distorted aggregates. The addition of anionic SDS to the latter mixture at a fixed dye concentration caused a pronounced spectral transformation which manifested itself in the gradual recovery of the monomer absorption. Furthermore, the absorption behaviour of **SQ13** was also studied as a function of dye concentration in the DMSO-water mixture = 5:95 at a fixed SDS concentration. With increasing concentration of **SQ13**, the intensity of the monomer band is reduced, and a concomitantly appearing bathochromically shifted new band revealed the aggregation of the dye. A well-defined isosbestic point occurs, clearly indicating the presence of thermodynamic equilibrium between monomeric and aggregated dye. As SDS represents a well-established

anionic surfactant with known parameters for micelle formation, Yefimova et al. could thus conclude on the size of the J-type aggregates, which were found to consist of dimers.

Conversely, Bonnet and co-workers have recently shown that in the polarity sensitive foldamer **SQ14**, the chromophores represented by the indolenine squaraine moiety form dimeric H-type aggregate π-stacks in aqueous solution, clearly emphasising the ambivalent aggregation nature of this chromophore type (Figure 12).[111]

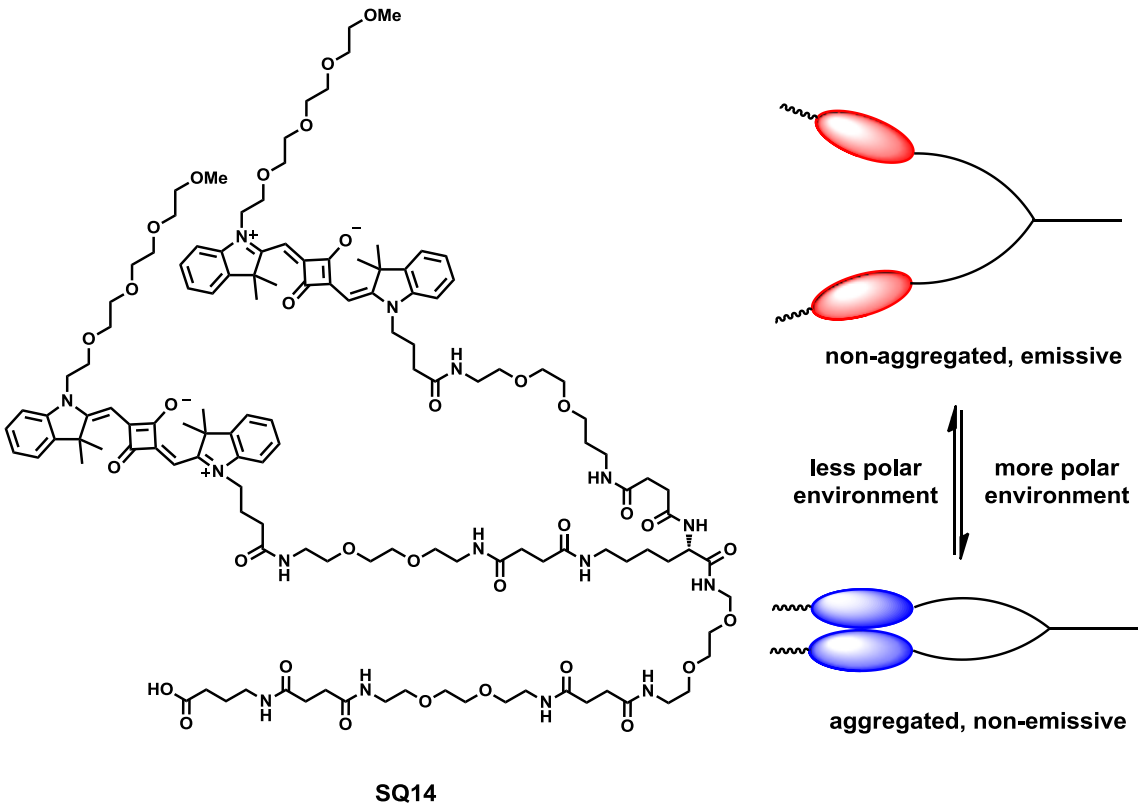

Figure 12: Chemical structure of polarity-sensitive foldamer **SQ14** and schematic illustration of its working principle.[111]

The squaraine dyes were attached to polyethylene glycol (PEG) chains, which are long enough to equip the chromophores with some flexibility but also short enough to enable their proper folding into stacked aggregates.

In summary, the latter, as well as all other aforementioned studies, showcase the high sensitivity of squaraine dyes towards the polarity of the environment to promote aggregation or deaggregation. Combined with strongly diverging photophysical profiles of monomeric and aggregated states, squaraine dyes have attracted not only interest for fundamental investigations, but have also proven an immense potential in the development of chemosensors in biological applications.[12]

A totally different strategy towards supramolecular squaraine aggregates was taken by Ajayaghosh and co-workers and involves the use of metal ions and podants to craft hierarchical self-assemblies in nanoscopic dimensions.[29-31] It was found that di- and tripodal squaraine dyes **SQ15 – SQ17** express a high affinity towards metal cations leading to various aggregate structures, such as spherical, micellar and helical architectures (Figure 13).

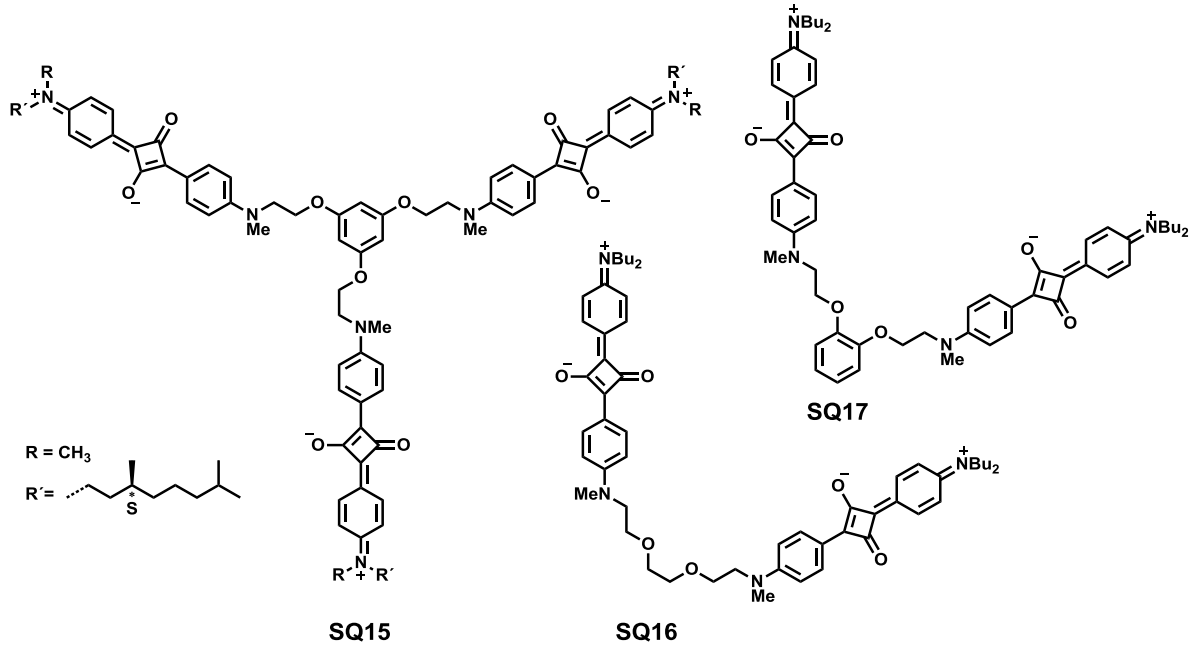

Figure 13: Chemical structures of squaraine podants **SQ15** – **SQ17**.

Notably, the response to metal ions afforded highly ordered aggregate structures with remarkably narrow H-aggregate absorption bands similar to SDS-assisted H-type aggregates of benzothiazole squaraine dye **SQ10**.

The brief glance at squaraine aggregates revealed that only a very limited number of studies were dedicated to the mechanistic and thermodynamic aspects of squaraine aggregation.[97,102,109] A quantitative understanding of the thermodynamics and structural features of the aggregates based on functional dyes plays a pivotal role for the precise control of the self-assembly process and thus for the optimization of the photophysical properties of self-associated systems.[126] The precise control of the self-organisation process in squaraine aggregates but also the control of the superstructure formation in covalently linked squaraine oligo- and polymers represent the main challenging tasks in this work.

.

2 Scope of the Work

This work partly follows the fundamental investigations of Völker et al. on a dicyano-vinylene-substituted polymeric squaraine dye, which showed a quite unusual spectroscopic behaviour in solution.[71] It was found that the absorption band manifold is strongly dependent on the solvent, giving rise to either blue- or red-shifted absorption bands with respect to the monomer absorption, which were assigned to intramolecular H- and J-type aggregates. Joint experimental and theoretical studies suggest that both spectral features are caused by zig-zag and helical conformations of the polymer.[73]

On account of the latter findings, this polymer is resynthesized in order to examine the exciton coupling effects in closer detail. Particularly, the influence of temperature on the absorption and thus on the folding of the polymer in solution will be investigated. Furthermore, the synthesis of oligomers with known molecular weight (dimer, trimer) will also be pursued to compare oligomer properties with those of analogous polymers, which might enable the design of polymers with tailor-made optical properties.

In a next step, the focus is directed on the control of the optical properties of squaraine polymers which aims at the selective formation of only one superstructure. One basic idea for controlling the folding behaviour constitutes the adequate design of monomer precursors. In this respect, it is assumed that the structure and the electronic properties of the donor moiety have a decisive impact on the conformer structure of the polymer. To this end, a screening of different donor-substituted squaraine monomers are given at the beginning of this work in which the optical properties are examined in detail to assess their eligibility for the polymer synthesis. Thus, these findings shall help to synthesise polymers whose optical properties are exclusively controlled by their inherent monomer structure.

The second part of this work deals with the synthesis and optical spectroscopy of squaraine homo- and heterodimers, in which different spacer units shall be implemented. By this, the influence of the different spacers on the exciton coupling strength will be examined, which manifests itself in the overall optical properties of the dimers. In addition, this section shall provide valuable insights into the specific design of squaraine oligomers with optical properties desired and how to optimise beneficial properties such as red-shifting and spectral broadening of absorptions bands. These aspects are a matter of particular interest for the design of optoelectronic devices and may be easily manipulated by the appropriate choice of spacer and/or monomer unit.

The following section provides a continuation of the previous chapter and considers exciton coupling interactions in alternating squaraine heterotrimers. In addition, the synthesis of a trimer bearing three disparate squaraine monomers covalently connected in a logical order is envisioned. This will give rise to a chromophore cascade which might be an ideal showcase for probing dynamic processes, i.e., energy transfer, by using ultra-fast time-resolved absorption spectroscopy. In particular, one may also be able to investigate the couplings between the states using two-dimensional (2D) spectroscopy, which, in contrast, are not accessible via classical transient absorption measurements.

The last chapter of this work follows previous studies by Ceymann et al. on star-like squaraine trimers and deals with squaraine oligomers arranged in a hexaarylbenzene framework.[69,93] This star-shape linkage motif deviates from the linear one established for all other systems in this thesis and might lead to enhanced electronic communication between the chromophore tentacles because of their closer distance as compared to analogous trimers. Two star-shaped hexasquarainyl benzenes are envisioned which differ in length, mutual distance and orientation of the squaraine tentacles. As exciton theory[74,75] predicts a high susceptibility of the coupling strength to alterations in the spatial arrangement of the transition moments, the two hexasquarainyl benzenes might exhibit completely different optical properties compared to each other and their monomers, and potentially to their linear congeners as well.

3 Results and Discussion

3.1 Reference Squaraine Monomers

3.1.1 Introduction

The synthesis of a broad selection of squaraine oligomers and polymers is generally preceded by the preparation of adequately functionalised squaraine monomers. Nevertheless, the preparation of non-functionalised squaraine monomers is considered equally important as these monomeric dyes were conceived to serve as reference dyes for the comparison of the spectroscopic properties. Even though the monomers are covalently linked to each other, these oligomers and polymers can be considered as chains of separate chromophores since the chemical and physical properties of the monomeric units are largely preserved within the polymers. Furthermore, non-functionalised chromophores are more suited for reference compounds than their functionalised analogues since substituents can significantly manipulate the optical properties of the dyes and the reasons for that are mostly not well understood. In this context, a striking halogen effect was previously reported about a series of squaraine dyes, which lead to unexpected superior fluorescence properties against the general belief about heavy atom quenching effects.[135] For these reasons, the synthesis and spectroscopy in the following will be discussed only in terms of the non-functionalised squaraine dyes.
At this point, it should explicitly be mentioned that other groups[49,136] have already reported about the following chromophores. Despite the fact, that these reference dyes have not all been studied in toluene and $CHCl_3$ so far, this chapter should solely provide a brief overview about the squaraine diversity and the possibilities to alter the optical properties, and on the other hand, a comparison of the dyes in order to select the ones with the most promising optical properties for subsequent functionalization and polymerization.

3.1.2 Synthesis

The synthesis of the basic heteroazole squaraine analogues **SQA** – **SQF** is straightforward and carried out in two steps. The commercial availability of the selected heteroazole building blocks makes the preparation of the respective heterocycles obsolete and the molecular design can thus be pursued by starting with the alkylation, respectively. In fact, the alkylation reaction of the heteroazole nitrogen plays a key role not only in terms of the solubility of

monomeric dyes, but also of higher oligomers and polymers. As it turned out, branched alkyl chains proofed to be superior compared to their linear analogues and thus allow the synthesis and spectroscopy of larger oligomers and polymers, and in a broader variety of solvents.[71] Taking advantage of these findings, 1-iodo-3,7-dimethyloctane was chosen as alkylating agent, which can be readily synthesized from the corresponding commercially available racemic, terpenoid alcohol.[137] The quaternization reaction of the heteroazole derivatives **1** – **5** is generally performed with an excess of alkylating agent in polar solvents, e.g. $MeNO_2$ or MeCN, at elevated temperatures (Scheme 2).

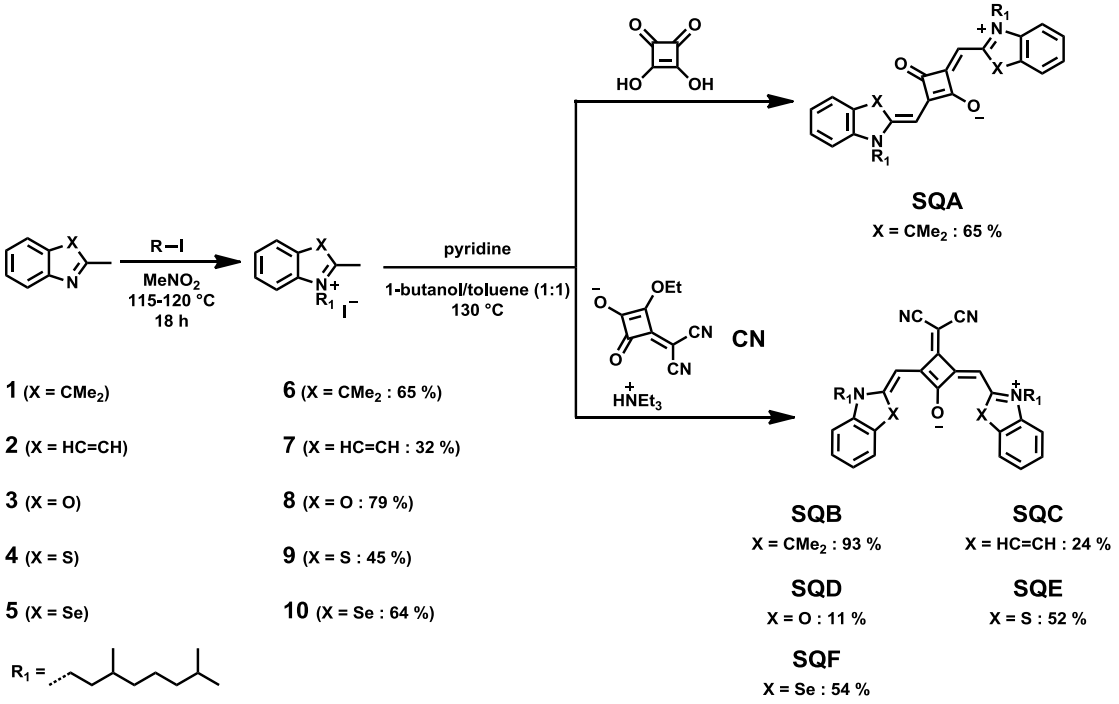

Scheme 2: Synthesis of reference squaraine monomers **SQA – SQF**.

The mechanism for the quaternization proceeds via a nucleophilic substitution of the halogen function by the nucleophilic nitrogen of the heteroazole moiety. The quaternary iodides were prepared in rather good yields, typically decreasing as the length and the degree of branching increases.[138] In this context, it is worth noting that the reaction with branched alkyl chains require higher temperatures than their linear congeners. The quaternary ammonium salts **6** – **10** bearing an activated methyl group in the 2-position, are considered to be the ultimate precursor for the synthesis of squaraine dyes. In situ deprotonation of the quaternary salts **6** – **10** at the 2-position using pyridine as base in a solvent mixture of toluene and 1-butanol (1:1) leads to the corresponding highly nucleophilic methylene base which reacts with squaric acid or dicyanovinylene-functionalised squaric acid (**CN**) in a double condensation reaction to the respective heteroazole squaraine dyes **SQA – SQF**. During the condensation reaction, the

reaction mixture becomes deeply coloured and the dyes are afterwards isolated and purified by flash column chromatography and subsequent recrystallization from *n*-hexane. Due to the steric demand of the dicyanovinylene-function, the squaraine dyes **SQB-SQF** exclusively occur in a *cis*-configuration, whereas **SQA** adopts a *trans*-configuration.

3.1.3 Absorption Spectroscopy

The basic absorption properties are given by the respective spectra of the non-functionalised reference dyes **SQA** – **SQF** in toluene according to Figure 14. The optical properties of all reference dyes are summarised in Table 1. The squared transition moments μ_{eg}^2 were obtained by integration of the main low energy absorption band and calculated according to equation (46):[139]

$$\mu_{eg}^2 = \frac{3hc\varepsilon_0 \ln 10}{2000\pi^2 N_{Av}} \frac{9n}{(n^2+2)^2} \int \frac{\varepsilon}{\tilde{\nu}} d\tilde{\nu} \qquad (46)$$

In this equation, h is Planck´s constant, c is the speed of light, N_{Av} is Avogadro´s constant, ε_0 is the permittivity, n is the refractive index of the solvent, and ε is the extinction coefficient. Owing to their characteristic donor-acceptor-donor structure, all squaraine dyes share the common feature of an intense main absorption band in the red region along with a shoulder from a vibronic progression located at the high energy side (Figure 14).[11] While the prominent main absorption band arises from a HOMO→LUMO transition, the vibronic progression originates from the coupling between electronic and vibrational degrees of freedom, in particular C-C stretching modes.[88]

Squaraine **SQA** has the most blue-shifted absorption maximum (15 500 cm^{-1}) and displays a very high extinction coefficient of 3.64×10^5 $M^{-1}cm^{-1}$ together with a squared transition moment of 127 D^2. By replacing one oxygen atom of the central squaric acid ring by a dicyanomethylene group, the electron acceptor strength of the central squaric acid moiety is increased which ultimately leads to an energetic decrease of the LUMO level and finally to a bathochromic shift of the absorption of ca. 1 200 cm^{-1} for **SQB**, as a result of the smaller band gap. The benzoxazole-substituted dye **SQD** effectively absorbs at same energy as **SQA** and thus represents the most blue-shifted reference for the series of *cis*-configured dyes. Starting from **SQD**, a progressive red-shift can be induced by implementing stronger donor moieties ($O < CMe_2 < S < Se$) into the squaraine framework. Besides, another approach to red-shift the absorption is an extension of the π-conjugated system, which could be achieved by using 2-methylquinolin as donor building block. In this context, the corresponding reference dye **SQC**

yields the lowest energy absorption maximum and thus represents the most red-shifted dye of the herein presented dicyanovinylene-functionalised derivatives. To sum up, all squaraine dyes can be sorted according to the energies of their main absorption band, which is done in descending order: **SQA** > **SQD** > **SQB** > **SQE** > **SQF** > **SQC**.

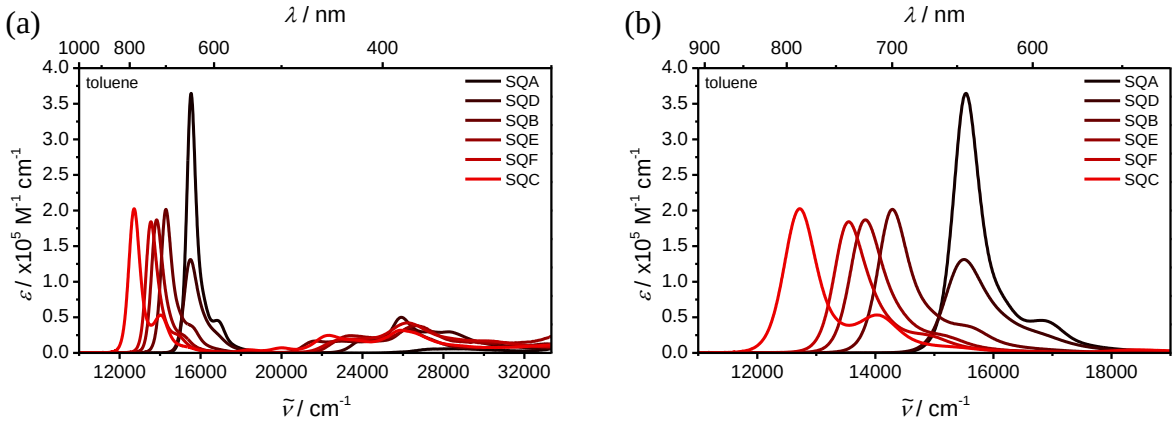

Figure 14: Absorption spectra in toluene of reference dyes **SQA – SQF**, sorted in descending order according to the energies of absorption maxima.

The squared transition moments range from 72.1 to 112 D^2 for **SQD** and **SQC**, respectively. Among the *cisoid*-analogues, the high energy shoulder at ca. 14 000 cm^{-1} is most prominent for **SQC** which should strictly speaking rather be considered as an additional maximum than a shoulder. The extinction coefficients for **SQB – SQF** (1.39-2.03×10^5) are almost 50 % smaller than for **SQA** (3.64×10^5). Besides the full widths at half maximum (FWHM) for the *cisoid*-derivatives (~ 720 cm^{-1}) are on average ~ 30 % larger than for **SQA** (540 cm^{-1}). When toluene is exchanged by the more polar solvent $CHCl_3$ (not shown), the absorption maxima shift towards higher energies and the extinction coefficients decreases while the squared transition moments slightly increase, yet are still very similar. These findings are summarised in Table 1.

Since all relevant features for the herein presented dyes are exclusively observed for the prominent main low energy absorption band, the spectral window for most of the absorption spectra shown in this work will be centred around the low energy band (10 000-22 000 cm^{-1}) without the high energy spectral range.

3.1.4 Fluorescence Spectroscopy

The normalised fluorescence spectra of reference dyes **SQA – SQF** in toluene are shown in Figure 15(a). For the convenience of representation, the normalised absorption spectra are additionally depicted in Figure 15(b). Generally, the fluorescence spectra of the squaraine dyes behave like mirror images to the corresponding absorption spectra and thus exhibit Strickler-Berg symmetry.[11,88] While the Stokes shifts are somewhat larger for the dicyanovinylene-functionalised squaraine dyes (200-400 cm^{-1}), **SQA** provides the smallest one of only about 100 cm^{-1}.

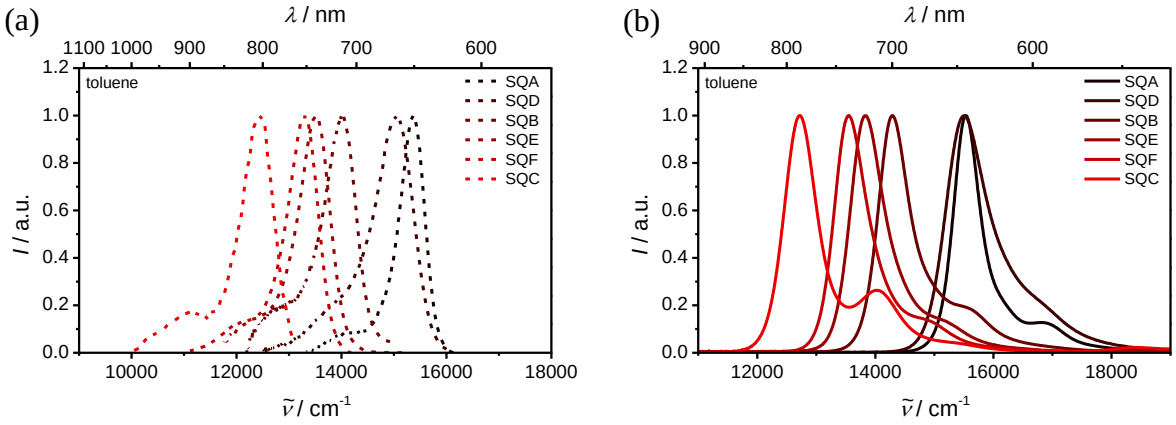

Figure 15: Normalised (a) fluorescence and (b) absorption spectra in toluene of reference dyes **SQA-SQF**, sorted in descending order according to the energies of absorption and fluorescence maxima, respectively.

Analogously to the absorption spectra, the emission spectra are slightly blue-shifted when measured in $CHCl_3$ (not shown). Yet, a significant solvent dependence on the fluorescence quantum yield Φ_{fl} is observed in both solvents. While high quantum yields of 0.62 and 0.75 are obtained for the indolenine squaraine dyes **SQA** and **SQB** in nonpolar solvent toluene, lower quantum yields of 0.51 and 0.55 are measured in the polar solvent $CHCl_3$, respectively. Interestingly, the opposite trend was found for the heteroazole derivatives **SQD – SQF**, where the highest quantum yields of 0.85-0.93 are observed in $CHCl_3$. Nevertheless, the quantum yields in toluene (0.75-0.89) are still very high. Quite remarkably and for unknown reasons, the quinoline-substituted squaraine dye **SQC** turns out to be a poor emitter in toluene and even more in $CHCl_3$. Thus, no reliable quantum yields could be stated due to the extremely week emissive character. The absolute determination of quantum yields in the scientific community is still a matter of debate.[140] Without a doubt, the values for the herein reported quantum yields are susceptible for errors, yet all samples were measured under very similar conditions which makes a relative comparison of all squaraine dyes reliable.

A considerably more exact method to characterise the fluorescence lifetime of a dye reflects time-correlated single photon counting (TCSPC). The acquired fluorescence lifetimes τ_{fl} show a monoexponential decay for dicyanovinylene-functionalised derivatives. **SQA** on the other hand has a biexponential decay with 1.71 ns (0.91) and 250 ps (0.09). In general, the lifetimes are twice as large for the *cisoid*-derivatives compared to *transoid*-**SQA**. Furthermore, the values nicely correlate with the quantum yields, meaning that a high quantum yield also induces a longer fluorescence lifetime. In toluene, the shortest and longest lifetimes of 40 ps and 4.50 ns were found for dyes **SQC** and **SQF**, respectively.

Table 1: Absorption maxima, extinction coefficients, transition moments, fluorescence maxima, fluorescence quantum yields, and fluorescence lifetimes of squaraine monomers **SQA**-**SQF** in $CHCl_3$ and toluene.

	solvent	$\tilde{\nu}_{abs}$ / cm^{-1}	λ_{abs} / nm	ε_{max} / $M^{-1}cm^{-1}$	μ_{eg}^2 / D^2	$\tilde{\nu}_{em}$ / cm^{-1}	λ_{em} / nm	Φ_{fl} / –	τ_{fl}[a] / ns
SQA	$CHCl_3$	15 700	637	3.45×10^5	129	15 500	645	0.51	0.26 (0.40) 1.47 (0.60)
	toluene	15 500	645	3.64×10^5	127	15 400	649	0.62	0.25 (0.09) 1.71 (0.91)
SQB	$CHCl_3$	14 600	685	1.96×10^5	98.6	14 200	704	0.55	2.40
	toluene	14 300	699	2.02×10^5	92.7	14 000	714	0.75	3.45
SQC	$CHCl_3$	13 100	763	1.95×10^5	115	12 700	787	–	< 0.04
	toluene	12 700	787	2.03×10^5	111	12 500	800	–	0.04
SQD	$CHCl_3$	16 000	625	1.46×10^5	78.5	15 500	645	0.90	4.02
	toluene	15 500	645	1.39×10^5	72.1	15 100	662	0.89	4.11
SQE	$CHCl_3$	14 200	704	1.77×10^5	102	13 900	719	0.93	4.59
	toluene	13 800	725	1.87×10^5	86.1	13 500	741	0.75	4.50
SQF	$CHCl_3$	13 900	719	1.72×10^5	88.8	13 500	741	0.85	4.64
	toluene	13 600	735	1.84×10^5	86.6	13 300	752	0.78	4.34

– not determined due to poor emission properties. [a](Multi-)exponential fit of fluorescence decay measured by TSCPC, excitation at 15 200 cm^{-1} (656 nm) for monomers **SQA**, **SQB**, **SQD** – **SQF**, and 12 800 cm^{-1} (783 nm) for **SQC**. Amplitudes are given in brackets.

3.1.5 Conclusion

Recapitulating, the reference squaraine dyes were synthesised in a linear and straightforward synthesis route following literature procedures. The absorption spectra for all squaraine dyes were measured in nonpolar and polar solvent toluene and $CHCl_3$, respectively. A progressive red-shift of the absorption could be achieved in both solvents by i) the introduction of a stronger acceptor unit, i.e., the dicyanovinylene-group, ii) stronger donor moieties (X = O < CMe_2 < S < Se), and iii) an extension of the π-system in the case of **SQC**. Thus, the largest bathochromic shift could be attained for the quinoline-substituted squaraine **SQC** exhibiting an absorption maximum in the NIR spectral region at 13 100 cm^{-1} ($CHCl_3$) and 12 700 cm^{-1} (toluene).

The fluorescence was also measured in $CHCl_3$ and toluene for this series of dyes and provided a minor red-shift and Strickler-Berg symmetry, respectively. Superior fluorescence properties (high quantum yields, long fluorescence lifetimes) were found for the indolenine squaraine derivatives **SQA** and **SQB** in toluene compared to $CHCl_3$. Even more promising fluorescence properties were found in toluene for the heteroazole derivatives. Yet against all expectations, the most outstanding properties were noted in polar $CHCl_3$ with quantum yields of 0.85-0.93 and lifetimes of 4.02-4.61 ns. On account of the latter findings, the three heteroazole-derivatives are considered to be the most promising squaraine dyes, e.g. for the development of highly demanded NIR emitting fluorescent polymers. Thus, the next chapter is exclusively dedicated to their functionalization.

3.2 Functionalised Heteroazole Squaraine Monomers

A widely applied synthetic strategy for the derivatisation of organic dyes is the introduction of functional groups to the existing dye scaffold. In this context, direct halogenation reactions generally reflect a common method to enable further functionalisation possibilities. However, reaction conditions, e.g. of a typical direct bromination reaction involving elemental Br_2 in glacial acetic acid are not tolerated by squaraine dyes and ultimately lead to the irreversible dye degradation. The latter aspect might be the essential criterion, that no literature procedures are reported so far for a selective halogenation reaction on the stage of a squaraine dye. In order to overcome this issue and to allow further derivatisation, the bromine function needs to be introduced at an earlier stage. Please note that the functionalisation with respect to

the herein presented squaraine dyes is always envisaged in the *para*-position with respect to the nitrogen.

During the processing of this project, the commercial availability of 6-bromo-2-methylheteroazole analogues was not yet given and diverse synthetic routes had thus to be attempted which start from smaller precursor molecules. This was part of the foregoing master thesis[141] to this work and for the sake of completeness, the synthesis and its associated problems are briefly described in the following.

In terms of 6-bromo-2-methylbenzo[*d*]oxazole **13**, 3-bromphenol was chosen as starting material in a linear synthesis route. According to Scheme 3, mild nitration in the *para*-position to the bromine function gave the respective nitro-phenol in 22 % yields.[142] Subsequent reduction with iron powder in HOAc led to the corresponding 2-amino-5-bromophenol, which was finally converted to 5-bromo-2-methylbenzoxazole **13** in an acid catalysed condensation reaction using triethyl orthoacetate.[143]

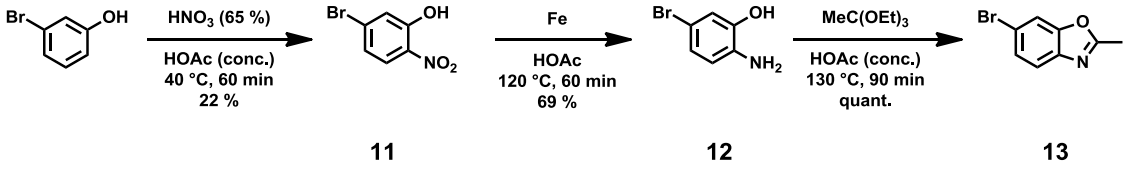

Scheme 3: Synthetic pathway to bromine-functionalised 2-methylbenzoxazole **13**.

On the other hand, the corresponding bromine-functionalised benzothiazole analogue **14** could be obtained in only one step, starting with the non-functionalised precursor 2-methylbenzothiazole (Scheme 4). The selective bromination in the *para*-position gave 6-bromo-2-methylbenzo[*d*]thiazole **14** in 21 % yields, using dibromoisocyanuric acid as bromination reagent, which is typically used for deactivated aromatic compounds.[144] Noteworthy, this reaction was also applied for the preparation of compound **13**, yet the desired compound was not isolated due to multiple bromination.

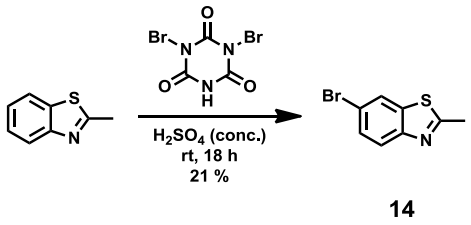

Scheme 4: Synthesis of 6-bromo-2-methylbenzothiazole **14**.

The synthesis of 6-bromo-2-methylbenzo[*d*]selenazole has in fact not been further pursued due to the lack of reliable synthetic protocols at that time. Nevertheless, the preparation of the

quaternary salts **15** and **16** was carried out as described above and the compounds were prepared in 15 % and 10 % yields, respectively (Scheme 5). Whereas the synthesis and purification of the benzothiazole-derived squaraine dye **SQE** proceeded without inconveniences (69 % yield), the formation of the symmetric squaraine **SQD** was accompanied by an undesired byproduct in form of the monobrominated analogue which was caused by debromination. According to NMR, the ratio of symmetrical to unsymmetrical squaraine dye was approximately 3:1. Preparative GPC and several recrystallizations were applied, but yet failed to enrich one of these two compounds. Due to the substantial amount of byproduct, the subsequent polymerization would have lead only to an extremely low degree of polymerization and thus to oligomers with low molecular weight. As the last reaction step suffers of poor yields and the separation of the byproduct proved to be not feasible, this project was not further investigated.

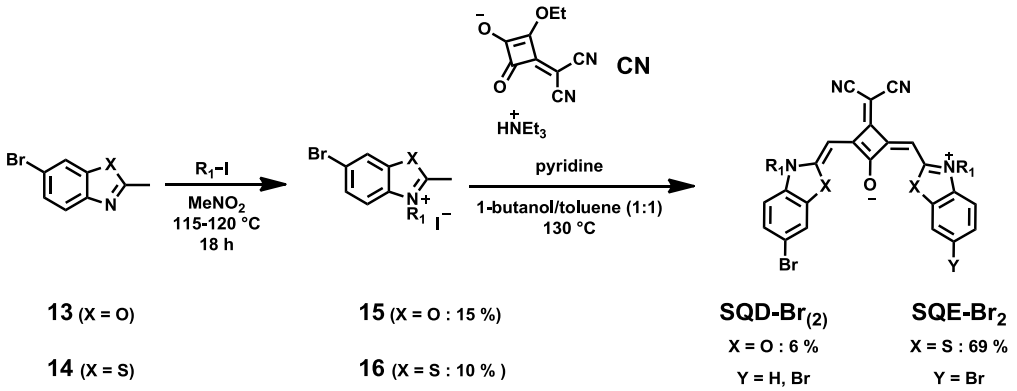

Scheme 5: Synthesis of brominated heteroazole squaraine dyes **SQD-Br$_{(2)}$** and **SQE-Br$_2$**.

The successful synthesis of symmetrical **SQE-Br$_2$** was indeed promising in order to employ the difunctionalised analogue for the subsequent polymerization reaction (not shown, see reference[141]). Unfortunately, the corresponding polymers proved to lack photostability and thus readily underwent photooxidative processes. This phenomenon has also been observed for *transoid*-configured benzothiazole squaraine monomers by other groups.[18,145-147] Accordingly, the heterocyclic moiety turned out to be the determining factor for the photostability. On account of these major drawbacks, polymers on the basis of benzothiazole derivatives were discarded and the focus was directed on the well-established indolenine squaraine dyes, which are known to be considerably photostable and chemically robust.[18]

3.3 Functionalised Indolenine Squaraine Monomers

3.3.1 Synthesis

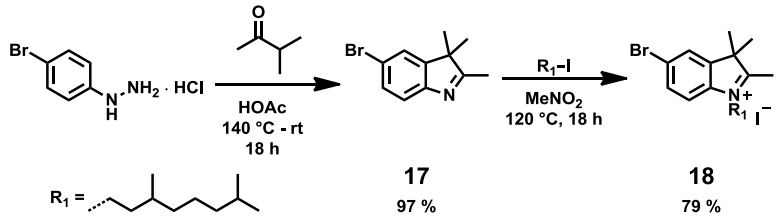

Scheme 6: Synthesis of bromine-functionalised indolenine precursors **17** and **18**.

For indolenine-derived squaraine dyes, the bromine function is typically introduced via the Fischer indole synthesis by using *p*-bromophenylhydrazine hydrochloride and isopropylmethyl ketone in glacial acetic acid to yield the bromine-functionalised indolenine precursor **17** similar to literature procedures in almost quantitative yields (Scheme 6).[148] This elegant method offers the incorporation of all relevant halogen functionalities due to the commercial availability of the corresponding halogenated hydrazine hydrochloride derivatives. Subsequent alkylation of the brominated indolenine **17** proceeds in a similar fashion and in decent yields as for non-functionalised indolenine **1**. Twofold condensation of the quaternary salt **18** with one equivalent of either squaric acid or **CN** gave the symmetrical difunctionalised *trans*- and *cis*-configured squaraine dyes **SQA-Br$_2$** and **SQB-Br$_2$** in good yields of ca. 80 %, respectively (Scheme 7).

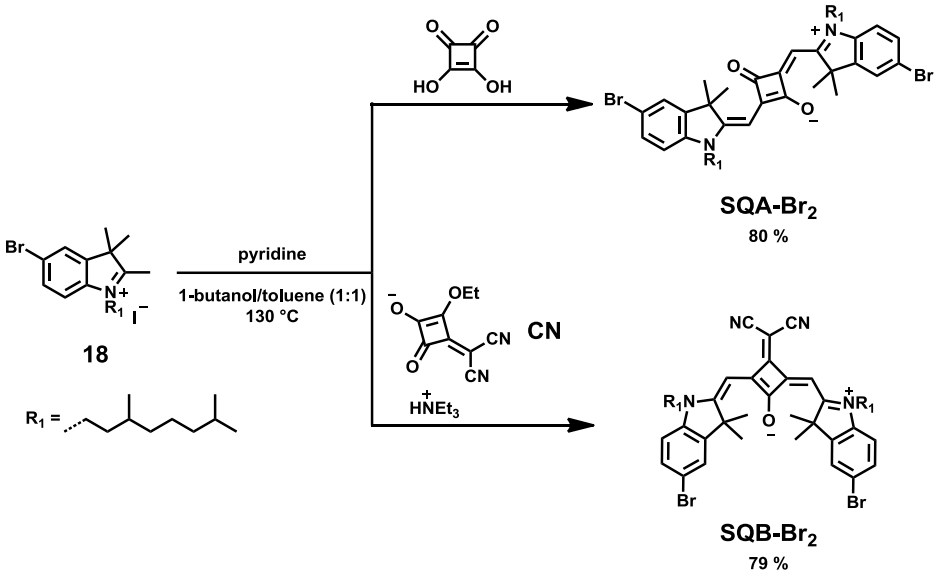

Scheme 7: Synthesis of symmetrical dibrominated indolenine squaraines **SQA-Br$_2$** and **SQB-Br$_2$**.

In order to obtain asymmetrical squaraine dyes, the synthetic route is somewhat more extensive and requires two more steps in comparison to the synthesis of their symmetrical analogues (Scheme 8). In this context, the reaction has to be stopped on the stage of the semisquaraine, which is generally not possible when using squaric acid or its dicyano derivative **CN** according to Scheme 2 and Scheme 7. As a matter of fact, the highly reactive intermediate semisquaraine readily reacts with a further equivalent of methylene base to a symmetrical squaraine dye and thus hampers the isolation of the corresponding semisquaraine.

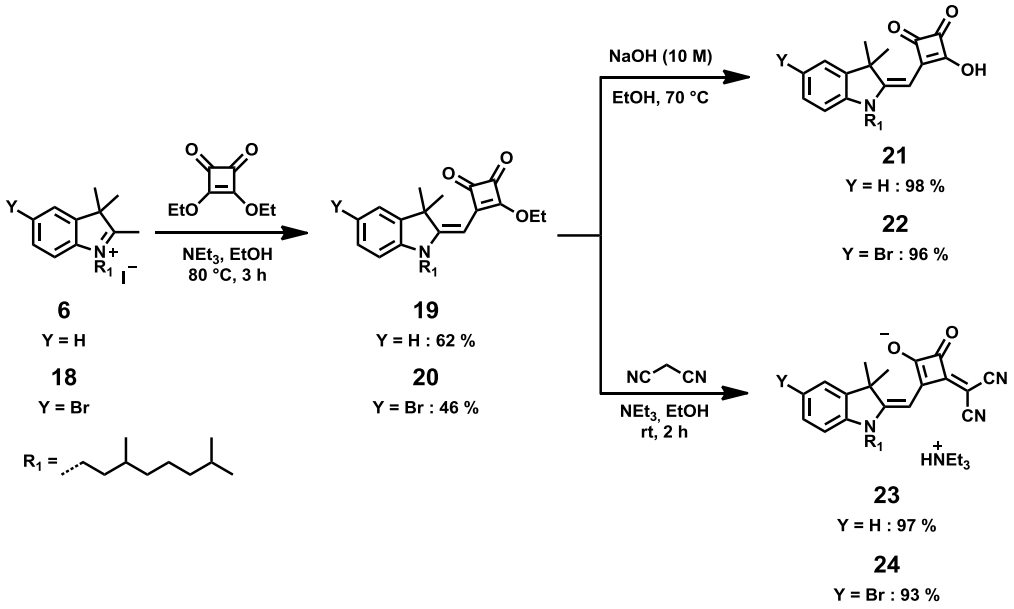

Scheme 8: Synthesis of semisquaraine dyes **19-24**.

For this purpose, the diethylester of squaric acid (3,4-diethoxy-3-cyclobutene-1,2-dione) is used to isolate the less reactive semisquaraine dyes **19** and **20**, respectively. With regard to the synthesis of the unsymmetrical *trans*-analogues, the semisquaraines were hydrolysed under basic conditions using 10 N NaOH to yield the respective semisquaraine acids **21** and **22** in high yields. In order to establish the *cis*-configuration, malononitrile reacted with the semisquaraine esters **13** and **14** under mild conditions to the corresponding dicyano semisquaraine salts **23** and **24**. Generally, the semisquaraine dyes **19-24** were purified by flash column chromatography and were directly used for the following condensation reaction. Accordingly, the bromine-functionalised semisquaraine dyes **22** and **24** were refluxed together with the non-brominated ammonium salt **6** to yield the corresponding asymmetrical squaraine dyes **SQA-Br** and **SQB-Br** (Scheme 9) in a similar fashion as outlined for symmetrical squaraine dyes in Scheme 2 and Scheme 7, respectively. As a matter of fact, the equivalent result can be achieved by the reverse route when using the non-brominated

semisquaraine dyes **21** or **23** together with the brominated indolenine salt **18**. Both ways are considered to be equally good.

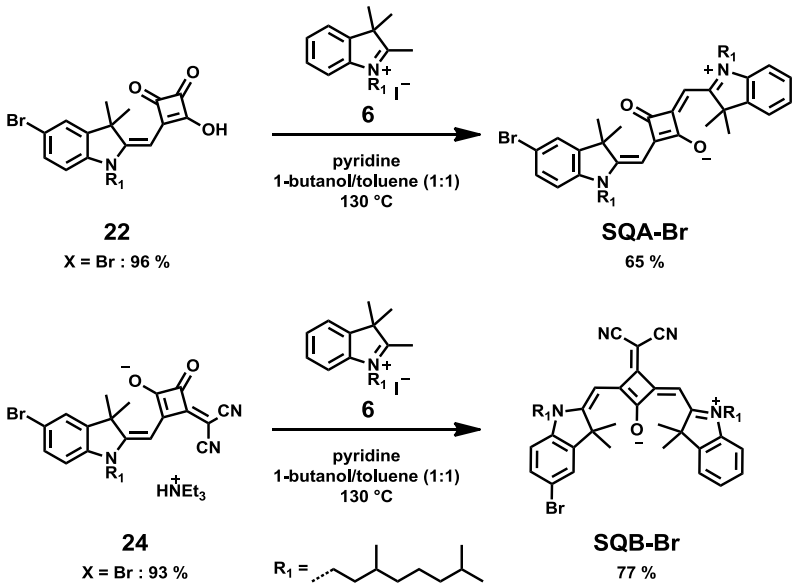

Scheme 9: Synthesis of asymmetrical mono-brominated squaraine dyes **SQA-Br** and **SQB-Br**.

Furthermore, the bromine-functionalised squaraine dyes **SQA-Br**$_{(2)}$ and **SQB-Br**$_{(2)}$ were effectively converted to their corresponding boronic esters via Pd-catalysed Miyaura borylation reaction throughout in high yields of 90 %, using bis(pinacolato)diboron, $Pd(PhCN)_2Cl_2$, 1,1´-bis(diphenylphosphino)ferrocene (dppf), and KOAc as base (Scheme 10). The borylated products were straightforwardly purified by flash column chromatography and subsequent recrystallization from *n*-hexane at low temperatures. The latter one was mandatory since the borylation reagent bis(pinacolato)diboron was hardly separable via column chromatography. Consequently, the successful synthesis of boronic ester derivatives enabled their use in potential Suzuki cross coupling reactions with brominated squaraine analogues to form homo- and heterodimers or even higher oligomers. This topic will be discussed in upcoming chapters.

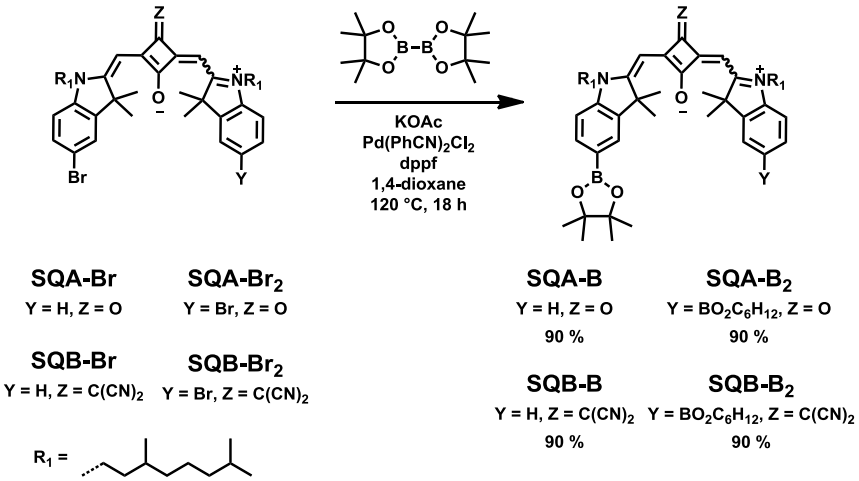

Scheme 10: Synthesis of symmetrical and asymmetrical borylated squaraine dyes **SQA-B**$_{(2)}$ and **SQB-B**$_{(2)}$.

Another possibility to promote further derivatisation was the introduction of alkyne functionalities, typically performed in the course of Sonogashira coupling reactions. In principal, twofold alkynylation of dibrominated squaraine dyes are possible but not envisaged in this work. Solely mono-alkynylation was of particular interest within the scope of this work.

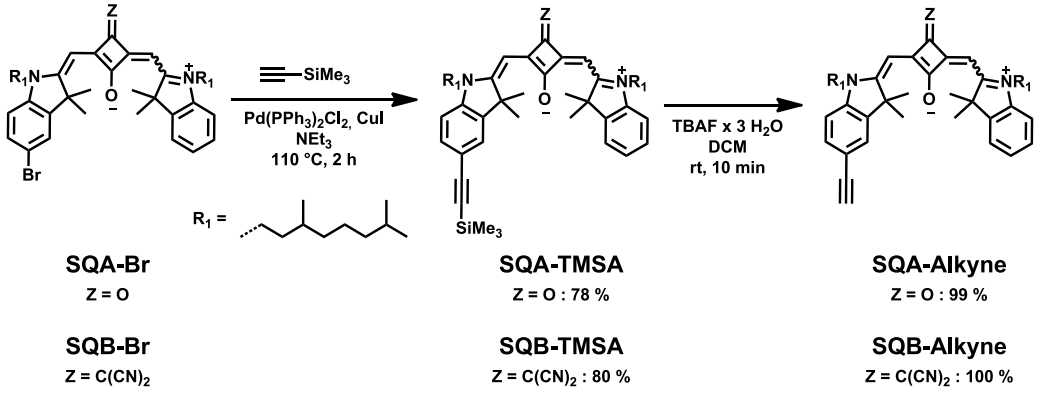

Scheme 11: Synthesis of unsymmetrical TMSA- and alkyne-functionalised squaraine monomers **SQA**(**B**)**-TMSA** and **SQA**(**B**)**-Alkyne**, respectively.

According to Scheme 11, the monobrominated squaraine analogues **SQA-Br** and **SQB-Br** were alkynylated in high yields using $Pd(PPh_3)_2Cl_2$ together with CuI as co-catalyst and NEt_3 as base and solvent.[149] The reaction proceeded without side products and the complete conversion of the starting material could easily be monitored by TLC. The TMSA functionalised squaraine dyes were purified in straightforward manner via rapid silica filtration. The TMS protecting group of **SQA** and **SQB** was subsequently removed, respectively, by using an excess of TBAF×3H_2O in DCM in quantitative yields to give the

terminal alkyne-functionalised squaraine derivatives **SQA-Alkyne** and **SQB-Alkyne** according to the literature procedure.[150]

3.3.2 Conclusion

To sum up, the preparation of symmetric and asymmetric squaraine dyes decorated with bromine, boronic ester-, or alkyne-functionalities are performed in a straightforward synthesis route throughout in decent yields. The synthesis of asymmetric dyes is marked by a somewhat more extensive route involving two additional stages. All functionalised (semi)squaraine derivatives could conveniently be purified via flash column chromatography and optionally by subsequent crystallisation if required, in analogy to their non-functionalised counterparts. The functionalised dyes proved to be chemically stable and robust without exception and thus paved the way for their further derivatisation and direct use in transition metal catalysed C-C cross couplings, such as Yamamoto, Suzuki and Sonogashira reactions, which will be subject of discussion in the following chapters.

3.4 Squaraine Polymers

3.4.1 Introduction

This chapter deals with the synthesis and optical spectroscopic properties of squaraine polymers. As already mentioned in Chapter 2, the fundamental investigations by Völker at al. on a *cis*-indolenine squaraine polymer gave the impetus for further studies regarding this polymer. It was found that the shape of the absorption band manifold of the polymer was strongly dependent on the solvent, which manifested itself in either blue- or red-shifted absorption bands with respect to the monomer absorption. These spectral features were interpreted to be caused by zig-zag and helical conformations of the polymer leading to intramolecular H- and J-type aggregate formation.[71,73]

This polymer is resynthesized following the synthetic procedure established by Völker et al. in order to engage further examinations but also to make a comparison to the prototype. In particular, the folding behaviour of the polymer and the operating factors driving the folding process will be investigated in more detail by subjecting the polymer to temperature dependent absorption studies. In addition, small molecular weight oligomers (dimer and trimer) will be synthesised in order to study the excitonic coupling effects involved in these reference systems and to compare them with the polymer properties. These model compounds are considered important as they may potentially contribute to a better understanding of the rather complex polymer.

The subsequent chapters exclusively deal with the control of the optical properties of polymers which is directly connected to the issue of different conformers in solution causing different spectral features. In this respect, the selective formation of only one superstructure irrespective of external influences (e.g. solvent) may be a plausible concept to overcome the scenario with diverse conformers. In order to approach this issue, it is proposed that the polymer conformer structure desired is inherently linked to its monomer structure. Therefore, it was a reasonable strategy to use different donor heteroazole building blocks as the monomers. Despite their highly promising optical properties, each heterocycle provides differences in terms of size and electronic structure, which might have led to polymers with different conformer structures. Unfortunately, lacking adequately functionalised precursors (6-bromo-2-methylbenzo[*d*]selenazole and **SQD-Br$_2$**) and photochemical stability (**SQE**-based homopolymer), the corresponding polymers could not be realised or investigated (Chapter 3.2). Therefore, new synthetic strategies and modification possibilities will be presented in the following how to chemically encode the essential steric or electronic

information into the monomer structure to achieve the superstructure and consequently the optical properties desired.

3.4.2 Indolenine Squaraine Homopolymer[VI]

3.4.2.1 Synthesis

The Ni-mediated Yamamoto homocoupling reaction is considered to be one of the most powerful and versatile methods for C-C bond formation, promising a convenient way for a sophisticated range of oligomers and polymers and was therefore selected for the synthesis of squaraine homopolymers. This kind of polycondensation reaction typically requires a dihaloaromatic compound as starting material, which is fulfilled by the dibrominated precursor monomer **SQB-Br$_2$**. According to Scheme 12, the reaction was performed by using stoichiometric amounts of Ni(COD)$_2$, 1,5-cyclooctadiene (COD), and 2,2´-bipyridine, respectively, in a solvent mixture of DMF and toluene (1:1) at 65 °C for 8 d to polymerise dicyanovinylene-substituted **SQB-Br$_2$**. After three consecutive Soxhlet extractions using *n*-hexane, MeOH, and acetone, the major part of the polymer remained in the latter fraction and was used for further investigations. In this way, crude **pSQB** was obtained in 78 % yields with a number average molecular weight M_n of ~ 5 610 and a degree of polymerisation X_n of ~ 8. In order to study the influence of molecular weight on the optical properties, the crude polymer was subsequently split via preparative recycling GPC ($CHCl_3$) into three polymer batches with varying molecular weight distribution. The polymer characteristics are summarised in Table 2. The polymer fractions **pSQB-1**, **2**, and **3** possess a number-average degree of 15 600, 5 870, and 2 270, respectively, and show comparably small polydispersities (M_w/M_n = 1.09-1.74) owing to preparative splitting. On the other hand, the crude polymer provides a larger *Đ* of 2.39. For ideal polycondensation reactions, a Flory distribution with *Đ* =2 is expected.

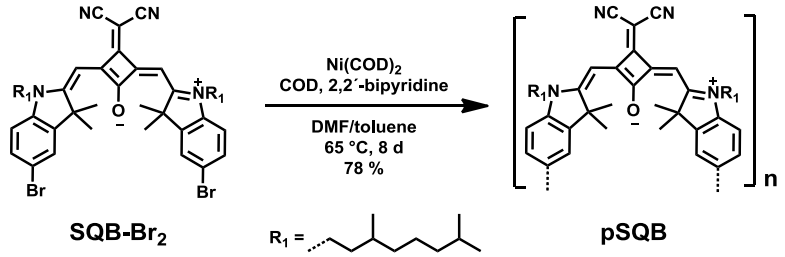

Scheme 12: Synthesis of homopolymer **pSQB**.

[VI] Parts of this chapter have been investigated in a bachelor thesis under the supervision of M. H. Schreck: A. Stoy, Bachelor Thesis, Julius-Maximilians Universität (Würzburg), **2014**.

The largest polymer fraction of the analogous polymer **pSQB-V** previously synthesised by Völker possesses a number-average degree of 25 600 along with an average degree of polymerisation of ~ 36.[71] Thus the four polymer fractions can be considered as a series of polymer fractions with an increasing degree of polymerisation. Besides, with an increasing degree of polymerisation the solubility usually decreases for polymers, yet even the longest polymer fraction shows considerable solubility in a large range of common organic solvents, such as $CHCl_3$, DCM, toluene, PhCN and DMF.

Table 2: Polymer characterisation: number-average molecular weight (M_n), number average degree of polymerisation (X_n), weight-average molecular weight (M_w), and polydispersity ($Đ = M_w/M_n$). Analysis was carried out in $CHCl_3$ with polystyrene as standard.

	M_n	X_n	M_w	$Đ$
pSQB (crude)	5 610	7.76	13 400	2.39
pSQB-V	25 600	35.5	46 700	1.82
pSQB-1	15 600	21.6	27 200	1.74
pSQB-2	5 870	8.12	8 150	1.39
pSQB-3	2 270	3.14	2 470	1.09

3.4.2.2 Synthesis of Reference Dyes

Squaraine dimer **dSQB-1** and trimer **tSQB** were conveniently prepared via a Suzuki cross coupling reaction in good yields of 65 % and 59 %, respectively, using $Pd(PPh_3)_4$ as catalyst and aqueous Na_2CO_3 as base in THF according to Scheme 13.

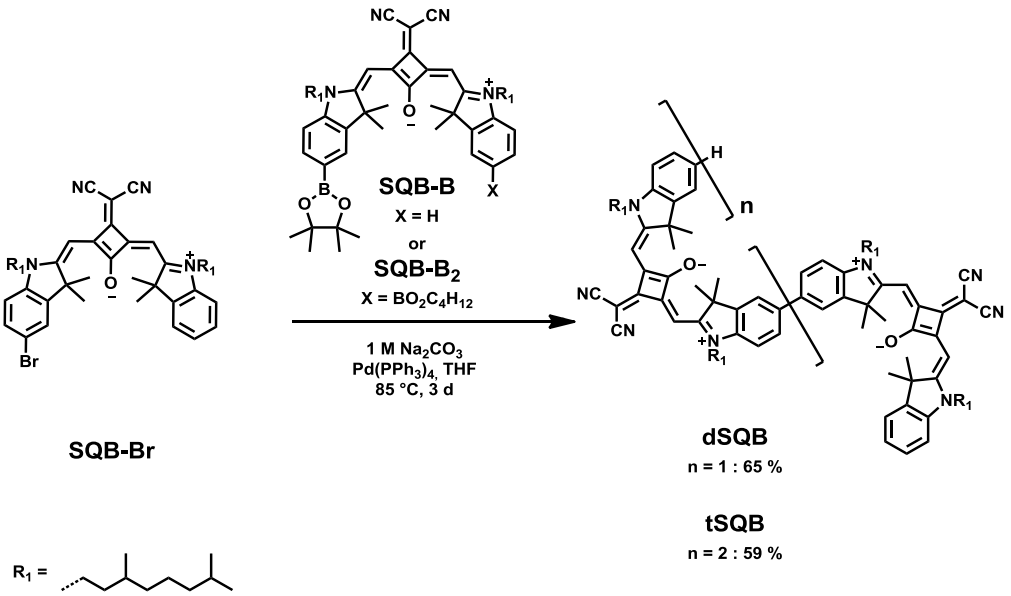

Scheme 13: Synthesis of squaraine oligomers **dSQB** and **tSQB**.

In terms of **dSQB**, the monofunctionalised squaraines **SQB-Br** and **SQB-B** served as starting materials, while the diborylated squaraine **SQB-B_2** was chosen together with **SQB-Br** in order to synthesise **tSQB**. Both crude oligomers were purified by a rapid column filtration and subsequent preparative GPC.

3.4.2.3 Absorption Spectroscopy

Absorption spectra of the complete *cisoid* dye series were recorded in $CHCl_3$ and toluene. The spectroscopic data are summarised in Table 4. The optical properties for **SQB** were already discussed in Chapter 3.1.3 and 3.1.4 and the focus is now directed on the corresponding oligomers and polymer.

In both solvents the dimer **dSQB-1**, the trimer **tSQB**, and the polymer **pSQB-1** exhibit a progressive red-shift of the lowest energy absorption band in comparison to the monomer **SQB**, along with a much larger bandwidth of the absorption (Figure 16). The red-shift is slightly more pronounced for the oligomers in toluene. The exciton coupling (estimated from the bandwidth using equations (4), (10), and (12) from Chapter 1.2, respectively) somewhat

decreases with increasing number of monomer units (toluene: dimer: 780 cm^{-1}, trimer: 640 cm^{-1}, polymer 620 cm^{-1}). The decrease of exciton coupling from dimer to polymer is most likely originate from the nearest-neighbour approximation in exciton theory.[87]

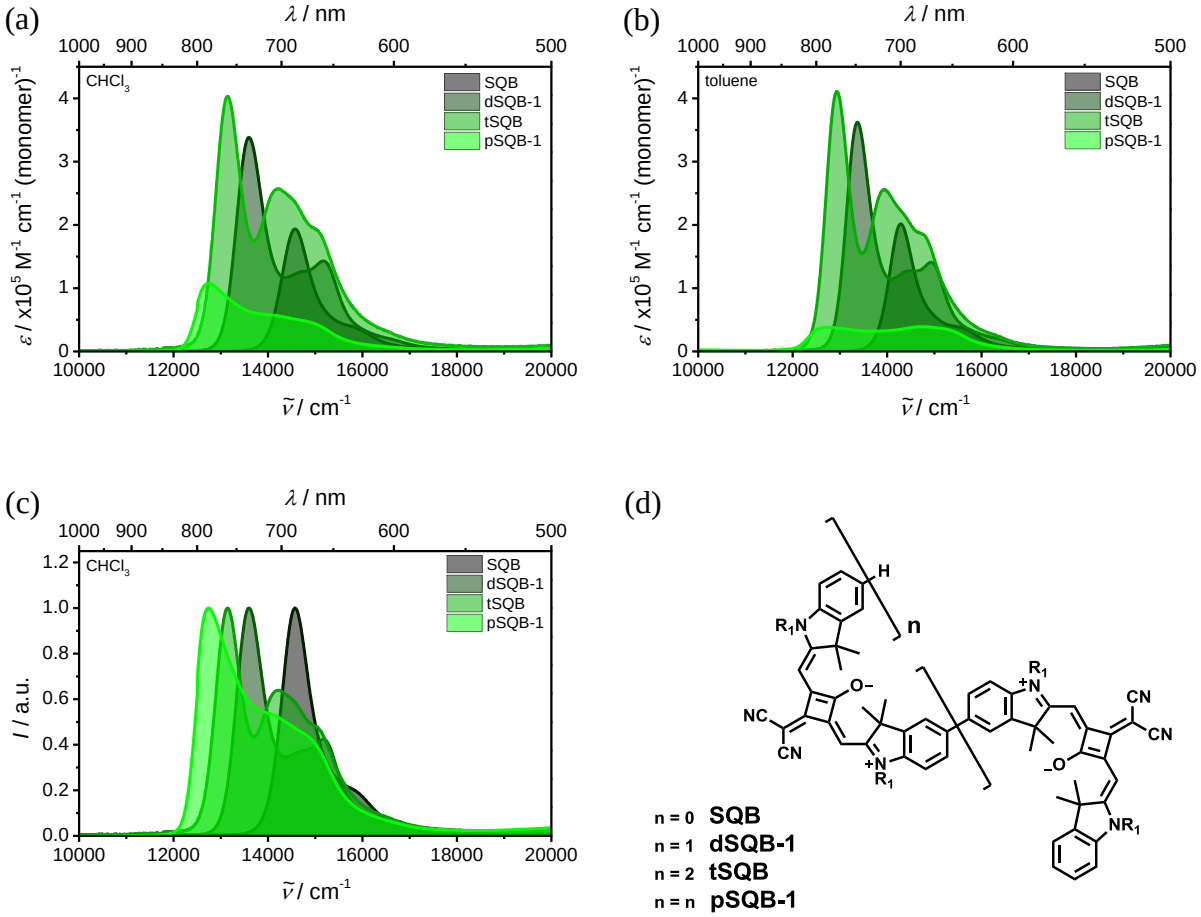

Figure 16: Absorption spectra of **SQB** and of corresponding oligomers and polymer in (a) $CHCl_3$ and (b) toluene, respectively. (c) Normalized absorption spectra in $CHCl_3$ and (d) corresponding chemical structures.

Moreover, the extinction coefficients gradually rise from the monomer to the trimer and are slightly larger in toluene, which was also observed earlier in this work for the reference dyes shown in Chapter 3.1.3. In $CHCl_3$ (toluene) the dimer and the trimer exhibit an extinction coefficient of 3.38×10^5 $M^{-1}cm^{-1}$ (3.62×10^5 $M^{-1}cm^{-1}$) and 4.03×10^5 $M^{-1}cm^{-1}$ (4.11×10^5 $M^{-1}cm^{-1}$), respectively.

For **dSQB-1** and **tSQB**, respectively, the shape of the absorption remains almost unchanged in both solvents. In $CHCl_3$ (toluene), the dimer displays a main absorption band at 13 200 cm^{-1} (13 400 cm^{-1}) together with two maxima located at higher energies at 14 700 cm^{-1} (14 500 cm^{-1}) and 15 100 cm^{-1} (14 900 cm^{-1}). In addition, the trimer has an absorption maximum at 13 100 cm^{-1} (12 900 cm^{-1}) and a local maximum at 14 200 cm^{-1} (13 900 cm^{-1}) accompanied by two shoulders at higher energies. The squared transition moments as

determined from the integration of the main absorption band for **dSQB-1** and **tSQB** are slightly larger in $CHCl_3$ (236 D^2 and 381 D^2) than in toluene (226 D^2 and 339 D^2), respectively. The values almost show additivity from the monomer which is in agreement with the Thomas-Reiche-Kuhn sum rule.[151]

Interestingly, the shape of the absorption dramatically differs for **pSQB-1** in both solvents. In $CHCl_3$, a broad absorption band with only one maximum at 12 700 cm^{-1} can be observed, whereas two maxima of almost equal intensity at 12 700 and 14 700 cm^{-1} are present in toluene. Even though the polymer provides distinctively smaller extinction coefficients (1.08×10^5 $M^{-1}cm^{-1}(monomer)^{-1}$ and 5.18×10^4 $M^{-1}cm^{-1}(monomer)^{-1}$) than the monomer in $CHCl_3$ and toluene, the calculated squared transition moments yield rather similar with values of 98.6 and 92.7 for **SQB**, and 112 and 88.9 for **pSQB-1**.

Due to the good solubility of the polymer, these interesting findings could be further pursued by recording the absorption of **pSQB-1** in a series of solvents that differ in polarity, viscosity, refractive index, etc. The spectra are shown in Figure 17(a). In contrast to $CHCl_3$ and DCM with an absorption maximum each at the low-energy side at 12 700 cm^{-1} and a shoulder at higher energies, the polymer shows significantly blue-shifted main absorption bands in the region from 15 500-15 800 cm^{-1} together with considerably less intense bands around 13 000 cm^{-1} in PhCN, DMF, and acetone, respectively. Interestingly, a small shoulder at 11 800 cm^{-1} might be attributed to the lower edge of the exciton band of the helix form. However, no correlation with any solvent parameter could be derived from the solvent-dependent absorption studies.

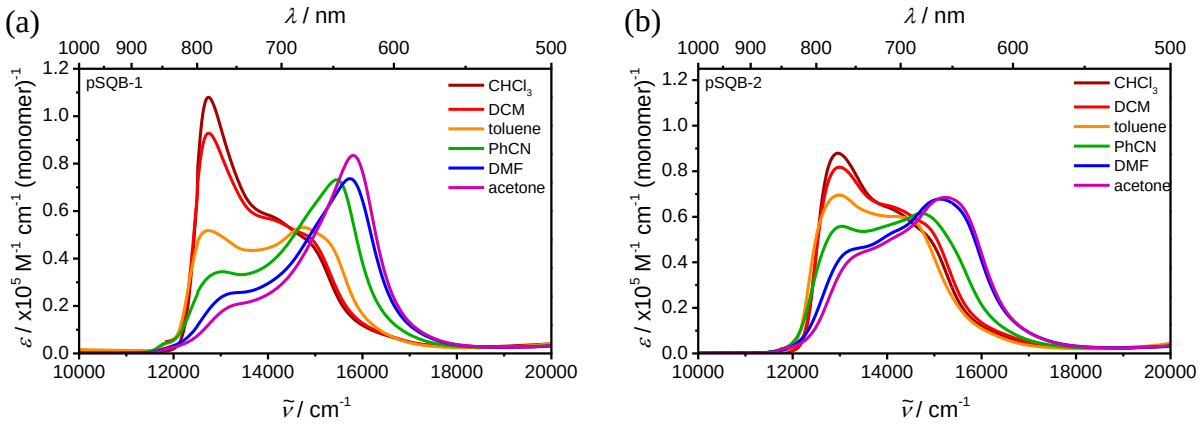

Figure 17: Absorption spectra of (a) **pSQB-1** and (b) **pSQB-2** in various solvents.

The spectral features of similar *transoid*-indolenine squaraine polymers were explained to be caused by exciton coupling of localized squaraine transitions rather than by conjugational effects.[6,44] As a matter of fact, electrochemical investigations provided evidence that only

weak electronic interactions are present between the squaraine chromophores in absence of redox centres, such as triarylamines or naphthalene diimides, etc.[44,67,70] Consequently, the spectral features of the present *cisoid* polymer were also discussed in terms of exciton coupling due to Coulomb interactions of transition densities. In order to assess these interactions, structural models of the polymer were required. For this purpose, two different hexameric superstructures were conceived to mimic possible polymer conformations: a helix and an elongated zig-zag structure. Semiempirical AM1/INDO calculations were carried out to enable assignments to the specific structural motifs.[71] Granted the simplicity of this method, the computed absorption spectra yet nicely correlate with the experimental spectra. Furthermore, more elaborated computational methods (DFT) additionally substantiated the former assignments of the spectral features to the structural motifs.[73] Accordingly, in chlorinated solvents, such as DCM and $CHCl_3$, elongated polymer chains prevail which cause a significant red-shifted absorption compared to the monomer absorption. This effect can be addressed to J-aggregate behaviour with a collinear (head-to-tail) alignment of transition moments. On the other hand, the blue-shifted absorption, for instance in PhCN, DMF, or acetone, can be referred to helix conformations and is caused by H-aggregate behaviour with a parallel (face-to-face) alignment of transition moments. The most extreme and contradictory effect was noticed in $CHCl_3$ and acetone, where mostly one of the two superstructure is favoured. Referring to Figure 17(a), it can be concluded that mixtures of both superstructures obviously exist within on polymer strand and the fractions to which these structures are formed can be operated via the solvent. However, as can be readily appreciated by Figure 17(b), the shape of the absorption band manifold is additionally dependent on the chain length of the polymers. The latter aspect was investigated in more detail for the second polymer fraction **pSQB-2**, providing a smaller average degree of polymerisation of ca. 8. For this purpose, the absorption of **pSQB-2** was recorded in the same solvents. Noteworthy, the absorption spectra of the third and shortest polymer fraction **pSQB-3** with the lowest average degree of polymerisation of ~ 3 mostly provided monomer-type characteristics and are therefore not shown. According to Figure 17(b), it is immediately evident that the dominance of the one aggregate band as observed for **pSQB-1** is strongly reduced in favour of the respective other aggregate band. Furthermore, the energy difference of the maxima of the excitonic bands of zig-zag and helix structures is significantly decreased for **pSQB-2**. In other words, **pSQB-1** exhibits a maximum at 12 700 cm^{-1} (15 800 cm^{-1}) in $CHCl_3$ (acetone), while **pSQB-2** provides a maximum at 13 000 cm^{-1} (15 200 cm^{-1}). In addition, the maxima are broadened and are not as sharp as for **pSQB-1**, which is accompanied by lower extinction

coefficients together with a considerable absorbance in the intermediate range around 14 000 cm^{-1}. The most severe differences are found in PhCN and toluene: In PhCN, almost the same ratios of J- and H-aggregate band are found, while in toluene, the J-aggregate band is favoured at the cost of the H-aggregate band.

As far as can be ascertained, the significant differences concerning the shape of the absorption band manifold of the two polymer fraction arise from a more heterogeneous polymer with more mixed conformations and more balanced fractions of helical and elongated zig-zag domains in the case of **pSQB-2**. Conversely, this means that with longer polymer chains, more homogeneous polymers are formed resulting in an enhanced prevalence of only one conformer and thus of one aggregate band.

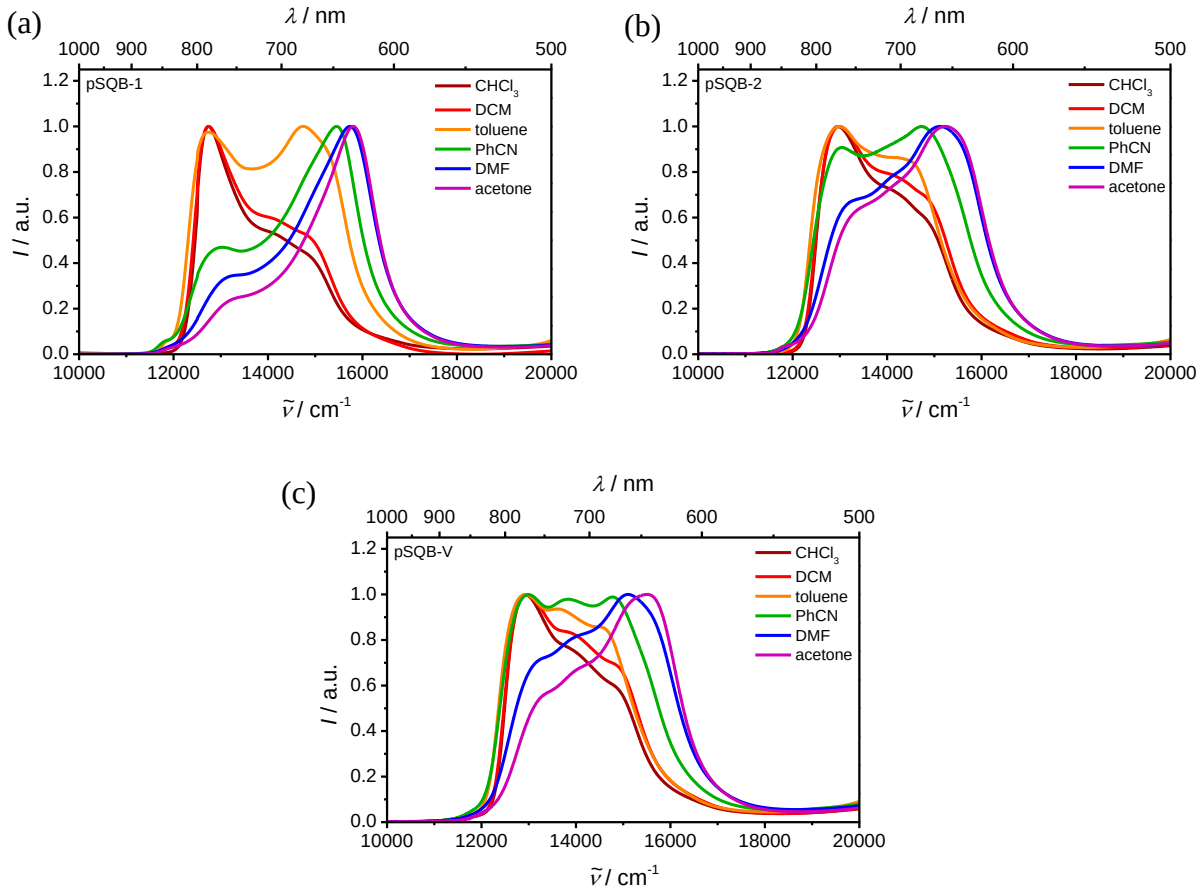

Figure 18: Normalised absorption of (a) **pSQB-1**, (b) **pSQB-2**, and (c) **pSQB-V** in various solvents, respectively.

In order to extend this study, analogous polymer **pSQB-V** (X_n = 36) which provides a somewhat higher polydispersity of 1.82 than **pSQB-1** (1.74), was chosen for further comparison. Intriguingly, Völker showed for his four polymer fractions with varying degrees of polymerisation (X_n =7-36), that the influence of the chain length on the optical properties was rather marginal. However, when comparing the spectra of **pSQB-1** and **pSQB-2** shown

in Figure 18(a) and (b), this previous finding does not hold true in the present case. Moreover, against expectation, the spectra recorded for **pSQB-V** (X_n = 36) closely resemble those of **pSQB-2** (X_n = 8) (Figure 18(c)), even though they strongly differ in chain length and polydispersity**. pSQB-1** on the other hand provides mostly one conformer in all considered solvents (except in toluene) and can thus be considered as more homogenous.

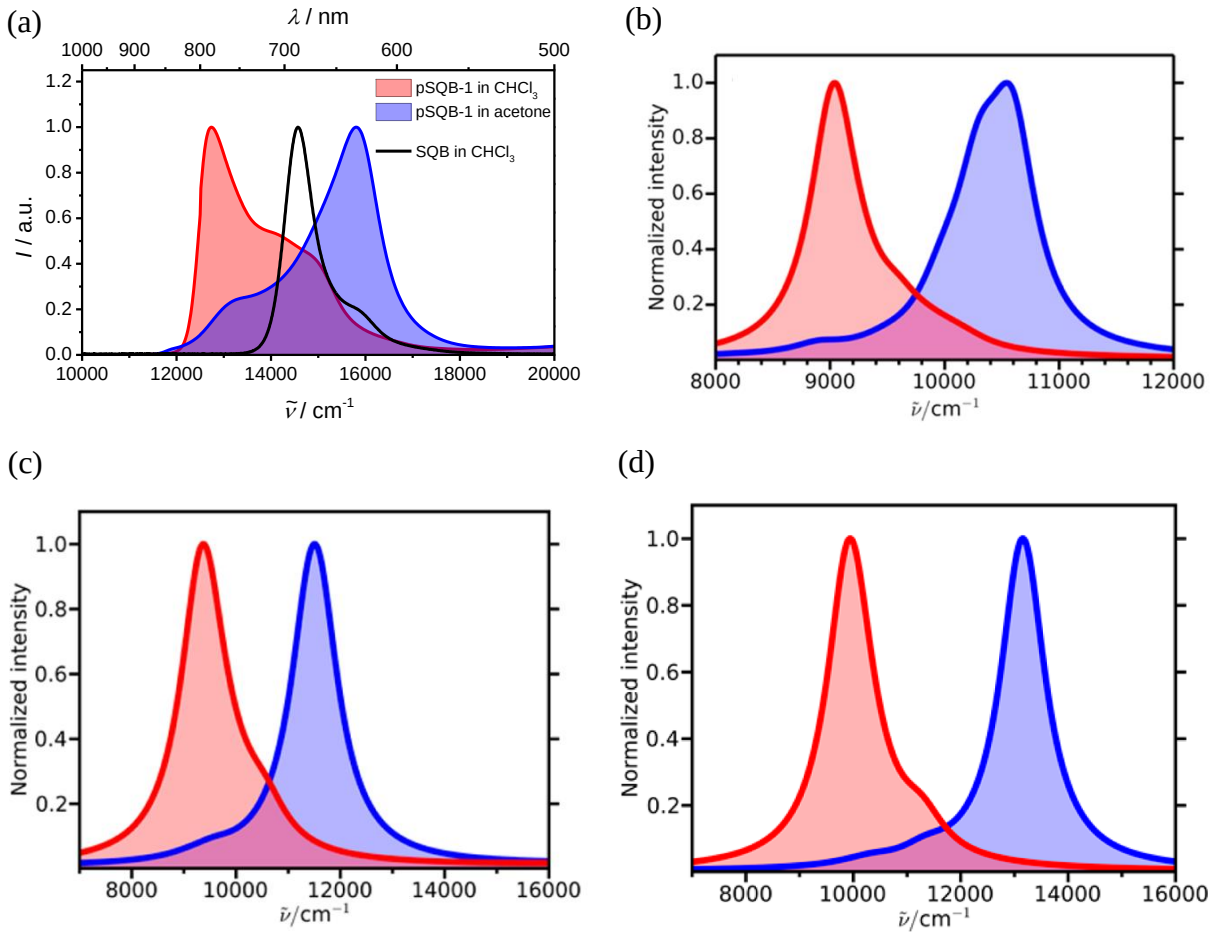

Figure 19: (a) Normalised absorption spectra of **pSQB-1** in $CHCl_3$ and acetone, and of **SQB** in $CHCl_3$. Comparison of the theoretical normalised absorption spectra for different zig-zag- and helix-oligomers: (b) 6mer, (c) 12mer, and (d) 22mer. Adapted with permission from *Energy Transfer Between Squaraine Polymer Sections: From Helix to Zigzag and All the Way Back*, C. Lambert, F. Koch, S. F. Völker, A. Schmiedel, M. Holzapfel, A. Humeniuk, M. I. S. Röhr, R. Mitric, T. Brixner, *J. Am. Chem. Soc*. **2015**, *137*, 7851-7861. Copyright © (2015) American Chemical Society.

As already mentioned, more elaborate computational methods were applied to further support the corresponding assignments. In this regard, the optical spectra of the zig-zag and helix form for oligomers of different length (6-, 12-, 22mer) were calculated by the Mitric group using the long-range-corrected tight-binding time-dependent density functional theory (lc-TDDFTB) (Figure 19). When comparing the computed spectra shown in Figure 19(b)-(d) with those recorded for **pSQB-1** (Figure 19(a)), it can be concluded that the overall shape for the experimental spectra could reasonably well be reproduced, substantiating the assignments

of the spectral features to the structural motifs. In particular, on account of the higher homogeneity without considerable amounts of mixed structures, the computed spectra rather fit better to **pSQB-1** than **pSQB-V.** Besides, with increasing oligomer length, the energy difference of the calculated maxima of the excitonic bands in both solvents increases and the bands become sharper and narrower, which may be caused by so-called exchange narrowing which is due to a delocalised exciton state. Both features nicely coincide with the experiments as illustrated above for **pSQB-1** and **pSQB-2** in Figure 18(a) and (b).

In order to shed more light on the folding behaviour of the polymer, the temperature influence on the optical properties was examined. Therefore, variable-temperature absorption measurements were performed in PhCN which provides an appropriately large temperature range. The temperature-dependent absorption experiments have been conducted in all the solvents indicated above, however, the most pronounced absorption changes were observed in PhCN for the polymer and are therefore exclusively shown. The other experiments are presented elsewhere.[152] Upon raising the temperature from 273-403 K according to Figure 20(a), a significant change of the spectra can be induced. In this context, the predominant H-aggregate band at 15 400 cm^{-1} decreases in favour of the concomitantly rising J-aggregate band at 12 600 cm^{-1}. At higher temperatures, the polymer thus favours elongated structures at the cost of helical arrangements in order to minimise the overall free energy of the system. The occurrence of an almost clean isosbestic point around 14 200 cm^{-1} indicates the presence of an equilibrium between two species, i.e., helix and zig-zag.

The temperature influence was also investigated for the largest oligomer **tSQB**. Similarly to **pSQB-1**, the measurements were carried out in PhCN and are presented in Figure 20(b). When increasing the temperature from 283 to 338 K, the main absorption band at 13 000 cm^{-1} and the broad band around 14 400 cm^{-1} slightly decrease. The observed spectral changes appear rather marginal and can be assigned to the small molecular size leading to limited conformer possibilities in comparison to the extended polymer chains in **pSQB-1**. Particularly, helical arrangements in the trimer might most likely involve too much molecular strain and would consequently not be energetically favoured. A systematic evaluation of 4 to 10mers would certainly provide more information about the required oligomer length for a helix formation.

It can be concluded that the features illustrated above are only present in the polymer and are caused by a reversible equilibrium of different polymer conformers, which can decisively be manipulated by either temperature or solvent (Figure 20(c)).

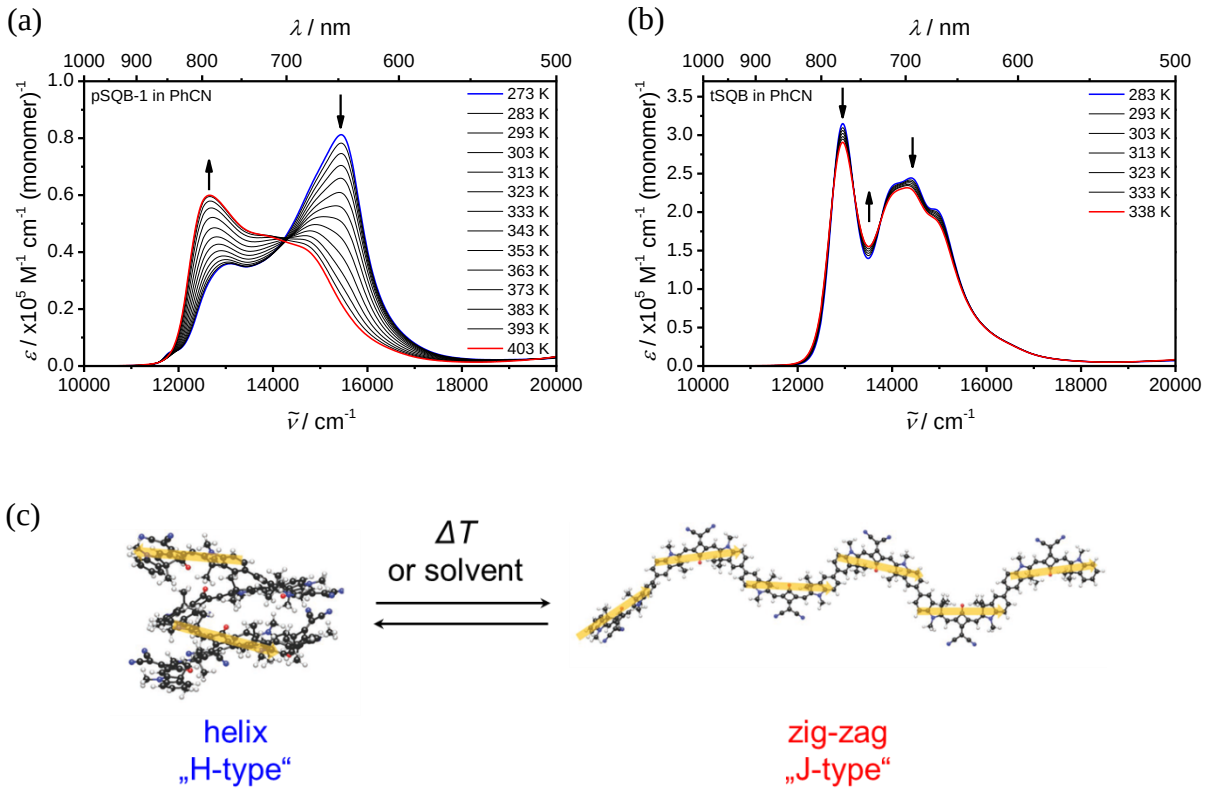

Figure 20: Absorption spectra of (a) **pSQB-1** and (b) **tSQB** in PhCN at different temperatures (density corrected). (c) AM1-computed model hexamer with transition moments indicated as yellow arrows.[6,71]

3.4.2.4 Fluorescence Spectroscopy

The fluorescence spectra and lifetimes of **SQB**, **dSQB-1**, **tSQB**, and **pSQB-1** were measured in $CHCl_3$ and toluene. The spectroscopic data is summarised in Table 4.

Similarly to absorption measurements, the dimer and the trimer show a gradual red-shift of the fluorescence with respect to the monomer (Figure 21). In $CHCl_3$ (toluene), the dimer and the trimer exhibit a maximum at 13 300 cm^{-1} (13 100 cm^{-1}) and 12 700 cm^{-1} (12 900 cm^{-1}), respectively. The fluorescence bands are no mirror images to the respective absorptions. They rather resemble the shape of monomer fluorescence yet shifted to lower energies. The Stokes shifts are in the range of 200-300 cm^{-1} and are somewhat smaller than for **SQB**. In both solvents, the fluorescence exclusively occurs from the lowest excitonic state and is thus in agreement with Kasha´s rule.[74,75] Besides, the FWHM of the emission bands of the squaraine dyes are generally smaller in toluene than in $CHCl_3$ and significantly decrease from the monomer (770 cm^{-1} in toluene) to the polymer (500 cm^{-1} in toluene) which can be assigned to exchange narrowing (Table 3).

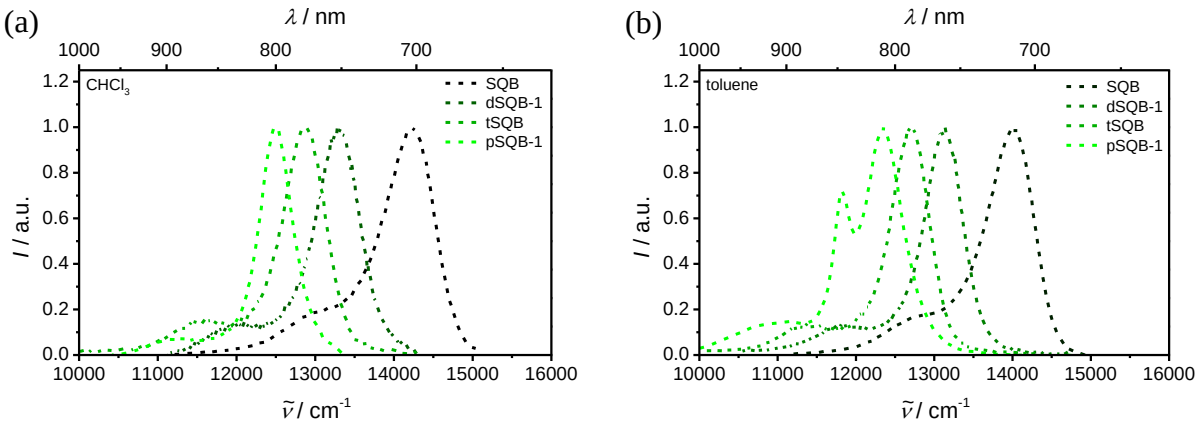

Figure 21: Normalised fluorescence spectra of squaraine dyes in (a) $CHCl_3$ and (b) toluene. Excitation of the oligomers and polymer was at 15 150 cm^{-1}, respectively.

The polymer on the other hand provides the most red-shifted fluorescence in this series of dyes. While in $CHCl_3$ the polymer exhibits a single monomer-type fluorescence at 12 500 cm^{-1}, two emission bands at 11 800 cm^{-1} and 12 400 cm^{-1} can be found in toluene. The excitation was at 15 150 cm^{-1} for the oligomers and the polymer in both solvents. As a matter of fact, **pSQB-V** solely exhibits one fluorescence band in toluene, similarly to **pSQB-1** in $CHCl_3$.

The occurrence of such a second emission band was rather surprising at first glance. However, as could be concluded from absorption studies, predominantly one superstructure is present in $CHCl_3$, i.e. zig-zag, which exhibits a characteristic J-aggregate band at 12 500 cm^{-1} (Figure 22(a)). In toluene, in contrast, **pSQB-1** exhibits two main bands, one at ca. 15 500 cm^{-1} with a hypochromic shoulder around 15 300 cm^{-1} and one at 12 700 cm^{-1}. The latter is attributed to the zig-zag form, which is in agreement with the spectrum in $CHCl_3$, while the former is assigned to the helix form. Yet, the excitation spectra presented in Figure 22(d) imply that the real absorption maximum of the helix is located around 15 300 cm^{-1} and thus corresponds to the above mentioned shoulder, and the maximum at 15 500 cm^{-1} originates from the spectral overlap of the exciton band of the helix. Furthermore, the relative strength of the two fluorescence peaks can be changed by the excitation energy (Figure 22(b) and (d)). Accordingly, the emission peak at 11 800 cm^{-1} reaches its maximum when the polymer is excited at 15 630 cm^{-1}, where absorption of the helix is expected to be dominant. Consequently, fluorescence can be assigned to the helix form, while the second fluorescence band at 11 830 cm^{-1} results from the zig-zag form.

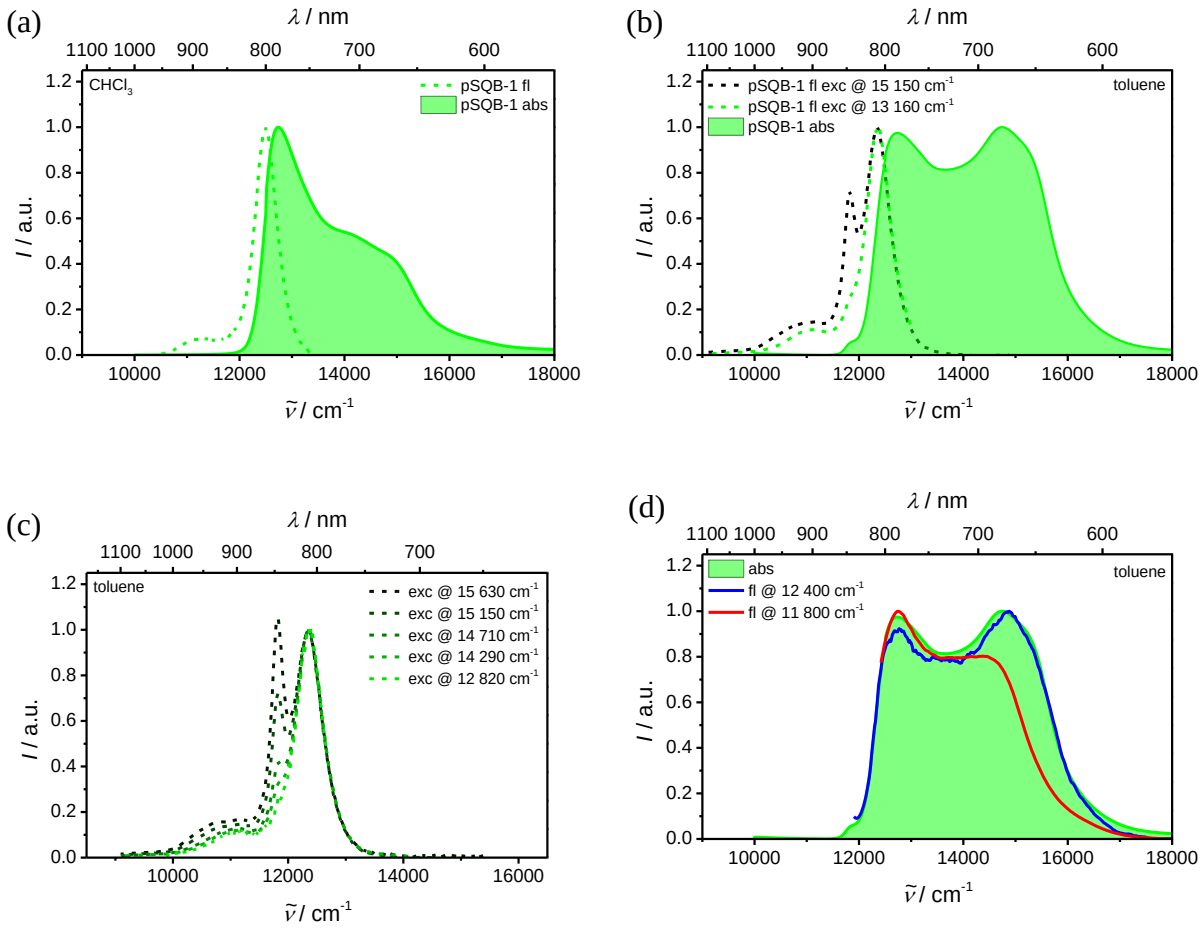

Figure 22: Normalised absorption and fluorescence emission spectra of **pSQB-1** in (a) $CHCl_3$ and (b) toluene at two different excitation energies 13 160 cm^{-1} (760 nm) and 15 150 cm^{-1} (660 nm). (c) Excitation dependent fluorescence emission spectra in toluene. (d) Normalised absorption and fluorescence excitation spectra of **pSQB-1** in toluene detected at 12 400 cm^{-1} (812 nm) and 11 820 cm^{-1} (846 nm). Excitation spectra are smoothed (40 points Savitzky-Golay algorithm) and offset-corrected.

The fluorescence quantum yield in toluene decreases from monomer (0.75) to dimer (0.68), and further to trimer (0.58). For a representative comparison with the oligomers, the same excitation energy (15 150 cm^{-1}) was chosen for **pSQB-1** and a quantum yield of 0.06 was determined. As shown above, the shape of the fluorescence is significantly depending on the excitation energy, which indeed affects the quantum yield as well. Accordingly, a quantum yield of 0.17 was determined upon excitation at lower energies at 13 510 cm^{-1}. These findings in toluene clearly indicate a rather slow energy transfer. Energy transfer is therefore assumed to occur between different polymer strands rather than between zig-zag und helical segments within one single polymer strand. The latter scenario would result in a fast energy transfer which is obviously not the case in toluene.

In $CHCl_3$, in contrast, the fluorescence quantum yield decreases from monomer (0.55) to dimer (0.20). Against expectations, no further decrease is observed for the trimer (0.20), and most remarkably for the polymer (0.21). Apparently, the quantum yield is invariant towards

the chain length in $CHCl_3$, while in toluene, a decrease is observed with increasing number of monomer units.

The lifetime measurements were fitted with (multi-)exponential decays. In case of the oligomers and polymer average lifetimes were additionally calculated by equation (47) using the amplitudes a_n and the corresponding lifetimes τ_n:

$$\bar{\tau} = \frac{a_1\tau_1^2 + a_2\tau_2^2 + a_n\tau_n^2}{a_1\tau_1 + a_2\tau_2 + a_n\tau_n} \tag{47}$$

The results of the fits are exclusively shown for toluene in Figure 23. The dimer and trimer show both biexponential decays with average lifetimes of 2.89 ns and 2.55 ns, respectively. In this context, the relative amplitude of the shorter component increases with increasing chain length, consequently the fluorescence lifetime shortens with increasing chromophore numbers.

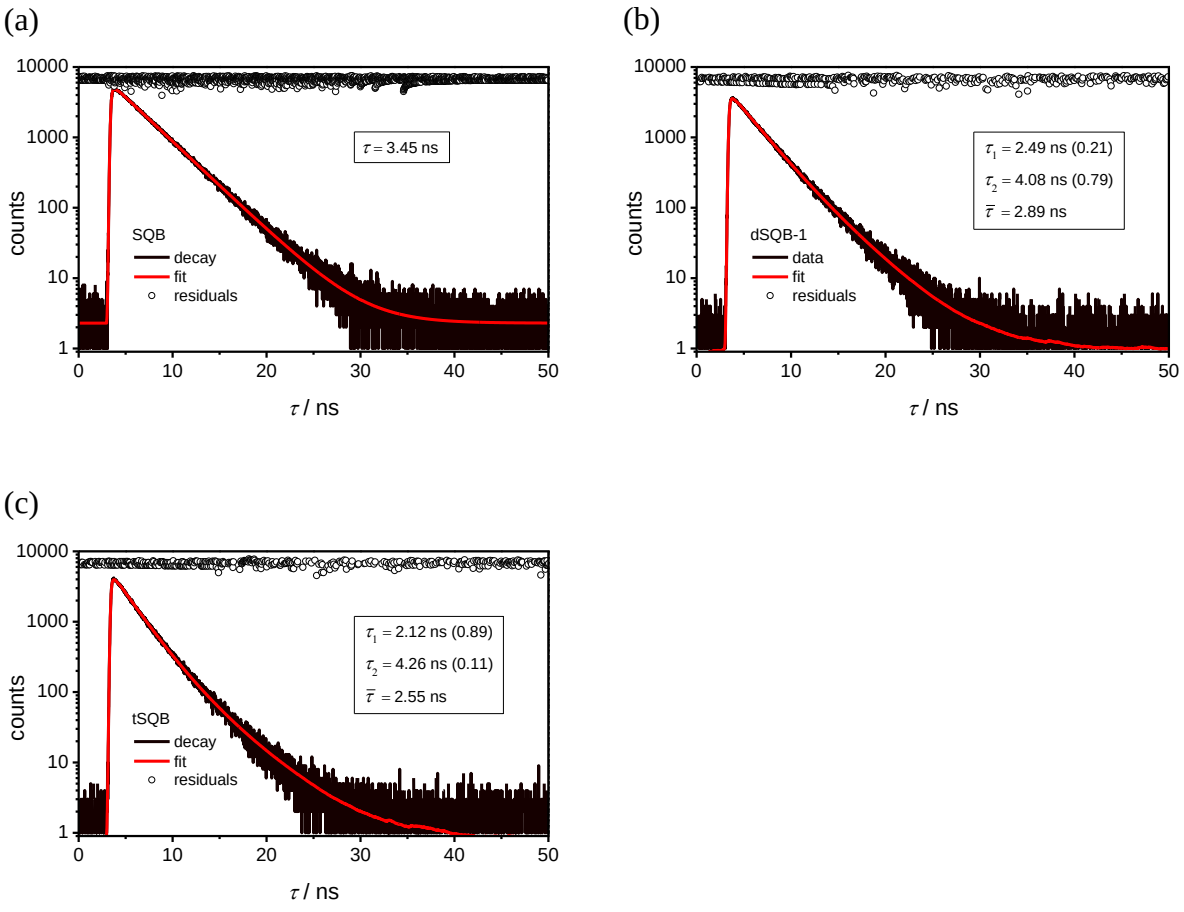

Figure 23: Fits of TCSCP data of (a) **SQB**, (b) **dSQB-1**, and (c) **tSQB**, in toluene with exponential functions. Insets: Resulting time constants τ_n and relative contributions of the corresponding amplitudes (in brackets). $\bar{\tau}$ represents the average fluorescence lifetime. Excitation was at 15 240 cm^{-1} (656 nm laser diode).

An alternative decay fit was performed applying the Kohlrausch equation (stretched exponential, equation (48)) with exponents β close to unity which turned out to be equally good for the dimer ($\bar{\tau}_{fl}$ = 2.56, β = 0.93) and trimer ($\bar{\tau}_{fl}$ = 2.05, β = 0.88) in toluene.[93]

$$I = I_0 \cdot e^{-\left(\frac{t}{\bar{\tau}_f}\right)^{\beta}} \tag{48}$$

As the polymer exhibits excitation energy-dependent dual fluorescence bands at 11 820 cm^{-1} and 12 330 cm^{-1}, the fluorescence lifetimes were therefore measured at these two energies, which is presented in Figure 24. Accordingly, biexponential decays are observed in both cases, with average lifetimes of 2.92 ns (11 820 cm^{-1}) and 2.15 ns (12 330 cm^{-1}). In addition, a significant increase of the longest lifetime (3.18 ns) together with an increase of the corresponding relative amplitude (0.72) is noted at 11 820 cm^{-1}. Consequently, the low energy fluorescence which was ascribed to the helix form is more long-lived than fluorescence at higher energies coming from the zig-zag form.

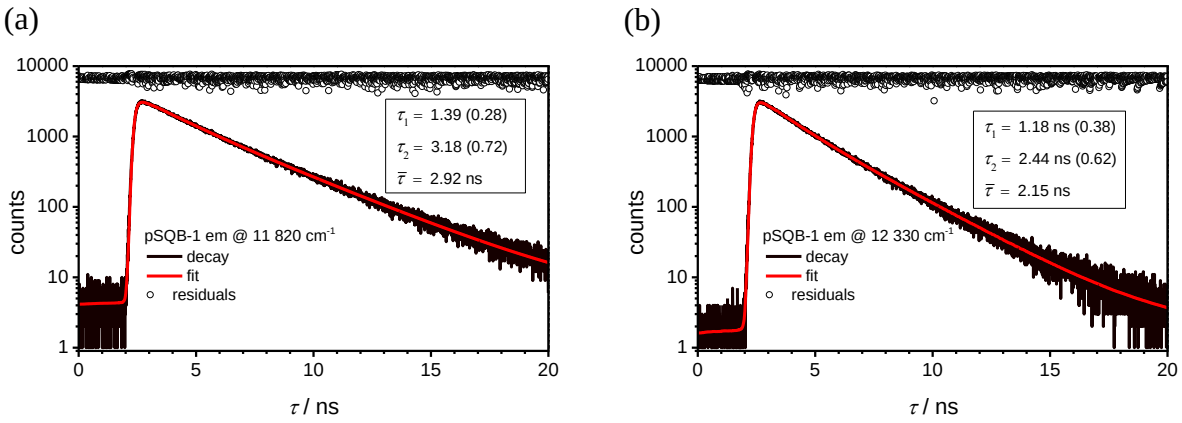

Figure 24: Fits of TCSCP data of **pSQB-1** in toluene with exponential functions. Emission detected at (a) 11 820 cm^{-1} and (b) 12 330 cm^{-1}. Insets: Resulting time constants τ_n and relative contributions of the corresponding amplitudes (in brackets). $\bar{\tau}$ represents the average fluorescence lifetime. Excitation was at 15 240 cm^{-1}.

Table 3: Full width at half maximum (FWHM) of absorption (abs) and emission (em) bands for different squaraine dyes.

	solvent	**FWHM** (abs) / **cm^{-1}**	**FWHM** (em) / **cm^{-1}**
SQB	$CHCl_3$	750	770
	toluene	660	730
dSQB-1	$CHCl_3$	740	660
	toluene	640	580
tSQB	$CHCl_3$	700	650
	toluene	610	570
pSQB-1	$CHCl_3$	–[a]	500
	toluene	–[a]	–[b]

– was not determined because of [a]overlapping absorption or [b]emission bands.

Table 4: Absorption maxima, extinction coefficients, transition moments, fluorescence maxima, fluorescence quantum yields, and fluorescence lifetimes of squaraine dyes in $CHCl_3$ and toluene. Extinction coefficients ε and transition moments μ_{eg} of the polymers are indicated per monomer unit.

	solvent	$\tilde{\nu}_{abs}$ / cm^{-1} (nm)	ε_{max} / $M^{-1}cm^{-1}$	μ_{eg}^2 / D^2	$\tilde{\nu}_{em}$ / cm^{-1} (nm)	Φ_{fl} / –	τ_{fl}[c] / ns
SQB	$CHCl_3$	14 600 (685)	1.96×10^5	98.6	14 200 (704)	0.55	2.40
	toluene	14 300 (699)	2.02×10^5	92.7	14 000 (714)	0.75	3.45
dSQB-1	$CHCl_3$	13 600 (735)	3.38×10^5	236	13 300 (751)	0.20	0.31 (0.21) 1.00 (0.79)
	toluene	13 400 (748)	3.62×10^5	226	13 100 (761)	0.68	2.49 (0.83)[d] 4.08 (0.17)[d]
tSQB	$CHCl_3$	13 200 (760)	4.03×10^5	381	12 900 (775)	0.20	0.90 (0.84) 1.30 (0.16)
	toluene	12 900 (774)	4.11×10^5	339	12 700 (786)	0.58	2.12 (0.89) 4.26 (0.11)
	PhCN	13 000 (769)	3.11×10^5	330	–	–	–
pSQB-1 X_n = 21.6	$CHCl_3$	12 700 (785)	1.08×10^5	112	12 500 (800)	0.21	0.05 (0.44) 0.47 (0.17) 0.96 (0.39)
	DCM	12 700 (785)	9.28×10^4	112	–	–	–
	toluene	12 700/14 700 (765/678)	$5.18/5.31\times10^4$	88.9	12 300 (810)	0.06[a] 0.17[b]	1.39 (0.28)[e] 3.18 (0.72)[e] 1.18 (0.38)[f] 2.44 (0.62)[f]
	PhCN	13 000/15 500 (767/647)	$3.44/7.32\times10^4$	90.3	–	–	–
	DMF	15 700 (636)	7.37×10^4	90.3	–	–	–
	acetone	15 800 (633)	8.35×10^4	92.2	–	–	–
pSQB-2 X_n = 8.12	$CHCl_3$	13 000 (771)	8.79×10^4	112	–	–	–
	DCM	13 000 (769)	8.18×10^4	114	–	–	–
	toluene	13 000 (771)	6.96×10^4	100	–	–	–
	PhCN	13 100/14 700 (766/679)	$5.59/6.15\times10^4$	100	–	–	–
	DMF	15 100 (661)	6.78×10^4	108	–	–	–
	acetone	15 200 (657)	6.85×10^4	108	–	–	–

– not determined. Excitation at [a]15150 cm^{-1}, [b]13510 cm^{-1}. [c](Multi-)exponential fit of fluorescence decay measured by TSCPC, excitation at 15 240 cm^{-1} (656 nm). Amplitudes are given in brackets. [d]Slightly different fluorescence lifetimes were previously reported in literature,[88] yet the values for the average fluorescence lifetime are very similar. Fluorescence was detected at [e]11 820 cm^{-1} (846 nm) or [f]12 330 cm^{-1} (811 nm).

3.4.2.5 Squaraine Dye Doped OLED[VII]

In collaboration with David J. Harkin and Prof. Henning Sirringhaus from the department of physics at the University of Cambridge, **tSQB** (**SQ3**) was applied as NIR emitter in an organic light emitting diode (OLED).[35] Poly(indacenodithiophene-*alt*-benzothiaidazole) (**IDTBT**, Figure 25) was used as host polymer in which **tSQB**, denoted as **SQ3** in the following, was incorporated as guest molecule. In this respect, a method was demonstrated to decouple electrical performance and electroluminescence using efficient resonance energy transfer (RET) from the high mobility polymer to the highly emissive near-infrared squaraine dye. The underlying mechanism of energy transfer was studied by photoluminescence (PL) and electroluminescence (EL) experiments.

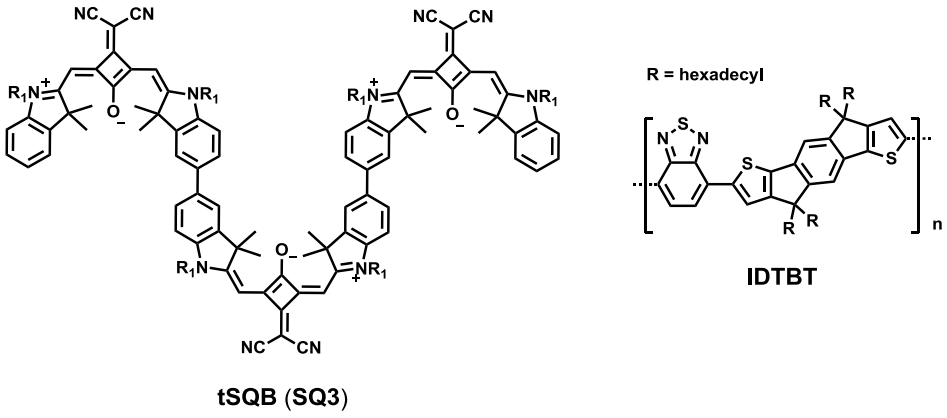

Figure 25: Chemical structures of **tSQB** (**SQ3**) and polymer **IDTBT**.

The IDTBT polymer was chosen as suitable transport medium because of its high mobility in transistor structures, high solubility (< 120 mg ml^{-1} *o*DCB) and the lack of long range structural order which was assumed to facilitate incorporation of the squaraine dye without impairing the charge transport.[153,154] In *o*DCB, the fluorescence quantum yield (FQY) of neat IDTBT is 0.18 with a lifetime of 1.3 ns. The FQY drops to 0.02 and the lifetime to around 90 ps when prepared in thin films, which hints towards strong non-radiative quenching processes in the solid state. The polymer exhibits a NIR fluorescence peak at 718 nm which can be appreciated in Figure 26 and has a HOMO and LUMO of –5.3 eV and –3.6 eV, respectively.[155] Owing to the relatively low bandgap of **IDTBT** (1.7 eV) the selection of a suitable acceptor molecule for efficient RET came down to **SQ3** due to its highly favourable optical properties, such as a high maximum molar absorption coefficient of 5.5×10^5 M^{-1} cm^{-1}

[VII] Reproduced or adapted in part with permission from *Decoupling Charge Transport and Electroluminescence in a High Mobility Polymer Semiconductor*, D. J. Harkin, K. Broch, M. H. Schreck, H. Ceymann, A. Stoy, C.-K. Yong, M. Nikolka, I. McCulloch, N. Stingelin, C. Lambert, and H. Sirringhaus, *Adv. Mater.* **2016**, *28*, 6378-6385. Copyright © (2016) WILEY-VCH Verlag GmbH & Co. KGaA, Weinheim..

at 780 nm in *o*-DCB along with high FQY of 0.58 (0.20) in toluene ($CHCl_3$) and a low band gap of 1.62 eV (in DCM). This ultimately offers the possibility to use ultralow concentrations of this dye as the emissive component. In addition, the energy levels of the all components implemented in the OLED show a good match (Figure 26(b)).

In general, RET describes a long range dipole coupling process in which a donor molecule transfers its excitation to an energetically suitable acceptor molecule.[156] RET typically acts over distances from 1-10 nm and its efficiency strongly correlates with the donor-acceptor spacing, donor FQY and the spectra overlap between the donor fluorescence spectrum and the acceptor absorption spectrum[34,157] In this respect, the Förster radius (R_0) is used to describe the coupling strength between two chromophores and defines the mean distance between donor and acceptor at which energy transfer is equally likely as decay of the excited donor molecule. For a randomly orientated medium equation (49) can be used to determine R_0:

$$R_0 = 0.197 \left(n^{-4} \, \Phi_D \, J(\lambda) \right)^{1/6} \tag{49}$$

R_0 is given in units of Å, n is the refractive index of the medium, Φ_D is the FQY of the donor in the absence of the acceptor.[157] $J(\lambda)$ is the spectral overlap between the fluorescence of the donor and the absorption of the acceptor in units of $m^{-1}cm^{-1}nm^4$. For stationary donor and acceptor molecules the exciton transfer efficiency can be calculated by equation (50):

$$\gamma = \frac{R_0^6}{R_0^6 + r^6} \tag{50}$$

where r is the donor-acceptor spatial separation. Since high mobility polymers suffer from low FQY the spectral overlap needs to be maximized in order to achieve high values of R_0.

According to Figure 26(a), **SQ3** is ideally suited for efficient resonance energy transfer from **IDTBT** due to the strong overlap with the fluorescence spectrum of **IDTBT**. The integrated spectral overlap was calculated to be 1.2×10^{17} M^{-1} cm^{-1} nm^4. Making use of equation (49) with an **IDTBT** FQY of 0.02 and an average refractive index of 2, the Förster radius was calculated to be 4.5 nm. Being aware of the very low FQY of neat **IDTBT** thin films, the Förster radius obtained is considered large for such a solid state organic system.[34]

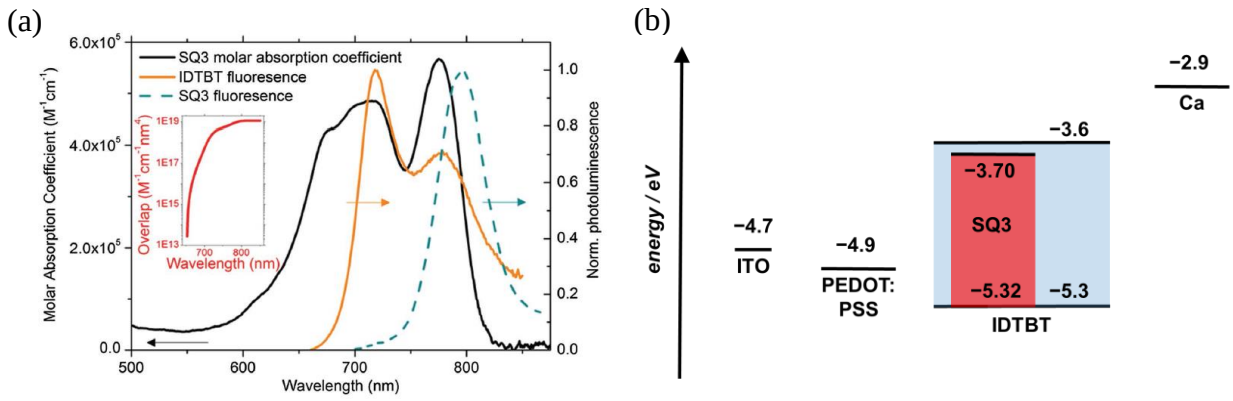

Figure 26: (a) **IDTBT** fluorescence spectrum with molar absorption and fluorescence spectra of **SQ3** in *o*-DCB showing the high spectral overlap between the two molecules of which the cumulative value is quantified in the inset. Copyright © (2016) The Authors. Published by WILEY-VCH Verlag GmbH & Co. KGaA, Weinheim. (b) Energy levels of the components implemented in the OLED.

Spin coated films of **IDTBT** with small concentrations of **SQ3** were prepared and the photophysics of the system are investigated. Figure 27(a) shows photoluminescence spectra of **SQ3**/**IDTBT** films with varying mass ratios of the dye (0.025, 0.075, 0.3 wt. %) along with the neat film. Accordingly, the emission peak of **SQ3** at 795 nm increases when increasing the dye loading. In this respect, the absorption spectra show no change even at high dye loading of 0.3 wt %. The increase of **SQ3** fluorescence without change in the absorption spectrum clearly points towards a strong energy transfer in the film. In order to distinguish whether it is an energy transfer process or direct excitation of the dye, photoluminescence excitation spectra were recorded of neat **IDTBT**, a solution of 0.01 wt % **SQ3** in *o*DCB as well as of a 0.3 wt. % **SQ3** blend film (Figure 27(b)).

Accordingly, the excitation spectra of the blended films nicely match the spectrum of the neat **IDTBT** rather than that of pure **SQ3** in *o*DCB. Indeed, this clearly indicates that the initial energy is absorbed by **IDTBT** and subsequently transferred to the squaraine dye. Furthermore, time-resolved fluorescence measurements were performed on neat **IDTBT** film as well as of **SQ3** doped films. Figure 27(c) shows a plot of the fluorescence decay of the 700 nm **IDTBT** component versus time. Accordingly, the exciton lifetime decreases with increasing concentration of **SQ3** (energy transfer). The experimental data show monoexponential decays with a lifetime of 90 ps for neat **IDTBT**, which further decrease to 25 ps in the films with increasing **SQ3** concentration (Inset Figure 27(c)). Figure 27(d) shows a plot of the energy transfer efficiency versus **SQ3** concentration. The calculation of the energy transfer efficiency can be carried out from the steady-state and time-resolved fluorescence data.[158] It can be seen that the process is efficient even at low concentrations of **SQ3**. From this plot it is apparent that 50 % energy transfer is reached at a **SQ3** loading of

0.3 wt. %. This unambiguously demonstrates a highly efficient energy transfer from a high mobility polymer to an acceptor chromophore.

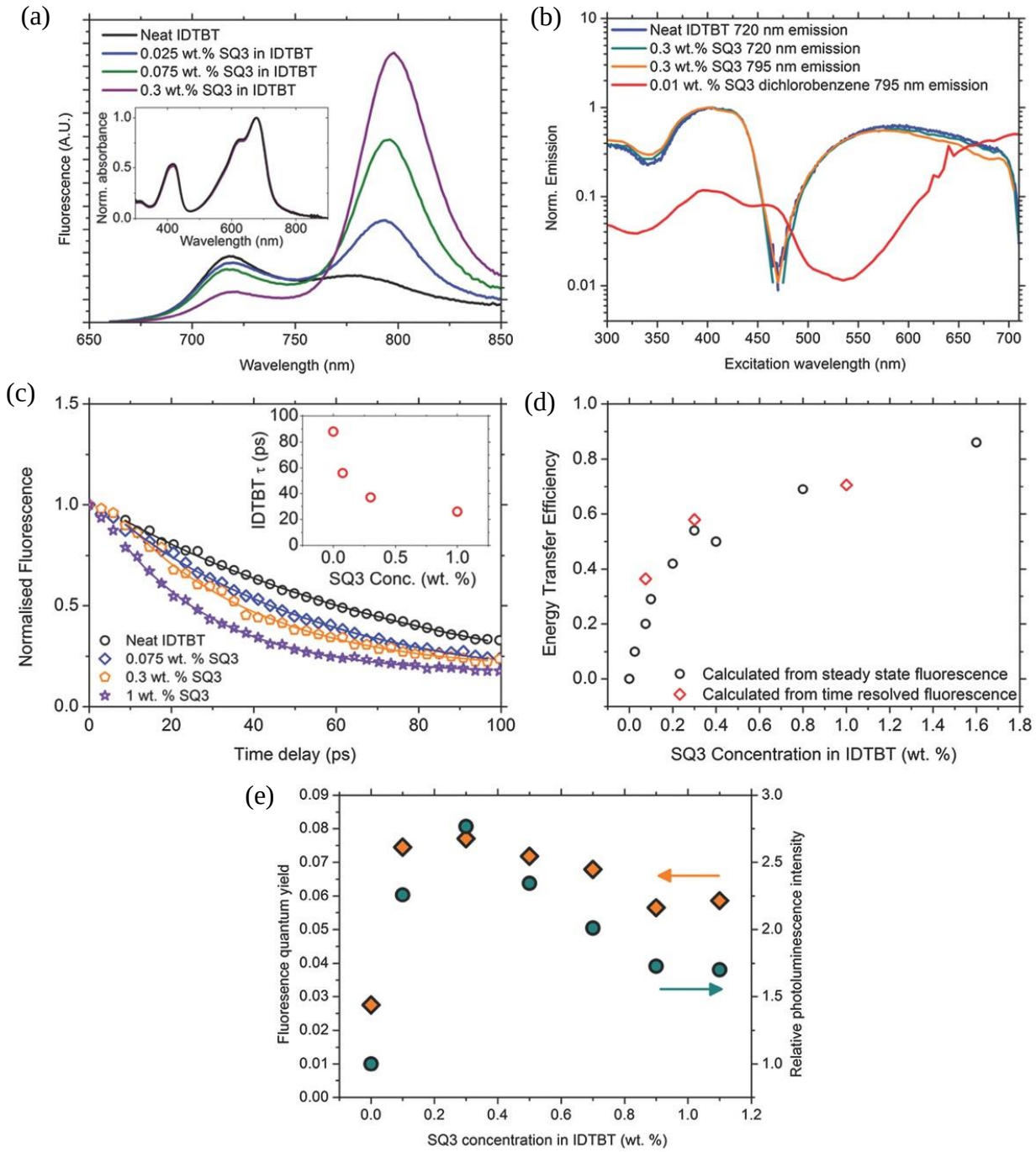

Figure 27: (a) PL spectra of neat **IDTBT** and films blended with low concentrations of **SQ3**. (b) Photoluminescence excitation spectra of neat **IDTBT** film, a solution of 0.01 wt % **SQ3** in *o*DCB as well as of a 0.3 wt. % **SQ3** blend. The fluorescence was probed either at 720 nm and 795 nm. (c) Plot of fluorescence decay of the 700 nm component of neat **IDTBT** and **IDTBT** blended with SQ3 versus time as well as monoexponential decays of which the lifetime is plotted versus concentration in the inset. (d) Exciton transfer efficiency versus **SQ3** concentration calculated from the steady-state and time-resolved fluorescence data. (e) Measured FQY and relative photoluminescence intensity of blended films.

Furthermore, FQY measurements were performed to elucidate, whether this energy transfer process gave rise to a fluorescence enhancement. Figure 27(e) shows a plot of FQY and relative integrated photoluminescence intensity of the blend films versus **SQ3** concentration. It can be appreciated that the FQY peaks at 0.077 at a **SQ3** loading of 0.3 wt. % reflecting a threefold enhancement in regard to neat **IDTBT** (0.02). This is among the highest FQYs hitherto reported for solid state organic systems with emission in the NIR.

In a next step, the blended films were embedded into organic light emitting diodes and the device performance was investigated. Electroluminescence spectra were recorded as a function of **SQ3** loading (Figure 28(a)). Accordingly, the emission of **IDTBT** is almost completely quenched at a dye loading of 0.3 wt. % indicating a highly efficient energy transfer process. In addition, the relative change of the external quantum efficiency (EQE) and hole field mobility was investigated. The spectra are shown in Figure 28(b). The EQE is increased by a factor of 8 at a dye loading of 0.3 wt. %. Simultaneously, the hole field mobility is not reduced and had consistently values of around 1.7 $cm^2 V^{-1} s^{-1}$ which is in accordance with values previously reported for this polymer.[159]

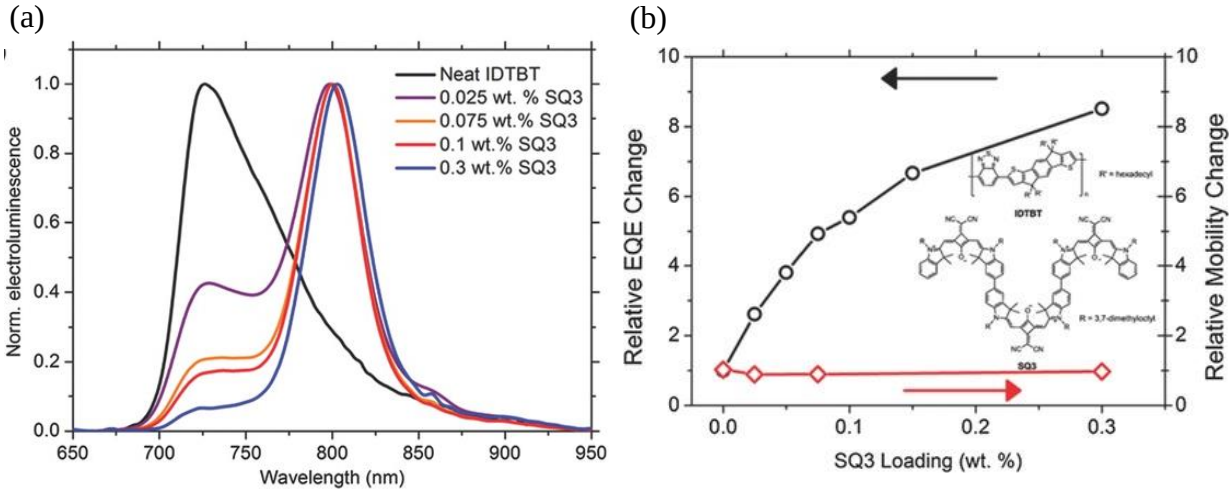

Figure 28: (a) Electroluminescence spectra of OLEDs with varying **SQ3** loadings. (b) Relative change in EQE and hole field effect mobility versus varying **SQ3** loadings. Copyright © (2016) The Authors. Published by WILEY-VCH Verlag GmbH & Co. KGaA, Weinheim.

In conclusion, it was demonstrated that **SQ3** could successfully be employed as NIR fluorophore in a solution processed film OLED with outstanding characteristics. In this respect, the fluorescence of the high-mobility polymer semiconductor (**IDTBT**) could be enhanced through efficient energy transfer to the highly emissive squaraine dye resulting in a maximum external quantum efficiency of 0.2 % and radiances up to 5 W str^{-1} m^{-2} at 800 nm, without reducing the charge-carrier mobility.

3.4.2.6 Conclusion

Taking advantage of the convenient access to homopolymers by means of Ni-mediated Yamamoto homocoupling reaction, a dicyanovinylene-substituted polymer **pSQB** was synthesised according to the literature known squaraine polymer **pSQB-V** by Völker. The crude polymer was split via preparative GPC into three batches of polymers with diverging molecular weight distribution. Only two of the three batches were studied in detail since the polymer batch **pSQB-3** solely provided a very low degree of polymerisation ($X_n \approx 3$). Furthermore, two discrete small molecular weight oligomers **dSQB-1** and **tSQB** were prepared via Pd-catalysed Suzuki cross coupling reaction in good yields of 65 % and 59 %, respectively. By this, a series of *cisoid* squaraine dyes with varying number of chromophore units could be generated, which enabled a comprehensive evaluation of the influence of molecular weight on the optical properties.

In comparison to the monomer **SQB**, the dimer **dSQB-1**, the trimer **tSQB**, and the polymer **pSQB-1** showed a progressive red-shift of the lowest main absorption band and a much larger bandwidth of the absorption which can be explained by exciton coupling of localised transition moments. Furthermore, the polymer **pSQB** displayed a strong dependency of the shape of the absorption band manifold on the solvent. The absorption features could best be explained by formation of an excitonic manifold due to at least two different conformers, i.e., a helix and a zig-zag chain. While the latter provided typical J-type behaviour, the former can be considered as an H-type aggregate. It was shown, that the fractions to which these conformers are formed dramatically depend on the solvent, chain length and temperature. Yet, a strong resemblance of the shape of the absorption band manifold was observed for the second polymer fraction **pSQB-2** and **pSQB-V**, even though they considerably differ in chain length ($X_n \approx 8$ and ≈ 36). In contrast, a strong difference was noted for **pSQB-1** with intermediate chain length, displaying sharper and more intense main absorption bands for the two extrema, helix and zig-zag, with substantially less absorbance in the spectral region of mixed structures. These features were referred to the presence of a rather homogenous polymer with ordered structures. This might be the reason that the computed spectra (TD-DFT) coincide very nicely with **pSQB-1**.

The fluorescence of **pSQB-1** provided another striking feature. While typical monomer shape fluorescence and decent quantum yields were observed for the oligomers in $CHCl_3$ and toluene, **pSQB-1** displayed in toluene a second fluorescence band located at lower energies which was assigned to the helix form. The relative intensity of this band can be reduced by using lower excitation energies, where absorption of the zig-zag form is predominant. Thus,

no substantial excitation energy transfer proceeds from the zig-zag to the helix form. In contrast, it was shown that the quantum yield is also dependent on the excitation energy. Thus, a higher quantum yield of 0.17 was obtained when exciting the zig-zag exciton manifold at lower energies. Therefore, it can be concluded, that a rather inefficient energy transfer occurs the opposite way, i.e., from helix to zig-zag.

3.4.3 Diphenylindolenine Squaraine Homopolymer[VIII]

3.4.3.1 Introduction

The previous chapter dealt with the ambivalent folding behaviour of *cisoid* squaraine polymers, which manifested itself in the formation of two different conformers in solution. Here, it became evident that the solvent as extrinsic factor proved to play a superior role. Now the question arises of how to chemically manipulate the dyes in order to gain intrinsic control over the folding process and thus to force the polymer exclusively into one superstructure. An answer to this question could possibly pave the way to polymers with tailor-made optical properties. Without doubt, the flexible biarlyaxes between two squaraine moieties is the reason for the emergence of different conformers. Now, the new strategy constitutes the encoding of the conformer structure already on the stage of the monomer. In this context, it is assumed that steric congestion might suppress helical domains in favour of elongated zig-zag structures due to steric repulsion between the dye moieties within the polymer strands. For this purpose, the steric demand of the dimethyl-groups in the 3-position of the indolenine donor is drastically increased by substitution with phenyl groups, giving rise to the corresponding 3,3-diphenyl-3*H*-indole (Scheme 14). The synthesis of such functionalised bulky squaraine dyes might enable polymers without collapsing to helical arrangements.

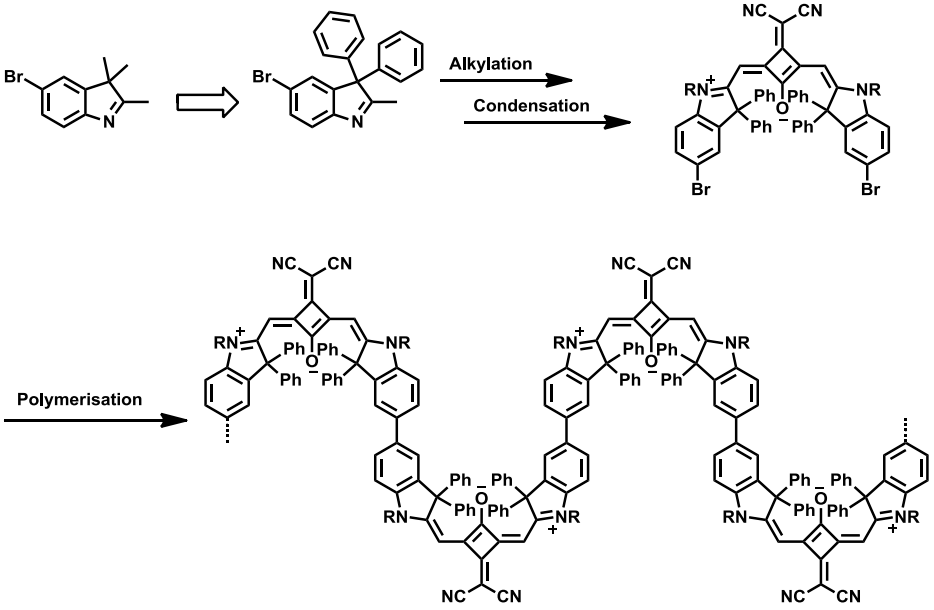

Scheme 14: Initially proposed synthetic route to bulky diphenylindolenine squaraine polymers.

[VIII] Parts of this chapter have been investigated in a bachelor thesis under the supervision of M. H. Schreck: L. Breitschwerdt, Bachelor Thesis, Julius-Maximilians Universität (Würzburg), **2016**.

3.4.3.2 Synthesis

Several attempts were made to prepare 2-methyl-3,3-diphenyl-3*H*-indole derivatives via conventional Fischer indole synthesis in the course of the foregoing master thesis, but failed owing to extremely low yields and laborious purification.[141] Apparently, sterically demanding ketones, such as 1,1-diphenylpropan-2-one are poorly tolerated in standard Fischer indole reactions. Hence, new synthetic strategies had to be developed for the introduction of bulky groups into the indole scaffold. One promising and elegant way comprises the Friedel-Crafts alkylation reaction of isatin (indoline-2,3-dione) with aromatics in superacidic triflic acid (TfOH) (Scheme 15).

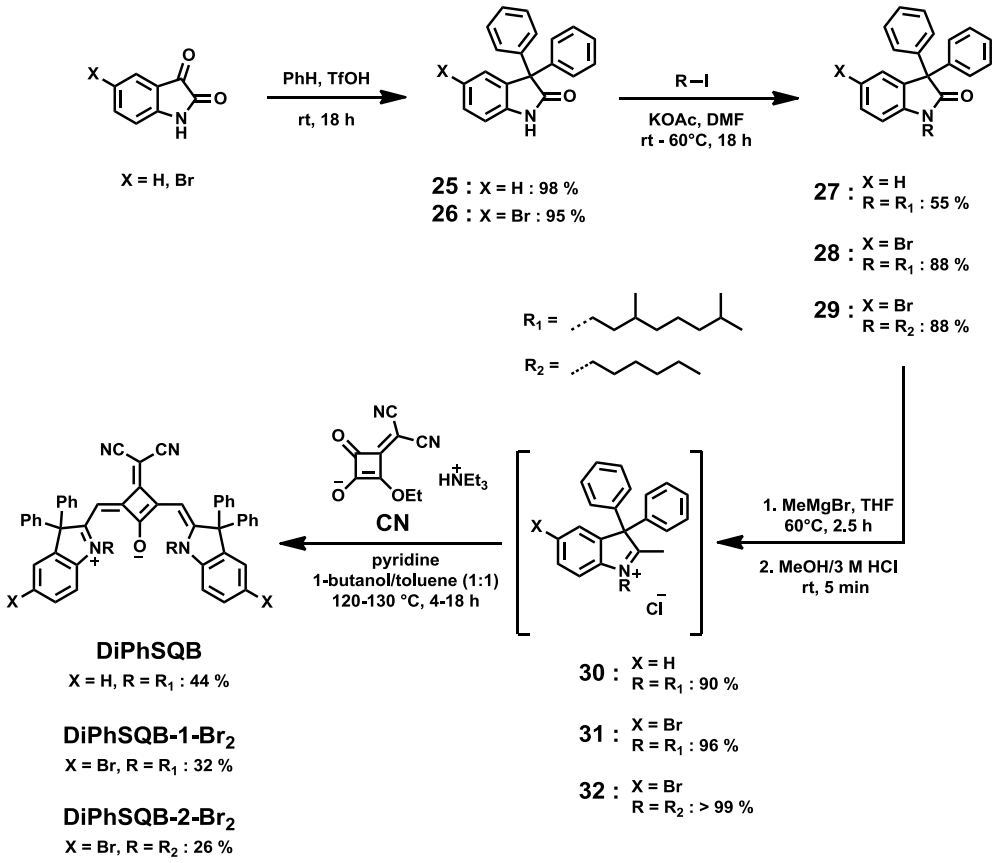

Scheme 15: Synthesis of diphenylindolenine squaraine dyes.

Olah and co-workers showed that the reaction proceeds in high to excellent yields and the condensation reaction exclusively occurs at the 3-carbonyl group of the isatin. Furthermore, it is highly regioselective in *para* attack on alkyl- and halogen-substituted aromatics. Interestingly, the reaction shows a crucial dependence on the acid strength, implying the formation of diprotonated, superelectrophilic intermediates. In this context, acids of lower strength only showed incomplete conversion to the product.[160] According to Scheme 15, the respective 3,3-diphenyloxindoles **25** and **26** were prepared in excellent yields following literature procedures.[160] It is assumed that the mechanism of the reaction involves a protolytic

activation of the 3-carbonyl group, followed by an electrophilic attack on benzene. The resulting Friedel-Crafts products are isolated in sufficient purity for further reactions or can optionally be purified by rapid column filtration.

In prospect of potential solubility issues of the respective polymer, the diphenyloxindoles were subsequently *N*-alkylated with standard alkylating agent 3,7-dimethlyoctyliodide under basic conditions to give compounds **27** and **28** in decent yields. However, the racemic nature of the stereo centre caused by the alkyl chain will produce squaraine diastereomers and thus hampers the possibility of structural elucidation by single crystal X-ray structure analysis. In order to address this issue, brominated oxindole **26** was also equipped with a linear hexyl chain. It is known that short and linear chains facilitate the crystallisation of organic compounds. For the same purpose, brominated oxindole **26** was used instead of non-functionalised indole derivative **25**. The iminium cations **30-32** were prepared by addition of MeMgBr to lactams **27-29** in THF at 60 °C for 2.5 h followed by treatment with 3 M HCl in MeOH. The quaternary salts were obtained as waxy colourless solids which readily turned red. These iminium salts proved to be unstable under ambient conditions. This observation was also reported by Maeda for a similar quaternary indole salt.[61] Therefore the compounds were used in the following condensation reaction without purification. The latter step is considered to be the key reaction step in this synthetic route which has not been applied so far in comparable synthetic protocols for squaraines. In this context, for the synthesis of novel benzo[*c*,*d*]indolenine squaraine dyes Maeda et al. developed a protocol which involves three additional stages in order generate the respective iminium salt.[61] Here, the reduction of the lactam function by simply using MeMgBr with aqueous acidic workup proves to be the more economic and convenient method.

Finally, the corresponding bulky squaraine dyes were synthesised in moderate yields (26-44 %). It is noteworthy that the bromine-functionalised squaraine dyes **DiPhSQB-1-Br$_2$** and **DiPhSQB-2-Br$_2$** were prone to undergo undesired debromination reactions when applying the standard protocol for the condensation reaction. To address this issue, the bromine-functionalised squaraine dyes were prepared under inert atmosphere with deaerated solvents and shorter reaction times (ca. 4 h). These measures were found to be very effective, thus no debromination reaction could be detected via NMR and mass spectrometry.

Furthermore, it was possible to grow crystals of both brominated species applying the layering technique. For this purpose, a highly concentrated solution of squaraine in DCM (~ 5-10 mg/0.5 ml) was placed in a NMR-tube and was carefully covered by *n*-hexane (1 ml) which served as antisolvent. The tube was afterwards sealed with parafilm and the crystal

growth was observed after 1 d. After several days, both squaraine dyes were obtained as green crystals while the non-brominated squaraine **DiPhSQB** gave a green powder. For the reason mentioned above, only **DiPhSQB-2-Br$_2$** was used for crystallography.

Single crystal X-ray structure analysis of squaraine **DiPhSQB-2-Br$_2$** revealed a striking finding (Figure 29). Against common expectations, the crystal structure of bulky **DiPhSQB-2-Br$_2$** proved to be totally different to all standard *cisoid* squaraine dyes found in literature.[11] While *cisoid* benzothiazole and quinoline squaraines display perfect planarity, 3,3-dimethylindolenine squaraine (Figure 30), decorated with a linear *n*-butyl alkyl chain, possesses a slight bending of the π-system out of planarity. The sterically demanding $C(CH_3)_2$ group induces a perceptible torsion of about 6°. In addition, the steric impact which is expressed by the angle β shows a value of 133° and thus reflects a deviation from ideal sp^2 hybridisation.

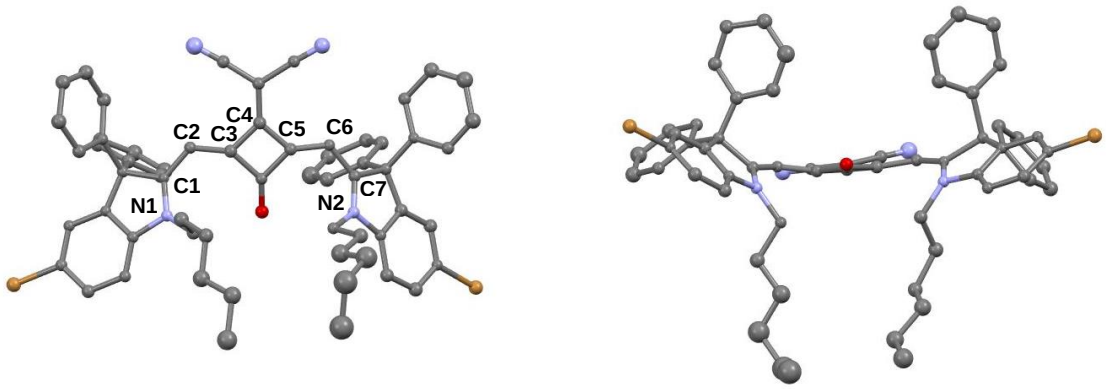

Figure 29: Molecular structure and side view of **DiPhSQB-2-Br$_2$**. H atoms are omitted for clarity; grey: C, blue: N, red: O, brown: Br.

The squaraine scaffold of **DiPhSQB-2-Br$_2$** is highly bent due to steric congestion and thus significantly deviates from the ideal planar geometry which is manifested by torsion of the indolenine donor on average of 149° in respect to the central squaric acid ring. This drastic change in geometry culminates in a unique distorted structure in which the bulky phenyl groups now face the dicyanovinylene group instead of the oxygen of the squaric acid ring. Interestingly, the structure which was anticipated in the first place and in which the electron-donating heterocycle is oriented away from the dicyanovinylene unit (Figure 30) is not formed. It is assumed that the steric repulsion potentially arising from the phenyl groups with the oxygen lead to a twist of the indolenine scaffold. DFT calculations[IX] (B3LYP/6-31G*) corroborate these experimental findings. Accordingly, the crystal structure was found to be 227 kJ mol^{-1} (2.36 eV) more stable than the expected structure. In a standard *cisoid*

[IX] DFT calculations were carried out by Dr. Marco Holzapfel.

conformation with typical C_{2v} symmetry, a considerable large open space is available in the vicinity of the dicyanovinylene group where usually the alkyl chains of the donor heterocycle are hosted. Here, this space is now occupied by the sterically demanding phenyl groups. As a consequence of this torsion, **DiPhSQB-2-Br$_2$** displays an average angle β of 126° (mean value of β_1 and β_2) which is significantly closer to ideal sp^2 hybridisation compared to the value of parent 3,3-dimethylindolenine squaraine.

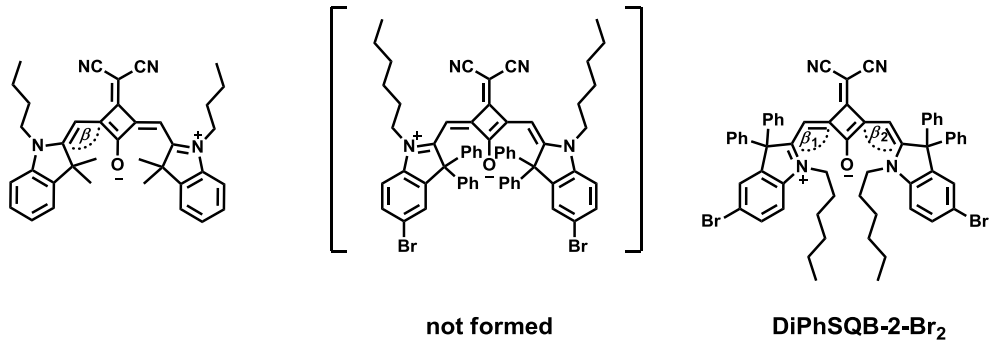

Figure 30: Chemical structures of squaraine dyes.

Moreover, the bond lengths along the polymethine chain between the nitrogen atoms N1 and N2 (Figure 29) show marginal bond length alteration (BLA), which can be readily appreciated by the crystallographic data presented in Table 5. The bond length distances are in the range 1.30-1.44 Å for **DiPhSQB-2-Br$_2$**. The BLA quantifies the average of the difference in the length between neighbouring bonds in the polymethine chain and can directly be determined from the crystallographic data. For literature squaraine dye a BLA of 0.02 Å was calculated, while a substantially larger value of 0.05 Å was obtained for **DiPhSQB-2-Br$_2$**. Both values are considerably lower than the values found for polyenes (0.11 Å) and stilbenes.[161]

Table 5: Bond lengths for the polymethine chain for squaraines **SQB**[b] and **DiPhSQB-2-Br$_2$** according to single crystal X-ray analysis.[c]

	N1-C1 / Å	C1-C2 / Å	C2-C3 / Å	C3-C4 / Å	C4-C5 / Å	C5-C6 / Å	C6-C7 / Å	N2-C7 / Å
SQB[a,b]	1.351	1.389	1.386	1.439	1.433	1.399	1.379	1.360
DiPhSQB-2-Br$_2$	1.303	1.429	1.365	1.435	1.424	1.396	1.395	1.339

[a]Crystallographic data taken from literature.[11] [b]**SQB** equipped with a *n*-butyl alkyl chain. [c]Atoms of polymethine chain are labelled from left to right as indicated in Figure 29.

Following the standard protocol for Ni-mediated Yamamoto homocoupling reactions according to Scheme 16, crude **pDiPhSQB** was synthesised and subsequently subjected to consecutive Soxhlet extractions using *n*-hexane, MeOH, and acetone. The major part

remained in the acetone fraction. Preparative GPC was used in order to get rid of small molecular weight oligomers. Finally, **pDiPhSQ** was synthesised in 48 % yield providing a number average molecular weight M_n of ~ 36 600 and a weight average molecular weight M_w of ~ 86 000 with a number average degree of polymerisation X_n of ~ 38. Furthermore, analytical GPC revealed a $Đ$ of 2.35, which reflects a slight deviation from the typical Flory-distribution. The polymer provides high solubility in common organic solvents, such as $CHCl_3$, DCM, DMF, PhCN, and *o*DCB, however, it is only partially soluble in toluene and acetone.

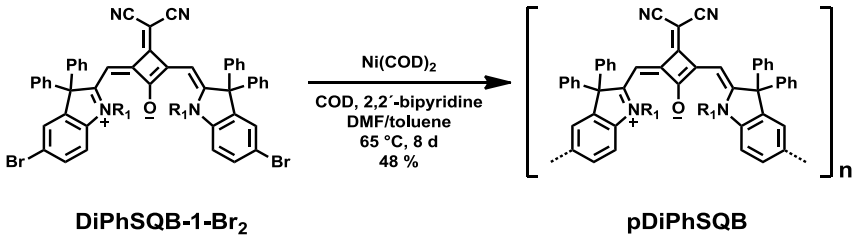

Scheme 16: Synthesis of diphenylindolenine squaraine homopolymer **pDiPhSQB**.

3.4.3.3 Absorption Spectroscopy

The absorption spectra of **DiPhSQB** in various solvents are depicted in Figure 31 and the corresponding optical data are presented in Table 6. Owing to the remarkable, highly twisted dye geometry, the monomer was investigated in more detail by measuring the absorption in a series of solvents that diverge in polarity, aromatic character, and hydrogen bond donor property.

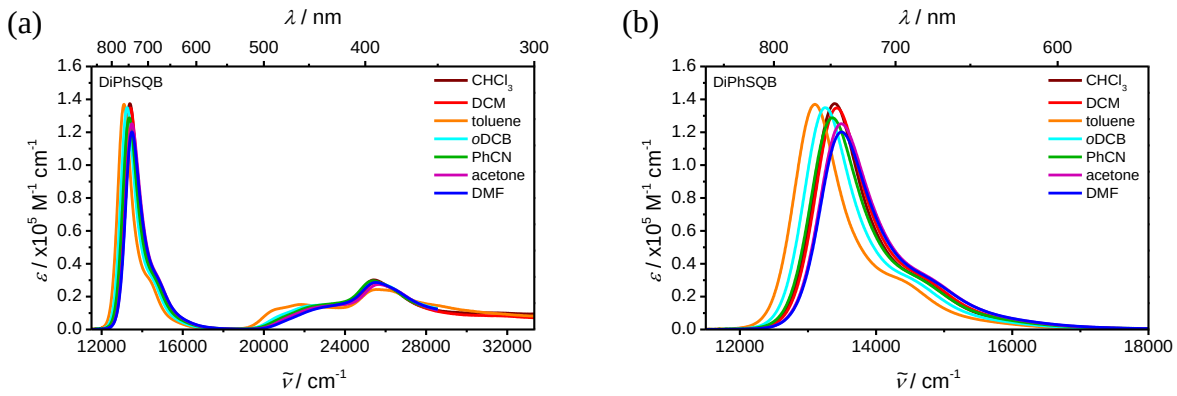

Figure 31: Absorption spectra of **DiPhSQB** in various solvents.

In all considered solvents, the monomer features typical characteristics of squaraine dyes, i.e., intense main absorption band along with a vibronic shoulder at higher energies. In addition, absorption bands at higher energies around 20 000-28 000 cm^{-1} are exhibited which can be

attributed to transitions into higher states and are commonly observed for dicyanovinylene substituted squaraine dyes.

Besides, the most red-shifted absorption band is found in toluene at 13 100 cm^{-1}, while the most blue-shifted absorption maximum is observed at 13 500 cm^{-1} in DMF and acetone, respectively. In comparison to parent squaraine **SQB**, **DiPhSQB** decorated with two phenyl groups per indolenine moiety exhibits a significant red-shift of about 1 200 cm^{-1} in toluene and $CHCl_3$ (Figure 32). On the other hand, considerably lower extinction coefficients are noticed for **DiPhSQB**. The highest and lowest extinction coefficient for **DiPhSQB** is found in toluene (1.35×10^5 M^{-1} cm^{-1}) and acetone (1.25×10^5 M^{-1} cm^{-1}), respectively. Similarly, lower squared transition moments are observed, that range from 79.2 D^2 in *o*DCB to 88.9 D^2 in acetone. Furthermore the absorption band of **DiPhSQB** appears to be broader which can be readily appreciated by a larger FWHM, which was estimated to be 830 cm^{-1} for **DiPhSQB** in toluene. In contrast, **SQB** provides a narrower absorption band with a FWHM of ca. 670 cm^{-1}. Consequently, the highly distorted structure of **DiPhSQB** which deviates from an ideal planar π-scaffold causes a significant red-shift and broadening of the absorption, accompanied by a decrease of molar absorptivity. In this context, a parallel may be drawn to ethylene, whose HOMO-LUMO gap also decreases upon gradually twisting the molecule.[162]

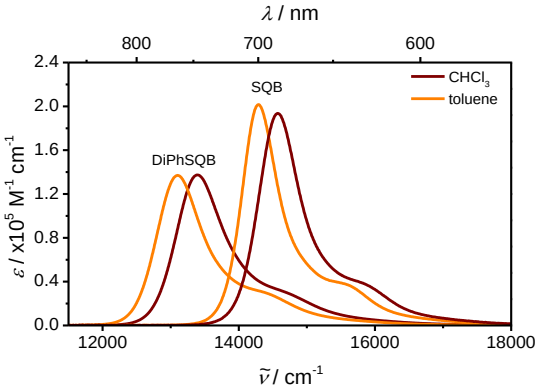

Figure 32: (a) Absorption spectra of **DiPhSQB** and **SQB** in $CHCl_3$ and toluene, respectively.

The absorption behaviour of the polymer was studied in the same solvents as shown for the monomer (Figure 33). However, due to rather low solubility in toluene and acetone, no extinction coefficients could be determined therein, respectively. The polymer exhibits a rather unstructured, broad absorption band from 11 000-16 000 cm^{-1}. The highest and lowest extinction coefficient is found in $CHCl_3$ (7.66×10^4 $M^{-1}cm^{-1}$) and *o*DCB (6.34×10^4 $M^{-1}cm^{-1}$), respectively. The calculation of the square of the transition moments of the whole exciton manifold yields comparable values (75.6-89.3 D^2) and thus indicate within experimental error that the integrated oscillator strength $f \sim \mu_{eg}^2$ is independent of the solvent. The squares of the transition moments also agree with the values obtained for the monomer. Besides, the

absorption spectra of the polymer show a red-shift of the main absorption peak in the range of 700-1 000cm^{-1} with respect to the monomer for the considered solvents and should be mainly due to the exciton splitting of the first excited state. In $CHCl_3$, for example, the red-shift of about 1 000 cm^{-1} coincides with the red-shift observed for **dSQB-1** (1 000 cm^{-1}) compared to its monomer. This finding speaks against a long delocalisation length as exciton theory predicts a larger splitting of the first excited state, when considering an exciton that is delocalised over several monomers.[26,27]

In contrary to **pSQB-1**, the absorption strength of **pDiPhSQB** is concentrated in the lower edge of the exciton band with no considerable contributions arising from the upper edge of the exciton band. This points towards J-aggregate behaviour with monomers allinged in a collinear (head-to-tail) fashion. Closer inspection of the band shapes yet reveal a double peak structure, which can be readily appreciated by Figure 33(b) and (c).

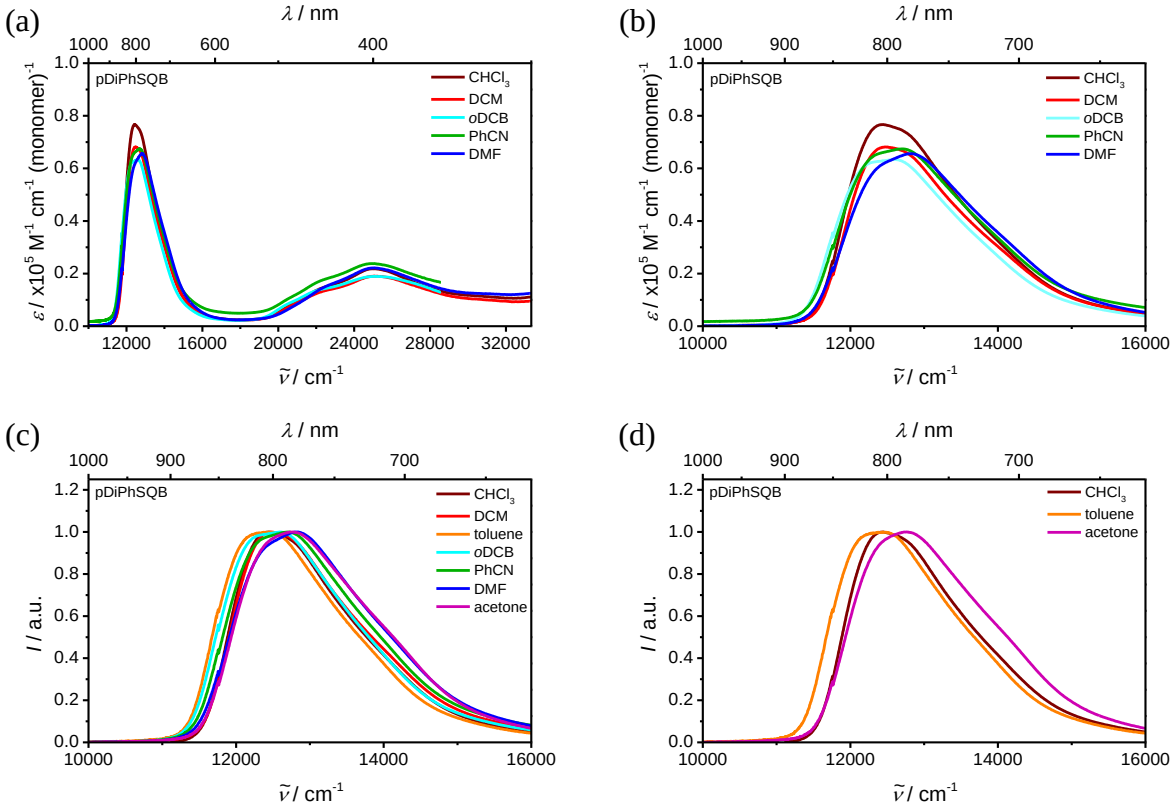

Figure 33: (a)(b) Complete and (c) normalised absorption spectra of **pDiPhSQB** in various solvents. (d) Normalised absorption spectra of **pDiPhSQB** in $CHCl_3$, toluene, and acetone.

While the most intense peak is located at the low energy side with a shoulder at higher energies in $CHCl_3$ and DCM, the situation is reverse in *o*DCB, PhCN, acetone, and DMF and displays a slightly blue-shifted absorption peak along with a shoulder at lower energies. Besides, an intermediate situtation can be observed for the polymer in toluene. Here, the absorption band proves to be rather broad and structureless, which might be the result of a

superposition of both features. Hence, the absorption can be devided in three solvent categories according to the spectral trends observed, i.e., $CHCl_3$, toluene, and acetone (Figure 33(d)). Recalling the absorption behaviour of **pSQB-1** (see Chapter 3.4.2.3) which is marked by a dramatic solvent dependency and a large exciton splitting, similar trends, albeit in a considerably weaker form and only present for the designated J-aggregate band are observed for **pDiPhSQB** in the same solvents. The existence of two different monomer-monomer conformations within the polymer strands, most likely enabled by the rotation around the relatively flexible biarylaxes, could possibly account for these spectral findings. However, much in contrast to **pSQB-1** which forms either elongated structures ($CHCl_3$) or helical arrangements (acetone), **pDiPhSQB** does not undergo H-aggregate formation (Figure 34). This could be successfully suppressed by steric hindrance induced by the phenyl groups. Thus, the polymer exclusively behaves as a J-aggregate in all considered solvents.

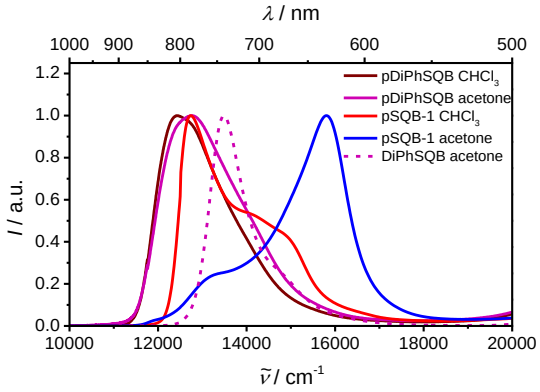

Figure 34: Normalised absorption spectra of **pDiPhSQB** and **pSQB-1** in $CHCl_3$ and acetone, respectively, and **DiPhSQB** in acetone for comparison.

3.4.3.4 Fluorescence Spectroscopy

The fluorescence spectra and lifetimes of **DiPhSQB** and **pDiPhSQB** were measured in $CHCl_3$ and toluene, respectively. The optical data are summarised in Table 6.

In both solvents, the monomer shows a typical squaraine-type fluorescence which is the mirror image to the main absorption band (Figure 35(a) and (b)). The Stokes shift in $CHCl_3$ is 400 cm^{-1} and thus twice as large as in toluene. Considerably low fluorescence quantum yields and short fluorescence lifetimes with high amplitudes for the sub-ns components are observed for the monomer, suggesting rapid and efficient non-radiative deactivation pathways. E.g., in toluene, the monomer exhibits a quantum yield of 0.04 together with a biexponential decay with lifetimes of 210 ps (0.90) and 2.94 ns (0.10), yielding an average fluorescence lifetime of about 1.87 ns. In $CHCl_3$, a quantum yield of 0.02 and lifetimes of 200 ps (0.97) and 1.81 ns

(0.03) with an average fluorescence lifetime of 550 ps were obtained. Thus, in non-polar solvent toluene, the fluorescence properties turned out to be superior to those in $CHCl_3$.

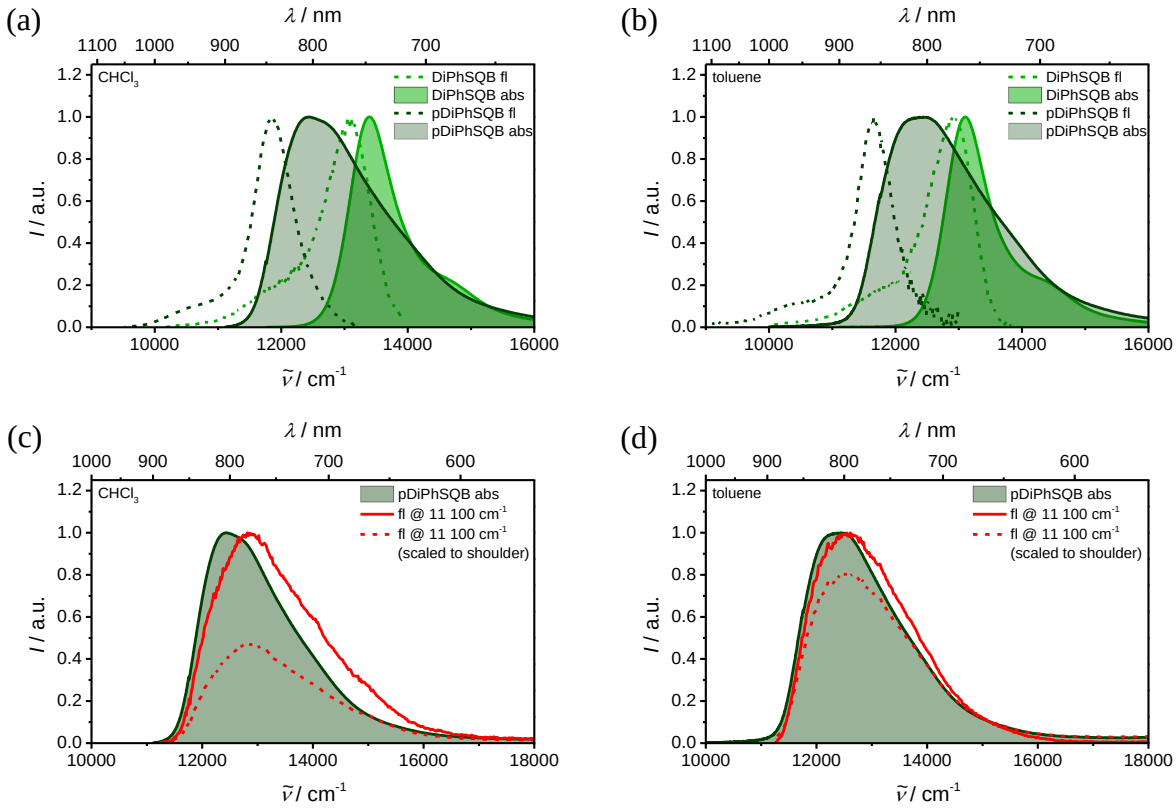

Figure 35: Normalised absorption and fluorescence emission spectra of **DiPhSQB** and **pDiPhSQB** in (a) $CHCl_3$ and (b) toluene, respectively. Normalised absorption and fluorescence excitation spectra of **pDiPhSQB** in $CHCl_3$ and toluene, respectively.

The fluorescence spectra of the polymer roughly resembles the shape of the monomer fluorescence and seems to exclusively stem from the lowest exciton state, providing a Stokes shift of ca. 600 cm^{-1} (700 cm^{-1}) in $CHCl_3$ (toluene) and is thus more pronounced than for the monomer (200-400 cm^{-1}). However, this is in contradiction with the findings of other J-aggregates, where a smaller Stokes shift is observed due to the delocalisation of the exciton compared to the corresponding monomers. The half width at half maximum (HWHM) of the monomer fluorescence is smaller than that of the polymer. In this context, the effective exciton delocalisation length N_{eff} can be estimated according to equation (51):[163]

$$\sqrt{N_{\mathrm{eff}}} = \frac{\Delta\tilde{\nu}_{\mathrm{HWHM}}(\mathrm{M})}{\Delta\tilde{\nu}_{\mathrm{HWHM}}(\mathrm{P})} \qquad (51)$$

The values for $\Delta\tilde{\nu}_{HWHM}(M)$ of the monomer and $\Delta\tilde{\nu}_{HWHM}(P)$ of the polymer were extracted from the corresponding fluorescence spectra, that are, 437 cm^{-1} and 713 cm^{-1} in $CHCl_3$, along with 430 cm^{-1} and 316 cm^{-1} in toluene. In $CHCl_3$, a delocalisation length of ~ 1.50 was estimated, while in toluene a somewhat larger value of ~ 1.85 was obtained. This means that the exciton is presumably delocalised in average over less than two monomer units within the

polymer. Admittedly, these values reflect rather rough estimations, yet the data clearly speak against a long delocalisation length of the exciton. Furthermore, the polymer exhibits very low fluorescence quantum yields, which are 0.02 in $CHCl_3$ and 0.04 in toluene, and are thus exactly same as for the monomer. In addition, biexponential decays are observed in $CHCl_3$ and toluene, with the most dominant amplitude for the shorter lifetime, respectively. Much in contrast to the monomer, the longer lifetimes are also in the sub-ns region. As a consequence, the average fluorescence lifetimes of 150 ps in $CHCl_3$ and 380 ps in toluene drastically deviate from the averaged lifetimes calculated for the monomer. Furthermore, fluorescence excitation spectra were recorded in $CHCl_3$ and toluene. The spectra are presented in Figure 35(c) and (d). For the sake of clarity, the spectra were also normalised to the shoulder of the absorption spectra. Remarkably, by recording the fluorescence at 11 100 cm^{-1}, the excitation spectra do not exactly match the absorption of the polymer in both solvents. From the spectra, it can be seen that this discrepancy is more pronounced in $CHCl_3$ than in toluene. This finding is highly likely caused by self-absorption effects due to a strong overlap of absorption and emission (Figure 35(a) and (b)). Besides, the spectra clearly show that the fluorescence in $CHCl_3$ and toluene exclusively stems from the lowest excitonic state and which is thus in agreement with Kasha´s rule.

Table 6: Absorption maxima, extinction coefficients, transition moments, fluorescence maxima, fluorescence quantum yields, and fluorescence lifetimes of squaraine dyes in $CHCl_3$ and toluene. Extinction coefficients ε and transition moments μ_{eg} of the polymer are indicated per monomer unit.

	solvent	$\tilde{\nu}_{abs}$ / cm^{-1} (nm)	ε_{max} / $M^{-1}cm^{-1}$	μ_{eg}^2 / D^2	$\tilde{\nu}_{em}$ / cm^{-1} (nm)	Φ_{fl} / –	τ_{fl}[c] / ns
DiPhSQB	$CHCl_3$	13 400 (746)	1.37×10^5	85.9	13 000 (766)	0.02	0.20 (0.97) 1.81 (0.03)
	DCM	13 400 (746)	1.35×10^5	87.7	–	–	–
	toluene	13 100 (763)	1.37×10^5	81.6	12 900 (755)	0.04	0.21 (0.90) 2.94 (0.10)
	*o*DCB	13 200 (758)	1.35×10^5	79.2	–	–	–
	PhCN	13 400 (746)	1.29×10^5	79.7	–	–	–
	DMF	13 500 (741)	1.35×10^5	81.8	–	–	–
	acetone	13 500 (741)	1.25×10^5	88.9	–	–	–
SQB	$CHCl_3$	14 600 (685)	1.96×10^5	98.6	14 200 (704)	0.55	2.40
	toluene	14 300 (699)	2.02×10^5	92.7	14 000 (714)	0.75	3.45
pDiPhSQB X_n = 37.7	$CHCl_3$	12 400 (806)	7.66×10^4	89.3	11 800 (847)	0.02 –	0.12 (0.94) 0.33 (0.06)
	DCM	12 500 (800)	6.82×10^4	84.0	–	–	–
	toluene	12 400 (806)	–	–	11 700 (855)	0.04	0.28 (0.88) 0.68 (0.12)
	*o*DCB	12 600 (794)	6.34×10^4	75.6	–	–	–
	PhCN	12 700 (787)	6.74×10^4	80.2	–	–	–
	DMF	12 800 (781)	6.56×10^4	75.6	–	–	–
	acetone	–	–	–	–	–	–
pSQB-1 X_n = 21.6	$CHCl_3$	12 700 (785)	1.08×10^5	112	12 500 (800)	0.21	0.05 (0.44) 0.47 (0.17) 0.96 (0.39)
	DCM	12 700 (785)	9.28×10^4	112	–	–	–
	toluene	12 700/14 700 (765/678)	$5.18/5.31\times10^4$	88.9	12 300 (810)	0.06[a] 0.17[b]	1.39 (0.28)[d] 3.18 (0.72)[d] 1.18 (0.38)[e] 2.44 (0.62)[e]
	PhCN	13 000/15 500 (767/647)	$3.44/7.32\times10^4$	90.3	–	–	–
	DMF	15 700 (636)	7.37×10^4	90.3	–	–	–
	acetone	15 800 (633)	8.35×10^4	92.2	–	–	–

– not determined. Excitation at [a]15150 cm^{-1}, [b]13510 cm^{-1}. [c](Multi-)exponential fit of fluorescence decay measured by TSCPC, excitation was at 15 240 cm^{-1} (656 nm) for the monomers and **pSQB-1**, and at 12 770 cm^{-1} (783 nm) for **pDiPhSQB**. Amplitudes are given in brackets. Fluorescence detected at [d]11 820 cm^{-1} (846 nm) or [e]12 330 cm^{-1} (811 nm).

3.4.3.5 Conclusion

A new synthetic protocol was developed in order to prepare diarylindolenine squaraine dyes, which are considered to be the first of its kind.

By replacing the standard branched alkyl chain by a short and linear one, it was possible to grow crystals of **DiPhSQB-2-Br$_2$** for single crystal X-ray analysis. It turned out that the solid state structure significantly deviates from common *cisoid* squaraine dyes. The squaraine displayed a highly bent structure with the donor moieties twisted of almost 150° in respect to the central squaric acid core plane. This unique structure is a result of steric congestion evoked by the bulky phenyl groups.

The absorption spectra of **DiPhSQB** featured the common squaraine characteristics, yet with a considerable broader and less intense main absorption band which is significantly shifted to lower energies of about 1 200 cm^{-1} (toluene) in comparison to parent **SQB**. The fluorescence spectra provided mirror image relation to the absorption. Extremely low quantum yields and very short-lived fluorescence decays were observed which may originate from the distorted π-system geometry giving rise to fast non-radiative relaxation processes.

The corresponding polymer **pDiPhSQB** was synthesised in a straightforward manner applying Yamamoto coupling methodology. Analytical GPC revealed a number average degree of polymerisation X_n of ~ 38 along with a $Đ$ of 2.35. Despite this high degree of polymerisation, the polymer showed high solubility in common organic solvents.

The absorption spectra of the polymer are shifted to lower energies of about 700-1 000 cm^{-1} in respect to the monomers in the considered solvents, which is caused by the exciton splitting of the first excited state. This shift is considered rather small and indicates a small delocalisation length of the exciton. Besides, the spectra of the polymer showed no dependence of the solvent a priori with no appreciable contribution from the upper edge of the exciton band. However, a closer inspection of this band revealed a double peak structure, whose shape was in fact dependent of the solvent. These findings suggested slightly different conformer structures, which were caused by the biarylaxes between adjacent monomers. In summary, it is assumed that the polymer behaves as J-aggregate with collinear arrangement of the monomer units. To conclude this chapter, the goal of intrinsic control of the optical polymer properties could thus be achieved, which manifested itself in the exclusive formation of J-type aggregates and the absence of H-type aggregates due to steric repulsion.

3.4.4 Benzodipyrrolenine Squaraine Polymers[X]

3.4.4.1 Introduction

According to the previous chapter, the synthetic approach of provoking solely zig-zag architectures by steric repulsion via bulky substituents proved to be very effective. Another synthetic approach represents a partial rigidification of the polymer backbone. Here, thought has been given to stiffen every second biarlyaxis by fusing two adjacent indolenine moieties to a single benzodipyrrolenine core unit.

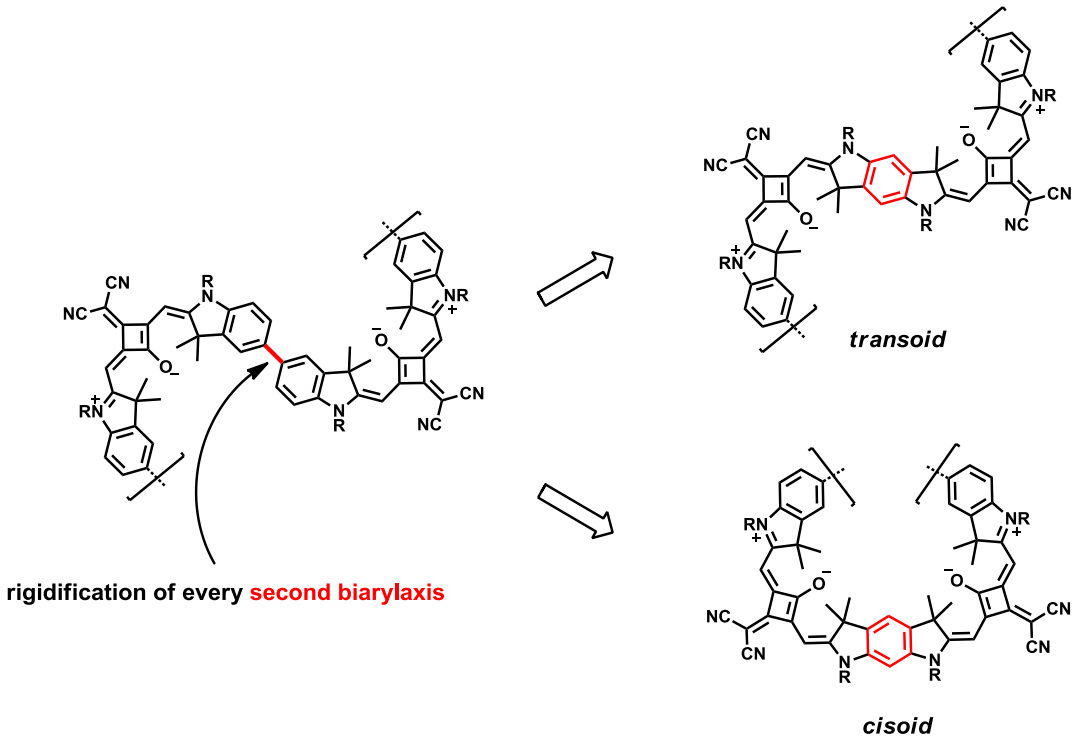

Scheme 17: Synthetic approach towards stiffening of the polymer backbone.

In principle, the flexible biaryaxis can be fused in two ways which ultimately yields two different regioisomeric benzodipyrrolenine analogues in either a *cisoid* or *transoid* configuration (Scheme 17). These two configurations could possibly give rise to different superstructures due to the strong structure-directing influence of the respective central core unit. It is assumed that the *cisoid* configuration will induce rather helical motifs, while the *transoid* configuration will most likely provoke zig-zag architectures. The synthesis of such *N*-heterocyclic compounds was first reported by the group of Boguslavskaya.[164] Terpetschnig and Patsenker extended this work and generated a plethora of benzodipyrrolenine-based bis-

[X] Parts of this chapter have been investigated in a bachelor thesis under the supervision of M. H. Schreck: L. Wittmann, Bachelor Thesis, Julius-Maximilians Universität (Würzburg), **2015**.

cyanine and bis-styryl dyes.[165,166] Now, these protocols were followed in order to prepare analogous bis-squaraine dyes.

3.4.4.2 Synthesis

The benzodipyrrolenine squaraine dyes **pySQB-1** and **pySQB-1-Br$_2$** were prepared in four stages via a convergent synthesis route according to Scheme 18.[167] Commercially available benzene-1,4-diamine reacted with 2 equivalents of 3-bromo-3-methylbutan-2-one in a nucleophilic substitution to provide compound **33** in 31 % yields. It is known that 3-anilo-3-methyl-2-butanone hydrochloride undergoes cyclisation to 2,3,3-trimethylindolenine upon heating.[168] Therefore, the bis-hydrochloride of **33** was generated and afterwards heated to 210 °C to give crude heterocycle **34** under release of water in 38 % yields. The compound turned out to be laborious to purify and was therefore used without further purification. Subsequent treatment with excess MeI gave the diquaternary salt **35** in 92 % yields. Finally, the benzodipyrrolenine squaraine dyes were obtained in a double condensation reaction using either dicyanovinylene-substituted semisquaraine salt **23** or **24** in boiling Ac_2O. The *transoid* configuration of the dyes was confirmed by ^{1}H-NMR which gave a singlet for the aromatic protons of the central benzene ring.

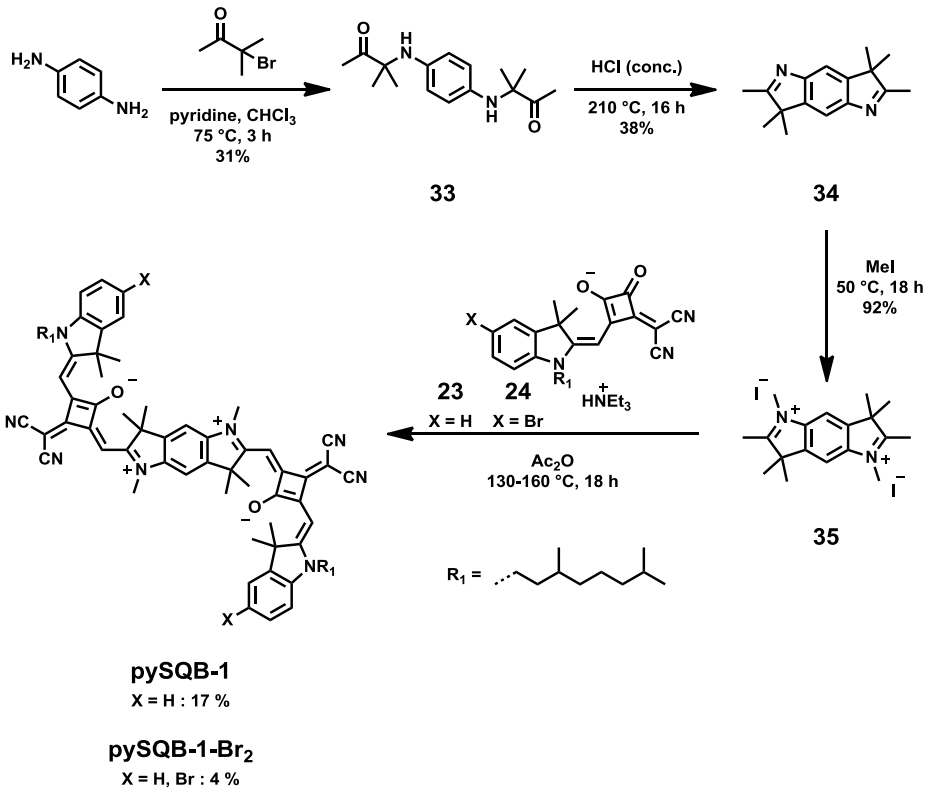

Scheme 18: Synthesis of benzodipyrrolenine squaraine dyes **pySQB-1** and **pySQB-1-Br$_2$**.

While **pySQB-1** was obtained in yields of 17 % and in a straight forward manner, the synthesis of bromine-functionalised **pySQB-1-Br$_2$** was carried out in 28 % yields, however, it was encountered by undesired debromination reaction. According to mass spectrometry analysis, 63 % of the product proved to be debrominated. In this context, the empirical correlation was found that higher reaction temperatures and longer reaction times promote the formation of the undesired byproduct. Yet, elevated temperatures were essential for this reaction. A compromise had to be made, involving lower temperatures around 130 °C instead of 160 °C. Thus, the desired compound was synthesised in low yields of 4 % but with less amount of byproduct (33 % debromination). Purification attempts applying crystallisation and preparative GPC were without success. However, 33 % byproduct is still considerably high and in view of subsequent polymerisation reaction, the substantial amount of debrominated species will ultimately lead to termination of chain elongation and thus to low molecular weight polymers. Nonetheless, the batch was used without further purification for a first attempt for the polymerisation reaction. As will be shown later, longer polymer chains would not have been expedient due to solubility issues. Consequently, no further effort has been made towards purification or to overcome the problem of debromination.

Ni-mediated Yamamoto homocoupling of crude **pySQB-1-Br$_2$** (33 % debrominated) gave the corresponding polymer in rather low yield of 18 % (Scheme 19).

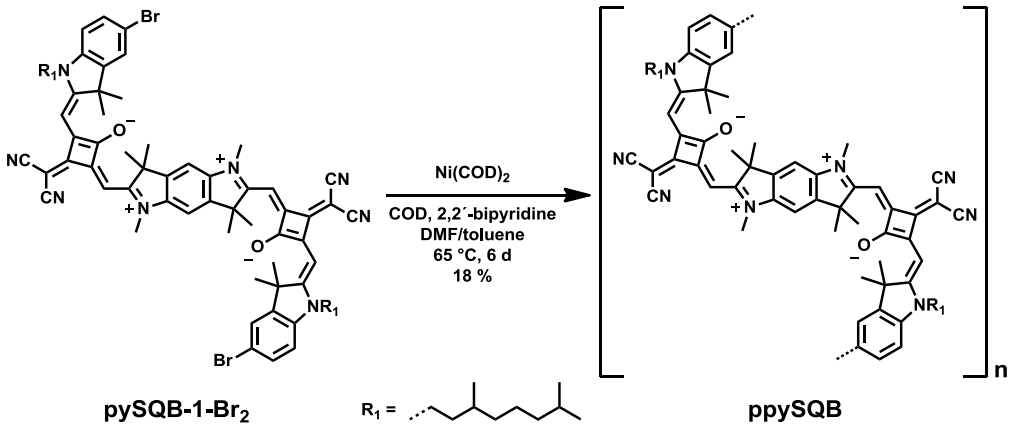

Scheme 19: Synthesis of *transoid* squaraine polymer **ppySQB**.

The solid that remained after Soxhlet extractions (*n*-hexane, MeOH, acetone) was used for GPC analysis. Accordingly, **ppySQB** possesses a number average molecular weight M_n of ~ 8 270 and a weight average molecular weight M_w of ~ 14 700 with a number average degree of polymerisation X_n of ~ 7.40 and a $Đ$ of 1.78. As anticipated, the analytical GPC data revealed a rather low degree of polymerisation which is certainly due to significant amount of debromination of the precursor. Consequently, end-group effects are clearly visible in the

^{1}H-NMR spectrum. However, the polymer proved to be poorly soluble in acetone and toluene. As a matter of fact, longer polymer chains would have decreased the solubility even further and thus hampered the characterisation by absorption spectroscopy. On account of these findings, no further attempts were made to completely suppress the debromination of precursor compound **pySQB-1-Br$_2$** (Scheme 18).

The synthesis of regioisomeric squaraine dye **pySQB-2** starts with the preparation of the hydrochloride salt of *m*-phenylenedihydrazine via azotization of *m*-phenylenediamine, followed by reduction of the resulting bis-diazonium salt yielding the corresponding *m*-phenylenedihydrazine hydrochloride according to literature procedures (Scheme 20).[169] The benzodipyrrolenine derivative **36** was prepared via Fischer indole reaction in 40 % yields (over 2 steps), using methyl isopropyl ketone in boiling HOAc in analogy to 2,3,3-trimethylindolenine **17**. Subsequent treatment with excess MeI gave the diquaternary salt **37** in 75 % yields. Squaraine dye **pySQB-2** was obtained in low yields of 6 % after condensation reaction of semisquaraine salt **9** and benzodipyrrolenine salt **37** in Ac_2O. Here, the reaction progress was carefully monitored by TLC and revealed no consummation of the starting materials. Apparently, compound **37** suffers from low reactivity in order to attack the carbonyl function of the semisquaraine. This might possibly explain the poor yields. Since the yields could not be increased by applying higher reaction temperatures (160 °C), the synthesis of the corresponding dibrominated analogue was not attempted. The *cisoid* configuration of **pySQB-2** was confirmed by ^{1}H-NMR which gave two singlets for the aromatic protons of the central benzene ring.

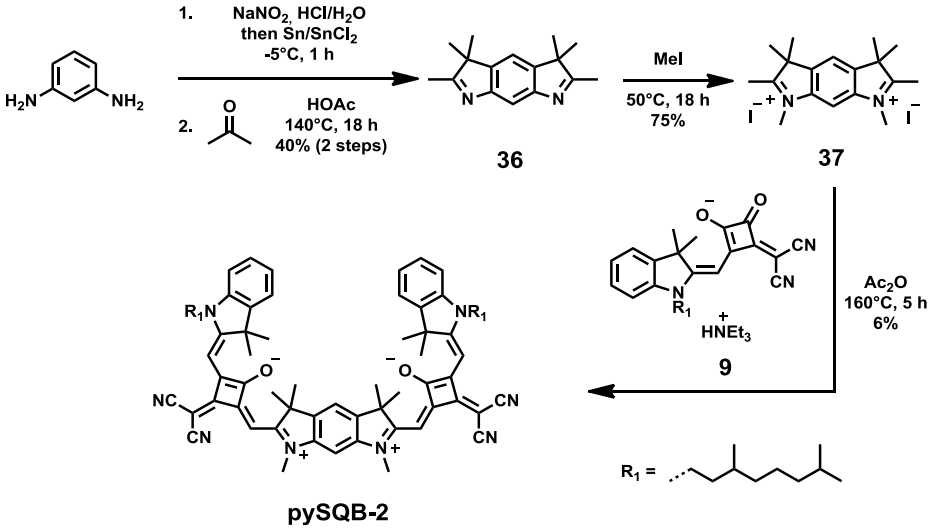

Scheme 20: Synthesis of *cisoid* benzodipyrrolenine squaraine dye **pySQB-2**.

3.4.4.3 Absorption Spectroscopy

The absorption behaviour of squaraine dye **pySQB-1** was examined in various solvents. The spectra are depicted in Figure 36 and the corresponding optical data are presented in Table 7.
In all solvents, squaraine dye **pySQB-1** exhibits a sharp and intense main absorption band in the red spectral region (12 100-12 400 cm^{-1}) with a subsidiary vibronic shoulder at higher energies around 13 500 cm^{-1}. Interestingly, the squaraine also displays a second, less intense maximum at even higher energies around 15 600 cm^{-1} accompanied by a vibronic progression at ca. 17 000 cm^{-1}. The extinction coefficient ranges from 3.33×10^5 $M^{-1}cm^{-1}$ in DMF to 4.92×10^5 $M^{-1}cm^{-1}$ in toluene and the calculated squared transition moments in all considered solvents show comparable values (216-272 D^2) within experimental error.
While the most intense low-energy absorption band can be ascribed to the $S_0\rightarrow S_1$ transition, the second maximum at higher energies belongs to the $S_0\rightarrow S_2$ transition. According to the Laporte selection rules for centrosymmetric dyes,[170] electronic transitions that conserve parity are dipole-forbidden. Consequently, the latter transition at higher energies clearly represents a violation of this rule. However, theoretically forbidden transitions can become allowed if the centre of symmetry is broken. The presence of asymmetric vibrations or vibronic transitions, which are caused by vibronic coupling, can possibly account for the weak allowed electronic transition.

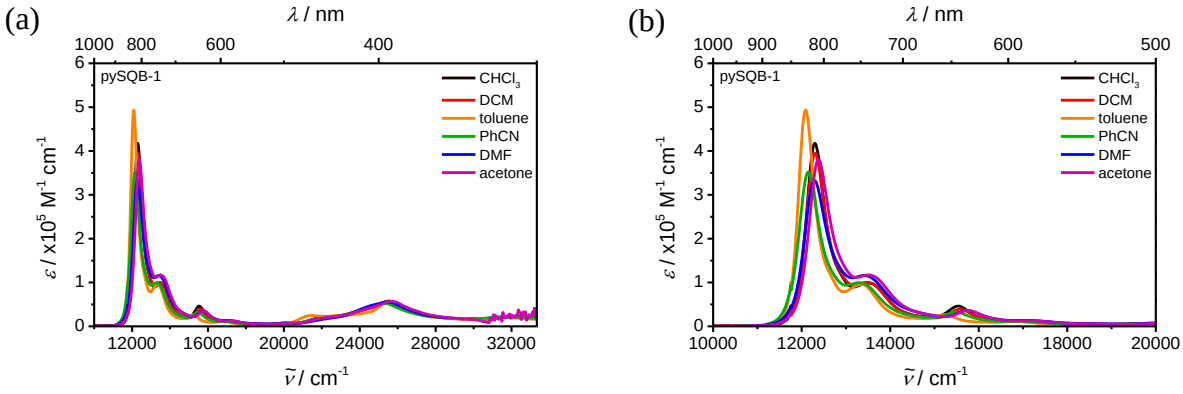

Figure 36: Absorption spectra of **pySQB-1** in various solvents.

The absorption spectrum of the polymer **ppySQB** in $CHCl_3$ displays a broad and red-shifted main absorption band of about 700 cm^{-1} compared to **pySQB-1** (Figure 37(a)) which is most likely caused by exciton coupling. The polymer additionally features two maxima and a weak shoulder at higher energies at ~ 13 000 cm^{-1}, ~ 15 000 cm^{-1}, and ~ 17 000 cm^{-1}, respectively. A closer inspection of the main absorption band reveals an additional shoulder at higher energies at around 12 000 cm^{-1}.

Furthermore, absorption spectra were recorded in various solvents in order to study the influence of solvent on intramolecular aggregate formation. Due to poor solubility, no extinction coefficients could be determined for **ppySQB** in toluene and acetone. The spectra are presented in Figure 37(b)-(d). The highest extinction coefficients of the polymer are found in $CHCl_3$ and DCM, which are 1.74 and 1.60×10^5 M^{-1} cm^{-1}. The spectra have practically the same shape with an intense main absorption peak and a shoulder at somewhat higher energies. In contrast, the spectra in PhCN and DMF show a broadened main absorption band, caused by a superposition of the main peak and the shoulder around 12 000 cm^{-1}, which are of almost the same intensity (Figure 37(c)). Remarkably, the spectrum recorded in toluene differs from all the other spectra, providing an extremely sharp and small bandwidth of the main absorption band (Figure 37(d)). However, the overall shape of the absorption band manifold and energetic position of the bands do not differ greatly for this series of solvents, indicative of almost the same polymer conformers and thus intramolecular aggregates in solution. The squared transition moments of the polymer (188-219 D^2) are in the same range as for the monomer (213-250 D^2) within the experimental uncertainty.

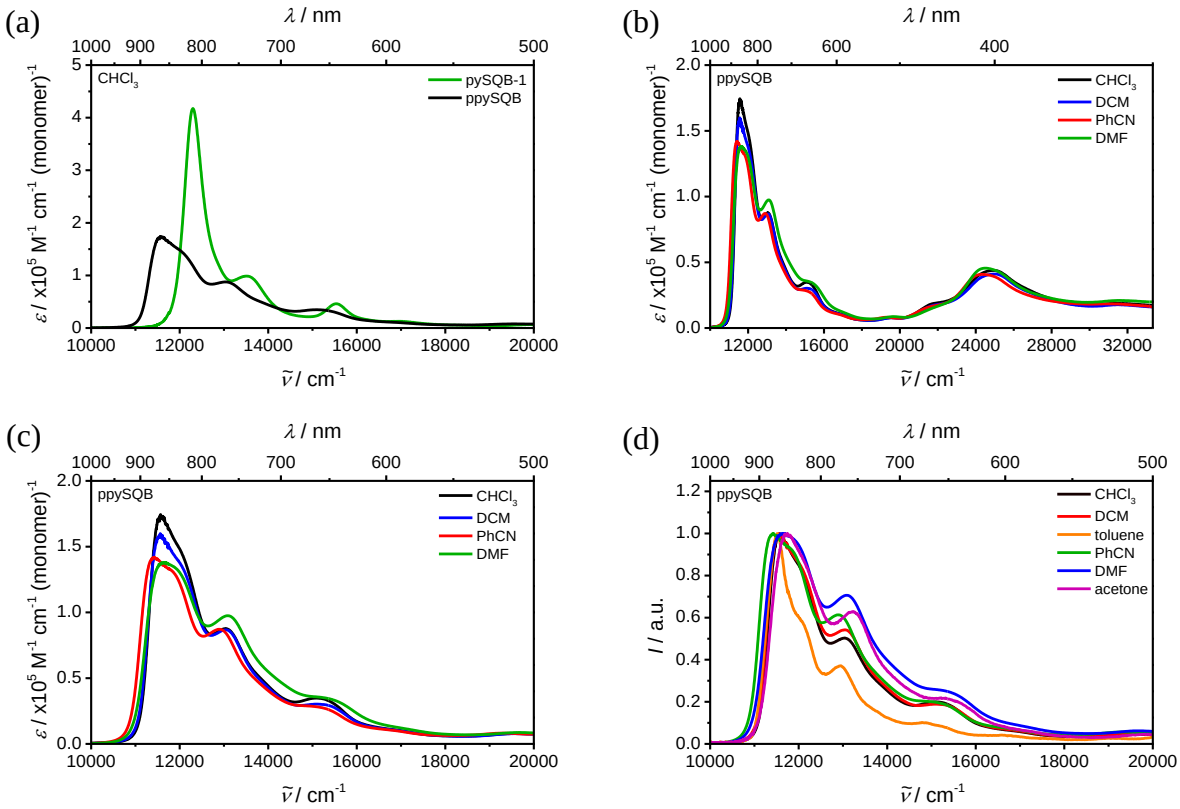

Figure 37: (a) Absorption spectrum of **pySQB-1** and **ppySQB** in $CHCl_3$. (b)(c) Complete and (d) normalised absorption spectra of **ppySQB** in various solvents.

In order to evaluate the nature of the aggregate band, the absorption spectra of **ppySQB** in $CHCl_3$ and acetone are first compared to the spectrum of the monomer unit **pySQB-1** in acetone (Figure 38). $CHCl_3$ and acetone were chosen due its antagonistic effect in terms of aggregate formation. Accordingly, the polymer spectra are both red-shifted with respect to **pySQB-1** and the absence of a blue-shifted band speaks against H-aggregate formation. Unlike the situation of parent squaraine polymer **pSQB-1** in $CHCl_3$ and acetone (Chapter 3.4.2.3), providing either J- or of H-aggregates due to different conformers in solution, the absorption spectra of **ppySQB** clearly indicate the formation of only one conformer structure, irrespective of the solvent. Obviously, the overall aggregate structure is controlled by the fused benzodipyrrolenine core unit which prevents the collapse to helical structures due to its rigid nature. Yet, owing to the low average degree of polymerisation of only ~ 7, the interpretation of the polymer spectra should be made with caution and solely in a qualitative manner.

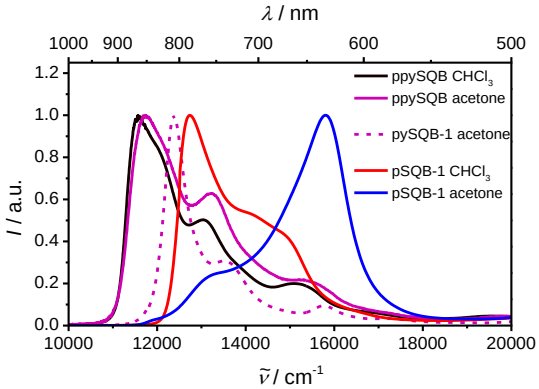

Figure 38: Normalised absorption spectra of **ppySQB** and **pSQB-1** in $CHCl_3$ and acetone. The absorption spectrum of **pySQB-1** in acetone is depicted for comparison.

The absorption behaviour of regioisomeric squaraine dye **pySQB-2** with C_{2v} symmetry was examined in the same solvents as **pySQB-1**. The spectra are depicted in Figure 39 and the corresponding optical data are presented in Table 7.

In all solvents, squaraine dye **pySQB-2** provides a sharp and intense main absorption band in the red spectral region (13 200-13 500 cm^{-1}) accompanied by a vibronic progression at higher energies around 14 500 cm^{-1}. Similarly to **pySQB-1**, a second less intense maximum at even higher energies around 15 600 cm^{-1} together with a subsidiary vibronic progression at ca. 16 500 cm^{-1} are observed. This weak band is attributed to the $S_0 \rightarrow S_2$ transition, which was also noticed for analogous cyanine dyes.[165] The extinction coefficients range from 3.09×10^5 $M^{-1}cm^{-1}$ in DMF to 4.92×10^5 $M^{-1}cm^{-1}$ in toluene and the calculated squared transition moments in all considered solvents reflect comparable values (174-236 D^2) within experimental error.

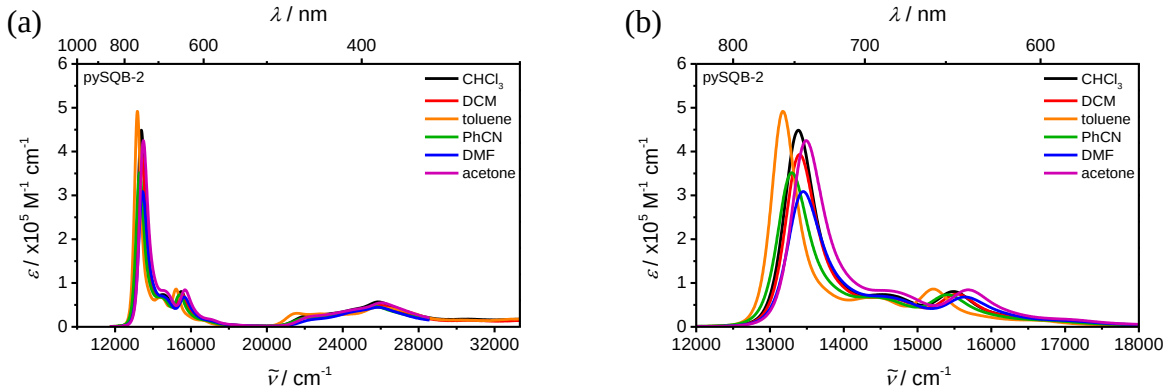

Figure 39: Absorption spectra of **pySQB-2** in various solvents.

Furthermore, the spectra of **pySQB-1** and **pySQB-2** dyes are compared to each other as well as to their parent squaraine monomer **SQB** and dimer **dSQB-1** in order to investigate the impact of the different benzodipyrrolenine core units (*transoid* versus *cisoid*) on the optical properties. The spectra are presented in Figure 40.

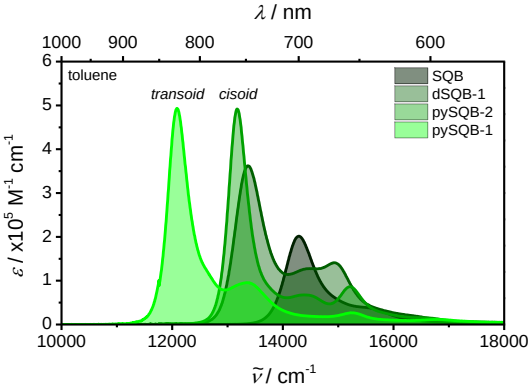

Figure 40: Absorption spectra of **SQB**, **dSQB-1**, **pySQB-2**, and **pySQB-1** in toluene.

In toluene, both benzopyrrolenine squaraine dyes display very intense main absorption bands with the same extinction coefficient of 4.92×10^5 $M^{-1}cm^{-1}$ yet with substantially different red-shifts of the main peak in respect to parent **SQB**. In this context, **pySQB-1** provides an extremely large red-shift of 2 200 cm^{-1} which is twice as large as that of **pySQB-2**. The great difference in red-shift originates from a disruption of conjugation due to the *meta*-substituted benzodipyrrolenine unit in **pySQB-2**. As a consequence, almost the same red-shift is obtained for **dSQB-1** in which conjugational effects do not play a role due to the flexible biarylaxis. In *transoid* **pySQB-1**, in contrast, the *para*-arrangement allows a complete conjugation over the rigid spacer unit, yielding an extension of the π-electron system. Thus, despite dipole-dipole interactions, the optical properties must be additionally considered to be influenced by conjugation. Moreover, both squaraine dyes **pySQB-1** and **pySQB-2** provide small bandwidths (FWHM) of ca. 460 cm^{-1} and 400 cm^{-1}, respectively, which can be explained by

the absence of conformers due to the rigid nature of the core unit. On the other hand, assuming considerable flexibility in **dSQB-1**, the spectrum displays a superposition of different conformers which causes a significantly larger bandwidth of 650 cm^{-1}. Besides, the squared transition moments of **pySQB-1** (216-272 D^2) are slightly larger than those of **pySQB-2** (174-236 D^2). Yet they do not differ greatly and show almost additivity to the monomer within the experimental error, respectively, which is in accordance to the Thomas-Reiche-Kuhn sum rule.[151]

Another interesting finding concerns the energetic position of the $S_0 \rightarrow S_2$ transitions for both benzodipyrrolenine dyes in toluene given in Figure 40. While a large energetic separation between both main absorption peaks ($S_0 \rightarrow S_1$) exists, the $S_0 \rightarrow S_2$ transitions occur at the same energy at 15 200 cm^{-1}. These transitions are energetically very close to the second exciton state S_1' of **dSQB-1** at ca. 15 000 cm^{-1}, which is a result of destructive, out-of-phase orientation of the monomeric transition moments.[88]

Furthermore, DFT calculations[XI] (B3LYP/6-31G*) reveal perfect planarity for both benzodipyrrolenine squaraine dyes in the gas phase with a different orientation of the transition moment (Figure 41).

(a)

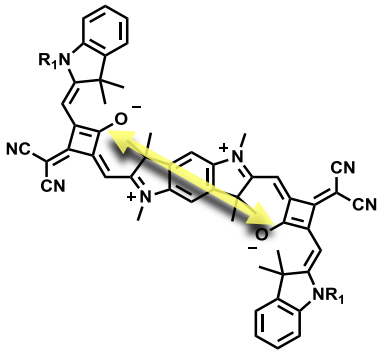

pySQB-1

(b)

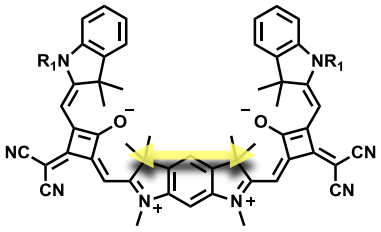

pySQB-2

Figure 41: Chemical structures of **pySQB-1** and **pySQB-2**. Transition moments were derived by DFT-calculations (B3LYP/6-31G*) and are given as yellow arrows.

[XI] DFT calculations were carried out by Dr. Marco Holzapfel.

3.4.4.4 Fluorescence Spectroscopy

Fluorescence emission and excitation spectra as well as fluorescence lifetimes of **pySQB-1**, **pySQB-2**, and **ppySQB** were recorded in $CHCl_3$ and toluene (Figure 42). However, no fluorescence lifetimes could be measured for **pySQB-2** and **ppySQB** in $CHCl_3$ due to the weak emission signal, respectively. The corresponding optical data is presented in Table 7.

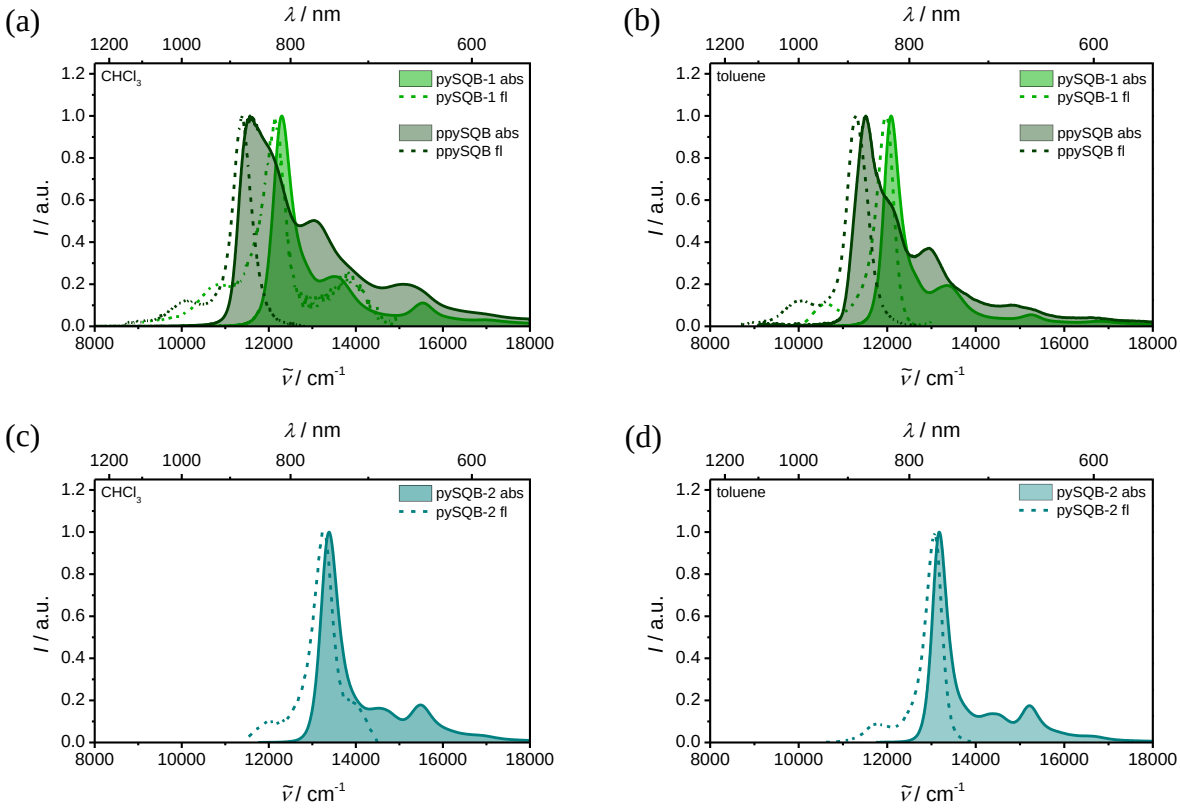

Figure 42: Absorption and fluorescence spectra of **pySQB-1** and **ppySQB** in (a) toluene and (b) $CHCl_3$, as well as of **pySQB-2** in (c) toluene and (d) $CHCl_3$, respectively.

In general, the fluorescence spectra of all three squaraine dyes in both solvents are red-shifted compared to the low energy edge of the respective absorptions (Figure 42). Applying the model of exciton coupling, it can be concluded that the fluorescence in toluene (Figure 42(b) and (d)) exclusively stems from the lower excitonic state, which is in accordance with J-aggregate behaviour. On the other hand, the fluorescence of **pySQB-1** and **pySQB-2** in polar $CHCl_3$ shows each an unusual, high-energy emission peak which originates from a higher state, which is very prominent in **pySQB-1**. The emergence of such residual fluorescence bands speaks against a quantitative internal conversion to the lowest excited state, from which the fluorescence mainly occurs. Besides, the absorption and fluorescence do not show mirror-image relationship, respectively, and thus no Strickler-Berg symmetry. The Stokes´ shifts are roughly twice as large in $CHCl_3$ (200 cm^{-1}) than in toluene (100 cm^{-1}). An increase of the solvent polarity from toluene to $CHCl_3$ considerably decreases the quantum yields.

Accordingly, the quantum yield of **pySQB-1** and **pySQB-2** in toluene are 0.26 and 0.80, while in $CHCl_3$ lower values of 0.06 and 0.07 were obtained, respectively. The extremely high quantum yield of 0.80 observed for *cisoid* **pySQB-2** even exceeds the quantum yield of 0.68 which was found for **dSQB-1**. The significant difference in quantum yield in toluene for both dipyrrolenine dyes can most likely attributed to an increased non-radiative transition caused by vibrationally induced internal conversion, which is known to considerably increase in the spectral window beyond 14 290 cm^{-1} (700 nm).[171]

The polymer displays very similar quantum yields of 0.04 in $CHCl_3$ and 0.16 in toluene as the corresponding monomer unit **pySQB-1** (0.06 and 0.26), respectively, which is due to the comparably small size difference of **pySQB-1** and **ppySQB** ($Đ$ ~7). Distinctively lower fluorescence quantum yields might be obtained with higher molecular weight polymers.

Monoexponential fluorescence decays were measured for **pySQB-1** and **pySQB-2** in contrast to **dSQB-1**, where the existence of conformers which is caused by the rotation around the central C-C bond, possibly causes biexponential decays. Following this assumption, a biexponential decay would have also been anticipated for **ppySQB**. Yet, this does not hold true. Apparently, the rigidity of the benzodipyrrolenine core within a single monomer unit also leads to an overall-stiffening of the polymer backbone which in turn causes very similar conformers. This is in agreement with previous absorption studies, where no significant solvent-dependence on the shape of the absorption band manifold was noticed. While the lifetimes in toluene for *transoid* **pySQB-1** and **ppySQB** were found to be in the sub-ns region, i.e., 860 ps and 690 ps, respectively, **pySQB-2** exhibits a comparatively long-lived fluorescence lifetime of 2.30 ns, which nicely correlates with the high quantum yield of 0.80.

The lifetimes were used to calculate the transition moment of the fluorescence μ_f by the Strickler-Berg equation (52) from the fluorescence quantum yield Φ_f:[172]

$$k_f = \frac{16 \times 10^6 \pi^3}{3h\varepsilon_0} \frac{n\,(n^2+2)^2}{9} \langle \tilde{\nu}_f^{-3} \rangle_{av}^{-1} \mu_f^2 \tag{52}$$

where $\langle \tilde{\nu}_f^{-3} \rangle_{av}^{-1} = \int I_f \, d\tilde{\nu} / \int \tilde{\nu}_f^{-3} I_f \, d\tilde{\nu}$ is the average cubic fluorescence energy and k_f is the radiative rate constant $k_f = \Phi_f / \tau_f$. The squares of the fluorescence transition moments of **pySQB-1** and **pySQB-2** are 204 D^2 and 177 D^2. The squares of absorption transition moments when only considering the respective S_1-state are 211 D^2 and 166 D^2, which reflect very similar values to those of the fluorescence within the limits of accuracy of the measurements. Furthermore, fluorescence excitation spectra of **pySQB-1** and **pySQB-2** were measured in toluene and are presented in Figure 43. As can be seen, the excitation spectra are

in agreement with the respective absorption spectra, corroborating the initial assumption that the fluorescence exclusively originates from the lowest excited state.

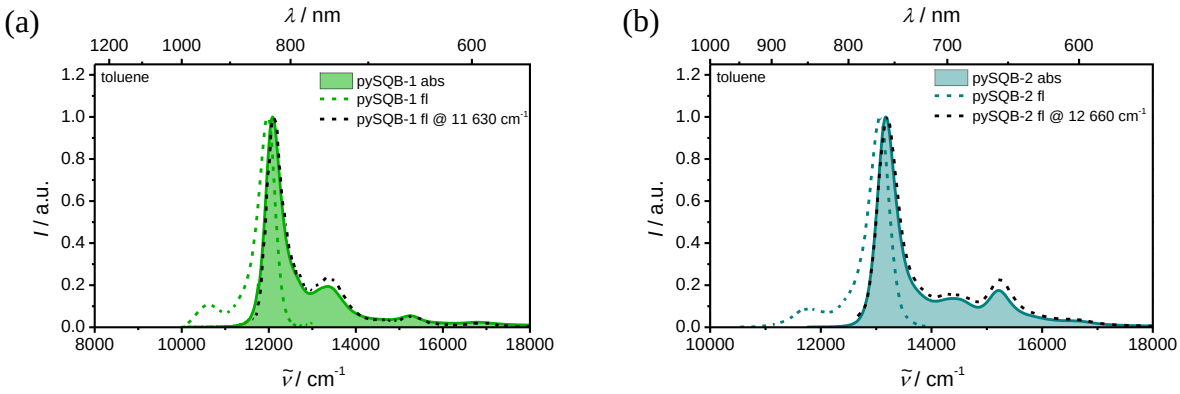

Figure 43: Absorption, fluorescence emission and excitation spectra of (a) **pySQB-1** and (b) **pySQB-2** in toluene, respectively. The excitation spectra were recorded by detecting the emission either at 11 630 cm^{-1} (**pySQB-1**) or 12 660 cm^{-1} (**pySQB-2**).

Table 7: Absorption maxima, extinction coefficients, transition moments, fluorescence maxima, fluorescence quantum yields, and fluorescence lifetimes of squaraine dyes in $CHCl_3$ and toluene. Extinction coefficients ε and transition moments μ_{eg} of the polymer are indicated per monomer unit.

	solvent	$\tilde{\nu}_{abs}$ / cm^{-1} (nm)	ε_{max} / $M^{-1}cm^{-1}$	μ_{eg}^2 [a] / D^2	$\tilde{\nu}_{em}$ / cm^{-1} (nm)	Φ_{fl} / –	τ_{fl} [b] / ns
	$CHCl_3$	12 300 (813)	4.18×10^5	243	12 100 (826)	0.06	0.25
	DCM	12 300 (813)	3.95×10^5	243	–	–	–
pySQB-1	toluene	12 100 (826)	4.92×10^5	231	12 000 (833)	0.26	0.86
	PhCN	12 200 (820)	3.52×10^5	216	–	–	–
	DMF	12 300 (813)	3.33×10^5	250	–	–	–
	acetone	12 400 (806)	3.80×10^5	272	–	–	–
	$CHCl_3$	13 400 (758)	4.49×10^5	214	13 200 (758)	0.07	–
	DCM	13 400 (758)	3.93×10^5	196	–		–
pySQB-2	toluene	13 200 (758)	4.92×10^5	195	13 100 (763)	0.80	2.30
	PhCN	13 300 (752)	3.52×10^5	174	–	–	–
	DMF	13 400 (746)	3.09×10^5	180	–	–	–
	acetone	13 500 (741)	4.25×10^5	236	–	–	–
SQB	$CHCl_3$	14 600 (685)	1.96×10^5	98.6	14 200 (704)	0.55	2.40
	toluene	14 300 (699)	2.02×10^5	92.7	14 000 (714)	0.75	3.45
dSQB-1	$CHCl_3$	13 600 (735)	3.38×10^5	236	13 300 (751)	0.20	0.31 (0.21) 1.00 (0.79)
	toluene	13 400 (748)	3.62×10^5	226	13 100 (761)	0.68	2.49 (0.83)[c] 4.08 (0.17)[c]
	$CHCl_3$	11 600 (862)	1.74×10^5	210	11 400 (877)	0.04	–
	DCM	11 600 (862)	1.60×10^5	204	–	–	–
ppySQB	toluene	11 500 (870)	–	–	11 300 (885)	0.16	0.69
X_n = 7.40	PhCN	11 400 (877)	1.42×10^5	188	–	–	–
	DMF	11 700 (855)	1.38×10^5	219	–	–	–
	acetone	11 700 (855)	–	–	–	–	–

– not determined. [a]was calculated by integrating the complete absorption in the low energy range. [b](Multi-)exponential fit of fluorescence decay measured by TSCPC, excitation at 15 240 cm^{-1} (656 nm) or 12 770 cm^{-1} (783 nm). Amplitudes are given in brackets. [c]Slightly different fluorescence lifetimes were previously reported in literature,[88] yet the values for the average fluorescence lifetime are very similar.

3.4.4.1 Conclusion

The successful synthesis of benzodipyrrolenine-based squaraine dyes **pySQB-1** and **pySQB-2** paved the way to long-wavelength absorbing and emitting bis-chromophores with high extinction coefficients $> 3.0\times10^5\ M^{-1}cm^{-1}$ and small bandwidths (FWHM) $\leq 460\ cm^{-1}$. In addition, a dramatic red-shift of ca. 2 000 cm^{-1} in respect to parent **SQB** was obtained for the *transoid* analogue, which proved to be almost twice as large as that of **pySQB-2** with *cisoid* configuration. The difference in shift was explained to be caused by a disruption of conjugation due to the *meta*-substituted benzodipyrrolenine core. Aside from the strong main absorption band at low energies, a second maximum at higher energies was observed for both dyes which was assigned to the $S_0\rightarrow S_2$ transition, respectively. The absorption and fluorescence spectra provided no Strickler-Berg symmetry and the stiff scaffold of both bis-chromophores presumably accounted for monoexponential fluorescence decays with lifetimes either in the sub-ns (**pySQB-1**) or ns (**pySQB-2**) region due to the lack of different conformers.

In the light of the low degree of polymerisation, the interpretation of the spectra of **ppySQB** should be made with caution. However, the spectral features, such as red-shifting of the absorption and absence of a hypsochromic aggregate band in polar (poor) solvents (DMF, acetone) as was seen for **pSQB-1**, suggested exclusive J-aggregate formation. Hence, the partial rigidification of the polymer backbone via a stiff benzodipyrrolenine core yields a similar effect on the intramolecular aggregate formation as the use of bulky substituents.

3.4.5 Quinoline-based Squaraine Polymers

3.4.5.1 Introduction

As became apparent in the last chapters, the control of the optical properties of squaraine polymers is directly associated with the control of the superstructure formation. The selective design of exclusively one superstructure was hitherto focused on elongated zig-zag structures which lead to predominant J-aggregate behaviour. In contrast, the design of squaraine polymers with a tendency toward H-aggregates involves opposing synthetic concepts. While steric repulsion between the bulky squaraine units was found to be favourable for elongated structures (Chapter 3.4.3), it is now suggested that attractive forces within the polymer strands might enable conformers with helical domains, in which the monomers are aligned in a parallel, face-to-face orientation. It is assumed, that the latter arrangement may be realised by strong π-π interactions between the squaraine units. In this regard, quinoline-derived squaraine dyes proved to show a pronounced propensity to form supramolecular π-stacks in non-polar solvent toluene, which can be ascribed to its perfectly planar geometry and the absence of bulky substituents.[173] Taking advantage of this property, polymers consisting of quinoline-derived squaraine dyes could possibly give rise to helical arrangements which would ultimately pave the way to H-aggregates.

3.4.5.2 Synthesis

The synthesis of unfunctionalised quinoline-substituted squaraine **SQC** has already been described in Chapter 3.1.2. and is therefore not part of the discussion. The corresponding dibrominated analogue was prepared in a similar fashion in two steps according to Scheme 21. Aside from flash chromatography, squaraine **SQC-Br**$_2$ was additionally be purified by precipitation from *n*-hexane. Very much in contrast to all other squaraine dyes, where the crystallisation process requires time and low temperatures, both quinoline-based dyes readily solidified upon dripping a concentrated solution of dye in DCM into *n*-hexane. Apparently, the large and planar π-surface of **SQC**-analogues significantly facilitates the crystallisation process. Squaraine **SQC-Br$_2$** was thus obtained in 63 % yield.

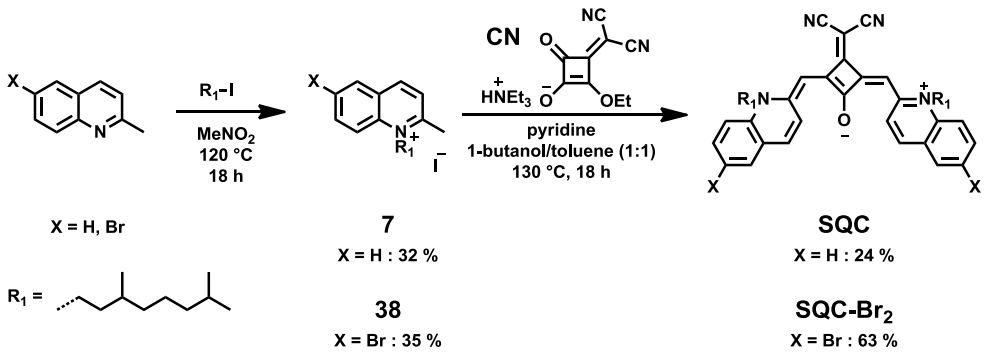

Scheme 21: Synthesis of quinoline-based squaraine monomers **SQC** and **SQC-Br$_2$**.

The subsequent polycondensation reaction was carried out according to the standard protocol (Scheme 22). After 8 d at 65 °C in a solvent mixture of toluene and DMF (1:1), a dark green solid was obtained, which was practically insoluble in all standard organic solvents and could not been analysed by GPC. It was assumed that the average degree of polymerisation and thus the average molecular weight of the polymers were too high leading to a dramatic deterioration of the solubility. The problem of solubility was encountered by a modified synthetic protocol, involving the use of only one solvent (DMF) and shorter reaction times (18 h) at room temperature, in order to provoke precipitation of the polymers at an earlier stage of the reaction to yield possibly shorter and thus better soluble polymers. The solubility could be somewhat increased yet proved to be restricted to chlorinated solvents. GPC analysis revealed a low average degree of only 7.80. On account of these major drawbacks, this project was considered to be not expedient and was therefore not pursued further.

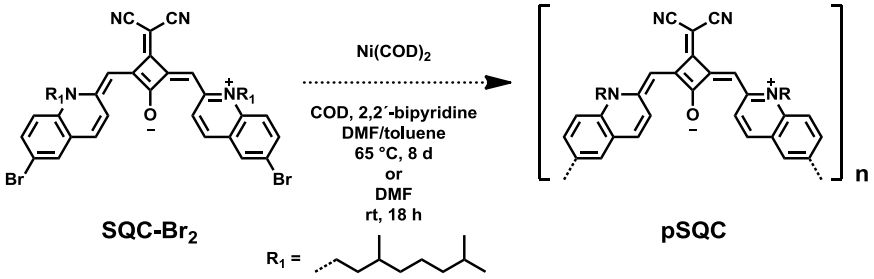

Scheme 22: Attempted syntheses of quinoline-based squaraine homopolymer **pSQC**.

Yet, as the standard indolenine-substituted squaraine polymer **pSQB-1** proved to be highly soluble in various solvents (Chapter 3.4.2), a copolymer comprising both indolenine and quinoline units might lead to a superior solubility compared to previously attempted **pSQC**. The copolymer was synthesised via Pd-catalysed Suzuki coupling reaction by using the diboronic ester squaraine analogue **SQB-B$_2$** and the dibrominated squaraine derivative **SQC-Br$_2$** according to Scheme 23.[72]

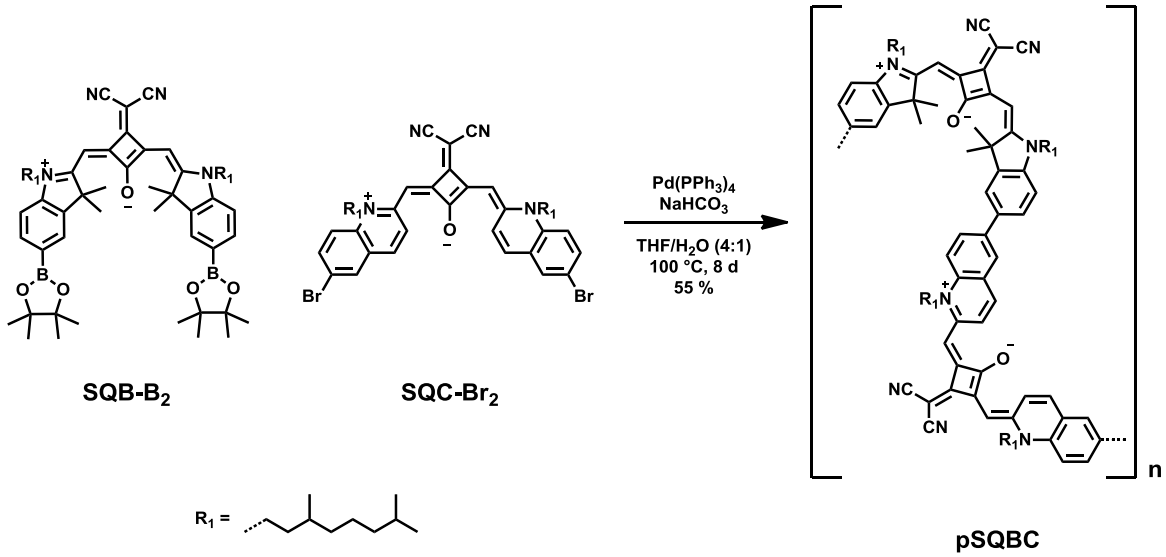

Scheme 23: Synthesis of indolenine-quinoline squaraine-squaraine copolymer **pSQBC**.

The reaction was carried out under aqueous conditions (THF/H_2O = 4:1) with $NaHCO_3$ as base and $Pd(PPh_3)_4$ at 110 °C for 8 d to give the copolymer **pSQBC** in 55 % yields (M_n ~ 30 500, M_w ~ 159 000, X_n ~ 21.8). Indeed, due to the incorporation of the indolenine moiety, the copolymer proved to be completely soluble now in $CHCl_3$, DCM, toluene, and PhCN.

Despite the copolymer, the corresponding monomer unit masked as a dimer is also of fundamental importance in order to get a whole picture of the excitonic coupling effects involved in these dyes. Hence, mono-functionalised species were required bearing either a boronic ester function or a bromine function. The general procedure of such dyes was already outlined in Chapter 3.3.1 for indolenine squaraine dyes. The synthesis of the quinoline-substituted squaraine dye **SQC-Br** proceeds similarly and is therefore not discussed explicitly (Scheme 24). The desired compound was obtained in poor yields of 6 %, most likely due to the low reactivity of compound **7**.

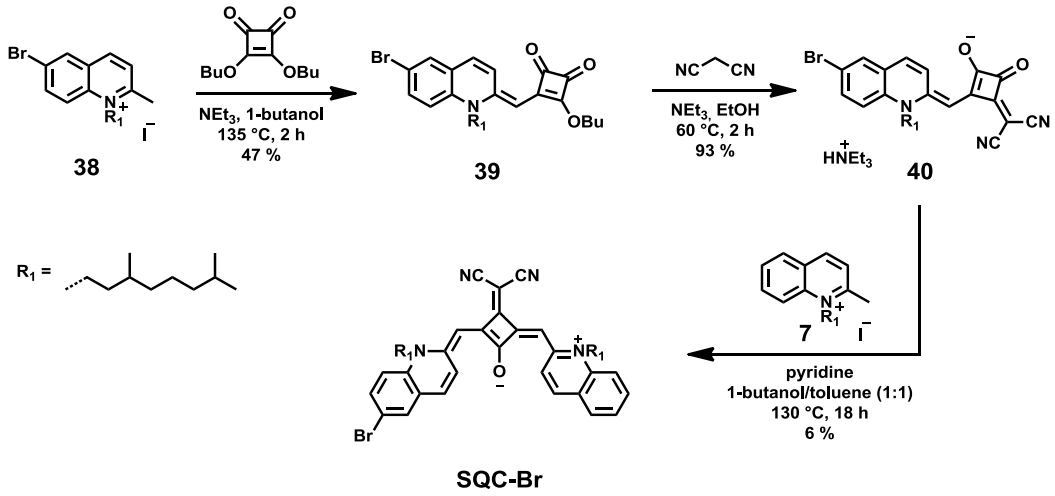

Scheme 24: Synthesis of unsymmetrical squaraine dye **SQC-Br**.

Finally, Suzuki coupling reaction of **SQB-B** and **SQC-Br** gave the corresponding dimer **dSQBC** in 52 % yields according to Scheme 25. The reaction was performed under aqueous conditions using $Pd(PPh_3)_4$ as Pd(0) source and Na_2CO_3 as base in THF. After flash column chromatography, the **dSQBC** was purified via preparative GPC followed by precipitation from *n*-hexane.

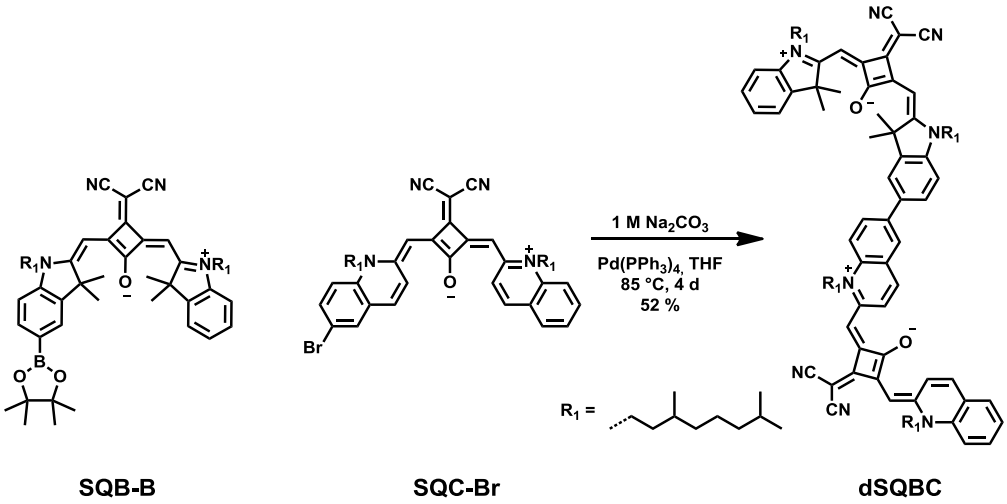

Scheme 25: Synthesis of squaraine dimer **dSQBC**.

3.4.5.3 Absorption Spectroscopy

Absorption spectra of **SQB**, **SQC**, **dSQBC**, as well as of **pSQBC** were measured in toluene and are depicted in Figure 44. The respective optical data are presented in Table 8. The optical properties of the monomers have already been discussed in Chapter 3.1.3 and 3.1.4. Hence, the focus will be directed at the dimer and subsequently at the polymer.

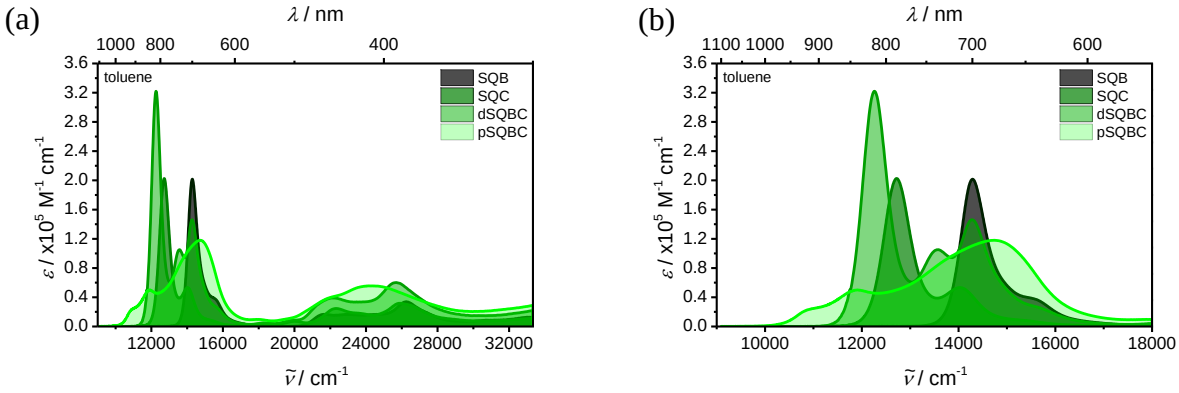

Figure 44: Absorption spectra of **SQB**, **SQC**, **dSQBC**, and **pSQBC** in toluene.

The heterodimer **dSQBC** exhibits a main absorption band at 12 250 cm^{-1} (3.22 ×10^5 $M^{-1}cm^{-1}$) which is red-shifted of ca. 400 cm^{-1} compared to **SQC**. Besides, two additional maxima yet of lower intensity are located at higher energies at 13 590 cm^{-1} (1.05×10^5 $M^{-1}cm^{-1}$) and

14 290 cm^{-1}(1.46×10^5 $M^{-1}cm^{-1}$). Exciton coupling of the two unequal monomers leads to the formation of two excitonic absorption bands which mostly correspond to the individual monomers, i.e., a S_1-state at 12 250 cm^{-1} that is mostly localised on the **SQC** unit and the S_1´-state at 14 290 cm^{-1} that is localised on the **SQB** unit, bearing less than half the intensity than the S_1-state. In this context, the S_1-state is slightly shifted to lower energies, while the S_1´-state turns out to be at the same energy as the maximum of **SQB** without any energetic shift upon exciton coupling. The coupling energy *J* between both monomers in the dimer can be approximated to 645 cm^{-1} from the dimer absorption (= 2 040 cm^{-1}) and the difference between the monomer absorption peaks of **SQB** (14 300 cm^{-1}) and **SQC** (12 720 cm^{-1}) by rearranging equation (12) to:

$$J_{\mathbf{dSQB}} = \sqrt{\left(\frac{\delta E_{\mathbf{dSQB}}}{2}\right)^2 - \Delta E^2} \tag{53}$$

Furthermore, the squared transition moments of the heterodimer in toluene, $CHCl_3$, and DCM yields comparable values (237-268 D^2) and the sum of the squared transition moments of the two isolated monomers **SQB** (92.7 D^2) and **SQC** (111 D^2) in toluene was found to be ca. 204 D^2 and is thus close to the value of 237 D^2 which was obtained for the **dSQBC**.

In contrast to **dSQBC**, the copolymer **pSQBC** has its main absorption band on the high energy side of the spectrum at 14 750 cm^{-1} (1.18×10^5 $M^{-1}cm^{-1}$) with a shoulder around 14 000 cm^{-1} (9.27 ×10^3 $M^{-1}cm^{-1}$). Besides, a much weaker peak is noticed around 11 910 cm^{-1} (5.00×10^4 $M^{-1}cm^{-1}$), which is assigned to the low energy edge of the exciton band. These findings point towards predominant H-type exciton coupling, where monomers are aligned in a parallel fashion which could be rationalised by helical-type arrangements. The splitting of 2 840 cm^{-1} between these peaks is larger than that of the heterodimer (2 040 cm^{-1}) and very close to the theoretically expected value under consideration of perfectly delocalised excitons, which would be ca. 2700 cm^{-1} in accordance to equation (12):

$$\delta E_{\mathbf{pSQBC}} = \sqrt{\Delta E^2 + 16\,J^2}, \tag{12}$$

where *J* corresponds to the heterodimer coupling (645 cm^{-1}).

The absorption of **pSQBC** was measured in $CHCl_3$, DCM, toluene, and PhCN in order to study the influence of the solvent on the shape of the absorption band manifold. Unfortunately, the copolymer was completely insoluble in acetone and DMF. The spectra are shown in Figure 45. A priori, the spectra show no great difference in shape, however, a closer inspection reveals a distinct difference between the spectra in PhCN and $CHCl_3$. In PhCN, the H-aggregate band is most pronounced and most blue-shifted within this series. In contrast, in

$CHCl_3$, the H-aggregate turns out to be more red-shifted, and more importantly, the J-aggregate band is more prominent than in the other solvents. Yet, as a matter of fact, the dependence of the solvent on the shape of the absorption band manifold is considered to be rather marginal, indicative of a very similar alignment of monomer units within the polymer strands. This leads to the conclusion, that the copolymer consisting of indolenine as well as of quinoline moieties predominantly shows H-aggregate behaviour.

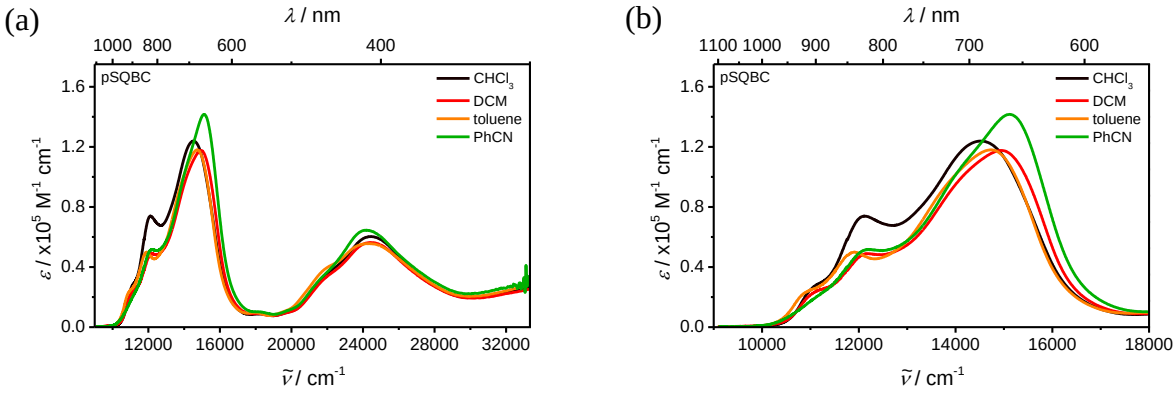

Figure 45: Absorption spectra of **pSQBC** in various solvents.

In order to further substantiate the formation of helical motifs, the spectral features of the copolymer are compared with those of the parent indolenine polymer **pSQB-1** in $CHCl_3$ and PhCN, respectively. As can be readily appreciated in Figure 46, the shape of both spectra of the copolymer in $CHCl_3$ and PhCN closely resembles that of **pSQB-1** in PhCN, where helical structures are found to be predominant.

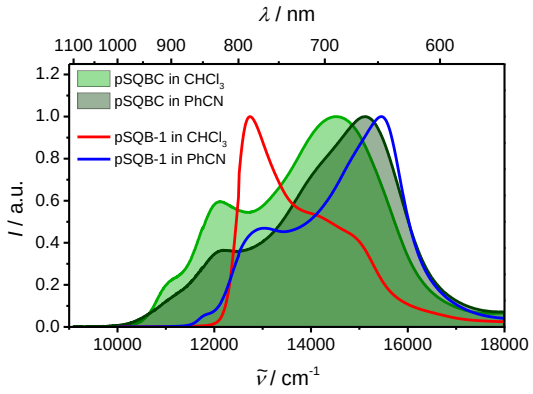

Figure 46: Absorption spectra of **pSQB-1** and **pSQBC** in $CHCl_3$ and PhCN, respectively.

Apparently, the incorporation of quinoline moieties ultimately favour the formation of intramolecular H-type aggregates, which can be explained by a face-to-face alignment of the monomer units possibly enabled by helical arrangements.

The absorption behaviour of **pSQBC** was further studied as a function of temperature. PhCN was chosen as solvent due to its high boiling point and for reasons of comparability with

parent indolenine polymer **pSQB-1** (Chapter 3.4.2.3). The spectra are shown in Figure 47. Starting at 273 K, the temperature was successively raised up to 433 K. Comparing the initial and the final spectrum at lowest and highest temperature, the H-aggregate band at ca. 15 000 cm^{-1} undergoes a energetic shift to lower energies of about 300 cm^{-1} and marginal increase in intensity, while the J-aggregate band at 12 200 cm^{-1} shows a significant increase in intensity and a marginal shift to lower energies. Similar trends were observed for the parent indolenine homopolymer in Chapter 3.4.2.3, where a change of the spectra from more H-type aggregate towards a mixture with more J-aggregate character is observed upon heating. However, here it was not possible to manipulate the ratio of the aggregate species in favour of the J-aggregates. This may be explained by the high driving force for π-π-interactions between the quinoline-moieties within the helical polymer strands. This assumption is corroborated by previous aggregation studies of 4-methylquinoline squaraine monomers, which showed a high propensity for self-assembly in toluene.[173]

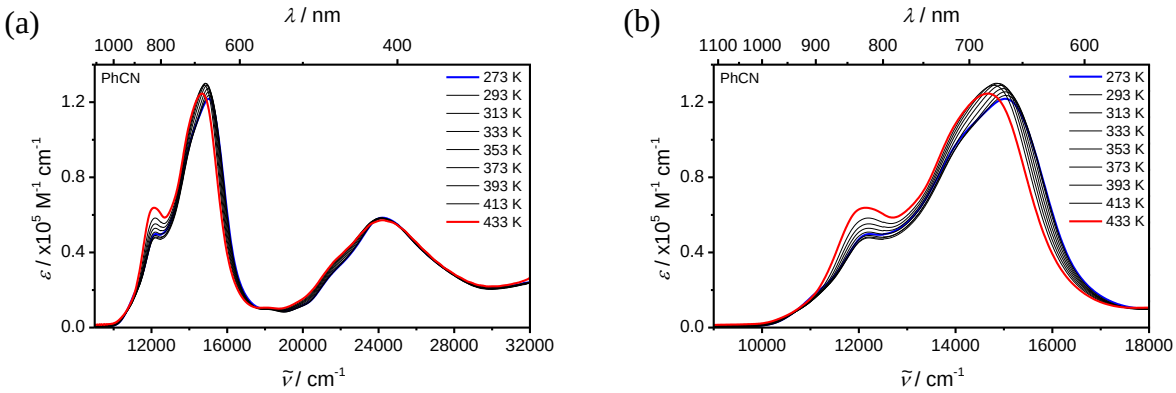

Figure 47: Absorption spectra of **pSQBC** in PhCN at different temperatures (density corrected).

3.4.5.4 Fluorescence Spectroscopy

Fluorescence emission spectra and lifetimes of **dSQBC** and **pSQBC** were recorded in DCM and toluene. The fluorescence properties of the monomers **SQB** and **SQC** have already been discussed in Chapter 3.1.4. Yet, it is worth mentioning that the determination of the quantum yield for the monomer **SQC** as well as for all quinoline-containing analogues was hampered by their weak emissive character, respectively. The optical data are presented in Table 8.

In DCM, the heterodimer **dSQBC** shows a red-shifted monomer-type fluorescence band at 12 300 cm^{-1} without Strickler-Berg symmetry (Figure 48(a)). Quite surprisingly, an additional fluorescence band of half the intensity is observed at higher energies at 13 900 cm^{-1}. While the former is assumed to arise from the lowest exciton state, the latter seems to stem from a higher state. A similar fluorescence spectrum was obtained in toluene, yet with rather two

peaks than one peak at higher energies at 13 200 cm^{-1} and 13 810 cm^{-1} which are considerably less intense than the main peak at 12 000 cm^{-1} (Figure 48(b)). In addition, the fluorescence excitation spectrum in toluene indicates no efficient energy relaxation from the $S_1´$- to the S_1-state. These findings in both solvents are in contradiction with Kasha´s rule where fluorescence is expected to occur exclusively from the lowest excitonic state.

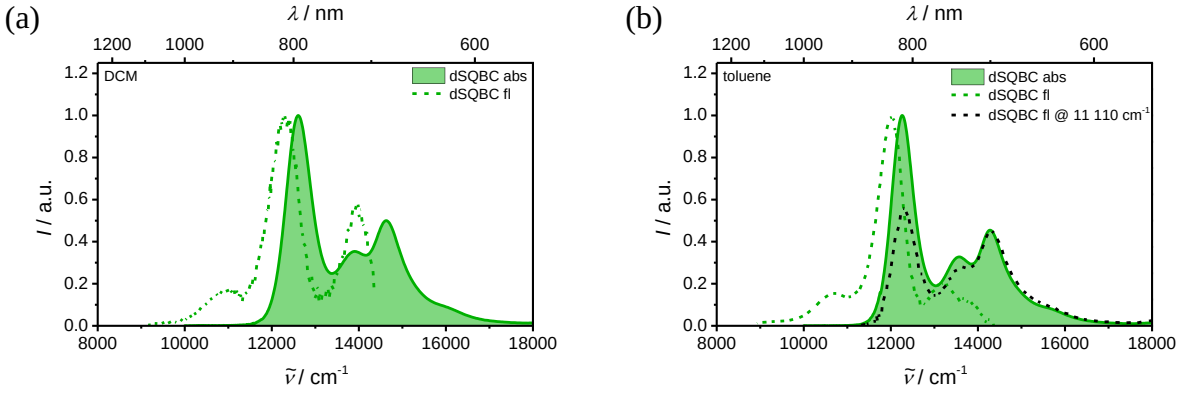

Figure 48: Normalised absorption and fluorescence spectra of **dSQBC** in (a) DCM and (b) toluene, respectively. (b) Fluorescence excitation spectrum of **dSQBC** in toluene.

The dimer exhibits very short-lived, monoexponential fluorescence decays with lifetimes of 30 ps in DCM and 80 ps in toluene, which are very similar to the lifetime of 40 ps of the monomer **SQC** in toluene. The extremely short lifetimes for the quinoline compounds go hand in hand with their weak emissive character.

According to Figure 49(a), the copolymer **pSQBC** exhibits a monomer-type fluorescence in DCM which provides a considerable red-shift of about 1 100 cm^{-1} with a maximum at 13 800 cm^{-1}. In this context, a monoexponential fluorescence decay with a lifetime of 1.92 ns was found, which is significant larger than those for the dimer and the monomer **SQC**.

In toluene, in conntrast, two further fluorescence peaks at lower energies at 10 400 cm^{-1} and 11 700 cm^{-1} are observed despite the main peak at 13 700 cm^{-1}. A biexponential fluorescence decay was found with lifetimes of 110 ps (0.37) and 3.12 ns (0.63) which is in line with the observation of more than one emission band.

Against expectations, the main contribution to the fluorescence in both solvents apparently originates from a state belonging to the H-aggregate band (shoulder at 14 000 cm^{-1}), respectively. This is in contradiction with exciton theory, which predicts no fluorescence in ideal H-aggregates.[74,75] Disorder caused by an inhomogeneous alignment of the monomer units probably leads to deviations from ideal H-aggregate behaviour. It must be kept in mind, that the polymer is conceived of two different monomers which inherently differ in shape and aggregation propensity. Thus, the polymer might be prone to adopt different conformers in

solution, which deviate from ideal H-aggregate behaviour to varying degrees, respectively. The emergence of at least three distinct transitions corroborates this assumption.

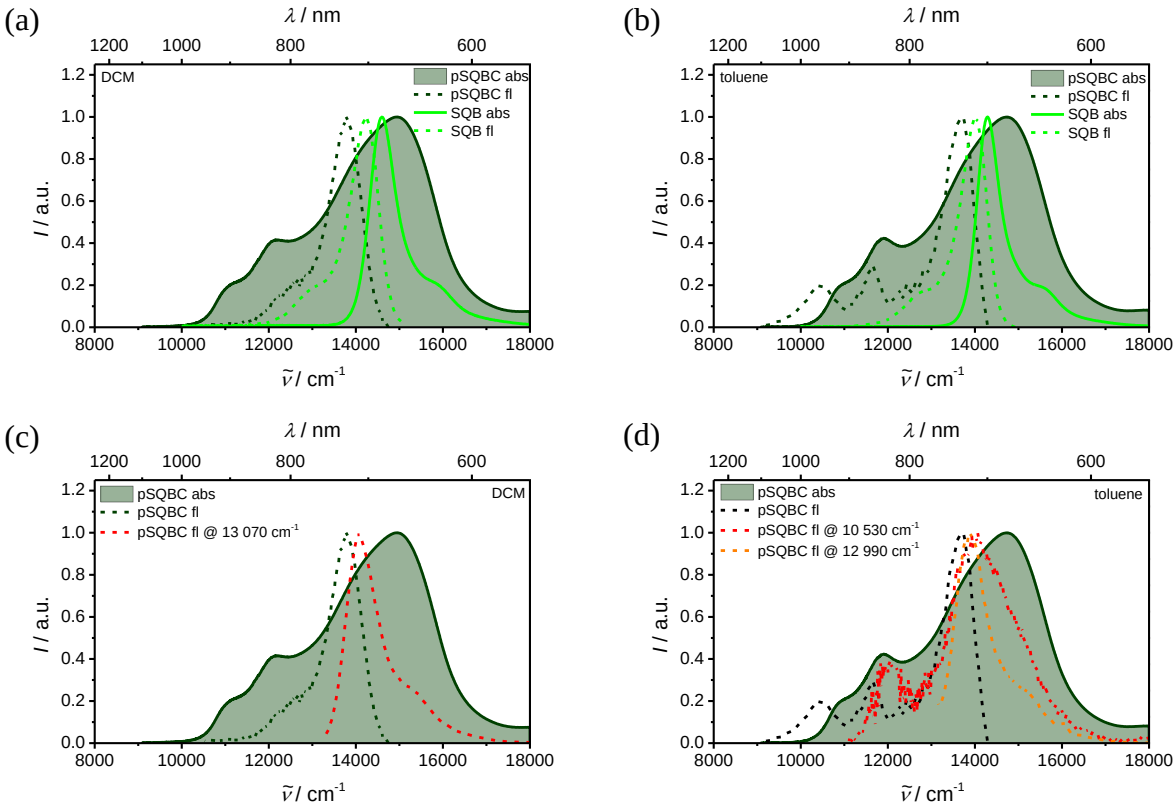

Figure 49: Normalised absorption and fluorescence spectra of **SQB** and **pSQBC** in (a) DCM and (b) toluene, respectively. Fluorescence excitation spectra of **pSQBC** in (c) DCM and (d) toluene at different emission energies.

In order to shed more light on the origin of theses emission bands, fluorescence excitation spectra were recorded in both solvents. According to Figure 49(c), the excitation spectrum in DCM resembles prima facie the absorption of a **SQB** monomer. A closer inspection yet reveals that the excitation spectrum of **pSQBC** is more red-shifted than the absorption of **SQB** in DCM which in turn excludes the presence of **SQB** monomers. In addition, smaller oligomers can also not be responsible for the spectral features as the shape of the spectrum and the red-shift of the absorption would be different and larger, respectively, as it was seen for **dSQBC**.

In toluene, due to the multiple fluorescence bands at lower energies, it was possible to measure excitation spectra as a function of different emission energies. The spectra are presented in Figure 49(d). While the excitation spectrum with higher emission energy (fl @ 12 990 cm^{-1}) closely resembles that in DCM and seems to originate from the shoulder at 14 000 cm^{-1}, the spectrum with lower emission energy (fl @ 10 530 cm^{-1}) covers more of the polymer absorption but does not fully reproduce the shape. Besides, the maximum of the excitation spectrum is more shifted towards the high energy edge of the H-band compared to

the former excitation spectrum. Now, with a more complete picture at hand, the Stokes shifts, which were initially considered to be unusually large, turned out to be rather common, since the emission peak at higher energies originates from the shoulder at around 14 000 cm^{-1} which is assigned to a second sort of H-aggregate. Ideal H-aggregates with perfectly aligned monomers in a face-to-face situation are believed to be the case for the main peak at around 15 000 cm^{-1}. Thus, the joint findings from the fluorescence emission and excitation spectra clearly indicate the presence of more than two types of H-aggregates.

Table 8: Absorption maxima, extinction coefficients, transition moments, fluorescence maxima, fluorescence quantum yields, and fluorescence lifetimes of squaraine dyes in $CHCl_3$ and toluene. Extinction coefficients ε and transition moments μ_{eg} of the polymer are indicated per monomer unit.

	solvent	$\tilde{\nu}_{abs}$ / cm^{-1} (nm)	ε_{max} / $M^{-1}cm^{-1}$	μ_{eg}^2 / D^2	$\tilde{\nu}_{em}$ / cm^{-1} (nm)	Φ_{fl} / –	τ_{fl}[c] / ns
	$CHCl_3$	14 600 (685)	1.96×10^5	98.6	14 200 (704)	0.55	2.40
SQB	DCM	14 600 (685)	1.96×10^5	103	–	–	–
	toluene	14 300 (699)	2.02×10^5	92.7	14 000 (714)	0.75	3.45
	$CHCl_3$	13 100 (763)	1.95×10^5	115	12 700	–	< 0.04
SQC	DCM	13 100 (763)	1.88×10^5	121	–	–	< 0.04
	toluene	12 700 (787)	2.03×10^5	111	12 500	–	0.04
	$CHCl_3$	12 600 (794)	3.12×10^5	253	–	–	–
dSQBC	DCM	12 600 (794)	3.08×10^5	268	12 300 (813)	–	0.03
	toluene	12 300 (813)	3.22×10^5	237	12 100 (826)	–	0.08
	$CHCl_3$	12 700 (785)	1.08×10^5	112	12 500 (800)	0.21	0.05 (0.44) 0.47 (0.17) 0.96 (0.39)
	DCM	12 700 (785)	9.28×10^4	112	–	–	–
pSQB-1 X_n = 21.6	toluene	12 700/14 700 (765/678)	$5.18/5.31\times10^4$	88.9	12 300 (810)	0.06[a] 0.17[b]	1.39 (0.28)[d] 3.18 (0.72)[d] 1.18 (0.38)[e] 2.44 (0.62)[e]
	PhCN	13 000/15 500 (767/647)	$3.44/7.32\times10^4$	90.3	–	–	
	DMF	15 700 (636)	7.37×10^4	90.3	–	–	
	acetone	15 800 (633)	8.35×10^4	92.2	–	–	
	$CHCl_3$	14. 500 (690)	1.24×10^5	237	–	–	–
pSQBC	DCM	14 900 (671)	1.18×10^5	213	13 800 (725)	–	1.92
X_n = 21.8	toluene	14 700 (680)	1.18×10^5	204	13 700 (730)	–	0.11 (0.37)
					–	–	3.12 (0.63)
	PhCN	15 100 (662)	1.42×10^5	225	–	–	–

– not determined. Excitation at [a]15150 cm^{-1}, [b]13510 cm^{-1}. [c](Multi-)exponential fit of fluorescence decay measured by TSCPC, excitation at 15 240 cm^{-1} (656 nm) or 12 770 cm^{-1} (783 nm). Amplitudes are given in brackets. Fluorescence was detected at [d]11 820 cm^{-1} (846 nm) or [e]12 330 cm^{-1} (811 nm).

3.4.5.5 Conclusion

On account of the poor solubility and the low degree of polymerisation of quinoline-substituted squaraine homopolymers, the synthetic approach towards H-aggregate polymers had to be somewhat changed by substituting every second quinoline squaraine unit by the parent 3,3-dimethylindolenine squaraine. Indeed, the resulting copolymer **pSQBC** showed improved solubility properties which allowed a comprehensive study in more solvents. Besides, the corresponding monomer unit masked as a heterodimer was synthesised to serve as reference compound.

The absorption of reference dimer **dSQBC** showed a red-shifted main absorption peak compared to the respective monomers, which was a result of exciton coupling of two unequal monomers giving rise to a S_1-state which is largely localised on the **SQC** moiety, while the S_1´-state is localised on the **SQB** subunit. Besides, multiple fluorescence emission bands were noticed which indicated a rather inefficient non-radiative energy relaxation from the S_1´- to the S_1-state, which was further corroborated by fluorescence excitation spectra. The extremely short fluorescence lifetimes of 80 ps (toluene) and 30 ps (DCM) are similar to that of **SQC** in toluene of 40 ps and underline once more the weak emissive character of quinoline analogues.

In contrast, the absorption spectra of the copolymer consistently showed a hypsochromic main peak in all solvents clearly indicating H-aggregate behaviour. It was assumed to be caused by a parallel alignment of transition moments enabled by helical domains. In analogy to **dSQBC**, multiple fluorescence bands were observed in toluene which were assigned to different sorts of H-aggregates that differ from ideal behaviour. Comparably long-lived fluorescence decays were found for the copolymer in both solvents which were in fact two orders of magnitude longer than all quinoline-containing compounds presented so far in this work.

In summary, the implementation of quinoline squaraine moieties into the polymeric scaffold proved to be highly structure-directing, which lead to predominant H-type aggregates. No solvent-dependency on the absorption was found which is indicative of very similar polymer conformers. The selective design of H-aggregates via a squaraine-squaraine copolymer together with that of J-aggregates described earlier in this work completed the picture of intramolecular aggregates. Indeed, it could be shown that the optical properties of squaraine polymers can be controlled intrinsically by adequately designed monomer units.

3.5 Squaraine Homo- and Heterodimers with Varying Spacer Units

3.5.1 Introduction

In this work, only oligomeric systems have hitherto been examined that bear a single C-C bond between the squaraine units, with the exception of the dipyrrolenine-containing squaraine dyes **pySQB-1** and **pySQB-2** which were presented in Chapter 3.4.4. Taking advantage of transition metal catalysed cross coupling reactions, a great variety of spacer units differing amongst others in length, structure, and electronic coupling can be introduced into the chromophore systems. In the light of the simpler synthetic access, only dimeric systems will be considered in this chapter. According to exciton theory, the variation of the spacer units should significantly affect the exciton coupling strength which will ultimately lead to an alteration of the overall optical properties. In theory, this examination should provide valuable information about how to chemically design a dimer in order to achieve an optical property desired. To this end, a systematic variation of the spacer part is envisaged spanning the range from singly-, over triply-, to phenyl-bound **SQA** and **SQB** homodimers as well as **SQA-SQB** heterodimers. In addition, an expansion of the **SQA** dimer pool should be realised in order to give a more exemplary picture of the exciton coupling effects involved in these dimeric chromophore systems.

3.5.2 Synthesis

The straightforward synthetic access to mono-brominated and -borylated squaraine monomers (Chapter 3.3.1) enables their use in Pd-catalysed Suzuki cross coupling reactions in order to generate systems of two coupled chromophores bridged via a C-C single bond. Following the synthetic procedure which was already described for the dimers **dSQB-1**[93] (3.4.2.2) and **dSQBC** (3.4.5.2), the homodimer **dSQA-1**[93] and the heterodimer **dSQAB-1**[88] were synthesised in similar yields of around 60 % (Scheme 26). A slight excess of the respective brominated analogue was typically used for these reactions to obtain better yields.

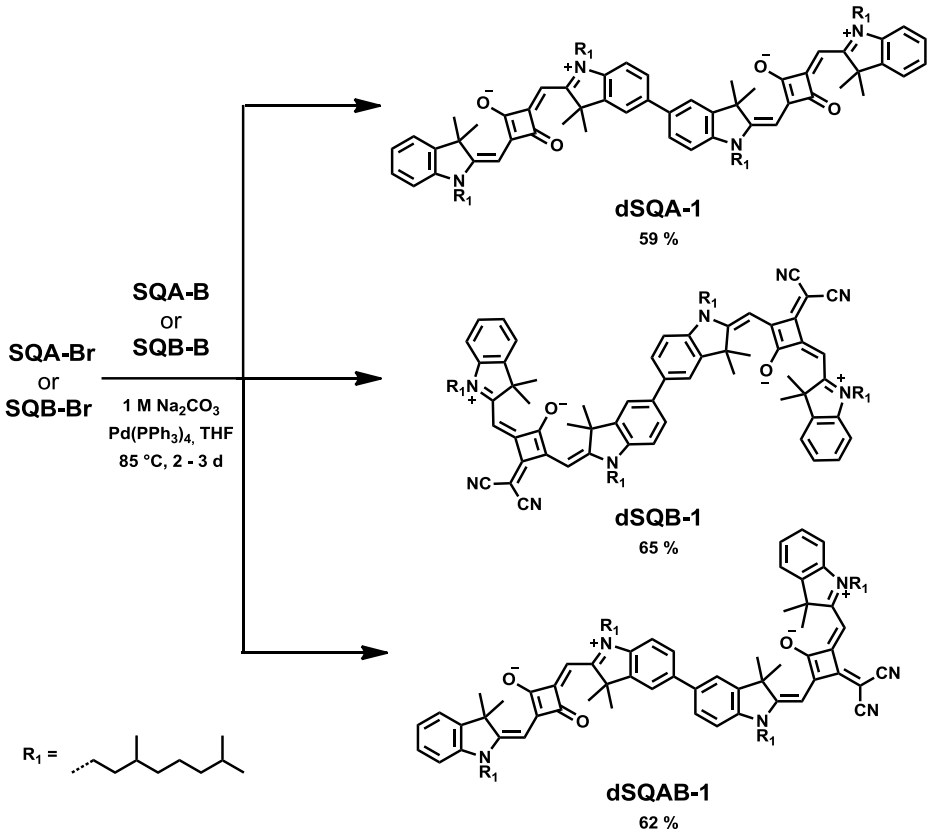

Scheme 26: Synthesis of squaraine dimers **dSQA-1**, **dSQB-1** and **dSQAB-1**.

In order to further expand the intrachromophore distance in comparison to the former dimers, the implementation of an ethynyl-spacer was envisaged. For this purpose, a terminal alkyne squaraine (Chapter 3.3.1) was coupled with a brominated squaraine analogue in a modified copper-free Sonogashira coupling reaction using $Pd(PPh_3)Cl_2$ and P*t*Bu_3 to supress the undesired Glaser homocoupling product as outlined in Scheme 27.[174] In addition the alkyne-derivative was added dropwise to the reaction mixture over a long period of time (~ 45 min) in a highly diluted manner to promote the formation of the desired dimer. The Glaser coupling byproduct occurred in all three reactions, yet it was only isolated in the case of the homodimer **dSQA-2**. The separation of the dimer from the corresponding byproduct was not feasible by flash column chromatography. Yet, it could effectively be realised by preparative GPC which is in fact the only way for these chromophore systems to be separated. The alkyne-bridged squaraine dimers **dSQA-2**, **dSQB-2**, and **dSQAB-2** were thus obtained in modest yields of 20-27 %.

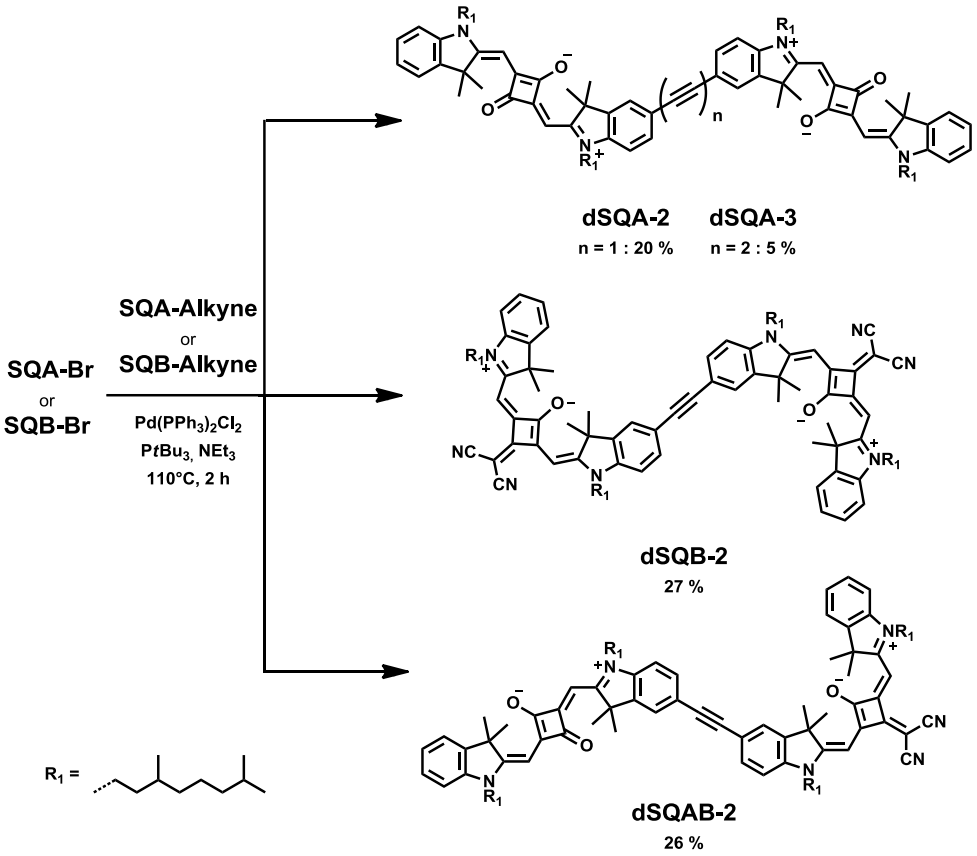

Scheme 27: Synthesis of squaraine dimers **dSQA-2**, **dSQA-3**, **dSQB-2**, and **dSQAB-2**.

The bridging unit was further varied via a phenyl spacer according to Scheme 28. Therefore, commercial 1,4-dibromobenzene was coupled with the boronic ester derivatives of **SQA** and **SQB**, respectively, to give the corresponding homodimers **dSQA-4** and **dSQB-3** in comparably lower yields than analogous biaryl-dimers mentioned above. Besides, the respective heterodimer was also of interest but required a stepwise synthesis over two stages according to Scheme 28 and Scheme 29. For this purpose, an excess of spacer was used in the Suzuki reaction in contrast to the synthesis of **dSQA-4** to obtain first the functionalised squaraine monomer **SQB-C_6H_4-Br** as main product (36 %) and the symmetrical dimer as side-product (15 %).

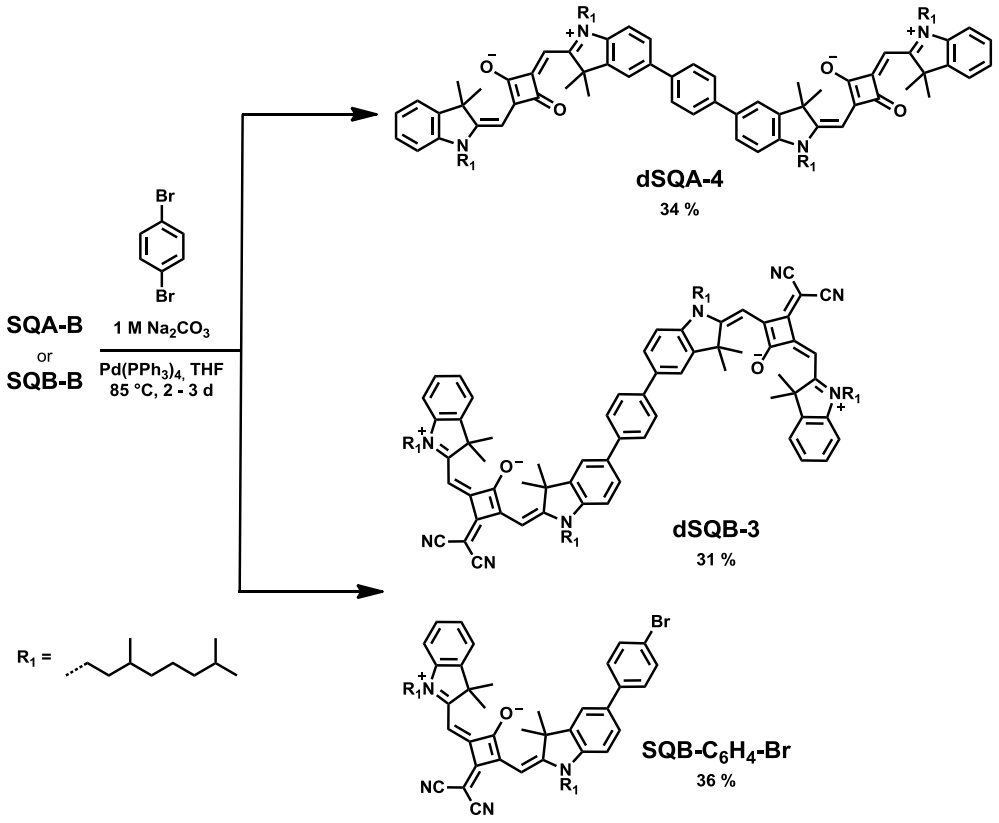

Scheme 28: Synthesis of squaraine homodimers **dSQA-4** and **dSQB-3**, as well as functionalised squaraine monomer **SQB-C_6H_4-Br**.

Finally, the functionalised squaraine monomer **SQB-C_6H_4-Br** reacted with **SQA-B** in a standard Suzuki coupling reaction and gave the corresponding heterodimer **dSQAB-3** in 34 % yields according to Scheme 29.

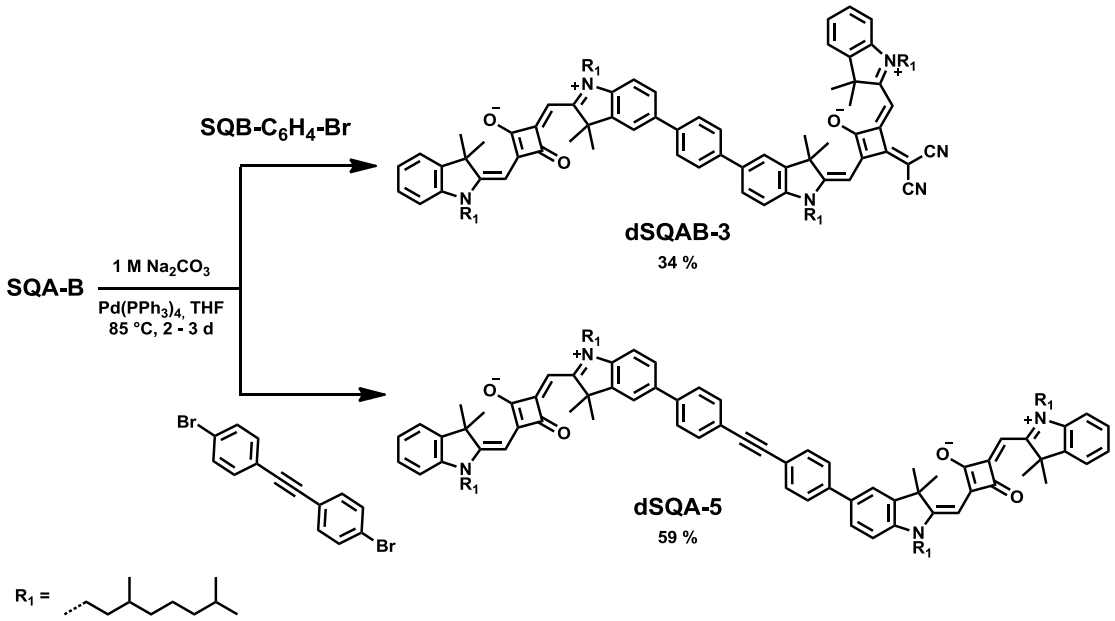

Scheme 29: Synthesis of squaraine heterodimer **dSQAB-3** and homodimer **dSQA-5**.

The pool of **SQA**-based homodimers was further expanded by employing commercially available 1,2-bis(4-bromophenyl)ethyne as spacer substrate. The Suzuki coupling reaction was performed under aqueous conditions in THF using a slight excess of borylated squaraine **SQA-B** (Scheme 29). By this means, the homodimer **dSQA-5** was obtained in good yields of almost 60 % providing the longest interchromophore distance within this series of dyes.

3.5.3 Absorption Spectroscopy

3.5.3.1 SQA-based Homodimers

Absorption spectra of **SQA**-based homodimers **dSQA-1** – **dSQA-5** were recorded in toluene and $CHCl_3$, and are presented in Figure 51. The chemical structures of the dimers are depicted in Figure 50. The optical data are summarised in Table 12.

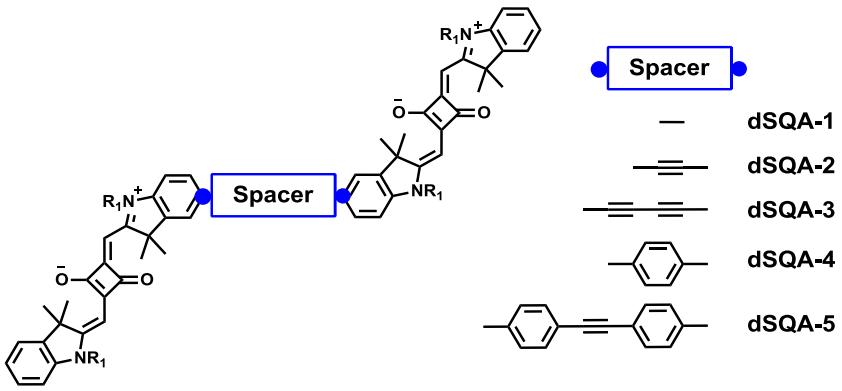

Figure 50: Chemical structures of **SQA**-based homodimers with varying spacers.

The absorption spectra of the dimers share the common feature of an intense main absorption band from 14 500-15 200 cm^{-1} in toluene and from 14 600-15 100 cm^{-1} in $CHCl_3$, which is red-shifted compared to that of the monomer **SQA**. Additional bands are observed at higher energies from 15 000-17 000 cm^{-1}, which can either be attributed to the subsidiary vibronic progression or to the S_1´-state. An exact assessment of these bands will be done below. The spectra in toluene show somewhat higher molar extinction coefficients compared to those in $CHCl_3$ and range from 4.65-6.25×10^5 $M^{-1}cm^{-1}$. In general, all **SQA**-based squaraine dimers show higher extinction coefficients than the parent monomer. The highest extinction coefficients are found for **dSQA-3** – **dSQA-5** (5.94-6.23×10^5 $M^{-1}cm^{-1}$) which considerably exceeds those of **dSQA-1** and **dSQA-2** (4.65 and 4.66×10^5 $M^{-1}cm^{-1}$). No significant solvent dependence can be ascertained as the spectra are very similar in shape in both solvents. The calculation of the square of the transition moments gives comparable values, i.e., 248-269 D^2

in toluene and 273-300 D^2 in $CHCl_3$, and shows nearly additive behaviour to **SQA** with 127 D^2 in toluene and 129 D^2 in $CHCl_3$.

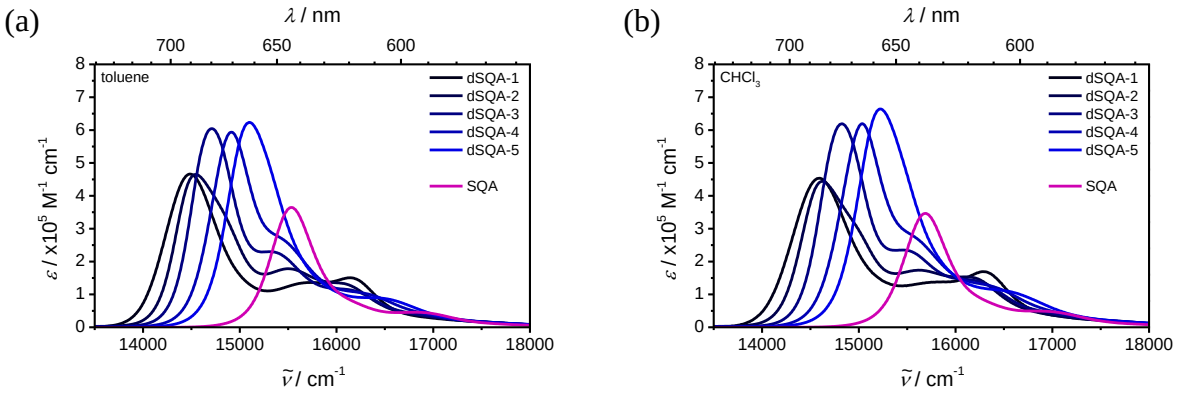

Figure 51: Absorption spectra of **SQA**-based homodimers with varying spacer unit in (a) toluene and (b) $CHCl_3$, respectively.

Table 9: Approximated spacer length[a] and experimental absorption maxima and coupling constants of **SQA**-based homodimers in $CHCl_3$ and toluene.

	spacer length / Å	**solvent**	$\tilde{\nu}_{abs1}$ **/ cm^{-1}**	$\tilde{\nu}_{abs2}$ **/ cm^{-1}**	$\|J\|$ **/ cm^{-1}**
dSQA-1	1.4	$CHCl_3$	14 600	16 290	850
		toluene	14 480	16 140	830
dSQA-2	3.8	$CHCl_3$	14 620	15 640	510
		toluene	14 550	15 500	480
dSQA-3	6.3	$CHCl_3$	14 830	15 480	330
		toluene	14 710	15 340	320
dSQA-4	5.6	$CHCl_3$	15 040	15 500[b]	230
		toluene	14 910	15 330[b]	210
dSQA-5	12.1	$CHCl_3$	15 220	–	–
		toluene	15 090	–	–

[a]Estimated with ChemBio3D Ultra (CambridgeSoft, Version 12.0.2.1076) by considering the outer carbon atoms of the spacers as shown in Figure 50. [b]Rough estimation in case of absence of a distinct peak maximum. – could not be determined.

The red-shift of the main absorption peak is caused by the exciton splitting of the first excited monomeric state. Accordingly, exciton coupling leads to the formation of a S_1-state which originates from a constructive coupling of monomeric transition moments with a collinear alignment. In contrast, the S_1´-state is caused by a destructive, out-of-phase orientation of the transition moments.[88] In case of **dSQA**-1, the S_1´-state can clearly be assigned to the maximum at higher energies at 16 140 cm^{-1}, while the intermediate band around 15 500 cm^{-1} is addressed to the vibronic progression. However, due to the gradually decreasing red-shift of

the absorption maxima in respect to **SQA** on going from **dSQA-1** to **dSQA-5**, the corresponding spectra become progressively compressed which leads to an enhanced mixing of vibronic and electronic states, culminating in a complete overlap in **dSQA-5**. For the other dimers, shoulders rather than distinct peaks (**dSQA-1**) are observed which hampers a precise assessment and localisation of the bands. The structural appearance of the dimers, which goes along with a deviation from ideal J-type aggregate behaviour, causes an intensity distribution giving rise to an energetically higher lying S_1'-state which should bear appreciable intensity.[88] The fact that the intermediate band around 15 400 cm^{-1} considerably increases on going from **dSQA-2** to **dSQA-5**, implicates that this band might originate from the S_1'-state.

In order to further substantiate the latter assumption, the energetic difference between the S_1-state and the vibronic progression of **SQA** was approximated to be ca. 1 300 cm^{-1}. This energetic splitting should also be preserved for the S_1-state and its subsidiary vibronic progression in all dimers. This leads to the conclusion that the intermediate bands around 15 400 cm^{-1} for the dimers **dSQA-2** – **dSQA-5** correspond to the respective S_1'-states, while the bands at even higher energies are caused by vibronic progression.

Considering the chemical structures of the dimers, the variation of the spacer units is also accompanied by a variation of the distance between the interacting chromophores which increases in the following order: **dSQA-1** < **dSQA-2** < **dSQA-4** < **dSQA-3** < **dSQA-5** (Table 9). Amongst geometrical factors, the exciton coupling strength is dependent on the distance between the chromophores ($J \sim r^{-3}$).[74,75] By rearranging equation (4) to (54), the coupling can be calculated for the dimers. For **dSQA-1** the energetic splitting can readily be evaluated from the absorption peaks at lowest and highest energy.

$$\delta E_{\text{homodimer}} = 2J \tag{4}$$

$$J = \frac{\delta E_{\text{homodimer}}}{2} \tag{54}$$

For **dSQA-2** – **dSQA-4**, the S_1'-state was roughly assessed from the intermediate band around 15 400 cm^{-1}. No coupling constant could be derived for **dSQA-5** due to an overlap of the respective transitions. The results are shown in Table 9. All estimated couplings in toluene are very similar to those in $CHCl_3$. Accordingly, the coupling of 830 cm^{-1} in **dSQA-1** bearing only a C-C single-bond is drastically reduced to 210 cm^{-1} in phenylene-bridged **dSQA-4** in toluene. However, the gradual decrease of exciton coupling strength on going from **dSQA-1** to **dSQA-4** does not completely correlate with increasing spacer length (see above). A slightly larger coupling of 320 cm^{-1} was obtained for the diyne-bridged dimer **dSQA-3** bearing a spacer length of ca. 6.3 Å, compared to 210 cm^{-1} in the phenylene-bridged dimer **dSQA-4**

with a length of only 5.6 Å. The smaller coupling in the latter one can be assigned to the disruption of π-conjugation between the two **SQA** monomers which is rationalised by a twist of the phenylene spacer out of planarity. Upon increasing the spacer length, the spectra of dimers tend to adopt the shape of the monomer, which is nicely illustrated by the spectrum of **dSQA-5** providing the longest interchromophore distance and thus the smallest exciton coupling strength.

To conclude, on going from **dSQA-1** to **dSQA-5**, the red-shift of the main absorption peaks decreases from 14 500-15 200 cm^{-1} in toluene and from 14 600-15 100 cm^{-1} in $CHCl_3$ which could be shown to correlate with a decrease in exciton coupling strength.

3.5.3.2 SQB-based Homodimers

In analogy to the **SQA**-dimers shown above, absorption studies of the **SQB**-based homodimers **dSQB-1**–**dSQB-3** were performed in toluene and $CHCl_3$. The systematic evaluation of the influence of varying spacers on the optical properties was carried out only for singly-, triply-, and phenylene-bound dimers. The corresponding chemical structures are given in Figure 52. The optical data are summarised in Table 13.

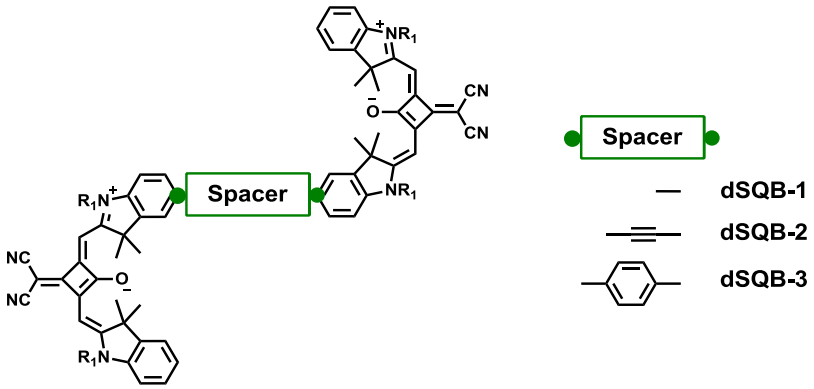

Figure 52: Chemical structures of **SQB**-based homodimers with varying spacers.

According to Figure 53, the **SQB**-based squaraine homodimers exhibit an intense main absorption band with two additional bands located at higher energies at around 14 000 cm^{-1} and 15 000 cm^{-1}, respectively. The molar extinction coefficients are in the range of 3.57-3.77×10^5 $M^{-1}cm^{-1}$ in toluene and 3.38-3.73×10^5 $M^{-1}cm^{-1}$ in $CHCl_3$ and show thus no great deviation. The squared transition moments provide very similar values, 226-227 D^2 in toluene and 235-239 D^2 in $CHCl_3$. In addition, the sum of the squared transition moments of the monomer **SQB** in toluene ($CHCl_3$) is 92.7 D^2 (98.6 D^2) are thus in agreement with those of dimers within experimental error. Furthermore, the red-shift compared to the monomer

absorption peak is caused by the exciton splitting of the first excited state. Non-collinear alignment of the transition moments gives rise to a second peak at higher energies. As argued above for the **SQA**-dimers, the assignment of the respective S_1´-states was carried out under consideration of the energetic difference between the maximum and the vibronic progression in the **SQB** monomer. The latter was estimated to 1 200 cm^{-1} which is in good agreement with the value assessed for **SQA** above. Based on that energy difference, the assignments of the second exciton states were made and the results are presented in Table 10. Upon varying the spacer unit, the coupling is reduced from 780 cm^{-1} in singly-bound **dSQA-1** to 500 cm^{-1} in alkyne-bridged **dSQA-2**, and to 190 cm^{-1} in phenylene-bridged **dSQA-3**. The obtained values for the couplings in toluene are similar to those in $CHCl_3$. The comparison between the couplings in **SQA**- and **SQB**-based homodimers bearing the same spacer does not provide a significant deviation, except for **dSQA-1** and **dSQB-1**. Here, the coupling of the former is by about 60 cm^{-1} (50 cm^{-1}) larger than that of **dSQB-1** in toluene ($CHCl_3$) (Table 9 and Table 10).

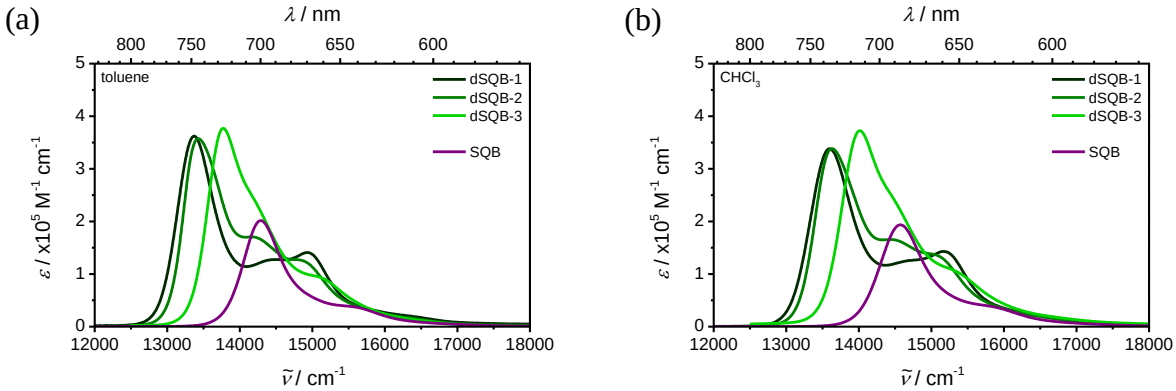

Figure 53: Absorption spectra of **SQB**-based homodimers with varying spacer unit in (a) toluene and (b) $CHCl_3$, respectively.

Table 10: Experimental absorption maxima and coupling constants of **SQB**-based homodimers in $CHCl_3$ and toluene.

	solvent	$\tilde{\nu}_{abs1}$ / cm^{-1}	$\tilde{\nu}_{abs2}$ / cm^{-1}	$\|J\|$ / cm^{-1}
dSQB-1	$CHCl_3$	13 600	15 170	790
	toluene	13 370	14 930	780
dSQB-2	$CHCl_3$	13 620	14 150	530
	toluene	13 430	14 420	500
dSQB-3	$CHCl_3$	14 020	14 410[a]	200
	toluene	13 770	14 140[a]	190

[a]Rough estimation in case of absence of a distinct peak maximum.

3.5.3.3 SQA-SQB-based Heterodimers

Absorption spectra of the heterodimers **dSQAB-1**–**dSQAB-3** were recorded in toluene and $CHCl_3$, and are shown in Figure 55. Identical spacer units were introduced as in **SQB**-homodimers. The corresponding chemical structures are given in Figure 54. The optical data are summarised in Table 13.

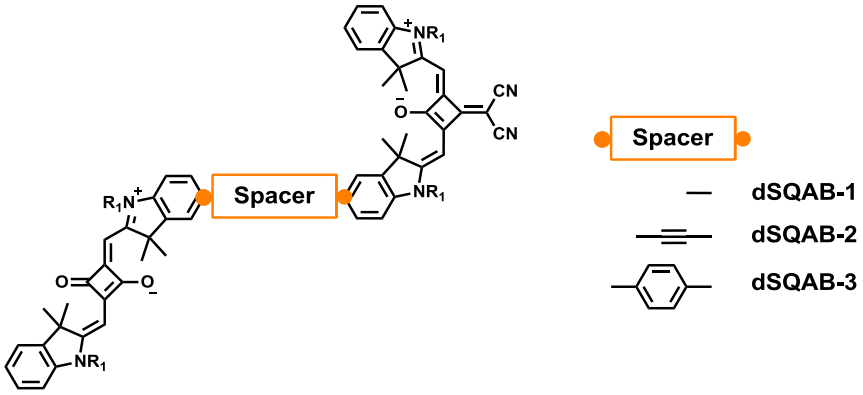

Figure 54: Chemical structures of **SQA**-**SQB**-based heterodimers with varying spacers.

The absorption spectra of the heterodimers feature two intense bands at around 14 000 cm^{-1} and 15 500 cm^{-1} with molar extinction coefficients of 2.87-3.13×10^5 $M^{-1}cm^{-1}$ and 2.15-2.93×10^5 $M^{-1}cm^{-1}$ in toluene, and 2.88-3.09×10^5 $M^{-1}cm^{-1}$ and 2.03-2.83×10^5 $M^{-1}cm^{-1}$ in $CHCl_3$, respectively. The emergence of two intense bands is caused by exciton coupling of two unequal monomers, i.e., **SQA** and **SQB**, which leads to the formation of a S_1-state which is mostly localised on the **SQB** subunit, and a S_1´-state which is mostly localised on the **SQA** subunit.[88] Upon increasing the spacer length from **dSQAB-1** to **dSQAB-3**, a significant increase of the second maximum at higher energies is observed, while the first maximum at lower energies slightly decreases. Simultaneously, the two absorption peaks at around 14 000 cm^{-1} and 15 500 cm^{-1} gradually shift towards higher and lower energies, respectively. The calculation of the square of the transition moments in toluene and $CHCl_3$ gives comparable values, i.e., 246-248 D^2 in toluene and 255-264 D^2 in $CHCl_3$. This indicates within the limits of accuracy of the measurements that the integrated oscillator strength is independent of the solvent. In addition, the values almost show additivity to the monomers units and thus follow the Thomas-Reiche-Kuhn sum rule.[151] In contrast to the homodimers, the assessment of the second exciton state is trivial. Thus, the coupling between the two monomers can be estimated from the energetic difference of the dimer absorption and the difference between the monomer absorption peaks of **SQA** and **SQB** using equation (53) from Chapter 3.4.5.3. The results are presented in Table 11.

As already proved above for the homodimers, the exciton coupling energy of the heterodimers also decreases with increasing spacer length. While **dSQAB-1** shows a somewhat smaller coupling of ca. 740 cm^{-1} than the respective homodimers **dSQA-1** (830 cm^{-1}) and **dSQB-1** (780 cm^{-1}), a larger coupling of 570 cm^{-1} was estimated for alkyne-bridged **dSQAB-2** in comparison to **dSQA-2** (480 cm^{-1}) and **dSQB-2** (500 cm^{-1}). The phenyl-bridged heterodimer exhibits a coupling of 240 cm^{-1} and is thus slightly larger than those of the homodimers (210 and 190 cm^{-1}). However, attention is drawn to the fact, that the determination of the coupling energies which was preceded by a rather rough estimation of the energetic positions of the S_1´-states in the case of the homodimers, should be considered with caution. The deviations in coupling energies are admittedly small when comparing dimers with the same spacer and should therefore be interpreted in a rather qualitative manner. Nonetheless, it could be shown that the variation of the spacer length directly affects the exciton coupling strength in squaraine homo- and heterodimers.

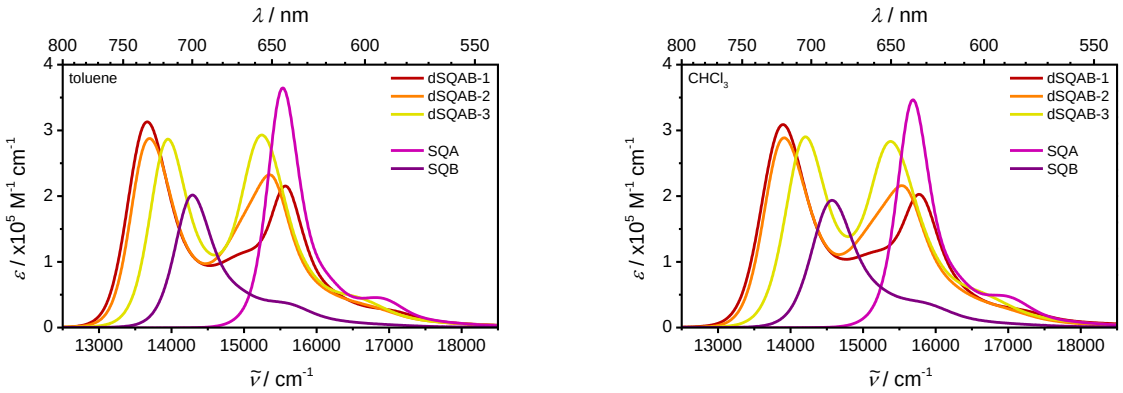

Figure 55: Absorption spectra of heterodimers with varying spacer unit in (a) toluene and (b) $CHCl_3$, respectively.

Table 11: Experimental absorption maxima and coupling constants of **SQA-SQB**-based heterodimers in $CHCl_3$ and toluene.

	solvent	$\tilde{\nu}_{abs1}$ / cm^{-1}	$\tilde{\nu}_{abs2}$ / cm^{-1}	$\|J\|$ / cm^{-1}
dSQAB-1	$CHCl_3$	13 900	15 770	760
	toluene	13 670	15 580	740
dSQAB-2	$CHCl_3$	13 920	15 530	590
	toluene	13 700	15 350	570
dSQAB-3	$CHCl_3$	14 200	15 370	200
	toluene	13 950	15 240	240

3.5.4 Fluorescence Spectroscopy

Steady-state and time-resolved fluorescence measurements were performed for all homo- and heterodimers in toluene and $CHCl_3$, respectively. The spectra of the investigated dimers are depicted only in toluene (Figure 56), as the spectra in $CHCl_3$ lack of novelty and were thus omitted. For the sake of completeness, the corresponding normalised absorption spectra are also presented in Figure 56.

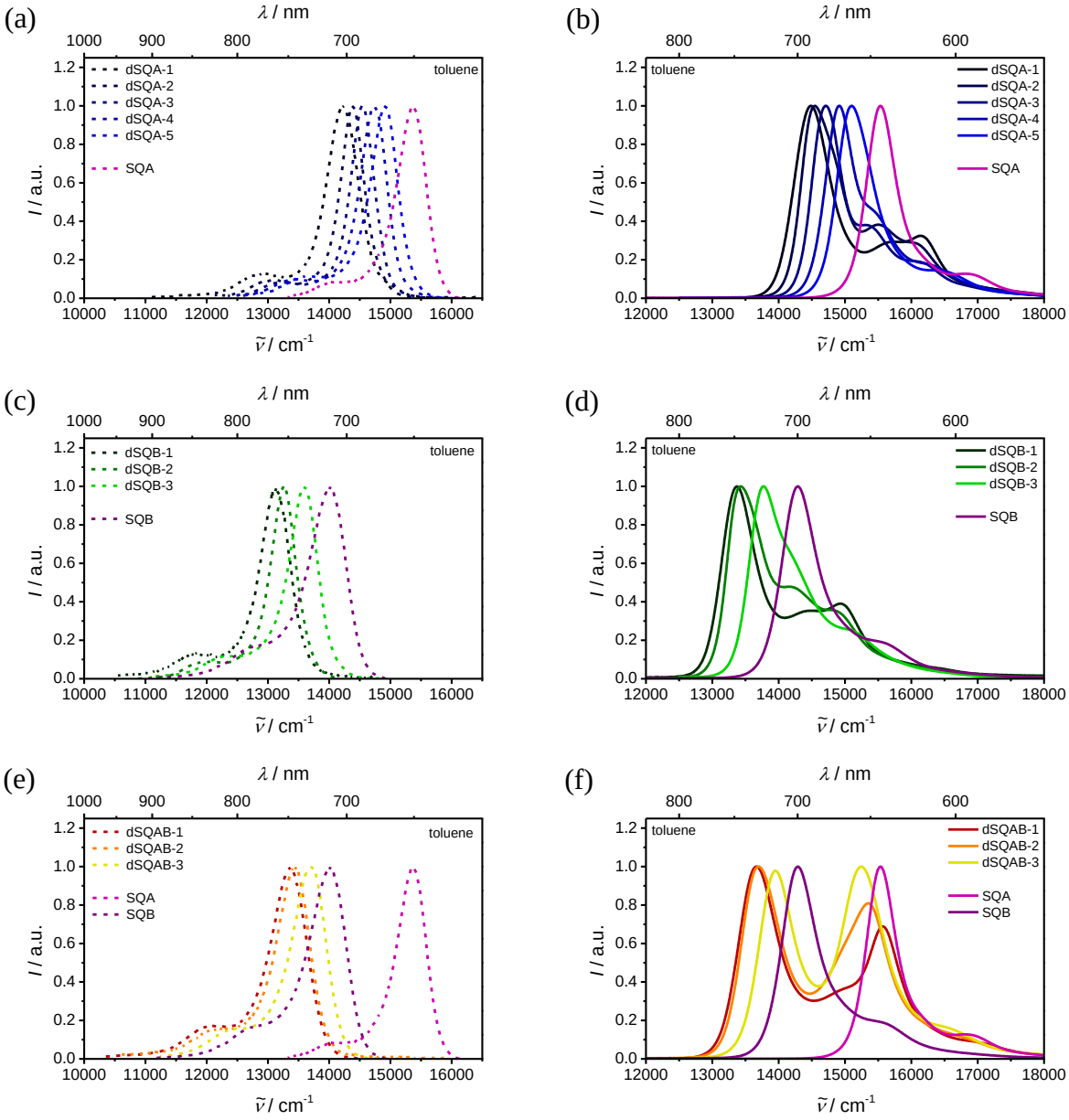

Figure 56: Normalised (a)(c)(e) fluorescence and (b)(d)(f) absorption spectra of **SQA**- and **SQB**-based homodimers, as well as of **SQA-SQB**-based heterodimers with varying spacer units in toluene, respectively.

In general, the fluorescence spectra of the dimers are reminiscent of the shape of the monomer fluorescence and thus provide no Strickler-Berg symmetry. A bathochromic shift compared to the low energy edge of the dimer absorption is observed proving that the fluorescence

exclusively originates from the lower exciton state. This is emphasised further by the excitation spectrum recorded for **dSQA-1**, which matches the absorption spectrum and therefore is a strong indicator of an efficient non-radiative relaxation from the S_1´- to the S_1-state.[69,88] While the Stokes shifts are in the range from 100-200 cm^{-1} in **SQA**-based homodimers, somewhat larger shifts from 100-300 cm^{-1} and from 200-400 cm^{-1} are found in **SQB**-based homodimers and **SQA**-**SQB**-based heterodimers, respectively. In toluene, the fluorescence quantum yields gradually decrease within the **SQA** series from 0.80 to 0.71. In contrast, the quantum yields increase from 0.40 to 0.65 in $CHCl_3$. This antagonistic tendency in both solvents is not observed for the **SQB** homodimers and **SQA**-**SQB** heterodimers. Albeit with some restrictions for the alkyne-bridged dimers **dSQB-2** and **dSQAB-2** , the quantum yields rather tend to increase in both solvents with increasing interchromophore distance, i.e., from 0.69-0.80 in toluene and from 0.20-0.53 for the **SQB** series, and from 0.69-0.81 in toluene and from 0.05-0.21 in $CHCl_3$ for the heterodimers.

Time-correlated single photon counting was used in order to measure the fluorescence lifetimes of the dimers. For comparative purposes, the averaged fluorescence lifetimes were determined according to equation (47). Accordingly, the lifetimes correlate with the fluorescence quantum yields in a qualitative manner, with the longest lifetimes generally exhibited in toluene. The averaged lifetimes within the **SQA** series decrease from 1.78 to 1.64 ns in toluene, and increase from 0.94 to 1.52 ns in $CHCl_3$. For the **SQB** homodimer series, an increase of lifetimes from 2.87 to 2.97 ns in toluene and from 0.95 to 1.99 ns in $CHCl_3$ is observed. In analogy, the lifetimes within the heterodimer series also increase from 2.14 to 2.83 ns in toluene and from 1.31 to 1.42 ns in $CHCl_3$.

Table 12: Absorption maxima, extinction coefficients, squares of the absorption transition moments, fluorescence maxima, fluorescence quantum yields, fluorescence lifetimes, expectation values of fluorescence lifetimes and squares of the fluorescence transition moments of **SQA**-based squaraine dyes in $CHCl_3$ and toluene.

	solvent	$\tilde{\nu}_{abs}$ / cm^{-1} (nm)	ε_{max} / $M^{-1}cm^{-1}$	μ^2_{abs} / D^2	$\tilde{\nu}_{em}$ / cm^{-1} (nm)	Φ_{fl} / –	τ_{fl}[a] / ns	$\bar{\tau}_{fl}$ / ns	μ^2_{fl} / D^2
SQA	$CHCl_3$	15 700 (637)	3.45×10^5	129	15 500 (645)	0.51	0.26 (0.40) 1.47 (0.60)	1.34	121[175]
	toluene	15 500 (645)	3.64×10^5	127	15 400 (649)	0.62	0.25 (0.09) 1.71 (0.91)	1.69	114[175]
dSQA-1	$CHCl_3$	14 600 (685)	4.54×10^5	274	14 300 (699)	0.40	0.11 (0.20) 0.96 (0.80)	0.937	172[175]
	toluene	14 500 (690)	4.66×10^5	248	14 200 (704)	0.80	1.22 (0.53)[88] 2.14 (0.47)	1.78	172[175]
dSQA-2	$CHCl_3$	14 600 (685)	4.44×10^5	273	14 500 (690)	0.50	0.08 (0.36) 1.25 (0.64)	1.21	172
	toluene	14 500 (690)	4.65×10^5	254	14 400 (694)	0.78	0.80 (0.22) 1.84 (0.78)	1.73	168
dSQA-3	$CHCl_3$	14 800 (676)	6.19×10^5	300	14 600 (685)	0.60	0.75 (0.18) 1.38 (0.82)	1.31	181
	toluene	14 700 (680)	6.04×10^5	269	14 500 (690)	0.74	0.63 (0.06) 1.61 (0.94)	1.59	168
dSQA-4	$CHCl_3$	15 000 (667)	6.20×10^5	290	14 800 (676)	0.64	0.62 (0.15) 1.43 (0.85)	1.37	180
	toluene	14 900 (671)	5.94×10^5	260	14 700 (680)	0.77	0.57 (0.13) 1.70 (0.87)	1.64	164
dSQA-5	$CHCl_3$	15 200 (658)	6.64×10^5	294	15 000 (667)	0.65	0.05 (0.25) 1.54 (0.75)	1.52	159
	toluene	15 100 (662)	6.23×10^5	252	14 900 (671)	0.71	0.27 (0.07) 1.66 (0.93)	1.64	147

[a]Multiexponential fit of fluorescence decay measured by TSCPC, excitation at 15 240 cm^{-1} (656 nm). Amplitudes are given in brackets.

Table 13: Absorption maxima, extinction coefficients, squares of the absorption transition moments, fluorescence maxima, fluorescence quantum yields, fluorescence lifetimes, expectation values of fluorescence lifetimes and squares of the fluorescence transition moments of squaraine monomers **SQA** and **SQB**, and **SQB**- and **SQA**-**SQB**-based squaraine dimers in $CHCl_3$ and toluene.

	solvent	$\tilde{\nu}_{abs}$ / cm^{-1} (nm)	ε_{max} / $M^{-1}cm^{-1}$	μ_{eg}^2 / D^2	$\tilde{\nu}_{em}$ / cm^{-1} (nm)	Φ_{fl} / –	τ_{fl}[a] / ns	$\bar{\tau}_{fl}$ / ns	μ_{fl}^2 / D^2
SQA	$CHCl_3$	15 700 (637)	3.45×10^5	129	15 500 (645)	0.51	0.26 (0.40) 1.47 (0.60)	1.34	121[175]
	toluene	15 500 (645)	3.64×10^5	127	15 400 (649)	0.62	0.25 (0.09) 1.71 (0.91)	1.69	114[175]
SQB	$CHCl_3$	14 600 (685)	1.96×10^5	98.6	14 200 (704)	0.55	2.40	2.40	102
	toluene	14 300 (699)	2.02×10^5	92.7	14 000 (714)	0.75	3.45	3.45	92.2[176]
dSQB-1	$CHCl_3$	13 600 (735)	3.38×10^5	235	13 300 (752)	0.20	0.31 (0.21) 1.00 (0.79)	0.95	112
	toluene	13 400 (746)	3.62×10^5	227	13 100 (763)	0.69	1.98 (0.42) 3.26 (0.58)	2.87	121
dSQB-2	$CHCl_3$	13 600 (735)	3.38×10^5	239	13 400 (746)	0.60	1.35	1.35	–
	toluene	13 400 (746)	3.57×10^5	226	13 300 (752)	0.80	2.83	2.83	135
dSQB-3	$CHCl_3$	14 000 (714)	3.73×10^5	238	13 800 (725)	0.53	1.99	1.99	128
	toluene	13 800 (725)	3.77×10^5	226	13 600 (735)	0.75	2.97	2.97	114
dSQAB-1	$CHCl_3$	13 900 (719)	3.09×10^5	261	13 600 (735)	0.05	1.82	1.82	–
	toluene	13 700 (730)	3.13×10^5	248	13 400 (746)	0.69	1.80 (0.51) 2.41 (0.49)	2.14	156
dSQAB-2	$CHCl_3$	13 900 (719)	2.88×10^5	255	13 600 (735)	0.08	0.08 (0.36) 1.25 (0.64)	1.18	–
	toluene	13 700 (730)	2.88×10^5	246	13 500 (741)	0.63	0.80 (0.22) 1.84 (0.78)	1.73	173
dSQAB-3	$CHCl_3$	14 200 (704)	2.90×10^5	264	13 800 (725)	0.21	0.70 (0.81) 0.98 (0.19)	0.77	129
	toluene	14 000 (714)	2.87×10^5	246	13 700 (730)	0.81	0.42 (0.24) 2.94 (0.76)	2.83	127

[a](Multi-)exponential fit of fluorescence decay measured by TSCPC, excitation at 15 240 cm^{-1} (656 nm). Amplitudes are given in brackets. – not determined.

3.5.5 Conclusion

A broad range of homo- and heterodimers were prepared by introducing different spacer units that vary in length, morphology, and electronic coupling behaviour. The dimers were synthesised via straightforward Pd-catalysed Suzuki- and Sonogashira cross coupling reactions. While three different **SQB** homo- and **SQA-SQB** heterodimers were prepared, respectively, a somewhat more extensive series of five **SQA** homodimers were generated in order to study the influence of spacer on the optical properties. The overall spectral features of the dimers were interpreted to be caused by exciton coupling of localised transition moments, while the decrease in red-shift of the absorption in comparison to the monomer was in particular explained by a gradual decrease in exciton coupling strength. Comparing dimers with the same spacer unit, almost the same effect on the exciton coupling strength was noticed. In summary, it could be shown that the optical properties of squaraine dimers can conveniently be tuned by a variation of the spacer unit and/or chromophore unit.

3.6 Squaraine Heterotrimers

3.6.1 Introduction

So far, this work has been dealing almost exclusively with the photophysical properties of homo- and heterodimeric and -polymeric chromophore systems in which amongst others favourable spectroscopic features such as spectral broadening and red-shifting of absorption bands came to light. These features were interpreted to be caused by exciton coupling of localised states within the covalently bound chromophore systems. Now, this chapter being considered as an extension of the foregoing ones involves the chemical derivatisation of the dimeric chromophore framework of **dSQAB-1** to yield a variety of squaraine heterotrimers. In this regard, the spectral features shall be altered through the coupling of an additional squaraine chromophore unit. Thus, preserving the alternating **SQA**-**SQB** sequence and deploying exclusively **SQA** and **SQB**, two trimers can be conceived which are depicted in Figure 57. The uneven ratio of monomers might exert disparate excitonic coupling effects requiring further in-depth investigations.

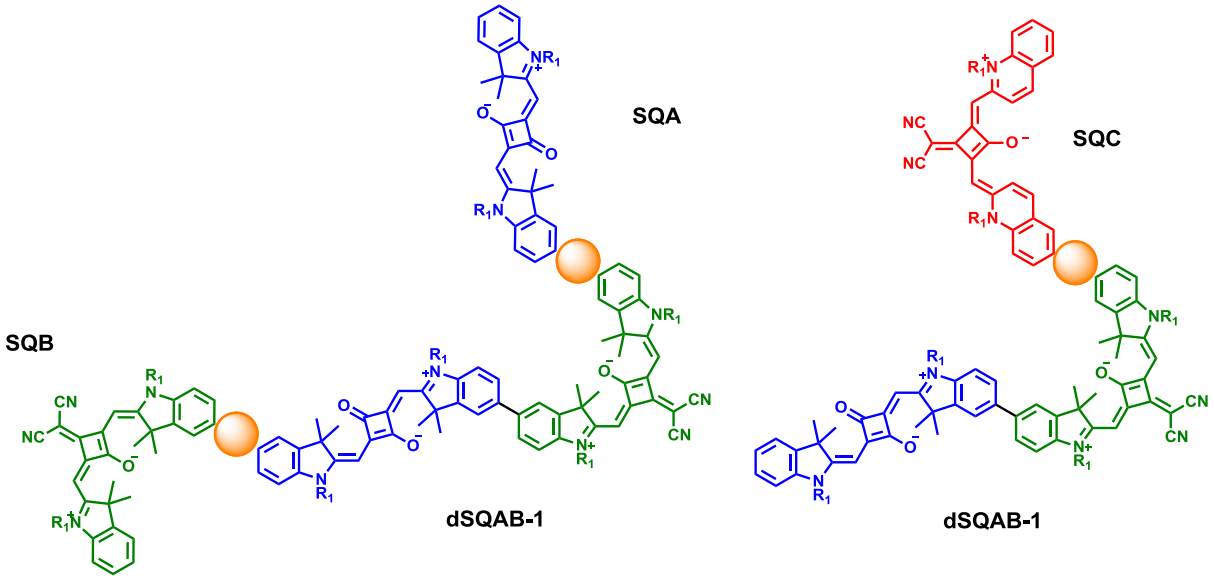

Figure 57: Coupling positions for additional squaraine dyes.

To go one step beyond, the implementation of a third squaraine dye deviating from the parent monomers **SQA** and **SQB** would give rise to a squaraine cascade with altered photophysical properties than pristine **dSQAB-1**. As to what extent this alteration impacts the spectral features of the cascade is crucially dependent on the electronic properties of the third squaraine dye. Inspired by recent works by Harriman[177,178] on artificial light-harvesting arrays and multicomponent systems with a well-defined sequence of chromophores with the ultimate

goal of directing electronic energy transfer, quinoline squaraine **SQC** was chosen to act as terminal acceptor of the cascade due to its suitable energetic position of the absorption maximum. Appreciating Figure 58(a), the implementation of **SQC** thus reflects a logical continuation of the **SQA-SQB** sequence in which the maximum of **SQA** is isoenergetic to the vibronic shoulder of **SQB**. Furthermore, the uncoupled monomers provide a spectral overlap between the emission and absorption of **SQA** and **SQB**, as well as between the emission and absorption of **SQB** and **SQC**, respectively (Figure 58(b)) and therefore fulfil an essential prerequisite for the approved approach for creating artificial cascades operating through the Förster resonance energy transfer (FRET).

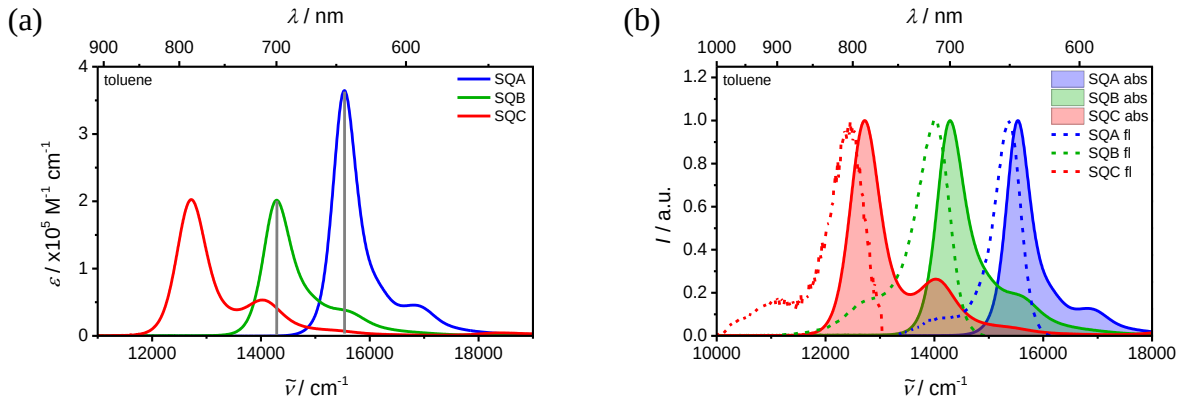

Figure 58: (a) Absorption spectra and (b) normalised absorption and fluorescence spectra of squaraine monomers **SQA**, **SQB**, and **SQC** in toluene. Vertical bars in grey illustrate the energetic position of the absorption maxima of **SQB** and **SQC**.

3.6.2 Synthesis

The synthesis of squaraine trimers providing two different sequences of **SQA** and **SQB** monomers is carried out via conventional Suzuki cross coupling reactions according to Scheme 30. While more than a twofold excess of brominated squaraine derivate was used for the synthesis of **tSQBAB**, almost equimolar amounts of monobrominated squaraine and diborylated squaraine were applied to yield the trimer **tSQABA** and the functionalised dimer **dSQAB-B**. Due to the stoichiometry chosen, the trimer was isolated as side product in 36 % yields and the functionalised dimer as major product in 48 % yields. In contrast, **tSQBAB** was obtained as major product. The corresponding functionalised dimer was also detected via TLC, yet it was of minor priority and therefore not isolated.

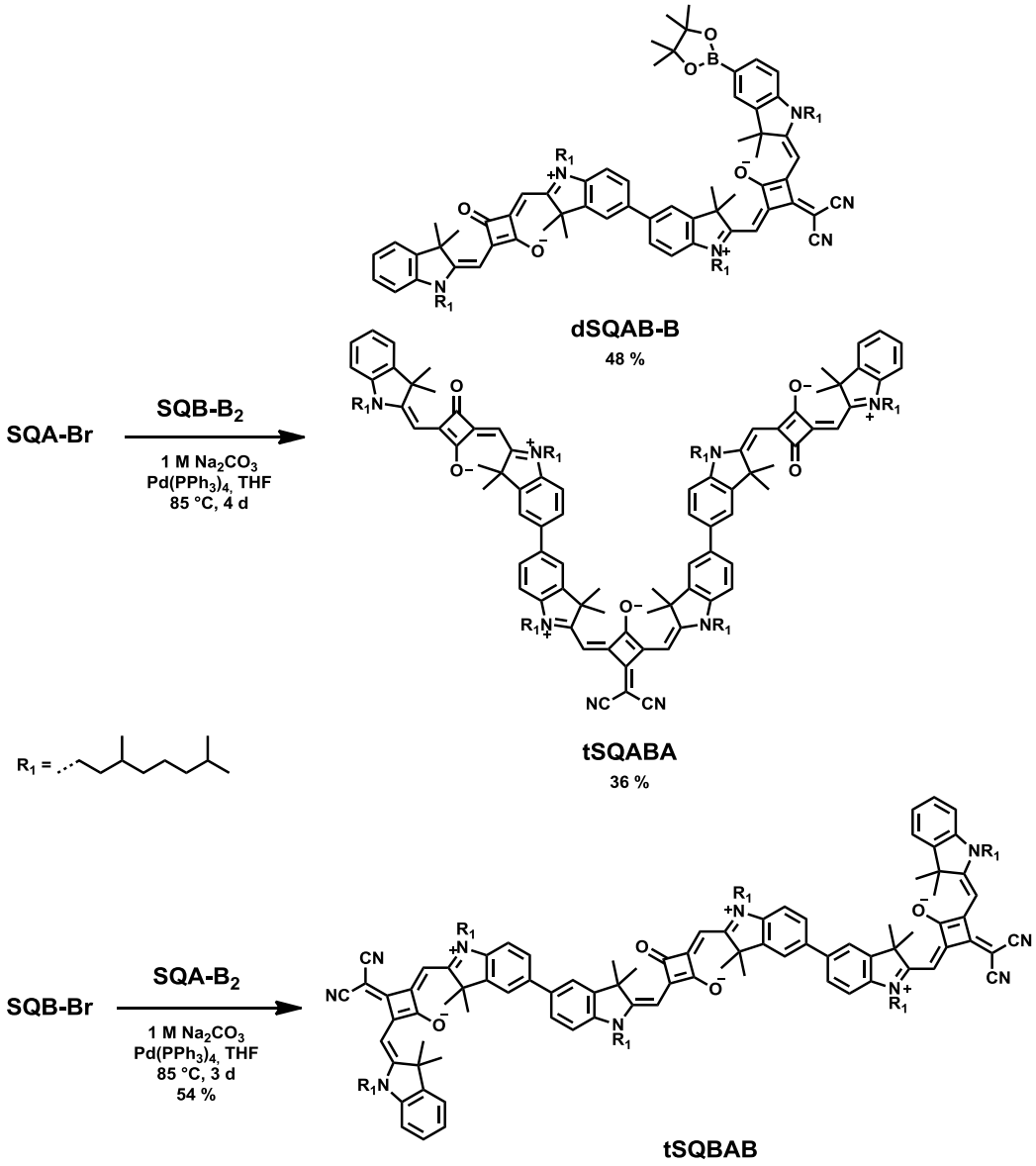

Scheme 30: Synthesis of borylated heterodimer **dSQAB-B** and trimer **tSQABA**, as well as of trimer **tSQBAB**.

The successful synthesis and isolation of the functionalised dimer **dSQAB-B** opened up the possibility to generate a squaraine cascade comprising three different squaraine monomers that are linked according to the energetic position of the respective absorption maxima. Using the standard protocol for Suzuki coupling reactions provided in this work along with a slight excess of the brominated squaraine species **SQC-Br**, the corresponding non-symmetric trimer **tSQABC** was synthesised in good yields of 55 % (Scheme 31). All squaraine oligomers presented in this chapter were subjected to preparative GPC for isolation and purification after short column filtrations.

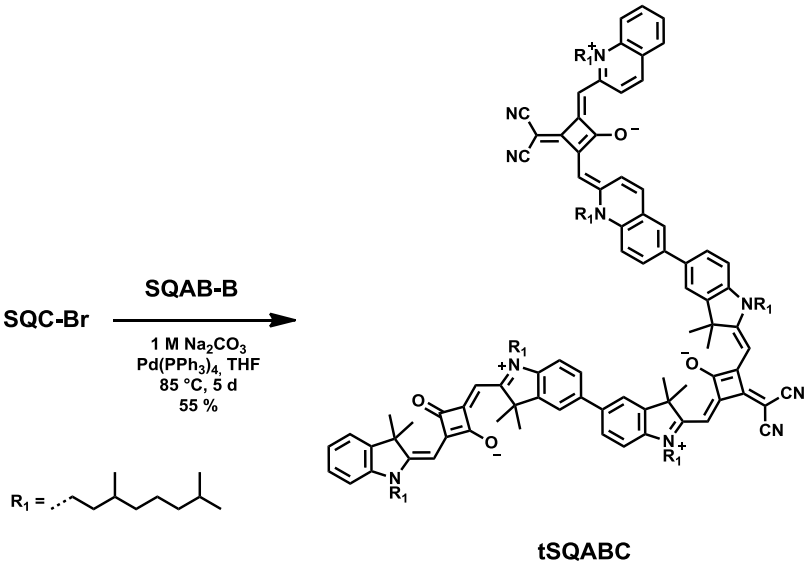

Scheme 31: Synthesis of squaraine heterotrimer **tSQABC** bearing three different squaraine units.

3.6.3 Absorption Spectroscopy

Absorption spectra of the trimers were recorded in toluene and $CHCl_3$. The corresponding spectra are depicted in Figure 59 (**tSQABA**, **tSQBAB**) and in Figure 60 (**tSQABC**). For the sake of comparison, the spectra of the monomers are additionally depicted. The optical data is summarised in Table 15. The spectra are discussed in toluene only, since the spectra in $CHCl_3$ are very similar.

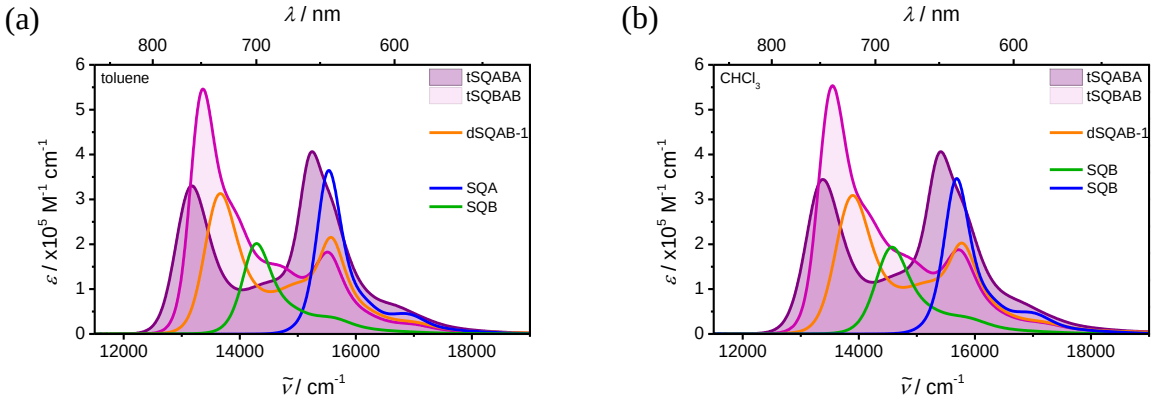

Figure 59: Absorption spectra of squaraine trimers **tSQABA** and **tSQBAB** in (a) toluene and (b) $CHCl_3$, respectively. For comparison purposes, the spectra of the monomers **SQA** and **SQB** as well as of the corresponding dimer **dSQAB-1** are additionally depicted.

According to Figure 59, squaraine trimer **tSQABA** features two intense absorption bands at 13 200 cm^{-1} and 15 200 cm^{-1}. The molar extinction coefficient of the high energy maximum (4.07×10^5 $M^{-1}cm^{-1}$) is higher than that at lower energies (3.30×10^5 $M^{-1}cm^{-1}$). Unlike trimer **tSQBAB**, which also features two maxima (13 400 cm^{-1} and 15 500 cm^{-1}) yet with a

considerably more intense low energy maximum (5.46×10^5 $M^{-1}cm^{-1}$) compared to that at higher energies. (1.83×10^5 $M^{-1}cm^{-1}$). Trimer **tSQABA** shows a red-shift of both maxima in respect to the corresponding monomer absorption peaks, while only the low energy maximum is shifted to lower energies in **tSQBAB**. The high energy maximum at 15 200 cm^{-1} is practically unaffected. This overall drifting apart of electronic transitions is assigned to exciton coupling of localised transition moments, respectively. The squared transition moments of the exciton manifold of the trimers **tSQABA** (377 D^2) and **tSQBAB** (361 D^2) reflect rough additivity from the monomers **SQA** (127 D^2) and **SQB** (92.7 D^2).

With the optical data at hand, the exciton coupling energy J in the heterotrimers can be estimated by rearranging equation (9) to (55):

$$\delta E_{\mathbf{tSQ}} = 2\sqrt{\Delta E^2 + 2J^2} \tag{9}$$

$$J = \sqrt{\frac{\delta E_{\mathbf{tSQ}}{}^2}{8} - \frac{\Delta E^2}{2}} \tag{55}$$

$\delta E_{\mathbf{tSQ}}$ can be approximated from the trimer absorption maxima at lowest and highest energy and $\Delta E = (E_{\mathbf{SQA}} - E_{\mathbf{SQB}})/2$. Thus, the couplings in toluene ($CHCl_3$) in **tSQABA** and **tSQBAB** were calculated to 590 cm^{-1} (610 cm^{-1}) and 630 cm^{-1} (660 cm^{-1}), respectively. The couplings of the trimers are somewhat larger in $CHCl_3$ than in toluene, which was also found for **dSQAB-1** (Table 14). Besides, the couplings in the trimers are smaller than in **dSQAB-1** (740 cm^{-1} and 760 cm^{-1}), however the exciton splittings are larger for the heterotrimers which is in agreement with the prediction of exciton theory.[74,75]

The spectra of **tSQABC** shows a broad band between 11 000 and 18 000 cm^{-1} referring to the exciton manifold with a distinct maximum on the low-energy side at 12 200 cm^{-1}. In contrast to the trimers which have just been discussed, trimer **tSQABC** provides even more peaks in the absorption spectrum, i.e., at 13 400, 13 900, and 15 500 cm^{-1}. The main maximum at 12 200 cm^{-1} bears almost twice the oscillator strength (3.65×10^5 $M^{-1}cm^{-1}$) than the other peaks and is red-shifted compared to that of the monomer **SQC** of about 500 cm^{-1}. As argued above, the shifting of the transitions can be attributed to J-type exciton coupling of localised transition moments, which are assumed to be oriented in a head-to-tail manner. The squared transition moment of **tSQABC** in toluene ($CHCl_3$) was calculated to be 398 D^2 (418 D^2) and is thus somewhat larger than the sum of the squares of the monomers.

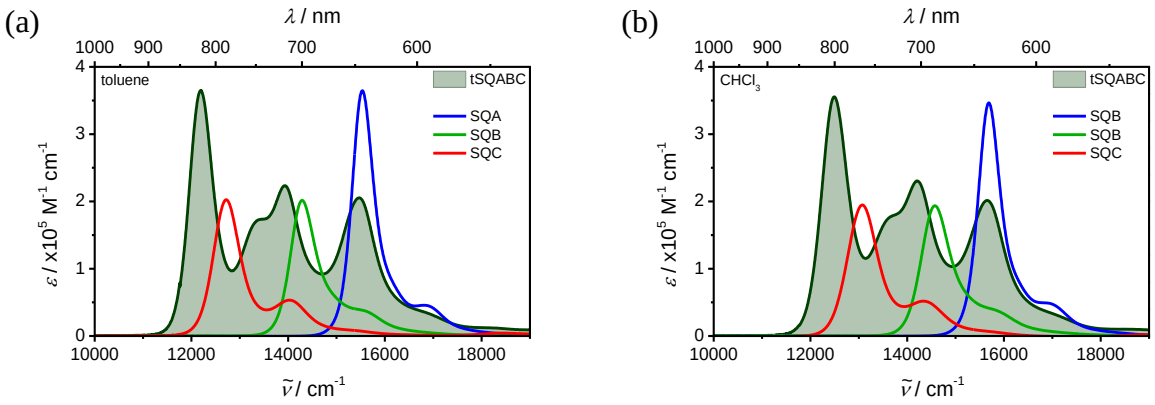

Figure 60: Absorption spectra of squaraine trimer **tSQABC** in (a) toluene and (b) $CHCl_3$. For comparison purposes, the spectra of the monomers **SQA**, **SQB**, and **SQC** are additionally depicted.

In case of **tSQABC**, the corresponding exciton interaction matrix differs from that of **tSQABA** and **tSQBAB** because two different couplings have to be considered now, i.e., the coupling between A and B (J_{AB}), as well as between B and C (J_{BC}). The matrix can be formulated according to equation (8) applying the nearest-neighbour approximation (coupling between A and C is set to zero) and neglecting dispersion between the chromophores in the ground state:[89]

$$\begin{vmatrix} E_A - \varepsilon & J_{AB} & 0 \\ J_{AB} & E_B - \varepsilon & J_{BC} \\ 0 & J_{BC} & E_C - \varepsilon \end{vmatrix} = 0 \qquad (56)$$

Rearranging equation (8) yields

$$(E_A - \varepsilon)(E_B - \varepsilon)(E_C - \varepsilon) - (E_A - \varepsilon){J_{BC}}^2 - (E_C - \varepsilon){J_{AB}}^2 = 0 \qquad (57)$$

where E_A, E_B, E_C and ε are the monomer absorption energies and exciton eigenvalues, respectively. Solving equation (57), one obtains three different eigenvalues for **tSQABC**, The validity of equation (57) was crosschecked by using the absorption data obtained for the trimer, that is, the exciton eigenvalues ε (= $\tilde{\nu}_{abs1}$, $\tilde{\nu}_{abs2}$, $\tilde{\nu}_{abs3}$ in Table 14). In addition, the couplings J_{AB} and J_{BC} in the trimer were approximated by the dimer couplings calculated for **dSQAB-1** and **dSQBC** (Table 14). However, equation (57) does not become zero when inserting the experimental values. This does not disprove the validity of the theory in general, but rather the approximations made for this calculation, e.g., neglecting the coupling between A and C in the trimer and using the couplings in the dimers.

Table 14: Experimental absorption maxima and coupling constants of **SQA**-**SQB**-based heterodimer **dSQAB-1** and of heterotrimers **tSQABA** and **tSQBAB** in $CHCl_3$ and toluene, respectively.

	solvent	$\tilde{\nu}_{abs1}$ / cm^{-1}	$\tilde{\nu}_{abs2}$ / cm^{-1}	$\tilde{\nu}_{abs3}$ / cm^{-1}	$\lvert J \rvert$ / cm^{-1}
dSQAB-1	$CHCl_3$	13 900	15 770	–	760
	toluene	13 670	15 580	–	740
dSQBC-1	$CHCl_3$	12 580	14 600	–	680
	toluene	12 250	14 290	–	650
tSQABA	$CHCl_3$	13 380	15 420	–	610
	toluene	13 180	15 240	–	590
tSQBAB	$CHCl_3$	13 550	15 720	–	660
	toluene	13 360	15 500	–	630
tSQABC	$CHCl_3$	12 490	14 200	15 650	–
	toluene	12 200	13 940	15 470	–

– not determined.

3.6.4 Fluorescence Spectroscopy

Steady-state and time-resolved fluorescence measurements were performed for **tSQABA** and **tSQBAB** in toluene and $CHCl_3$. The spectra are depicted in Figure 61. Due to the extremely week emission properties of **tSQABC**, no fluorescence lifetimes and quantum yields could be acquired. Therefore, the measurements were restricted to steady-state fluorescence emission and excitation spectra which were recorded in toluene only (Figure 62). The optical data of the trimers are presented in Table 15.

Upon excitation in the high energy absorption band, trimer **tSQBAB** exhibits a monomer-type fluorescence in toluene and $CHCl_3$, which is red-shifted compared to the low energy edge of the absorption with a Stokes shift of ca. 200-300 cm^{-1} (Figure 61(c) and (d)). This proves that the fluorescence exclusively occurs from the lowest exciton state. In contrast, the fluorescence spectra of **tSQABA** provide some differences in $CHCl_3$. Beside the monomer-type fluorescence band with a Stokes shift of ca. 300 cm^{-1} originating from the delocalised lowest energy state, the spectra of the trimer **tSQABA** feature an additional fluorescence peak at higher energies at around 15 000 cm^{-1} that strongly overlaps with the absorption (Figure 61(b)). Similar observations have been made earlier in this work for heterodimer **dSQBC** and copolymer **pSQBC** in Chapter 3.4.5.4, respectively.

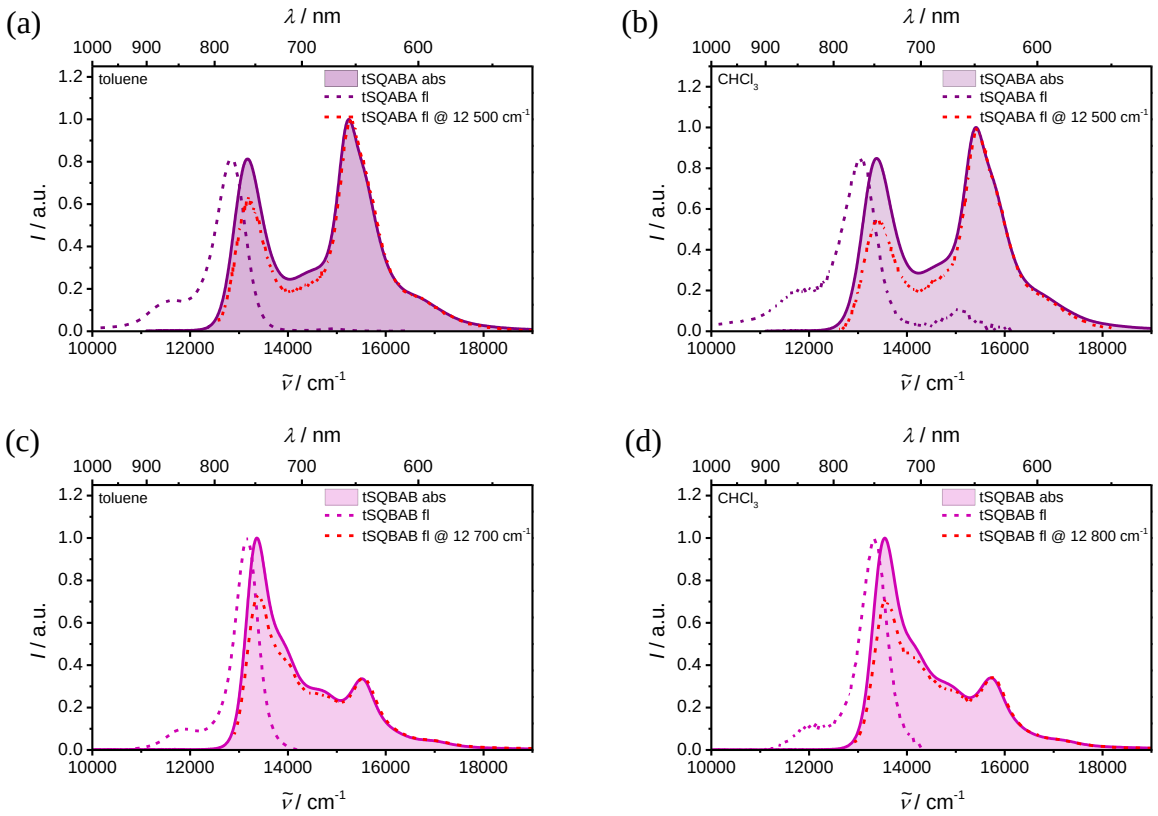

Figure 61: Normalised absorption and fluorescence spectra of squaraine trimers (a)(b) **tSQABA** and (c)(d) **tSQBAB** in toluene and $CHCl_3$, respectively. Excitation was at 17 000 cm^{-1} (**tSQABA**) and 15 700 cm^{-1} (**tSQBAB**).

The fluorescence excitation spectra of the trimers (red dashed curve) in Figure 61 feature a less intense low-energy absorption band and thus do not exactly reproduce the absorption spectra and, respectively. This discrepancy is attributed to self-absorption effects even though highly diluted samples were used for the measurements ($OD_{max} < 0.02$). Similar effects have also been noticed for **pDiPhSQB** in chapter 3.4.3.4.

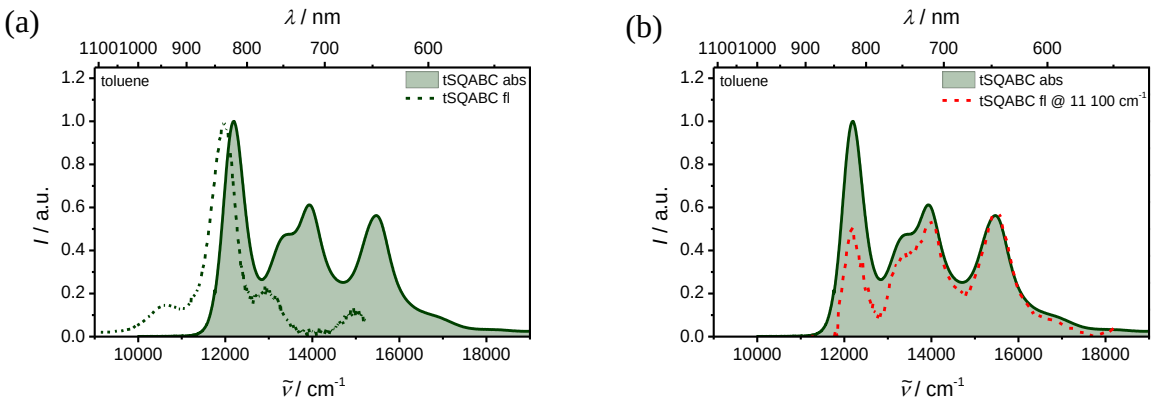

Figure 62: (a) Normalised absorption and fluorescence spectrum of **tSQABC**. Excitation was at 15 500 cm^{-1}. (b) Normalised absorption and fluorescence excitation spectrum of **tSQABC**, fluorescence was probed at 11 100 cm^{-1}.

After excitation into the high energy absorption band at 15 500 cm^{-1}, the fluorescence emission spectrum of **tSQABC** in toluene shows a red-shifted monomer-type fluorescence with two additional emission peaks at higher energies at 12 900 cm^{-1} and 15 000 cm^{-1} stemming from localised higher states. Furthermore, recent studies by Ceymann on star-like squaraine heterotrimers also showed analogous spectral features involving emission from localised higher states. Here, it was found that introduction of **SQA** and **SQB** monomers into the star-like framework causes a population of localised states that thwart the delocalised states generated by exciton coupling. An explanation was given that static disorder or dynamic fluctuations rather than different conformers may evoke localisation of excitation, which could possibly account for the spectral features observed in the present cases, too.[69]

Fluorescence lifetimes were measured by TCSPC and mostly gave biexponential decays. For the sake of comparison, the average fluorescence lifetime was calculated for the relevant cases. Accordingly, lifetimes of 1.89 ns (220 ps) and 2.05 ns (280 ps) were obtained for **tSQABA** and **tSQBAB** in toluene ($CHCl_3$), respectively. The fluorescence quantum yields of the trimers are very similar and correlate with the acquired lifetimes. Thus, low quantum yields of 0.10 and 0.08 were obtained in $CHCl_3$, while high quantum yields of 0.73 and 0.74 were measured in toluene. The fluorescence data acquired are quite similar to those of the dimer **dSQAB-1** with exception of its significantly longer lifetime in $CHCl_3$ which is 1.82 ns.

As already outlined above, the poor emission properties of squaraine cascade **tSQABC** decisively hampered the measurement of fluorescent quantum yields as well as of lifetimes. Given the fact that squaraine monomer **SQC** is a very weak emitter, the fluorescence quantum yield and lifetime of the cascade are estimated to be even lower and more short-lived, i.e., < 1 % and < 40 ps, respectively.

3.6.5 Conclusion

Suzuki coupling methodology allowed the sequential arrangement of squaraine monomers to three linearly linked squaraine trimers providing on the one hand two different sequences of **SQA**-**SQB** conjugates, and on the other hand a cascade-type architecture being conceived of three different monomers **SQA**, **SQB**, and **SQC**.

The trimers with alternating **SQA**-**SQB** monomer sequences showed both two distinct peak maxima in the absorption, yet with an appreciable difference. In **tSQABA**, the band at higher energies is slightly more intense than the one at lower energies. In contrast, **tSQBAB** featured a low energy maximum bearing considerably more oscillator strength than the high energy

peak. Besides, the spectra of **tSQABC** exhibited several bands, of which the highest in intensity was located at lower energies. In general, all squaraine trimers presented in this section shared the common feature of a red-shifted low energy absorption band compared to the respective monomers which was explained to be caused by J-type exciton coupling of localised transition moments.

The steady-state fluorescence emission spectra of **tSQABA** and **tSQABC** provided some striking features. While trimer **tSQBAB** solely displayed emission from the delocalised lowest exciton state, the other trimers both showed additional emission peaks spotted at higher energies. This was explained to be caused by an incomplete intraband energy relaxation process within the exciton manifold resulting in a localisation of excitation. In addition, the fluorescence excitation spectra of all trimers did not exactly reproduce the respective absorption spectra. These findings were attributed to self-absorption effects.

Table 15: Absorption maxima, extinction coefficients, transition moments, fluorescence maxima, fluorescence quantum yields, fluorescence lifetimes and expectation values of fluorescence lifetimes of squaraine monomers **SQA**, **SQB**, and **SQC**, as well as of squaraine heterotrimers **tSQABA**, **tSQBAB**, and **tSQABC** in $CHCl_3$ and toluene.

	solvent	$\tilde{\nu}_{abs}$ / cm^{-1} (nm)	ε_{max} / $M^{-1}cm^{-1}$	μ_{eg}^2 / D^2	$\tilde{\nu}_{em}$ / cm^{-1} (nm)	Φ_{fl} / –	τ_{fl} [a] / ns	$\bar{\tau}_{fl}$ / ns
SQA	$CHCl_3$	15 700 (637)	3.45×10^5	129	15 500 (645)	0.51	0.26 (0.40) 1.47 (0.60)	1.34
	toluene	15 500 (645)	3.64×10^5	127	15 400 (649)	0.62	0.25 (0.09) 1.71 (0.91)	1.69
SQB	$CHCl_3$	14 600 (685)	1.96×10^5	98.6	14 200 (704)	0.55	2.40	2.40
	toluene	14 300 (699)	2.02×10^5	92.7	14 000 (714)	0.75	3.45	3.45
SQC	$CHCl_3$	13 100 (763)	1.95×10^5	115	12 700 (787)	–	< 0.04	< 0.04
	toluene	12 700 (787)	2.03×10^5	111	12 500 (800)	–	0.04	0.04
dSQAB-1	$CHCl_3$	13 900 (719)	3.09×10^5	261	13 600 (735)	0.05	1.82	1.82
	toluene	13 700 (730)	3.13×10^5	248	13 400 (746)	0.69	1.80 (0.51) 2.41 (0.49)	2.14
tSQABA	$CHCl_3$	13 400 (746)	3.44×10^5	420	13 100 (763)	0.10	0.22	0.22
	toluene	13 200 (758)	3.30×10^5	377	12 900 (775)	0.73	1.88 (0.99) 2.84 (0.01)	1.89
tSQBAB	$CHCl_3$	13 600 (735)	5.54×10^5	405	13 300 (752)	0.08	0.24 (0.99) 1.18 (0.01)	0.28
	toluene	13 400 (746)	5.46×10^5	361	13 200 (758)	0.74	1.82 (0.79) 2.64 (0.21)	2.05
tSQABC	$CHCl_3$	12 500 (800)	3.55×10^5	418	–	–	–	–
	toluene	12 200 (820)	3.65×10^5	398	12 000 (833)	–	–	–

– not determined. [a](Multi-)exponential fit of fluorescence decay measured by TSCPC, excitation at 15 240 cm^{-1} (656 nm). Amplitudes are given in brackets.

3.7 Star-Shaped Hexasquarainyl Benzenes[XII]

3.7.1 Introduction

This chapter follows recent studies on squaraine trimers that were covalently linked to a central benzene or nitrogen core unit.[69,93] The resulting star-like arrangement of squaraine chromophores differs from the linear linkage motif used so far in this thesis. Similar to the linear congeners, the absorption features of the star-shaped trimers such as spectral broadening and red-shifting of absorption bands were discussed in terms of exciton coupling of localised transition moments. Appreciating the structure of **tSQA-benz** in Figure 63 in which the squaraine tentacles undergo rather weak exciton coupling due to the *meta*-substitution pattern, a multichromophoric system was envisioned bearing the maximal number of six squaraine chromophores at the benzene core with the goal to enhance the mutual electronic communication.

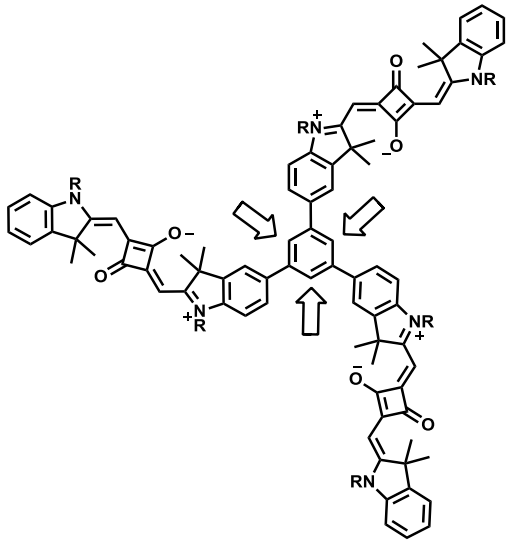

Figure 63: Chemical structure of squaraine trimer **tSQA-benz** synthesised by Ceymann.[93] Arrows indicate free positions for additional squaraine chromophores.

The most elegant way to synthesise such a star-shaped hexaarylbenzene with six squaraine chromophores (= hexasquarainyl benzene) constitutes the dicobaltoctacarbonyl catalysed cyclotrimerisation reaction of an appropriate tolan derivative. In this respect, the tolan squaraine dimers **dSQA-2** and **dSQA-5**, which were already described in Chapter 3.5.2, offer themselves as ideal candidates for their use in the cyclotrimerisation reaction while the *cisoid*

[XII] Manuscript in preparation: *Self-Assembly of a Star-Shaped Squaraine Dye in Well-defined Dimeric Aggregates*, Maximilian H. Schreck, Merle I. S. Röhr, Timothy Clark, Vladimir Stepanenko, Frank Würthner, Christoph Lambert.

analogue **dSQB-2** might be more prone to steric interference of adjacent squaraine chromophores because of the C_{2v} configuration.

3.7.2 Synthesis

The cyclotrimerisation reaction of the two tolan squaraine dimers **dSQA-2** and **dSQA-5** was carried out under inert atmosphere in deaerated 1,4-dioxane at 120 °C overnight according to Scheme 32. The crude products were isolated and purified by flash chromatography followed by subsequent preparative GPC ($CHCl_3$) and precipitation from *n*-hexane. The corresponding hexasquarainyl benzenes were synthesised in good yields of 50 and 53 % yields, respectively.

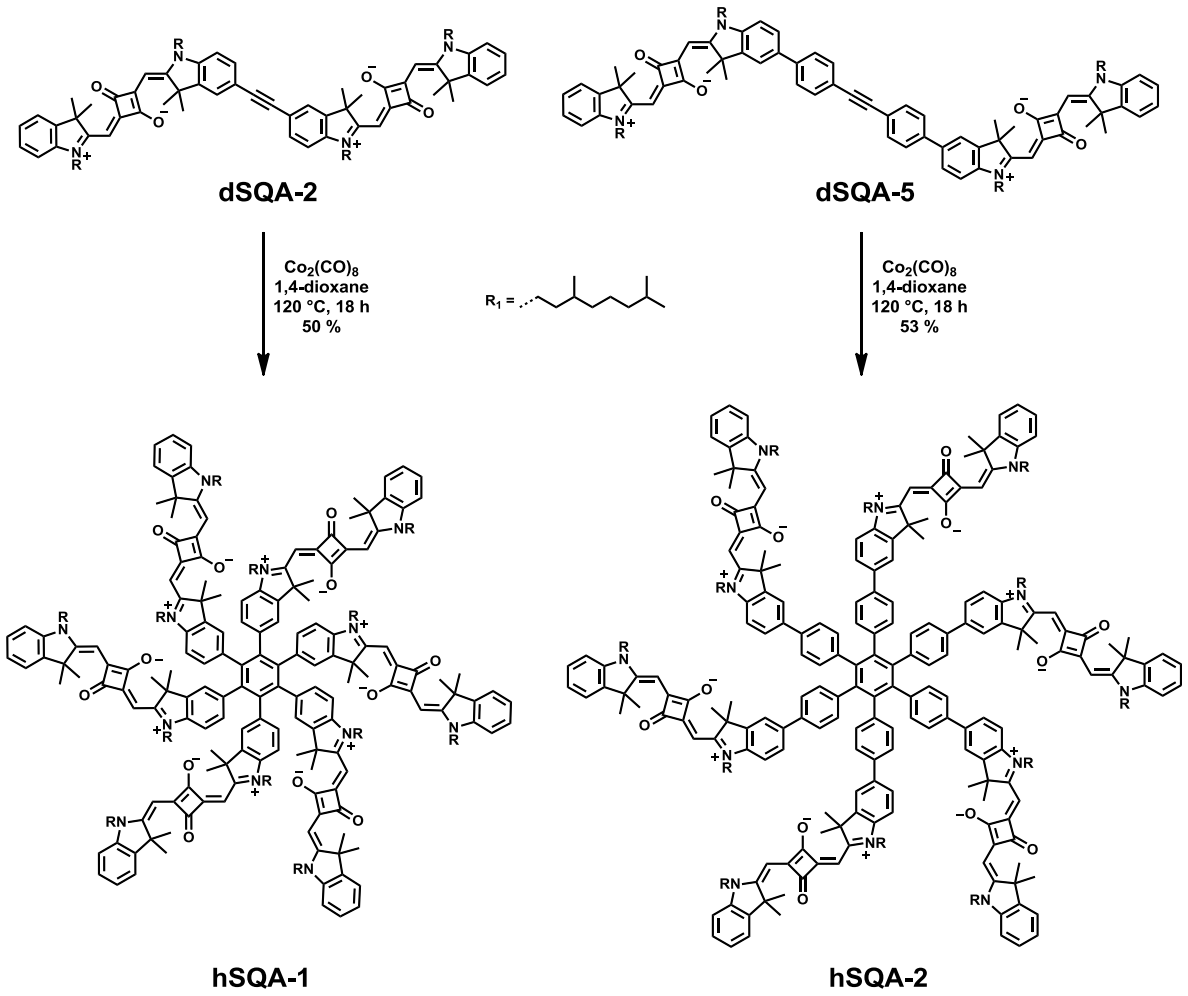

Scheme 32: Synthesis of hexasquarainyl benzenes **hSQA-1** and **hSQA-2**.

At first glance, the structures of the hexasquarainyl benzenes appear rather complex, therefore smaller reference compounds were synthesised being decorated with two squaraine tentacles only. Following the standard protocol for Suzuki coupling reactions, the 1,2-disubstitued

benzenes **dSQA-6** and **dSQA-7** were synthesised in 62 and 17 % yields (Scheme 33) using the borylated squaraine **SQA-B** and the respective dibrominated benzene derivative. In case of **dSQA-7**, the dibrominated substrate **HAB-Br$_2$** needed to be prepared from 1,2-bis(4-bromophenyl)ethyne and 2,3,4,5-tetraphenylcyclopenta-2,4-dienone in a Diels-Alder cycloaddition reaction, which was performed in high-boiling Ph_2O at high temperatures.

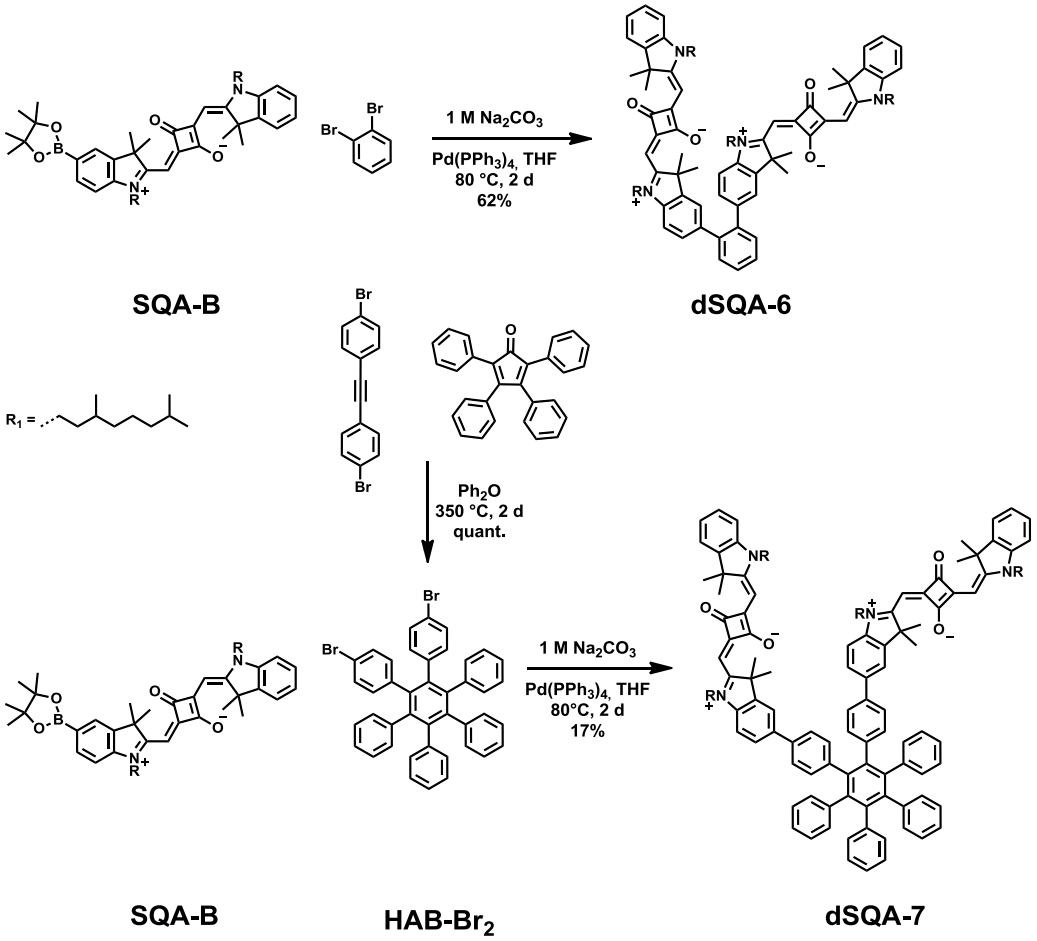

Scheme 33: Synthesis of reference dyes **dSQA-6** and **dSQA-7**.

3.7.3 Absorption Spectroscopy

Steady-state absorption spectroscopy was performed for monomer **SQA** and model dyes **dSQA-6** and **dSQA-7**, as well as for star-shaped hexasquarainyl benzenes **hSQA-1** and **hSQA-2**. The spectra are shown in Figure 64.

In chloroform, the hexasquarainyl benzenes **hSQA-1** and **hSQA-2** show a sharp and intense main absorption band at 15 300 cm^{-1}. While the smaller hexasquarainyl benzene displays a second maximum at 17 100 cm^{-1} along with two additional shoulders, one at the lower energy side at 14 900 cm^{-1} and the other at higher energies at 16 200 cm^{-1}, the larger hexasquarainyl

benzene solely exhibits one blue-shifted shoulder at 16 500 cm^{-1}, most likely originating from vibronic progression.

The absorption spectra of the model dyes **dSQA-6** and **dSQA-7** reveal some distinct differences to each other, as well as to their corresponding hexasquarainyl benzenes. Squaraine dye **dSQA-6** possesses one main absorption band at 15 000 cm^{-1} and two further maxima at 15 800 cm^{-1} and 16 400 cm^{-1}. In contrast, reference dye **dSQA-7** only exhibits a broad main absorption band around 15 400 cm^{-1} and a shoulder located at higher energies. As the result of exciton coupling, the main absorption band of both model dyes and hexasquarainyl benzenes are broadened and red-shifted in $CHCl_3$ compared to their monomer unit **SQA**. The squared transition moments of **SQA**, **dSQA-6**, **dSQA-7**, **hSQA-1** and **hSQA-2** are 129, 266, 241, 792 and 848 D^2, respectively. For the model dyes and hexasquarainyl benzenes, the squared transition moments of the exciton manifold reflect almost additivity from **SQA** which is in agreement with the Thomas-Reiche-Kuhn sum rule, meaning that no other transitions are involved except those caused by exciton coupling.[151]

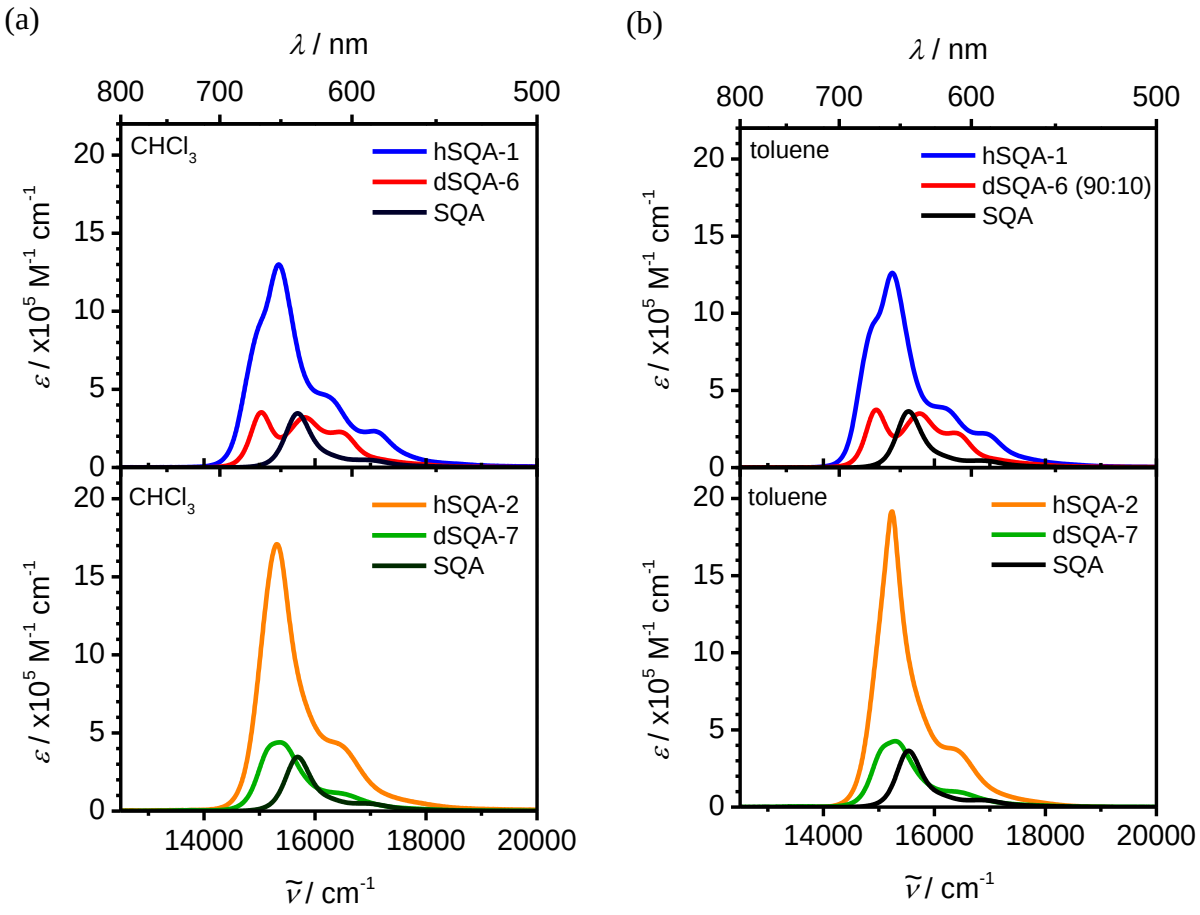

Figure 64: Absorption spectra of squaraine dyes **SQA**, **dSQA-6**, **dSQA-7**, **hSQA-6**, and **hSQA-2** in (a) $CHCl_3$ and (b) toluene. Absorption of **dSQA-6** was recorded in the mixture toluene/$CHCl_3$ = 90:10 (*v*:*v*) due to poor solubility.

Furthermore, the absorption behaviour of these dyes was studied in the less polar solvent toluene. All squaraine chromophores exhibit a similar band shape as monitored in $CHCl_3$, except for the smaller **hSQA-1**. Here, upon dissolving the solid compound, a dark blue colour was noted that gradually turned light blue. In order to gain more insight into these time-dependent colour changes, a series of absorption spectra of a freshly prepared solution of **hSQA-1** was recorded after fixed time intervals at 293 K. The results are displayed in Figure 65(a). The initially observed absorption bands at 17 900 cm^{-1} and 16 100 cm^{-1} gradually decrease, while the band at the lower energy side at 15 200 cm^{-1} rises in intensity. The pronounced spectral changes share a well-defined isosbestic point at 15 800 cm^{-1}, indicating a dynamic process between only two distinct species. The final absorption spectrum (shown in red) strongly resembles that recorded in $CHCl_3$, which is assumed to be that of the monomeric squaraine dye **hSQA-1**.

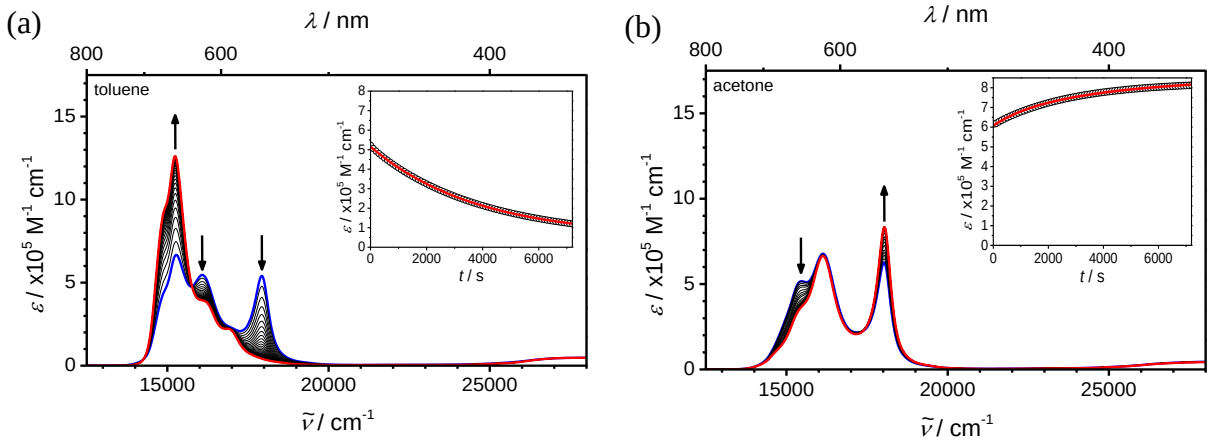

Figure 65: Time-dependent absorption spectra of **hSQA-1** in (b) toluene and (d) acetone (1.49×10^{-6} M) at 293 K. Initial and final curve is given in blue and red, respectively. Insets: Plot of molar absorptivity versus time of the aggregate band at 17 900 cm^{-1} in toluene and at 18 000 cm^{-1} in acetone (0-7200 s). Data points are indicated as open circles and the fitting curves according to equations (63) and (68) (Appendix Chapter 9.2.5) are drawn in red.

The same experiment was repeated for **hSQA-1** in the polar solvent acetone Figure 65(b). Here, the spectral changes of the absorption bands at 15 500 cm^{-1} and 18 000 cm^{-1}, which are comparable to those at 15 200 cm^{-1} and 17 900 cm^{-1} in toluene, show the opposite trend. Whereas the band at the lower-energy side significantly decreases with time, that located at higher energies grows concomitantly. The intermediate band at 16 100 cm^{-1} is hardly affected by this dynamic transformation. Remarkably, the final spectrum in acetone lacks the typical long-wavelength squaraine absorption and displays a very unusual blue-shifted, rather narrow absorption band with a full width at half maximum (FWHM) of only ca. 560 cm^{-1}. For comparison, FWHM of **hSQA-1** in acetone is ca. 600 cm^{-1}. The appearance of a

hypsochromic band points towards H-type aggregation of **hSQA-1**, as has been observed for other squaraine dyes.[95,108,109,126,135] On the other hand, the small band width of the H-type band suggests well-ordered aggregates. Such narrow bands have frequently been observed for H-type aggregate bands and may be caused by so-called exchange narrowing which is due to a delocalised exciton state.[29,112,179-183] Furthermore, because of the latter findings, the dynamic process observed in toluene can reasonably be attributed to a dissociation process of aggregates into monomers. Interestingly, kinetic experiments in acetone and toluene both indicate that these processes start from a mixture of monomer and aggregate.

3.7.4 NMR Studies

The dynamic self-assembly of squaraine **hSQA-1** is directly linked to the question of the corresponding aggregate structure. However, the structure of the pure monomer **hSQA-1** must first be dehtermined. Because of flexible biaryl-axes between the inner benzene core unit and the squaraine moieties, the six squaraine tentacles are able to point either above or below the central benzene plane, which may consequently lead to eight possible conformers with regard to the position of the squaraine chromophore units (up and down) and independently of the specific dihedral angle.

In order to elucidate the structural situation in the **hSQA-1** monomer and aggregate, ^{1}H-NMR spectra of **hSQA-1** were recorded at 295 K in low viscosity solvents CD_2Cl_2 and in highly viscous 1,1,2,2-tetrachloroethane-d_2 (TCE-d_2). TCE-d_2 is much more nonpolar than $CHCl_3$, in which the optical spectra were recorded, however, it can be seen from the absorption spectra (Appendix, Figure 82) that aggregation is also suppressed in TCE-d_2. A significant difference between the NMR spectra in the two solvents is shown in Figure 66. The spectrum obtained in CD_2Cl_2 exhibits sharp and resolved signals with complex higher-order splitting patterns. In contrast, the spectrum recorded in TCE-d_2 exhibits spectral broadening and resembles the coalescence regime, most likely because the higher solvent viscosity leads to a slower interconversion of the conformers. These observations indicate dynamic exchange processes within the monomeric **hSQA-1**, probably caused by the existence of different conformers. In addition, ^{1}H-^{13}C HSQC measurements (see Appendix, Figure 88) reveal slightly broadened ^{13}C-signals for each complex set of proton signals. This would agree with the presence of very similar conformers, yielding almost the same chemical shifts for corresponding ^{13}C signals.

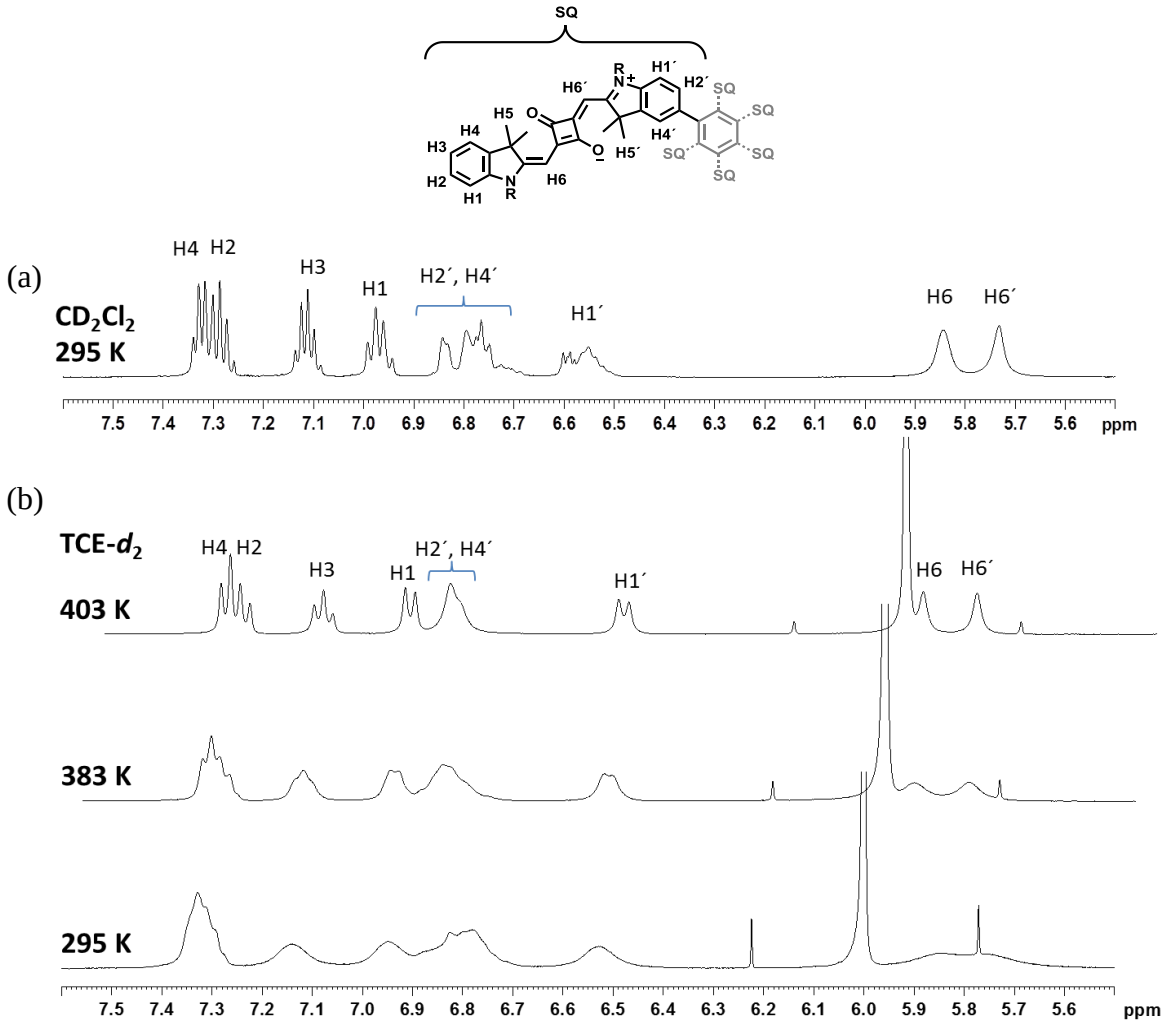

Figure 66: (a) ^{1}H-NMR spectrum of **hSQA-1** in CD_2Cl_2 at 295 K and (b) temperature-dependent ^{1}H-NMR spectra of **hSQA-1** in 1,1,2,2-tetrachloroethane-d_2 at a concentration of ~ 3×10^{-4} M, respectively. The spectra at 295 K proved to be the same before and after heating. Assignments of significant protons refer to the aromatic region only (7.5-5.5 ppm).

Moreover, the influence of temperature on the exchange rate was studied by variable-temperature NMR measurements in TCE-d_2 from 295 K to 403 K (Figure 66(b)). Noteworthy, the spectrum at 295 K before and after heating turned out to be the same, clearly indicating the reversibility of the process. At 403 K, due to the fast exchange at elevated temperatures, a single, averaged data set was obtained with sharp and intense signals that resemble those in CD_2Cl_2 at 295 K very closely. The temperature dependence of the exchange rate clearly corroborates the dynamic of this process. At 295 K, the signals coalesce and become very broad and remained unchanged despite further cooling. Therefore the regime of slow exchange in TCE-d_2 was not reached. However, measurements in chlorinated solvents suggest the presence of at least two different conformers that cannot interconvert rapidly on the NMR time scale at 295 K.

In order to unravel the aggregate structure of **hSQA-1** in acetone, a series of ^{1}H-NMR spectra at temperatures from 219-323 K were recorded. These are shown in Figure 67(a). Similarly to the observations in TCE-d_2, the broad and unresolved spectra at low temperatures considerably sharpen upon heating. Consequently, the spectrum at the highest possible temperature (327 K) was chosen for further structural evaluations, even though it still suffers from rather broad and overlapping signals. While the monomer spectrum in CD_2Cl_2 yields seven aromatic protons (7.4-6.4 ppm) per squaraine tentacle, the spectrum recorded in acetone exhibits a double set of signals. Considering symmetry, it follows that the aggregate structure has to be composed of two different **hSQA-1** monomers. This assumption is further corroborated by the fact that an overall number of 14 aromatic CH-signals are observed in the ^{13}C-NMR spectrum (136-104 ppm, Appendix, Figure 90). Thus, each ^{13}C-signal splits into a set of two signals on going from the monomer to the fully aggregated state. For further structural assignments, we performed 2D-NMR experiments (^{1}H-^{1}H COSY, ^{1}H-^{13}C HSQC), which are shown in the Appendix, Figure 91 and Figure 92.

Because of the flexible biaryl axes and thus different conformer possibilities, the ^{1}H-NMR spectrum appears to be consistent with an unsymmetrical structure at first glance. Nonetheless, the small FWHM of the blue-shifted absorption peak in the UV/vis spectra of **hSQA-1** in acetone is highly suggestive of ordered, relatively rigid and uniform aggregates. Rotating-frame Overhauser effect (ROESY) NMR experiments in acetone-d_6 were performed which provide information about proximate protons coupling through space within the aggregate. However, the spectra only exhibited cross-signals of adjacent protons within one tentacle, and thus did not help elucidate the aggregate structure. Furthermore, the size of **hSQA-1** aggregates was estimated in acetone at a concentration of 3×10^{-4} M by means of diffusion ordered (DOSY) NMR at 293 K. A hydrodynamic radius of 1.64 nm was determined based on the acquired diffusion coefficients using the Stokes-Einstein equation (61) (Appendix, Chapter 9.2.2). For comparison, a radius of 1.43 nm was measured for pure monomeric **hSQA-1** in CD_2Cl_2. From these radii, a volume ratio of 1.5:1 for the aggregate in acetone-d_6 vs. monomer in CD_2Cl_2 was deduced which appears reasonable, considering a dimer structure of two stacking **hSQA-1** with all six squaraine tentacles of one monomer pointing in the same direction. From this point of view, the picture of stacked **hSQA-1** should indeed possess less than twice the volume of a monomer and is in accordance with the observation made by NMR, which reveals two sets of signals caused by two slightly different **hSQA-1**.

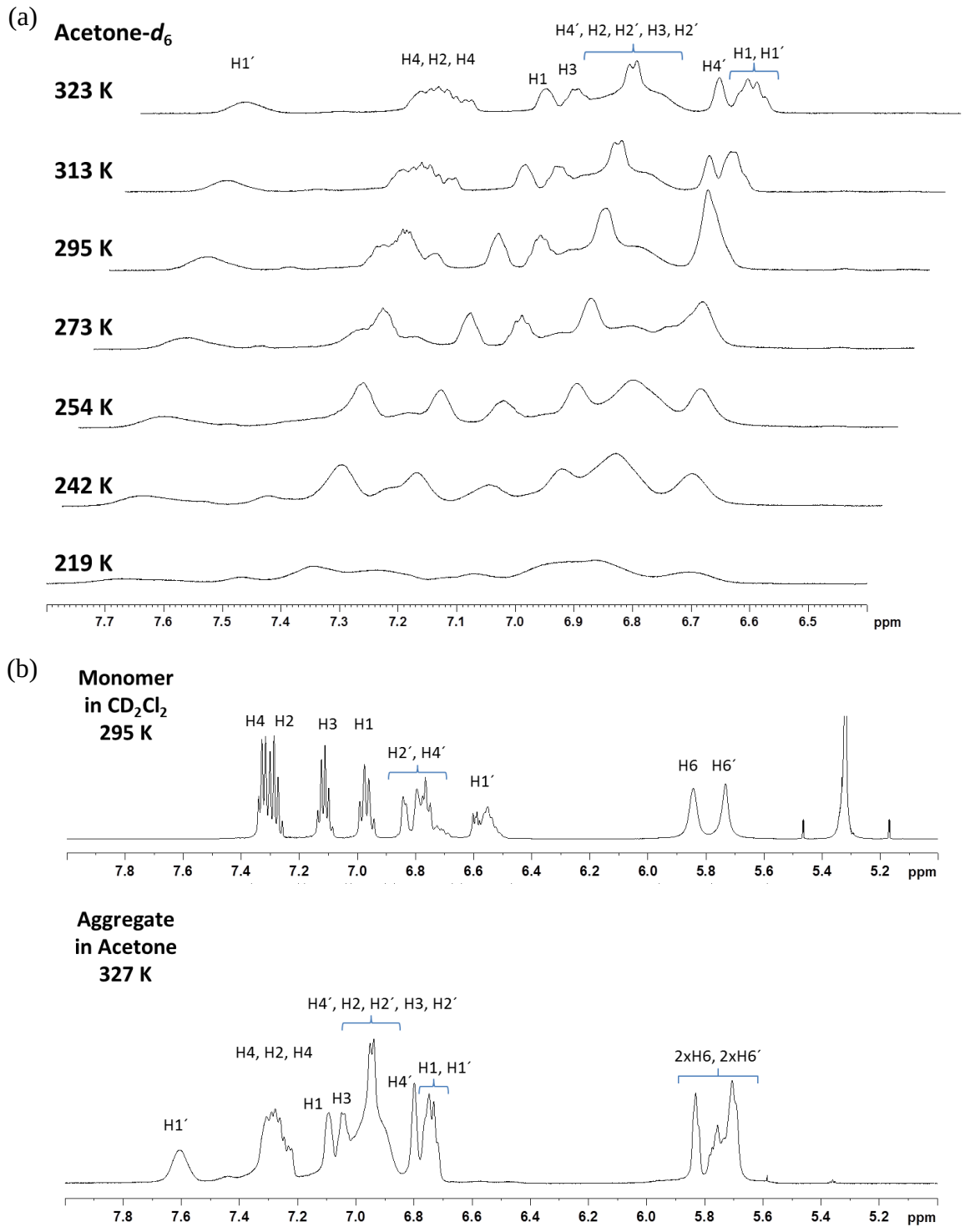

Figure 67: (a) Temperature-dependent 600 MHz ^{1}H-NMR spectra of **hSQA-1** at $c = 3\times10^{-4}$ M in acetone-d_6. (b) ^{1}H-NMR spectra of **hSQA-1** in CD_2Cl_2 and acetone-d_6 at $c = 3\times10^{-4}$ M, respectively.

At this point, it has to be mentioned that **dSQA-7** and **hSQA-2** are also prone to self-association in acetone. However, the NMR-spectra of both compounds in the aggregated state provide an excessive number of signals with complex splitting patterns that hampers proper and accurate assignments. Further structural examinations of these two squaraine dyes will be

carried out through other experimental techniques (below). Nevertheless, in order to evaluate the aggregate size in solution of **hSQA-2**, DOSY NMR measurements were carried out in acetone at a dye concentration of about 3×10^{-4} M similarly to **hSQA-1**. Analysis of the DOSY data revealed a hydrodynamic radius of 2.06 nm. In contrast, a radius of 1.73 nm was obtained in CD_2Cl_2. This equals a volume ration of 1.7:1 for the aggregate in acetone-d_6 vs. monomer in CD_2Cl_2, reflecting similar findings as for **hSQA-1** (1.5:1). Consequently, DOSY NMR experiments also confirm the absence of assemblies larger than dimers of **hSQA-2**.

3.7.5 Atomic Force Microscopy Studies[XIII]

To gain a deeper insight into the morphology and size of hexasquarainyl benzene aggregates in the solid state, Atomic Force Microscopy (AFM) experiments were performed. As the hydrodynamic radii acquired from DOSY NMR measurements yield comparable values for **hSQA-1** and **hSQA-2** aggregates, the measurements were carried out for **hSQA-1** in a representative way. The results are presented in Figure 68.

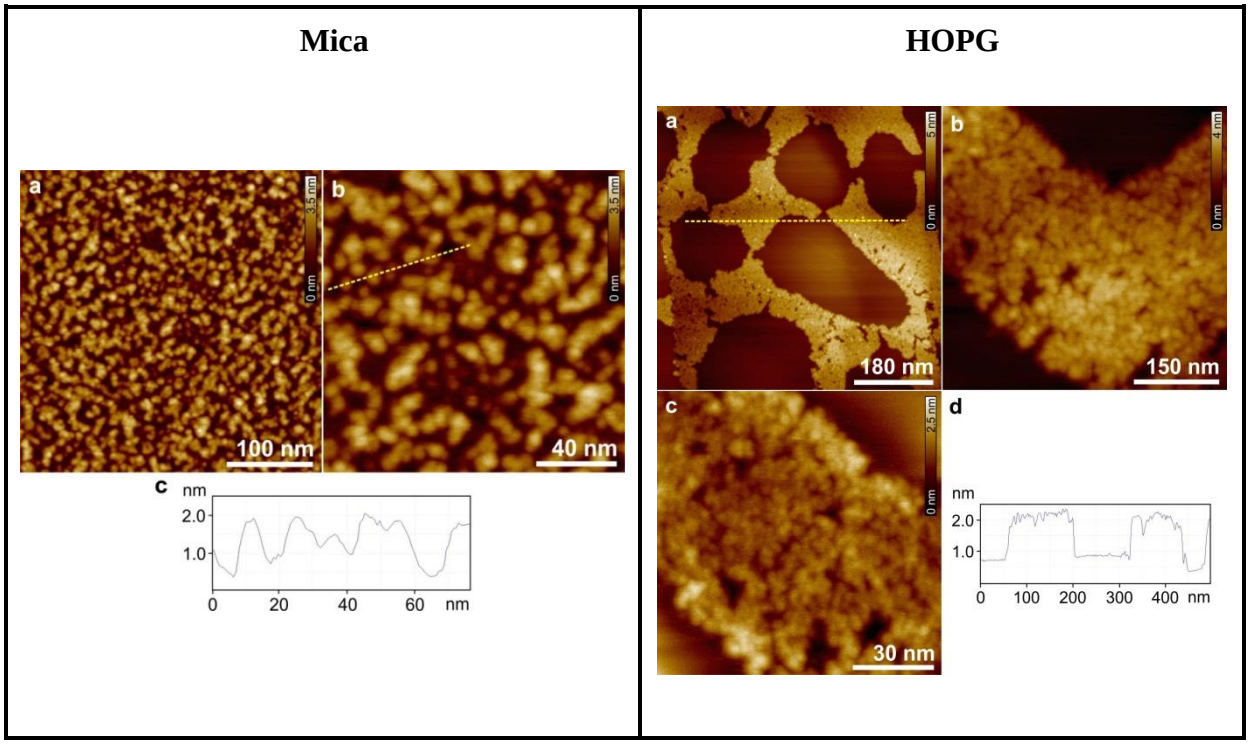

Figure 68: Mica: Height AFM images of sample **hSQA-1** prepared by spin-coating a MCH solution of the dye (3×10^{-4} M) onto mica. *Z* scale is 3.5 nm. Image (c) shows the cross-section analysis from the yellow dashed line in image (b). **HOPG**: Height AFM images of sample **hSQA-1** prepared by spin-coating a MCH solution of the dye onto HOPG. *Z* scale is 5 nm (a), 4 nm (b) and 2.5 nm (c). Image (d) shows the cross-section analysis from the yellow dashed line in image (a).

[XIII] AFM-Measurements and analysis were performed by Dr. Vladimir Stepanenko

The samples were prepared by spin-coating a methylcyclohexane (MCH) solution of **hSQA-1** onto mica and highly oriented pyrolytic graphite (HOPG). It is noteworthy that **hSQA-1** self-assembles in MCH analogously to acetone and gave very similar absorption spectral features (Appendix, Figure 84). MCH is considered more suitable for AFM measurements due to its lower vapour pressure. Accordingly, the thin films on hydrophilic and negatively charged mica surface consisted of small, round nanoparticles with an average diameter of 3.5±0.3 nm. The height of the particles could be measured to be 1.42-1.46 nm. Furthermore, the thin films obtained on hydrophobic HOPG surface also showed small, round nanoparticles with an average diameter of 3.0±0.3 nm with a height of 1.46-1.56 nm. For each measurement, a tip-broadening effect was taken into account.

The results obtained on both surfaces show practically no deviation. Thus, the nanoparticles observed are supposed to consist of a similar structure. Consequently, the results obtained in the solid state clearly substantiate the results obtained in solution by DOSY NMR and UV/vis absorption measurements, indicating no larger aggregates than dimeric species for **hSQA-1**. It is highly likely that **hSQA-2** behaves the same way.

3.7.6 Computations[XIV]

As will be shown later, the absorption features of **dSQA-7** and **hSQA-2** in the aggregated state are located energetically very close to the monomer features which severely hamper structural elucidation via theoretical calculations and computations. In the following, all theoretical evaluations were carried out for **hSQA-1** only since the spectral signatures of aggregate and monomer are clearly separated due to their large splitting.

The optical spectroscopic features of a monomeric and dimeric **hSQA-1** are encoded in the mutual orientation of the squaraine tentacles and, consequently, their state energies and transition moments. This relative orientation influences the intramolecular exciton coupling and thereby the optical spectra.[74,75] A comparison of computed and experimental absorption spectra helps elucidate the dimer structure further.

The geometries of both the monomeric species and dimeric aggregates were optimized using the self-consistent charge-density-functional tight binding (SCC-DFTB) methodology and the 3-ob-freq-1-2 parameter set,[184-187] as implemented in the ADF2017/DFTB Package[188] along with Grimme's D3 dispersion correction with Becke-Johnson damping (see also Appendix 9.2.4).[189] Simulations of the absorption spectra have been carried out using the lc-TDDFTB

[XIV] Computations and calculations were performed by Dr. Merle I.S. Röhr.

method[190] as implemented in the DFTBaby program package[191] which has proven to give good results in the description of the optical properties of squaraine oligomers.[73]

Two starting configurations were considered for the monomers out of the eight possible conformers with respect to the position of the squaraine tentacles (up or down relative to the central benzene ring): i) a structure in which all six squaraine units exhibit the same orientation with respect to the central benzene core unit ("all-up" **hSQA-1-1**) and ii) a structure with alternating orientations of the six squaraine chromophores relative to the central benzene ("up-down" **hSQA-1-2**). As initial structures for the dimer aggregates, three scenarios were considerd: a "bowl-like" aggregate consisting of two stacked **hSQA-1-1**, a "folded hands" formed by two **hSQA-1-1** with interdigitating squaraine "fingers", and a "mixed"-dimer consisting of two **hSQA-1-2** monomers with alternating squaraines up and down.

(a) **hSQA-1-1** with Dsp. (b) **hSQA-1-1** w/o Dsp.

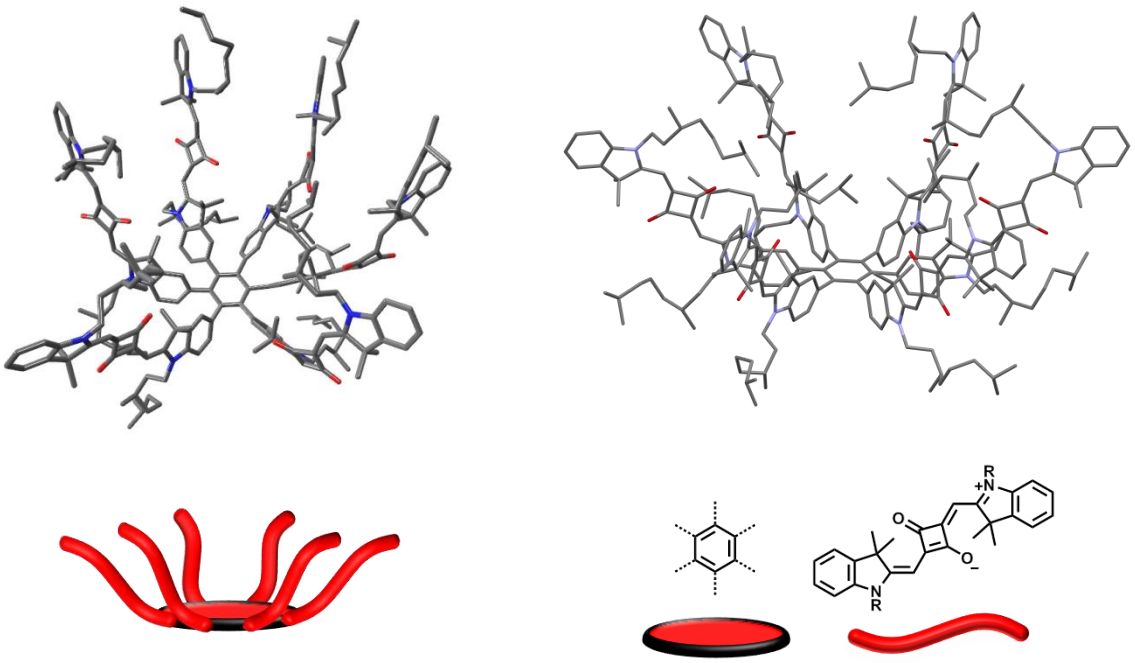

Figure 69: Geometry-optimised monomeric structures of **hSQA-1-1** ("all-up") isomer (a) with and (b) without dispersion correction, and schematic illustration. The **hSQA-1-2** ("up-down") structures are shown in the Appendix Figure 85.

The resulting DFTB optimised structures are shown in detail in the Appendix (Table 20). For the monomers, the **hSQA-1-1** isomer ("all-up") was found to be slightly more stable than **hSQA-1-2** ("up-down") (+0.2 eV). In the **hSQA-1-1** isomer, the calculations give a relaxed structure with neighbouring squaraine units forming dimer stacks (Figure 69(a)). These interactions provide stabilization with respect to the **hSQA-1-2** structure (Appendix Figure 85). Since solvation effects were not considered in the model calculations but may interfere

with the dimer formation of two squaraines in **hSQA-1**, the gas-phase relative energies of the two species are only indicative of stabilities in solution but not definitive. In fact, for squaraine systems the strong solvent-dependence of structure formation has been reported in previous publications that show reduced aggregation in $CHCl_3$.[71,108,109]

In order to account for this solvation effect in the calculation of optical properties, as a rough approximation, additional optimizations of the monomers without dispersion correction were carried out; these yielded structures with the squaraine units almost uniformly distributed around the centred benzene core as one would expect for solvation with a good solvent (see Figure 69(b)).

The experimental absorption spectra in $CHCl_3$ and acetone ($c = 1.49 \times 10^{-6}$ M) are shown together with the calculated spectra for all monomer and dimer species in Figure 71(a) and in Figure 71(b)-(d), respectively. In order to simplify the calculations of the absorption spectra, the dimethyloctyl chains were replaced in all cases by methyl groups but the geometry of the chromophores was left unchanged otherwise. This simplification has no significant influence on the computed spectra, as can be seen in Figure 71(b) for one selected example. The formation of dimer stacks in the structure of **hSQA-1-1** leads to excitonic coupling, resulting in a series of electronic states between 13 000 cm^{-1} and 17 000 cm^{-1}, with the latter being by far the most intense Figure 71(c). In contrast, the **hSQA-1-1** structure optimized without dispersion correction as the model structure for a solvated monomer gives rise to a spectrum with two prominent transitions located at 13 800 cm^{-1} and 14 600 cm^{-1} (Figure 71(c)).

In case of the "up-down" **hSQA-1-2**, the structure calculated without dispersion correction yields an absorption spectrum that exhibits one transition located at 13 300 cm^{-1} (Figure 71(c)), while that calculated with dispersion again shows two slightly separated transitions at 13 100 cm^{-1} and 13 400 cm^{-1} but at the same spectral position as the calculation without dispersion (Figure 71(b)). This demonstrates that dispersion interactions have almost no influence in **hSQA-1-2** because the up-down arrangement of the squaraine tentacles prevents direct squaraine-squaraine interactions (dimer stacking).

Although all three computed spectra of **hSQA-1-1** (without dispersion correction) and **hSQA-1-2** (with and without dispersion correction) are somewhat shifted to lower energies with respect to the recorded experimental spectra, the narrow shape of the band is similar to the experimentally recorded one. Here, it has to be taken into account that the computational methodology cannot reproduce the vibrational progression observed between 16 000-18 000 cm^{-1} in the experimental spectrum.

In contrast, the computed spectrum of **hSQA-1-1** optimised with dispersion correction, and consequently squaraine-dimer stacking, clearly deviates significantly from the experimental spectra and this structure, although it is the more stable in the gas phase, can therefore be ruled out as the solution structure. However, based on the computed monomer spectra, which agree with the experimental spectra, it cannot be concluded anything about the specific monomer structure ("up-down" or "all-up") because the squaraine tentacles are too far away from each other to interact strongly enough in the **hSQA-1** system. Other conformers are indeed conceivable but no significantly different spectral behaviour is expected for these conformers. From a thermodynamic point of view, it is assumed that in reality a mixture of quickly interconverting (see NMR above) conformers is present in solution, and that **hSQA-1-1** and **hSQA-1-2** are just two of them.

In case of the dimers, structure optimization including dispersion indicates the "folded hands"-dimer to be the most stable aggregate followed by the "bowls"-dimer and the "mixed"-dimer, which has the highest energy (see Figure 70 below and Table 20 in the Appendix). This ordering is directly connected to the strength of dispersion interaction. The "hands"- and the "bowls"-configurations allow for better overlap of the squaraine units, while in the "mixed"- dimer only three of the six squaraines per monomer can interact.

Comparison of the computed spectra (Figure 71(d)) with the experimental data (Figure 71(a)) unambiguously indicates the predominance of the "bowls"-dimer in solution. The theoretical spectrum nicely matches the envelope of the measured one, comprising an intense main absorption band at ca. 16 500 cm^{-1} together with two closely located bands of lower intensity around 14 900 cm^{-1}. The whole spectrum is slightly shifted towards lower energy of about 1 500 cm^{-1} but the overall bandwidth is in good agreement. The spectrum of the "folded hands" dimer is very similar indeed to the one of the "bowls"-dimer and a conclusion about the structure cannot be made based exclusively on the computed spectra. However, the NMR experiments (see above) revealed two sets of different squaraine protons, which are only conceivable with the unsymmetrical structure of the "bowls"-dimer.

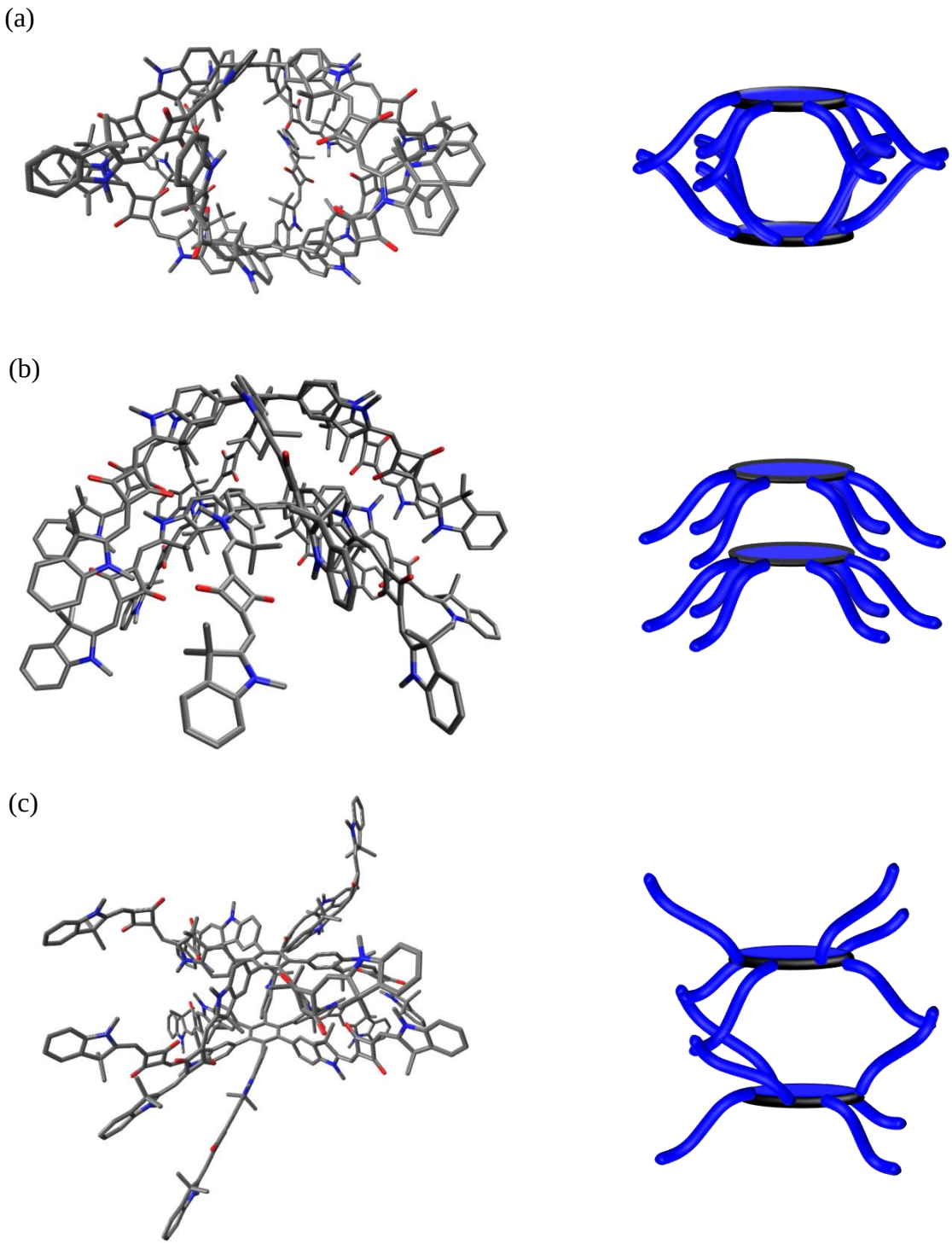

Figure 70: Geometry optimized structures of (a) “folded hands”-, (b) “bowls”-, and (c) “mixed”-dimeric aggregates and corresponding schematic illustration (dimers are shown in blue). The side chains were omitted for clarity and replaced by methyl groups, respectively.

The spectra of the two isolated **hSQA-1-1** monomers were also computed based on the “bowls”-dimer by deleting one of the monomers in each case. The spectra of these monomers are denoted **hSQA-1-1-bottom** and **hSQA-1-1-top** and differ somewhat in shape, as can easily be seen in Figure 71(e). While **hSQA-1-1-bottom** features a maximum at ca.

15 100 cm^{-1} together with a second intense band at lower energies, **hSQA-1-1-top** exhibits a maximum at higher energies at 15 700 cm^{-1} and two additional peaks of intermediate and lower intensity at lower energies. The difference in the spectra reflects the slightly different geometries of the monomers within the **hSQA-1** "bowls"-dimer. From this point of view, it becomes evident that binding a third **hSQA-1-1** is not favourable since it would require a drastic expansion of the **hSQA-1-1-bottom** geometry. Another explanation for the absence of higher aggregates is provided by the steric shielding of the alkyl chains due to the interdigitating **hSQA-1-1**, which hampers a further binding event (Figure 71(f) side view). Accordingly, the two interdigitating **hSQA-1-1** monomers are shown in different colours (grey and yellow) for the sake of clarity. The absorption maxima of the spectra of **hSQA-1-1-top** and **hSQA-1-1-bottom** are slightly shifted towards higher energies relative to **hSQA-1-1** optimised without dispersion (Figure 71(c)), indicative of H-type aggregate formation within the isolated **SQ6-1** monomers. Remarkably, the superposition of the two spectra neither matches the experimental one nor the computed spectrum of the "bowls"-dimer. This inevitably leads to the conclusion that the spectral features of the aggregates in solution are caused by both intra- and intermolecular interactions of the 12 squaraine tentacles.

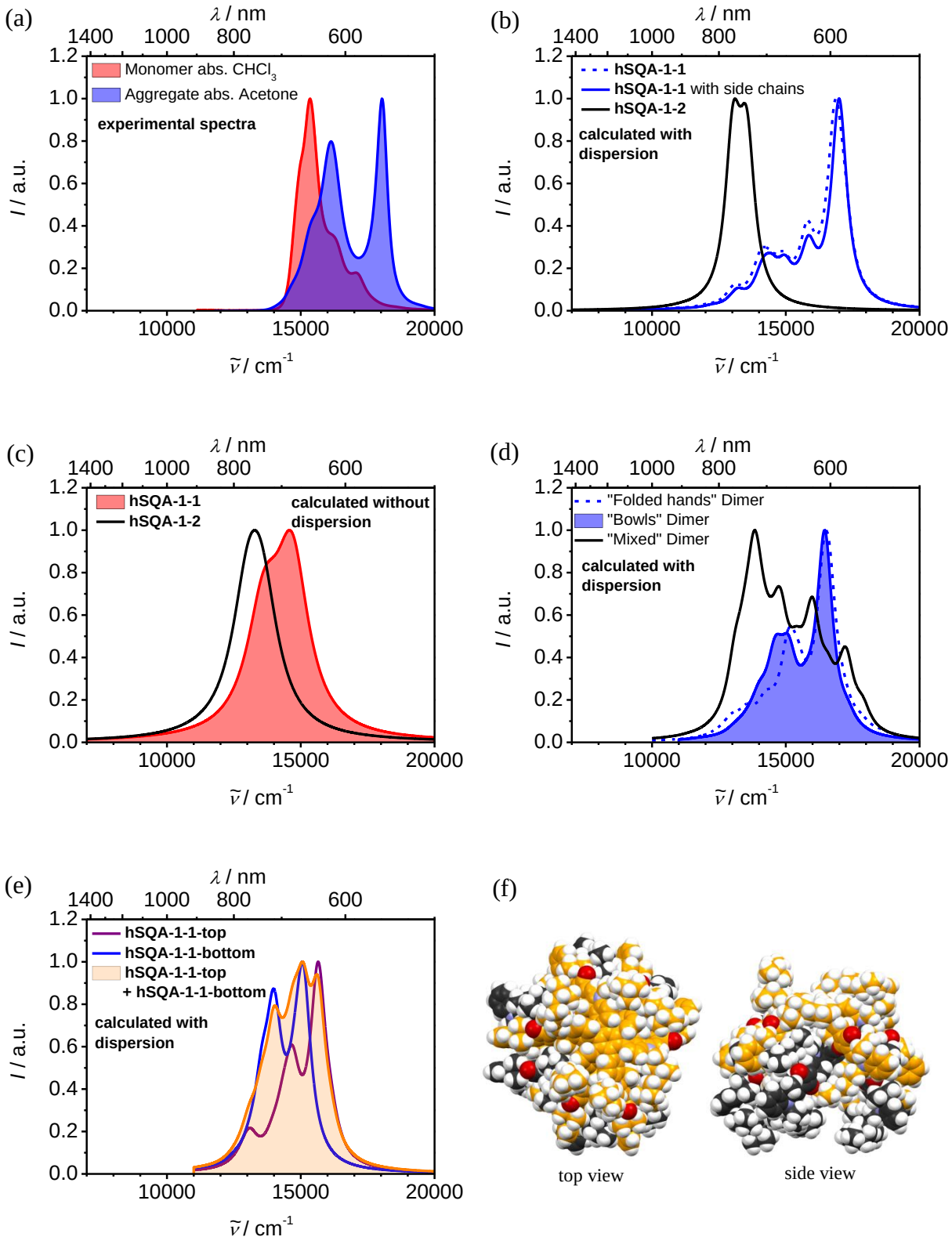

Figure 71: (a) Normalized absorption spectra of **hSQA-1** in $CHCl_3$ and acetone (c =1.49×10^{-6} M). Calculated spectra of "all up" **hSQA-1-1**) "up-down" (**hSQA-1-2**) monomers (b) with and (c) without dispersion. (d) Calculated spectra of different dimeric aggregates. Side chains were replaced by methyl groups for calculations. (e) Absorption spectra of the isolated **hSQA-1-1** monomers (**hSQA-1-1-bottom** and **hSQA-1-1-top**) based on the geometry-optimised "bowls"-dimer structure and superposition thereof. (f) Optimised structure of "bowls"-dimer shown as spacefilling model with alkyl chains in two perspectives (top and side view). Monomers are shown in grey and yellow.

3.7.7 Kinetics

To assess the activation parameters for the assembly and disassembly process of **hSQA-1** in solution quantitatively, kinetic experiments were performed by monitoring the time-dependent absorption changes at a fixed wavelength (toluene: 17 900 cm^{-1} and acetone: 18 000 cm^{-1}), when a defined amount of solid was dissolved in the appropriate volume of pre-tempered solvent reservoir (cuvette). Analogously to recent kinetic studies on the deaggregation of a quadruple π stack of two perylene bisimide tweezers,[192] this disassembly process was considered as a first-order fragmentation reaction. In contrast, a second-order reaction was found to be suitable to describe the assembly process from monomers into dimers in acetone (for detailed information of the fitting routines see Appendix, Chapter 9.2.5). For both cases, when fitting the apparent absorption coefficient $OD(t)/(c \cdot d)$ values for a given temperature versus time t with the corresponding fit function, the rate constant k is accessible. The correlation coefficients obtained are highly reliable, with values better than 0.99. In this way, in toluene at 293 K, a rate constant value of 2.65×10^{-4} s^{-1} along with a half-life time of $t_{1/2}$ = 2620 s (43.7 min) were found for the disassembly. In acetone, a rate constant of 214 M^{-1} s^{-1} and a half-life time of $t_{1/2}$ = 3130 s (52.2 min) were determined for the dimerization process at 293 K. Subsequently, the temperature-dependence of the rate constant k for both processes was examined. For this purpose, the same experiment was repeated at different temperatures, that is between 288 and 313 K for toluene and between 283 and 303 K for acetone in 2.5 K steps, respectively (see Appendix, Chapter 9.2.5).

$$\ln\frac{k}{T} = -\frac{\Delta H^{\ddagger}}{R}\frac{1}{T} + \ln\frac{k_B}{h} + \frac{\Delta S^{\ddagger}}{R} \qquad (58)$$

An Eyring plot of $\ln(k/T)$ vs $1/T$ together with equation (58) gave the activation parameters for the dissociation $\Delta H^{\ddagger}_{diss}$ = 60.0 ± 1.86 kJ mol^{-1} and $\Delta S^{\ddagger}_{diss}$ = -109 ± 6.24 J mol^{-1} K^{-1} and from those $\Delta G^{\ddagger}_{diss}$ = 91.8 ± 1.87 kJ mol^{-1} at 293 K. In the same way, $\Delta H^{\ddagger}_{ass}$ = 95.2 ± 2.94 kJ mol^{-1}, $\Delta S^{\ddagger}_{ass}$ = 124 ± 6.24 J mol^{-1} K^{-1} and $\Delta G^{\ddagger}_{ass}$ = 58.7 ± 2.94 kJ mol^{-1} were obtained for the association process at 293 K (Figure 72). The results for the Gibbs activation energy for both processes are very similar to those for a quadruple π-stack of two perylene bisimide tweezers[192] and quadruply hydrogen-bonded 2-ureido-4[1*H*]-pyrimidinone dimers[193] in $CHCl_3$, respectively.

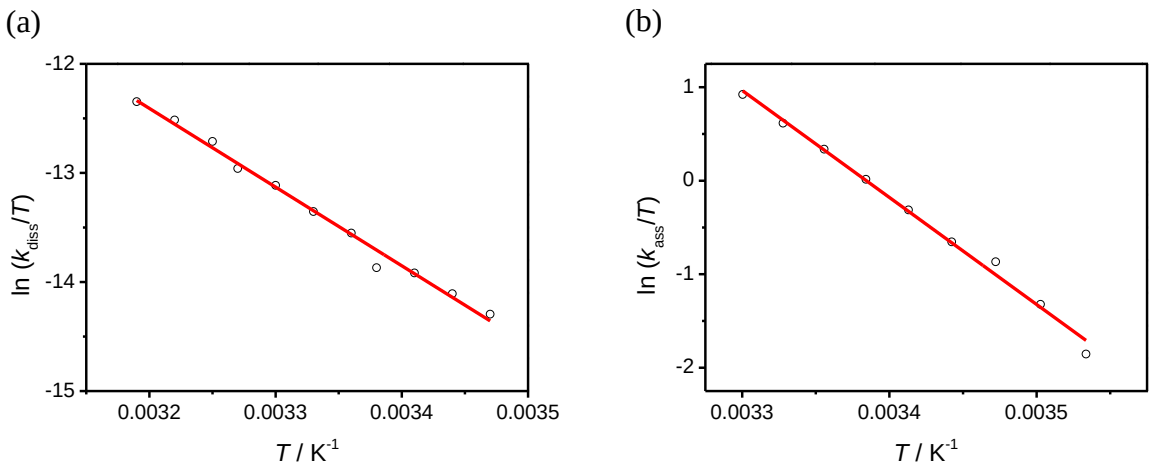

Figure 72: Eyring plot for the temperature dependence of the disassembly and assembly rate constants k_{diss} and k_{ass} in (a) toluene and (b) acetone for **hSQA-1**. Measured data points are indicated as black circles and fitting curve is drawn in red.

3.7.8 Concentration-Dependent Absorption Studies

While the experiments described above yield information about the kinetics of aggregate formation/dissociation of **hSQA-1**, the thermodynamics of these processes are investigated in the following. This was done in three ways, by measuring absorption spectra in (i) a variety of solvent mixtures of a good ($CHCl_3$) and a bad (acetone) solvent, (ii) a large concentration range in a specific $CHCl_3$/acetone mixture, and (iii) a range diverse temperatures. These experiments were not only performed for **hSQA-1** but also for **dSQA-7** and **hSQA-2**.

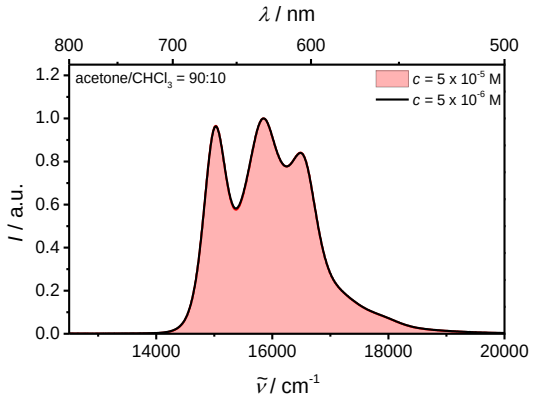

Figure 73: Normalized absorption spectra of **dSQA-6** in acetone/$CHCl_3$ = 90:10 at different concentrations.

The model dye **dSQA-6** is only poorly soluble in pure acetone therefore the binary solvent mixture acetone/$CHCl_3$ = 90:10 was used (Figure 73). The absorption spectra at the two different concentrations bear a strong resemblance to the one recorded in pure $CHCl_3$ (Figure 64(a)), and show no concentration dependence, indicating the absence of any self-assembly of

dSQA-6. In contrast, **hSQA-1** strongly self-assembles in acetone with a pronounced kinetic effect.

The solvent-dependent absorption spectra of **hSQA-1** in acetone/$CHCl_3$ mixtures ranging from 100:0 to 50:50 (*v*:*v*) were acquired at a fixed concentration of 5.39×10^{-6} M (Figure 74(a)). With increasing volume fraction of $CHCl_3$, the aggregate band at 18 000 cm^{-1} decreases, while the monomer band at 15 400 cm^{-1} increases concomitantly. The marked spectral changes are examined in more detail in Figure 74(b) for the aggregate band at 18 000 cm^{-1}. The plot of apparent molar absorptivity against solvent composition reveals a sigmoidal curve with a decrease from 893 000 M^{-1} cm^{-1} in pure acetone to 54 800 M^{-1} cm^{-1} in the mixture acetone/$CHCl_3$ = 50:50. Thus, the solvent composition directly affects the aggregation constant and the corresponding Gibbs energy.

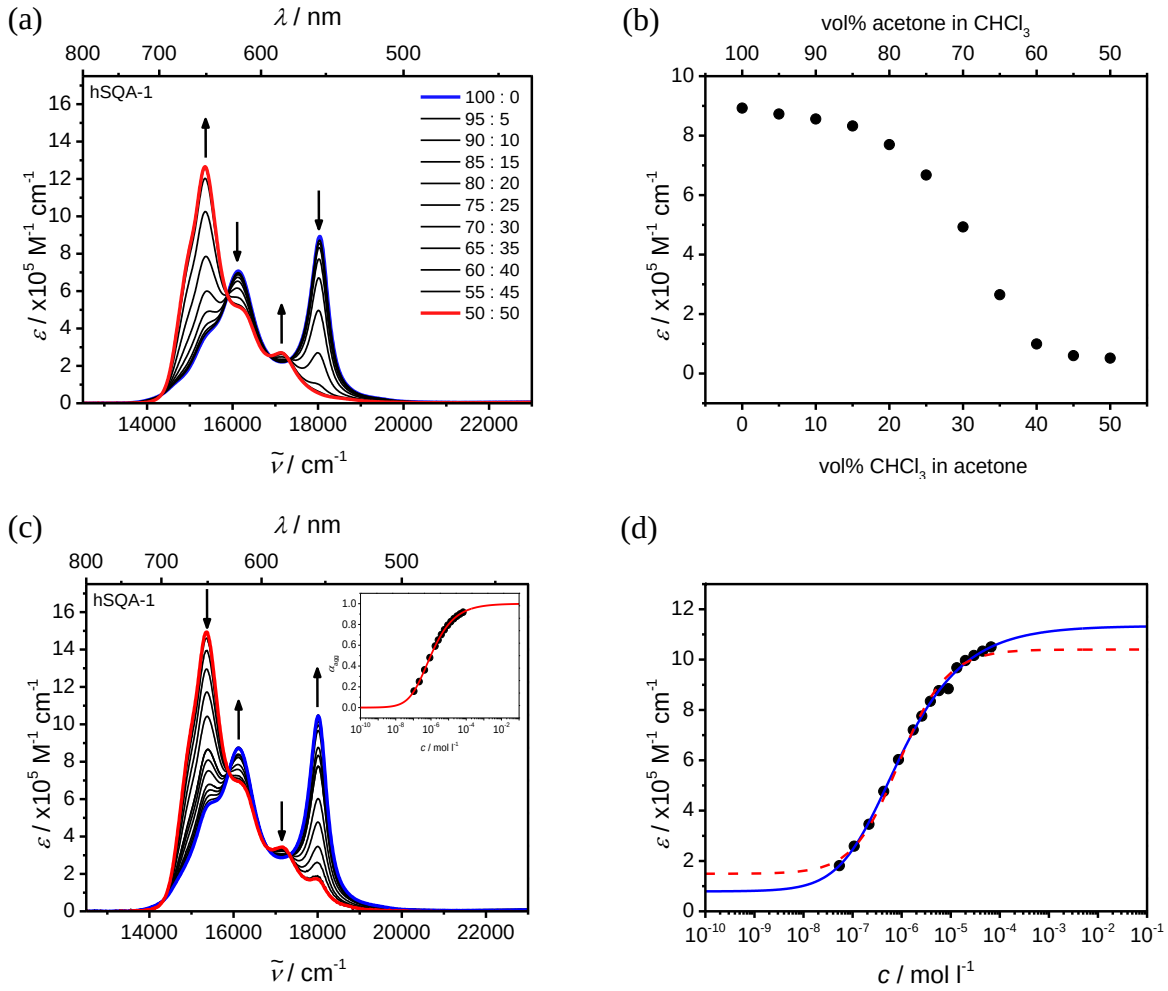

Figure 74: (a) Solvent-dependent absorption spectra of squaraine dye **hSQA-1** (5.39×10^{-6} M) in acetone/$CHCl_3$ mixtures from pure acetone (blue curve) to 50:50 (red curve) (*v*:*v*). (b) Plot of apparent molar absorptivity at 18 000 cm^{-1} versus vol% $CHCl_3$ in acetone at 293 K. (c) Concentration-dependent absorption spectra (10^{-7} – 10^{-5} M) in acetone/$CHCl_3$ = 75:25 recorded at 293 K. The red and blue spectra are the calculated monomer and dimer spectra according to the dimerization model. Inset: Plot of degree of aggregation against concentration. (d) Analysis of the concentration-dependent extinction data at 18 000 cm^{-1} according to the dimerization (blue curve, R^2 = 0.998) and isodesmic (red dashed line, R^2 = 0.993) models.

Taking advantage of these findings, the solvent ratio 75:25 was considered suitable for the following concentration-dependent studies. At this ratio, almost identical extinction coefficients are obtained for the aggregate and monomer bands. The absorption studies were carried out over a concentration range from 6.66×10^{-5} to 2.16×10^{-7} M. At first glance, the spectra depicted in Figure 74(c) clearly resemble those of the solvent-dependent measurements, revealing the same spectral trends, both upon increasing concentration and upon increasing acetone content. The acquired set of spectra exhibit well defined isosbestic points at 15 900 cm^{-1}, 16 800 cm^{-1} and 17 300 cm^{-1}, again indicating aggregation equilibrium between two discrete species only, i.e., monomeric and aggregated **hSQA-1**. Non-linear least-square analysis of the concentration-dependent absorption data was applied according to equation (21) and gave a good fit to the dimerization model for the aggregate band at 18 000 cm^{-1} (blue curve, Figure 74(d)):

$$\frac{OD\,(\lambda)}{c\cdot d} = (\varepsilon_{\mathrm{M}} - \varepsilon_{\mathrm{agg}})\,\frac{\sqrt{8K_{\mathrm{dim}}\,c+1}-1}{4K_{\mathrm{dim}}c} + \varepsilon_{\mathrm{agg}} \tag{21}$$

where c is the total concentration of all molecules, d the path length of the cuvette, K_{dim} the dimerization constant, $OD(\lambda)/(c\cdot d)$ the apparent extinction coefficient, and ε_{M} and $\varepsilon_{\mathrm{agg}}$ the extinction coefficients obtained by this regression analysis for the molar absorptivity of a pure monomer and dimer at a fixed wavelength, respectively. For the lowest and highest concentration regimes, it turned out that the dimerization model describes the aggregation process more accurately than the alternative isodesmic model (red dashed curve in Figure 74(d)) which entails the stepwise formation of larger aggregates with identical aggregation constant for each step. The dimerization model goes hand in hand with the DOSY NMR measurements and calculations shown above. For this reason, no higher aggregates than dimers are expected to be formed. The resulting dimerization constant K_{dim} is 1.11×10^{6} M^{-1}. Furthermore, extinction coefficients for monomer and dimer at 18 000 cm^{-1} are 79 100 $M^{-1}cm^{-1}$ and 1.13×10^{6} $M^{-1}cm^{-1}$, respectively. The same fit procedure was carried out for the monomer band at 15 400 cm^{-1} and gave comparable results (see Table 16). The averaged dimerization constant $\overline{K}_{\mathrm{dim}}$ was used to calculate the Gibbs free dimerization energy $\Delta\overline{G}^{\mathrm{o}}_{\mathrm{dim}}$ to be –33.7 kJ mol^{-1} at 293 K.

$$\alpha_{\mathrm{agg}} = \frac{OD(\lambda)/(c\cdot d) - \varepsilon^{\mathrm{max}}_{\mathrm{agg}}}{\varepsilon^{\mathrm{min}}_{\mathrm{agg}} - \varepsilon^{\mathrm{max}}_{\mathrm{agg}}} \tag{59}$$

By inserting these values for $\varepsilon^{\mathrm{max}}_{\mathrm{agg}}$ and $\varepsilon^{\mathrm{min}}_{\mathrm{agg}}$ into equation (59) the corresponding degree of aggregation α_{agg} was calculated. The high dimerization constant points towards an almost complete dimerization of 92 % at the highest used concentration (6.66×10^{-6} M). Using the

experimental absorption data for α_{agg} from 25 to 92 %, the spectra of the pure monomer (red curve) and aggregate (blue curve) could be calculated.

For the larger hexasquarainyl benzene **hSQA-2**, solvent-dependent absorption spectra were initially recorded in analogy to **hSQA-1** (Figure 75(a)). The former suffers from poor solubility in pure acetone, the ratio 95:5 was therefore chosen as a starting point and the $CHCl_3$ volume fraction was gradually increased up to 60 %. Compared to the smaller hexasquarainyl benzene, the spectral changes and the exciton splitting are not as pronounced as for **hSQA-1**. The absorption with the highest acetone content (blue curve) is characterized by a maximum at 15 200 cm^{-1}, together with a prominent aggregate shoulder at 14 800 cm^{-1} and a vibronic progression at higher energies. Upon increasing the $CHCl_3$ content, the aggregate band decreases while the main maximum shifts towards higher energies and gains in intensity concomitantly. A rise in intensity is also noted for the vibronic progression. Furthermore, the spectral changes were monitored in more detail for the aggregate band according to Figure 75(b). Very similar to **hSQA-1**, a sigmoidal curve is recorded for this titration experiment. The extinction coefficients range from 1.04×10^6 $M^{-1}cm^{-1}$ to 39 500 $M^{-1}cm^{-1}$ for the lowest and highest chloroform contents.

In order to shed light into the fundamental aggregation mechanism for **hSQA-2**, concentration-dependent absorption studies in a ratio of 80:20 were performed, which provided very similar spectral features to previous solvent-dependent studies (Figure 75(c)). With increasing concentration of squaraine dye **hSQA-2**, a rise of the aggregate band at 148 200 cm^{-1} was observed, accompanied by a shift towards lower energies and a decrease of the monomer band at 15 300 cm^{-1}. An almost clean isosbestic point was detected at 15 200 cm^{-1}. According to Figure 75(d), non-linear least-square analysis of the collected absorption data revealed a good fit to the dimerization model with a correlation coefficient of $R^2 = 0.998$. Closer inspection shows, that the dimerization model fits the collected absorption data more precisely than the isodesmic model, in particular for the lowest and highest concentration regimes. In addition and complementary to concentration-dependent studies, DOSY NMR indicates no higher aggregates than dimeric species for the larger hexasquarainyl benzene **hSQA-2**, which was also found for **hSQA-1**. By means of the dimer fit at 14 800 cm^{-1}, the dimerization constant K_{dim} along with the extinction coefficients for the pure monomeric and aggregated species were determined to be 2.18×10^6 M^{-1}, 486 000 $M^{-1}cm^{-1}$, and 1.25×10^6 $M^{-1}cm^{-1}$, respectively. An aggregation degree α_{agg} of 10 and 95 % were calculated for the lowest and highest measured concentration, revealing an almost

complete dimerization at highest concentration. The high dimerization constant stresses the high propensity of **hSQA-2** to form aggregates in mixtures with high acetone content.

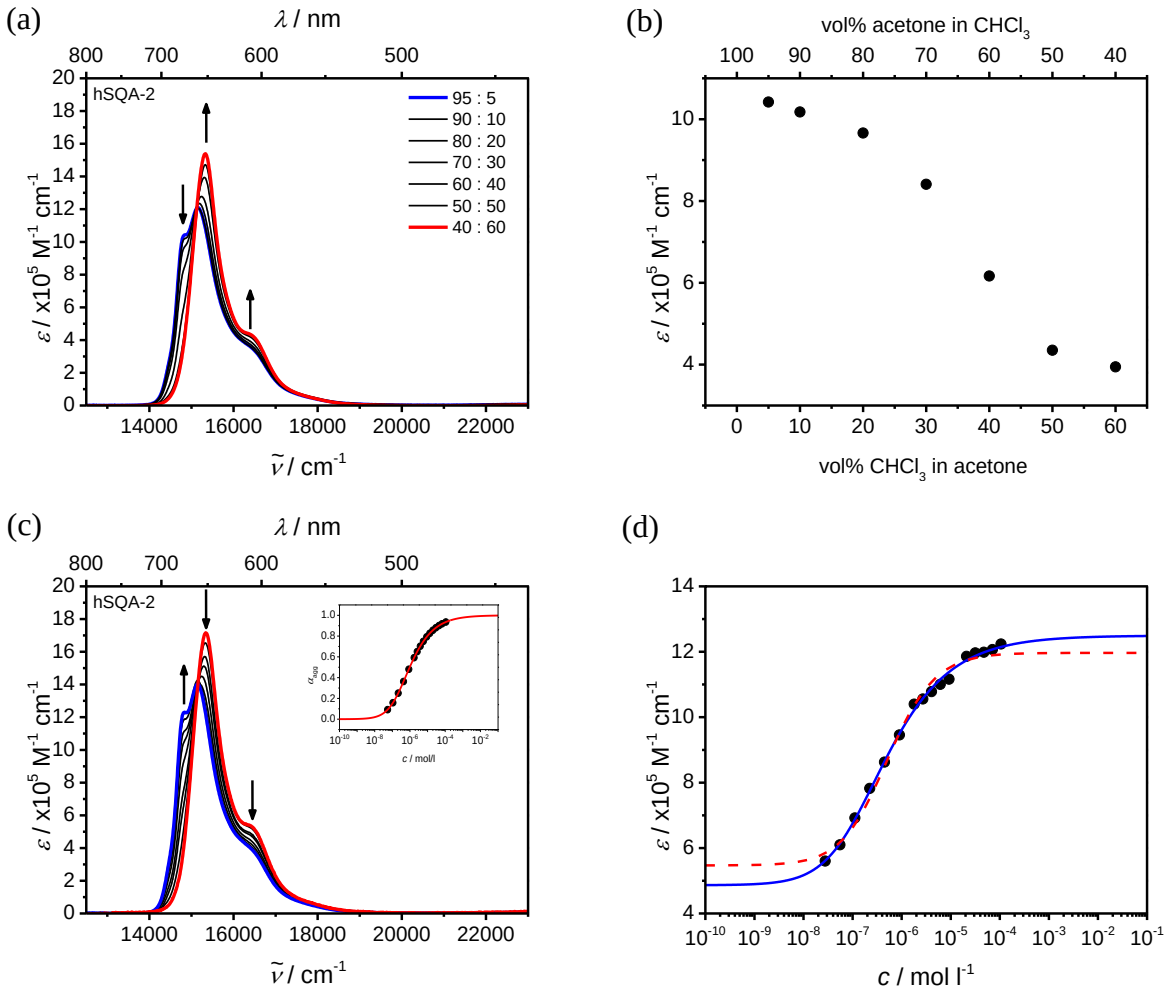

Figure 75: (a) Solvent-dependent absorption spectra of squaraine dye **hSQA-2** (4.97×10^{-6} M) in actone/$CHCl_3$, starting in 95:5 (blue curve) and gradually increasing the volume fraction of $CHCl_3$ in steps of 5 and 10 vol% up to 60 vol% (red curve). Arrows indicate the spectral changes upon increasing the volume fraction of $CHCl_3$. (b) Plot of molar absorptivity at 676 nm (14 800 cm^{-1}) versus vol% $CHCl_3$ in acetone at 293 K. (c) Concentration-dependent absorption spectra (10^{-8} – 10^{-4} M) in acetone/$CHCl_3$ = 80:20 recorded at 293 K. Red and blue spectrum is the calculated monomer and dimer absorptions from available data according to the dimerization model, respectively. Arrows indicate the spectral changes upon increasing concentration. Inset: Plot of degree of aggregation against concentration. (d) Analysis of the concentration-dependent extinction data at 14 800 cm^{-1} according to the dimer (blue curve, R^2 = 0.998) and isodesmic (red dashed line, R^2 = 0.988) models.

Model dye **dSQA-7** also showed concentration-dependent absorption spectra in acetone. On account of the excellent solubility in acetone, the measurements could be performed in the pure solvent. The absorption studies were carried out over a concentration range from 2.49×10^{-7} to 2.44×10^{-4} M. With increasing concentration, the intensity of the monomer band at 15 400 cm^{-1} and the subsidiary vibronic progression are reduced, and a concomitantly appearing of bathochromically shifted new bands at 14 500 and 15 200 cm^{-1} reveals the aggregation of the dye (Figure 76(a)). The isosbestic point at 15 300 cm^{-1} imply the presence

of an equilibrium between two discrete species, i.e. monomer and aggregate. Furthermore, the dimerization model (red curve) turned out to be the most suitable aggregation model according to Figure 76(b). Consistent with both hexasquarainyl benzenes, the isodesmic model (dashed red curve) describes the aggregation process inadequately for the lowest and highest dye concentrations. For **dSQA-7**, monomer and aggregate extinction coefficients of 28 100 and 129 000 $M^{-1}cm^{-1}$ together with a dimerization constant K_{dim} of 218 000 M^{-1} were obtained from non-linear least squares analysis for the aggregate band at 14 500 cm^{-1}. With the lowest and highest utilized concentrations, aggregation degrees of 9 and 91 % could be reached, indicating an almost complete transformation from monomer to dimer. On the basis of the acquired absorption data, the spectra of the pure monomeric and dimeric species could be calculated and are shown in red and blue, respectively (Figure 76(a)).

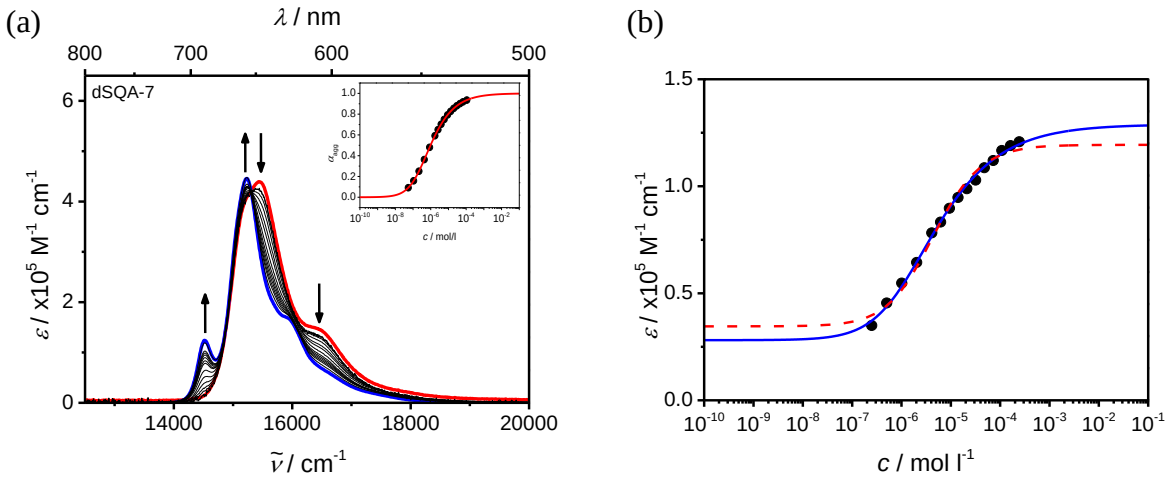

Figure 76: (a) Concentration-dependent absorption spectra (2.49×10^{-7} – 2.44×10^{-4} M) in acetone recorded at 293 K. The red and blue spectra are the calculated monomer and dimer spectra according to the dimerization model. Inset: Plot of degree of aggregation against concentration. (b) Analysis of the concentration-dependent extinction data at 14 500 cm^{-1} according to the dimerization (blue curve, R^2 = 0.997) and isodesmic (red dashed line, R^2 = 0.988) models.

3.7.9 Temperature-Dependent Absorption Studies

The self-assembly of squaraine dyes **hSQA-1**, **hSQA-2**, and **dSQA-7** was additionally studied by absorption spectroscopy as a function of temperature. The same solvent and solvent mixtures were chosen as for the concentration-dependent measurements. Moreover, the temperature-dependent data were acquired over a large temperature range in small temperature steps of 5 K, in order to precisely describe the respective boundaries of fully aggregated (at low *T*) and molecularly dissolved states (at high *T*).

In particular, due to the remarkably high kinetic stability of **hSQA-1** aggregates, each data acquisition step turned out to require extremely long equilibration times up to 300 min. According to Figure 77(a), the marked spectral changes are observed for the monomer and aggregate band at 15 400 cm^{-1} and 18 000 cm^{-1}. Starting at 328 K (red curve) and gradually decreasing the temperature down to 243 K (blue curve), the aggregate band significantly increases at the expense of the monomer band. Interestingly, no clear isosbestic points can be assigned which indicates that thermodynamic equilibrium between two explicit species has not achieved at each temperature which is a consequence of the slow kinetics of the aggregation/deaggregation process. In this context, the final spectrum at 243 K does not match the shape of the ones obtained by solvent- and concentration-dependent studies, where the monomer band has completely vanished in favour of the aggregate band at lowest chloroform content and highest dye concentration, respectively.

Referring to **hSQA-2** in Figure 77(b), the spectrum obtained at 318 K (red curve) can be ascribed to **hSQA-2** monomer with a main absorption at 15 300 cm^{-1} and subsidiary vibronic progression at higher energies. Upon decreasing the temperature, the spectral features of the aggregated state become apparent. Accordingly, the monomeric band shifts to higher energies and a second prominent band at 14 800 cm^{-1} along with a small shoulder at even lower energies arise at 198 K (blue curve). The transformation is marked by a distinctive isosbestic point at 15 200 cm^{-1}, indicating an equilibrium of two explicit species. In comparison to **hSQA-1** (328-243 K), a significant larger temperature span had to be covered for **hSQA-2** (318-198 K) to guarantee a complete transformation from molecularly dissolved to fully aggregated states.

In case of **dSQA-7**, temperature-dependent absorption spectra were recorded from 318-183 K in steps of 5 K. The initial (high *T*) and final (low *T*) spectra are shown in red and blue, respectively. A clear sigmoidal curve was obtained by monitoring the spectral changes at the aggregate band at 14 500 cm^{-1}, indicating a complete conversion of monomers into dimers (Figure 77(f)). Moreover, the initial spectrum of **dSQA-7** displays a broad and diffuse band shape. The spectrum at lowest temperatures exhibits a narrow and fine-structured band and resembles the one recorded at high dye concentrations, yet without such an intense band at 15 200 cm^{-1} and an additional maximum at 15 900 cm^{-1}.

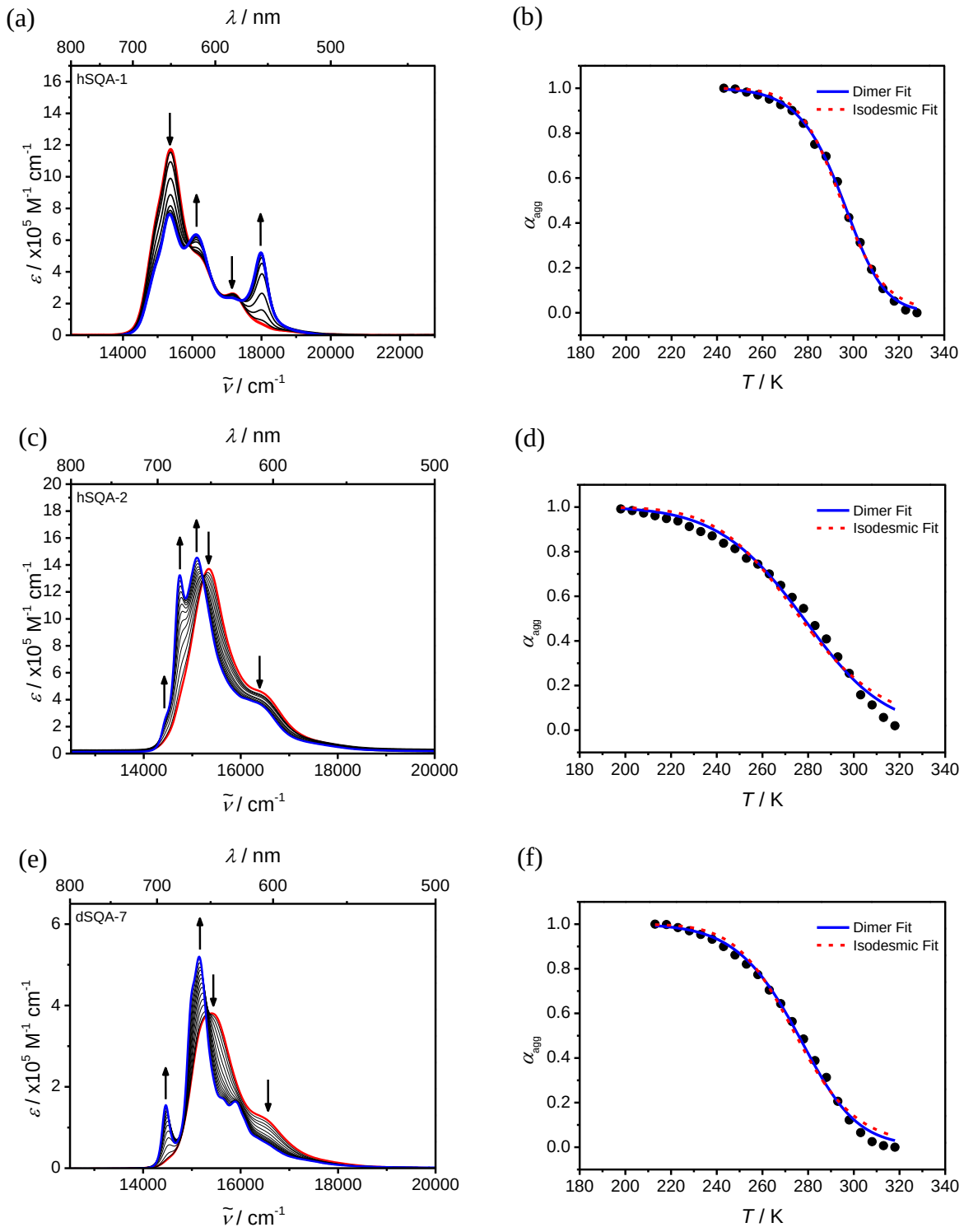

Figure 77: Temperature-dependent absorption spectra of squaraine dye (a) **hSQA-1** (3.25×10^{-7} M) in acetone/$CHCl_3$ = 75:25, (c) **hSQA-2** (3.47×10^{-7} M) in acetone/$CHCl_3$ = 80:20, and of (e) **dSQA-7** (9.13×10^{-7} M) in pure acetone, starting at high temperatures and gradually decreasing the temperature in 5 K steps. Initial and final spectra are shown in red and blue, respectively. Arrows indicate the spectral changes with decreasing temperature. Corresponding plot of degree of aggregation against temperature at (b) 18 000 cm^{-1}(**hSQA-1**), (d) 15 800 cm^{-1} (**hSQA-2**), and (f) 14 500 cm^{-1} (**dSQA-7**). Non-linear least squares analysis of the temperature-dependent data according to the dimerization model (equation (19)) and isodesmic model (equation (29)).

In order to verify the temperature-dependent measurements and to compare the data with those obtained by concentration-dependent studies, non-linear least squares analysis was carried out using the dimerization model and the isodesmic model according to equation (9) and (19), respectively (Figure 77 (b)(d)(f)). For both models, the fits gave consistently unreliable results for the concentrations c used in the experiments ($c_{Fit} \ll c_{exp}$), as well as for the Gibbs free energies obtained by concentration-dependent studies ($\Delta\overline{G}^{o}_{Fit} \ll \Delta\overline{G}^{o}_{dim}$ (Table 16)). This indicates that the temperature- and concentration-dependent results are not internally consistent and that the temperature-driven aggregation processes for all three dyes most likely occurred under strong kinetic rather than thermodynamic control. Consequently, reliable thermodynamic data could only be collected by concentration-dependent studies.

Table 16: Absorption Maxima $\tilde{\nu}_{mon}$ and $\tilde{\nu}_{agg}$, Minimum and Maximum Extinction Coefficients of Monomer ε_{mon} and Aggregate ε_{agg}, Dimerization Constants K_{dim}, Mean Value of Dimerization Constants $\overline{K}_{dim}$, and Gibbs Free Dimerization Energies $\Delta_{dim}G°$ for Squaraines **hSQA-1**, **hSQA-2**, and **dSQA-7** from Concentration-dependent Absorption Studies at 293 K in the Mixtures Acetone/$CHCl_3$ = 75:25 (*v*:*v*) (**hSQA-1**) and 80:20 (**hSQA-2**), and in Pure Acetone (**dSQA-7**).

	$\tilde{\nu}_{mon}$ / cm^{-1} λ_{mon} / nm	$\tilde{\nu}_{agg}$ / cm^{-1} λ_{agg} / nm	ε_{mon} (min) / $M^{-1}cm^{-1}$	ε_{mon} (max) / $M^{-1}cm^{-1}$	ε_{agg} (min) / $M^{-1}cm^{-1}$	ε_{agg} (max) / $M^{-1}cm^{-1}$	K_{dim} ($\tilde{\nu}_{mon}$) K_{dim} ($\tilde{\nu}_{agg}$) ($\overline{K}_{dim}$) / M^{-1}	$\Delta\overline{G}^{o}_{dim}{}^{o}$ [b] / kJ mol^{-1}
Concentration-dependent Absorption Data[a]								
hSQA-1	15 400 649	18 000 556	466 000 ±5 930	1.55×10^6 ±10 700	79 100 ±16 800	1.13×10^6 ±8 320	956 000 ±53 300 1.11×10^6 ±95 900 (1.03×10^6)	–33.7
hSQA-2	15 300 654	14 800 676	1.21×10^6 ±6 150	1.72×10^6 ±18 900	486 000 ±15 000	1.25×10^6 ± 5 890	2.85×10^6 ±505 000 2.18×10^6 ±221 000 (2.52×10^6)	–35.9
dSQA-7	16 500 606	14 500 690	69 000 ±796	147 000 ±2 870	28 100 ±1 990	129 000 ±1 120	129 000 ±86 400 218 000 ±23 800 (174 000)	–29.4

[a]Values obtained by non-linear regression analysis according to the dimerization model. [b]Averaged dimerization constant $\overline{K}_{dim}$ was used to calculate the Gibbs free dimerization energy $\Delta\overline{G}^{o}_{dim}$.

3.7.10 Fluorescence Spectroscopy

Steady-state and time-resolved fluorescence spectra were recorded of reference dyes **dSQA-6** and **dSQA-7**, as well as of hexasquarainyl benzenes **hSQA-1** and **hSQA-2** in toluene and $CHCl_3$. Fluorescence emission and excitation spectra are depicted in toluene only (Figure 78), since the spectra in $CHCl_3$ very similar. The optical data is summarised in Table 17.

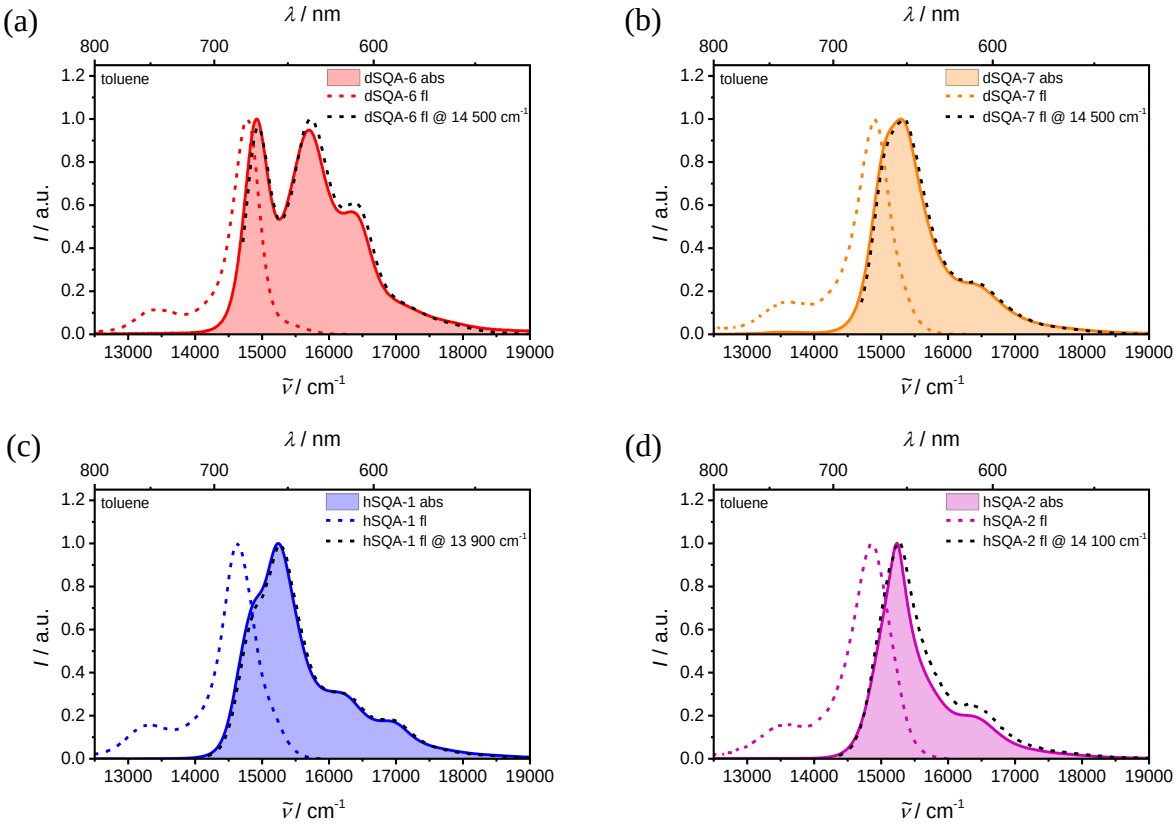

Figure 78: Normalised absorption, fluorescence emission and excitation spectra of (a) **dSQA-6**, (b) **dSQA-7**, (c) **hSQA-1**, and (d) **hSQA-2** in toluene.

According to Figure 78, the fluorescence emission spectra of all squaraine dyes resemble the shape of the monomer fluorescence and are red-shifted compared to the low energy edge of the absorption. This proves that fluorescence exclusively stems from the lowest energy level of the exciton manifold. This finding is further corroborated by the excitation spectra which are in very good agreement with the respective absorption spectrum, clearly indicating an efficient non-radiative relaxation process from the highest to the lowest exciton state without any appreciable radiative transitions from localised higher states. While reference dye **dSQA-6** provides a small Stokes shift of about 100 cm^{-1} in both solvents, larger Stokes shifts of ca. 400 cm^{-1} (**dSQA-7**, **hSQA-2**) and 600 cm^{-1} (**hSQA-1**) are found for the other congeners.

All squaraine dyes exhibit decent fluorescence quantum yields Φ_{fl} in toluene ranging from 0.53 to 0.68. Lower quantum yields of 0.18 and 0.11 are found in $CHCl_3$ for **dSQA-6** and

hSQA-1, while comparably high quantum yields of 0.53 and 0.41 were obtained for the larger dye analogues **dSQA-7** and **hSQA-2**, respectively.

Fluorescence lifetimes τ_{fl} were found to be in the ns and sub-ns time regime. For all squaraine dyes multiexponential fluorescence decays are observed. The calculation of the expectation values of the fluorescence lifetime gave values of 2.18-2.99 ns in toluene and 0.81-1.75 ns in $CHCl_3$. Thus, the lifetimes nicely correlate with the measured quantum yields.

Further investigations into the fluorescence properties of **dSQA-7**, **hSQA-1** and **hSQA-2** aggregates were carried out in pure acetone. The spectra are shown in Figure 79 for **hSQA-1** in a representative way. Upon excitation at 18 000 cm^{-1} (aggregate band), no emission could be detected for **hSQA-1**, while a very weak monomer-type fluorescence could be observed after excitation at lower energies at 16 700 cm^{-1}. The excitation spectrum probed at 13 900 cm^{-1} resembles the monomer absorption in $CHCl_3$ very closely. However, the spectrum also features a band at 18 000 cm^{-1} which can be assigned to **hSQA-1** aggregates. The origin of this weak band in the excitation spectrum is up to now not known. The other dyes also exhibited weak monomer-type fluorescence spectra similar to those in toluene and $CHCl_3$. In summary, the aggregates only show extremely weak fluorescence while the fluorescence observed almost exclusively originates from molecularly dissolved monomer species.

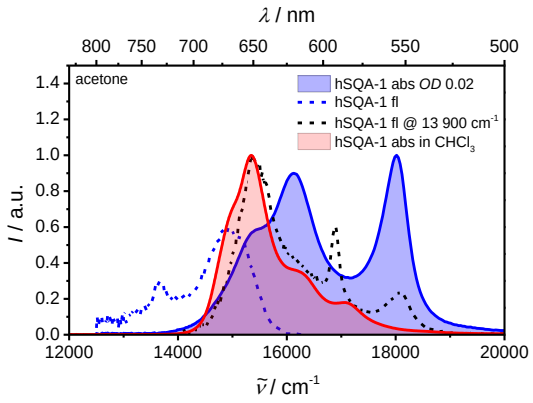

Figure 79: Normalised absorption as well as fluorescence emission and excitation spectra of **hSQA-1** at an optical density of ~ 0.02. Excitation was at 16 700 cm^{-1}. The fluorescence was probed at 14 3000 cm^{-1}. Sharp peaks at 13 700 and 16 900 cm^{-1} are caused by Raman scattering. Absorption spectrum of **hSQA-1** in $CHCl_3$ is shown for the sake of clarity.

In order to gain a deeper insight into the energy-transfer processes in both hexasquarainyl benzenes, fluorescence excitation anisotropy measurements were performed in highly viscous polyTHF (pTHF), respectively, to prevent rotational reorientation.[93,194] But before the focus is directed on the anisotropy measurements, the results of the fluorescence excitation spectra in pTHF in absence of any polarisation are briefly discussed.

The spectra are given in Figure 80. For the sake of comparison the absorption spectra of **hSQA-1** and **hSQA-2** in toluene are also depicted. In both cases, the fluorescence was probed at 14 100 cm^{-1}. The shape of the excitation spectra are in agreement with the respective monomer absorption in toluene. Given the findings in toluene and acetone from above, the excitation spectra of both chromophores in pTHF demonstrate once more that the emission exclusively originates from isolated monomers, respectively. A closer inspection of the band structure of **hSQA-1** reveals a significantly narrower bandwidth than the corresponding absorption spectrum in toluene (Figure 80(b)). Very remarkably, the excitation spectrum does not feature shoulders at lower and higher energies as observed in toluene and is therefore reminiscent of the monomer absorption of **SQA** only red-shifted.

Much in contrast, the excitation spectrum of **hSQA-2** is broader than the absorption and features a more pronounced vibronic progression at higher energies which can be readily appreciated in Figure 80(d).

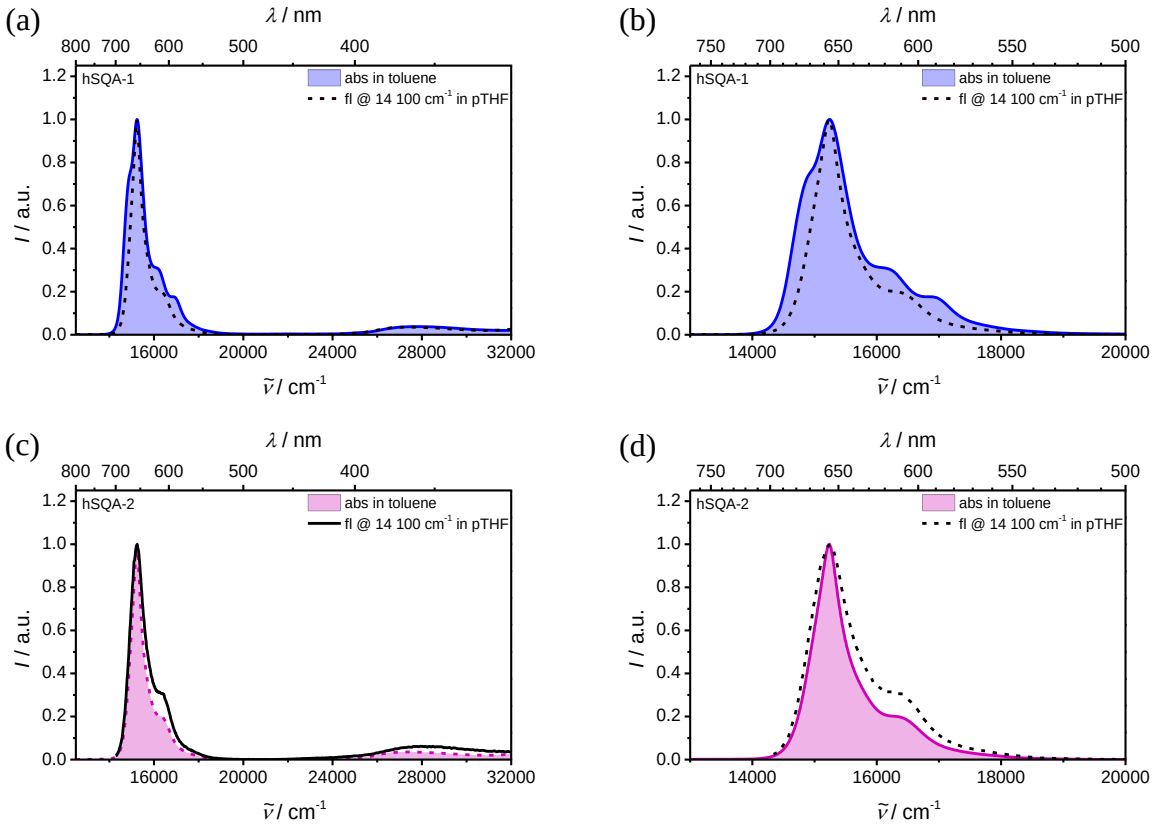

Figure 80: Complete and partial fluorescence excitation spectra of (a)(b) **hSQA-1** and (c)(d) **hSQA-2** in pTHF as well as normalised absorption spectra in toluene. Fluorescence was probed at 14 100 cm^{-1}, respectively.

In general, fluorescence excitation anisotropy measurements yield information about the spectral positions of optical transitions and the orientation of the transition moments. The fluorescence anisotropy r is defined by equation (60) in which I_{VV} and I_{VH} is the fluorescence

intensity with excitation and emission polariser aligned vertically or horizontally, respectively, while the grating factor G is a device-specific correction factor. The anisotropy r can be set into relation to the angle Θ, which describes the angular displacement between absorption and emission transition moment. Depending on this angle, r can adopt values between 0.4 (Θ = 0 °) and –0.2 (Θ = 90 °).[157,195]

$$r = \frac{I_{VV} - I_{VH} \cdot G}{I_{VV} + 2I_{VH} \cdot G} = \frac{2}{5} \cdot \frac{3\cos^2\theta - 1}{2} \tag{60}$$

The spectra are given in Figure 81. The absorption in toluene for both hexasquarainyl benzenes is plotted in a logarithmic scale to better pinpoint potential optical transitions. The fluorescence was probed at 14 100 cm^{-1} analogously to the measurements above. According to Figure 81(a), **hSQA-1** shows anisotropy of almost 0.4 at the low energy edge of the absorption band. Thus, it can be concluded that emission and absorption transition moments are aligned almost in a parallel fashion, i.e., excitation occurs into the same state from which emission is observed.

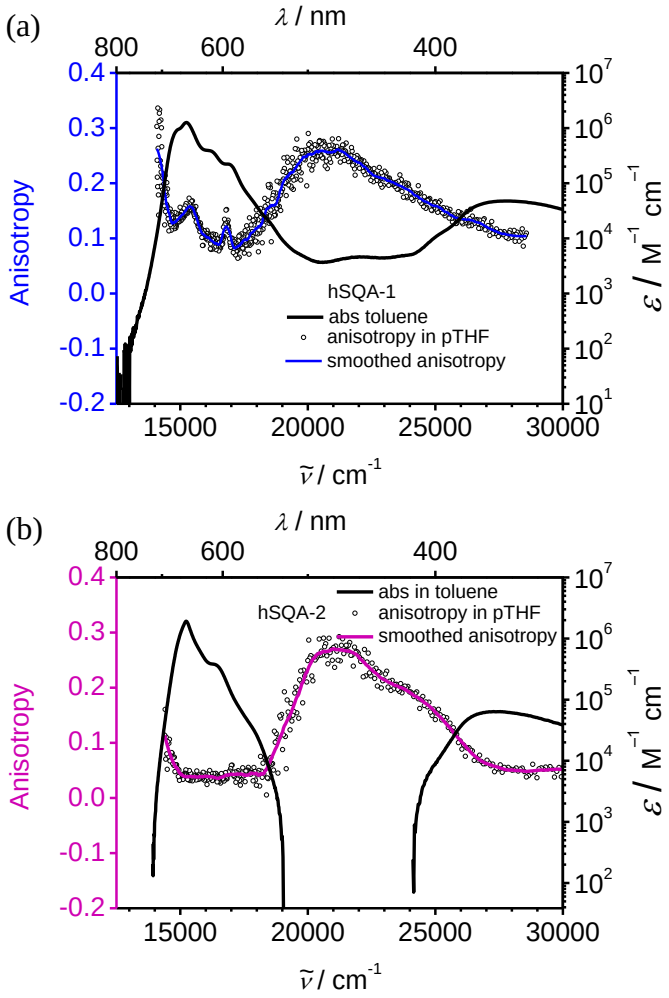

Figure 81: Absorption spectra in toluene and fluorescence excitation anisotropy spectra in polyTHF (pTHF) of (a) **hSQA-1** and (b) **hSQA-2**. Fluorescence was probed at 14 100 cm^{-1}, respectively.

Deviations from an ideal r = 0.4 may be due to partial energy transfer between different molecules or molecular rearrangement during the lifetime of the excited state.[195] The excitation anisotropy spectrum exhibits a sharp decrease and thus a strong depolarisation to a value of 0.13 on going from 14 100 cm^{-1} to 14 800 cm^{-1}. Such a "red-edge excitation effect"[195-197] has frequently observed in multidimensional chromophore systems and originates from energy transfer between different energy levels of somewhat different energy within one single chromophore. Then the anisotropy slightly increases to 0.16 (15 200 cm^{-1}) at the peak maximum in toluene. From 14 800 cm^{-1} to 17 200 cm^{-1} the anisotropy decreases further and oscillates around 0.1, until it increases considerably to 0.26 at around 20 000 cm^{-1}. There, it remains constant till 21 000 cm^{-1} and then steadily drops to 0.1 on moving to the high energy side of the spectrum. In this context, a value of r = 0.1 can be related to a two-dimensional depolarisation.[157] This value particularly appears in the spectral region of the main absorption band and can be attributed to energy transfer.

A similar scenario is observed for **hSQA-2** which can be seen in Figure 81(b). Accordingly, a constant value of 0.05 being close to 0.1 (**hSQA-1**) is reached in the spectral range of the main absorption from 15 000 cm^{-1} to 18 500 cm^{-1}, together with a steep rise to r =0.27 at intermediate energies (20 000 cm^{-1}) and a gradually decrease to 0.05 at high energies. However, some distinguishing features compared to the anisotropy of **hSQA-1** were noticed. First, the "red-excitation effect" is less pronounced, yielding a maximum value of only 0.16. Higher values as noticed for **hSQA-1** are most likely be observable when probing the fluorescence at even lower energies (< 14 100 cm^{-1}). Second, a constant value is observed within the spectral range of the main absorption while in **hSQA-1** each transition has slightly different anisotropy values indicating slightly different polarisations. These minor changes in the anisotropy reflect the fairly complex nature of the main transitions, which are a result of exciton coupling. In general, the values obtained for **hSQA-1** are somewhat smaller yet comparable to those of **hSQA-2** and describe a scenario between two- and three-dimensional (r = 0) depolarisation due to energy transfer occurring between the chromophore tentacles.

3.7.11 Conclusion

Two star-shaped hexasquarainyl benzenes were synthesised via convenient dicobaltoctacarbonyl-catalysed cyclotrimerisation reaction based on the respective tolan derivatives **dSQA-2** and **dSQA-5**. Two reference dyes labelled as **dSQA-6** and **dSQA-7** were also synthesised applying Suzuki coupling methodology. In contrast to reference dye

dSQA-6, comprehensive concentration- and temperature dependent studies showed that both hexasquarainyl benzenes and the reference **dSQA-7** exhibit a strong tendency towards self-organisation in polar solvent acetone. In particular, the aggregate spectrum of **hSQA-1** revealed a large hypsochromic shift of the absorption of ca. 2 700 cm^{-1}, indicating H-type exciton coupling. The aggregate band is marked by a very narrow bandwidth of only 560 cm^{-1} which was explained to be caused by exchange narrowing. While **hSQA-2** and **dSQA-7** instantaneously formed stable aggregates, the absorption spectra of **hSQA-1** in acetone and toluene turned out to be time-dependent. The process of aggregation (acetone) and deaggregation (toluene) was assessed for **hSQA-1**, revealing a pronounced kinetic stability of the aggregates with half-lifetimes of 52.2 min and 43.7 min, respectively.

The exclusive formation of **hSQA-1** dimeric aggregates in solution was unambiguously proved by concentration-dependent UV/vis studies and DOSY NMR measurements. Providing clear isosbestic points, the absorption data was successfully fitted to the dimerization model which turned out to be superior to the isodesmic model, revealing an extremely high binding constant in excess of 10^6 M^{-1}. This high driving force for self-assembly was rather unexpected, appreciating the unfavourable bulky 3,3-dimethyl-groups within the indolenine scaffold that prevent aggregation of e.g. cyanine dyes.[126] Such high binding constants are typically found for phthalocyanines, merocyanines, and perylene bisimides dyes only which substantially profit from their larger π-surface and dipolar/quadrupolar interactions. Joint computational and NMR studies were performed in order to unravel the aggregate structure, which turned out to be the "bowls"-dimer being composed of two stacked **hSQA-1**. Further structural assignments by NMR were hampered by the use of a racemic alkyl chain, which ultimately led to a complex mixture of diastereoisomers in the rigidized aggregate structure.

In contrast to **hSQA-1**, the structural elucidation of **hSQA-2** and **dSQA-7** aggregates by NMR failed due to complex ^{1}H- and ^{13}C- NMR spectra which were governed by a substantial amount of signals. However, DOSY NMR studies indicated the presence of dimeric **hSQA-2** aggregates similar to the smaller hexasquarainyl benzene. The absorption spectra of **dSQA-7** and **hSQA-2** aggregates are very similar but different to **hSQA-1**, featuring two intense bands which were marginally red-shifted compared to the monomer spectrum, respectively. These findings pointed towards J-type aggregate formation, however, these bands may also be of vibronic origin. A clear and representative assessment by computational methods was not feasible as the aggregate bands were not sufficiently enough separated from the monomer band in both cases. Nevertheless, the absorption data of **hSQA-2** and **dSQA-7** which showed

almost clear isosbestic points could be fitted to the dimerization model, respectively. The resulting high binding constants of 1.74×10^5 and 2.52×10^6 clearly emphasised the high driving force for self-assembly for **dSQA-7** and **hSQA-2**, respectively, in analogy to **hSQA-1**. Given the simplicity of the dimerization model for such complex and extended chromophore architectures, it proved to be a good approach to assess the basic parameters of the underlying aggregation processes. More sophisticated computational methods in combination with further spectroscopic techniques are required to elucidate the aggregate structures of **hSQA-2** and **dSQA-7** which were found to be highly complex according to NMR.

Furthermore, it could be shown that the reference dyes and hexasquarainyl benzenes possess decent fluorescence properties in toluene and $CHCl_3$, respectively. In each case, the emission exclusively occurred from the lowest energy state of the exciton manifold. In addition, the fluorescence was studied in acetone where aggregation of the dyes is observed. Accordingly, the fluorescence observed almost exclusively stemmed from molecularly dissolved monomer species. Fluorescence excitation anisotropy measurements in highly viscous pTHF revealed a strong depolarisation in the spectral region of the main absorption band of both hexasquarainyl benzenes. Anisotropy values of 0.1 (**hSQA-1**) and almost zero (**hSQA-2**) hinted towards a 2D and 3D-depolarisation which was attributed to energy transfer between adjacent squaraine tentacles.

Table 17: Absorption maxima, extinction coefficients, transition moments, fluorescence maxima, fluorescence quantum yields, fluorescence lifetimes and expectation values of fluorescence lifetimes of squaraine dyes **SQA**, **dSQA-6**, **dSQA-7**, **hSQA-1**, and of **hSQA-2** in $CHCl_3$ and toluene.

	solvent	$\tilde{\nu}_{abs}$ / cm^{-1} (nm)	ε_{max} / $M^{-1}cm^{-1}$	μ_{eg}^2 / D^2	$\tilde{\nu}_{em}$ / cm^{-1} (nm)	Φ_{fl} / –	τ_{fl}[a] / ns	$\bar{\tau}_{fl}$ / ns
SQA	$CHCl_3$	15 700 (637)	3.45×10^5	129	15 500 (645)	0.51	0.26 (0.40) 1.47 (0.60)	1.34
	toluene	15 500 (645)	3.64×10^5	127	15 400 (649)	0.62	0.25 (0.09) 1.71 (0.91)	1.69
dSQA-6	$CHCl_3$	15 000 (667)	3.53×10^5	266	14 900 (671)	0.18	0.02 (0.33) 0.52 (0.23) 1.10 (0.44)	0.97
	toluene	14 900 (671)	–[b]	–[b]	14 800 (676)	0.68	1.18 (0.38) 3.01 (0.58)	2.64
dSQA-7	$CHCl_3$	15 400 (649)	4.40×10^5	241	15 000 (667)	0.53	0.20 (0.09) 0.88 (0.24) 1.91 (0.67)	1.75
	toluene	15 300 (654)	4.27×10^5	221	14 900 (671)	0.62	0.98 (0.27) 2.36 (0.73)	2.18
hSQA-1	$CHCl_3$	15 300 (654)	1.30×10^6	792	14 700 (680)	0.11	0.18 (0.59) 0.97 (0.41)	0.81
	toluene	15 200 (658)	1.26×10^6	719	14 600 (685)	0.62	1.24 (0.29) 3.26 (0.71)	2.99
hSQA-2	$CHCl_3$	15 300 (654)	1.71×10^6	848	14 900 (671)	0.41	0.48 (0.25) 1.84 (0.75)	1.73
	toluene	15 200 (658)	1.92×10^6	770	14 800 (676)	0.53	0.63 (0.37) 2.45 (0.69)	2.23

– not determined. [a]Multi-exponential fit of fluorescence decay measured by TSCPC, excitation at 15 240 cm^{-1} (656 nm). Amplitudes are given in brackets. [b]Only partially soluble in toluene.

4 Summary

In this thesis, the synthesis and photophysics of a great variety of squaraine dyes were presented. This variety was based on four parent squaraines containing either indolenine or quinoline heterocycles. Among the donor moiety of the monomer units, the acceptor moiety was also varied by substituting the carbonyl-function of the squaric acid ring in **SQA** by a dicyanovinylene-group in **SQB**, **SQC**, and **DiPhSQB**. This ultimately led to a change in the overall molecular geometry from *transoid* (C_{2h}) to *cisoid* (C_{2v}) and caused a significant red-shift of the main absorption. By a suitable choice of the donor and acceptor unit, the optical properties could already be adapted to the properties desired on the stage of the monomer. An excerpt of this broad variety is given below.

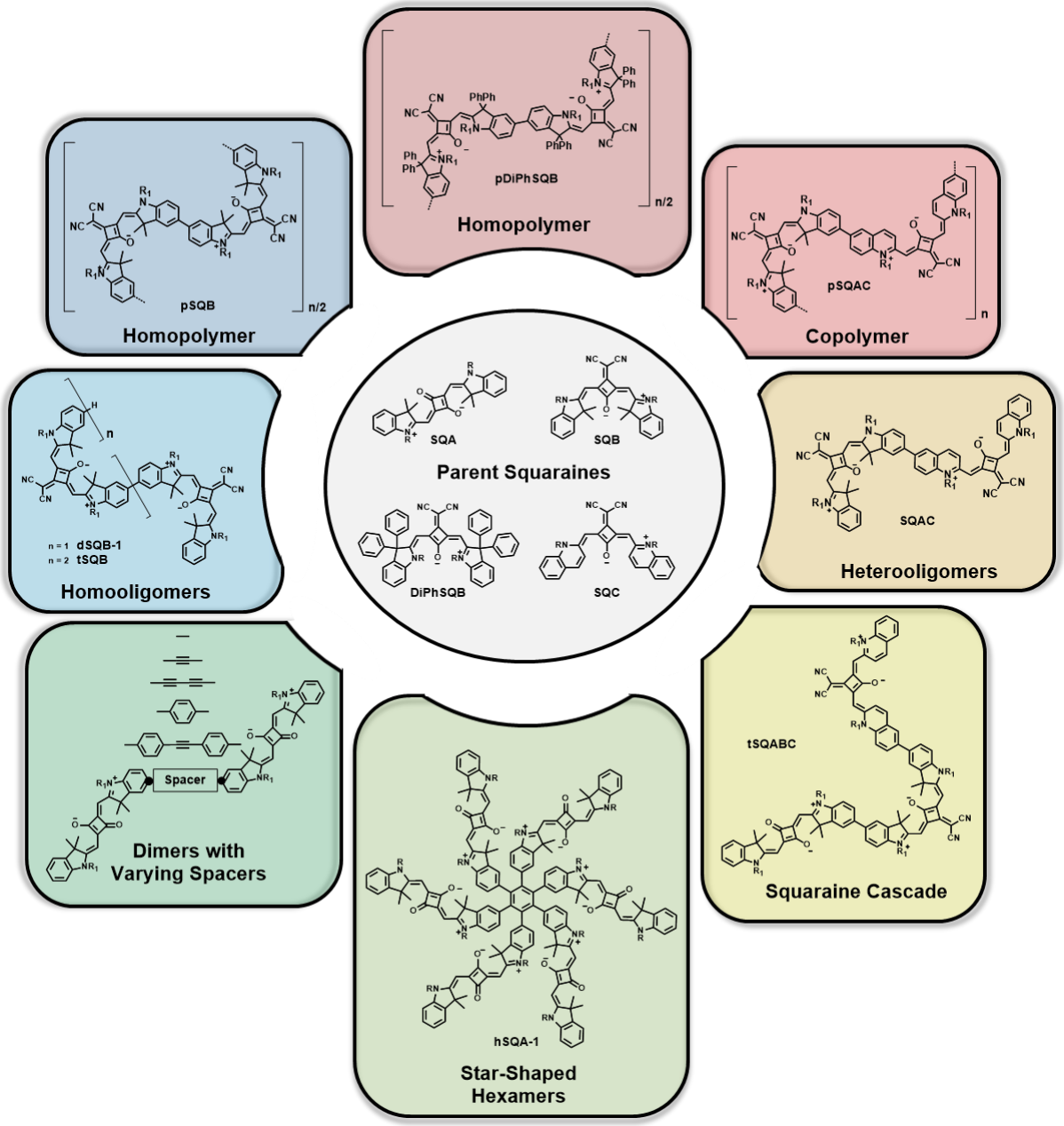

To promote a further derivatisation of these dyes, diverse functional groups were attached to the monomers using transition metal-catalysed C-C coupling reactions. However, this had to be preceded by the synthesis of bromine-functionalised derivatives as a direct halogenation of squaraine dyes is not feasible. Therefore, the halogen function was already introduced in precursor molecules. Finally, a molecular building block system could be realised containing bromine-, boronic ester-, and alkyne-functionalised monomer units, which paved the way to a plethora of squaraine oligomers and polymers. In the following, the results of this work are briefly summarised.

In chapter 3.1 an overview of literature-known squaraine monomers was given and their photophysical properties were investigated in order to evaluate their eligibility for the polymer synthesis. It was found that among the classic indolenine squaraines **SQA** and **SQB**, the benzoxazole (**SQD**), -thiazole (**SQE**), and –selenazole (**SQF**) analogues provide highly promising NIR-absorbing and -emitting properties. In particular, the latter three dyes exhibit high fluorescence quantum yields along with fluorescence lifetimes longer than 4 ns, which consequently made them highly interesting for the subsequent polymer synthesis.

Requiring dihalogenated monomer species, the following chapter 3.2 exclusively dealt with the attempts to introduce bromine-functionalities into these three monomers. The synthesis of the functionalised benzoxazole squaraine, starting from commercially available 3-bromophenol was hampered by poor yields of 11 % occurring in the last dicondensation reaction. Moreover, the small quantities of crude product were contaminated with considerable amounts of an inseparable side product formed by monodebromination. This would have consequently led to polymers with an extremely low degree of polymerisation, and for this reason, the project was not further pursued. Furthermore, the synthesis of benzothiazole-substituted squaraine polymers failed due to their photoinstability which was already noticed for analogous dimers. Due to the lack of synthetic protocols for either a systematic enlargement from brominated precursors or a direct bromination method of commercially available 2-methylbenzoselenazole, the variety of squaraine monomer units was reduced to indolenine and quinoline derivatives.

The following chapter dealt with the synthetic methodologies for functionalising indolenine squaraine dyes. In this respect, boronic ester and alkyne functionalities were attached at the periphery of the dyes applying Pd-catalysed Suzuki and Sonogashira coupling reaction. The resulting mono- and difunctionalised indolenine derivatives provided the basis for most of the herein presented oligomer and polymer systems.

Drawing from this diversity of functionalities, the indolenine homopolymer **pSQB-1** as well as the corresponding small molecular weight oligomers **dSQB-1** and **tSQB** were synthesized applying Ni-mediated Yamamoto and Pd-catalysed Suzuki coupling methodologies, respectively. The motivation for this project relied on the fundamental investigations by Völker et al. on **pSQB-V**. A progressive red-shift of the lowest energy absorption maximum from the dimer to the polymer was observed in $CHCl_3$ compared to the monomer. With increasing number of monomer units, the exciton coupling decreased from the dimer to the polymer. In addition, the shape of the absorption band manifold showed a strong dependence on the solvent, which was also observed by Völker et al. J-type aggregate behavior was found in chlorinated solvents such as $CHCl_3$ and DCM, whereas H-type aggregates were formed in acetone. Temperature-dependent absorption studies in PhCN revealed a reversible equilibrium of diverse polymer conformers, which manifested itself in a gradual change from H-aggregate behavior to a mixture with a more pronounced J-aggregate behavior upon raising the temperature. It was assumed that both characteristic aggregate bands correlate in borderline cases with two polymer structures which can be assigned to a zig-zag and a helical structure. As no experimental evidence for these structures could hitherto be provided by NMR, TD-DFT computations on oligomers (22-mers) could reproduce very closely the characteristic features of the spectra for the two conformational isomers.

The subsequent chapters 3.4.3-3.4.5 were motivated by the goal to influence the optical properties through a control of the superstructure and thus of the intramolecular aggregate formation.

On the one hand, bulky groups were implemented in the 3-position of the indolenine scaffold to provoke steric repulsion and thus favoring J-aggregate behavior at the expense of helical arrangements. The resulting homopolymers **pDiPhSQB** bearing two phenyl groups per indolenine exhibited J-type aggregate behavior with red-shifted absorption maxima in all considered solvents which was explained to be caused by the formation of elongated zig-zag structures. Furthermore, single-crystal X-ray analysis of monomer **DiPhSQB-2-Br$_2$** revealed a torsion of the indolenine moieties as a consequence of steric congestion. The twist of the molecular geometry and the resulting loss of planarity led to a serious deterioration of the fluorescence properties, however a significant bathochromic shift of ca. 1 200 cm^{-1} of the lowest absorption band was observed compared to parent **SQB**, which is even larger than the shift for **dSQB-1** (ca. 1 000 cm^{-1}).

On the other hand, a partial stiffening of the polymer backbone was attempted to create a bias for elongated polymer chains. In this respect, the synthetic approach was to replace every

second biarylaxis with the rigid *transoid* benzodipyrrolenine unit. Despite a rather low average degree of polymerization < 10, exclusively red-shifted absorption maxima were observed in all solvents used.

In order to complete the picture of intramolecular aggregates through the selective design of H-aggregates, a squaraine-squaraine copolymer was synthesised containing the classic *cisoid* indolenine as well as the *cisoid* quinoline building block. Taking advantage of the highly structure directing self-assembly character of the quinoline moiety, the copolymer **pSQBC** indeed showed a broad, blue-shifted main absorption band in comparison with the monomer unit **dSQBC**. The shape of the absorption band manifold solely exhibited a minor solvent and temperature dependence indicating a persistent H-aggregate behaviour. Hence, as a proof of concept, it was shown that the optical properties of the polymers (H- and J-aggregate) and the corresponding superstructure could be inherently controlled by an adequate design of monomer precursors.

In the following chapter 3.5 the optical properties of small **SQA** and **SQB** homo- and heterodimers could be fine-tuned likewise through a systematic variation of the spacer unit. As a result, the largest exciton coupling was obtained for dimers bearing a single biarylaxis, while dimers with larger spacers and consequently a larger interchromophore distances significantly exhibit lower couplings.

Furthermore, the exciton coupling effects were also studied in squaraine heterotrimers. Based on the findings from previous chapter, the trimers were prepared via Suzuki coupling, in which the chromophores were covalently linked through a biarylaxis in order to gain a stronger electronic communication. Among **tSQABA** and **tSQBAB**, the trimer **tSQABC** is particularly of interest as it provided the possibility to study energy transfer in a cascade exclusively consisting of squaraine dyes. Steady-state fluorescence studies revealed aside from emission from a delocalised lowest energy state, radiative transitions from higher localised states, disproving a complete and efficient intraband energy transfer. Because of the considerably red-shifted absorption of **tSQABC**, the underlying ultrafast dynamics could hitherto not be investigated by time-resolved 2D spectroscopy as part of a cooperation, since the experimental set-up was not yet optimised for measurements in the spectral regime of 700-900 nm.

The last chapter 3.7 of this work dealt, in contrast to all other chapters, with intermolecular aggregates. It was shown that the two star-shaped hexasquarainyl benzenes **hSQA-1** and **hSQA-2** exhibited a strong propensity for self-organisation. Concentration- and temperature-dependent studies revealed a great driving force for self-assembly in acetone. While the larger

hSQA-2 instantaneously formed stable aggregates, the aggregates of **hSQA-1** showed a pronounced kinetic stability. Taking advantage of the kinetic persistency of these aggregates, the corresponding kinetic activation parameters for aggregation and deaggregation could be assessed. The absorption spectra of both hexasquarainyl benzenes in the aggregated state revealed some striking differences. While **hSQA-1** featured an intensive, very narrow and blue-shifted absorption band, two red-shifted bands were observed for **hSQA-2**, which are closely located at the monomer absorption. The very small bandwidth of **hSQA-1** was interpreted to be caused by exchange narrowing and pointed towards highly ordered supramolecular aggregates. The concentration-dependent data of the two hexasquarainyl benzenes could be fitted to the dimer-model with excellent correlation coefficients, yielding binding constants in excess of 10^6 M^{-1}, respectively. Such high binding constants are very surprising, considering the unfavourable bulky 3,3-dimethyl groups of the indolenine units which should rather prevent aggregation. Joint theoretical and NMR spectroscopic methods were applied to unravel the supramolecular aggregate structure of **hSQA-1**, which was shown to consist of two stacked hexasquarainyl benzenes resembling the picture of two stacked bowls.

5 Experimental Section

5.1 Materials and Methods

5.1.1 Steady-State Absorption Spectroscopy

- JASCO V670 UV/vis/NIR-Spectrophotometer (software SpectraManager v. 2.08.04)
- Agilent Technologies Cary 5000 UV-vis-NIR spectrophotometer (software Agilent Cary WinUV Analysis and Bio v. 4.2)

Solvents for spectroscopic studies were of spectroscopic grade und used as received from Acros Organics. Absorption spectra were measured on a JASCO V670 UV/vis/NIR-Spectrophotometer in quartz cuvettes with path lengths of 0.1-10 mm at 293 K. For concentration-dependent studies, freshly prepared stock solutions were subsequently diluted to adjust the desired concentration. An Agilent Technologies Cary 5000 UV/vis/NIR spectrophotometer was used for kinetic experiments. For the kinetic experiments, the samples were prepared by dissolving the appropriate amount of solid in a defined volume of pre-tempered solvent reservoir (cuvette) using a cryostat RUL 80 (MGW-Lauda). The time-dependent absorption changes were subsequently monitored for a specific wavelength. Variable temperature absorption measurements were executed with an external cryostat OptistatDN (Oxford Instruments Nanoscience, England). The cryostat was accurately placed into the beam path of the Agilent Technologies Cary 5000 UV/vis/NIR spectrophotometer. The temperature was manually regulated with an electronic temperature control unit. The measuring cell was purged with argon prior to inserting the sample and sealed with a cuff to exclude moisture.

5.1.2 Steady-State Emission Spectroscopy

- Edinburgh Instruments FLS980 fluorescence lifetime spectrometer (software F980 version 1.2.2); 450 W Xenon lamp/PMT (R928P)
- Edinburgh Instruments FLS920 fluorescence lifetime spectrometer (software F900 version 7.2.1); 450 W Xenon lamp/PMT (R5509-42)

Steady-state emission spectra were recorded at 298 K in 10 mm quarts cells from Starna (Pfungstadt, Germany). The emission and excitation spectra were measured with strongly diluted samples (λ_{max}< 0.05 OD) in order to prevent self-absorption. The fluorescence

quantum yields were determined with optically dense samples in an integrating sphere. The observed fluorescence quantum yields were afterwards corrected for self-absorption applying the method of Bardeen et al.[140]

5.1.3 Time Dependent Fluorescence-Emission

- Edinburgh Instruments FLS980 fluorescence lifetime spectrometer (software F980 version 1.2.2); 450 W Xenon lamp/PMT (R928P)
- 15 240 cm^{-1} (656 nm) and 12 770 (783 nm) pulsed Laser Diodes/PMT (H10720)

The samples were prepared similarly to the steady-state emission experiments. Fluorescence lifetimes were determined by time-correlated single-photon counting (TCSPC). The samples were excited by a pulsed laser diode under magic angle conditions and the fluorescence was detected with a high-speed PMT detector (H10720). Deconvolution of the data (4096 channels) was conducted by measuring the instrument response function with a scatterer solution consisting of colloidal silicon in deionised water (LUDOX). The FAST software (version 3.4.2) was used to fit the decay curves with exponential decay functions.

5.1.4 Polarised Steady-State Fluorescence Excitation Spectroscopy

- Edinburgh Instruments FLS980 fluorescence lifetime spectrometer (software F980 version 1.2.2); 450 W Xenon lamp/PMT (R928P)

The fluorescence excitation anisotropy measurements were conducted using two polarisation filters for excitation and emission. The compounds were dissolved in highly viscous polyTHF (M_n ~ 650, CAS 25190-06-1, Sigma Aldrich) in 10 mm quartz cells from Starna (Pfungstadt, Germany) and measured at 298 K.

5.1.5 Cyclic Voltammetry (CV)

- Gamry Instruments Reference 600 Potentiostat/Galvanostat/ZRA (v. 6.2.2, Warminster, PA, USA)

Cyclic voltammograms were measured under an argon atmosphere using sample concentrations of ca. 1-3 mM. A standard three electrode set-up with a platinum disc working electrode (Ø = 1 mm), a Ag/AgCl “leak free” reference electrode (Warner Instruments,

Hamden, CT, USA) and a platinum wire counter electrode was used. The electrochemical cell was dried in an oven at 150 °C and flushed with argon prior to use. The reference electrode was measured against decamethylferrocene/decamethylferoccenium and afterwards referenced against the ferrocene/ferrocenium (Fc/Fc^+) redox couple.[198] A scan rate of 250 mV s^{-1} was applied for all CV measurements. The HOMO and LUMO energy levels ($E_{HOMO/LUMO}$) were acquired from the half-wave potential of the cyclic voltammetry measurements. The potential of the ferrocene/ferrocenium (Fc/Fc^+) redox couple in DCM/$^nBu_4NPF_6$ is 0.46 V vs. the saturated calomel electrode (SEC).[199] Moreover, the potential of SCE is 0.244 V vs. the normal hydrogen electrode (NHE),[200] having an absolute potential of 4.46 eV vs. vacuum.[201] Consequently, the energy levels and the electrochemically derived band gap E_{gap} in DCM are calculated as follows:

$$E_{HOMO/LUMO} = -5.16\ \text{eV} - E_{1/2}^{ox1/red1}$$

$$E_{gap} = E_{LUMO} - E_{HOMO}$$

5.1.6 NMR Spectroscopy

- Avance III HD 400 FT-Spectrometer (^1H: 400.13 MHz, ^{13}C: 100.61 MHz) with a Bruker Ultrashield magnet
- Avance III HD 400 FT-Spectrometer (^1H: 400.03 MHz, ^{13}C: 100.59 MHz) with a Bruker Ascend magnet
- Avance III HD 600 FT-Spectrometer (^1H: 600.13 MHz, ^{13}C: 150.90 MHz) with an Oxford Instrument magnet
- Avance III HD 600 FT-Spectrometer (^1H: 600.43 MHz, ^{13}C: 150.98 MHz) with a Bruker Ascend magnet

^1H and ^{13}C spectra were recorded with one of the spectrometers listed above using high sample concentration of > 0.1 mM in deuterated solvents (e.g. $CDCl_3$, CD_2Cl_2, acetone-d_6, dimethylsulfoxid-d_6). Deuterated solvents were used without further purification. ^1H-chemical shifts are indicated in ppm relative to the residual non-deuterated solvent signal (^1H: $CHCl_3$: δ 7.26 ppm, CH_2Cl_2: δ 5.32 ppm, acetone: δ 2.05 ppm, dimethlysulfoxide: δ 2.50 ppm; ^{13}C: $CHCl_3$: δ 77.16 ppm, CH_2Cl_2: δ 53.84 ppm, acetone: δ 29.84 ppm).[202] The Abbreviations used for the spin multiplicities and C-atom descriptions are: s = singlet, d =doublet, m = multiplet, dd = doublet of doublet, ddd = doublet of doublet of doublet; prim = primary, sec =secondary, tert =tertiary, quart =quaternary. Multiplet signals or overlapping multiplet signals in ^1H-NMR spectra which could not be assigned to first order

couplings are indicated as (-). The coupling constants are given in Hertz (Hz). Order of description for ^{1}H-NMR spectra: chemical shift (spin multiplicity, coupling constant, number of protons, assignment).

5.1.7 Mass Spectrometry

- Bruker Daltonics microTOF focus (ESI)
- Bruker Daltonics autoflex II (MALDI)

Mass spectra were recorded with a Bruker Daltonics autoflex II (MALDI) in positive mode (POS) utilizing a DCTB (*trans*-2-[3-(4-*tert*-butylphenyl)-2-methyl-2-propenyl-idene]malononitrile) matrix. High resolution mass spectrometry was performed on a Bruker Daltonic microTOF focus (ESI). All mass spectrometry peaks are reported as m/z. For calculation of the respective mass values of the isotopic distribution, the software Compass 1.1 from Bruker Daltonics GmbH (Bremen, Germany) was used. Calculated (calc.) and measured (found) peak values always refer to the most intense peak of the isotopic distribution.

5.1.8 Atomic Force Microscopy (AFM)[XV]

AFM measurements were performed under ambient conditions using a Bruker Multimode 8 SPM system operating in tapping mode in air. Silica cantilevers (OMCL-AC200TS, Olympus) with a resonance frequency of ~ 150 kHz and a spring constant of ~ 10 Nm^{-1} were used. The samples were prepared by spin-coating of methylcyclohexane (MCH) solution onto mica and highly oriented pyrolytic graphite (HOPG) with 2 000 rpm.

5.1.9 Recycling Gel Permeation Chromatography (GPC)

Shimadzu GPC System

- Model SPD-M20A diode array detector
- CBM-20A system controller
- LC-20AD solvent delivery unit
- DGU 20A9 online degasser

[XV] AFM-measurements and analysis were carried out by Dr. Vladimir Stepanenko.

Gel permeation chromatography (GPC) was carried out at 293 K in chloroform (HPLC grade). Preparative chromatography was performed in recycling mode on two consecutive SDV columns (PSS preparative 50 Å and 500 Å, dimensions 20×600 mm) from PSS (Mainz, Germany) with a flow rate of 1 and 4 ml min^{-1}. Analytical chromatography was executed with a SDV column (mixed bed, "Linear S", 5 µm particle size, 8×300 nm) from PSS. Polystyrene solutions of different molecular weight (~ 1 mg ml^{-1}) were used as calibration standard.

5.2 Synthesis

All reactions were carried out in standard glassware and chemicals purchased from commercial suppliers were used without further purification. All reactions being conducted under nitrogen atmosphere were performed in oven-dried vessels. The solvents were dried according to standard literature procedures and stored under nitrogen atmosphere. The nitrogen was dried over Sicapent® from Merck and oxygen was removed by copper oxide catalyst R3-11 from BASF). Flash column chromatography was carried out on silica gel (60 Å, 40-63 µm, Macherey-Nagel "Silica 60 M") in glass columns.

5.2.1 Synthesis of Precursors

The precursors 5-bromo-2,3,3,trimethyl-3*H*-indole **1**,[148] 1-iodo-3,7-dimethyloctane,[137] quaternary salts **6**-**10**,[11,44,71] semisquaraine ethyl esters **19** and **20**,[68] semisquaraine acid derivates **21** and **22**,[203] dicyano-functionalized semisquaraine salts **23** and **24**,[136] 3,3'-(1,4-phenylenebis(azanediyl))bis(3-methylbutan-2-one) **33**,[204] 2,3,3,6,7,7-hexamethyl-3,7-dihydropyrrolo[2,3-*f*]indole **34**,[204] bis-iodo salt of 2,3,3,6,7,7-hexamethyl-3,7-dihydropyrrolo[2,3-*f*]indole **35**,[204] 2,3,3,5,5,6-hexamethyl-3,5-dihydropyrrolo[3,2-*f*]indole **36**,[169] bis-iodo salt of 2,3,3,5,5,6-hexamethyl-3,5-dihydropyrrolo[3,2-*f*]indole **37**,[204] semisquaraine butyl ester **39**,[68] dicyano-functionalized semisquaraine salt **40**,[11] and 4,4''-dibromo-3',4',5',6'-tetraphenyl-1,1':2',1''-terphenyl[205] **HAB-Br$_2$** were synthesized according to given literature procedures.

CN

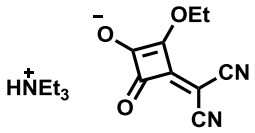

CAS: 1788877-12-2

Synthesis according to given literature.[206]

Malononitrile (382 mg, 5.78 mmol) was dissolved in benzene (30 ml) and 3,4-diethoxycyclobut-3-ene-1,2-dione (1.00 g, 5.88 mmol), and triethylamine (792 ml, 5.68 mmol) were consecutively added dropwise over a period of 5 min, respectively. The reaction was stirred at ambient temperature for 10 min and allowed to stand in the freezer at -25 °C overnight. The resulting solid was filtered off and dried under high vacuum.

Yield: 1.57 g (5.39 mmol, 95 %) of a light yellow solid.

$C_{15}H_{21}N_3O_3$ [291.35]

^{1}H-NMR (400.1 MHz, DMSO):

δ [ppm] = 8.83 (s, 1H, N*H*), 4.61 (q, ^3J = 7.1 Hz, 2H, OC*H*$_2$CH$_3$), 3.10 (q, ^3J = 7.2 Hz, 6H, 3 × HNC*H*$_2$CH$_3$), 1.34 (t, ^3J = 7.1 Hz, 3H, OCH$_2$C*H*$_3$), 1.18 (t, ^3J = 7.2 Hz, 9H, 3 × HNCH$_2$C*H*$_3$).

3,3-diphenylindolin-2-one

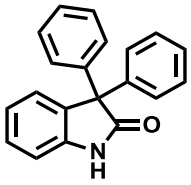

CAS: 1922-79-8

Synthesis based on given literature.[160]

Under a nitrogen atmosphere indoline-2,3-dione (500 mg, 3.40 mmol) was dissolved in TfOH (10.0 ml, 113 mmol) and benzene (5.00 ml, 55.7 mmol) was subsequently added dropwise over a period of 5 min. The resulting mixture was stirred at ambient temperature for 18 h. The reaction was poured on ice (100 g) and extracted with $CHCl_3$ (3 × 50 ml). The organic layer was washed with H_2O (50 ml) and saturated NaCl-solution (50 ml). The combined organic phases were dried over $MgSO_4$ and the solvent was removed under reduced pressure. The crude product was purified by flash chromatography (DCM/EA = 20:1).

Yield: 950 mg (3.33 mmol, 98 %) of a colourless solid.

$C_{20}H_{15}NO$ [285.34]

^{1}H-NMR (400.1 MHz, $CDCl_3$):

δ [ppm] = 7.61 (s, 1H, N*H*), 7.35-7.21 (-, 12H, 12 × C*H*), 7.07 (dd, ^3J = 6.6 Hz, ^4J = 1.0 Hz, 1H, C*H*), 6.95 (m, 1H, C*H*).

5-bromo-3,3-diphenylindolin-2-one

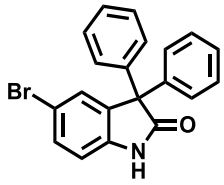

CAS: 63483-15-8

Synthesis based on given literature.[160]

Under a nitrogen atmosphere 5-bromoindoline-2,3-dione (154 mg, 681 µmol) was dissolved in TfOH (2.00 ml, 22.5 mmol) and benzene (1.00 ml, 11.1 mmol) was subsequently added dropwise. The resulting mixture was stirred at rt for 18 h. The reaction was poured on ice (25 g) and extracted with $CHCl_3$ (3 × 50 ml). The organic layer was washed with H_2O (50 ml) and saturated NaCl-solution (50 ml). The combined organic phases were dried over $MgSO_4$ and the solvent was removed under reduced pressure. The crude product was purified by flash chromatography (DCM/EA = 20:1).

Yield: 236 mg (648 µmol, 95 %) of a colourless solid.

$C_{20}H_{14}BrNO$ [364.24]

^{1}H-NMR (400.1 MHz, $CDCl_3$):

δ [ppm] = 7.52 (s, 1H, N*H*), 7.39 (dd, ^3J = 8.2 Hz, ^4J = 1.9 Hz, 1H, C*H*), 7.36-7.22 (-, 11H, 11 × C*H*), 6.58 (d, ^3J = 8.3 Hz, 1H, C*H*).

1-(3,7-dimethyloctyl)-3,3-diphenylindolin-2-one

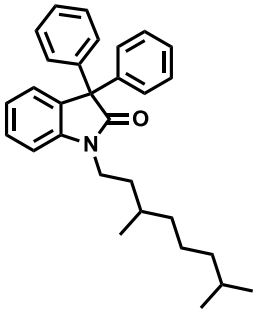

Synthesis based on given literature.[61]

Under a nitrogen atmosphere 3,3-diphenylindolin-2-one (950 mg, 3.33 mmol) and oven-dried anhydrous K_2CO_3 (4.60 g, 33.3 mmol) were suspended in dry DMF (10 ml) and stirred at ambient temperature for 30 min. 1-Iodo-3,7-dimethyloctane (1.79 g, 8.09 mmol) was subsequently added and the reaction was heated at 60 °C in a sealed tube for 18 h. The cooled reaction was quenched with H_2O (50 ml) and extracted with $CHCl_3$ (3 × 50 ml). The organic layer was dried over Na_2SO_4 and the solvent was evaporated under reduced pressure. The crude product was purified by flash chromatography (PE/EA = 20:1).

Yield: 826 mg (1.94 mmol, 58 %) of a colourless oil.

$C_{30}H_{35}NO$ [425.61]

^{1}H-NMR (400.1 MHz, CD_2Cl_2):

δ [ppm] = 7.32 (dd, ^3J = 7.8 Hz, 1H, C*H*), 7.31-7.19 (-, 11H, 11 × C*H*), 7.07 (dd, ^3J = 7.6 Hz, ^4J = 1.0 Hz, 1H, C*H*), 6.96 (d, ^3J = 7.9 Hz, 1H, C*H*), 3.87-3.70 (m, 2H, NCH_2), 1,79-1.66 (m, 1H, NCH_2CH), 1.53-1.42 (-, 3H, 2 × C*H*, NCH_2CH), 1.38- 1.08 (-, 6H, 3 × CH_2), 0.97 (d, ^3J = 6.4 Hz, 3H, CH_3), 0.85 (d, ^3J = 6.6 Hz, 6H, 2 × CH_3).

^{13}C-NMR (100.6 MHz, CD_2Cl_2):

δ [ppm] = 177.3 (quart), 143.0 (quart), 142.55 (quart)*, 142.50 (quart)*, 133.4 (quart), 128.79 (tert)*, 128.77 (tert)*, 128.73 (tert)*, 128.72 (tert)*, 128.70 (tert), 127.6 (tert), 126.4 (tert), 122.8 (tert), 109.3 (tert), 62.7 (quart), 39.5 (sec), 39.0 (sec),

37.4 (sec), 34.7 (sec), 31.1 (tert), 28.4 (tert), 25.0 (sec), 22.83 (prim)*, 22.75 (prim)*, 19.6 (prim).

* The signals of the primary, tertiary, and quaternary C-atoms split into two signals of equal intensity.

MALDI-MS pos: [$M^{\cdot+}$]

calc.: 425.271 m/z

found: 425.228 m/z

5-bromo-1-(3,7-dimethyloctyl)-3,3-diphenylindolin-2-one

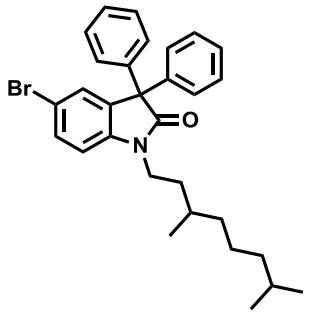

Synthesis based on given literature.[61]

Under a nitrogen atmosphere 5-bromo-3,3-diphenylindolin-2-one (3.35 g, 9.19 mmol) and oven-dried anhydrous K_2CO_3 (12.7 g, 91.9 mmol) were suspended in dry DMF (25 ml) and stirred at rt for 30 min. 1-Iodo-3,7-dimethyloctane (4.93 g, 18.4 mmol) was subsequently added and the reaction was heated at 60 °C in a sealed tube for 18 h. The cooled reaction was quenched with H_2O (100 ml) and extracted with $CHCl_3$ (3 × 50 ml). The organic layer was dried over Na_2SO_4 and the solvent was evaporated under reduced pressure. The crude product was purified by flash chromatography (PE/EA = 20:1).

Yield: 3.36 g (6.66 mmol, 72 %) of a colourless oil.

$C_{30}H_{34}BrNO$ [504.50]

^{1}H-NMR (400.1 MHz, $CDCl_3$):

δ [ppm] = 7.40 (dd, ^3J = 8.3 Hz, ^4J = 2.0 Hz, 1H, C*H*), 7.32 (d, ^4J = 2.0 Hz, 1H, C*H*), 7.32-7.31 (-, 10H, 10 × C*H*), 6.78 (d, ^3J = 8.3 Hz, 1H, CH), 3.84-3.65 (m, 2H, NCH_2), 1.75-1.61 (m, 1H, NCH_2CH), 1.54-1.40 (-, 3H, NCH_2CH, 2 × C*H*),

1.34-1.04 (-, 6H, 3 × CH_2), 0.93 (d, ^3J = 6.2 Hz, 3H, CH_3), 0.82 (d, ^3J = 6.6 Hz, 6H, 2 × CH_3).

^{13}C-NMR (100.6 MHz, CD_2Cl_2):

δ [ppm] = 176.9 (quart), 142.1 (quart)*, 141.83 (quart)*, 141.77 (quart), 135.5 (quart), 131.6 (tert), 129.4 (tert), 128.88 (tert)*, 128.87 (tert)*, 128.72 (tert)*, 128.70 (tert)*, 127.9 (tert), 115.3 (quart), 110.9 (tert), 62.8 (quart), 39.5 (sec), 39.1 (sec), 37.4 (sec), 34.5 (sec), 31.1 (tert), 28.3 (tert), 25.0 (sec), 22.8 (prim)*, 22.7 (prim)*, 19.6 (prim).

* The signals of the primary, tertiary, and quaternary C-atoms split into two signals of equal intensity.

MALDI-MS pos: [$M^{\cdot+}$]

calc.: 505.180 m/z

found: 505.170 m/z

5-bromo-1-hexyl-3,3-diphenylindolin-2-one

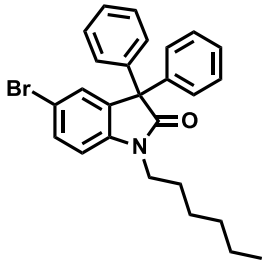

Synthesis based on given literature.[61]

Under a nitrogen atmosphere 5-bromo-3,3-diphenylindolin-2-one (1.00 g, 2.75 mmol) and oven-dried anhydrous K_2CO_3 (3.79 g, 27.4 mmol) were suspended in dry DMF (25 ml) and stirred at ambient temperature for 30 min. 1-Iodohexane (1.79 g, 8.44 mmol) was subsequently added and the reaction was heated at 60 °C in a sealed tube for 18 h. The cooled reaction was quenched with H_2O (100 ml) and extracted with $CHCl_3$ (3 × 50 ml). The organic layer was dried over Na_2SO_4 and the solvent was evaporated under reduced pressure. The crude product was purified by flash chromatography (PE/EA = 20:1).

Yield: 764 mg (1.70 mmol, 62 %) of a colourless solid.

$C_{26}H_{26}NOBr$ [448.40]

^{1}H-NMR (400.1 MHz, CD_2Cl_2):

δ [ppm] = 7.45 (dd, ^3J = 8.3 Hz, ^4J = 2.0 Hz, 1H, C*H*), 7.35 (dd, ^4J = 2.0 Hz, ^5J = 0.3 Hz, 1H, C*H*), 7.34-7.26 (-, 6H, 6 × C*H*), 7.24-7.14 (-, 4H, 4 × C*H*), 6.86 (d, ^3J = 8.3 Hz, 1H, C*H*), 3.74 (t, ^3J = 7.3 Hz, 2H, NCH_2), 1.69 (m, 2H, NCH$_2$CH_2), 1.37-1.20 (-, 6H, 3 × CH_2), 0.85 (t, ^3J = 7.0 Hz, 3H, CH_3).

^{13}C-NMR (100.6 MHz, CD_2Cl_2):

δ [ppm] = 177.0 (quart), 142.2 (quart), 141.8 (quart), 135.5 (quart), 131.5 (tert), 129.4 (tert), 128.9 (tert), 128.7 (tert), 127.9 (tert), 115.3 (quart), 110.9 (tert), 62.8 (quart), 40.8 (sec), 31.7 (sec), 27.6 (sec), 26.8 (sec), 22.9 (sec), 14.1 (prim).

MALDI-MS pos: [$M^{\cdot+}$]

calc.: 449.118 m/z

found: 449.150 m/z

5.2.2 Synthesis of Squaraine Monomers

Squaraine monomers **SQA**,[72] **SQB**,[71] **SQD**,[11] and **SQF**[11] were synthesized according to literature procedures.

SQC

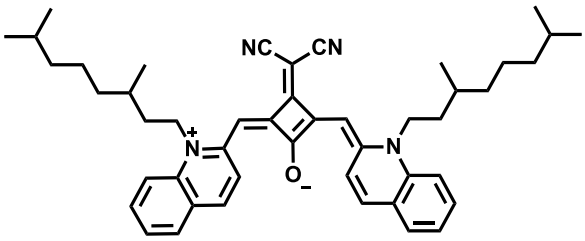

1-(3,7-Dimethyloctyl)-2-methylquinolin-1-ium iodide (**7**) (610 mg, 1.48 mmol) and dicyanovinylene salt **CN** (207 mg, 710 µmol) were dissolved in pyridine (3 ml) and a mixture of *n*-butanol and toluene (1:1, 20 ml) and heated under reflux for 18 h using a *Dean-Stark* trap. The cooled reaction mixture was concentrated *in vacuo* and the residue purified by flash chromatography (DCM). The crude product was dissolved in a small amount of DCM and dripped into an excess of *n*-hexane. The precipitate formed was filtered off and washed with *n*-hexane.

Yield: 118 mg (170 µmol, 24 %) of a green solid.

$C_{47}H_{56}N_4O$ [692.98]

^{1}H-NMR (400.1 MHz, CD_2Cl_2):

δ [ppm] = 9.11 (d, ^{3}J =9.6 Hz, 2H, 2 × C*H*), 7.63-7.56 (-, 6H, 6 × C*H*), 7.46 (d, ^{3}J =8.8 Hz, 2H, 2 × C*H*), 7.37-7.27 (m, 2H, 2 × C*H*), 6.24 (s, 2H, 2 × C*H*), 4.39-4.11 (m, 4H, 2 × NCH_2), 1.92-1.79 (m, 4H, 2 × NCH_2CH_2), 1.79-1.63 (m, 2H, 2 × C*H*), 1.63-1.49 (m, 2H, C*H*), 1.49-1.17 (-, 12H, 6 × CH_2), 1.10 (d, ^{3}J =6.5 Hz, 6H, 2 × CH_3), 0.89 (d, ^{3}J =6.5 Hz, 12H, 4 × CH_3).

^{13}C-NMR (150.9 MHz, CD_2Cl_2):

δ [ppm] = 175 (quart), 165.7 (quart), 163.5 (quart), 151.5 (quart), 140.0 (quart), 134.5 (tert), 132.0 (tert), 129.3 (tert), 126.0 (tert), 125.7 (quart), 124.8 (tert), 119.3

(quart), 115.3 (tert), 94.4 (tert), 48.4 (sec), 40.5 (quart), 39.6 (sec), 37.5 (sec), 34.0 (sec), 31.7 (tert), 28.4 (tert), 25.0 (sec), 22.84 (prim)*, 22.78 (prim)*, 19.4 (prim).

* The signal of the primary C-atom splits into two signals of equal intensity.

ESI-MS pos (high resolution): [$M^{\cdot+}$]

calc.: 692.44486 m/z

found: 692.44468 m/z Δ = 0.26 ppm

SQE

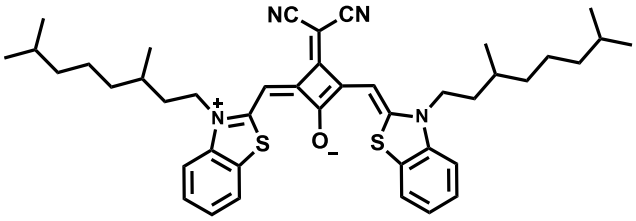

3-(3,7-Dimethyloctyl)-2-methylbenzo[*d*]thiazol-3-ium iodide (**9**) (2.00 g, 4.79 mmol) and dicyanovinylene salt **CN** (661 mg, 2.27 mmol) were dissolved in pyridine (10 ml) and a mixture of *n*-butanol and toluene (1:1, 25 ml) and heated under reflux for 18 h using a *Dean-Stark* trap. The cooled reaction mixture was concentrated *in vacuo* and the residue purified by flash chromatography (DCM/MeOH = 99:1).

Yield: 869 mg (1.23 mmol, 54 %) of a green solid.

$C_{43}H_{52}N_4OS_2$ [705.03]

^{1}H-NMR (600.1 MHz, CD_2Cl_2):

δ [ppm] = 7.62 (dd, ^3J = 7.8 Hz, ^4J = 0.6 Hz, 2H, C*H*), 7.47-7.41 (m, 2H, 2 × C*H*), 7.29-7.25 (m, 2H, 2 × C*H*), 7.23 (d, ^3J = 8.4 Hz, 2H, 2 × C*H*), 6.26 (s, 2H, 2 × C*H*), 4.18-4.06 (m, 4H, 2 × NCH_2), 1.85-1.76 (m, 2H, 2 × NCH_2CH), 1.70-1.58 (-, 4H, 2 × NCH_2CH, 2 × C*H*), 1.54 (m, 2H, 2 × C*H*), 1.42-1.11 (- , 12 H, 6 × CH_2), 1.05 (d, ^3J = 6.4 Hz, 6H, 2 × CH_3), 0.87 (d, ^3J = 6.6 Hz, 12 H, 4 × CH_3).

^{13}C-NMR (150.9 MHz, CD_2Cl_2):

δ [ppm] = 174.1 (quart), 164.5 (quart), 162.5 (quart), 160.8 (quart), 141.2 (quart), 128.9 (quart), 127.8 (tert), 124.9 (tert), 122.7 (tert), 119.0 (quart), 112.3 (tert), 87.0 (tert), 45.8 (sec), 40.2 (quart), 39.5 (sec), 37.4 (sec), 34.4 (sec), 31.5 (tert), 28.4 (tert), 25.0 (sec), 22.8 (prim)*, 22.7 (prim)*, 19.6 (prim).

* The signal of the primary C-atom splits into two signals of equal intensity.

MALDI-MS pos: [$M^{\cdot+}$]

calc.: 704.358 m/z

found: 704.182 m/z

DiPhSQB

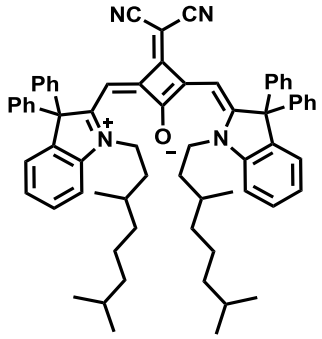

Under a nitrogen atmosphere MeMgBr (5.24 ml, 7.34 mmol, 1.4 M in 3:1 toluene/THF) was added dropwise to 1-(3,7-dimethyloctyl)-3,3-diphenylindolin-2-one (780 mg, 1.83 mmol) in dry THF (10 ml), and the reaction was heated to 60 °C for 2.5 h. The reaction was allowed to cool. MeOH (10 ml) was subsequently added and the reaction was concentrated under reduced pressure. The resulting residue was treated with HCl (3 M, 30 ml) and extracted with DCM (3 × 50 ml). The combined organic phases were dried over Na_2SO_4 and the solvent was removed under reduced pressure to yield crude 1-(3,7-dimethyloctyl)-2-methyl-3,3-diphenyl-3*H*-indol-1-ium chloride as a green foam (759 mg, 1.65 mmol, 90 %), which was used without further purification due to rapid decomposition when exposed to moist air.

1-(3,7-Dimethyloctyl)-2-methyl-3,3-diphenyl-3*H*-indol-1-ium chloride (759 mg, 1.65 mmol) and dicyanovinylene salt **CN** (200 mg, 686 µmol) were suspended in pyridine (3 ml) and a mixture of toluene and 1-butanol (1:1, 50 ml) and heated under reflux for 18 h using a *Dean-*

Stark trap. The solvent was removed under reduced pressure and the residue was purified by flash chromatography (DCM). The crude product was recrystallized from *n*-hexane.

Yield: 321 mg (330 μmol, 48 %) of a green solid.

$C_{69}H_{72}N_4O$ [973.34]

^{1}H-NMR (600.1 MHz, CD_2Cl_2):

δ [ppm] = 7.38 (dd, ^{3}J = 8.0 Hz, ^{4}J = 1.2 Hz, 2H, 2 × C*H*), 7.33-7.27 (-, 12H, 12 × C*H*), 7.26-7.12 (-, 14H, 14 × C*H*), 6.06 (s, 2H, 2 × C*H*), 4.69-4.19 (m, 4H, 2 × NCH_2), 1.76-1.64 (m, 2H, 2 × NCH_2C*H*), 1.52-1.43 (-, 4H, 2 × CH, 2 × NCH_2C*H*), 1.43-1.32 (m, 2H, 2 × C*H*), 1.31-1.19 (-, 4H, 2 × CH_2), 1.16-1.03 (-, 8H, 4 × CH_2), 0.88 (d, ^{3}J = 6.5 Hz, 6H, 2 × CH_3), 0.84 (d, ^{3}J = 6.7 Hz, 12H, 4 × CH_3).

^{13}C-NMR (150.9 MHz, CD_2Cl_2):

δ [ppm] = 175.2 (quart), 170.9 (quart), 166.15 (quart), 166.07 (quart), 143.6 (quart), 142.05 (quart)*, 141.99 (quart)*, 139.8 (quart), 129.1 (tert), 129.0 (tert), 128.0 (2 × tert), 125.9 (tert), 125.5 (tert), 118.3 (quart), 112.2 (tert), 92.5 (tert), 68.5 (quart), 45.4 (sec), 41.7 (quart), 39.6 (sec), 37.44 (sec)*, 37.42 (sec)*, 34.6 (sec), 31.0 (tert), 28.4 (tert), 24.99 (sec)*, 24.98 (sec)*, 22.8 (prim)*, 22.7 (prim)*, 19.7 (prim).

* The signals of the primary, secondary, and quaternary C-atoms split into two signals of equal intensity.

ESI-MS pos (high resolution): [$M^{\cdot+}$]

calc.: 972.57006 m/z

found: 972.57101 m/z Δ = 0.98 ppm

5.2.3 Synthesis of Functionalised Squaraine Dyes

Functionalized squaraine dyes **SQA-Br**,[68] **SQA-Br$_2$**,[44] **SQA-B$_2$**,[68] **SQB-Br$_2$**,[71] were synthesized according to literature procedures.

SQA-B

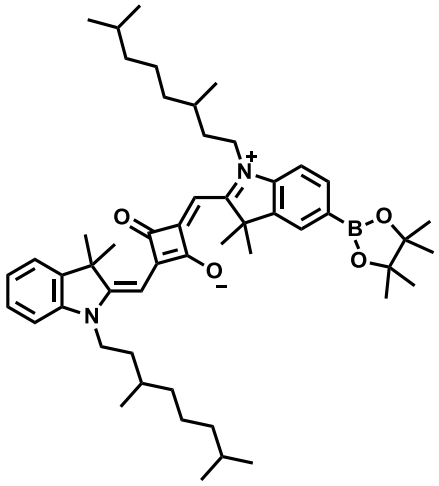

Synthesis based on given literature.[68]

Under a nitrogen atmosphere squaraine **SQA-Br** (810 mg, 1.07 mmol), bis(pinacolato)diboron (381 mg, 1.50 mmol) and KOAc (335 mg, 3.41 mmol) were suspended in dry 1,4-dioxane (15 ml). The mixture was purged in a gentle stream of nitrogen for 15 min. $Pd(PhCN)_2Cl_2$ (21.0 mg, 54.7 µmol) and 1,1´-bis(diphenylphosphino)ferrocene (dppf) (30.0 mg, 54.1 µmol) were added and the reaction was continuously heated at 85 °C in a sealed tube for 18 h. The solvent was removed *in vacuo* and the residue purified by flash chromatography (PE/EA 1:1). The crude product was dissolved in a small amount of DCM and dripped into an excess of *n*-hexane. The mixture was allowed to stand at 4 °C in the refrigerator overnight. The precipitate formed was separated by filtration and dried under high vacuum.

Yield: 773 mg (963 µmol, 90 %) of a blue solid.

$C_{52}H_{75}BN_2O_4$ [802.98]

^{1}H-NMR (400.1 MHz, CD_2Cl_2):

δ [ppm] = 7.78 (dd, ^{3}J = 8.0 Hz, ^{4}J = 1.2 Hz, 1H, C*H*), 7.76-7.73 (m, 1H, C*H*), 7.36 (dd, ^{3}J = 7.7 Hz, ^{4}J = 0.9 Hz, 1H, C*H*), 7.31 (ddd, ^{3}J = 7.7 Hz, ^{3}J = 7.7 Hz, ^{4}J = 1.0 Hz, 1H, C*H*), 7.15 (ddd, ^{3}J = 7.5 Hz, ^{3}J = 7.5 Hz, ^{4}J = 0.7 Hz, 1H, C*H*), 6.97 (d, ^{3}J = 8.3 Hz, 1H, C*H*), 6.93 (d, ^{3}J = 8.3 Hz, 1H, C*H*), 5.98 (s, 1H, C*H*), 5.96 (s, 1H, C*H*), 4.07-3.92 (-, 4H, 2 × NCH_2), 2.08-1.89 (-, 2H, 2 × NCH_2C*H*), 1.85-1.46 (-, 18H, 2 × NCH_2C*H*, 4 × C*H*, 4 × CH_3), 1.36 (s, 12H, 4 × CH_3), 1.42-1.10 (-, 12H, 6 × CH_2), 1.05 (d, ^{3}J = 5.7 Hz, 3H, CH_3), 1.03 (d, ^{3}J = 5.7 Hz, 3H, CH_3), 0.87 (d, ^{3}J = 6.4 Hz, 6H, 2 × CH_3), 0.86 (d, ^{3}J = 6.4 Hz, 6H, 2 × CH_3).

^{13}C-NMR (100.6 MHz, CD_2Cl_2):

δ [ppm] = 182.0 (2 × quart), 181.8 (quart), 180.1 (quart), 170.7 (quart), 169.4 (quart), 145.5 (quart), 142.73 (quart), 142.70 (quart), 141.8 (quart), 135.3 (tert), 128.4 (tert), 128.2 (tert), 124.2 (tert), 124.0 (quart), 122.6 (tert), 109.9 (tert), 109.0 (tert), 87.2 (tert), 87.0 (tert), 84.2 (quart), 49.7 (quart), 49.2 (quart), 42.5 (sec), 42.3 (sec), 39.5 (2 × sec), 37.5 (2 × sec), 34.1 (sec), 34.0 (sec), 31.50 (tert), 31.48 (tert), 28.4 (2 × tert), 27.2 (prim), 27.0 (prim), 25.08 (2 × sec), 25.06 (prim), 22.8 (prim), 22.7 (prim), 19.78 (prim), 19.77 (prim).

MALDI-MS pos: [$M^{\cdot+}$]

calc.: 802.976 m/z

found: 802.625 m/z

SQA-TMSA

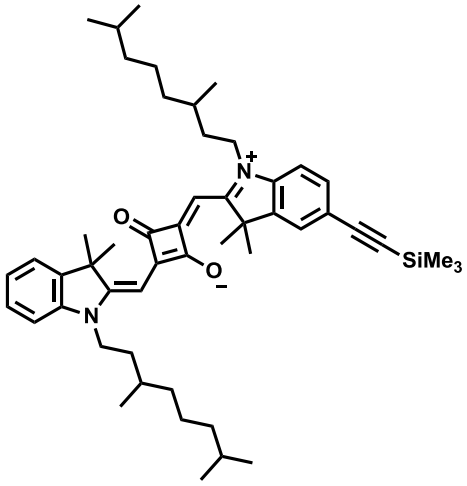

Synthesis based on given literature.[149]

Under a nitrogen atmosphere squaraine **SQA-Br** (364 mg, 482 µmol) was dissolved in dry NEt_3 (15 ml). The deep blue solution was degassed in a gentle stream of nitrogen for 20 min. CuI (2.76 mg, 14.5 µmol), $Pd(PPh_3)_2Cl_2$ (10.2 mg, 14.5 µmol), and trimethylsilylacetylene (267 µl, 1.92 mmol) were subsequently added and the reaction mixture was heated under reflux for 2 h. After cooling to room temperature the solvent was removed *in vacuo* and the residue was subjected to a rapid silica filtration (DCM/MeOH = 99:1).

Yield: 290 mg (375 µmol, 78 %) of a blue solid.

$C_{51}H_{72}N_2O_2Si$ [773.22]

^{1}H-NMR (400.1 MHz, CD_2Cl_2):

δ [ppm] = 7.45-7.36 (-, 3H, 3 × C*H*), 7.33 (ddd, ^3J = 7.7 Hz, ^3J = 7.7 Hz, ^4J = 1.2 Hz, 1H, C*H*), 7.18 (ddd, ^3J = 7.4 Hz, ^3J = 7.4 Hz, ^4J = 0.8 Hz, 1H, C*H*), 7.04 (d, ^3J = 7.9 Hz 1H, C*H*), 6.90 (dd, ^3J = 8.6 Hz, ^4J = 0.6 Hz, 1H, C*H*), 5.96 (s, 1H, C*H*), 5.90 (s, 1H, C*H*), 4.13-4.00 (m, 2H, NCH_2), 4.00-3.80 (m, 2H, NCH_2), 1.88-1.69 (-, 14H, 2 × NCH_2CH, 4 × CH_3), 1.69-1.59 (-, 4H, 2 × NCH_2CH, 2 × C*H*), 1.59-1.48 (-, 2H, 2 × C*H*), 1.45-1.13 (-, 12H, 6 × CH_2), 1.09-1.02 (-, 6H, 2 × CH_3), 0.90-0.82 (-, 12H, 4 × CH_3), 0.25 (s, 9H, $Si(CH_3)_3$).

^{13}C-NMR (100.6 MHz, CD_2Cl_2):

δ [ppm] = 181.9 (2 × quart), 181.8 (quart), 179.4 (quart), 171.3 (quart), 168.8 (quart), 144.2 (quart), 143.2 (quart), 142.8 (quart), 142.6 (quart), 132.3 (tert), 128.2 (tert), 126.1 (tert), 124.5 (tert), 122.6 (tert), 117.9 (quart), 110.1 (tert), 109.3 (tert), 105.5 (quart), 94.2 (quart), 87.3 (2 × tert), 49.9 (quart), 49.1 (quart), 42.6 (sec), 42.4 (sec), 39.5 (2 × sec), 37.5 (2 × sec), 34.2 (sec), 34.0 (sec), 31.49 (tert), 31.47 (tert), 28.4 (2 × tert), 27.2 (prim), 27.0 (prim), 25.1 (2 × sec) 22.8 (prim), 22.7 (prim), 19.8 (2 × prim), 0.04 (prim).

MALDI pos: [$M^{\cdot+}$]

calc.: 773.536 m/z

found: 772.549 m/z

SQA-Alkyne

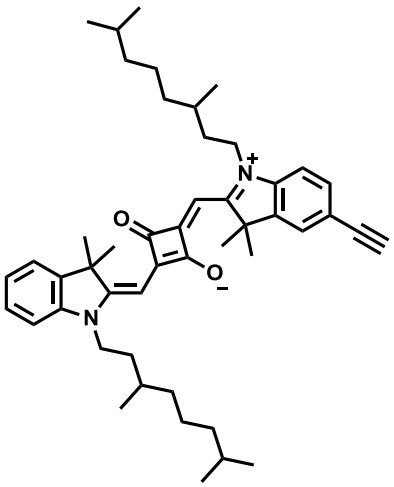

Synthesis based on given literature.[150]

A mixture of squaraine **SQA-TMSA** (290 mg, 375 mmol) and tetrabutylammonium fluoride trihydrate (829 mg, 2.63 mmol) in DCM (15 ml) was stirred at ambient temperature for 10 min. The reaction was diluted with DCM (20 ml) and washed with H_2O (2 × 20 ml). The organic phase was dried over $MgSO_4$ and evaporated under reduced pressure. The crude product was used without further purification.

Yield: 261 mg (372 mmol, 99%) of a blue solid.

$C_{48}H_{64}N_2O_2$ [701.04]

^{1}H-NMR (400.1 MHz, $CDCl_3$):

δ [ppm] = 7.46-7.41 (-, 2H, 2 × C*H*), 7.37 (dd, ^3J = 7.4 Hz, ^4J = 0.8 Hz, 1H, C*H*), 7.33 (ddd, ^3J = 7.7 Hz, ^3J = 7.7 Hz, ^4J = 1.2 Hz, 1H, C*H*), 7.17 (ddd, ^3J = 7.5 Hz, ^3J = 7.5 Hz, ^4J = 0.7 Hz, 1H, C*H*), 7.00 (d, ^3J = 7.8 Hz, 1H, C*H*), 6.86 (d, ^3J = 8.6 Hz, 1H, C*H*), 6.00 (s, 1H, C*H*), 5.95 (s, 1H, C*H*), 4.15-3.83 (-, 4H, 2 × NCH_2), 3.10 (s, 1H, ≡C*H*), 1.85-1.69 (-, 12H, 4 × CH_3), 1.68-1.56 (-, 6H, 2 × NCH_2CH_2, 2 × C*H*), 1.55-1.44 (-, 2H, 2 × C*H*), 1.44-1.11 (-, 12H, 6 × CH_2), 1.08-1.00 (-, 6H, 2 × CH_3), 0.89-0.83 (-, 12H, 4 × CH_3).

^{13}C-NMR (100.6 MHz, CD_2Cl_2):

δ [ppm] = 182.2 (2 × quart), 182.1 (quart), 179.6 (quart), 171.2 (quart), 168.5 (quart), 143. 5 (quart), 142.8 (quart), 142.6 (quart), 142.5 (quart), 132.6 (tert), 128.2 (tert), 126.3 (tert), 124.4 (tert), 122.6 (tert), 116.6 (quart), 110.1 (tert), 109.2 (tert), 87.3 (tert), 87.2 (tert), 84.1 (tert), 77.0 (quart), 49.9 (quart), 49.0 (quart), 42.6 (sec), 42.3 (sec), 39.5 (2 × sec), 37.4 (2 × sec), 34.2 (sec), 34.0 (sec), 31.50 (tert), 31.47 (tert), 28.4 (2 × tert), 27.2 (prim), 27.0 (prim), 25.1 (2 × sec), 22.8 (prim), 22.7 (prim), 19.7 (2 × prim).

MALDI-MS pos: [$M^{\cdot+}$]

calc.: 700.036 m/z

found: 700.488 m/z

SQB-Br

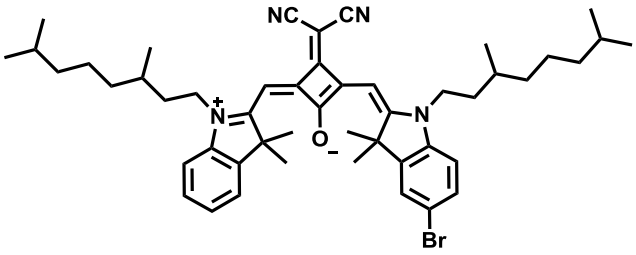

Synthesis based on given literature.[68]

Semisquaraine **24** (1.84 g, 2.95 mmol) and 1-(3,7-dimethyloctyl-)-3,3-dimethyl-3*H*-indol-1-ium iodide (1.29 g, 3.02 mmol) were dissolved in pyridine (11 ml) and a mixture of toluene and 1-butanol (1:1, 50 ml) and heated under reflux using a *Dean-Stark* trap for 18 h. The solvent was removed *in vacuo* and the residue purified by flash chromatography (DCM).

Yield: 1.83 g (2.28 mmol, 77 %) of a green solid.

$C_{49}H_{63}BrN_4O$ [803.96]

^{1}H-NMR (600.1 MHz, CD_2Cl_2):

δ [ppm] = 7.48 (d, ^{4}J = 1.9 Hz, 1H, C*H*), 7.46 (dd, ^{3}J = 8.3 Hz, ^{4}J = 1.9 Hz, 1H, C*H*), 7.41 (dd, ^{3}J = 7.4 Hz, ^{4}J = 0.7 Hz, 1H, C*H*), 7.37 (ddd, ^{3}J = 7.7 Hz, ^{3}J = 7.7 Hz, ^{4}J = 1.1 Hz, 1H, C*H*), 7.24 (ddd, ^{3}J = 7.5 Hz, ^{3}J = 7.5 Hz ^{4}J = 0.8 Hz, 1H, C*H*), 7.10 (d, ^{3}J = 7.9 Hz, 1H, C*H*), 6.90 (d, ^{3}J = 8.4 Hz, 1H, C*H*), 6.51 (s, 1H, C*H*), 6.41 (s, 1H, C*H*), 4.11-3.91 (-, 4H, 2 × NCH_2), 1.85-1.73 (-, 14H, 2 × NCH$_2$C*H*, 4 × CH_3), 1.66-1.55 (-, 4H, 2 × NCH$_2$C*H*, 2 × C*H*), 1.54-1.48 (-, 2H, C*H*), 1.41-1.12 (-, 12H, 6 × CH_2), 1.02 (d, ^{3}J = 6.5 Hz, 3H, CH_3), 1.01(d, ^{3}J = 6.5 Hz, 3H, CH_3), 0.86 (-, 12H, 4 × CH_3).

^{13}C-NMR (150.9 MHz, CD_2Cl_2):

δ [ppm] = 173.3 (quart), 173.1 (quart), 170.5 (quart), 167.9 (quart), 167.8 (quart), 166.0 (quart), 144.7 (quart), 143.0 (quart), 142.1 (quart), 141.6 (quart), 131.2 (tert), 128.4 (tert), 126.0 (tert), 125.3 (tert), 122.7 (tert), 119.03 (quart), 119.01 (quart), 117.2 (quart), 111.5 (tert), 110.8 (tert), 89.8 (tert), 89.3 (tert), 50.1 (quart), 49.6 (quart), 43.5 (sec), 43.2 (sec), 40.8 (quart), 39.5 (2 × sec), 37.4

(2 × sec), 34.4 (sec), 34.1 (sec), 31.3 (tert), 31.2 (tert), 28.4 (2 × tert), 26.79 (prim)*, 26.75 (prim)*, 26.50 (prim)*, 26.47 (prim)*, 25.01 (sec), 25.00 (sec), 22.80 (prim), 22.7 (prim), 19.8 (2 × prim).

* The signal of the primary C-atom splits into two signals of equal intensity.

ESI-MS pos (high resolution): $[M^{\cdot+}]$

calc.: 804.417072 m/z

found: 804.417450 m/z Δ = 0.47 ppm

SQB-B

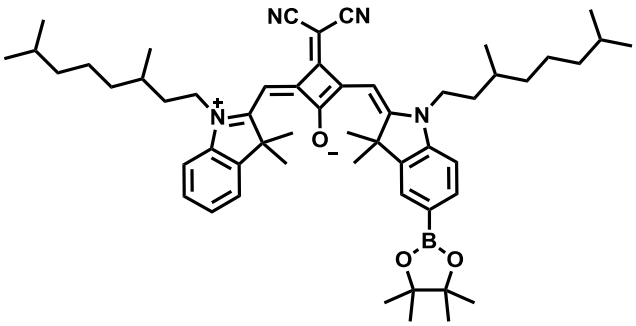

Synthesis based on given literature.[68]

Under a nitrogen atmosphere squaraine **SQB-Br** (1.58 g, 1.97 mmol), bis(pinacolato)diboron (699 mg, 2.75 mmol) and KOAc (615 mg, 6.27 mmol) were suspended in dry 1,4-dioxane (25 ml). The mixture was purged in a gentle stream of nitrogen for 15 min. $Pd(PhCN)_2Cl_2$ (38.0 mg, 99.1 µmol) and dppf (54.0 mg, 97.4 µmol) were added and the resulting mixture was continuously heated at 120 °C in a sealed tube for 18 h.. The solvent was removed *in vacuo* and the residue purified by flash chromatography (PE/EA 1:1). The crude product was dissolved in a small amount of DCM and dripped into an excess of *n*-hexane. The mixture was allowed to stand at -30 °C in the freezer overnight. The precipitate formed was separated by filtration and dried under high vacuum.

Yield: 1.51 g (1.77 mmol, 90 %) of a shiny ruby solid.

$C_{55}H_{75}BN_4O_3$ [851.02]

^{1}H-NMR (400.1 MHz, CD_2Cl_2):

δ [ppm] = 7.77 (dd, ^{3}J = 8.0 Hz, ^{4}J = 1.1 Hz, 1H, C*H*), 7.75-7.73 (m, 1H, C*H*), 7.41 (dd, ^{3}J = 7.5 Hz, ^{4}J = 0.8 Hz, 1H, C*H*), 7.37 (ddd, ^{3}J = 7.7 Hz, ^{3}J = 7.7 Hz, ^{4}J = 1.3 Hz, 1H, C*H*), 7.23 (ddd, ^{3}J = 7.5 Hz, ^{3}J = 7.7 Hz, ^{4}J = 0.8 Hz, 1H, C*H*), 7.10 (d, ^{3}J = 7.9 Hz, 1H, C*H*), 7.04 (d, ^{3}J = 8.1 Hz, 1H, C*H*), 6.51 (s, 1H, C*H*), 6.46 (s, 1H, C*H*), 4.14-3.94 (-, 4H, 2 × NCH_2), 1.84-1.72 (-, 14H, 2 × NCH_2CH, 4 × CH_3), 1.70-1.55 (-, 4H, 2 × NCH_2CH, 2 × C*H*), 1.56-1.46 (-, 2H, 2 × C*H*), 1.35 (s, 12H, 4 × CH_3), 1.42-1.11 (-, 12H, 6 × CH_2), 1.05 (d, ^{3}J = 6.4 Hz, 3H, CH_3), 1.03 (d, ^{3}J = 6.3 Hz, 3H, CH_3), 0.86 (d, ^{3}J = 6.6 Hz, 6H, 2 × CH_3), 0.85 (d, ^{3}J = 6.6 Hz, 6H, 2 × CH_3).

^{13}C-NMR (100.6 MHz, CD_2Cl_2):

δ [ppm] = 173.4 (quart), 172.8 (quart), 171.7 (quart), 168.0 (quart), 167.6 (quart), 166.4 (quart), 145.0 (quart), 143.0 (quart), 142.2 (quart), 142.0 (quart), 135.4 (tert), 128.39 (2 × tert), 125.1 (quart), 125.2 (tert), 122.7 (tert), 119.12 (quart), 119.08 (quart), 110.7 (tert), 109.7 (tert), 89.7 (tert), 89.5 (tert), 84.3 (quart), 50.0 (quart), 49.5 (quart), 43.4 (sec), 43.2 (sec), 40.7 (quart), 39.5 (2 × sec), 37.5 (2 × sec), 34.4 (sec), 34.3 (sec), 31.32 (tert), 31.29 (tert), 28.4 (2 × tert), 26.83 (prim), 26.79 (prim), 26.59 (prim), 26.55 (prim), 25.05 (prim), 25.02 (2 × sec), 22.8 (prim), 22.7 (prim), 19.80 (prim), 19.78 (prim).

MALDI-MS pos: [$M^{\cdot+}$]

calc.: 850.594 m/z

found: 850.616 m/z

SQB-B_2

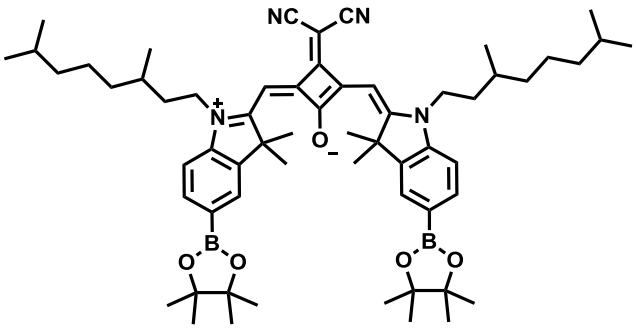

Synthesis based on given literature.[68]

Under a nitrogen atmosphere squaraine **SQB-Br_2** (700 mg, 793 µmol), bis(pinacolato)-diboron (562 mg, 2.21 mmol) and KOAc (248 mg, 2.53 mmol) were suspended in dry 1,4-dioxane (15 ml). The mixture was purged in a gentle stream of nitrogen for 15 min. $Pd(PhCN)_2Cl_2$ (15.0 mg, 39.1 µmol) and dppf (22.0 mg, 39.7 µmol) were added and the resulting mixture was continuously heated at 120 °C in a sealed tube for 18 h. The solvent was removed *in vacuo* and the residue purified by flash chromatography (eluent: PE/EA = 1:1). The crude product was dissolved in a small amount of DCM and dripped into an excess of *n*-hexane. The mixture was allowed to stand at -30 °C in the freezer overnight. The precipitate formed was separated by filtration and dried under high vacuum.

Yield: 700 mg (716 µmol, 90 %) of shiny ruby crystals.

$C_{61}H_{86}B_2N_4O_5$ [976.98]

^{1}H-NMR (600.1 MHz, CD_2Cl_2):

δ [ppm] = 7.78 (dd, ^3J = 7.9 Hz, ^4J = 1.1 Hz, 2H, 2 × C*H*), 7.77-7.75 (m, 2H, 2 × C*H*), 7.07 (d, ^3J = 7.9 Hz, 2H, 2 × C*H*), 6.49 (s, 2H, 2 × C*H*), 4.09-3.98 (m, 4H, 2 × NCH_2), 1.82-1.70 (-, 14H, 2 × NCH_2CH, 4 × CH_3), 1.62-1.55 (-, 4H, 2 × NCH_2CH, 2 × C*H*), 1.54-1.46 (m, 2H, 2 × C*H*), 1.41-1.30 (-, 28H, 2 × CH_2, 8 × CH_3), 1.28-1.12 (-, 8H, 4 × CH_2), 1.01 (d, ^3J = 6.5 Hz, 6H, 2 × CH_3), 0.86 (d, ^3J = 6.6 Hz, 12H, 4 × CH_3).

^{13}C-NMR (105.9 MHz, CD_2Cl_2):

δ [ppm] = 173.3 (quart), 172.4 (quart), 168.0 (quart), 167.3 (quart), 144.8 (quart), 142.1 (quart), 135.4 (tert), 128.4 (tert), 125.4 (quart), 119.0 (quart), 109.9 (tert), 89.9 (tert), 84.3 (quart), 49.6 (quart), 43.3 (sec), 40.8 (quart), 39.5 (sec), 37.4 (sec), 34.3 (sec), 31.3 (tert), 28.4 (tert), 26.72 (prim), 26.70 (prim), 25.04 (prim), 25.00 (sec), 22.8 (prim), 22.7 (prim), 19.8 (prim).

MALDI-MS pos: [$M^{\cdot+}$]

calc.: 976.680 m/z

found: 976.579 m/z

SQB-TMSA

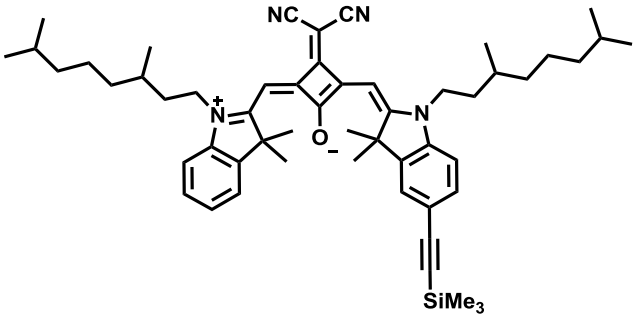

Synthesis based on given literature.[149]

Under a nitrogen atmosphere **SQB-Br** (100 mg, 124 µmol) was dissolved in dry NEt_3 (15 ml). The deep green solution was degassed in a gentle stream of nitrogen for 20 min. CuI (711 µg, 3.73 µmol), $Pd(PPh_3)_2Cl_2$ (260 µg, 370 nmol), and trimethylsilylacetylene (69.0 µl, 499 µmol) were subsequently added and the reaction mixture was heated under reflux for 2 h. After cooling to room temperature the solvent was removed *in vacuo* and the residue was subjected to a rapid silica filtration (DCM).

Yield: 82.0 mg (99.8 µmol, 80 %) of a green solid.

$C_{54}H_{72}N_4OSi$ [821.26]

^{1}H-NMR (400.1 MHz, CD_2Cl_2):

δ [ppm] = 7.47-7.40 (-, 3H, 3 × C*H*), 7.38 (dd, ^{3}J = 7.7 Hz, ^{4}J = 1.2 Hz, 1H, C*H*), 7.29-7.20 (m, 1H, C*H*), 7.11 (d, ^{3}J = 8.0 Hz, 1H, C*H*), 6.96 (d, ^{3}J = 8.6 Hz, 1H, C*H*) 6.52 (s, 1H, C*H*), 6.44 (s, 1H, C*H*), 4.26-3.80 (-, 4H, 2 × NCH_2), 1.88-1.70 (-, 14H, 2 × NCH_2CH, 4 × CH_3), 1.69-1.58 (-, 4H, 2 × NCH_2CH, 2 × C*H*), 1.58-1.46 (-, 2H, 2 × C*H*), 1.46-1.13 (-, 12H, 6 × CH_2), 1.03 (d, ^{3}J = 6.2 Hz, 3H, CH_3), 1.01 (d, ^{3}J = 6.3 Hz, 3H, CH_3), 0.89-0.84 (-, 12H, 4 × CH_3), 0.26 (s, 9H, $Si(CH_3)_3$).

^{13}C-NMR (100.6 MHz, CD_2Cl_2):

δ [ppm] = 173.4 (quart), 173.1 (quart), 170.9 (quart), 168.0 (quart), 167.9 (quart), 166.0 (quart), 143.1 (quart), 142.8 (quart), 142.6 (quart), 142.1 (quart), 132.5 (tert), 128.5 (tert), 126.1 (tert), 125.3 (tert), 122.7 (tert), 119.1 (quart), 119.0 (quart), 118.9 (quart), 110.8 (tert), 110.0 (tert), 105.3 (quart), 94.8 (quart), 89.9 (tert), 89.6 (tert), 50.1 (quart), 49.3 (quart), 43.5 (sec), 43.2 (sec), 40.8 (quart), 39.5 (2 × sec), 37.5 (2 × sec), 34.5 (sec), 34.3 (sec), 31.32 (tert), 31.29 (tert), 28.4 (2 × tert), 26.83 (prim)*, 26.79 (prim)*, 26.53 (prim)*, 26.50 (prim)*, 25.0 (2 × sec) 22.8 (prim), 22.7 (prim), 19.8 (2 × prim), 0.03 (prim).

* The signal of the primary C-atom splits into two signals of equal intensity.

MALDI pos: [$M^{\cdot+}$]

calc.: 820.547 m/z

found: 820.518 m/z

SQB-Alkyne

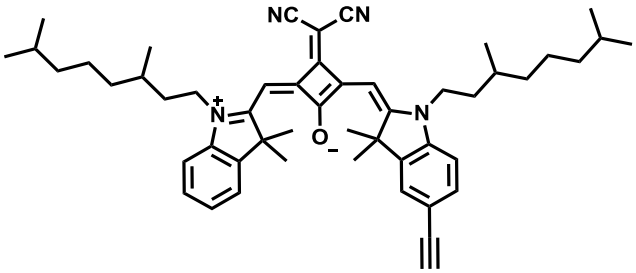

Synthesis based on given literature.[150]

A mixture of **SQB-TMSA** (82.0 mg, 99.8 µmol) and tetrabutylammonium fluoride trihydrate (221 mg, 700 µmol) in DCM (15 ml) was stirred at ambient temperature for 10 min. The reaction was diluted with DCM (20 ml) and washed with H_2O (2 × 20 ml). The organic phase was dried over $MgSO_4$ and evaporated under reduced pressure. The crude product was used without further purification.

Yield: 74.7 mg (99.7 µmol, 100 %) of a green solid.

$C_{51}H_{64}N_4O$ [749.08]

^{1}H-NMR (400.1 MHz, $CDCl_3$):

δ [ppm] = 7.47 (dd, ^3J = 8.2 Hz, ^4J = 1.6 Hz, 1H, C*H*), 7.43 (d, ^4J = 1.4 Hz, 1H, C*H*), 7.40-7.33 (-, 2H, 2 × C*H*), 7.23 (ddd, ^3J = 7.4 Hz, ^3J = 7.4 Hz, ^4J = 0.8 Hz, 1H, C*H*), 7.07 (d, ^3J = 7.9 Hz, 1H, C*H*), 6.93 (d, ^3J = 8.2 Hz, 1H, C*H*), 6.55 (s, 1H, C*H*), 6.47 (s, 1H, C*H*), 4.14-3.91 (-, 4H, 2 × NC*H*$_2$), 3.13 (s, 1H, ≡C*H*), 1.85-1.70 (-, 14H, 2 × NCH$_2$C*H* 4 × C*H*$_3$), 1.70-1.56 (-, 4H, 2 × NCH$_2$C*H*, 2 × C*H*), 1.55-1.45 (-, 2H, 2 × C*H*), 1.43-1.11 (-, 12H, 6 × C*H*$_2$), 1.03 (d, ^3J = 6.3 Hz, 3H, C*H*$_3$), 1.01 (d, ^3J = 6.3 Hz, 3H, C*H*$_3$), 0.87-0.84 (-, 12H, 4 × C*H*$_3$).

^{13}C-NMR (100.6 MHz, CD_2Cl_2):

δ [ppm] = 173.31 (quart), 173.27 (quart), 170.8 (quart), 168.05 (quart), 167.95 (quart), 165.9 (quart), 143.1 (quart), 142.9 (quart), 142.8 (quart), 142.1 (quart), 132.7 (tert), 128.4 (tert), 126.3 (tert), 125.4 (tert), 122.7 (tert), 119.0 (quart), 118.97 (quart), 117.6 (quart), 110.8 (tert), 110.0 (tert), 89.9 (tert), 89.5 (tert), 83.8 (tert), 77.5 (quart), 50.1 (quart), 49.3 (quart), 43.5 (sec), 43.2 (sec), 40.8

(quart), 39.5 (2 × sec), 37.432 (sec), 37.426 (sec), 34.4 (sec), 34.2 (sec), 31.3 (tert), 31.2 (tert), 28.4 (2 × tert), 26.80 (prim)*, 26.76 (prim)*, 26.5 (prim)*, 26.4 (prim)*, 24.99 (sec), 24.98 (sec), 22.8 (prim), 22.7 (prim), 19.75 (prim), 19.74 (prim).

* The signal of the primary C-atom splits into two signals of equal intensity.

MALDI-MS pos: [$M^{\cdot+}$]

calc.: 748.507 m/z

found: 748.652 m/z

SQC-Br

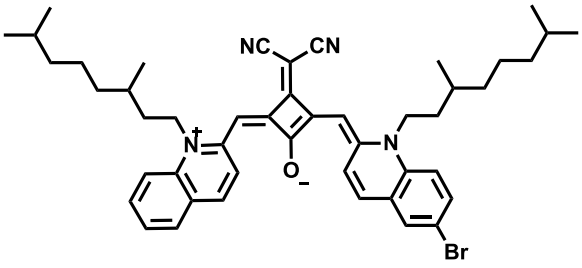

Synthesis based on given literature.[68]

Semisquaraine **40** (722 mg, 1.40 mmol) and 1-(3,7-dimethyloctyl)-2-methylquinolin-1-ium iodide (538 mg, 1.31 mmol) were dissolved in pyridine (5 ml) and a mixture of *n*-butanol and toluene (1:1, 20 ml) and heated under reflux for 18 h using a *Dean-Stark* trap. The cooled reaction mixture was concentrated *in vacuo* and the residue purified by flash chromatography (DCM). The crude product was dissolved in small amount of DCM and dripped into an excess of *n*-hexane. The precipitate formed was filtered off and washed with *n*-hexane.

Yield: 65.0 mg (84.2 µmol, 6 %) of a bronze solid.

$C_{47}H_{55}BrN_4O$ [771.87]

^{1}H-NMR (600.1 MHz, CD_2Cl_2):

δ [ppm] = 9.15 (d, ^3J = 9.4 Hz, 1H, C*H*), 9.07 (d, ^3J = 9.4 Hz, 1H, C*H*), 9.15 (d, ^3J = 9.4 Hz, 1H, C*H*), 7.69 (d, ^3J = 9.5 Hz, 1H, C*H*), 7.67-7.60 (-, 3H, 3 × C*H*),

7.52 (d, ^3J = 8.6 Hz, 1H, C*H*), 7.38 (d,^3J = 7.4 Hz, 1H, C*H*), 7.37 (d, ^3J = 10 Hz, 1H, C*H*), 7.23 (d, ^3J = 8.4 Hz, 1H, C*H*), 6.30 (s, 1H, C*H*), 6.16 (s, 1H, C*H*), 4.44-4.10 (-, 4H, 2 × NCH_2), 1.90-1.60 (-, 6H, 2 × C*H*, 2 × NCH_2CH_2), 1.60-1.51 (-, 2H, C*H*), 1.50-1.17 (-, 12H, 6 × CH_2), 1.10 (d, ^3J = 6.5 Hz, 3H, CH_3), 1.08 (d, ^3J = 6.5 Hz, 3H, CH_3), 0.90-0.88 (-, 12H, 4 × CH_3).

^{13}C-NMR (150.9 MHz, CD_2Cl_2):

δ [ppm] = 174.9 (quart), 165.76 (quart), 164.36 (quart), 162.4 (quart), 152.0 (quart), 150.4 (quart), 139.7 (quart), 139.1 (quart), 135.4 (tert), 134.4 (tert), 132.4 (tert), 132.3 (tert), 131.1 (tert), 129.5 (tert), 127.4 (tert), 127.0 (quart), 125.96 (tert), 125.89 (quart), 125.3 (tert), 119.09 (quart), 119.06 (quart), 117.2 (quart), 116.8 (tert), 115.6 (tert), 95.1 (tert), 94.4 (tert), 48.7 (sec), 48.3 (sec), 41.2 (quart), 39.6 (2 × sec), 37.5 (2 × sec), 34.2 (sec), 33.7 (sec), 31.7 (2 × tert), 28.4 (2 × tert), 25.0 (2 × sec), 22.84 (2 × prim)*, 22.77 (2 × prim)*, 19.5 (2 × prim).

* The signal of the primary C-atom splits into two signals of equal intensity.

ESI-MS pos (high resolution): [$M^{\cdot+}$]

calc.: 772.35439 m/z

found: 772.35834 m/z Δ = 5.11 ppm

SQC-Br_2

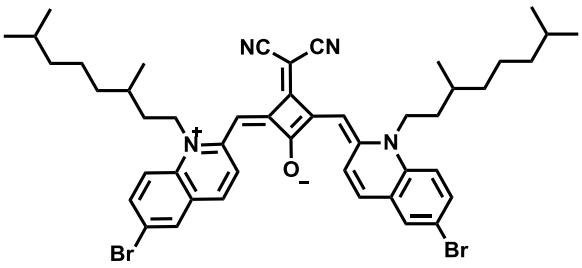

Synthesis based on given literature.[71]

Dicyanovinylene salt **CN** (234 mg, 803 µmol) and 6-bromo-1-(3,7-dimethyloctyl)-2-methylquinolin-1-ium iodide (**38**) (789 mg, 1.61 mmol) were dissolved in pyridine (3 ml) and a mixture of *n*-butanol and toluene (1:1, 20 ml) and heated under reflux for 18 h using a

Dean-Stark trap. The cooled reaction mixture was concentrated *in vacuo* and the residue purified by flash chromatography (DCM). The crude product was dissolved in a small amount of DCM and dripped into an excess of *n*-hexane. The precipitate formed was filtered off and washed with *n*-hexane.

Yield: 430 mg (505 µmol, 63 %) of a green solid.

$C_{47}H_{54}Br_2N_4O$ [850.77]

^{1}H-NMR (600.1 MHz, CD_2Cl_2):

δ [ppm] = 9.10 (d, ^3J = 9.5 Hz, 2H, 2 × C*H*), 7.70-7.62 (-, 4H, 4 × C*H*), 7.45 (d, ^3J = 9.5 Hz, 2H, 2 × C*H*), 7.28 (d, ^3J = 8.8 Hz, 2H, 2 × C*H*), 6.18 (s, 2H, 2 × C*H*), 4.30-4.06 (m, 4H, 2 × NCH_2), 1.93-1.63 (-, 6H, 2 × C*H*, 2 × NCH_2CH_2), 1.63-1.54 (m, 2H, C*H*), 1.49-1.36 (m, 4H, 2 × CH_2), 1.35-1.24 (m, 4H, 2 × CH_2), 1.24-1.16 (m, 4H, 2 × CH_2), 1.08 (d, ^3J = 6.5 Hz, 6H, 2 × CH_3), 0.89 (d, ^3J = 6.7 Hz, 12H, 4 × CH_3).

^{13}C-NMR (150.9 MHz, CD_2Cl_2):

δ [ppm] = 174.7 (quart), 165.7 (quart), 163.6 (quart), 151.0 (quart), 138.9 (quart), 134.7 (tert), 133.1 (tert), 131.2 (tert), 127.3 (tert), 127.2 (quart), 118.9 (quart), 117.8 (quart), .117.1 (tert), 95.2 (tert), 48.6 (sec), 41.4 (quart), 39.6 (sec), 37.5 (sec), 33.9 (sec), 31.7 (tert), 28.4 (tert), 25.0 (sec), 22.84 (prim)*, 22.77 (prim)*, 19.4 (prim).

* The signal of the primary C-atom splits into two signals of equal intensity.

ESI-MS pos (high resolution): [$M^{\cdot+}$]

calc.: 850.26441 m/z

found: 850.26427 m/z Δ = 0.16 ppm

DiPhSQB-1-Br_2

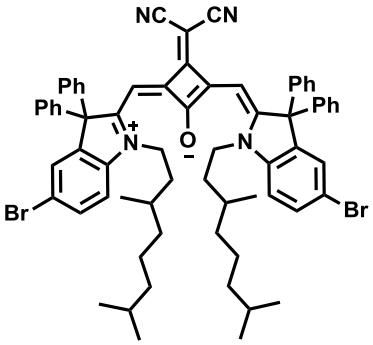

Under a nitrogen atmosphere MeMgBr (15.3 ml, 21.4 mmol, 1.4 M in 3:1 toluene/THF) was added dropwise to 5-bromo-1-(3,7-dimethyloctyl)-3,3-diphenylindolin-2-one (2.69 g, 5.34 mmol) in dry THF (85 ml), and the reaction was heated to 60 °C for 2.5 h. The reaction was allowed to cool. MeOH (12 ml) was subsequently added and the reaction was concentrated under reduced pressure. The resulting residue was treated with HCl (3 M, 80 ml) and extracted with DCM (3 × 50 ml). The combined organic phases were dried over Na_2SO_4 and the solvent was removed under reduced pressure to yield crude 5-bromo-1-(3,7-dimethyloctyl)-2-methyl-3,3-diphenyl-3*H*-indol-1-ium chloride as a green foam (2.73 g, 5.07 mmol, 95 %) which was used without further purification since it readily decomposes when exposed to moist air.

Under a nitrogen atmosphere 5-bromo-1-(3,7-dimethyloctyl)-2-methyl-3,3-diphenyl-3*H*-indol-1-ium chloride (200 mg, 371 µmol) and dicyanovinylene salt **CN** (51.0 mg, 175 µmol) were suspended in pyridine (1 ml) and a mixture of toluene and 1-butanol (1:1, 10 ml). The suspension was degassed in a gentle stream of nitrogen for 15 min. The reaction was heated at 130 °C for 3 h. The solvent was removed under reduced pressure and the residue was purified by flash chromatography (DCM). The crude product was recrystallized from *n*-hexane.

Yield: 64.0 mg (56.6 µmol, 32 %) of dark green crystals.

$C_{69}H_{70}Br_2N_4O$ [1131.13]

^{1}H-NMR (600.1 MHz, CD_2Cl_2):

δ [ppm] = 7.50 (dd, ^3J = 8.4 Hz, ^4J = 1.8 Hz, 2H, 2 × C*H*), 7.37-7.14 (-, 22H, 22 × C*H*), 7.04 (d, ^3J = 8.5 Hz, 2H, 2 × C*H*), 6.07 (s, 2H, 2 × C*H*), 4.60-4.16 (m, 4H,

2 × NC*H*$_2$), 1.74-1.61 (m, 2H, 2 × NCH$_2$C*H*), 1.52-1.05 (-, 18H, 2 × NCH$_2$C*H*, 6 × C*H*$_2$, 4 × C*H*), 0.87 (d, ^3J = 6.2 Hz, 6H, 2 × C*H*$_3$), 0.83 (d, ^3J = 6.6 Hz, 12H, 4 × C*H*$_3$).

^{13}C-NMR (150.9 MHz, CD_2Cl_2):

δ [ppm] = 175.0 (quart), 170.5 (quart), 166.6 (quart), 166.2 (quart), 142.7 (quart), 141.9 (quart), 141.4 (quart)*, 141.3 (quart)*, 132.1 (tert), 129.3 (tert), 129.0 (2 × tert), 128.3 (tert), 118.5 (quart), 118.0 (quart), 113.5 (tert), 93.0 (tert), 68.3 (quart), 45.6 (sec), 42.2 (quart), 39.6 (sec), 37.40 (sec)*, 37.39 (sec)*, 34.5 (sec), 31.0 (tert), 28.4 (tert), 24.98 (sec)*, 24.97 (sec)*, 22.8 (prim)*, 22.7 (prim)*, 19.7 (prim).

* The signals of the primary, secondary, and quaternary C-atoms split into two signals of equal intensity.

ESI-MS pos (high resolution): [M$^{\cdot+}$]

calc.: 1130.39017 m/z

found: 1130.38998 m/z Δ = 0.17 ppm

DiPhSQB-2-Br$_2$

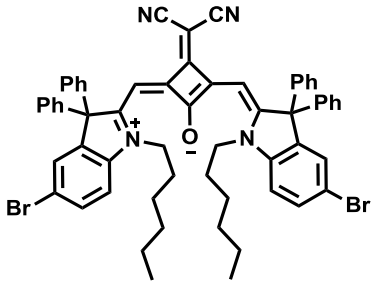

Under a nitrogen atmosphere MeMgBr (4.80 ml, 6.72 mmol, 1.4 M in 3:1 toluene/THF) was added dropwise to 5-bromo-1-hexyl-3,3-diphenylindolin-2-one (754 mg, 1.68 mmol) in dry THF (15 ml), and the reaction was heated to 60 °C for 2.5 h. The reaction was allowed to cool. MeOH (5 ml) was subsequently added and the reaction was concentrated under reduced pressure. The resulting residue was treated with HCl (3 M, 30 ml) and extracted with DCM (3 × 50 ml). The combined organic phases were dried over Na_2SO_4 and the solvent was removed under reduced pressure to yield crude 5-bromo-1-hexyl-2-methyl-3,3-diphenyl-3*H*-

indol-1-ium chloride as a green foam (812 mg, 1.68 mmol, 99 %) which was used without further purification since it readily decomposes when exposed to moist air.

Under a nitrogen atmosphere 5-bromo-1-hexyl-2-methyl-3,3-diphenyl-3*H*-indol-1-ium chloride (812 mg, 1.68 mmol) and dicyanovinylene salt **CN** (254 mg, 872 µmol) were suspended in pyridine (2 ml) and a mixture of toluene and 1-butanol (1:1, 20 ml). The suspension was degassed in a gentle stream of nitrogen for 15 min. The reaction was heated at 130 °C for 3.5 h. The solvent was removed under reduced pressure and the residue was purified by flash chromatography (DCM). The crude product was recrystallized from *n*-hexane.

Yield: 230 mg (226 µmol, 26 %) of dark green crystals.

$C_{61}H_{54}Br_2N_4O$ [1018.92]

^{1}H-NMR (600.1 MHz, CD_2Cl_2):

δ [ppm] = 7.50 (dd, ^{3}J = 8.5 Hz, ^{4}J = 1.9 Hz, 2H, 2 × C*H*), 7.35-7.30 (-, 14H, 14 × C*H*), 7.27- 7.15 (-, 8H, 8 × C*H*), 7.05 (d, ^{3}J = 8.5 Hz, 2H, 2 × C*H*), 6.08 (s, 2H, 2 × C*H*), 4.56-4.13 (m, 4H, 2 × NCH_2), 1.78-1.61 (m, 4H, 2 × NCH$_2$CH_2), 1.27-1.20 (-, 12H, 6 × CH_2), 0.83 (t, ^{3}J = 6.9 Hz, 6H, 2 × CH_3).

^{13}C-NMR (150.9 MHz, CD_2Cl_2):

δ [ppm] = 174.6 (quart), 170.0 (quart), 166.7 (quart), 166.3 (quart), 142.8 (quart), 141.8 (quart), 141.4 (quart), 132.1 (tert), 129.3 (tert), 129.02 (tert), 128.96 (tert), 128.2 (tert), 118.4 (quart), 118.1 (quart), 113.5 (tert), 93.0 (tert), 68.3 (quart), 47.05 (sec), 41.9 (quart), 31.8 (sec), 27.5 (sec), 26.7 (sec), 22.8 (sec), 14.1 (prim).

ESI-MS pos (high resolution): [$M^{\cdot+}$]

calc.: 1018.26474 m/z

found: 1018.26305 m/z Δ = 1.66 ppm

pySQB-1-Br_2

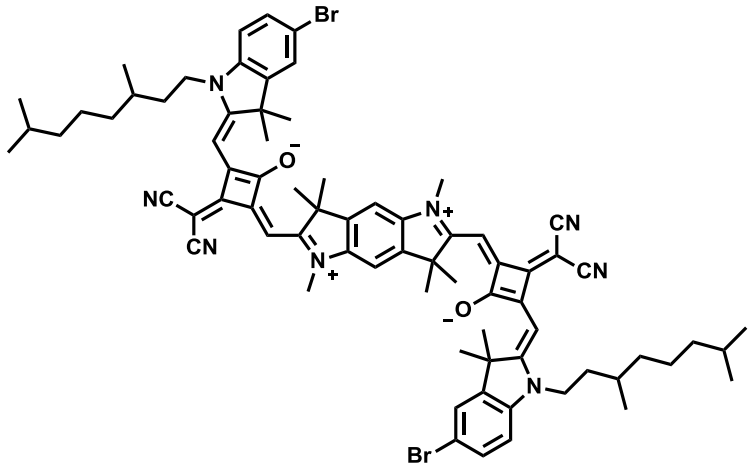

Synthesis based on given literature.[136]

Pyrrolo salt **35** (413 mg, 788 µmol) and semisquaraine dye **24** (1.06 mg, 2.03 mmol) were dissolved in Ac_2O (15 ml) and refluxed for 18 h. The solvent was removed *in vacuo* and the dark green residue was purified by flash chromatography (DCM/MeOH = 99:1) and subsequent preparative recycling GPC ($CHCl_3$). The crude product was recrystallized from *n*-hexane.

Yield: 40.0 mg (31.3 µmol, 4 %) of a dark green solid.

$C_{74}H_{84}Br_2N_8O_2$ [1277.32]

^{1}H-NMR (400.1 MHz, CD_2Cl_2):

δ [ppm] = 7.50 (d, ^4J = 1.8 Hz, 2H, 2 × C*H*), 7.48 (dd, ^3J = 8.3 Hz, ^4J = 1.9 Hz, 2H, 2 × C*H*), 7.10 (s, 2H, 2 × C*H*), 6.93 (d, ^3J = 8.3 Hz, 2H, 2 × C*H*), 6.80-5.90 (-, 4H, 4 × C*H*), 4.10-3.50 (-, 10H, 2 × NCH_2, 2 × NCH_3), 1.83-1.60 (-, 30H, 2 × NCH_2CH_2, 8 × CH_3, 2 × C*H*), 1.60-1.47 (m, 2H, 2 × C*H*), 1.41-1.13 (-, 12H, 6 × CH_2), 1.02 (d, ^3J = 6.4 Hz, 6H, 2 × CH_3), 0.86 (d, ^3J = 6.6 Hz, 12H, 4 × CH_3).

MALDI-MS pos: [$M^{\cdot+}$]

calc.: 1276.507 m/z

found: 1276.535 m/z

5.2.4 Synthesis of Squaraine Homodimers (SQA)

Squaraine dimer **dSQA-1**[93] was synthesized according to literature procedures.

dSQA-2 and **dSQA-3**

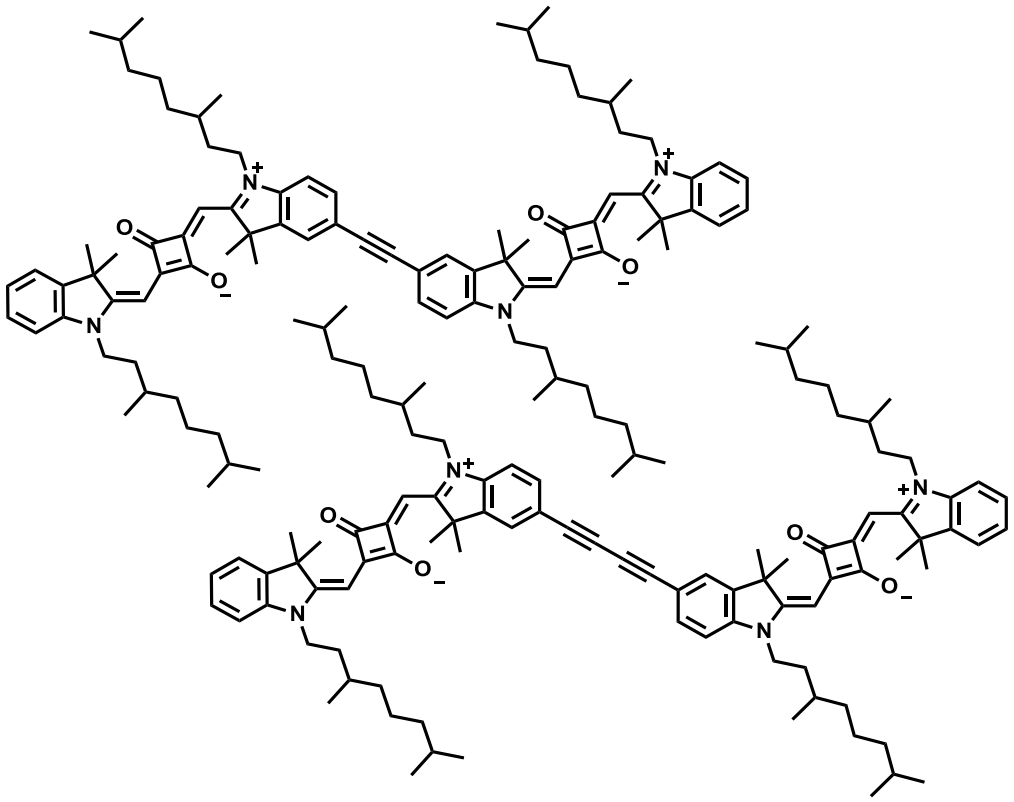

Under a nitrogen atmosphere functionalized squaraine dye **SQA-Br** (623 mg, 824 µmol) was dissolved in dry NEt_3 (25 ml). The deep blue solution was degassed in a gentle stream of nitrogen for 20 min. P*t*Bu_3 (1 M in solution, 35.3 µl, 35.3 µmol) and $Pd(PPh_3)_2Cl_2$ (24.8 mg, 35.3 µmol) were subsequently added and the mixture was heated to 60 °C. A degassed solution of **SQA-Alkyne** (413 mg, 589 µmol) in dry NEt_3 (30 ml) was carefully added dropwise over a period of 45 min. After complete addition, the reaction mixture was heated to reflux for 2 h. The solvent was removed *in vacuo* and the residue purified by flash chromatography (DCM/MeOH = 99:1). Preparative recycling GPC ($CHCl_3$) was used to separate both compounds **dSQA-2** and **dSQA-3**. Each batch was finally recrystallized from *n*-hexane.

dSQA-2:

Yield: 163 mg (118 µmol, 20 %) of a blue powder.

$C_{94}H_{126}N_4O_4$ [1376.03]

^{1}H-NMR (600.1 MHz, CD_2Cl_2):

δ [ppm] = 7.53-7.46 (-, 4H, 4 × C*H*), 7.39 (d, ^{3}J = 7.4 Hz, 2H, 2 × C*H*), 7.36-7.30 (m, 2H, 2 × C*H*), 7.22-7.13 (m, 2H, 2 × C*H*), 7.04 (d, ^{3}J = 7.3 Hz, 2H, C*H*), 6.96 (d, ^{3}J = 7.3 Hz, 2H, 2 × C*H*), 5.96 (s, 2H, 2 × C*H*), 5.91 (s, 2H, 2 × C*H*), 4.23-3.80 (-, 8H, 4 × NCH_2), 1.85-1.71 (-, 28H, 4 × NCH_2CH, 8 × CH_3), 1.68-1.57 (-, 8H, 4 × NCH_2CH, 4 × C*H*), 1.57-1.49 (-, 4H, 4 × C*H*), 1.44-1.13 (-, 24H, 12 × CH_2), 1.10-1.03 (-, 12H, 4 × CH_3), 0.87 (d, ^{3}J = 6.6 Hz, 12H, 4 × CH_3), 0.86 (d, ^{3}J = 6.7 Hz, 12H, 4 × CH_3).

^{13}C-NMR (150.9 MHz, CD_2Cl_2):

δ [ppm] = 182.0 (2 × quart), 181.6 (quart), 179.6 (quart), 171.0 (quart), 168.5 (quart), 143.1 (quart), 142.8 (quart), 142.7 (quart), 142.3 (quart), 131.8 (quart), 128.1 (tert), 125.6 (tert), 124.3 (tert), 122.7 (tert), 122.5 (tert), 110.0 (tert), 109.5 (tert), 90.0 (quart), 87.4 (tert), 87.2 (tert), 49.8 (quart), 49.1 (quart), 42.6 (2 × sec), 39.5 (2 × sec), 37.5 (2 × sec), 34.1 (2 × sec), 31.5 (2 × tert), 28.4 (2 × tert), 27.2 (2 × prim), 27.0 (2 × prim), 25.1 (2 × sec), 22.8 (2 × prim), 22.7 (2 × prim), 19.8 (2 × prim).

ESI-MS pos (high resolution): [MH^{+}]

calc.: 1376.9885 m/z

found: 1376.9904 m/z Δ = 1.38 ppm

dSQA-3:

Yield: 44.0 mg (31.4 µmol, 5 %) of a blue powder.

$C_{94}H_{126}N_4O_4$ [1400.06]

^{1}H-NMR (600.1 MHz, CD_2Cl_2):

δ [ppm] = 7.52-7.46 (-, 4H, 4 × C*H*), 7.40 (dd, ^{3}J = 7.4 Hz, ^{4}J = 0.6 Hz, 2H, 2 × C*H*), 7.34 (ddd, ^{3}J = 7.7 Hz, ^{3}J = 7.7 Hz, ^{4}J = 1.2 Hz, 2H, 2 × C*H*), 7.19 (ddd, ^{3}J = 7.4 Hz, ^{3}J = 7.7 Hz, ^{4}J = 0.7 Hz, 2H, 2 × C*H*), 7.06 (d, ^{3}J = 8.0 Hz, 2H, 2 × C*H*), 6.92 (d, ^{3}J = 8.2 Hz, 2H, 2 × C*H*), 5.98 (s, 2H, 2 × C*H*), 5.91 (s, 2H, 2 × C*H*), 4.15-4.00 (m, 4H, 2 × NCH_2), 4.00-3.86 (m, 4H, 2 × NCH_2), 1.87-1.70 (-, 28H, 4 × NCH_2C*H*, 8 × CH_3), 1.68-1.58 (-, 8H, 4 × NCH_2C*H*, 4 × C*H*), 1.56-1.50 (-, 4H, 4 × C*H*), 1.45-1.13 (-, 24H, 12 × CH_2), 1.10-1.02 (-, 12H, 4 × CH_3), 0.87 (d, ^{3}J = 6.6 Hz, 12H, 4 × CH_3), 0.86 (d, ^{3}J = 6.6 Hz, 12H, 4 × CH_3).

^{13}C-NMR (150.9 MHz, CD_2Cl_2):

δ [ppm] = 181.9 (2 × quart), 179.2 (quart), 171.5 (quart), 167.9 (quart), 143.9 (quart), 142.82 (quart), 142.77 (quart), 142.6 (quart), 133.2 (tert), 128.2 (tert), 126.5 (tert), 124.5 (tert), 122.7 (tert), 116.0 (quart), 110.2 (tert), 109.3 (tert), 87.6 (tert), 87.4 (tert), 82.8 (quart), 74.2 (quart), 50.0 (quart), 48.9 (quart), 42.7 (sec), 42.3 (sec), 39.52 (sec), 39.51 (sec), 37.5 (sec), 37.4 (sec), 34.2 (sec), 34.0 (sec), 31.50 (tert), 31.47 (tert), 28.4 (2 × tert), 27.3 (prim), 26.93 (prim)*, 26.92 (prim)*, 25.08 (sec), 25.07 (sec), 22.82 (prim)*, 22.81 (prim)*, 22.72 (prim), 19.8 (prim), 19.7 (prim).

* The signal of the primary C-atoms splits into two signals of equal intensity.

ESI-MS pos (high resolution): [$M^{\cdot+}$]

calc.: 1399.98067 m/z

found: 1399.97979 m/z Δ = 0.63 ppm

dSQA-4

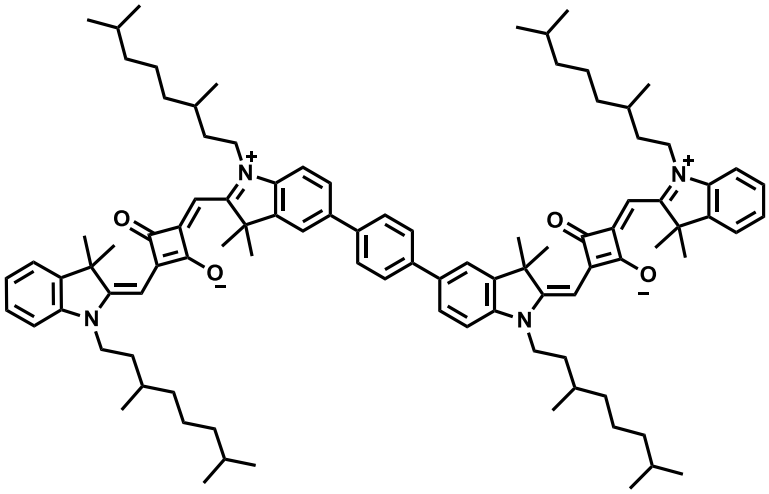

Functionalized squaraine dye **SQA-B** (100 mg, 125 µmol) and 1,4-dibromobenzene (13.0 mg, 55.1 µmol) were dissolved in peroxide-free THF (8 ml) under a nitrogen atmosphere. An aqueous solution of Na_2CO_3 (1 M, 336 µl, 336 µmol) was added and the mixture was purged in a gentle stream of nitrogen for 15 min. $Pd(PPh_3)_4$ (6.54 mg, 5.66 µmol) was added and the reaction was heated at 85 °C in a sealed tube for 2 d. The solvent was removed *in vacuo* and the residue purified by flash chromatography (DCM/MeOH = 99:1) and subsequent preparative recycling GPC ($CHCl_3$). Finally, the product was dissolved in a small amount of DCM and dripped into an excess of *n*-hexane. The mixture was allowed to stand in the refrigerator at 4 °C overnight. The precipitate formed was filtered off and dried under high vacuum.

Yield: 27.0 mg (18.9 µmol, 34 %) of a blue powder.

$C_{98}H_{130}N_4O_4$ [1428.11]

^{1}H-NMR (600.1 MHz, CD_2Cl_2):

δ [ppm] = 7.73-7.72 (m, 4H, 4 × C*H*), 7.65 (d, ^4J = 1.6 Hz, 2H, 2 × C*H*), 7.63 (dd, ^3J = 8.2 Hz, ^4J = 1.8 Hz 2H, 2 × C*H*), 7.38 (dd, ^3J = 7.4 Hz, ^4J = 0.6 Hz, 2H, 2 × C*H*), 7.34 (ddd, ^3J = 7.7 Hz, ^3J = 7.7 Hz, ^4J = 1.1 Hz, 2H, 2 × C*H*), 7.20-7.13 (m, 2H, 2 × C*H*), 7.09 (d, ^3J = 8.2 Hz, 2H, 2 × C*H*), 7.02 (d, ^3J = 7.9 Hz, 2H, 2 × C*H*), 6.07-5.80 (-, 4H, 4 × C*H*), 4.21-3.84 (-, 8H, 4 × NCH_2), 1.89-1.73 (-, 28H, 4 × NCH_2CH, 8 × CH_3), 1.69-1.60 (-, 8H, 4 × C*H*, 4 × NCH_2CH),

1.57-1.49 (-, 4H, 4 × C*H*), 1.46-1.14 (-, 24H, 12 × CH_2), 1.09 (d, ^3J = 6.3 Hz, 6H, 2 × CH_3), 1.07 (d, ^3J = 6.3 Hz, 6H, 2 × CH_3), 0.88 (d, ^3J = 6.6 Hz, 12H, 4 × CH_3), 0.87 (d, ^3J = 6.7 Hz, 12H, 4 × CH_3).

^{13}C-NMR (150.9 MHz, CD_2Cl_2):

δ [ppm] = 182.0 (2 × quart), 180.9 (quart), 180.0 (quart), 170.2 (quart), 169.5 (quart), 143.4 (quart), 142.8 (quart), 142.6 (quart), 142.5 (quart), 139.8 (quart), 136.4 (quart), 128.1 (tert), 127.6 (tert), 126.9 (tert), 124.0 (tert), 122.6 (tert), 121.2 (tert), 109.9 (tert), 109.8 (tert), 87.1 (tert), 86.9 (tert), 49.64 (quart), 49.57 (quart), 42.51 (sec), 42.45 (sec), 39.54 (sec), 39.53 (sec), 37.49 (sec), 37.47 (sec), 34.14 (sec), 34.11 (sec), 31.5 (2 × tert), 28.38 (tert), 28.37 (tert), 27.3 (prim), 27.1 (prim), 25.10 (sec), 25.08 (sec), 22.83 (prim)*, 22.82 (prim)*, 22.74 (prim)*, 22.73 (prim)*, 19.80 (prim), 19.76 (prim).

* The signals of the primary C-atoms split into two signals of equal intensity.

ESI-MS pos (high resolution): [$M^{\cdot+}$]

calc.: 1428.0120 m/z

found: 1428.0111 m/z Δ = 0.63 ppm

dSQA-5

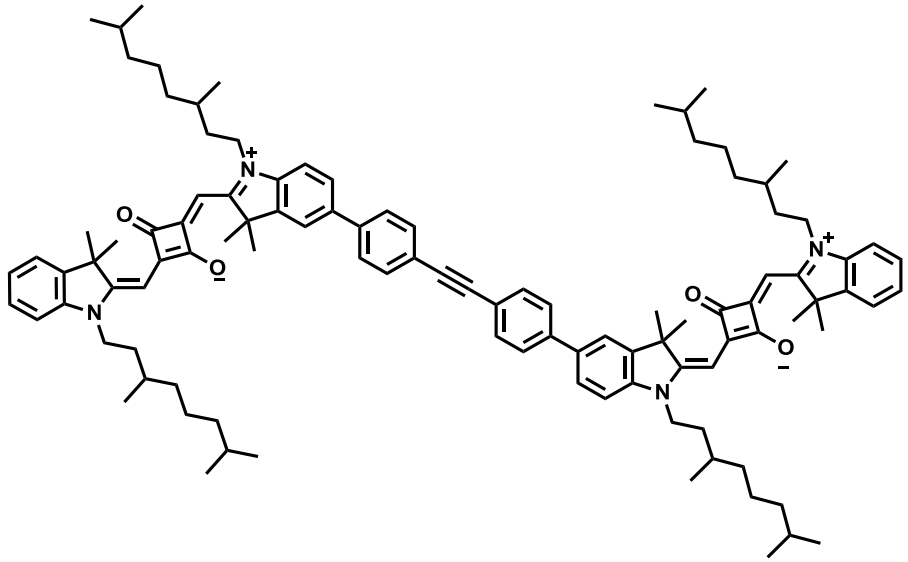

Under a nitrogen atmosphere functionalized squaraine dye **SQ-B** (205 mg, 255 µmol) and 1,2-bis(4-bromophenyl)ethyne (43.0 mg, 128 µmol) were dissolved in peroxide-free THF (8 ml). An aqueous solution of Na_2CO_3 (1 M, 758 µl, 758 µmol) was added and the mixture was purged in a gentle stream of nitrogen for 15 min. $Pd(PPh_3)_4$ (15.0 mg, 13.0 µmol) was added and the reaction was heated at 85 °C in a sealed tube for 2 d. The solvent was removed *in vacuo* and the residue purified by flash chromatography (DCM/MeOH = 99:1) and subsequent preparative recycling GPC ($CHCl_3$). Finally, the product was dissolved in a small amount of DCM and dripped into an excess of *n*-hexane. The mixture was allowed to stand in the refrigerator at 4 °C overnight. The precipitate formed was filtered off and dried under high vacuum.

Yield: 116 mg (75.9 µmol, 59 %) of a shiny purple solid.

$C_{106}H_{134}N_4O_4$ [1528.23]

^{1}H-NMR (600.1 MHz, CD_2Cl_2):

δ [ppm] = 7.68-7.57 (-, 12H, 12 × C*H*), 7.38 (d, ^3J = 7.1 Hz, 2H, 2 × C*H*), 7.36-7.30 (m, 2H, 2 × C*H*), 7.22-7.12 (m, 2H, 2 × C*H*), 7.08 (d, ^3J = 6.7 Hz, 2H, 2 × C*H*), 7.02 (d, ^3J = 6.7 Hz, 2H, 2 × C*H*), 6.10-5.72 (-, 4H, 4 × C*H*), 4.50-3.70 (-, 8H, 4 × NCH_2), 1.92-1.70 (-, 28H, 4 × NCH_2CH, 8 × CH_3), 1.69-1.60 (-, 8H,

4 × NCH_2CH, 4 × C*H*), 1.57-1.48 (-,4H, 4 × C*H*), 1.45-1.15 (-, 24H, 12 × CH_2), 1.11-1.04 (-, 12H, 4 × CH_3), 0.87 (d, ^3J = 6.6 Hz, 12H, 4 × CH_3), 0.86 (d, ^3J = 6.6 Hz, 12H, 4 × CH_3).

^{13}C-NMR (150.9 MHz, CD_2Cl_2):

δ [ppm] = 182.0 (2 × quart), 181.4 (quart), 180.1 (quart), 170.4 (quart), 169.3 (quart), 143.4 (quart), 142.78 (2 × quart), 142.77 (quart), 141.0 (quart), 136.0 (quart), 132.4 (2 × tert), 128.1 (tert), 127.1 (2 × tert), 127.0 (tert), 124.1 (tert), 122.6 (tert), 122.2 (quart), 121.2 (tert), 109.9 (2 × tert), 90.4 (quart), 87.2 (tert), 87.0 (tert), 49.7 (quart), 49.5 (quart), 42.5 (2 × sec), 39.5 (2 × sec), 37.5 (2 × sec), 34.1 (2 × sec), 31.5 (2 × tert), 29.380 (tert), 29.377 (tert), 27.3 (prim), 27.1 (prim), 25.1 (2 × sec), 22.8 (prim), 22.7 (prim), 19.80 (prim), 19.77 (prim).

ESI-MS pos (high resolution): [$M^{\cdot+}$]

calc.: 1528.0433 m/z

found: 1528.0447 m/z Δ = 0.92 ppm

dSQA-6

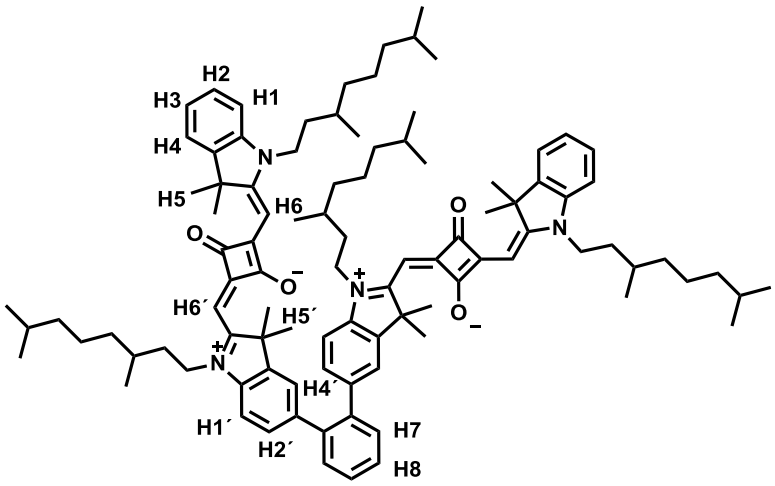

Functionalized squaraine dye **SQA-B** (100 mg, 125 µmol) and 1,2-dibromobenzene (6.73 µl, 13.0 mg, 55.1 µmol) were dissolved in peroxide-free THF (8 ml) under a nitrogen atmosphere. An aqueous solution of Na_2CO_3 (1 M, 336 µl, 336 µmol) was added and the mixture was purged in a gentle stream of nitrogen for 15 min. $Pd(PPh_3)_4$ (6.54 mg, 5.66 µmol) was added and the reaction was heated at 85 °C in a sealed tube for 2 d. The solvent was removed *in vacuo* and the residue purified by flash chromatography (DCM/MeOH = 99:1) and subsequent preparative recycling GPC ($CHCl_3$). Finally, the product was dissolved in a small amount of DCM and dripped into an excess of *n*-hexane. The mixture was allowed to stand in the refrigerator at 4 °C overnight. The precipitate formed was filtered off and dried under high vacuum to afford analytically pure squaraine dimer **dSQA-6**.

Yield: 50.0 mg (35.0 µmol, 64 %) of a dark green powder.

$C_{98}H_{130}N_4O_4$ [1428.11]

^{1}H-NMR (600.1 MHz, CD_2Cl_2):

δ [ppm] = 7.50-7.46 (m, 2H, 2 × H7), 7.46-7.42 (m, 2H, 2 × H8), 7.35 (dd, $^3J_{3\text{-}4}$ = 7.4 Hz, $^4J_{2\text{-}4}$ = 1.2 Hz, 2H, 2 × H4), 7.30 (ddd, $^3J_{1\text{-}2}$ = 7.8 Hz, $^3J_{2\text{-}3}$ = 7.4 Hz, $^4J_{2\text{-}4}$ = 1.2 Hz, 2H, 2 × H2), 7.21 (dd, $^3J_{1'\text{-}2'}$ = 8.1 Hz, $^4J_{2'\text{-}4'}$ = 1.6 Hz, 2H, 2 × H2´), 7.13 (ddd, $^3J_{2\text{-}3}$ = 7.4 Hz, $^3J_{3\text{-}4}$ = 7.4 Hz, $^4J_{1\text{-}3}$ = 0.7 Hz, 2H, 2 × H3), 6.99 (d,

$^{3}J_{1\text{-}2}$ = 7.8 Hz, 2H, 2 × H1), 6.96 (d, $^{4}J_{2'\text{-}4'}$ = 1.6 Hz, 2H, 2 × H4´), 6.90 (d, $^{3}J_{1'\text{-}2'}$ = 8.1 Hz, 2H, 2 × H1´), 5.87 (s, 2H, 2 × H6), 5.83 (s, 2H, 2 × H6´), 4.09-3.83 (-, 8H, 4 × NCH_2) 1.80-1.74 (-, 4H, 4 × NCH_2CH), 1.72 (s, 12H, 4 × CH_3), 1.65-1.57 (-, 8H, 4 × C*H*, 4 × NCH_2CH), 1.57-1.46 (-, 16H, 4 × C*H*, 4 × CH_3), 1.42-1.11 (-, 24H, 12 × CH_2), 1.04 (d, ^{3}J = 6.2 Hz, 6H, 2 × CH_3), 1.03 (d, ^{3}J = 6.3 Hz, 6H, 2 × CH_3), 0.85 (-, 24H, 8 × CH_3).

^{13}C-NMR (150.9 MHz, CD_2Cl_2):

δ [ppm] = 181.9 (2 × quart), 180.8 (quart), 180.3 (quart), 170.0 (quart), 169.5 (quart), 142.8 (quart), 142.6 (quart), 142.3 (quart), 141.5 (quart), 140.8 (quart), 137.4 (quart), 130.7 (tert), 129.5 (tert), 128.1 (tert), 128.0 (tert), 124.8 (tert), 123.9 (tert), 122.6 (tert), 109.7 (tert), 109.1 (tert), 87.0 (tert), 86.8 (tert), 49.6 (quart), 49.1 (quart), 42.4 (2 × sec), 39.51 (sec), 39.49 (sec), 37.4 (sec), 37.3 (sec), 34.1 (sec), 34.0 (sec), 31.5 (2 × tert), 28.4 (2 × tert), 27.1 (2 × prim), 25.08 (sec), 25.06 (sec), 22.84 (prim)*, 22.82 (prim)*, 22.75 (prim)*, 22.73 (prim)*, 19.7 (2 × prim).

* The signals of the primary C-atoms split into two signals of equal intensity.

ESI-MS pos (high resolution): [$M^{\cdot+}$]

calc.: 1428.0120 m/z

found: 1428.0136 m/z Δ = 1.12 ppm

dSQA-7

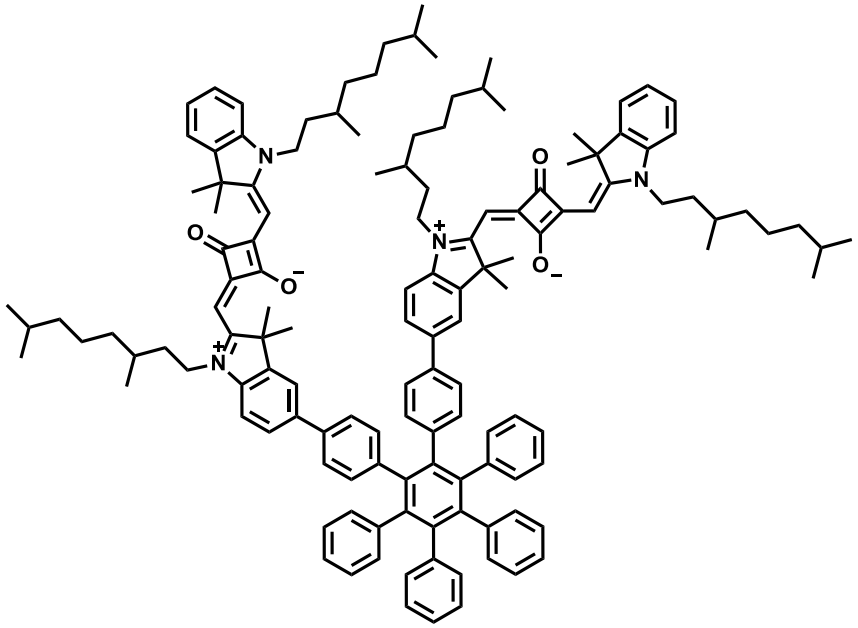

Functionalized squaraine dye **SQA-B** (100 mg, 125 µmol) and 4,4''-dibromo-3',4',5',6'-tetraphenyl-1,1':2',1''-terphenyl (43.0 mg, 62.1 µmol) were dissolved in peroxide-free THF (10 ml) under a nitrogen atmosphere. An aqueous solution of Na_2CO_3 (1 M, 370 µl, 370 µmol) was added and the mixture was purged in a gentle stream of nitrogen for 15 min. $Pd(PPh_3)_4$ (7.20 mg, 6.23 µmol) was added and the reaction was heated at 85 °C in a sealed tube for 2 d. The solvent was removed *in vacuo* and the residue purified by flash chromatography (DCM/MeOH = 99:1) and subsequent preparative recycling GPC ($CHCl_3$). Finally the product was dissolved in a small amount of DCM and dripped into an excess of *n*-hexane. The mixture was allowed to stand in the refrigerator at 4 °C overnight. The precipitate formed was filtered off and dried under high vacuum to afford analytically pure squaraine dimer **dSQA-7**.

Yield: 20.0 mg (10.6 µmol, 17 %) of a purple powder.

$C_{134}H_{154}N_4O_4$ [1884.69]

^{1}H-NMR (600.1 MHz, CD_2Cl_2):

δ [ppm] = 7.48-7.43 (s, 2H, 2 × C*H*), 7.40 (d, ^3J = 7.8 Hz, 2H, 2 × C*H*), 7.36 (d, ^3J = 7.0 Hz, 2H, 2 × C*H*), 7.34-7.28 (d, ^3J = 7.4 Hz, ^3J = 7.4 Hz, 2H, 2 × C*H*), 7.20

(d, ^{3}J = 8.0 Hz, 4H, 4 × C*H*), 7.17-7.08 (m, 2H, 2 × C*H*), 7.00 (-, 6H, 6 × C*H*), 6.96-6.80 (-, 22H, 22 × C*H*), 6.00-5.80 (-, 4H, 4 × C*H*), 4.20-3.80 (-, 8H, 4 × NCH_2), 1.90-1.62 (-, 28H, 4 × NCH_2CH, 8 × CH_3), 1.63-1.55 (-, 8H, 4 × NCH_2CH, 4 × C*H*), 1.55-1.44 (-, 4H, 4 × C*H*), 1.44-1.09 (-, 24H, 12 × CH_2), 1.09-0.97 (-, 12H, 4 × CH_3), 0.86 (d, ^{3}J = 6.5 Hz, 12H, 4 × CH_3), 0.83 (d, ^{3}J = 6.5 Hz, 12H, 4 × CH_3).

^{13}C-NMR (150.9 MHz, CD_2Cl_2):

δ [ppm] = 181.9 (2 × quart), 180.4 (quart), 180.1 (quart), 170.0 (quart), 169.6 (quart), 143.2 (quart), 142.8 (quart), 142.6 (quart), 142.1 (quart), 141.084 (quart), 141.077 (quart), 140.88 (quart), 140.84 (quart), 140.24 (quart), 140.16 (quart), 137.3 (quart), 136.3 (quart), 132.4 (tert), 131.8 (tert), 131.7 (tert), 128.1 (tert), 127.0 (tert), 126.9 (tert), 126.4 (tert), 125.7 (tert), 125.6 (tert), 125.1 (tert), 123.9 (tert), 122.5 (tert), 120.7 (tert), 109.7 (2 × tert), 87.0 (2 × tert), 49.5 (2 × quart), 42.4 (2 × sec), 39.51 (sec), 39.49 (sec), 37.5 (2 × sec), 34.1 (2 × sec), 31.48 (tert), 31.44 (tert), 28.35 (tert), 28.33 (tert), 27.1 (2 × prim), 25.1 (2 × sec), 22.81 (prim), 22.73 (prim), 19.8 (2 × prim).

ESI-MS pos (high resolution): [$M^{\cdot+}$]

calc.: 1884.19979 m/z

found: 1884.20039 m/z Δ = 0.32 ppm

5.2.5 Synthesis of Squaraine Homodimers (SQB)

dSQB-1

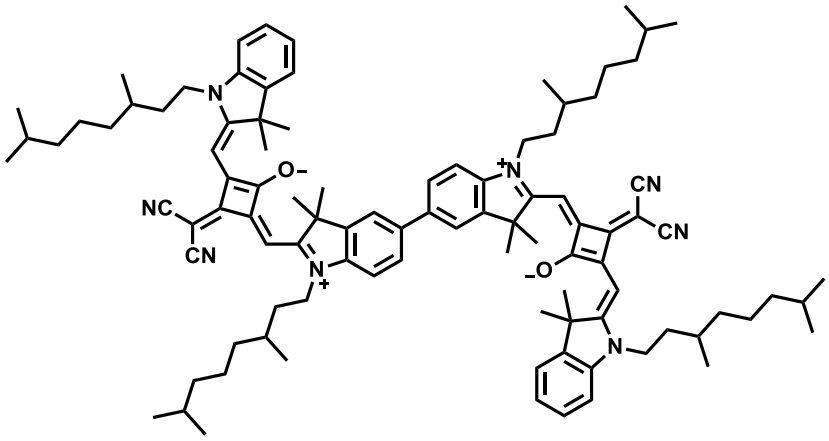

Synthesis according to given literature.[93]

Under a nitrogen atmosphere squaraine **SQB-Br** (46.0 mg, 57.2 µmol) and squaraine **SQB-B** (41.0 mg, 48.2 µmol) were dissolved in peroxide-free THF (8 ml). An aqueous solution of Na_2CO_3 (1 M, 323 µl, 323 µmol) was added and the mixture was purged in a gentle stream of nitrogen for 15 min. $Pd(PPh_3)_4$ (5.57 mg, 4.82 µmol) was added and the green solution was continuously heated at 85 °C in a sealed tube for 3 d. The solvent was removed in vacuo and the green residue was purified by flash chromatography (DCM/MeOH = 99:1) and subsequent preparative recycling GPC ($CHCl_3$). Finally the crude product was dissolved in a small amount of DCM and dripped into an excess of *n*-hexane. The mixture was allowed to stand at 4 °C in the refrigerator overnight. The precipitate formed was separated by filtration and dried under high vacuum.

Yield: 45.0 mg (31.1 µmol, 65 %) of a green powder.

$C_{98}H_{126}N_8O_2$ [1448.11]

^{1}H-NMR (400.1 MHz, CD_2Cl_2):

δ [ppm] = 7.62-7.58 (-, 4H, 4 × C*H*), 7.41 (dd, ^3J = 7.2 Hz, ^4J = 0.6 Hz, 2H, 2 × C*H*), 7.39-7.34 (m, 2H, 2 × C*H*), 7.26-7.20 (m, 2H, 2 × C*H*), 7.14 (d, ^3J = 8.4 Hz, 2H, 2 × C*H*), 7.09 (d, ^3J = 7.8 Hz, 2H, 2 × C*H*), 6.495 (s, 2H, 2 × C*H*), 6.489

(s, 2H, 2 × C*H*), 4.16-3.97 (-, 8H, 4 × NCH_2), 1.86-1.72 (-, 28H, 4 × NCH$_2$C*H*, 8 × CH_3), 1.71-1.57 (-, 8H, 4 × NCH$_2$C*H*-, 4 × C*H*), 1.57-1.47 (-, 4H, 4 × C*H*), 1.46-1.14 (-, 24H, 12 × CH_2), 1.05 (d, ^3J = 6.6 Hz, 6H, 2 × CH_3), 1.03 (d, ^3J = 6.6 Hz, 6H, 2 × CH_3), 0.87 (d, ^3J = 6.6 Hz,12H, 4 × CH_3), 0.86 (d, ^3J = 6.6 Hz, 12H, 4 × CH_3).

^{13}C-NMR (100.6 MHz, CD_2Cl_2):

δ [ppm] = 173.5 (quart.), 172.4 (quart.), 171.4 (quart.), 167.9 (quart.), 166.2 (quart.) 143.7 (quart.), 142.9 (quart.), 142.3 (quart.), 141.9 (quart.), 137.5 (quart.), 128.4 (tert.), 127.2 (tert.), 125.0 (tert.), 122.6 (tert.), 121.1 (tert.), 119.14 (quart.), 119.12 (quart.), 110.7 (tert.), 110.6 (tert.), 89.55 (tert.), 89.51 (tert.), 49.9 (quart.), 49.8 (quart.), 43.4 (2x sec.), 40.6 (2x quart.), 39.52 (sec.), 39.51 (sec.), 37.48 (sec.), 37.46 (sec.), 34.4 (2x sec.), 31.3 (2x tert.), 28.39 (tert.), 28.38 (tert.), 26.87 (prim.)*, 26.83 (prim.)*, 26.61 (prim.)*, 26.60 (prim.)*, 25.04 (sec.), 25.01 (sec.), 22.82 (prim.)*, 22.81 (prim.)*, 22.73 (prim.)*, 22.72 (prim.)*, 19.82 (prim.), 19.77 (prim.).

* The signals of the primary C-atoms split into two signals of equal intensity.

ESI-MS pos (high resolution): [$M^{\cdot+}$]

calc.: 1448.00305 m/z

found: 1448.00449 m/z Δ = 0.99 ppm

dSQB-2

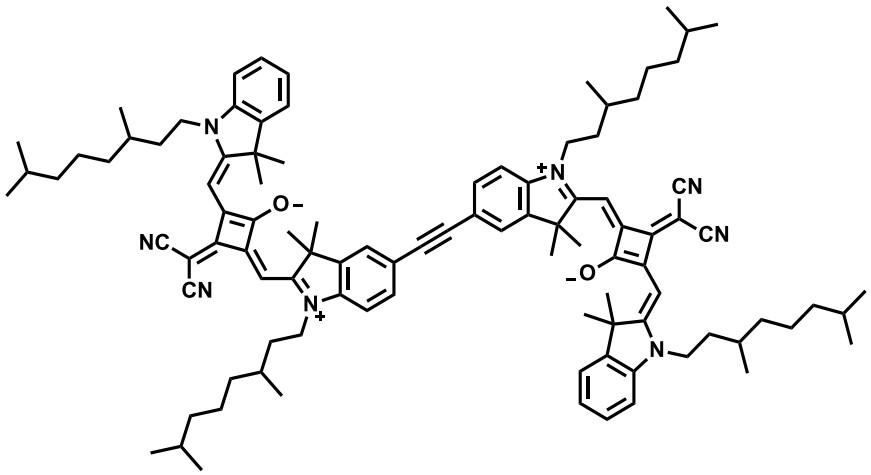

Under a nitrogen atmosphere squaraine **SQB-Br** (50.0 mg, 62.2 µmol) was dissolved in dry NEt_3 (25 ml). The deep green solution was degassed in a gentle stream of nitrogen for 20 min. P*t*Bu_3 (1 M in solution, 4.00 µl, 4.00 µmol) and $Pd(PPh_3)_2Cl_2$ (2.80 mg, 3.99 µmol) were subsequently added and the mixture was heated to 60 °C. A degassed solution of squaraine **SQB-Alkyne** (50.0 mg, 66.7 µmol) in dry NEt_3 (25 ml) was carefully added dropwise over a period of 45 min. After complete addition the reaction mixture was heated to reflux for 2 h. The solvent was removed *in vacuo* and the residue purified by flash chromatography (DCM/MeOH = 99:1) and subsequent preparative recycling GPC ($CHCl_3$). Finally, the product was dissolved in a small amount of DCM and dripped into an excess of *n*-hexane. The mixture was allowed to stand in the refrigerator at 4 °C overnight. The precipitate formed was filtered off and dried under high vacuum.

Yield: 25.0 mg (17.0 µmol, 27 %) of a dark green solid.

$C_{100}H_{126}N_8O_2$ [1472.13]

^{1}H-NMR (400.1 MHz, CD_2Cl_2):

δ [ppm] = 7.57-7.50 (-, 4H, 4 × C*H*), 7.42 (dd, ^3J = 7.5 Hz, ^4J = 0.7 Hz, 2H, 2 × C*H*), 7.38 (ddd, ^3J = 7.7 Hz, ^3J = 7.7 Hz, ^4J = 1.2 Hz, 2H, 2 × C*H*), 7.25 (ddd, ^3J = 7.5 Hz, ^3J = 7.7 Hz, ^4J = 0.7 Hz, 2H, 2 × C*H*), 7.11 (d, ^3J = 8.0 Hz, 2H, 2 × C*H*), 7.03 (d, ^3J = 8.7 Hz, 2H, 2 × C*H*), 6.53 (s, 2H, 2 × C*H*), 6.46 (s, 2H,

2 × C*H*), 4.18-3.88 (-, 8H, 4 × NCH_2), 1.86-1.73 (-, 28H, 4 × NCH_2C*H*, 8 × CH_3), 1.71-1.58 (-, 8H, 4× NCH_2C*H*, 4 × C*H*), 1.58-1.46 (-, 4H, 4 × C*H*), 1.45-1.13 (-, 24H, 12 × CH_2), 1.06-1.01 (-, 12H, 4 × CH_3), 0.87 (d, ^3J = 6.7 Hz, 12H, 4 × CH_3), 0.86 (d, ^3J = 6.6 Hz, 12H, 4 × CH_3).

^{13}C-NMR (100.6 MHz, CD_2Cl_2):

δ [ppm] = 173.4 (quart), 173.1 (quart), 170.7 (quart), 168.0 (quart), 167.8 (quart), 165.9 (quart), 143.08 (quart), 143.06 (quart), 142.5 (quart), 142.2 (quart), 132.0 (tert), 128.5 (tert), 125.7 (tert), 125.3 (tert), 122.7 (tert), 119.06 (quart), 119.04 (quart), 118.99 (quart), 110.8 (tert), 110.2 (tert), 90.2 (quart), 89.9 (tert), 89.7 (tert), 50.1 (quart), 49.4 (quart), 43.5 (sec), 43.3 (sec), 40.8 (quart), 39.54 (sec), 39.52 (sec), 37.49 (sec), 37.47 (sec), 34.5 (sec), 34.3 (sec), 31.33 (tert), 31.31 (tert), 28.402 (tert), 28.396 (tert), 26.88 (prim)*, 26.84 (prim)*, 26.54 (prim)*, 26.50 (prim)*, 25.04 (sec), 25.02 (sec), 22.83 (prim)*, 22.82 (prim)*, 22.74 (prim)*, 22.73 (prim)*, 19.80 (prim), 19.78 (prim).

* The signal of the primary C-atoms splits into two signals of equal intensity.

ESI-MS pos (high resolution): [$MH^{\cdot\cdot+++}$]

calc.: 736.5052 m/z

found: 736.5062 m/z Δ = 1.36 ppm

SQB-C_6H_4-Br and **dSQB-3**

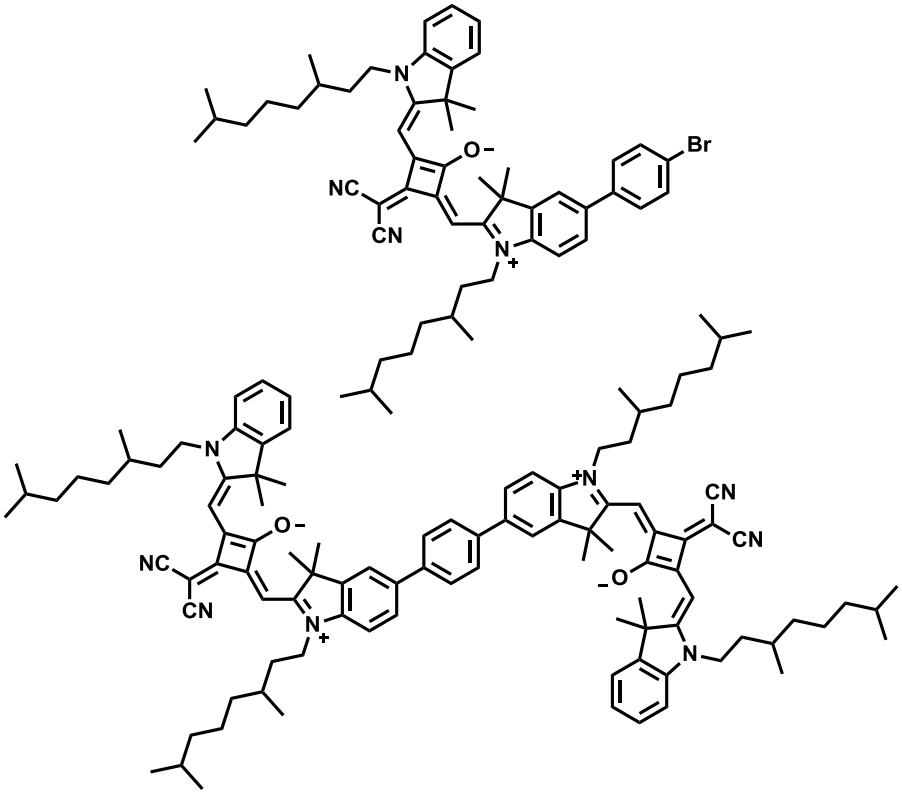

Functionalized squaraine dye **SQB-B** (128 mg, 150 µmol) and 1,4-dibromobenzene (35.0 mg, 148 µmol) were dissolved in peroxide-free THF (10 ml) under a nitrogen atmosphere. An aqueous solution of Na_2CO_3 (1 M, 451 µl, 451 µmol) was added and the mixture was purged in a gentle stream of nitrogen for 15 min. $Pd(PPh_3)_4$ (17.0 mg, 14.7 µmol) was added and the reaction was heated at 85 °C in a sealed tube for 2 d. The solvent was removed *in vacuo* and the residue purified by flash chromatography (DCM/MeOH = 99:1) and subsequent preparative recycling GPC ($CHCl_3$) to separate both compounds **SQB-C_6H_4-Br** and **dSQB-3**. Each batch was dissolved in a small amount of DCM and dripped into an excess of *n*-hexane. The precipitate formed was filtered off and dried under high vacuum, respectively.

SQB-C_6H_4-Br:

Yield: 47.0 mg (53.4 µmol, 36 %) of a green solid.

$C_{55}H_{67}BrN_4O$ [880.05]

^{1}H-NMR (400.1 MHz, CD_2Cl_2):

δ [ppm] = 7.65-7.54 (-, 4H, 4 × C*H*), 7.54-7.44 (-, 2H, 2 × C*H*), 7.44-7.31 (-, 2H, 2 × C*H*), 7.31-6.96 (-, 3H, 3 × C*H*), 6.82-6.03 (-, 2H, 2 × C*H*), 4.56-3.50 (-, 4H, 2 × NCH_2), 1.90-1.72 (-, 14H, 2 × NCH_2CH, 4 × CH_3), 1.72-1.58 (-, 4H, 2 × NCH_2CH, 2 × C*H*), 1.58-1.46 (-, 2H, 2 × C*H*), 1.46-1.10 (-, 12H, 6 × CH_2), 1.04 (d, ^{3}J = 6.4 Hz, 3H, CH_3), 1.03 (d, ^{3}J = 6.4 Hz, 3H, CH_3), 0.90-0.82 (-, 12H, 4 × CH_3).

^{13}C-NMR (100.6 MHz, CD_2Cl_2):

δ [ppm] = 173.5 (quart), 172.5 (quart), 171.5 (quart), 167.9 (quart), 167.2 (quart), 166.3 (quart), 143.6 (quart), 143.0 (quart), 142.3 (quart), 142.2 (quart), 139.9 (quart), 136.7 (quart), 132.3 (tert), 128.9 (tert), 128.4 (tert), 127.2 (tert), 125.1 (tert), 122.6 (tert), 121.7 (quart), 121.1 (tert), 119.1 (2 × quart), 110.7 (tert), 110.6 (tert), 89.6 (tert), 89.5 (tert), 50.0 (quart), 49.8 (quart), 43.40 (sec), 43.35 (sec), 40.7 (quart), 39.5 (2 × sec), 37.5 (2 × sec), 34.40 (sec), 34.37 (sec), 31.3 (2 × tert), 28.4 (2 × tert), 26.9 (prim)*, 26.8 (prim)*, 26.61 (prim)*, 26.58 (prim)*, 25.03 (sec), 25.02 (sec), 22.8 (2 × prim)*, 22.7 (2 × prim)*, 19.82 (prim), 19.78 (prim).

* The signals of the primary C-atoms split into two signals of equal intensity.

MALDI-MS pos: [$M^{\cdot+}$]

calc.: 880.449 m/z

found: 880.404 m/z

dSQB-3:

Yield: 35.0 mg (23.0 μmol, 31 %) of a dark green solid.

$C_{104}H_{130}N_8O_2$ [1524.20]

^{1}H-NMR (400.1 MHz, CD_2Cl_2):

δ [ppm] = 7.77-7.72 (-, 4H, 4 × C*H*), 7.69-7.64 (-, 4H, 4 × C*H*), 7.41 (dd, ^{3}J = 7.5 Hz, ^{4}J = 0.8 Hz, 2H, 2 × C*H*), 7.37 (ddd, ^{3}J = 7.7 Hz, ^{3}J = 7.7 Hz ^{4}J = 1.2 Hz, 2H,

2 × C*H*), 7.23 (ddd, ^{3}J = 7.5 Hz, ^{3}J = 7.5 Hz ^{4}J = 0.8 Hz, 2H, 2 × C*H*), 7.16 (d, ^{3}J = 8.8 Hz, 2H, 2 × C*H*), 7.09 (d, ^{3}J = 8.0 Hz, 2H, 2 × C*H*), 6.53-6.46 (-, 4H, 4 × C*H*), 4.18-3.96 (-, 8H, 4 × NCH_2), 1.90-1.73 (-, 28H, 4 × NCH_2CH, 8 × CH_3), 1.73-1.59 (-, 8H, 4 × NCH_2CH, 4 × C*H*), 1.57-1.47 (-, 4H, 4 × C*H*), 1.47-1.12 (-, 24H, 12 × CH_2), 1.05 (d, ^{3}J = 6.4 Hz, 6H, 2 × CH_3), 1.03 (d, ^{3}J = 6.4 Hz, 6H, 2 × CH_3), 0.87 (d, ^{3}J = 6.6 Hz, 12H, 4 × CH_3), 0.86 (d, ^{3}J = 6.6 Hz, 12H, 4 × CH_3).

^{13}C-NMR (100.6 MHz, CD_2Cl_2):

δ [ppm] = 173.5 (quart), 172.4 (quart), 171.6 (quart), 167.9 (quart), 167.0 (quart), 166.3 (quart), 143.7 (quart), 143.0 (quart), 142.3 (quart), 142.0 (quart), 139.8 (quart), 137.3 (quart), 128.4 (tert), 127.8 (tert), 127.2 (tert), 125.0 (tert), 122.6 (tert), 121.2 (tert), 119.2 (2 × quart), 110.7 (tert), 110.6 (tert), 89.6 (tert), 89.5 (tert), 49.9 (quart), 49.8 (quart), 43.40 (sec), 43.37 (sec), 40.7 (quart), 39.54 (sec), 39.53 (sec), 37.50 (sec), 37.48 (sec), 34.4 (2 × sec), 31.3 (2 × tert), 28.4 (2 × tert), 26.9 (prim)*, 26.8 (prim)*, 26.64 (prim)*, 26.61 (prim)*, 25.05 (sec), 25.02 (sec), 22.8 (prim), 22.7 (prim), 19.8 (prim), 19.8 (prim).

* The signals of the primary C-atoms split into two signals of equal intensity.

ESI-MS pos (high resolution): [$M^{\cdot+}$]

calc.: 1524.0344 m/z

found: 1524.0299 m/z Δ = 2.95 ppm

pySQB-1

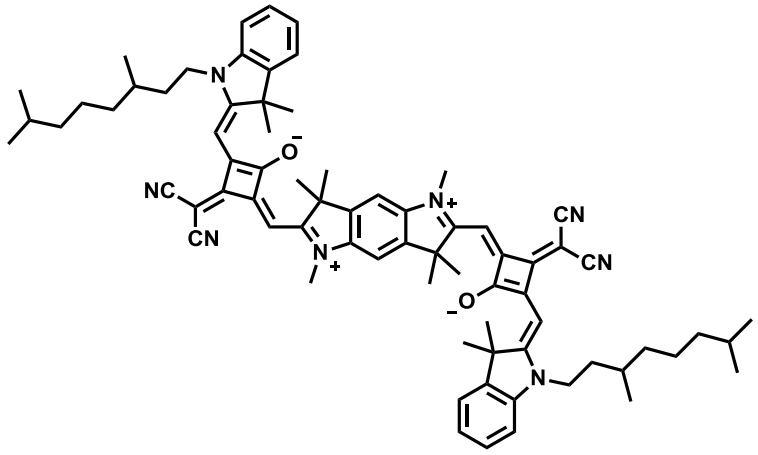

Pyrrolo salt **35** (200 mg, 382 µmol) and semisquaraine dye **23** (520 mg, 1.17 µmol) were dissolved in Ac_2O (15 ml) and refluxed for 18 h. The solvent was removed *in vacuo* and the dark green residue was purified by flash chromatography (DCM/MeOH = 99:1) and subsequent preparative recycling GPC ($CHCl_3$). The crude product was recrystallized from *n*-hexane.

Yield: 74.0 mg (66.1 µmol, 17 %) of a dark green solid.

$C_{74}H_{86}N_8O_2$ [1119.53]

^{1}H-NMR (600.1 MHz, CD_2Cl_2):

δ [ppm] = 7.41 (dd, ^3J = 7.4 Hz, ^4J = 0.7 Hz, 2H, 2 × C*H*), 7.37 (ddd, ^3J = 7.7 Hz, ^3J = 7.7 Hz, ^4J = 1.0 Hz, 2H, 2 × C*H*), 7.23 (ddd, ^3J = 7.4 Hz, ^3J = 7.4 Hz, ^4J = 0.7 Hz, 2H, 2 × C*H*), 7.09 (d, ^3J = 7.9 Hz, 2H, 2 × C*H*), 7.06 (s, 2H, 2 × C*H*), 6.49 (s, 2H, 2 × C*H*), 6.46 (s, 2H, 2 × C*H*), 4.12-3.98 (m, 4H, 2 × NCH_2), 3.65 (s, 6H, NCH_3), 1.83-1.70 (-, 26H, 2 × NCH_2CH, 8 × CH_3), 1.58-1.56 (-, 4H, 2 × NCH_2CH, 2 × C*H*), 1.56-1.48 (m, 2H, 2 × C*H*), 1.43-1.13 (-, 12H, 6 × CH_2), 1.03 (d, ^3J = 6.4 Hz, 6H, 2 × CH_3), 0.86 (d, ^3J = 6.6 Hz, 12H, 4 × CH_3).

^{13}C-NMR (150.9 MHz, CD_2Cl_2):

δ [ppm] = 173.6 (quart), 172.5 (quart), 171.5 (quart), 168.0 (quart), 167.2 (quart), 165.7 (quart), 143.2 (quart), 143.0 (quart), 142.3 (quart), 140.4 (quart), 128.4 (tert), 125.1 (tert), 122.6 (tert), 119.4 (quart), 119.0 (quart), 110.7 (tert), 104.9 (tert), 89.7 (tert), 89.6 (tert), 50.0 (quart), 49.7 (quart), 43.4 (sec), 40.6 (quart), 39.5 (sec), 37.5 (sec), 34.4 (sec), 31.3 (tert), 31.0 (prim), 28.4 (tert), 27.0 (prim), 26.59 (prim)*, 26.56 (prim)*, 25.0 (sec), 22.8 (prim)*, 22.7 (prim)*, 19.8 (prim).

* The signals of the primary C-atoms split into two signals of equal intensity.

ESI-MS pos (high resolution): [$M^{\cdot+}$]

calc.: 1118.68683 m/z

found: 1118.68665 m/z Δ = 0.16 ppm

pySQB-2

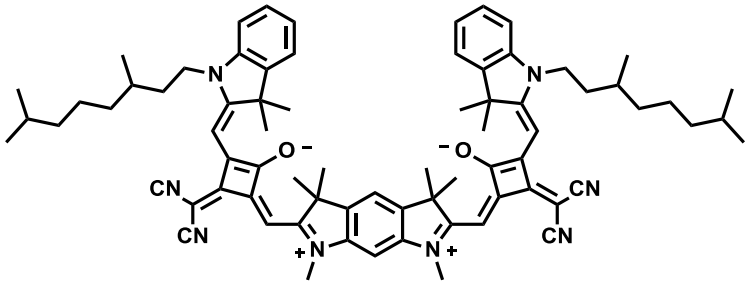

Pyrrolo salt **37** (92.0 mg, 175 µmol) and semisquaraine dye **23** (219 mg, 495 µmol) were dissolved in Ac_2O (25 ml) and refluxed for 4.5 h. The solvent was removed *in vacuo* and the dark green residue was purified by flash chromatography (DCM/MeOH = 99:1) and subsequent preparative recycling GPC ($CHCl_3$). The crude product was recrystallized from *n*-hexane.

Yield: 11.0 mg (9.83 µmol, 6 %) of a dark green solid.

$C_{74}H_{86}N_8O_2$ [1119.53]

^{1}H-NMR (600.1 MHz, CD_2Cl_2):

δ [ppm] = 7.42 (dd, ^{3}J = 7.5 Hz, ^{4}J = 0.6 Hz, 2H, 2 × C*H*), 7.38 (ddd, ^{3}J = 7.7 Hz, ^{3}J = 7.7 Hz, ^{4}J = 1.2 Hz, 2H, 2 × C*H*), 7.29 (s, 1H, C*H*), 7.25 (ddd, ^{3}J = 7.4 Hz, ^{3}J = 7.7 Hz, ^{4}J = 0.8 Hz, 2H, 2 × C*H*), 7.11 (d, ^{3}J = 7.9 Hz, 2H, 2 × C*H*), 6.72 (s, 1H, C*H*), 6.52 (s, 2H, 2 × C*H*), 6.45 (s, 2H, 2 × C*H*), 4.12 – 4.01 (m, 4H, 4 × NCH_2), 3.63 (s, 6H, 2 × NCH_3), 1.83-1.78 (m, 2H, 2 × NCH$_2$C*H*), 1.76 (s, 12H, 4 × CH_3), 1.75 (s, 12H, 4 × CH_3) 1.58-1.49 (-, 4H, 2 × NCH$_2$C*H*, 2 × C*H*), 1.56-1.48 (m, 2H, 2 × C*H*), 1.43-1.41 (-, 12H, 6 × CH_2), 1.03 (d, ^{3}J = 6.5 Hz, 6H, 2 × CH_3), 0.86 (d, ^{3}J = 6.6 Hz, 12H, 4 × CH_3).

^{13}C-NMR (150.9 MHz, CD_2Cl_2):

δ [ppm] = 173.5 (quart), 173.0 (quart), 172.3 (quart), 168.1 (quart), 168.0 (quart), 166.1 (quart), 143.5 (quart), 143.1 (quart), 142.6 (quart), 142.2 (quart), 128.5 (tert), 125.3 (tert), 122.7 (tert), 119.3 (quart), 119.0 (quart), 116.2 (tert), 110.8 (tert), 92.6 (tert), 89.9 (tert), 89.4 (tert), 50.1 (quart), 49.4 (quart), 43.5 (sec), 40.7 (quart), 39.5 (sec), 37.5 (sec), 34.5 (sec), 31.3 (tert), 31.0 (prim), 28.4 (tert), 27.1 (prim), 26.54 (prim)*, 26.51 (prim)*, 25.0 (sec), 22.8 (prim)*, 22.7 (prim)*, 19.8 (prim).

* The signal of the primary C-atoms splits into two signals of equal intensity.

ESI-MS pos (high resolution): [$M^{\cdot+}$]

calc.: 1118.68683 m/z

found: 1118.68724 m/z Δ = 0.37 ppm

5.2.6 Synthesis of Squaraine Heterodimers

dSQAB-1

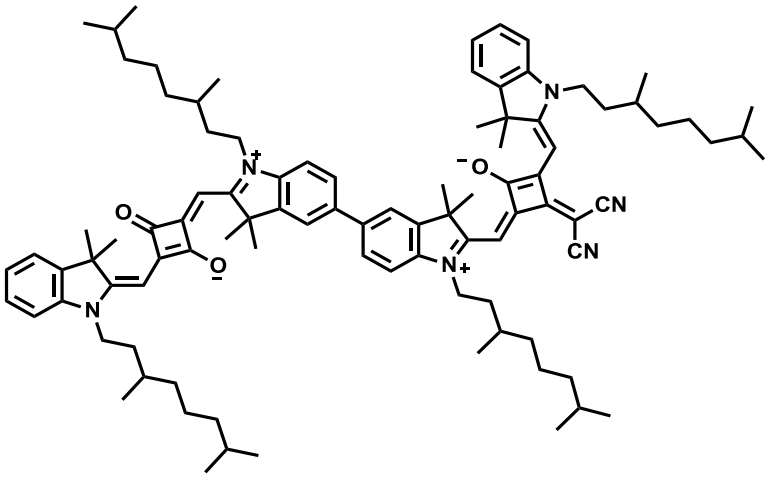

Synthesis according to given literature.[88]

Under a nitrogen atmosphere squaraine **SQA-Br** (70.0 mg, 92.6 µmol) and squaraine **SQB-B** (95.0 mg, 112 µmol) were dissolved in peroxide-free THF (7 ml). An aqueous solution of Na_2CO_3 (1 M, 278 µl, 278 µmol) was subsequently added and the mixture was purged in a gentle stream of nitrogen for 20 min. $Pd(PPh_3)_4$ (10.7 mg, 9.26 µmol) was added and the reaction was continuously heated at 85 °C in a sealed tube for 2 d. The solvent was removed *in vacuo* and the residue purified by flash chromatography (DCM/MeOH = 99:1) and subsequent preparative recycling GPC ($CHCl_3$). Finally the product was dissolved in a small amount of DCM and dripped into an excess of *n*-hexane. The mixture was allowed to stand in the refrigerator at 3 °C overnight. The precipitate formed was filtered off and dried under high vacuum.

Yield: 80.0 mg (57.1 µmol, 62 %) of a bronze solid.

$C_{95}H_{126}N_6O_3$ [1400.06]

^{1}H-NMR (600.1 MHz, CD_2Cl_2):

δ [ppm] = 7.62-7.56 (-, 4H, 4 × C*H*), 7.42-7.31 (-, 4H, 4 × C*H*), 7.22 (dd, ^3J = 7.4 Hz, ^4J = 0.7 Hz, 1H, C*H*), 7.18-7.12 (-, 2H, 2 × C*H*), 7.08 (d, ^3J = 7.9 Hz, 1H, C*H*), 7.07 (d, ^3J = 8.2 Hz, 1H, C*H*), 7.02 (d, ^3J = 8.0 Hz, 1H, C*H*), 6.490 (s, 1H,

C*H*), 6.487 (s, 1H, C*H*), 5.93-5.91 (-, 2H, 2 × C*H*), 4.14-3.95 (-, 8H, 4 × NCH_2), 1.88-1.72 (-, 28H, 4 × NCH_2CH, 8 × CH_3), 1.72-1.57 (-, 8H, 4 × NCH_2CH, 4 × C*H*), 1.57-1.48 (-, 4H, 4 × C*H*), 1.46-1.13 (-, 24H, 12 × CH_2), 1.08 (d, ^3J = 6.3 Hz, 3H, CH_3), 1.07 (d, ^3J = 6.4 Hz, 3H, CH_3), 1.05 (d, ^3J = 6.4 Hz, 3H, CH_3), 1.03 (d, ^3J = 6.5 Hz, 3H, CH_3), 0.89-0.84 (-, 24H, 8 × CH_3).

^{13}C-NMR (150.9 MHz, CD_2Cl_2):

δ [ppm] = 181.2 (2 × quart), 180.1 (quart), 179.4 (quart), 173.5 (quart), 172.3 (quart), 171.6 (quart), 170.3 (quart), 169.2 (quart), 167.9 (quart), 166.9 (quart), 166.3 (quart), 143.7 (quart), 142.9 (2 × quart), 142.8 (quart), 142.7 (quart), 142.5 (quart), 142.3 (quart), 141.7 (quart), 137.8 (quart), 136.5 (quart), 128.4 (tert), 128.2 (tert), 127.1 (tert), 127.0 (tert), 124.9 (tert), 124.1 (tert), 122.63 (tert), 122.61 (tert), 121.2 (tert), 121.1 (tert), 119.18 (quart), 119.16 (quart), 110.8 (tert), 110.6 (tert), 109.9 (tert), 109.8 (tert), 89.6 (tert), 89.5 (tert), 87.1 (tert), 87.0 (tert), 49.89 (quart), 49.88 (quart), 49.7 (quart), 49.5 (quart), 43.4 (sec), 43.3 (sec), 42.5 (2 × sec), 40.6 (quart), 39.5 (4 × sec), 37.5 (2 × sec), 37.49 (sec), 37.47 (sec), 34.42 (sec), 34.39 (sec), 34.1 (2 × sec), 31.5 (2 × tert), 31.3 (2 × tert), 28.41 (tert), 28.40 (tert), 29.39 (tert), 28.38 (tert), 27.3 (2 × prim), 27.1 (2 × prim), 26.9 (prim), 26.8 (prim), 26.7 (prim), 26.6 (prim), 25.11 (sec), 25.09 (sec), 25.06 (sec), 25.03 (sec), 22.83 (2 × prim), 22.82 (2 × prim), 22.7 (4 × prim), 19.84 (prim), 19.81 (prim), 19.79 (prim), 19.77 (prim).

ESI-MS pos (high resolution): [$M^{\cdot+}$]

calc.: 1399.99186 m/z

found: 1399.99225 m/z Δ = 0.28 ppm

dSQAB-2

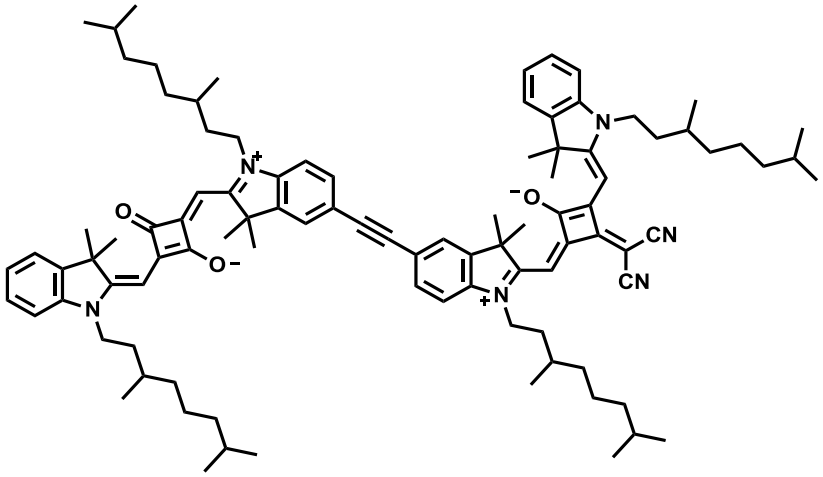

Under a nitrogen atmosphere squaraine **SQB-Br** (34.0 mg, 42.3 µmol) was dissolved in dry NEt_3 (10 ml). The dark green solution was degassed in a gentle stream of nitrogen for 20 min. CuI (239 µg, 1.25 µmol) and $Pd(PPh_3)_2Cl_2$ (881 µg, 1.26 µmol) were subsequently added and the mixture was heated to 60 °C. A degassed solution of squaraine **SQA-Alkyne** (44.0 mg, 62.8 µmol) in dry NEt_3 (10 ml) was carefully added dropwise over a period of 45 min. After complete addition the reaction mixture was heated to reflux for 2 h. The solvent was removed *in vacuo* and the residue purified by flash chromatography (DCM/MeOH = 99:1) and subsequent preparative GPC ($CHCl_3$).

Yield: 16.0 mg (11.2 µmol, 26 %) of a shiny red solid.

$C_{97}H_{126}N_6O_3$ [1424.08]

^{1}H-NMR (400.1 MHz, CD_2Cl_2):

δ [ppm] = 7.57-7.47 (-, 4H, 4 × C*H*), 7.45-7.30 (-, 4H, 4 × C*H*), 7.25 (ddd, ^3J = 7.5 Hz, ^3J = 7.5 Hz, ^4J = 0.7 Hz, 1H, C*H*), 7.22-7.15 (m, 1H, C*H*), 7.11 (d, ^3J = 7.9 Hz, 1H, C*H*), 7.18-6.99 (-, 2H, 2 × C*H*), 6.96 (d, ^3J = 7.1 Hz, 1H, C*H*), 6.52 (s, 1H, C*H*), 6.46 (s, 1H, C*H*), 5.96 (s, 1H, C*H*), 5.91 (s, 1H, C*H*), 4.17-3.86 (-, 8H, 4 × NCH_2), 1.86-1.71 (-, 28H, 4 × NCH_2CH, 8 × CH_3), 1.70-1.58 (-, 8H, 4 × C*H*, 4 × NCH_2CH), 1.56-1.45 (-, 4H, 4 × C*H*), 1.44-1.11 (-, 24H, 12 × CH_2), 1.11-1.05 (-, 6H, 2 × CH_3), 1.05-1.00 (-, 6H, 2 × CH_3), 0.90-0.83 (-, 24H, 8 × CH_3).

^{13}C-NMR (100.6 MHz, CD_2Cl_2):

δ [ppm] = 182.2 (2 × quart), 180.7 (quart), 179.6 (quart), 173.4 (quart), 173.0 (quart), 171.1 (quart), 170.8 (quart), 168.4 (quart), 168.0 (quart), 167.7 (quart), 166.0 (quart), 143.2 (quart), 143.1 (2 × quart), 142.8 (quart), 142.8 (quart), 142.7 (quart), 142.3 (quart), 142.2 (quart), 132.0 (tert), 131.9 (tert), 128.4 (tert), 128.2 (tert), 125.8 (tert), 125.6 (tert), 125.3 (tert), 124.4 (tert), 122.8 (tert), 122.7 (tert), 119.2 (quart), 119.07 (quart), 118.5 (quart), 118.0 (quart), 110.8 (tert), 110.3 (tert), 110.1 (tert), 109.5 (tert), 89.9 (quart), 89.8 (tert), 89.73 (quart), 89.66 (tert), 87.5 (tert), 87.3 (tert), 50.1 (quart), 49.9 (quart), 49.4 (quart), 49.1 (quart), 43.5 (sec), 43.3 (sec), 42.6 (sec), 42.4 (sec), 40.8 (quart), 39.54 (2 × sec), 39.53 (2 × sec), 37.48 (2 × sec), 37.47 (2 × sec), 34.5 (sec), 34.3 (sec), 34.2 (sec), 34.0 (sec), 31.5 (2 × tert), 31.3 (2 × tert), 28.39 (2 × tert), 28.38 (2 × tert), 27.2 (2 × prim)*, 27.0 (2 × prim)*, 26.9 (prim)*, 26.8 (prim)*, 26.55 (prim)*, 26.52 (prim)*, 25.1 (2 × sec), 25.03 (sec), 25.02 (sec), 22.825 (prim), 22.819 (prim), 22.74 (prim), 22.73 (prim), 19.79 (prim), 19.78 (2 × prim), 19.75 (prim).

* The signal of the primary C-atoms splits into two signals of equal intensity.

ESI-MS pos (high resolution): [$M^{\cdot+}$]

calc.: 1423.99186 m/z

found: 1423.99209 m/z Δ = 0.16 ppm

dSQAB-3

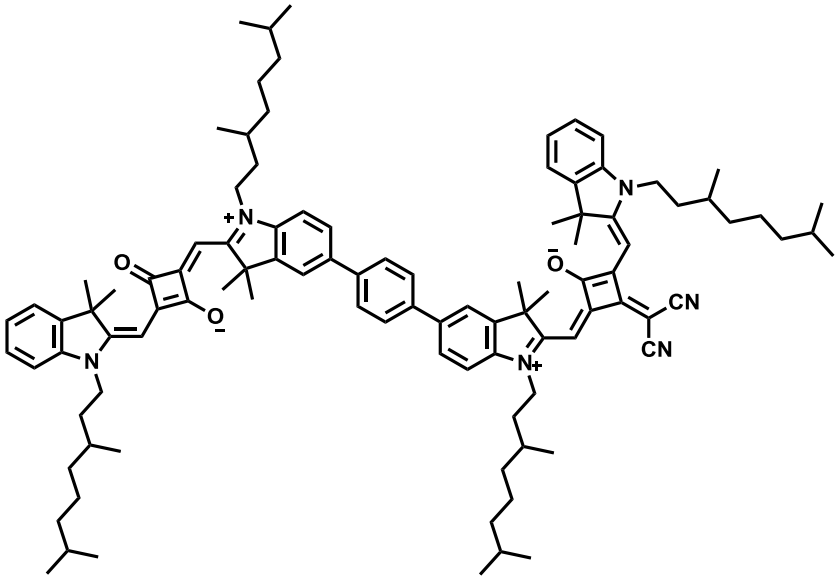

Synthesis according to given literature.[88]

Functionalized squaraine dye **SQA-B** (25.0 mg, 31.1 µmol) and squaraine **SQB-C_6H_4-Br** (36.0 mg, 40.9 µmol) were dissolved in peroxide-free THF (7 ml) under a nitrogen atmosphere. An aqueous solution of Na_2CO_3 (1 M, 93.0 µl, 93.0 µmol) was added and the mixture was purged in a gentle stream of nitrogen for 15 min. $Pd(PPh_3)_4$ (3.60 mg, 3.12 µmol) was added and the reaction was heated at 85 °C in a sealed tube for 2 d. The solvent was removed *in vacuo* and the residue purified by flash chromatography (DCM/MeOH = 99:1) and subsequent preparative recycling GPC ($CHCl_3$). Finally the product was dissolved in a small amount of DCM and dripped into an excess of *n*-hexane. The mixture was allowed to stand in the refrigerator at 4 °C overnight. The precipitate formed was filtered off and dried under high vacuum.

Yield: 10.0 mg (6.77 µmol, 22 %) of a green solid.

$C_{101}H_{130}N_6O_3$ [1476.16]

^{1}H-NMR (400.1 MHz, CD_2Cl_2):

δ [ppm] = 7.77-7.70 (-, 4H, 4 × C*H*), 7.69-7.60 (-, 4H, 4 × C*H*), 7.43-7.29 (-, 4H, 4 × C*H*), 7.22 (ddd, ^3J = 7.5 Hz, ^3J = 7.5 Hz, ^4J = 0.7 Hz, 1H, C*H*), 7.19-7.12 (-, 2H, 2 × C*H*), 7.12-7.05 (-, 2H, 2 × C*H*), 7.05-6.96 (m, 1H, C*H*), 6.497 (s, 1H, C*H*), 6.493 (s, 1H, C*H*), 6.08-5.80 (-, 2H, 2 × C*H*), 4.20-3.89 (-, 8H,

4 × NC*H*$_2$), 1.90-1.71 (-, 28H, 4 × NCH$_2$C*H*, 8 × C*H*$_3$), 1.71-1.60 (-, 8H, 4 × NCH$_2$C*H*, 4 × C*H*), 1.59-1.47 (-, 4H, 4 × C*H*), 1.47-1.13 (-, 24H, 12 × C*H*$_2$), 1.12-1.07 (-, 6H, 2 × C*H*$_3$), 1.05 (d, ^3J = 6.4 Hz, 3H, C*H*$_3$), 1.03 (d, ^3J = 6.4 Hz, 3H, C*H*$_3$), 0.90-0.84 (-, 24H, 8 × C*H*$_3$).

^{13}C-NMR (100.6 MHz, CD_2Cl_2):

δ [ppm] = 182.0 (2 × quart), 181.3 (quart), 180.1 (quart), 173.5 (quart), 172.3 (quart), 171.6 (quart), 170.4 (quart), 169.2 (quart), 167.9 (quart), 167.0 (quart), 166.4 (quart), 143.7 (quart), 143.4 (quart), 142.9 (quart), 142.8 (quart), 142.7 (quart), 142.5 (quart), 142.3 (quart), 142.0 (quart), 141.4 (quart), 139.9 (quart), 139.6 (quart), 137.4 (quart), 128.4 (2 × tert), 127.7 (2 × tert), 127.2 (2 × tert), 125.0 (2 × tert), 122.6 (2 × tert), 121.2 (2 × tert), 119.2 (2 × quart), 110.7 (tert), 110.6 (tert), 109.9 (tert), 109.8 (tert), 89.6 (tert), 89.5 (tert), 87.2 (tert), 87.0 (tert), 49.9 (2 × quart), 49.8 (2 × quart), 43.4 (2 × sec), 43.3 (2 × sec), 40.6 (quart), 39.54 (2 × sec), 39.53 (2 × sec), 37.50 (2 × sec), 37.48 (2 × sec), 34.41 (2 × sec), 34.39 (2 × sec), 31.5 (2 × tert), 31.3 (2 × tert), 28.40 (tert), 28.39 (tert), 28.38 (tert), 28.37 (tert), 26.86 (prim), 26.82 (prim), 26.65 (prim), 26.62 (prim), 25.1 (2 × sec), 25.04 (sec), 25.02 (sec), 22.8 (2 × prim), 22.7 (2 × prim), 19.83 (2 × prim), 19.79 (2 × prim).

ESI-MS pos (high resolution): [MH$^{\cdot+}$]

calc.: 1477.0310 m/z

found: 1477.0294 m/z Δ = 1.08 ppm

dSQBC

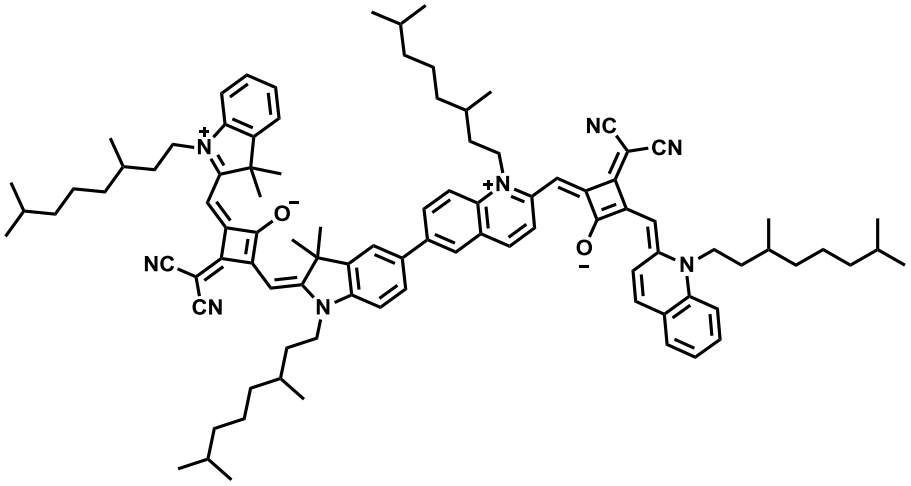

Under a nitrogen atmosphere squaraine **SQC-Br** (20.0 mg, 25.9 µmol) and squaraine **SQB-B** (44.0 mg, 51.7 µmol) were dissolved in peroxide-free THF (8 ml). An aqueous solution of Na_2CO_3 (1 M, 154 µl, 154 µmol) was added and the mixture was purged in a gentle stream of nitrogen for 15 min. $Pd(PPh_3)_4$ (2.99 mg, 2.59 µmol) was subsequently added and the mixture heated at 85 °C in a sealed tube for 4 d. The reaction was concentrated *in vacuo* and the crude product was purified by flash chromatography (DCM/MeOH = 99:1) and preparative recycling GPC ($CHCl_3$). The product was dissolved in a small amount of DCM and dripped into an excess of *n*-hexane. The voluminous precipitate formed was filtered off and dried under high vacuum.

Yield: 19.0 mg (13.4 µmol, 52 %) of a green solid.

$C_{96}H_{118}N_8O_2$ [1416.02]

^{1}H-NMR (600.1 MHz, CD_2Cl_2):

δ [ppm] = 9.14 (-, 2H, 2 × C*H*), 7.88 (dd, ^3J = 8.8 Hz, ^4J = 1.2 Hz, 1H, C*H*), 7.80 (s, 1H, C*H*), 7.68-7.59 (-, 6H, 6 × C*H*), 7.53-7.46 (-, 2H, 2 × C*H*), 7.41 (d, ^3J = 7.3 Hz, 1H, C*H*), 7.39-7.32 (-, 2H, 2 × C*H*), 7.26-7.21 (-, 1H, C*H*), 7.13 (d, ^3J = 8.7 Hz, 1H, C*H*), 7.10 (d, ^3J = 8.1 Hz, 1H, C*H*), 6.51 (s, 1H, C*H*), 6.49 (s, 1H, C*H*), 6.38-6.14 (-, 2H, 2 × C*H*), 4.45-4.14 (-, 4H, 2 × NCH_2), 4.14-3-98 (-, 4H, 2 × NCH_2), 1.94-1.72 (-, 20H, 4 × C*H*, 4 × NCH_2CH, 4 × CH_3) 1.71-1.61 (-, 4H, 4 × NCH_2CH), 1.61-1.49 (-, 4H, 4 × C*H*), 1.48-1.15 (-, 24H, 12 × CH_2),

1.12 (d, ^{3}J = 6.8 Hz, 3H, CH_3), 1.10 (d, ^{3}J = 6.8 Hz, 3H, CH_3), 1.05 (d, ^{3}J = 6.6 Hz, 3H, CH_3), 1.03 (d, ^{3}J = 6.6 Hz, 3H, CH_3), 0.91-0.88 (-, 12H, 4 × CH_3), 0.88-0.85 (-, 12H, 4 × CH_3).

^{13}C-NMR (150.9 MHz, CD_2Cl_2):

δ [ppm] = 175.1 (quart), 173.9 (quart), 173.5 (quart), 172.7 (quart), 171.2 (quart), 168.0 (quart), 167.4 (quart), 166.1 (quart), 165.8 (quart), 163.5 (quart), 162.8 (quart), 151.6 (quart), 150.7 (quart), 143.8 (quart), 143.0 (quart), 142.4 (quart), 142.2 (quart), 139.9 (quart), 139.3 (quart), 136.7 (quart), 135.6 (2 × quart), 134.7 (tert), 134.2 (tert), 132.2. (2 × tert), 130.7 (2 × tert), 129.4 (tert), 128.4 (tert), 127.1 (tert), 126.5 (tert), 126.1 (2 × tert), 125.1 (tert), 122.7 (tert), 121.0 (2 × quart), 119.1 (2 × quart), 115.9 (tert), 115.5 (tert), 110.8 (tert), 110.7 (tert), 94.5 (2 × tert), 89.7 (2 × tert), 50.0 (quart), 49.7 (quart), 48.5 (quart), 43.44 (2 × sec), 43.36 (2 × sec), 40.7 (quart), 39.6 (2 × sec), 39.5 (2 × sec), 37.5 (4 × sec), 34.4 (2 × sec), 34.0 (2 × sec), 31.7 (2 × tert), 31.3 (tert), 31.0 (tert), 28.4 (4 × tert), 26.9 (2 × prim), 26.6 (2 × prim), 25.0 (4 × sec), 22.83 (2 × prim), 22.77 (2 × prim), 19.8 (2 × prim)*, 19.5 (2 × prim)*.

ESI-MS pos (high resolution): [$M^{\cdot+}$]

calc.: 1415.94045 m/z

found: 1415.94064 m/z Δ = 0.13 ppm

5.2.7 Synthesis of Squaraine Trimers

tSQB

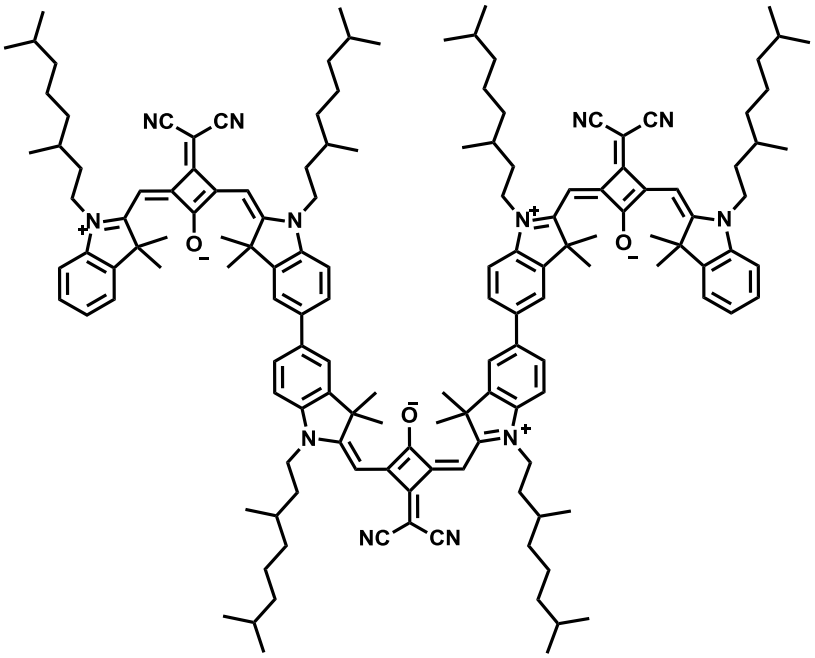

Synthesis according to given literature.[158]

Under a nitrogen atmosphere squaraine **SQB-B$_2$** (100 mg, 102 µmol) and squaraine **SQB-Br** (181 mg, 225 µmol) were dissolved in peroxide-free THF (8 ml). An aqueous solution of Na_2CO_3 (1 M, 60.8 µl, 60.8 µmol) was added and the mixture was purged in a gentle stream of nitrogen for 15 min. $Pd(PPh_3)_4$ (9.11 mg, 7.88 µmol) was added and the reaction was continuously heated at 85 °C in a sealed tube for 3 d. The solvent was removed *in vacuo* and the residue purified by flash chromatography (eluent: DCM/MeOH = 99:1) and subsequent preparative recycling GPC ($CHCl_3$).

Yield: 130 mg (59.9 µmol, 59 %) of a green solid.

$C_{147}H_{188}N_{12}O_3$ [2171.14]

^{1}H-NMR (600.1 MHz, CD_2Cl_2):

δ [ppm] = 7.62-7.59 (-, 8H, 8 × C*H*), 7.41 (d, ^3J = 7.3 Hz, 2H, 2 × C*H*), 7.37 (dd, ^3J = 7.8 Hz, ^4J = 1.0 Hz, 2H, 2 × C*H*), 7.25-7.20 (m, 2H, 2 × C*H*), 7.18-7.13 (-, 4H, 4 × C*H*), 7.09 (d, ^3J = 8.0 Hz, 2H, 2 × C*H*), 6.52-6.49 (-, 6H, 6 × C*H*),

4.16- 3.99 (-, 12H, 6 × NC*H*$_2$), 1.88-1.75 (-, 42H, 6 × NCH$_2$C*H*, 12 × C*H*$_3$), 1.72-1.57 (-, 12H, 6 × NCH$_2$C*H*, 6 × C*H*), 1.57-1.49 (-, 6H, 6 × C*H*), 1.44-1.32 (-, 12H, 6 × C*H*$_2$), 1.32-1.21 (-, 12H, 6 × C*H*$_2$), 1.21-1.19 (-, 12H, 6 × C*H*$_2$), 1.05 (d, ^3J = 6.3 Hz, 6H, 2 × C*H*$_3$), 1.05 (d, ^3J = 6.3 Hz, 6H, 2 × C*H*$_3$), 1.03 (d, ^3J = 6.4 Hz, 6H, 2 × C*H*$_3$), 0.89-0.85 (-, 36H, 12 × C*H*$_3$).

^{13}C-NMR (150.9 MHz, CD_2Cl_2):

δ [ppm] = 173.54 (quart), 173.50 (quart), 172.4 (quart), 171.7 (quart), 171.4 (quart), 168.0 (quart), 167.9 (quart), 167.1 (quart), 166.5 (quart), 166.2 (quart), 143.8 (quart), 143.7 (quart), 142.9 (quart), 142.3 (quart), 141.9 (quart), 141.8 (quart), 137.7 (quart), 137.4 (quart), 128.4 (tert), 127.3 (2 × tert), 125.0 (tert), 122.6 (2 × tert), 121.2 (tert), 119.1 (2 × quart), 110.9 (tert), 110.7 (tert), 110.6 (tert), 89.6 (tert), 89.3 (tert), 49.92 (quart), 49.91 (quart), 49.8 (quart), 43.47 (sec), 43.37 (2 × sec), 40.75 (quart), 40.66 (quart), 39.53 (2 × sec), 39.52 (sec), 37.49 (2 × sec), 37.47 (sec), 34.45 (sec), 34.40 (2 × sec), 31.3 (2 × tert), 28.40 (2 × tert), 28.39 (tert), 26.89 (prim), 26.85 (2 × prim), 26.81 (prim), 26.62 (prim), 26.59 (prim), 25.05 (2 × sec) 25.02 (sec), 22.83 (2 × prim), 22.82 (prim), 22.74 (2 × prim), 22.73 (prim), 19.83 (2 × prim), 19.78 (prim).

ESI-MS pos (high resolution): [$M^{\cdot+}$]

calc.: 2171.498628 m/z

found: 2171.495970 m/z Δ = 1.22 ppm

dSQAB-B and **tSQABA**

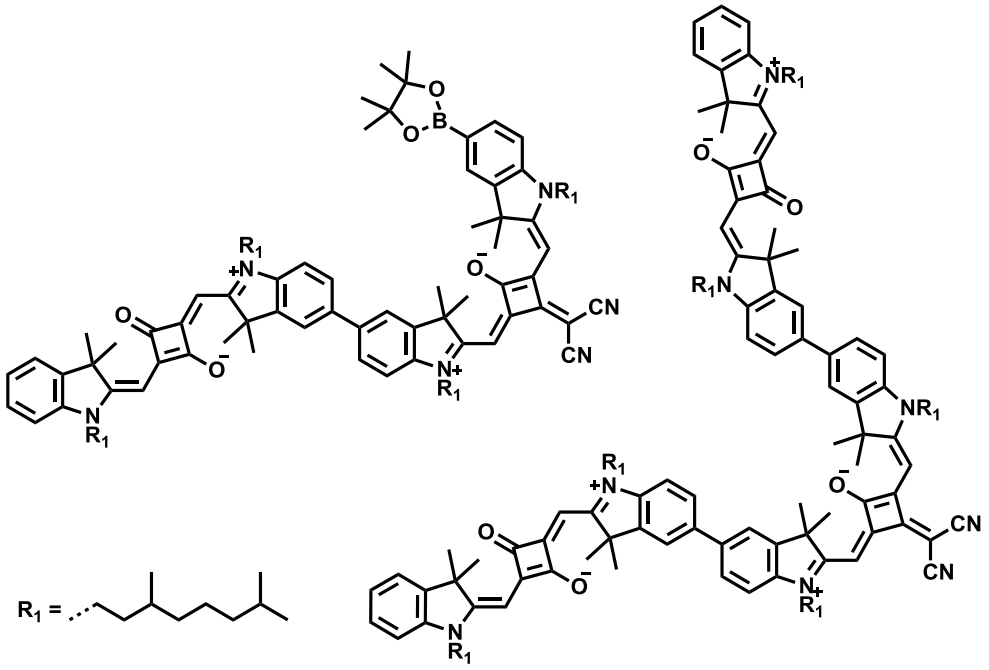

Squaraine **SQA-Br** (267 mg, 353 µmol), squaraine **SQB-B$_2$** (384 mg, 393 µmol), and Na_2CO_3 (1 M, 1.18 ml, 1.18 mmol) were dissolved in dry THF (15 ml) under a nitrogen atmosphere. The mixture was purged in a gentle stream of nitrogen for 15 min. $Pd(PPh_3)_4$ (23.0 mg, 19.9 µmol) was subsequently added and the reaction was continuously heated at 85 °C in a sealed tube for 4 d. The reaction was concentrated *in vacuo* and the residue was purified by flash chromatography (DCM/MeOH = 99:1) and preparative recycling GPC ($CHCl_3$) to isolate the functionalized squaraine dimer **dSQAB-B** and the symmetric squaraine trimer **tSQABA**.

dSQAB-B

Yield: 266 mg (174 µmol, 49 %) of a green solid.

$C_{101}H_{137}BN_6O_5$ [1526.02]

^{1}H-NMR (600.1 MHz, CD_2Cl_2):

δ [ppm] = 7.78 (dd, ^3J = 7.9 Hz, ^4J = 1.1 Hz, 1H, C*H*), 7.76-7.75 (-, 1H, C*H*), 7.63-7.56 (-, 4H, 4 × C*H*), 7.38 (dd, ^3J = 7.4 Hz, ^4J = 0.6 Hz, 1H, C*H*), 7.33 (ddd, ^3J = 7.7 Hz, ^3J = 7.7 Hz, ^4J = 1.2 Hz, 1H, C*H*), 7.19-7.15 (-, 2H, 2 × C*H*), 7.08 (d, ^3J = 8.5 Hz, 1H, C*H*), 7.06 (d, ^3J = 7.9 Hz, 1H, C*H*), 7.03 (d, ^3J = 8.0 Hz,

1H, C*H*), 6.53 (s, 1H, C*H*), 6.49 (s, 1H, C*H*), 5.96-5.93 (-, 2H, 2 × C*H*), 4.15-3.96 (-, 8H, 4 × NCH_2), 1.88-1.58 (-, 28H, 4 × NCH_2CH, 8 × CH_3), 1.70-1.57 (-, 8H, 4 × NCH_2CH, 4 × C*H*), 1.58-1.48 (-, 4H, 4 × C*H*), 1.32-1.12 (-, 36H, 12 × CH_2, 4 × CH_3), 1.08 (d, ^3J = 6.3 Hz, 3H, CH_3), 1.07 (d, ^3J = 6.4 Hz, 3H, CH_3), 1.05 (d, ^3J = 6.4 Hz, 3H, CH_3), 1.02 (d, ^3J = 6.4 Hz, 3H, CH_3), 0.89-0.85 (-, 24H, 8 × CH_3).

^{13}C-NMR (150.9 MHz, CD_2Cl_2):

δ [ppm] = 182.1 (2 × quart), 181.0 (quart), 179.8 (quart), 173.5 (quart), 172.2 (quart), 171.9 (quart), 170.4 (quart), 169.3 (quart), 168.0 (quart), 167.1 (quart), 166.6 (quart), 144.9 (quart), 143.8 (quart), 143.5 (quart), 142.8 (quart), 142.5 (quart), 142.1 (quart), 141.7 (quart), 141.6 (quart), 138.2 (quart), 136.4 (quart), 135.4 (tert), 128.4 (tert), 128.2 (tert), 127.3 (tert), 127.2 (tert), 124.1 (tert), 122.6 (tert), 121.2 (tert), 121.1 (tert), 119.13 (quart), 119.08 (quart), 111.0 (tert), 110.0 (tert), 109.9 (tert), 109.8 (tert), 90.0 (tert), 89.7 (tert), 87.2 (tert), 87.0 (tert), 84.3 (quart), 50.1 (quart), 49.7 (quart), 49.6 (quart), 49.5 (quart), 43.6 (sec), 43.2 (sec), 42.5 (2 × sec), 40.7 (quart), 39.54 (2 × sec), 39.53 (2 × sec), 37.50 (2 × sec), 37.48 (2 × sec), 34.5 (sec), 34.4 (sec), 34.1 (2 × sec), 31.5 (2 × tert), 31.33 (tert), 31.30 (tert), 28.41 (tert), 28.40 (tert), 28.39 (tert), 28.38 (tert), 27.3 (2 × prim)*, 27.07 (prim)*, 27.06 (prim)*, 26.82 (prim)*, 26.79 (prim)*, 26.78 (prim)*, 26.75 (prim)*, 25.11 (sec), 25.09 (sec), 25.6 (prim, sec), 25.02 (sec), 22.84 (prim), 22.83 (prim), 2 × 22.7 (2 × prim), 19.83 (prim), 19.81 (2 × prim), 19.80 (prim).

* The signal of the primary C-atoms splits into two signals of equal intensity.

MALDI-MS pos (high resolution): [$M^{\cdot+}$]

calc.: 1526.078 m/z

found: 1526.005 m/z

tSQABA

Yield: 132 mg (63.6 µmol, 36 %) of a green solid.

$C_{141}H_{188}N_8O_5$ [2075.06]

^{1}H-NMR (600.1 MHz, CD_2Cl_2):

δ [ppm] = 7.65-7.59 (-, 8H, 8 × C*H*), 7.38 (d, ^3J = 7.3 Hz, 2H, 2 × C*H*), 7.33 (dd, ^3J = 7.7 Hz, ^4J = 1.0 Hz, 2H, C*H*), 7.19-7.15 (-, 4H, 4 × C*H*), 7.10 (d, ^3J = 8.0 Hz, 2H, 2 × C*H*), 7.03 (d, ^3J = 8.0 Hz, 2H, 2 × C*H*), 6.54 (s, 2H, 2 × C*H*), 6.00-5.93 (-, 4H, 4 × C*H*), 4.17-3.96 (-, 12H, 6 × NC*H*$_2$), 1.90-1.74 (-, 42H, 6 × NCH$_2$C*H*, 12 × C*H*$_3$), 1.74-1.59 (-, 12H, 6 × C*H*, 6 × NCH$_2$C*H*), 1.59-1.48 (-, 6H, C*H*),1.48-1.15 (-, 36H, C*H*$_2$), 1.10 (d, ^3J = 6.1 Hz, 6H, 2 × C*H*$_3$), 1.08 (d, ^3J = 6.1 Hz, 6H, 2 × C*H*$_3$), 1.07 (d, ^3J = 6.3 Hz, 6H, 2 × C*H*$_3$). 0.90-0.88 (-, 18H, 6 × C*H*$_3$), 0.88-0.87 (-,18H, 6 × C*H*$_3$).

^{13}C-NMR (150.9 MHz, CD_2Cl_2):

δ [ppm] = 182.0 (2 × quart), 181.1 (quart), 180.0 (quart), 173.6 (quart), 171.7 (quart), 170.3 (quart), 169.2 (quart), 168.0 (quart), 166.4 (quart), 143.8 (quart), 142.5 (quart), 142.8 (quart), 142.6 (quart), 142.5 (quart), 141.7 (quart), 137.9 (quart), 136.5 (quart), 128.2 (tert), 127.2 (tert), 127.0 (tert), 124.1 (tert), 122.6 (tert), 121.2 (tert), 121.1 (tert), 119.2 (quart), 110.9 (tert), 109.0 (tert), 109.8 (tert), 89.8 (tert), 87.2 (tert), 87.0 (tert), 49.9 (quart), 49.7 (quart), 49.5 (quart), 43.5 (sec), 42.48 (sec), 42.45 (sec), 40.7 (quart), 39.54 (sec), 39.53 (sec), 39.52 (sec), 37.51 (sec), 37.50 (sec), 37.46 (sec), 34.5 (sec), 34.13 (sec), 34.11 (sec), 31.5 (2 × tert), 31.3 (tert), 28.40 (tert), 28.37 (tert), 28.36 (tert), 27.33 (prim)*, 27.32 (prim)*, 27.09 (prim)*, 27.08 (prim)*, 26.87 (prim)*, 26.84 (prim)*, 25.10 (sec), 25.07 (sec), 25.05 (sec), 22.87 (prim)*, 22.86 (prim)*, 22.85 (prim)*, 22.777 (prim)*, 22.773 (prim)*, 22.76 (prim)*, 19.86 (prim), 19.83 (prim), 19.79 (prim).

* The signal of the primary C-atoms splits into two signals of equal intensity.

ESI-MS pos (high resolution): [$M^{\cdot+}$]

calc.: 2074.47300 m/z

found: 2074.47490 m/z Δ = 0.92 ppm

tSQBAB

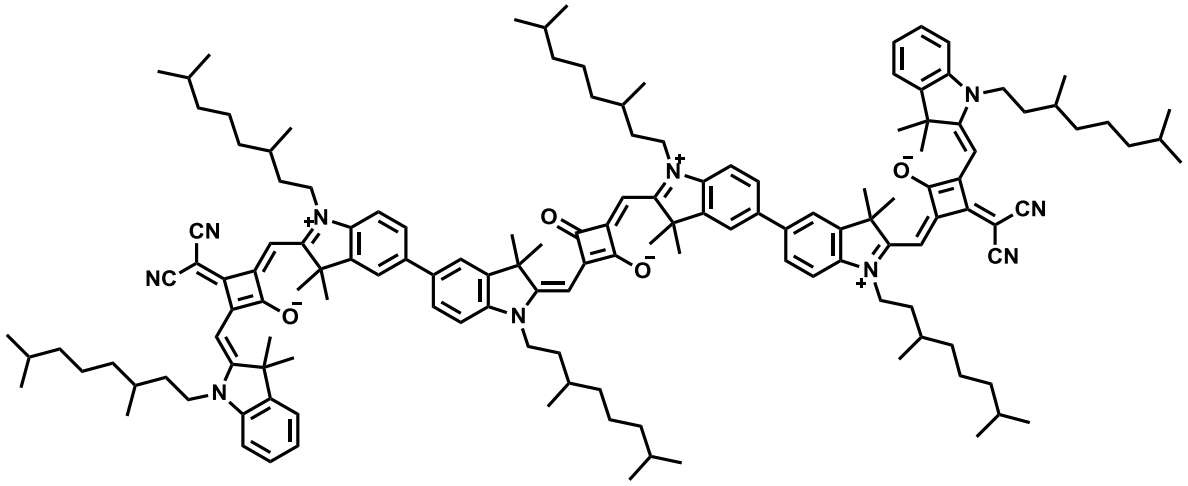

Under a nitrogen atmosphere squaraine **SQA-B$_2$** (100 mg, 108 µmol) and squaraine **SQB-Br** (190 mg, 236 µmol) were dissolved in peroxide-free THF (10 ml). An aqueous solution of Na_2CO_3 (1 M, 323 µl, 323 µmol) was added and the mixture was purged in a gentle stream of nitrogen for 15 min. $Pd(PPh_3)_4$ (9.11 mg, 7.88 µmol) was added and the reaction was continuously heated at 85 °C in a sealed tube for 3 d. The solvent was removed *in vacuo* and the residue purified by flash chromatography (eluent: DCM/MeOH = 99:1) and preparative recycling GPC ($CHCl_3$). The crude product was dissolved in a small amount of DCM and dripped into an excess of *n*-hexane. The mixture was allowed to stand overnight in the refrigerator at 4 °C. The precipitate formed was filtered off and dried under high vacuum.

Yield: 123 mg (57.9 µmol, 54 %) of a bronze solid.

$C_{144}H_{188}N_{10}O_4$ [2123.10]

^{1}H-NMR (600.1 MHz, CD_2Cl_2):

δ [ppm] = 7.60-7.47 (-, 8H, 8 × C*H*), 7.40-7.32 (-, 4H, 4 × C*H*), 7.24-7.18 (m, 2H, 2 × C*H*), 7.10 (d, ^3J = 8.2 Hz, 2H, 2 × C*H*), 7.07-7.02 (-, 4H, 4 × C*H*), 6.56-6.48 (-, 4H, 4 × C*H*), 6.02 (s, 2H, 2 × C*H*), 4.17-3.95 (-, 12H, 6 × NCH_2), 1.90-1.72 (-, 42H, 6 × NCH$_2$C*H*, 12 × CH_3), 1.72-1.56 (-, 12H, 6 × NCH$_2$C*H*, 6 × C*H*), 1.56-1.46 (-, 6H, 6 × C*H*), 1.46-1.11 (-, 36H, 18 × CH_2), 1.10-1.01 (-, 18H, 6 × CH_3), 0.91-0.83 (-, 36H, 12 × CH_3).

^{13}C-NMR (150.9 MHz, CD_2Cl_2):

δ [ppm] = 182.5 (quart), 179.7 (quart), 173.4 (quart), 172.1 (quart), 171.2 (quart), 169.6 (quart), 167.9 (quart), 166.9 (quart), 166.2 (quart), 143.4 (2 × quart), 142.7 (quart), 142.0 (2 × quart), 141.5 (quart), 137.6 (quart), 136.7 (quart), 128.2 (tert), 127.1 (tert), 126.9 (tert), 124.8 (tert), 122.5 (tert), 121.1 (tert), 121.0 (tert), 119.06 (quart), 119.04 (quart), 110.4 (tert), 110.2 (tert), 109.7 (tert), 89.4 (tert), 89.4 (tert), 87.2 (tert), 49.7 (quart), 49.6 (quart), 49.5 (quart), 43.13 (sec), 43.11 (sec), 42.4 (sec), 41.0 (quart), 39.31 (2 × sec), 39.30 (sec), 37.29 (sec), 37.27 (2 × sec), 34.3 (2 × sec), 34.1 (sec), 31.3 (tert), 31.0 (2 × tert), 28.131 (tert), 28.126 (2 × tert), 27.3 (prim), 26.93 (prim)*, 26.90 (prim)*, 26.68 (prim)*, 26.67 (prim)*, 24.84 (sec), 24.78 (sec), 24.76 (sec), 22.85 (prim), 22.84 (prim), 22.76 (prim)*, 22.75 (prim)*, 19.87 (prim), 19.83 (prim), 19.78 (prim).

* The signals of the primary C-atoms split into two signals of equal intensity.

ESI-MS pos (high resolution): [$M^{\cdot+}$]

calc.: 2122.48421 m/z

found: 2122.48459 m/z Δ = 0.18 ppm

tSQABC

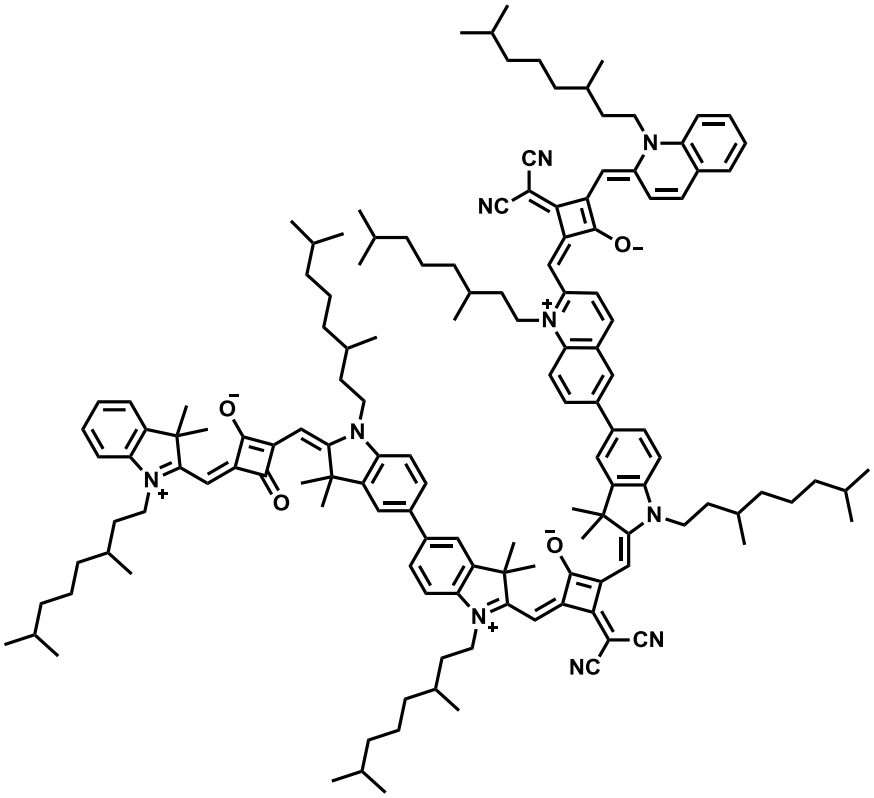

Under a nitrogen atmosphere squaraine **SQC-Br** (56.0 mg, 72.6 µmol) and squaraine dimer **dSQAB-B** (122 mg, 79.9 µmol) were dissolved in peroxide-free THF (10 ml). An aqueous solution of Na_2CO_3 (1 M, 430 µl, 430 µmol) was subsequently added and the mixture was purged in a gentle stream of nitrogen for 20 min. $Pd(PPh_3)_4$ (8.38 mg, 7.25 µmol) was added and the reaction was continuously heated at 85 °C in a sealed tube for 5 d. The solvent was removed *in vacuo* and the residue purified by flash chromatography (DCM/MeOH = 99:1) and subsequent preparative recycling GPC ($CHCl_3$). Finally the product was dissolved in a small amount of DCM and dripped into an excess of *n*-hexane. The resulting precipitate was separated by filtration and dried under high vacuum.

Yield: 84.0 mg (40.2 µmol, 55 %) of a dark green solid.

$C_{142}H_{180}N_{10}O_4$ [2091.02]

^{1}H-NMR (600.1 MHz, CD_2Cl_2):

δ [ppm] = 9.17 (d, ^{3}J = 9.4 Hz, 1H, C*H*), 9.15 (d, ^{3}J = 9.5 Hz, 1H, C*H*), 7.93 (dd, ^{3}J = 8.9 Hz, ^{4}J = 2.2 Hz, 1H, C*H*), 7.83 (d, ^{4}J = 2.2 Hz, 1H, C*H*), 7.71-7.59 (-,10 × 10H, C*H*), 7.57 (d, ^{3}J = 9.1 Hz, 1H, C*H*), 7.50 (^{3}J = 8.8 Hz, 1H, C*H*), 7.42 (dd, ^{3}J = 7.5 Hz, ^{4}J = 0.7 Hz, 1H, C*H*), 7.39-7.35 (-, 2H, 2 × C*H*), 7.22-7.18 (-, 2H, 2 × C*H*), 7.16 (d, ^{3}J = 8.2 Hz, 1H, C*H*), 7.11 (d, ^{3}J = 8.2 Hz, 1H, C*H*), 7.06 (d, ^{3}J = 8.0 Hz, 1H, C*H*), 6.56 (s, 1H, C*H*), 6.53 (s, 1H, C*H*), 6.30 (s, 1H, C*H*), 6.29 (s, 1H, C*H*), 6.01-5.94 (s, 2H, 2 × C*H*), 4.44-4.20 (-, 4H, 2 × NCH_2), 4.20-4.00 (-, 8H, 4 × NCH_2), 1.92-1.65 (-, 42H, 6 × NCH_2CH_2, 8 × CH_3, 6 × C*H*), 1.64-1.54 (-, 6H, 6 × C*H*), 1.50-1.20 (-, 36H, 18 × CH_2), 1.17-1.08 (-, 18H, 6 × CH_3), 0.95-0.90 (-, 36H, 12 × CH_3).

^{13}C-NMR (150.9 MHz, CD_2Cl_2):

δ [ppm] = 181.6 (2 × quart), 180.8 (quart), 179.5 (quart), 174.7 (quart), 173.1 (quart), 171.7 (quart), 170.8 (quart), 170.0 (quart), 168.8 (quart), 167.6 (quart), 166.5 (quart), 165.7 (quart), 165.3 (quart), 163.0 (quart), 162.4 (quart), 162.4 (quart), 151.1 (quart), 150.3 (quart), 143.4 (quart), 143.1 (quart), 142.4 (quart), 142.3 (quart), 142.2 (quart), 141.9 (quart), 141.2 (quart), 139.5 (quart), 138.9 (quart), 137.7 (quart), 136.3 (quart), 135.9 (quart), 135.3 (quart), 134.3 (tert), 133.8 (tert), 131.8 (tert), 130.3 (tert), 128.9 (tert), 127.8 (tert), 126.8 (tert), 126.7 (tert), 126.6 (tert), 126.12 (tert), 126.07 (tert), 125.8 (quart), 125.6 (tert), 125.3 (quart), 124.5 (tert), 123.7 (tert), 122.2 (tert), 120.8 (tert), 120.7 (tert), 120.6 (tert), 118.8 (2 × quart), 118.7 (2 × quart), 115.5 (tert), 115.0 (tert), 110.6 (tert), 110.4 (tert), 109.53 (tert), 109.46 (tert), 94.2 (2 × tert), 89.6 (tert), 89.4 (tert), 86.8 (tert), 86.6 (tert), 49.7 (quart), 49.4 (quart), 49.3 (quart), 49.1 (quart), 48.1 (sec), 48.0 (sec), 43.2 (sec), 43.0 (sec), 42.1 (2 × sec), 40.6 (quart), 40.4 (quart), 39.23 (sec), 39.21 (sec), 39.2 (3 × sec), 39.1 (sec), 37.11 (4 × sec), 37.07 (2 × sec), 34.1 (sec), 34.0 (sec), 33.73 (2 × sec), 33.67 (sec), 33.62 (sec), 31.3 (tert), 31.1 (2 × tert), 30.94 (tert), 30.93 (tert), 30.6 (tert), 28.04 (tert), 28.03 (tert), 28.02 (2 × tert), 27.99 (tert), 27.98 (tert), 26.93 (prim)*, 26.91 (prim)*, 26.67 (prim)*, 26.66 (prim)*, 26.54 (prim)*, 26.50 (prim)*, 26.40 (prim)*, 26.36 (prim)*, 24.7 (sec), 24.69 (sec), 24.66 (2 × sec), 24.63 (sec), 24.60 (sec), 22.47 (prim)*, 22.454 (prim)*, 22.447 (2 × prim)*, 22.440 (prim)*, 22.43 (prim)*, 22.39 (prim)*, 22.38 (prim)*, 22.36 (2 × prim)*, 22.35

(prim)*, 22.34 (prim)*, 19.442 (prim), 19.436 (prim), 19.41 (prim), 19.37 (prim), 19.1 (2 × prim).

* The signals of the primary C-atoms split into two signals of equal intensity.

ESI-MS pos (high resolution): $[M^{\cdot+}]$

calc.: 2090.42160 m/z

found: 2090.42070 m/z Δ = 0.43 ppm

5.2.8 Synthesis of Hexasquarainyl Benzenes

hSQA-1

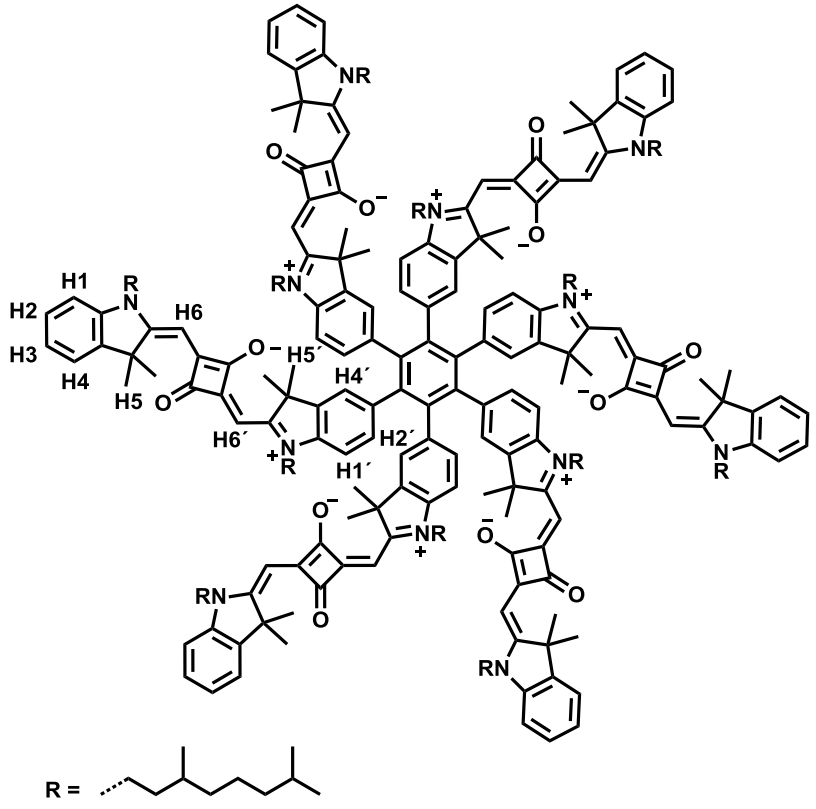

To a degassed solution of squaraine dimer **dSQA-2** (103 mg, 74.9 µmol) in dry 1,4-dioxane (7 ml) dicobaltoctacarbonyl (90 %, 3.13 mg, 8.24 µmol) was added and the reaction mixture heated under reflux for 18 h. The solvent was removed *in vacuo* and the residue purified by flash chromatography (DCM/MeOH = 98:2) and subsequent preparative recycling GPC ($CHCl_3$). Finally the product was dissolved in a small amount of DCM and dripped into an excess of *n*-hexane. The mixture was allowed to stand at -30 °C in the freezer overnight. The precipitate formed was filtered off and dried under high vacuum to afford analytically pure hexasquarainyl benzene **hSQA-1**.

Yield: 52.0 mg (12.6 µmol, 50 %) of a dark blue powder.

$C_{282}H_{378}N_{12}O_{12}$ [4128.10]

^{1}H-NMR (600.1 MHz, CD_2Cl_2):

δ [ppm] = 7.38-7.22 (-, 12H, 6 × H4 and 6 × H2), 7.17-7.06 (m, 6H, 6 × H3), 7.02-6.91 (m, 6H, 6 × H1), 6.87-6.67 (-, 12H, 6 × H4´and 6 × H2´), 6.64-6.46 (m, 6H, 6 × H1´), 5.92-5.78 (bs, 6H, 6 × H6), 5.78-5.61 (bs, 6H, 6 × H6´), 4.07-3.86 (m, 12H, 6 × NC*H*$_2$), 3.86-3.62 (m, 12H, 6 × NC*H*$_2$), 1.80-1.66 (-, 42H, 6 × NCH_2CH, 12 × C*H*$_3$), 1.64-1.44 (-, 36H, 24 × C*H*, 12 × NCH_2CH), 1.44-1.07 (-, 114H, 6 × NCH_2CH, 12 × C*H*$_3$, 36 × CH_2), 1.06-0.98 (m, 18H, 6 × C*H*$_3$), 0.96-0.89 (m, 18H, 6 × C*H*$_3$), 0.88-0.78 (-, 72H, 24 × C*H*$_3$).

Complete assignment of ^{13}C-NMR signals could not be made due to the complexity of the spectrum most likely caused by different isomers.

hSQA-2

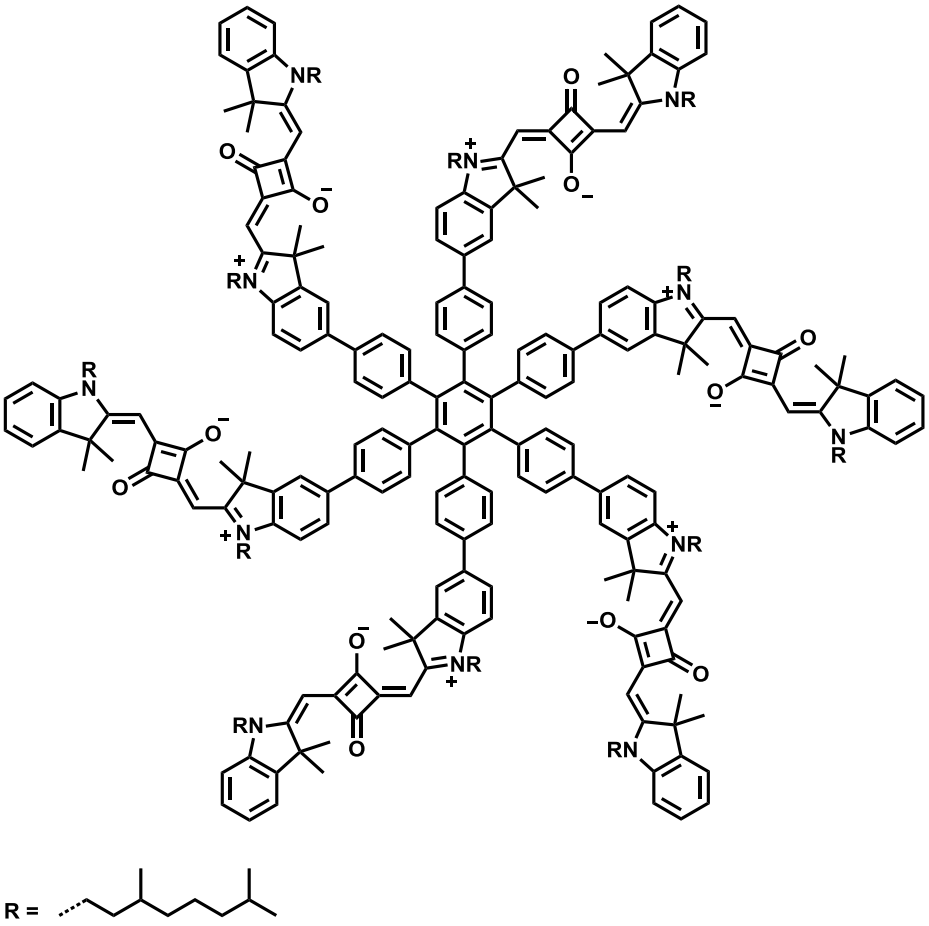

To a degassed solution of squaraine dimer **dSQA-5** (75.0 mg, 49.1 µmol) in dry 1,4-dioxane (5 ml) dicobaltoctacarbonyl (90 %, 2.05 mg, 5.40 µmol) was added and the reaction mixture stirred at 120 °C in a sealed tube for 2 d. The solvent was removed *in vacuo* and the residue purified by flash chromatography (DCM/MeOH = 98:2) and subsequent preparative recycling GPC ($CHCl_3$). Finally the product was dissolved in a small amount of DCM and dripped into an excess of *n*-hexane. The mixture was allowed to stand in the refrigerator at 4 °C overnight. The precipitate formed was filtered off and dried under high vacuum to afford analytically pure squaraine hexasquarainyl benzene **hSQA-2**.

Yield: 40 mg (8.72 µmol, 53 %) of a shiny violet solid.

$C_{318}H_{402}N_{12}O_{12}$ [4584.68]

^{1}H-NMR (600.1 MHz, CD_2Cl_2):

δ [ppm] = 7.49-7.44 (m, 6H, 6 × C*H*), 7.41 (d, ^{3}J = 7.5 Hz, 6H, 6 × C*H*), 7.35 (d, ^{3}J = 7.0 Hz, 6H, 6 × C*H*), 7.31 (dd, ^{3}J = 7.6 Hz, ^{3}J = 7.6 Hz, 6H, 6 × C*H*), 7.29-7.18 (m, 12H, 12 × C*H*), 7.13 (dd, ^{3}J = 7.4 Hz, ^{3}J = 7.4 Hz, 6H, 6 × C*H*), 7.11-7.01 (m, 12H, 12 × C*H*), 6.99 (d, ^{3}J = 8.0 Hz, 6H, 6 × C*H*), 6.93 (d, ^{3}J = 7.3 Hz, 6H, 6 × C*H*), 5.89 (s, 6H, 6 × C*H*), 5.87 (s, 6H, 6 × C*H*), 4.13-3.82 (-, 24H, 12 × NCH_2), 1.80-1.65 (-, 84H, 12 × NCH_2CH, 24 × CH_3), 1.60-1.41 (-, 36H, 12 × NCH_2CH, 12 × $CHCH_3$, 12 × $CH(CH_3)_2$), 1.40-1.09 (-, 72H, 36 × CH_2), 1.04 (d, ^{3}J = 6.2 Hz, 18H, 6 × CH_3), 1.01 (d, ^{3}J = 6.1 Hz, 18H, 6 × CH_3), 0.84 (d, ^{3}J = 6.6 Hz, 36H, 12 × CH_3), 0.81 (d, ^{3}J = 6.6 Hz, 36H, 12 × CH_3).

^{13}C-NMR (150.9 MHz, CD_2Cl_2):

δ [ppm] = 181.9 (2 × quart), 180.7 (quart), 180.3 (quart), 170.0 (quart), 169.5 (quart), 143.2 (quart), 142.8 (quart), 142.6 (quart), 142.2 (quart), 140.7 (quart), 140.1 (quart), 137.5 (quart), 136.2 (quart), 132.5 (2 × tert), 128.1 (tert), 126.5 (tert), 125.2 (2 × tert), 123.9 (tert), 122.6 (tert), 120.7 (tert), 109.7 (2 × tert), 87.1 (tert), 86.9 (tert), 49.6 (quart), 49.5 (quart), 42.4 (sec), 42.4 (sec), 39.50 (sec), 39.46 (sec), 37.44 (sec), 37.41 (sec), 34.1 (2 × sec), 31.5 (tert), 31.4 (tert), 28.34 (tert), 29.31 (tert), 27.2 (prim), 27.1 (prim), 25.05 (sec), 25.04 (sec), 22.81 (prim)*, 22.80 (prim)*, 22.73 (prim)*, 22.72 (prim)*, 19.8 (2 × prim).

* The signal of the primary C-atoms splits into two signals of equal intensity.

ESI-MS pos (high resolution): [$M^{\cdot\cdot+++}$]

calc.: 2292.06517 m/z

found: 2292.06471 m/z Δ = 0.43 ppm

5.2.9 Synthesis of Squaraine Polymers

Squaraine polymers **pSQB**,[71] **pDiPhSQB**,[71] **ppySQB**,[71] and **pSQBC**[72] were synthesized following literature procedures.

pSQB

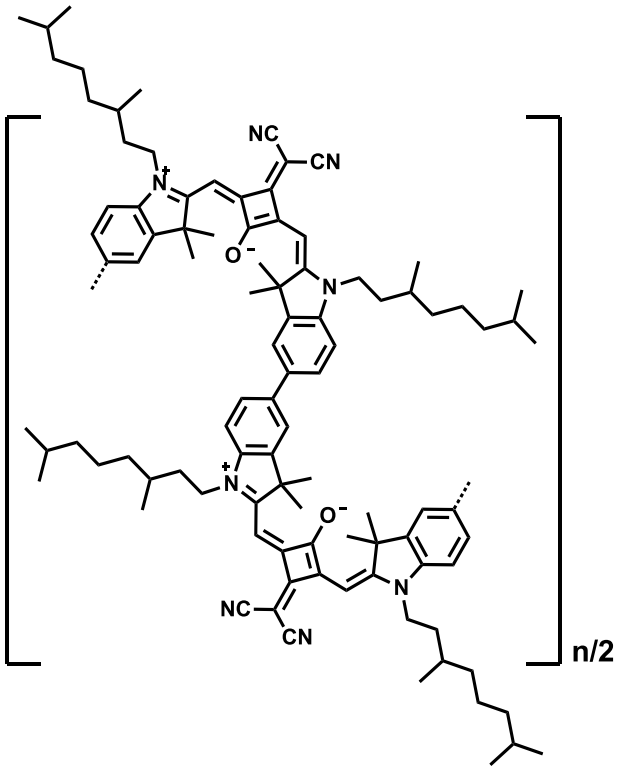

A mixture of $Ni(COD)_2$ (224 mg, 814 µmol), 2,2'-bipyridine (127 mg, 813 µmol), 1,5-cyclooctadiene (88.0 mg, 813 µmol), degassed toluene (2 ml), and degassed DMF (2 ml) was stirred at 65 °C under a nitrogen atmosphere for 30 min. A solution of squaraine **SQB-Br$_2$** (200 mg, 227 µmol) in degassed toluene (4 ml) and degassed DMF (4 ml) was added dropwise and the reaction mixture was continuously heated at 65 °C for 8 d. The cooled reaction mixture was poured into MeOH/HCl (20%) (4:1, 500 ml) and stirred for 5 h. The resulting purple precipitate was filtered off and washed consecutively with hexane, MeOH and acetone using a *Soxhlet* extractor. Each washing ran overnight. The major part remained in the acetone fraction with marginal amounts of solid that remained insoluble in acetone. Subsequent preparative GPC was used to separate the acetone fraction into three polymer batches of different molecular weight.

Yield: Fraction I: 50.0 mg (~ 69.2 µmol, 30 %) of a dark green solid.
Fraction II: 64.0 mg (~ 88.5 µmol, 39 %) of a dark green solid.
Fraction III: 25.0 mg (~ 34.6 µmol, 15 %) of a dark green solid.

$(C_{49}H_{62}N_4O)_n$ $[723.04]_n$

^{1}H-NMR (400.1 MHz, $CDCl_3$):
δ [ppm] = 7.61-7.53 (2H, 2 × C*H*), 7.53-7.46 (2H, 2 × C*H*), 7.17-7.06 (2H, 2 × C*H*), 6.59-6.49 (2H, 2 × C*H*), 4.25-3.94 (4H, 4 × C*H*), 1.89-1.74 (14H, 2 × NCH_2CH, 4 × CH_3), 1.73-1.60 (4H, 2 × NCH_2CH, 2 × C*H*), 1.57-1.48 (2H, 2 × C*H*), 1.42-1.14 (12H, 6 × CH_2), 1.09-0.98 (6H, 2 × CH_3), 0.92-0.79 (12H, 4 × CH_3).

pDiPhSQB

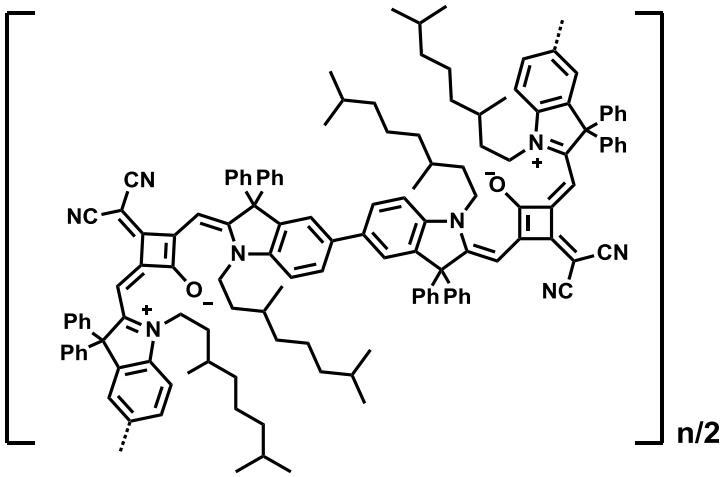

A mixture of $Ni(COD)_2$ (138 mg, 502 µmol), 2,2'-bipyridine (99.0 mg, 634 µmol), 1,5-cyclooctadiene (78.0 mg, 721 µmol), degassed toluene (2 ml), and degassed DMF (2 ml) was stirred at 65°C under nitrogen atmosphere for 30 min. A solution of squaraine **DiPhSQB-Br$_2$** (145 mg, 128 µmol) in degassed toluene (5 ml) and degassed DMF (5 ml) was added dropwise and the reaction mixture was continuously heated at 65 °C for 6 d under exclusion of light. The cooled reaction mixture was poured into MeOH/HCl (20%) (4:1, 500 ml) and stirred for 2 h. The resulting green precipitate was filtered off and washed consecutively with *n*-hexane, MeOH and acetone using a *Soxhlet* extractor, until no colouring of the solvent could be observed anymore, respectively. The *n*-hexane and MeOH-fraction were both

discarded. The acetone-fraction was dissolved in a small amount of DCM and dripped into an excess of MeOH/HCl (5 %, 4:1). The green precipitate was filtered off and washed with MeOH.

Yield: 60.0 mg (~ 61.8 µmol, 48 %) of a green solid.

$(C_{69}H_{70}N_4O)_n$ $[971.32]_n$

^{1}H-NMR (400.1 MHz, CD_2Cl_2):
δ [ppm] = 7.49-6.91 (26H, 26 × C*H*), 6.04 (2H, 2 × C*H*), 4.83-4.04 (4H, 2 × NCH_2), 1.77-1.60 (2H, 2 × NCH_2C*H*), 1.51-1.31 (6H, 2 × NCH_2C*H*, 4 × C*H*), 1.31-1.00 (12H, 6 × CH_2), 0.92-0.76 (18H, 6 × CH_3).

ppySQB

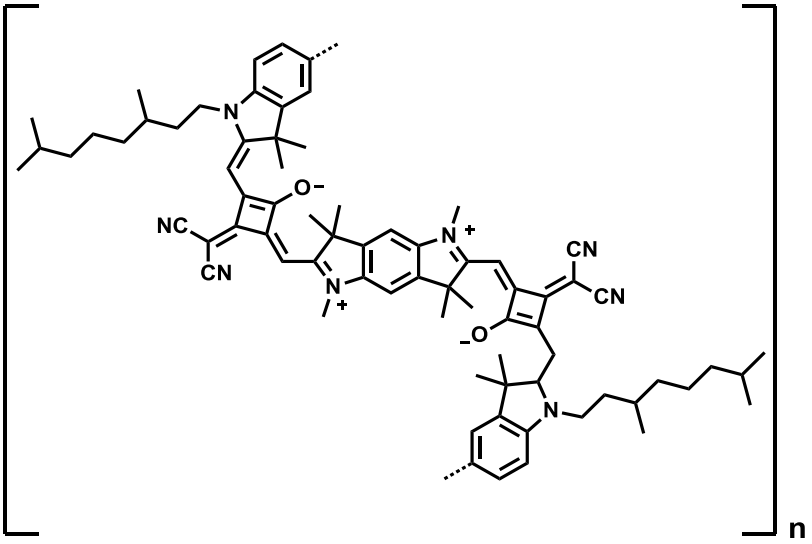

A mixture of $Ni(COD)_2$ (52.0 mg, 189 µmol), 2,2'-bipyridine (30.0 mg, 192 µmol), 1,5-cyclooctadiene (21.0 mg, 194 µmol), degassed toluene (4 ml), and degassed DMF (4 ml) was stirred at 65 °C under a nitrogen atmosphere for 30 min. A solution of squaraine **pySQB-1-Br_2** (101 mg, 79.1 µmol) in degassed toluene (3 ml) and degassed DMF (3 ml) was added dropwise and the reaction mixture was continuously heated at 65 °C for 6 d under exclusion of light. The cooled reaction mixture was poured into MeOH/HCl (15%) (4:1, 500 ml) and stirred for 5 h. The resulting dark green precipitate was filtered off and washed consecutively

with *n*-hexane, MeOH and acetone using a *Soxhlet* extractor, until no colouring of the solvent could be observed anymore, respectively. The remaining solid in the extraction thimble was dissolved in a small amount of DCM and dripped into an excess of *n*-hexane. The dark green precipitate was filtered off and dried in high vacuum.

Yield: 16.0 mg (~ 14.3 µmol, 18 %) of a dark green solid.

$(C_{74}H_{84}N_8O_2)_n$ $[1117.51]_n$

^{1}H-NMR (400.1 MHz, CD_2Cl_2):
δ [ppm] = 7.69-7.55 (4H, 4 × C*H*), 7.20-7.13 (2H, 2 × C*H*), 7.12-7.05 (2H, 2 × C*H*), 6.55-6.45 (4H, 4 × C*H*), 4.19-3.95 (4H, 2 × NCH_2), 3.73-3.55 (6H, 2 × NCH_3), 1.90-1.72-1.62 (30H, 2 × NCH_2CH_2, 8 × CH_3, 2 × C*H*), 1.60-1.46 (2H, 2 × C*H*), 1.43-1.13 (12H, 6 × CH_2), 1.08-1.04 (6H, 2 × CH_3), 0.89-0.85 (12H, 4 × CH_3).

pSQAC

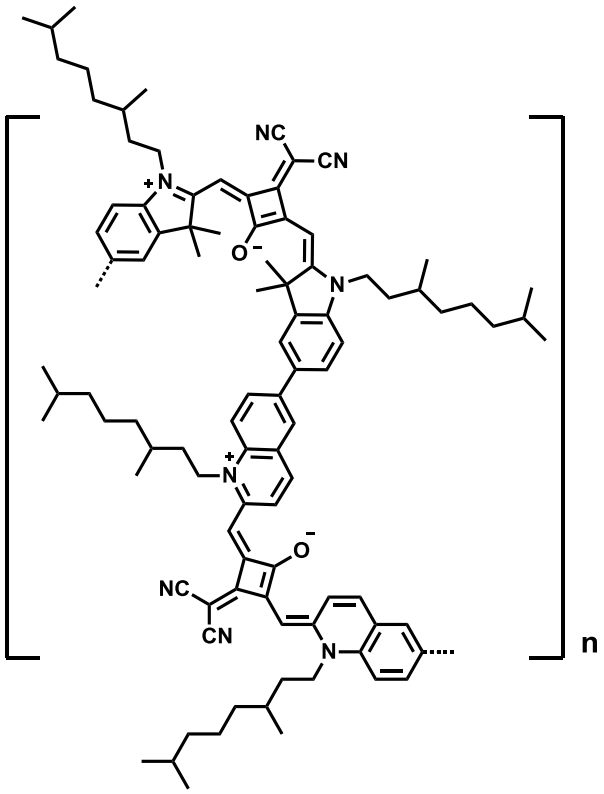

Squaraine **SQC-Br$_2$** (151 mg, 177 µmol), squaraine **SQB-B$_2$** (173 mg, 177 µmol), and $NaHCO_3$ (596 mg, 7.09 mmol) were dissolved in dry THF (16 ml) and H_2O (4 ml) under a nitrogen atmosphere. The mixture was purged in a gentle stream of nitrogen for 15 min and $Pd(PPh_3)_4$ (4.10 mg, 3.55 µmol) was added. The solution was stirred at 100 °C for 8 d. H_2O (25 ml) and DCM (25 ml) were subsequently added to the cooled reaction mixture and the layers were separated. The organic layer was washed with H_2O (2 × 20 ml) and the solvent was removed *in vacuo*. The residue was dissolved in a small amount of $CHCl_3$ and dripped into an excess of *n*-hexane. The precipitate formed was filtered through a blue ribbon filter and consecutively washed with *n*-hexane, MeOH and acetone using a *Soxhlet* extractor. Each extraction was carried out overnight. The remaining solid was dissolved in a small amount $CHCl_3$ and dripped into an excess of *n*-hexane. The precipitate was filtered through a blue ribbon filter and washed with *n*-hexane.

Yield: 137 mg (~ 96.9 µmol, 55 %) of a dark green solid.

$(C_{96}H_{116}N_8O_2)_n$ $[1414.00]_n$

Assessment of ^{1}H-NMR spectrum (CD_2Cl_2) was hampered by considerable signal broadening.

6 Literature

(1) Peceli, D.; Hu, H.; Fishman, D. A.; Webster, S.; Przhonska, O. V.; Kurdyukov, V. V.; Slominsky, Y. L.; Tolmachev, A. I.; Kachkovski, A. D.; Gerasov, A. O.; Masunov, A. E.; Hagan, D. J.; Van Stryland, E. W. *J. Phys. Chem. A* **2013**, *117*, 2333.

(2) Schmidt, A. H. *Synthesis* **1980**, 961.

(3) Lee, G.; Kim, J.; Kim, S. Y.; Kim, D. E.; Joo, T. *ChemPhysChem* **2017**, *18*, 670.

(4) Keil, T. H. *Phys. Rev.* **1965**, *140*, A601.

(5) Richards, J. L.; Rice, S. A. *J. Chem. Phys.* **1971**, *54*, 2014.

(6) Brixner, T.; Hildner, R.; Köhler, J.; Lambert, C.; Würthner, F. *Adv. Energy Mater.* **2017**, *7*, 1700236.

(7) Yagi, S.; Nakazumi, H. In *Top. Heterocycl. Chem.*; Strekowski, L., Ed.; Springer Berlin Heidelberg: Berlin, Heidelberg, 2008, p 133.

(8) Beverina, L.; Salice, P. *Eur. J. Org. Chem.* **2010**, 1207.

(9) Ajayaghosh, A. *Acc. Chem. Res.* **2005**, *38*, 449.

(10) Sreejith, S.; Carol, P.; Chithra, P.; Ajayaghosh, A. *J. Mater. Chem.* **2008**, *18*, 264.

(11) Mayerhöffer, U.; Gsänger, M.; Stolte, M.; Fimmel, B.; Würthner, F. *Chem. Eur. J.* **2013**, *19*, 218.

(12) Sun, W.; Guo, S.; Hu, C.; Fan, J.; Peng, X. *Chem. Rev.* **2016**, *116*, 7768.

(13) Volkova, K. D.; Kovalska, V. B.; Tatarets, A. L.; Patsenker, L. D.; Kryvorotenko, D. V.; Yarmoluk, S. M. *Dyes Pigm.* **2007**, *72*, 285.

(14) Tatarets, A. L.; Fedyunyayeva, I. A.; Dyubko, T. S.; Povrozin, Y. A.; Doroshenko, A. O.; Terpetschnig, E. A.; Patsenker, L. D. *Anal. Chim. Acta* **2006**, *570*, 214.

(15) Terpetschnig, E.; Szmacinski, H.; Ozinskas, A.; Lakowicz, J. R. *Anal. Biochem.* **1994**, *217*, 197.

(16) Thomas, J.; Sherman, D. B.; Amiss, T. J.; Andaluz, S. A.; Pitner, J. B. *Bioconjugate Chem.* **2007**, *18*, 1841.

(17) Renard, B.-L.; Aubert, Y.; Asseline, U. *Tetrahedron Lett.* **2009**, *50*, 1897.

(18) Terpetsching, E.; Szmacinski, H.; Lakowicz, J. R. *Anal. Chim. Acta* **1993**, *282*, 633.

(19) Arunkumar, E.; Fu, N.; Smith, B. D. *Chem. Eur. J.* **2006**, *12*, 4684.

(20) Gassensmith, J. J.; Arunkumar, E.; Barr, L.; Baumes, J. M.; DiVittorio, K. M.; Johnson, J. R.; Noll, B. C.; Smith, B. D. *J. Am. Chem. Soc.* **2007**, *129*, 15054.

(21) Xiang, Z.; Nesterov, E. E.; Skoch, J.; Lin, T.; Hyman, B. T.; Swager, T. M.; Bacskai, B. J.; Reeves, S. A. *J. Histochem. Cytochem.* **2005**, *53*, 1511.

(22) Jisha, V. S.; Arun, K. T.; Hariharan, M.; Ramaiah, D. *J. Am. Chem. Soc.* **2006**, *128*, 6024.

(23) Jisha, V. S.; Arun, K. T.; Hariharan, M.; Ramaiah, D. *J. Phys. Chem. B* **2010**, *114*, 5912.

(24) Grande, V.; Doria, F.; Freccero, M.; Würthner, F. *Angew. Chem. Int. Ed.* **2017**, *56*, 7520.

(25) Law, K. Y. *Chem. Rev.* **1993**, *93*, 449.

(26) Emmelius, M.; Pawlowski, G.; Vollmann, H. W. *Angew. Chem. Int. Ed.* **1989**, *28*, 1445.
(27) Ros-Lis, J. V.; Martínez-Máñez, R.; Sancenón, F.; Soto, J.; Spieles, M.; Rurack, K. *Chem. Eur. J.* **2008**, *14*, 10101.
(28) Ros-Lis, J. V.; Martinez-Manez, R.; Soto, J. *Chem. Commun.* **2002**, 2248.
(29) Ajayaghosh, A.; Chithra, P.; Varghese, R. *Angew. Chem.* **2007**, *119*, 234.
(30) Ajayaghosh, A.; Chithra, P.; Varghese, R.; Divya, K. P. *Chem. Commun.* **2008**, 969.
(31) Arunkumar, E.; Chithra, P.; Ajayaghosh, A. *J. Am. Chem. Soc.* **2004**, *126*, 6590.
(32) Radaram, B.; Mako, T.; Levine, M. *Dalton Trans.* **2013**, *42*, 16276.
(33) Ananda Rao, B.; Kim, H.; Son, Y.-A. *Sens. Actuators B Chem.* **2013**, *188*, 847.
(34) Stender, B.; Völker, S. F.; Lambert, C.; Pflaum, J. *Adv. Mater.* **2013**, *25*, 2943.
(35) Harkin, D. J.; Broch, K.; Schreck, M.; Ceymann, H.; Stoy, A.; Yong, C.-K.; Nikolka, M.; McCulloch, I.; Stingelin, N.; Lambert, C.; Sirringhaus, H. *Adv. Mater.* **2016**, *28*, 6378.
(36) Odom, S. A.; Webster, S.; Padilha, L. A.; Peceli, D.; Hu, H.; Nootz, G.; Chung, S.-J.; Ohira, S.; Matichak, J. D.; Przhonska, O. V.; Kachkovski, A. D.; Barlow, S.; Brédas, J.-L.; Anderson, H. L.; Hagan, D. J.; Van Stryland, E. W.; Marder, S. R. *J. Am. Chem. Soc.* **2009**, *131*, 7510.
(37) Ohira, S.; Rudra, I.; Schmidt, K.; Barlow, S.; Chung, S.-J.; Zhang, Q.; Matichak, J.; Marder, S. R.; Brédas, J.-L. *Chem. Eur. J.* **2008**, *14*, 11082.
(38) Toro, C.; Boni, L. D.; Yao, S.; Ritchie, J. P.; Masunov, A. E.; Belfield, K. D.; Hernandez, F. E. *J. Chem. Phys.* **2009**, *130*, 214504.
(39) Webster, S.; Fu, J.; Padilha, L. A.; Przhonska, O. V.; Hagan, D. J.; Van Stryland, E. W.; Bondar, M. V.; Slominsky, Y. L.; Kachkovski, A. D. *Chem. Phys.* **2008**, *348*, 143.
(40) Webster, S.; Odom, S. A.; Padilha, L. A.; Przhonska, O. V.; Peceli, D.; Hu, H.; Nootz, G.; Kachkovski, A. D.; Matichak, J.; Barlow, S.; Anderson, H. L.; Marder, S. R.; Hagan, D. J.; Van Stryland, E. W. *J. Phys. Chem. B* **2009**, *113*, 14854.
(41) Webster, S.; Peceli, D.; Hu, H.; Padilha, L. A.; Przhonska, O. V.; Masunov, A. E.; Gerasov, A. O.; Kachkovski, A. D.; Slominsky, Y. L.; Tolmachev, A. I.; Kurdyukov, V. V.; Viniychuk, O. O.; Barrasso, E.; Lepkowicz, R.; Hagan, D. J.; Van Stryland, E. W. *J. Phys. Chem. Lett.* **2010**, *1*, 2354.
(42) Belfield, K. D.; Bondar, M. V.; Haniff, H. S.; Mikhailov, I. A.; Luchita, G.; Przhonska, O. V. *ChemPhysChem* **2013**, *14*, 3532.
(43) Scherer, D.; Dorfler, R.; Feldner, A.; Vogtmann, T.; Schwoerer, M.; Lawrentz, U.; Grahn, W.; Lambert, C. *Chem. Phys.* **2002**, *279*, 179.
(44) Völker, S. F.; Uemura, S.; Limpinsel, M.; Mingebach, M.; Deibel, C.; Dyakonov, V.; Lambert, C. In *Macromol. Chem. Phys.* 2010; Vol. 211, p 1098.
(45) Silvestri, F.; Irwin, M. D.; Beverina, L.; Facchetti, A.; Pagani, G. A.; Marks, T. J. *J. Am. Chem. Soc.* **2008**, *130*, 17640.
(46) Merritt, V. Y.; Hovel, H. J. *Appl. Phys. Lett.* **1976**, *29*, 414.
(47) Morel, D. L.; Ghosh, A. K.; Feng, T.; Stogryn, E. L.; Purwin, P. E.; Shaw, R. F.; Fishman, C. *Appl. Phys. Lett.* **1978**, *32*, 495.

(48) Wang, S.; Mayo, E. I.; Perez, M. D.; Griffe, L.; Wei, G.; Djurovich, P. I.; Forrest, S. R.; Thompson, M. E. *Appl. Phys. Lett.* **2009**, *94*, 233304.
(49) Mayerhöffer, U.; Deing, K.; Gruß, K.; Braunschweig, H.; Meerholz, K.; Würthner, F. *Angew. Chem., Int. Ed.* **2009**, *48*, 8776.
(50) Fan, B.; Maniglio, Y.; Simeunovic, M.; Kuster, S.; Geiger, T.; Hany, R.; Nüesch, F. *Int. J. Photoenergy* **2009**, *2009*, 7.
(51) Wei, G.; Lunt, R. R.; Sun, K.; Wang, S.; Thompson, M. E.; Forrest, S. R. *Nano Lett.* **2010**, *10*, 3555.
(52) Wei, G.; Wang, S.; Renshaw, K.; Thompson, M. E.; Forrest, S. R. *ACS Nano* **2010**, *4*, 1927.
(53) Wei, G.; Wang, S.; Sun, K.; Thompson, M. E.; Forrest, S. R. *Adv. Energy Mater.* **2011**, *1*, 184.
(54) Beverina, L.; Drees, M.; Facchetti, A.; Salamone, M.; Ruffo, R.; Pagani, G. A. *Eur. J. Org. Chem.* **2011**, *2011*, 5555.
(55) Wang, S.; Hall, L.; Diev, V. V.; Haiges, R.; Wei, G.; Xiao, X.; Djurovich, P. I.; Forrest, S. R.; Thompson, M. E. *Chem. Mater.* **2011**, *23*, 4789.
(56) Wei, G.; Xiao, X.; Wang, S.; Sun, K.; Bergemann, K. J.; Thompson, M. E.; Forrest, S. R. *ACS Nano* **2012**, *6*, 972.
(57) Chen, C.-H.; Cheng, W.-T.; Tsai, M.-L.; Huang, K.-T. *Ind. Eng. Chem. Res.* **2012**, *51*, 3630.
(58) Deing, K. C.; Mayerhöffer, U.; Würthner, F.; Meerholz, K. *Phys. Chem. Chem. Phys.* **2012**, *14*, 8328.
(59) Kylberg, W.; Zhang, Y.; Aebersold, A.; Castro, F. A. d.; Geiger, T.; Heier, J.; Kuster, S.; Ma, C.-Q.; Bäuerle, P.; Nüesch, F.; Tisserant, J.-N.; Hany, R. *Org. Electron.* **2012**, *13*, 1204.
(60) Maeda, T.; Tsukamoto, T.; Seto, A.; Yagi, S.; Nakazumi, H. *Macromol. Chem. Phys.* **2012**, *213*, 2590.
(61) Maeda, T.; Nitta, S.; Sano, Y.; Tanaka, S.; Yagi, S.; Nakazumi, H. *Dyes Pigm.* **2015**, *122*, 160.
(62) Maeda, T.; Hamamura, Y.; Miyanaga, K.; Shima, N.; Yagi, S.; Nakazumi, H. *Org. Lett.* **2011**, *13*, 5994.
(63) Maeda, T.; Nakao, H.; Kito, H.; Ichinose, H.; Yagi, S.; Nakazumi, H. *Dyes Pigm.* **2011**, *90*, 275.
(64) Maeda, T.; Shima, N.; Tsukamoto, T.; Yagi, S.; Nakazumi, H. *Synth. Met.* **2011**, *161*, 2481.
(65) Maeda, T.; Arikawa, S.; Nakao, H.; Yagi, S.; Nakazumi, H. *New J. Chem.* **2013**, *37*, 701.
(66) Bagnis, D.; Beverina, L.; Huang, H.; Silvestri, F.; Yao, Y.; Yan, H.; Pagani, G. A.; Marks, T. J.; Facchetti, A. *J. Am. Chem. Soc.* **2010**, *132*, 4074.
(67) Völker, S. F.; Renz, M.; Kaupp, M.; Lambert, C. *Chem. Eur. J.* **2011**, *17*, 14147.
(68) Völker, S. F.; Dellermann, T.; Ceymann, H.; Holzapfel, M.; Lambert, C. *J. Polym. Sci., Part A: Polym. Chem.* **2014**, *52*, 890.
(69) Ceymann, H.; Balkenhohl, M.; Schmiedel, A.; Holzapfel, M.; Lambert, C. *Phys. Chem. Chem. Phys.* **2016**.
(70) Völker, S. F.; Schmiedel, A.; Holzapfel, M.; Böhm, C.; Lambert, C. *Phys. Chem. Chem. Phys.* **2013**, *15*, 19831.

(71) Völker, S. F.; Lambert, C. *Chem. Mater.* **2012**, *24*, 2541.
(72) Völker, S. F.; Schmiedel, A.; Holzapfel, M.; Renziehausen, K.; Engel, V.; Lambert, C. *J. Phys. Chem. C* **2014**, *118*, 17467.
(73) Lambert, C.; Koch, F.; Völker, S. F.; Schmiedel, A.; Holzapfel, M.; Humeniuk, A.; Röhr, M. I. S.; Mitric, R.; Brixner, T. *J. Am. Chem. Soc.* **2015**, *137*, 7851.
(74) Kasha, M. *Radiat. Res.* **1963**, *20*, 55.
(75) Kasha, M.; Rawls, H.; Ashraf El-Bayoumi, M. *The exciton model in molecular spectroscopy, Pure Appl. Chem.11, 371-392*, 1965; Vol. 11.
(76) Beaujuge, P. M.; Amb, C. M.; Reynolds, J. R. *Acc. Chem. Res.* **2010**, *43*, 1396.
(77) Dou, L.; Liu, Y.; Hong, Z.; Li, G.; Yang, Y. *Chem. Rev.* **2015**, *115*, 12633.
(78) Ajayaghosh, A.; Eldo, J. *Org. Lett.* **2001**, *3*, 2595.
(79) Eldo, J.; Ajayaghosh, A. *Chem. Mater.* **2002**, *14*, 410.
(80) Ajayaghosh, A. *Chem. Soc. Rev.* **2003**, *32*, 181.
(81) Kuster, S.; Geiger, T. *Dyes Pigm.* **2012**, *95*, 657.
(82) Balbo Block, M. A.; Khan, A.; Hecht, S. *J. Org. Chem.* **2003**, *69*, 184.
(83) Balbo Block, M. A.; Hecht, S. *Macromolecules* **2004**, *37*, 4761.
(84) Zhang, W.; Tao, F.; Meng, K.-g.; Wang, Z.; Xi, L.-y.; Li, Y.; Jiang, Q. *J. Mater. Sci.* **2011**, *46*, 5363.
(85) Zhang, W.; Tao, F.; Meng, K.; Xi, L.; Wang, Z.; Li, Y.; Jiang, Q. *Polym. Bull.* **2012**, *68*, 349.
(86) Müllen, K.; Wegner, G. *Electronic Materials: The Oligomer Approach* **1998**, Wiley VCH: Weinheim (Germany).
(87) McRae, E. G.; Kasha, M. In *Physical Processes in Radiation Biology*; Augenstein, L., Mason, R., Rosenberg, B., Eds.; Academic Press: 1964, p 23.
(88) Röhr, M. I. S.; Marciniak, H.; Hoche, J.; Schreck, M. H.; Ceymann, H.; Mitric, R.; Lambert, C. *J. Phys. Chem. C* **2018**, *122*, 8082.
(89) Lambert, C.; Scherpf, T.; Ceymann, H.; Schmiedel, A.; Holzapfel, M. *J. Am. Chem. Soc.* **2015**, *137*, 3547.
(90) Ottiger, P.; Leutwyler, S. *J. Chem. Phys.* **2012**, *137*, 204303.
(91) Ottiger, P.; Köppel, H.; Leutwyler, S. *Chem. Sci.* **2015**, *6*, 6059.
(92) Würthner, F.; Kaiser, T. E.; Saha-Möller, C. R. *Angew. Chem. Int. Ed.* **2011**, *50*, 3376.
(93) Ceymann, H.; Rosspeintner, A.; Schreck, M. H.; Mützel, C.; Stoy, A.; Vauthey, E.; Lambert, C. *Phys. Chem. Chem. Phys.* **2016**, *18*, 16404.
(94) Baldereschi, A. *Phys. Rev. B* **1973**, *7*, 5212.
(95) Buncel, E.; McKerrow, A. J.; Kazmaier, P. M. *J. Chem. Soc., Chem. Commun.* **1992**, 1242.
(96) Wojtyk, J.; McKerrow, A.; Kazmaier, P.; Buncel, E. *Can. J. Chem.* **1999**, *77*, 903.
(97) Chen, H.; Herkstroeter, W. G.; Perlstein, J.; Law, K.-Y.; Whitten, D. G. *J. Phys. Chem.* **1994**, *98*, 5138.
(98) Liang, K.; Law, K.-Y.; Whitten, D. G. *J. Phys. Chem.* **1994**, *98*, 13379.
(99) Chen, H.; Law, K.-Y.; Perlstein, J.; Whitten, D. G. *J. Am. Chem. Soc.* **1995**, *117*, 7257.
(100) Chen, H.; Farahat, M. S.; Law, K.-Y.; Whitten, D. G. *J. Am. Chem. Soc.* **1996**, *118*, 2584.

(101) Das, S.; Kamat, P. V.; De la Barre, B.; Thomas, K. G.; Ajayaghosh, A.; George, M. V. *J. Phys. Chem.* **1992**, *96*, 10327.
(102) Das, S.; Thanulingam, T. L.; Thomas, K. G.; Kamat, P. V.; George, M. V. *J. Phys. Chem.* **1993**, *97*, 13620.
(103) Das, S.; Thomas, K. G.; Thomas, K. J.; Madhavan, V.; Liu, D.; Kamat, P. V.; George, M. V. *J. Phys. Chem.* **1996**, *100*, 17310.
(104) Alex, S.; Basheer, M. C.; Arun, K. T.; Ramaiah, D.; Das, S. *J. Phys. Chem. A* **2007**, *111*, 3226.
(105) Arun, K. T.; Epe, B.; Ramaiah, D. *J. Phys. Chem. B* **2002**, *106*, 11622.
(106) Dimitriev, O. P.; Dimitriyeva, A. P.; Tolmachev, A. I.; Kurdyukov, V. V. *J. Phys. Chem. B* **2005**, *109*, 4561.
(107) Stoll, R. S.; Severin, N.; Rabe, J. P.; Hecht, S. *Adv. Mater.* **2006**, *18*, 1271.
(108) Jyothish, K.; Hariharan, M.; Ramaiah, D. *Chem. Eur. J.* **2007**, *13*, 5944.
(109) Mayerhoffer, U.; Würthner, F. *Chem. Sci.* **2012**, *3*, 1215.
(110) Yefimova, S.; Lebed, A.; Sorokin, A.; Guralchuk, G.; Borovoy, I.; Malyukin, Y. *J. Mol. Liq.* **2012**, *165*, 113.
(111) Karpenko, I. A.; Collot, M.; Richert, L.; Valencia, C.; Villa, P.; Mély, Y.; Hibert, M.; Bonnet, D.; Klymchenko, A. S. *J. Am. Chem. Soc.* **2015**, *137*, 405.
(112) Xu, Y.; Li, Z.; Malkovskiy, A.; Sun, S.; Pang, Y. *J. Phys. Chem. B* **2010**, *114*, 8574.
(113) Xu, Y.; Panzner, M. J.; Li, X.; Youngs, W. J.; Pang, Y. *Chem. Commun.* **2010**, *46*, 4073.
(114) Xu, Y.; Li, B.; Xiao, L.; Li, W.; Zhang, C.; Sun, S.; Pang, Y. *Chem. Commun.* **2013**, *49*, 7732.
(115) Grande, V.; Shen, C.-A.; Deiana, M.; Dudek, M.; Olesiak-Banska, J.; Matczyszyn, K.; Würthner, F. *Chem. Sci.* **2018**.
(116) Ashwell, G. J.; Jefferies, G.; Hamilton, D. G.; Lynch, D. E.; Roberts, M. P. S.; Bahra, G. S.; Brown, C. R. *Nature* **1995**, *375*, 385.
(117) Law, K. Y.; Chen, C. C. *J. Phys. Chem.* **1989**, *93*, 2533.
(118) Ashwell, G. J.; Bahra, G. S.; Brown, C. R.; Hamilton, D. G.; Kennard, C. H. L.; Lynch, D. E. *J. Mater. Chem.* **1996**, *6*, 23.
(119) Law, K. Y. *J. Phys. Chem.* **1988**, *92*, 4226.
(120) Bernstein, J.; Goldstein, E. *Mol. Cryst. Liq. Cryst.* **1988**, *164*, 213.
(121) Tristani-Kendra, M.; Eckhardt, C. J. *J. Chem. Phys.* **1984**, *81*, 1160.
(122) Gsänger, M.; Kirchner, E.; Stolte, M.; Burschka, C.; Stepanenko, V.; Pflaum, J.; Würthner, F. *J. Am. Chem. Soc.* **2014**, *136*, 2351.
(123) Würthner, F.; Yao, S.; Debaerdemaeker, T.; Wortmann, R. *J. Am. Chem. Soc.* **2002**, *124*, 9431.
(124) Gershberg, J.; Fennel, F.; Rehm, T. H.; Lochbrunner, S.; Würthner, F. *Chem. Sci.* **2016**, *7*, 1729.
(125) Martin, R. B. *Chem. Rev.* **1996**, *96*, 3043.
(126) Chen, Z.; Lohr, A.; Saha-Moller, C. R.; Würthner, F. *Chem. Soc. Rev.* **2009**, *38*, 564.
(127) Baxter, N. J.; Williamson, M. P.; Lilley, T. H.; Haslam, E. *J. Chem. Soc., Faraday Trans.* **1996**, *92*, 231.
(128) Heyn, M. P.; Nicola, C. U.; Schwarz, G. *J. Phys. Chem.* **1977**, *81*, 1611.
(129) Kaiser, T. E.; Stepanenko, V.; Würthner, F. *J. Am. Chem. Soc.* **2009**, *131*, 6719.

(130) Zhao, D.; Moore, J. S. *Org. Biomol. Chem.* **2003**, *1*, 3471.
(131) Smulders, M. M. J.; Nieuwenhuizen, M. M. L.; de Greef, T. F. A.; van der Schoot, P.; Schenning, A. P. H. J.; Meijer, E. W. *Chem. Eur. J.* **2010**, *16*, 362.
(132) De Greef, T. F. A.; Smulders, M. M. J.; Wolffs, M.; Schenning, A. P. H. J.; Sijbesma, R. P.; Meijer, E. W. *Chem. Rev.* **2009**, *109*, 5687.
(133) Prince, R. B.; Brunsveld, L.; Meijer, E. W.; Moore, J. S. *Angew. Chem. Int. Ed.* **2000**, *39*, 228.
(134) Gillard, R. D. *Analyst* **1963**, *88*, 825.
(135) Mayerhöffer, U.; Fimmel, B.; Würthner, F. *Angew. Chem., Int. Ed.* **2012**, *51*, 164.
(136) Tatarets, A. L.; Fedyunyaeva, I. A.; Terpetschnig, E.; Patsenker, L. D. *Dyes Pigm.* **2005**, *64*, 125.
(137) Bennett, C. J.; Caldwell, S. T.; McPhail, D. B.; Morrice, P. C.; Duthie, G. G.; Hartley, R. C. *Biorg. Med. Chem.* **2004**, *12*, 2079.
(138) Pardal, A. C.; Ramos, S. S.; Santos, P. F.; Reis, L. V.; Almeida, P. *Molecules* **2002**, *7*, 320.
(139) Lewis, J. E.; Maroncelli, M. *Chem. Phys. Lett.* **1998**, *282*, 197.
(140) Ahn, T.-S.; Al-Kaysi, R. O.; Müller, A. M.; Wentz, K. M.; Bardeen, C. J. *Rev. Sci. Instrum.* **2007**, *78*, 086105.
(141) Schreck, M. H. *Master Thesis* **2014**, Universität Würzburg.
(142) Kozic, J.; Novotná, E.; Volková, M.; Stolaříková, J.; Trejtnar, F.; Wsól, V.; Vinšová, J. *Eur. J. Med. Chem.* **2012**, *56*, 108.
(143) Nagarathnam, D. *PCT Int. Appl.* **2012**, *WO 2012151525 A1*, 128.
(144) Lawrentz, U. *Diploma Thesis* **1996**, Universität Braunschweig.
(145) Avirah, R.; Jayaram, D.; Nagappanpillai, A.; Ramaiah, D. *Org. Biomol. Chem* **2011**, *10*, 911.
(146) Rapozzi, V.; Beverina, L.; Salice, P.; Pagani, G. A.; Camerin, M.; Xodo, L. E. *J. Med. Chem.* **2010**, *53*, 2188.
(147) Heilig, G.; Lüttke, W. *Chem. Ber.* **1988**, *121*, 407.
(148) Reddington, M. V. *Bioconjugate Chem.* **2007**, *18*, 2178.
(149) Walkey, M. C.; Byrne, L. T.; Piggott, M. J.; Low, P. J.; Koutsantonis, G. A. *Dalton Trans.* **2015**, *44*, 8812.
(150) Zieschang, F.; Schreck, M. H.; Schmiedel, A.; Holzapfel, M.; Klein, J. H.; Walter, C.; Engels, B.; Lambert, C. *J. Phys. Chem. C* **2014**, *118*, 27698.
(151) Parson, W. W. *Modern Optical Spectroscopy* **2009**, *Springer*, 293.
(152) Stoy, A. *Bachelor Thesis* **2014**, Universität Würzburg.
(153) Zhang, W.; Smith, J.; Watkins, S. E.; Gysel, R.; McGehee, M.; Salleo, A.; Kirkpatrick, J.; Ashraf, S.; Anthopoulos, T.; Heeney, M.; McCulloch, I. *J. Am. Chem. Soc.* **2010**, *132*, 11437.
(154) Zhang, X.; Bronstein, H.; Kronemeijer, A. J.; Smith, J.; Kim, Y.; Kline, R. J.; Richter, L. J.; Anthopoulos, T. D.; Sirringhaus, H.; Song, K.; Heeney, M.; Zhang, W.; McCulloch, I.; DeLongchamp, D. M. *Nat. Commun.* **2013**, *4*, 2238.
(155) Ashraf, R. S.; Schroeder, B. C.; Bronstein, H. A.; Huang, Z.; Thomas, S.; Kline, R. J.; Brabec, C. J.; Rannou, P.; Anthopoulos, T. D.; Durrant, J. R.; McCulloch, I. *Adv. Mater.* **2013**, *25*, 2029.
(156) Förster, T. *Ann. Phys.* **1948**, *437*, 55.

(157) Lakowicz, J. R. *Principles to Fluorescence Spectroscopy*; 3rd ed.; Springer: Berlin, 2006.
(158) Harkin, D. J.; Broch, K.; Schreck, M.; Ceymann, H.; Stoy, A.; Yong, C.-K.; Nikolka, M.; McCulloch, I.; Stingelin, N.; Lambert, C.; Sirringhaus, H. *Adv. Mater.* **2016**, n/a.
(159) Venkateshvaran, D.; Nikolka, M.; Sadhanala, A.; Lemaur, V.; Zelazny, M.; Kepa, M.; Hurhangee, M.; Kronemeijer, A. J.; Pecunia, V.; Nasrallah, I.; Romanov, I.; Broch, K.; McCulloch, I.; Emin, D.; Olivier, Y.; Cornil, J.; Beljonne, D.; Sirringhaus, H. *Nature* **2014**, *515*, 384.
(160) Klumpp, D. A.; Yeung, K. Y.; Prakash, G. K. S.; Olah, G. A. *J. Org. Chem.* **1998**, *63*, 4481.
(161) Marder, S. R.; Cheng, L.-T.; Tiemann, B. G.; Friedli, A. C.; Blanchard-Desce, M.; Perry, J. W.; Skindhøj, J. *Science* **1994**, *263*, 511.
(162) Lindholm, E.; Åsbrink, L. *Molecular orbitals and their energies, studied by the semiempirical HAM method*; Springer-Verlag, 1985.
(163) Knapp, E. W. *Chem. Phys.* **1984**, *85*, 73.
(164) Mikhailenko, F. A.; Boguslavskaya, A. N. *Chemistry of Heterocyclic Compounds* **1971**, *7*, 574.
(165) Klochko, O. P.; Fedyunyayeva, I. A.; Khabuseva, S. U.; Semenova, O. M.; Terpetschnig, E. A.; Patsenker, L. D. *Dyes Pigm.* **2010**, *85*, 7.
(166) Fedyunyayeva, I. A.; Klochko, O. P.; Semenova, O. M.; Khabuseva, S. U.; Povrozin, Y. A.; Sokolyk, O. O.; Stepanenko, O. Y.; Terpetschnig, E. A.; Patsenker, L. D. *Dyes Pigm.* **2011**, *90*, 201.
(167) Patsenker, L.; Terpetschnig, E.; Fedyunyaeva, I.; Kolosova, O.; Klochko, A. 2007; Vol. US2007/0281363A1.
(168) Garry, M. *Comptes Rend.* **1940**, *211*, 399.
(169) Rajca, A.; Olankitwanit, A.; Rajca, S. *J. Am. Chem. Soc.* **2011**, *133*, 4750.
(170) Laporte, O.; Meggers, W. F. *J. Opt. Soc. Am.* **1925**, *11*, 459.
(171) Aleksandr, A. I. *Russ. Chem. Rev.* **1991**, *60*, 865.
(172) Strickler, S. J.; Berg, R. A. *J. Chem. Phys.* **1962**, *37*, 814.
(173) Mayerhöffer, U. *Disseration Thesis* **2011**, Universtität Würzburg.
(174) Böhm, Volker P. W.; Herrmann, Wolfgang A. *Eur. J. Org. Chem.* **2000**, *2000*, 3679.
(175) Ceymann, H. *Dissertation Thesis* **2016**, Universität Würzburg.
(176) Auerhammer, N.; Schmiedel, A.; Holzapfel, M.; Lambert, C. *J. Phys. Chem. C* **2018**, *122*, 11720.
(177) Harriman, A.; Mallon, L.; Ziessel, R. *Chem. Eur. J.* **2008**, *14*, 11461.
(178) Harriman, A. *Chem. Commun.* **2015**, *51*, 11745.
(179) Ryu, N.; Okazaki, Y.; Pouget, E.; Takafuji, M.; Nagaoka, S.; Ihara, H.; Oda, R. *Chem. Commun.* **2017**, *53*, 8870.
(180) Würthner, F.; Yao, S.; Beginn, U. *Angew. Chem. Int. Ed.* **2003**, *42*, 3247.
(181) Fernández, G.; Stolte, M.; Stepanenko, V.; Würthner, F. *Chem. Eur. J.* **2013**, *19*, 206.
(182) Lohr, A.; Uemura, S.; Würthner, F. *Angew. Chem. Int. Ed.* **2009**, *48*, 6165.
(183) Liess, A.; Lv, A.; Arjona-Esteban, A.; Bialas, D.; Krause, A.-M.; Stepanenko, V.; Stolte, M.; Würthner, F. *Nano Lett.* **2017**, *17*, 1719.
(184) Gaus, M.; Goez, A.; Elstner, M. *J. Chem. Theory Comput.* **2013**, *9*, 338.

(185) Gaus, M.; Lu, X.; Elstner, M.; Cui, Q. *J. Chem. Theory Comput.* **2014**, *10*, 1518.
(186) Lu, X.; Gaus, M.; Elstner, M.; Cui, Q. *J. Phys. Chem. B* **2015**, *119*, 1062.
(187) Kubillus, M.; Kubař, T.; Gaus, M.; Řezáč, J.; Elstner, M. *J. Chem. Theory Comput.* **2015**, *11*, 332.
(188) ADF DFTB 2017, S., Theoretical Chemistry, Vrije Universiteit, Amsterdam, The Netherlands, http://www.scm.com.
(189) Grimme, S.; Ehrlich, S.; Goerigk, L. *J. Comput. Chem.* **2011**, *32*, 1456.
(190) Humeniuk, A.; Mitrić, R. *J. Chem. Phys.* **2015**, *143*, 134120.
(191) Humeniuk, A.; Mitrić, R. *Comput. Phys. Commun.* **2017**, *221*, 174.
(192) Shao, C.; Stolte, M.; Würthner, F. *Angew. Chem. Int. Ed.* **2013**, *52*, 7482.
(193) Söntjens, S. H. M.; Sijbesma, R. P.; van Genderen, M. H. P.; Meijer, E. W. *J. Am. Chem. Soc.* **2000**, *122*, 7487.
(194) Liu, T.; Bondar, M. V.; Belfield, K. D.; Anderson, D.; Masunov, A. E.; Hagan, D. J.; Stryland, E. W. V. *J. Phys. Chem. C* **2016**, *120*, 11099.
(195) Lambert, C.; Ehbets, J.; Rausch, D.; Steeger, M. *J. Org. Chem.* **2012**, *77*, 6147.
(196) Verbouwe, W.; Van der Auweraer, M.; De Schryver, F. C.; Piet, J. J.; Warman, J. M. *J. Am. Chem. Soc.* **1998**, *120*, 1319.
(197) Valeur, B.; Weber, G. *J. Chem. Phys.* **1978**, *69*, 2393.
(198) Noviandri, I.; Brown, K. N.; Fleming, D. S.; Gulyas, P. T.; Lay, P. A.; Masters, A. F.; Phillips, L. *J. Phys. Chem. B* **1999**, *103*, 6713.
(199) Connelly, N. G.; Geiger, W. E. *Chem. Rev.* **1996**, *96*, 877.
(200) Pavlishchuk, V. V.; Addison, A. W. *Inorg. Chim. Acta* **2000**, *298*, 97.
(201) Tsiplakides, D.; Archonta, D.; Vayenas, C. G. *Top. Catal.* **2007**, *44*, 469.
(202) Fulmer, G. R.; Miller, A. J. M.; Sherden, N. H.; Gottlieb, H. E.; Nudelman, A.; Stoltz, B. M.; Bercaw, J. E.; Goldberg, K. I. *Organometallics* **2010**, *29*, 2176.
(203) Matsui, M.; Mase, H.; Jin, J.-Y.; Funabiki, K.; Yoshida, T.; Minoura, H. *Dyes Pigm.* **2006**, *70*, 48.
(204) Patsenker, L.; Terpetschnig, E.; Fedyunyaeva, I.; Kolosova, O.; Klochko, A.; Google Patents: 2007.
(205) Terazono, Y.; Liddell, P. A.; Garg, V.; Kodis, G.; Brune, A.; Hambourger, M.; Moore, A. L.; Moore, T. A.; Gust, D. *J. Porphyr. Phthalocyanines* **2005**, *09*, 706.
(206) Zubatyuk, R. I.; Baumer, V. N.; Tatarets, A. L.; Patsenker, L. D.; Shishkin, O. V. *Acta Crystallographica Section E* **2004**, *60*, o2252.

7 Table of Formulas

Precursors

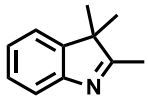

1

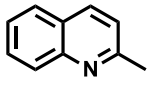

2

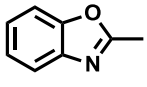

3

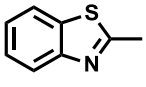

4

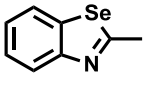

5

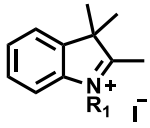

6

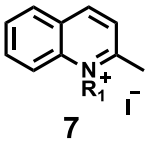

7

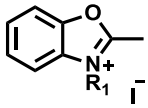

8

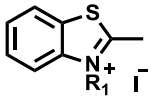

9

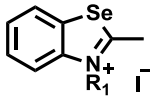

10

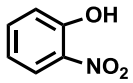

11

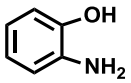

12

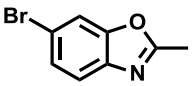

13

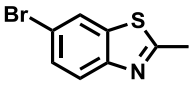

14

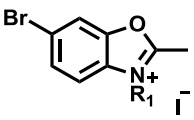

15

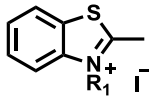

16

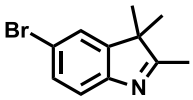

17

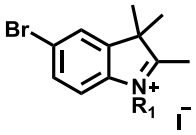

18

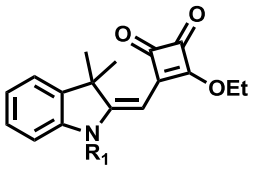

19

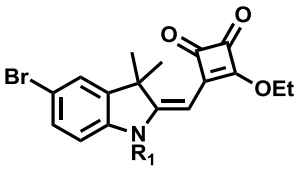

20

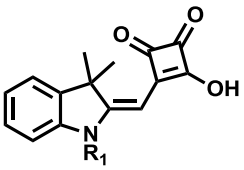

21

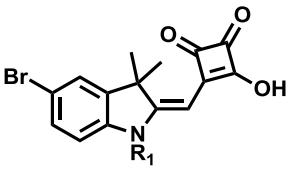

22

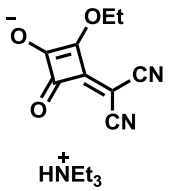

CN

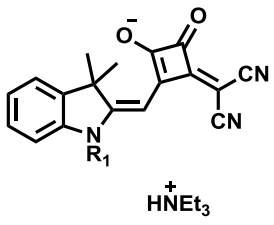

23

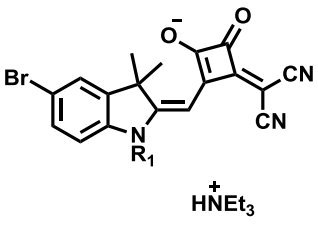

24

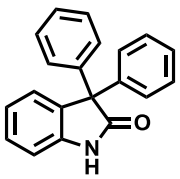

25

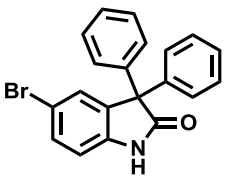

26

27

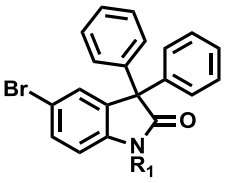

28

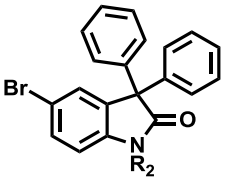

29

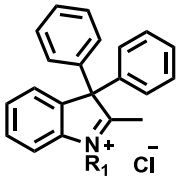

30

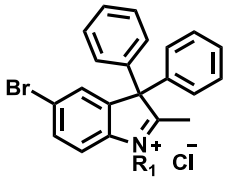

31

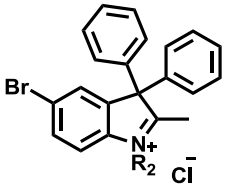

32

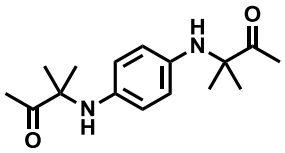

33

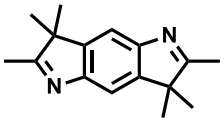

34

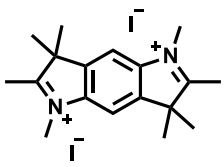

35

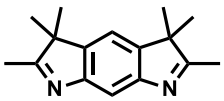

36

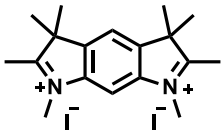

37

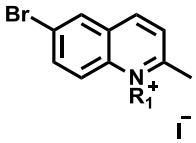

38

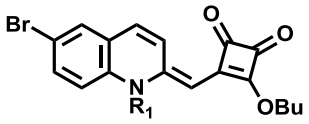

40

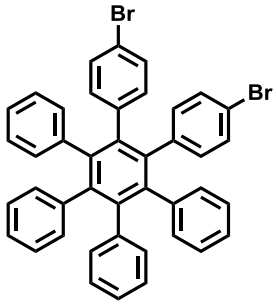

HAB-Br_2

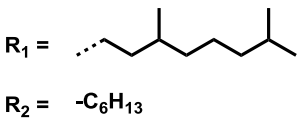

Squaraine Monomers

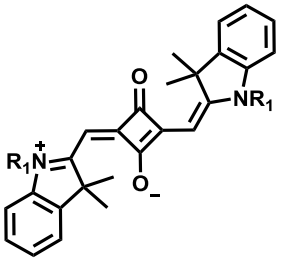

SQA

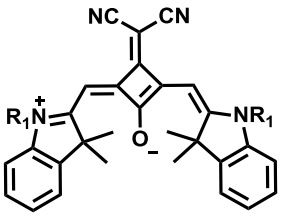

SQB

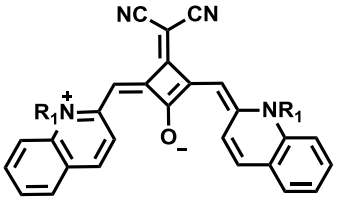

SQC

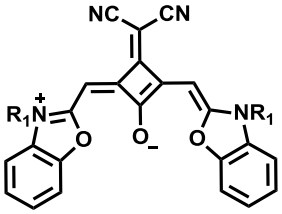

SQD

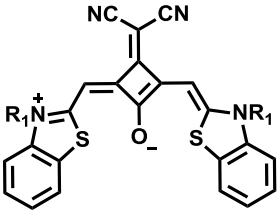

SQE

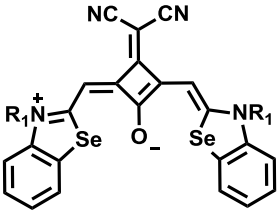

SQF

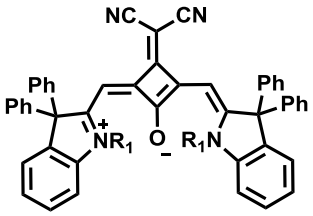

DiPhSQB

Functionalized Squaraine Dyes

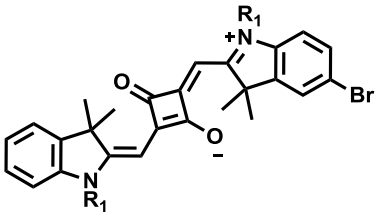

SQA-Br

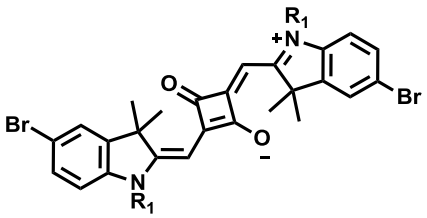

SQA-Br$_2$

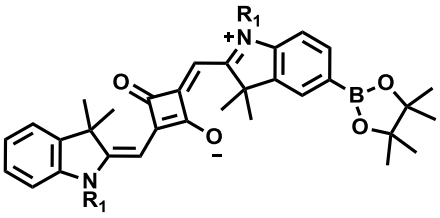

SQA-B

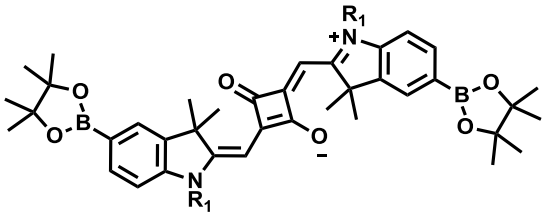

SQA-B$_2$

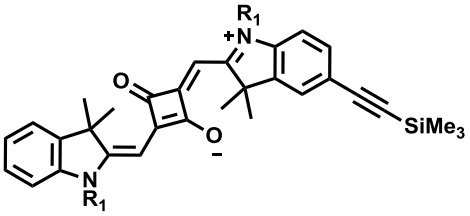

SQA-TMSA

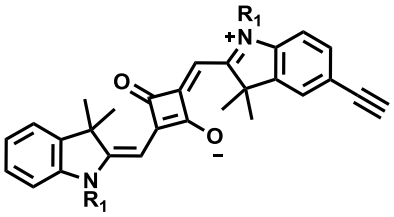

SQA-Alkyne

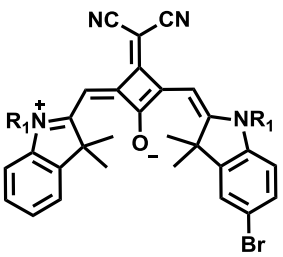

SQB-Br

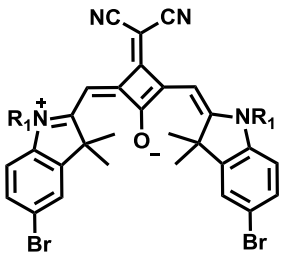

SQB-Br$_2$

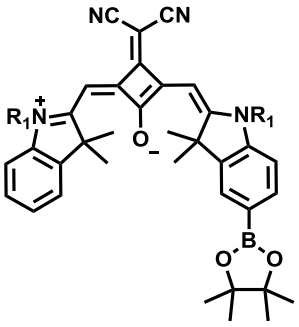

SQB-B

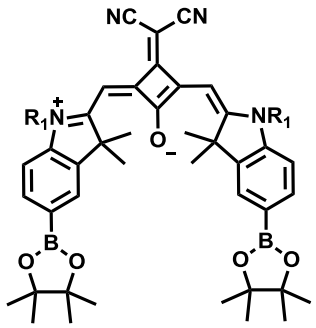

SQB-B_2

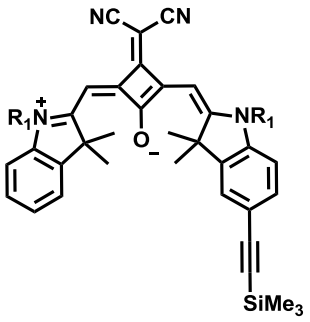

SQB-TMSA

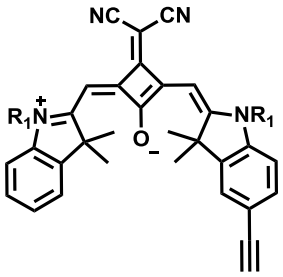

SQA-Alkyne

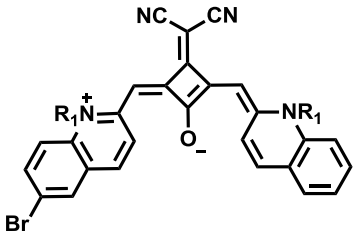

SQC-Br

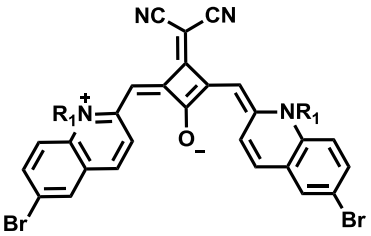

SQC-Br_2

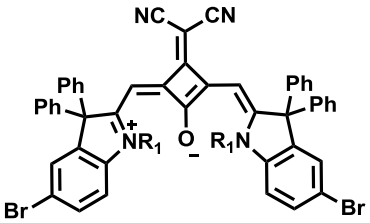

DiPhSQB-Br_2

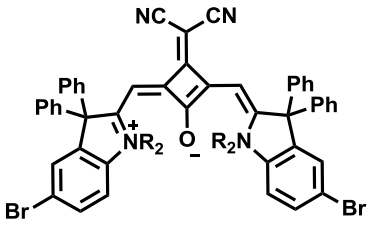

DiPhSQB-Br_2

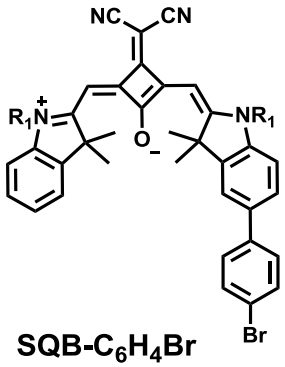

SQB-C_6H_4Br

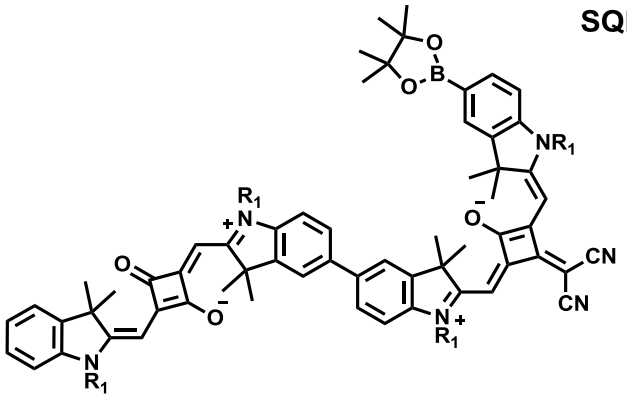

dSQAB-B

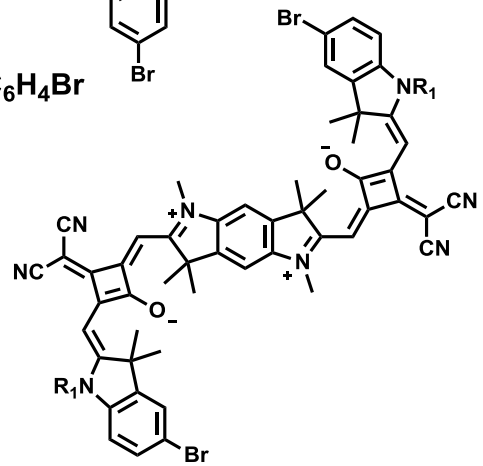

pySQB-1-Br_2

Squaraine Homodimers (SQA)

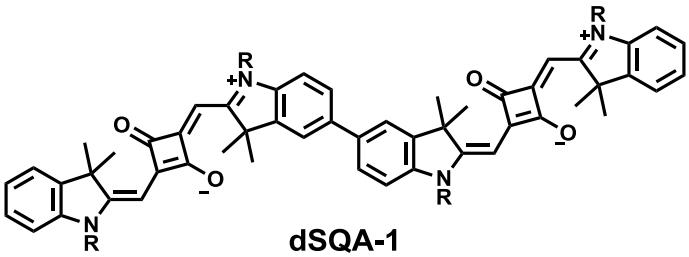

dSQA-1

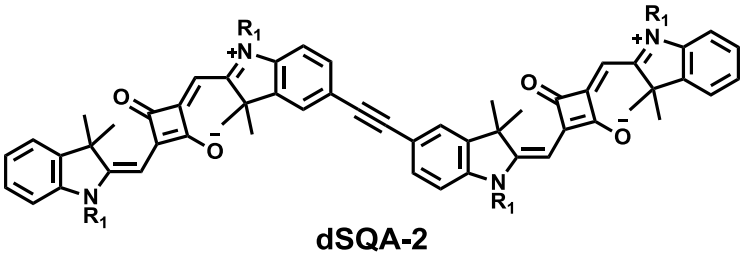

dSQA-2

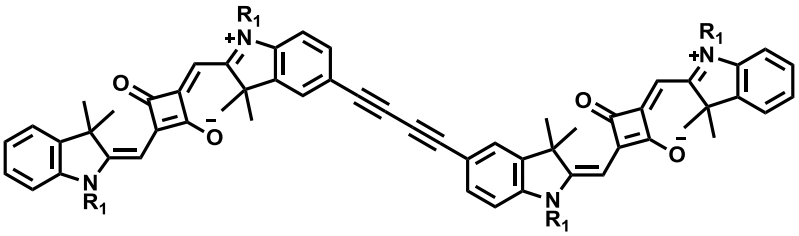

dSQA-3

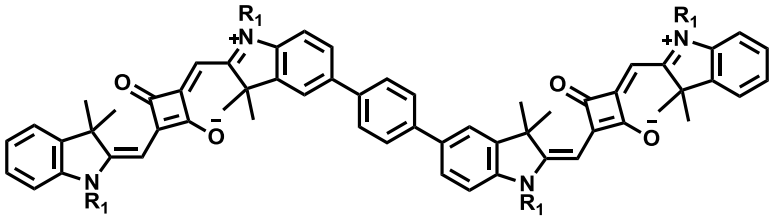

dSQA-4

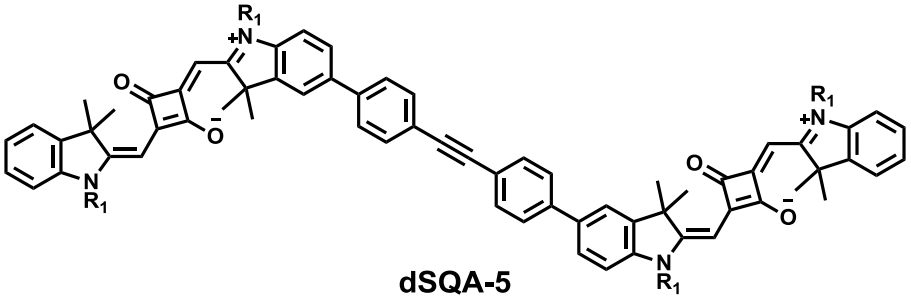

dSQA-5

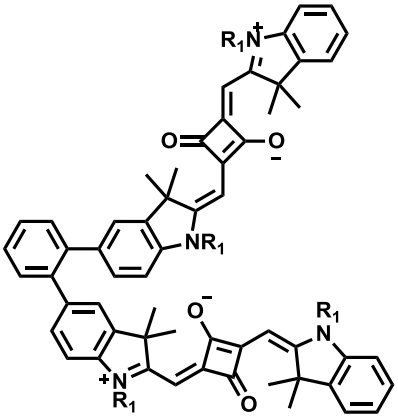

dSQA-6

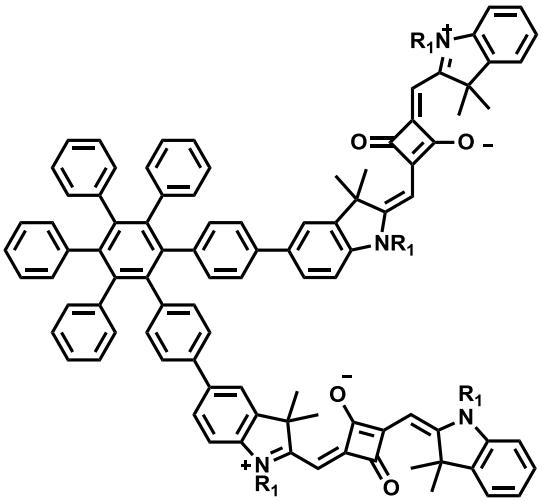

dSQA-7

Squaraine Homodimers (SQB)

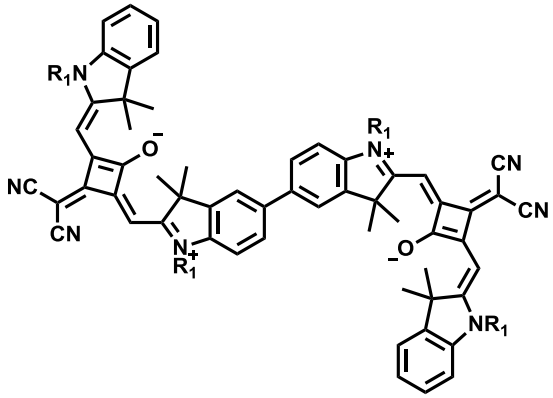

dSQB-1

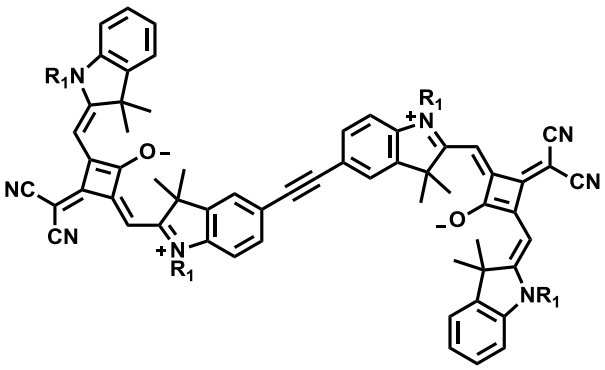

dSQB-2

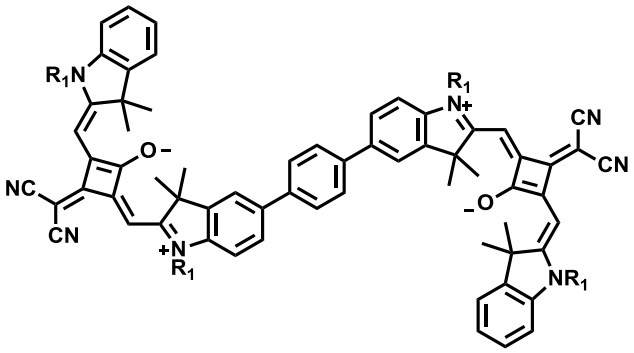

dSQB-3

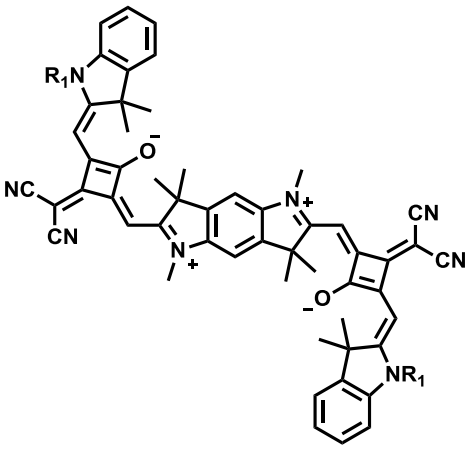

pySQB-1

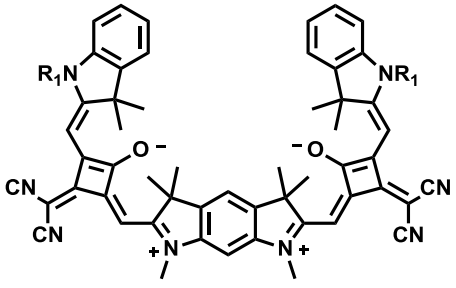

pySQB-2

Squaraine Heterodimers

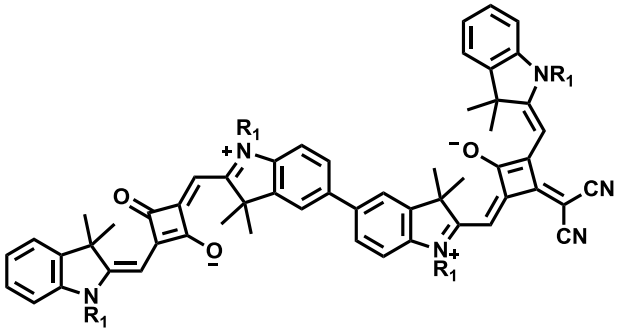

dSQAB-1

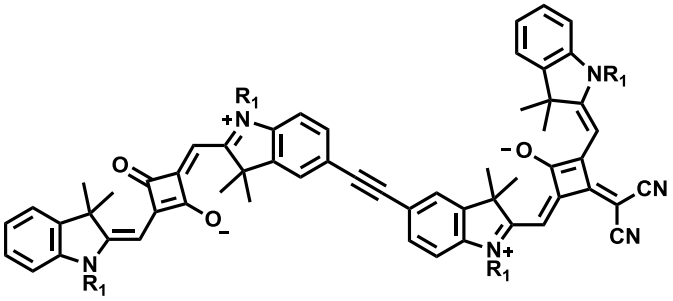

dSQAB-2

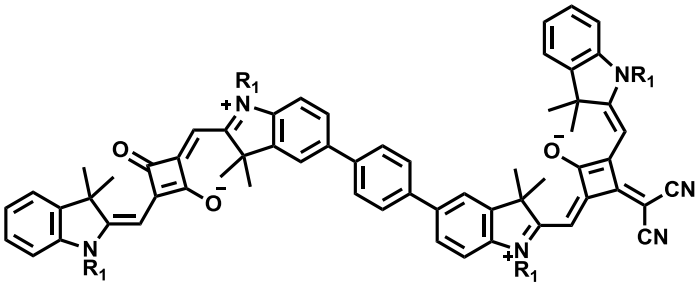

dSQAB-3

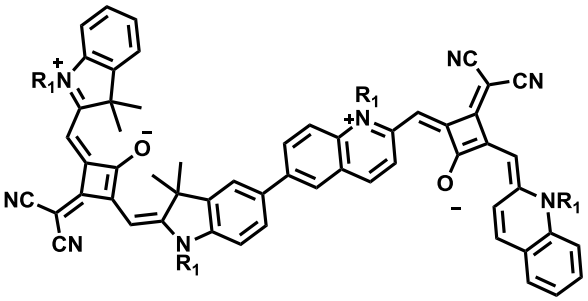

dSQBC

Squaraine Trimers

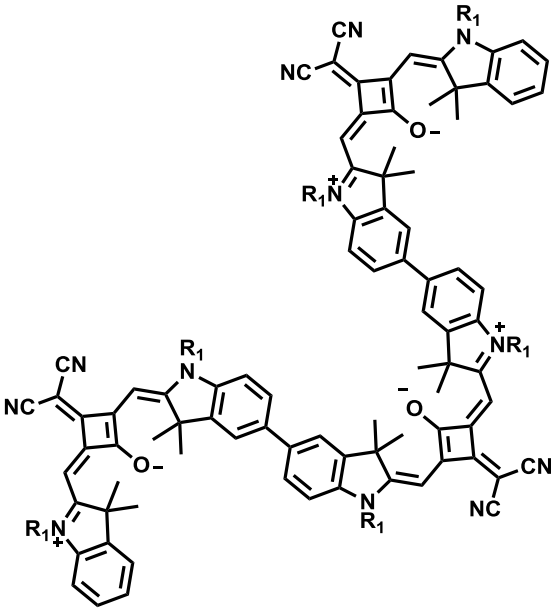

tSQB

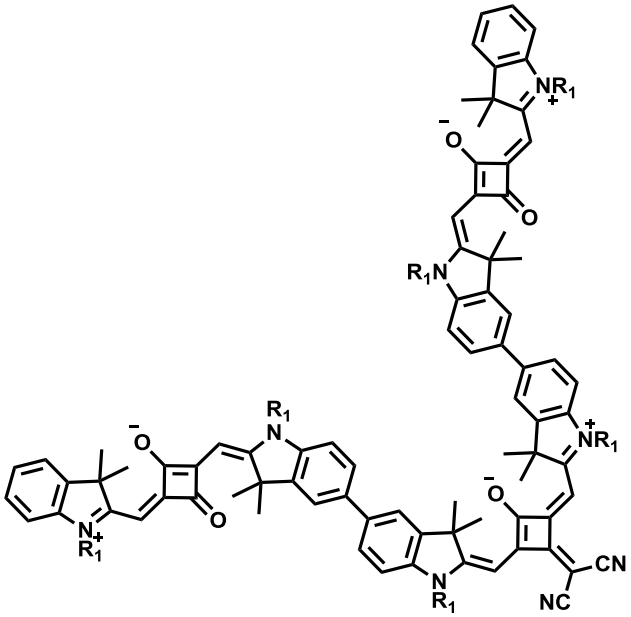

tSQABA

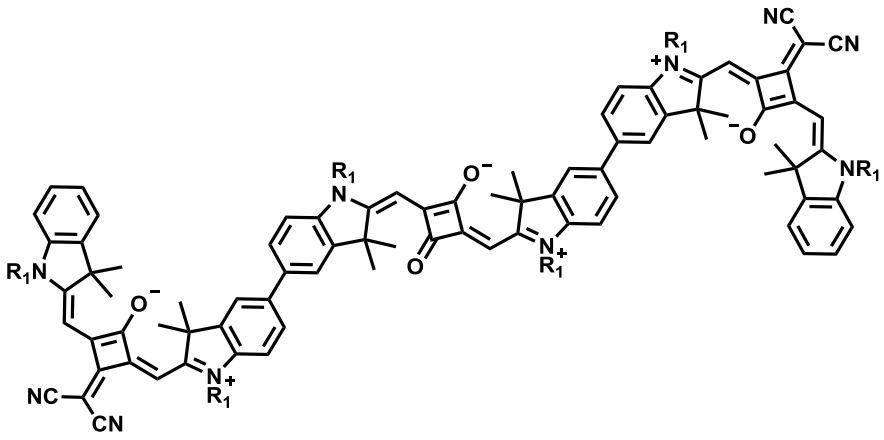

tSQBAB

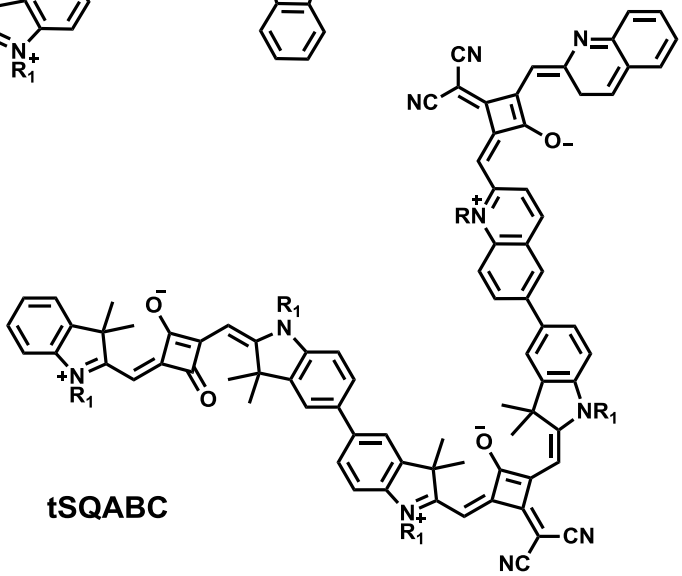

tSQABC

Hexasquarainyl Benzenes

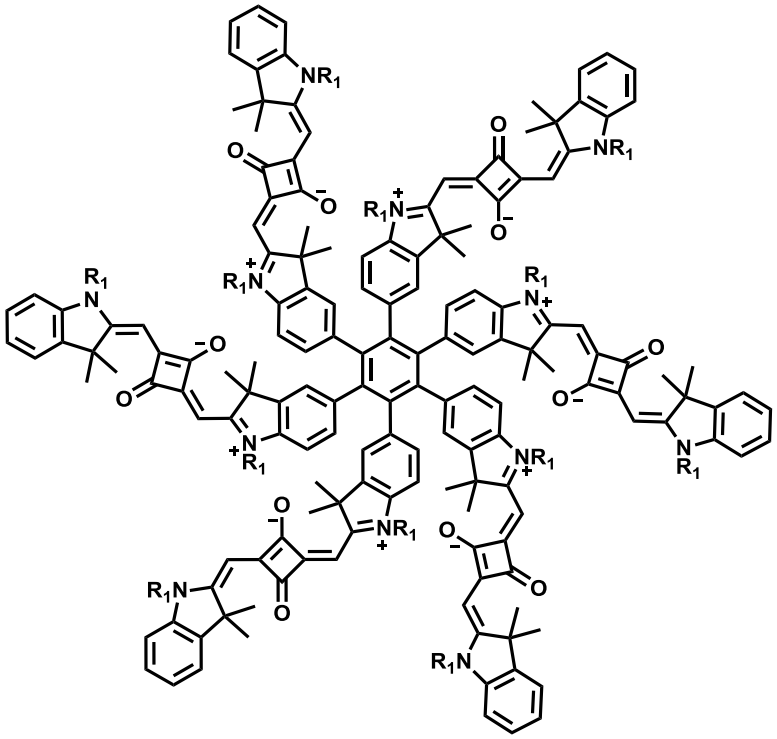

hSQA-1

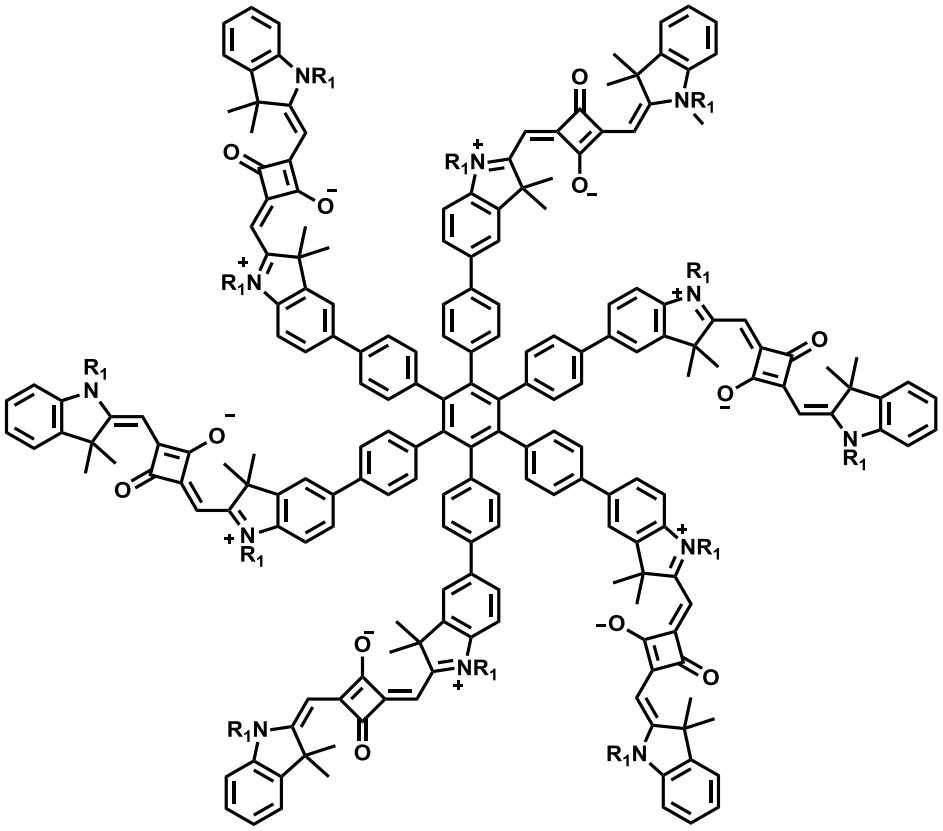

hSQA-2

Squaraine Polymers

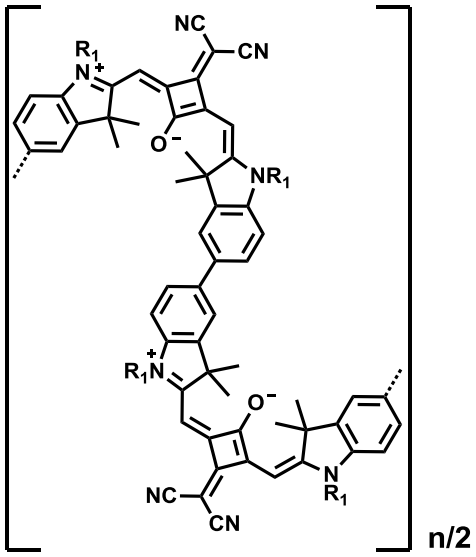

pSQB

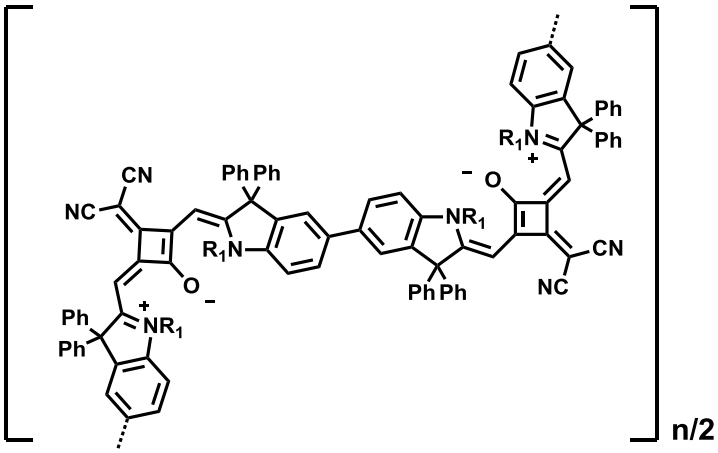

pDiPhSQB

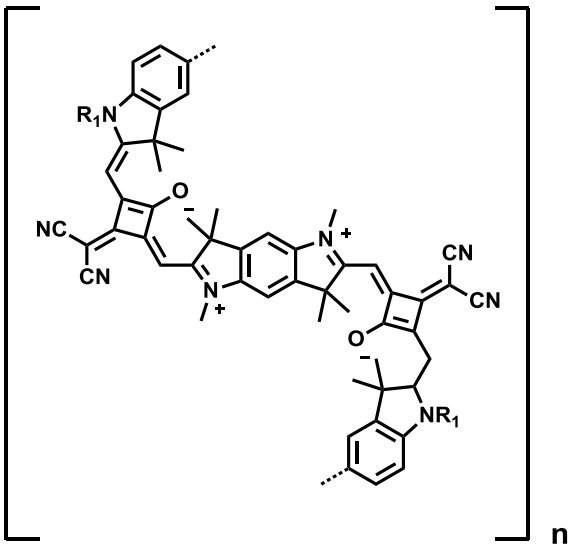

ppySQB

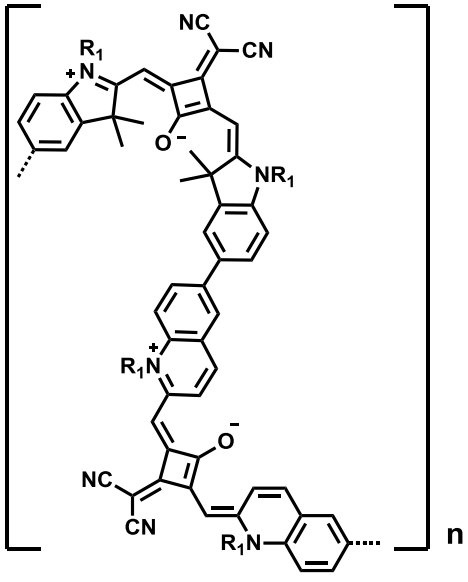

pSQAC

8 Zusammenfassung

Im Rahmen dieser Arbeit wurde die Synthese sowie photophysikalischen Untersuchungen einer Vielzahl von Squarainfarbstoffen präsentiert. Diese Vielfalt erwuchs aus vier monomeren Stammverbindungen, die auf Indolenin- bzw. Chinolin-Heterozyklen gründeten. Ein Querschnitt dieser Vielfalt ist im Folgenden abgebildet:

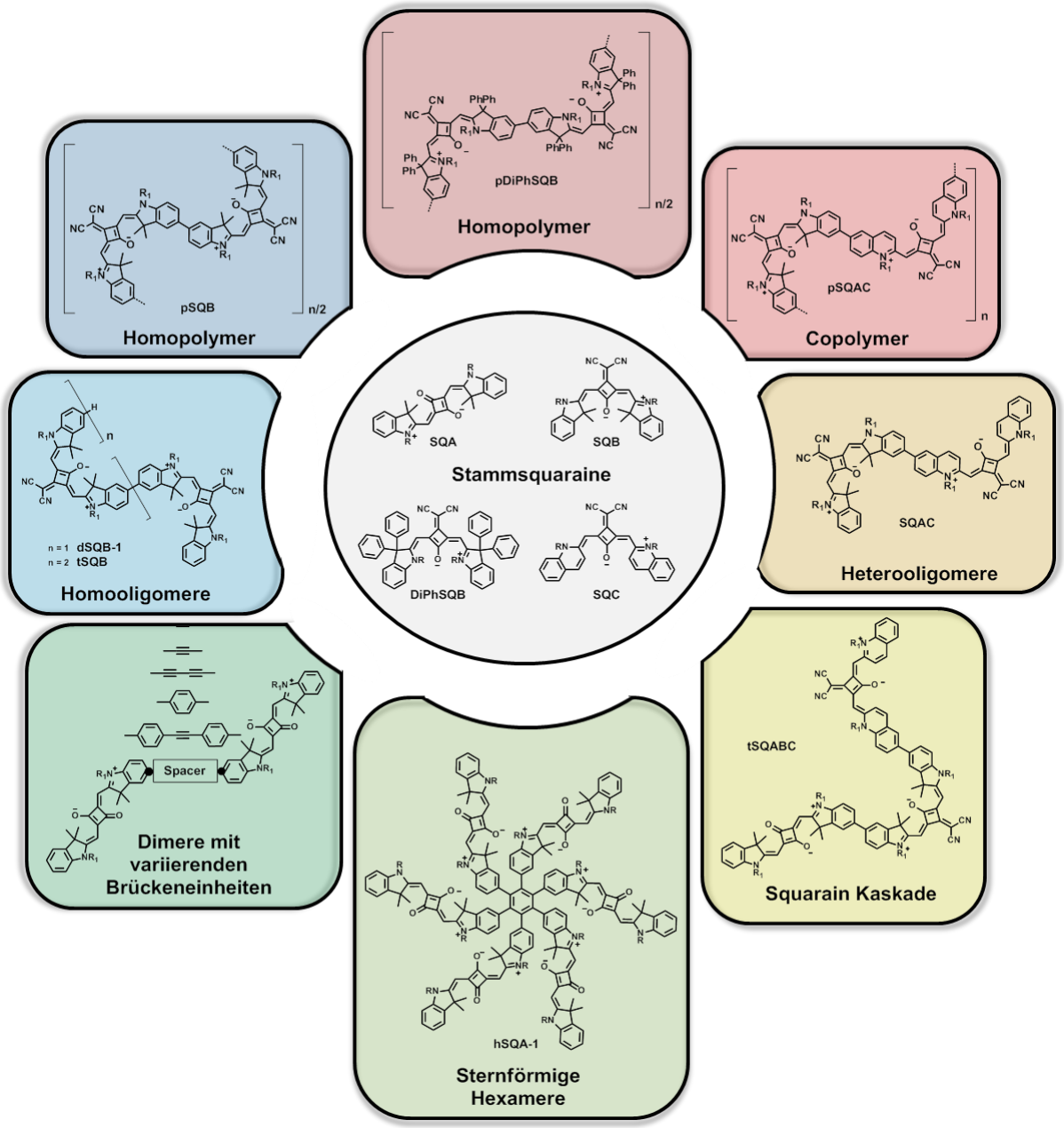

Neben der Donoreinheit dieser Monomerbausteine, wurde auch deren Akzeptoreinheit variiert. So ergab die Substitution der C=O Gruppe der zentralen Quadratsäureeinheit in **SQA** durch eine Dicyanovinylen-Einheit in **SQB**, **SQC** und **DiPhSQB** nicht nur eine Strukturänderung von *transoid* (C_{2h}) zu *cisoid* (C_{2v}), sondern auch eine signifikante Rotverschiebung der Hauptabsorptionsbande. Durch eine geeignete Wahl des Akzeptors und

Donors konnten so die optischen Eigenschaften bereits auf der Stufe des Monomers an die gewünschten Eigenschaften der späteren Zielverbindung angepasst werden.
Um die Derivatisierung der Monomere weiter voranzutreiben, wurden diese durch geeignete funktionelle Gruppen unter der Verwendung von übergangsmetallkatalysierten C-C Kupplungsreaktionen chemisch modifiziert. Dieser ging jedoch die Synthese Brom-funktionalisierter Vorstufen voraus. So musste die Halogenfunktion bereits in den Vorläufermolekülen eingeführt werden, da eine selektive, direkte Halogenierung auf der Stufe des Squarains nicht möglich ist. Schlussendlich konnte somit ein molekularer Baukasten entwickelt werden, der, bestückt mit Monomerbausteinen mit Brom-, Borester-, und Alkinfunktionen, den Weg zu diversen oligomeren und polymeren Squarainfarbstoffen ebnete. Die einzelnen Ergebnisse der Arbeit werden nun im Folgenden zusammengefasst.

Kapitel 3.1 stellt eine Übersicht von Squarain-Monomeren dar, die im Anschluss ihrer Synthese hinsichtlich ihrer photophysikalischen Eigenschaften untersucht wurden. Hierbei stellte sich heraus, dass neben den klassischen Indolenin-Squarainen **SQA** und **SQB**, die Benzoxazol (**SQD**), –thiazol (**SQE**), und –selenazol (**SQF**) Analoga vielversprechende Eigenschaften als NIR-Absorber und Emitter aufzeigten. Insbesondere besitzen Letztere exzellente Fluoreszenzquantenausbeuten um 90 % ($\geq$ 75 %) in $CHCl_3$ (Toluol) sowie eine Fluoreszenzlebenszeit über 4 ns, was sie folglich in den Fokus für die anschließende Polymersynthese rücken ließen.
Das anschließende Kapitel 3.2 widmete sich ausschließlich der Funktionalisierung der drei letztgenannten Monomerbausteine, für deren Einsatz in der Ni-untersützten Yamamoto Kupplungsreaktion eine dihalogenierte Spezies erforderlich war. Die Synthese des dibromierten Benzoxazol-Squarains, ausgehend von 3-Bromphenol, wurde durch die sehr geringen Ausbeuten von 11 % in der Dikondensationsreaktion erschwert. Das eigentliche Problem stellte allerdings das Auftreten eines nicht abzutrennenden Nebenprodukts dar. Neben den insgesamt geringen Mengen an Rohprodukt, zeigte ein erheblicher Anteil Monodebromierung, was zu einem sehr kleinen Polymerisationsgrad im Folgenden geführt hätte. Angesichts dieser Nachteile wurde das Projekt nicht weiter verfolgt. Des Weiteren konnten keine Polymere auf Basis von Benzothiazolen synthetisiert werden, da diese bereits auf der Stufe des Dimers zur Photoinstabilität neigten. Ebenso scheiterte die Synthese von Benzoselenazol-substituierten Polymeren, da eine direkte Bromierung des 2-Methylbenzoselenazols und der systemische Aufbau aus bromierten Vorstufen nicht literaturbekannt war. Aufgrund dessen reduzierte sich der Pool an potentiellen Monomerbausteinen auf die literaturbekannten Indolenin und Chinolin Analoga.

Das anschließende Kapitel handelte von der Funktionalisierung der Indolenin Squarainderivate. Mittels Pd-katalysierten Suzuki- und Sonogashira Reaktionen wurden in guten bis exzellenten Ausbeuten sowohl Borester- als auch Alkinfunktionen in die Peripherie der Bausteine angebracht. Die resultierenden mono- und difunktionalisierten Indolenin Derivate bildeten die Grundlage für die meisten der hier beschriebenen Oligo- und Polymersysteme.

Aus dieser Vielzahl an Funktionalitäten schöpfend, wurde sowohl das Indolenin Squarain Homopolymer **pSQB-1**, als auch die entsprechenden niedermolekularen Oligomerverbindungen **dSQB-1** und **tSQB** mittels der Ni-unterstützten Yamamoto bzw. Pd-katalysierte Suzuki Kupplung dargestellt. Die bereits durch Völker et al. erfolgten spektroskopischen Untersuchungen an **pSQB-V** wurden im Rahmen dieser Arbeit fortgesetzt. Im Vergleich zum Monomer, zeigten das Dimer, Trimer und das Polymer in $CHCl_3$ eine progressive Rotverschiebung der niedrigsten, intensivsten Absorptionsbande. Mit steigender Anzahl der **SQB**-Monomereinheiten nahm die Exzitonenkopplung im Dimer bis hin zum Polymer ab. Wie auch bereits Völker et al. zeigen konnten, war die Form der Absorption des Exzitonenbandes von **pSQB-1** stark lösemittelabhängig. Während J-Aggregat ähnliches Verhalten in $CHCl_3$ und DCM beobachtet wurde, zeigte das Polymer in Aceton H-Aggregat ähnliches Verhalten. Temperaturabhängige Absorptionsmessungen in PhCN zeigten ein reversibles thermodynamisches Gleichgewicht von verschiedenen Polymerstrukturen, welches sich mit steigender Temperatur durch einen sukzessiven Übergang von H-Aggregat zu einer Mischung mit mehr J-Aggregat Charakter manifestierte. Es wird angenommen, dass das Auftreten der charakteristischen Aggregatsbanden im Grenzfall mit zwei Polymerkonformeren korreliert, die einer Zick-Zack- und einer Helix-Struktur entsprechen. Da hierfür keine experimentellen Beweise durch NMR bis dato vorliegen, wurden TD-DFT Kalkulationen an Oligomereinheiten (22-er) durchgeführt, die die wesentlichen Merkmale der Absorptionsspektren der zwei Konformere reproduzieren konnten.

Die anschließenden Kapitel 3.4.3–3.4.5 erwuchsen aus der Motivation heraus, die optischen Eigenschaften der Polymere über die Kontrolle der Strukturbildung und somit der intramolekularen Aggregatsbildung zu beeinflussen.

Um einerseits J-Aggregat Verhalten zu provozieren wurde zunächst der Ansatz verfolgt, durch sterisch anspruchsvolle Gruppen in der 3-Position des Indolenin Gerüsts, den Kollaps zu helikalen Stukturen zu vermeiden. Das resultierende Homopolymer **pDiPhSQB** mit zwei Phenylgruppen pro Indolenin Einheit zeigte in allen untersuchten Lösemitteln bathochrom verschobene Absorptionsmaxima, was mit der Ausbildung von ausschließlich ausgedehnten

Zick-Zack-Ketten begründet wurde. Darüber hinaus zeigte die Einkristall-Röntgenstrukturanalyse des Monomers **DiPhSQB-2-Br$_2$** als Konsequenz der sterischen Überfrachtung eine Torsion des Indolenin Gerüsts. Die Verdrillung der Molekülgeometrie und der daraus resultierende Verlust an Planarität, führte zu einer erheblichen Verschlechterung der Fluoreszenzeigenschaften, jedoch wurde eine signifikante Rotverschiebung der Monomerbande von ca. 1 200 cm^{-1} im Vergleich zu **SQB** beobachtet, welche sogar größer als die für **dSQB-1** ist.

Zum anderen sollte der Ansatz einer partiellen Versteifung des Polymerrückgrades ebenfalls die Ausbildung von ausgedehnten Polymerketten begünstigen. Dieser Ansatz wurde insofern verfolgt, als dass jede zweite Biarylachse zwischen zwei Monomereinheiten in **pSQB-1** durch eine rigide *transoide* Benzodipyrrolenin Brücke ersetzt wird. Trotz eines eher geringen durchschnittlichen Polymerisationsgrades von < 10 konnte dennoch eine Rotverschiebung der niederenergetischsten Absorptionsbande in allen Lösemitteln beobachtet werden.

Um das Bild der intramolekularen Aggregate zu vervollständigen, wurde das gezielte Design von H-Aggregaten verfolgt. Hierfür wurde ein Squarain-Squarain Copolymer synthetisiert, das zum einen aus dem klassischen *cisoiden* Indolenin und zum anderen aus dem *cisoiden* Chinolin Squarain aufgebaut ist. Diesbezüglich wollte man sich die Triebkraft des Chinolin Bausteins für Aggregation als strukturdirigierende Komponente zu Nutze machen, um helikale Konformationen der Polymerstränge zu erzeugen. Das Copolymer **pSQBC** zeigte in der Tat eine verbreiterte, hypsochrom verschobene Hauptabsorptionsbande im Vergleich zur Monomereinheit **dSQBC**. Die Form der Absorption des Exzitonenbandes zeigte eine geringe Lösemittelabhängigkeit, die ebenfalls nur marginal durch die Temperatur beeinflusst werden konnte. Schlussendlich deuten diese Befunde auf ein stark-ausgeprägtes H-Aggregat ähnliches Verhalten hin, was die zu anfangs formulierte These belegt, dass sich die optischen Eigenschaften der Polymere (H- und J-Aggregate) und deren Strukturbildung durch ein adäquates Moleküldesign der Monomerbausteine kontrollieren lassen.

Im nächsten Kapitel 3.5 wurde gezeigt, dass sich die optischen Eigenschaften auch in niedermolekularen **SQA** und **SQB** Homo- und Heterodimeren durch eine systematische Variation der Brückeneinheit feinabstimmen lassen. In diesem Zusammenhang beobachtete man die stärkste Exzitonenkopplung in Dimeren mit Biarylachse, während beispielsweise geringere Kopplungen mit Brückeneinheiten auftraten, die u.a. einen großen intramolekularen Abstand der Chromophore zueinander aufwiesen.

Neben Homo- und Heterodimeren, wurde im folgenden Kapitel 3.6 die exzitonische Kopplung auch in Squarain Heterotrimeren untersucht. Aufbauend auf den Befunden des

vorherigen Kapitels, wurden drei Trimere mittels Suzuki-Kupplung synthetisiert, in denen die Chromophore durch Biarylachsen verknüpft sind, um so eine stärkere elektronische Kommunikation zu erzeugen. Neben **tSQABA** und **tSQBAB**, ist das Trimer **tSQABC** insbesondere von Interesse, da erstmalig die Möglichkeit bestand, Energietransfer in einer Kaskade nur auf Squarainen basierend zu untersuchen. In diesem Zusammenhang zeigten stationäre Fluoreszenzmessungen neben Emission aus dem niedrigsten, delokalisierten Zustand, auch strahlende Übergänge aus höheren, lokalisierten Zuständen, was eindeutig auf einen eher ineffizienten Energietransfer innerhalb dieses exzitonisch-gekoppelten Systems hinweist. Aufgrund der extrem rotverschobenen Absorptionsbande des Trimers konnten bis dato die zugrunde liegenden Dynamiken mittels zeitaufgelöster 2D Spektroskopie im Rahmen einer Kooperation noch nicht untersucht werden, da der experimentelle Aufbau zum Zeitpunkt der Anfertigung dieser Arbeit noch nicht für Messungen im Bereich für 700-900 nm optimiert war.

Das letzte Kapitel 3.7 dieser Arbeit stand im Gegensatz zu den vorherigen Kapiteln ausschließlich im Fokus von intermolekularen Aggregaten. Wie gezeigt werden konnte, neigten die Squaraine **hSQA-1** und **hSQA-2**, in ein sternförmiges Hexaarylbenzol-Gerüst gebettet zur Selbstorganisation. Konzentration- und temperaturabhängige Studien der beiden synthetisierten Hexasquarainyl-Benzole offenbarten eine starke Triebkraft zur Aggregation in Aceton. Während **hSQA-2** instantan thermodynamisch stabile Aggregate bildete, zeigten **hSQA-1** Aggregate eine ausgeprägte kinetische Stabilität. Dies konnte man sich zu Nutze machen um die kinetischen Aktivierungsparameter der Aggregation und Deaggregation zu bestimmen. Die Absorptionsspektren der beiden Hexasquarainyl-Benzole im aggregierten Zustand zeigten extreme Unterschiede auf. Während **hSQA-1** eine intensive, sehr schmale und stark hypsochrom verschobene Bande zeigte, beobachtete man für das größere Hexasquarainyl-Benzol zwei bathochrom verschobene Banden, die allerdings energetisch sehr nahe der Monomerbande lokalisiert waren. Die sehr geringe Halbwertsbreite der Aggregatsbande in **hSQA-1** wurde durch die sog. Austauschverschmälerung erklärt und deutet auf hochgeordnete supramolekulare Aggregate hin. Die konzentrationsabhängigen Messdaten der beiden Chromophore konnten sehr gut mit Hilfe des Dimer-Modells angepasst werden, welches für beide Systeme eine hohe Bindungskonstante von über 10^6 M^{-1} ergab. In Anbetracht der Tatsache, dass die raumgreifenden 3,3-Dimethylgruppen im Indoleningerüst extrem hinderlich für den Aggregationsprozess sind, ist die starke Triebkraft zur Selbstorganisation, welche sich in den hohen Bindungskonstanten niederschlägt, äußerst bemerkenswert. Theoretische Modellierungen und Rechnungen in Kombination mit NMR-

spektroskopischen Untersuchungen von **hSQA-1** ergaben eine Aggregatsstruktur aus zwei sich stapelten Hexasquarainylbenzolmonomeren, die dem Bild zweier gestapelter Schüsseln entspricht.

9 Appendix

9.1 X-Ray Crystallographic Data of DiPhSQB-2-Br_2[XVI]

($C_{61}H_{54}Br_2N_4O$): *M*r = , crystal size: 0.230×0.124×0.037 mm, monoclinic space group P2(1)/n, a =12.3578(5) Å, α = 90°, b = 19.6171(8) Å, β = 93.8074, c = 24.1612(8) Å, γ = 90°, V =5844.3(4) $Å^3$, Z = 4, ρ (calcd) = 1.3535 $g \cdot cm^{-3}$, μ =3.535 mm^{-1}, $F_{(000)}$ =2392, *GooF* (F^2) = 1.144, R_1 = 0.0395, wR^2 = 0.1133 for $I > 2\sigma(I)$, R_1 = 0.0413, wR^2 = 0.1147 for all data, 11 929 unique reflections [Θ = 67.679°] with a completeness of 99.5 % and 683 parameters, 5 restraints.

Table 18: Atomic coordinates (× 10^4) and equivalent isotropic displacement parameters ($Å^2$ × 10^3) for twin crystal. *U*(eq) is defined as one third of the trace of the orthogonalised U_{ij} tensor.

	x	y	z	*U*(eq)
Br(1)	4371(1)	921(1)	22(1)	22(1)
Br(2)	4483(1)	986(1)	24(1)	24(1)
O(1)	6174(2)	2175(1)	22(1)	22(1)
N(1)	6881(3)	2125(2)	16(1)	16(1)
N(2)	6595(3)	2078(2)	16(1)	16(1)
N(3)	8151(4)	4994(2)	33(1)	33(1)
N(4)	7482(4)	5034(2)	30(1)	30(1)
C(1)	6346(3)	1755(2)	16(1)	16(1)
C(2)	6331(3)	1057(2)	18(1)	18(1)
C(3)	5728(3)	823(2)	18(1)	18(1)
C(4)	5182(3)	1271(2)	17(1)	17(1)
C(5)	5190(3)	1973(2)	17(1)	17(1)
C(6)	5787(3)	2206(2)	14(1)	14(1)
C(7)	5886(3)	2918(2)	14(1)	14(1)
C(8)	6654(3)	2788(2)	16(1)	16(1)
C(9)	6984(3)	3307(2)	16(1)	16(1)
C(10)	7042(3)	3234(2)	15(1)	15(1)
C(11)	7232(3)	3698(2)	16(1)	16(1)
C(12)	6891(3)	3209(2)	16(1)	16(1)

[XVI] X-ray crystallography was carried out by Dr. David Schmidt.

C(13)	6635(3)	2726(2)	16(1)	16(1)
C(14)	6664(3)	3267(2)	16(1)	16(1)
C(15)	6387(3)	2761(2)	15(1)	15(1)
C(16)	5738(3)	2917(2)	16(1)	16(1)
C(17)	5660(3)	2210(2)	16(1)	16(1)
C(18)	5162(3)	1998(2)	18(1)	18(1)
C(19)	5162(3)	1305(2)	18(1)	18(1)
C(20)	5637(3)	833(2)	18(1)	18(1)
C(21)	6145(3)	1044(2)	18(1)	18(1)
C(22)	6145(3)	1742(2)	16(1)	16(1)
C(23)	7540(3)	4380(2)	18(1)	18(1)
C(24)	7865(3)	4727(2)	21(1)	21(1)
C(25)	7527(3)	4746(2)	20(1)	20(1)
C(31)	6378(3)	3454(2)	16(1)	16(1)
C(32)	7021(3)	3249(2)	21(1)	21(1)
C(33)	7511(4)	3728(2)	28(1)	28(1)
C(34)	7375(4)	4421(2)	28(1)	28(1)
C(35)	6747(4)	4625(2)	27(1)	27(1)
C(36)	6263(3)	4148(2)	21(1)	21(1)
C(41)	4750(3)	3098(2)	18(1)	18(1)
C(42)	4017(3)	3464(2)	21(1)	21(1)
C(43)	2969(3)	3569(2)	27(1)	27(1)
C(44)	2632(3)	3310(2)	30(1)	30(1)
C(45)	3358(4)	2942(2)	29(1)	29(1)
C(46)	4410(3)	2833(2)	23(1)	23(1)
C(51)	6355(3)	3438(2)	17(1)	17(1)
C(52)	6198(3)	4137(2)	20(1)	20(1)
C(53)	6806(4)	4603(2)	25(1)	25(1)
C(54)	7572(4)	4380(2)	27(1)	27(1)
C(55)	7746(4)	3687(2)	26(1)	26(1)
C(56)	7146(3)	3217(2)	21(1)	21(1)
C(61)	4568(3)	3128(2)	19(1)	19(1)
C(62)	4102(3)	2924(2)	26(1)	26(1)
C(63)	3015(4)	3052(3)	34(1)	34(1)
C(64)	2384(3)	3390(2)	34(1)	34(1)
C(65)	2849(4)	3596(2)	29(1)	29(1)
C(66)	3924(3)	3457(2)	23(1)	23(1)
C(71)	7471(3)	1764(2)	16(1)	16(1)

C(72)	8572(3)	1942(2)	27(1)	27(1)
C(73)	9508(4)	1599(2)	32(1)	32(1)
C(74)	9619(3)	837(2)	30(1)	30(1)
C(75)	10427(5)	499(3)	39(1)	39(1)
C(76)	10505(5)	-263(3)	46(1)	46(1)
C(81)	7732(3)	1802(2)	19(1)	19(1)
C(82)	8735(4)	1649(3)	32(1)	32(1)
C(83)	9568(4)	1277(3)	34(1)	34(1)
C(84)	10490(20)	951(17)	47(3)	47(3)
C(85)	11230(20)	514(19)	62(4)	62(4)
C(86)	10750(30)	-187(17)	63(4)	63(4)
C(83B)	9568(4)	1277(3)	34(1)	34(1)
C(84B)	10660(8)	1199(8)	47(3)	47(3)
C(85B)	11433(10)	720(9)	62(4)	62(4)
C(86B)	11103(13)	-33(7)	63(4)	63(4)
C(101)	264(6)	5935(4)	60(2)	60(2)
Cl(1)	195(2)	5641(1)	78(1)	78(1)
Cl(2)	1511(2)	6291(2)	120(1)	120(1)
C(102)	309(8)	3854(4)	71(2)	71(2)
Cl(3)	188(3)	3002(1)	131(2)	131(2)
Cl(4)	1552(2)	4134(1)	71(1)	71(1)

Table 19: Anisotropic displacement parameters ($Å^2 \times 10^3$) for twin crystal.

	U_{11}	U_{22}	U_{33}	U_{23}	U_{13}	U_{12}
Br(1)	25(1)	21(1)	20(1)	-5(1)	-3(1)	-4(1)
Br(2)	27(1)	25(1)	20(1)	4(1)	9(1)	-6(1)
O(1)	30(2)	16(1)	21(1)	-1(1)	-1(1)	-7(1)
N(1)	21(2)	16(2)	12(1)	1(1)	-1(1)	4(1)
N(2)	20(2)	13(1)	14(1)	-2(1)	6(1)	-1(1)
N(3)	50(2)	21(2)	29(2)	6(2)	12(2)	-2(2)
N(4)	49(2)	17(2)	23(2)	-3(1)	-4(2)	-6(2)
C(1)	18(2)	14(2)	15(2)	0(1)	2(1)	-1(1)
C(2)	23(2)	14(2)	18(2)	3(1)	4(1)	2(2)
C(3)	22(2)	11(2)	21(2)	-1(1)	6(2)	-2(1)
C(4)	16(2)	20(2)	15(2)	-2(1)	2(1)	-3(1)
C(5)	21(2)	15(2)	15(2)	2(1)	0(1)	1(1)

C(6)	17(2)	12(2)	15(2)	0(1)	4(1)	-1(1)
C(7)	20(2)	10(2)	13(2)	0(1)	-1(1)	0(1)
C(8)	18(2)	16(2)	14(2)	2(1)	2(1)	3(1)
C(9)	20(2)	13(2)	15(2)	2(1)	1(1)	2(1)
C(10)	15(2)	13(2)	17(2)	1(1)	3(1)	2(1)
C(11)	18(2)	17(2)	13(2)	1(1)	-1(1)	2(2)
C(12)	18(2)	14(2)	16(2)	3(1)	3(1)	2(1)
C(13)	19(2)	16(2)	14(2)	1(1)	1(1)	0(2)
C(14)	22(2)	12(2)	14(2)	-1(1)	3(1)	-2(1)
C(15)	16(2)	15(2)	14(2)	-1(1)	2(1)	1(1)
C(16)	21(2)	14(2)	15(2)	0(1)	6(1)	-2(1)
C(17)	18(2)	13(2)	17(2)	-1(1)	2(1)	-1(1)
C(18)	17(2)	20(2)	17(2)	-2(1)	5(1)	0(1)
C(19)	17(2)	20(2)	16(2)	3(1)	2(1)	-7(1)
C(20)	20(2)	12(2)	22(2)	1(1)	2(1)	-4(1)
C(21)	21(2)	14(2)	20(2)	-4(1)	4(1)	-2(2)
C(22)	16(2)	16(2)	15(2)	0(1)	1(1)	-1(1)
C(23)	21(2)	15(2)	18(2)	1(1)	0(1)	-2(2)
C(24)	26(2)	15(2)	23(2)	2(2)	2(2)	0(2)
C(25)	24(2)	12(2)	23(2)	4(2)	-2(2)	-3(2)
C(31)	19(2)	14(2)	14(2)	1(1)	-3(1)	0(1)
C(32)	26(2)	20(2)	17(2)	-1(2)	2(2)	1(2)
C(33)	33(2)	31(2)	20(2)	2(2)	5(2)	-3(2)
C(34)	36(2)	25(2)	24(2)	9(2)	0(2)	-7(2)
C(35)	35(2)	16(2)	30(2)	5(2)	-5(2)	-2(2)
C(36)	27(2)	18(2)	19(2)	1(1)	-2(2)	1(2)
C(41)	22(2)	13(2)	19(2)	-4(1)	-2(1)	3(1)
C(42)	24(2)	16(2)	22(2)	-2(1)	-4(2)	2(2)
C(43)	23(2)	23(2)	34(2)	-5(2)	-7(2)	4(2)
C(44)	21(2)	33(2)	35(2)	-9(2)	4(2)	1(2)
C(45)	31(2)	36(2)	22(2)	-2(2)	5(2)	-3(2)
C(46)	24(2)	24(2)	19(2)	2(2)	-1(2)	2(2)
C(51)	24(2)	14(2)	14(2)	-2(1)	8(1)	1(1)
C(52)	26(2)	15(2)	20(2)	-1(1)	8(2)	-1(2)
C(53)	35(2)	14(2)	25(2)	-3(2)	10(2)	-4(2)
C(54)	32(2)	28(2)	23(2)	-8(2)	8(2)	-11(2)
C(55)	28(2)	30(2)	20(2)	-2(2)	7(2)	-2(2)
C(56)	24(2)	18(2)	21(2)	-1(2)	6(2)	0(2)

C(61)	22(2)	14(2)	22(2)	0(1)	6(2)	-2(1)
C(62)	23(2)	28(2)	26(2)	-4(2)	3(2)	2(2)
C(63)	31(2)	40(3)	30(2)	-1(2)	-2(2)	2(2)
C(64)	19(2)	36(2)	46(3)	10(2)	2(2)	6(2)
C(65)	26(2)	21(2)	41(2)	1(2)	14(2)	4(2)
C(66)	25(2)	19(2)	24(2)	1(2)	9(2)	-4(2)
C(71)	22(2)	13(2)	14(2)	-2(1)	6(1)	5(1)
C(72)	25(2)	29(2)	25(2)	-5(2)	-2(2)	0(2)
C(73)	24(2)	35(2)	37(2)	2(2)	4(2)	-1(2)
C(74)	25(2)	35(2)	31(2)	6(2)	7(2)	5(2)
C(75)	45(3)	39(3)	34(2)	8(2)	14(2)	12(2)
C(76)	48(3)	38(3)	54(3)	8(2)	13(3)	18(3)
C(81)	23(2)	18(2)	14(2)	1(1)	-3(1)	5(2)
C(82)	28(2)	48(3)	19(2)	3(2)	1(2)	9(2)
C(83)	28(2)	50(3)	22(2)	1(2)	1(2)	10(2)
C(84)	34(4)	82(9)	26(3)	1(5)	2(3)	13(5)
C(85)	30(5)	130(12)	26(3)	-1(7)	3(4)	29(6)
C(86)	56(9)	87(8)	46(7)	2(5)	6(5)	49(7)
C(83B)	28(2)	50(3)	22(2)	1(2)	1(2)	10(2)
C(84B)	34(4)	82(9)	26(3)	1(5)	2(3)	13(5)
C(85B)	30(5)	130(12)	26(3)	-1(7)	3(4)	29(6)
C(86B)	56(9)	87(8)	46(7)	2(5)	6(5)	49(7)
C(101)	52(4)	37(3)	93(5)	-5(4)	15(4)	5(3)
Cl(1)	71(1)	59(1)	106(2)	17(1)	33(1)	5(1)
Cl(2)	51(1)	142(3)	166(3)	102(2)	4(2)	-7(1)
C(102)	63(5)	78(6)	74(5)	25(4)	8(4)	19(5)
Cl(3)	100(2)	57(1)	226(4)	27(2)	-64(2)	-12(2)
Cl(4)	54(1)	88(2)	70(1)	-10(1)	10(1)	8(1)

9.2 Hexasquarainyl Benzenes

9.2.1 Absorption Spectra of hSQA-1 in $CHCl_3$, DCM and TCE

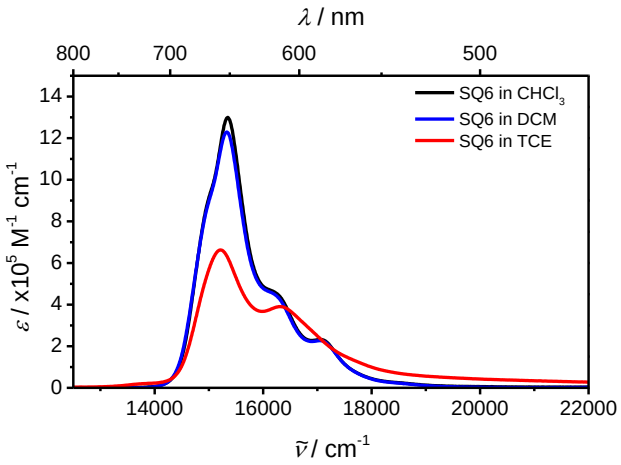

Figure 82: Absorption spectra of **hSQA-1** in $CHCl_3$, DCM and TCE.

9.2.2 DOSY-NMR Measurements

The hydrodynamic radii R_0 of **hSQA-1** and **hSQA-2** were determined in CD_2Cl_2 and acetone-d_6, respectively, from the corresponding diffusion coefficients D according to the Stokes-Einstein equation at 293 K:

$$D = \frac{k_B T}{6\pi\eta R_0} \qquad \text{Stokes-Einstein equation (61)}$$

where k_B represents the Boltzmann constant, T the temperature, and η the viscosity of the solvent. The diffusion constants for each compound were acquired from DOSY NMR measurements in dichloromethane ($\eta_{293\,K}$ = 4.40×10^{-4} Nsm^{-2}) and acetone ($\eta_{293\,K}$ = 3.20×10^{-4} Nsm^{-2}), respectively. For each measurement, the dye concentration was ca. 10^{-3} M. For **hSQA-1**, hydrodynamic radii of 1.43 nm and 1.64 nm in CD_2Cl_2 and acetone were determined, respectively. For **hSQA-2**, radii of 1.73 nm and 2.06 nm were analogously calculated, respectively.

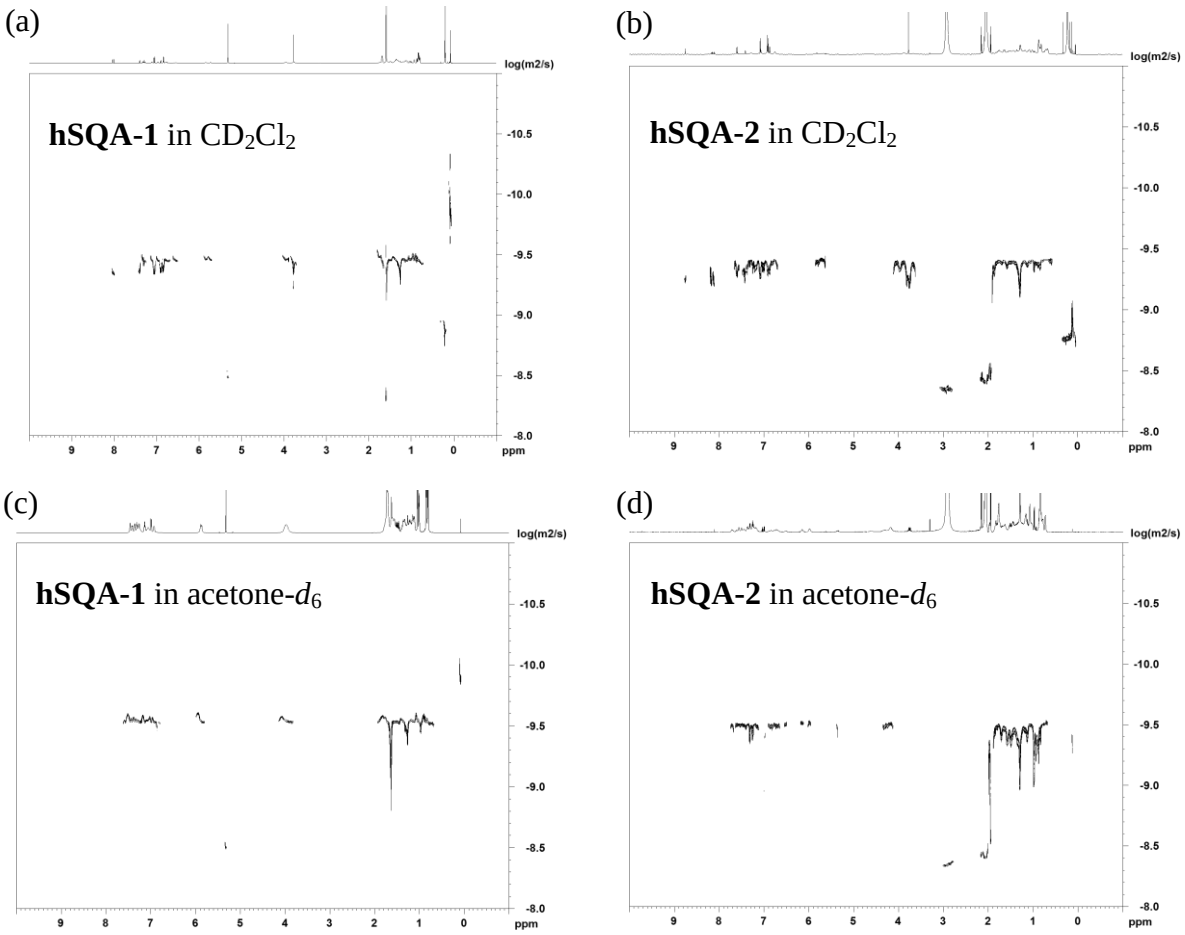

Figure 83: DOSY NMR spectra of (a)(c) **hSQA-1** and (b)(d) **hSQA-2** in CD_2Cl_2 and acetone-d_6, respectively, recorded at 600.1 MHz at 293 K. The logarithm of the diffusion coefficients D [m^2s^{-1}] are plotted against the chemical shift δ [ppm].

9.2.3 Absorption Spectra of hSQA-1 in Acetone and Methylcyclohexane

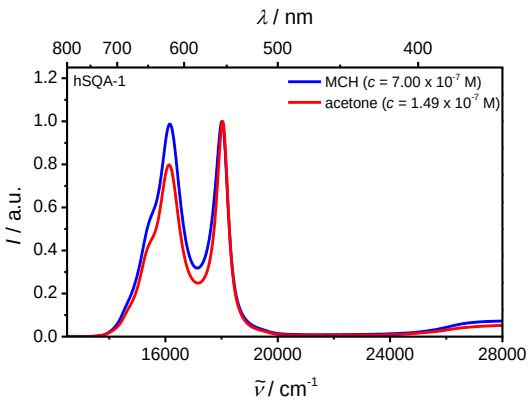

Figure 84: Normalised absorption spectra of **hSQA-1** in acetone and methylcyclohexane (MCH) at different concentrations.

9.2.4 Computational Methods[XVII]

For the calculation of optical properties, we considered the optimized geometries and replaced the alkyl chains by methyl groups. Simulations of the absorption spectra then have been carried out using the lc-TDDFTB method[190] as implemented in the DFTBaby program package.[191] This methodology accounts for a correct description of charge transfer states by introducing a long-range correction to the time-dependent DFTB (TDDFTB). An active space of 30 occupied and 30 virtual orbitals was chosen for the simulations and the individual transitions have been convoluted by a Lorentzian function with a width of 700 cm^{-1}, except for the "non-dispersive" monomer structures where a Lorentzian function with a width of 1 500 cm^{-1} was used to match the experimental spectral width.

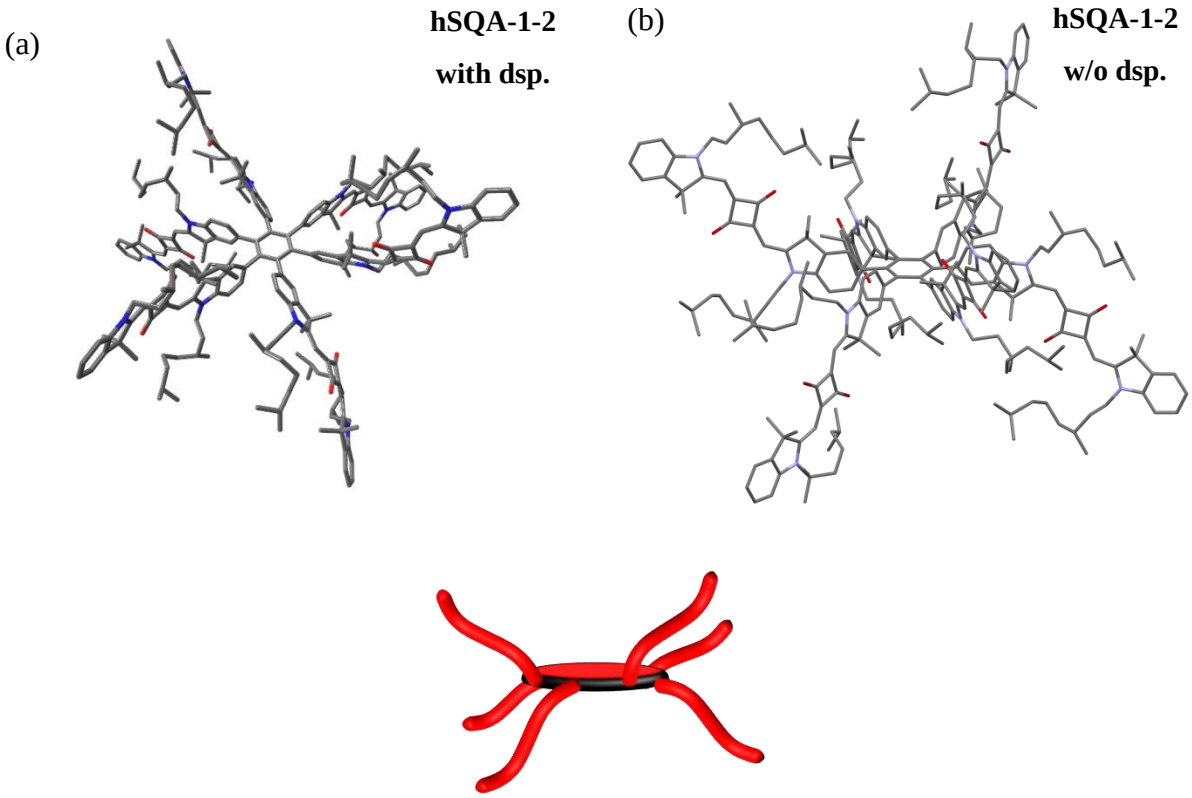

Figure 85: Geometry optimized monomeric structures of **hSQA-1-2** ("all-up") isomer (a) with and (b) without dispersion correction.

[XVII] Computations were carried out by Dr. Merle I. S. Röhr.

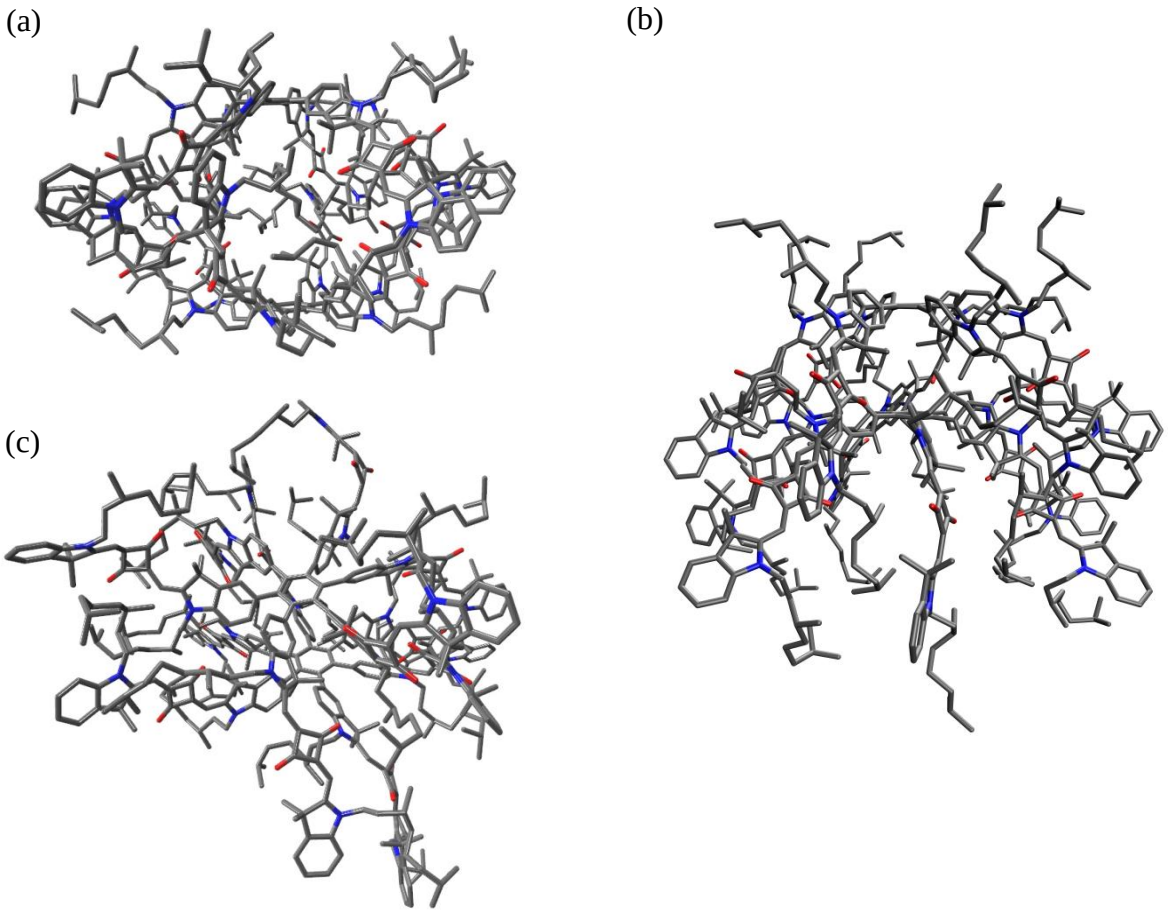

Figure 86: Geometry optimized structures of (a) “folded hands”-, (b) “bowls”-, and (c) “mixed”-dimeric aggregates with side chains, respectively.

Table 20: Overview of calculated energies (DFTB level using Grimme dispersion correction).

	DFTB Final Energy / eV	Electronic Energy / eV	Dispersion Energy / eV	Repulsion Energy / eV	Coulomb Energy / eV
hSQA-1-1	–18 859.027	–18 864.603	–30.591	24.982	11.185
2 × **hSQA-1-1**	–37 718.055	–37 729.207	–61.183	49.964	22.370
hSQA-1-1 w/o dispersion	–18 829.494	–18 862.782	0.000	21.576	11.712
hSQA-1-2	–18 858.832	–18 865.850	–29.597	24.975	11.641
hSQA-1-2 w/o dispersion	–18 829.561	–18 863.031	0.000	21.708	11.762
Dimer "Folded Hands" (**hSQA-1-1**)	–37 731.126	–37 727.378	–75.407	50.043	21.615
Dimer "Bowls" (**hSQA-1-1**)	–37 729.069	–37 728.019	–73.177	49.829	21.915
Dimer "Mixed" (**hSQA-1-2**)	–37 727.282	–37 728.051	–70.975	49.829	21.915

9.2.5 Kinetic Fitting Routines

9.2.5.1 Disassembly of hSQA-1-Dimers into Monomers in Toluene

We used the same fitting routine as already introduced and successfully applied for the disassembly of a bimolecular perylene bisimide tweezer by *Würthner et al*. For a detailed deduction of the fitting routine, we like to refer to the corresponding literature.[192] In general, a disassembly reaction of a dimer into two monomers can be regarded as a first-order defragmentation reaction according to equation (62) with a single rate constant k_{diss} and is described by an exponential function.

$$D \xrightarrow{k_{diss}} M+M \tag{62}$$

The following equation (63) was used to fit the absorption data as a function of time t':

$$\frac{OD(\lambda,t')}{c \cdot d} = \varepsilon_M + \left(\frac{\varepsilon_D}{2} - \varepsilon_M\right) e^{-kt^0} e^{-kt'} = \varepsilon_M + C e^{-kt'} \tag{63}$$

where c is the concentration, d the path length of the cuvette, $OD(\lambda)/(c \cdot d)$ the apparent extinction coefficient, and ε_M and ε_D the extinction coefficients of monomer and dimer,

respectively. The effect of a dead time of $t^0 = t - t'$ between the ideal time t and the recorded time t' is considered and incorporated in a constant value C together with the absorption relationship of $\varepsilon_D/2$ and ε_M.

Table 21: Monomer absorption coefficient ε_M, constant C and disassembly rate constant k_{diss} received from non-least squares analysis according to equation (63) at 18 000 cm^{-1} for different temperatures. In terms of a first-order reaction, the half-life time of the disassembly process was determined according to $t_{1/2} = \ln 2/k$. The concentration of each measurement was 1.49×10^{-6} M.

T / K	ε_M / $M^{-1}cm^{-1}$	C / $M^{-1}cm^{-1}$	k_{diss} / s^{-1}	$t_{1/2}$ /s	Correlation Coefficient R^2
288.0	66 600	493 000	1.78×10^{-4}	3894	0.99994
290.5	56 000	489 000	2.17×10^{-4}	3194	0.99994
293.0	52 200	463 000	2.65×10^{-4}	2616	0.99994
295.5	47 700	496 000	2.80×10^{-4}	2476	0.99996
298.0	43 200	484 000	3.88×10^{-4}	1786	0.99997
300.5	44 400	503 000	4.77×10^{-4}	1453	0.99994
303.0	44 100	499 000	6.11×10^{-4}	1134	0.99995
305.5	43 500	502 000	7.19×10^{-4}	964	0.99991
308.0	41 100	482 000	9.29×10^{-4}	746	0.99994
310.5	40 400	497 000	1.14×10^{-3}	608	0.99995
313.0	41 700	494 000	1.36×10^{-3}	510	0.99994

9.2.5.2 Assembly of hSQA-1-Monomers into Dimers in Acetone

A dimerization reaction of two identical monomers that form a dimer in a single elementary step can be written as follows:

$$M + M \xrightarrow{k_{ass}} D \tag{64}$$

where k_{ass} is the assembly rate constant. The reaction rate r is given by $r = k_{ass}[M]^2$ and depends quadratically on the monomer concentration. The integrated second order rate law is given by equation (65):

$$[M] = \frac{[M]_0}{[M]_0 k_{ass} t + 1} \tag{65}$$

Where [M] = c_M denotes the monomer concentration as a function of time and $[M]_0 = c_{M0}$ the initial monomer concentration.

The ensemble absorption $OD(t)$ recorded at time t can be regarded as the superposition of the monomer and dimer absorption of the dye in solution according to equation (66):

$$OD(t) = \varepsilon_M d c_M + \varepsilon_D d \frac{1}{2}(c_{M0} - c_M) \tag{66}$$

where d is the path length of the cuvette (10 mm). Combining equations (65) and (66) and dividing both sides by $(d \cdot c_{M0})$ we obtain equation (67):

$$\frac{OD(t)}{d \cdot c_{M0}} = \frac{\varepsilon_D}{2} + \left(\varepsilon_M - \frac{\varepsilon_D}{2}\right) \frac{1}{c_{M0} k_{ass} t + 1} \tag{67}$$

After setting $(\varepsilon_M - \varepsilon_D/2)$ as constant C, we finally obtain equation (68) which can be used to fit the absorption data:

$$\frac{OD(t)}{d \cdot c_{M0}} = \frac{\varepsilon_D}{2} + C \frac{1}{c_{M0} k_{ass} t + 1} \tag{68}$$

Table 22: Monomer absorption coefficient ε_D, constant C and assembly rate constant k_{ass} received from non-least squares analysis according to equation (68) at 18 000 cm^{-1} for different temperatures. In terms of a second-order reaction, the half-life time of the assembly process was determined according to $t_{1/2} = 1/(c_{M0} k_{ass})$. The initial concentration of each measurement was 1.49×10^{-6} M.

T / K	ε_D / $M^{-1}cm^{-1}$	C / $M^{-1}cm^{-1}$	k_{ass} / $M^{-1}s^{-1}$	$t_{1/2}$ / s	Correlation Coefficient R^2
283.0	963 000	–318 000	44.3	15 100	0.99950
285.5	907 000	–300 000	76.1	8 810	0.99977
288.0	889 000	–275 000	121	5 550	0.99972
290.5	920 000	–314 000	151	4 440	0.99960
293.0	907 000	–300 000	214	3 130	0.99920
295.5	887 000	–295 000	300	2 240	0.99871
298.0	866 000	–274 000	418	1 610	0.99891
300.5	857 000	–281 000	556	1 210	0.99850
303.0	857 000	–281 000	765	877	0.99902

9.2.6 NMR-Spectroscopy

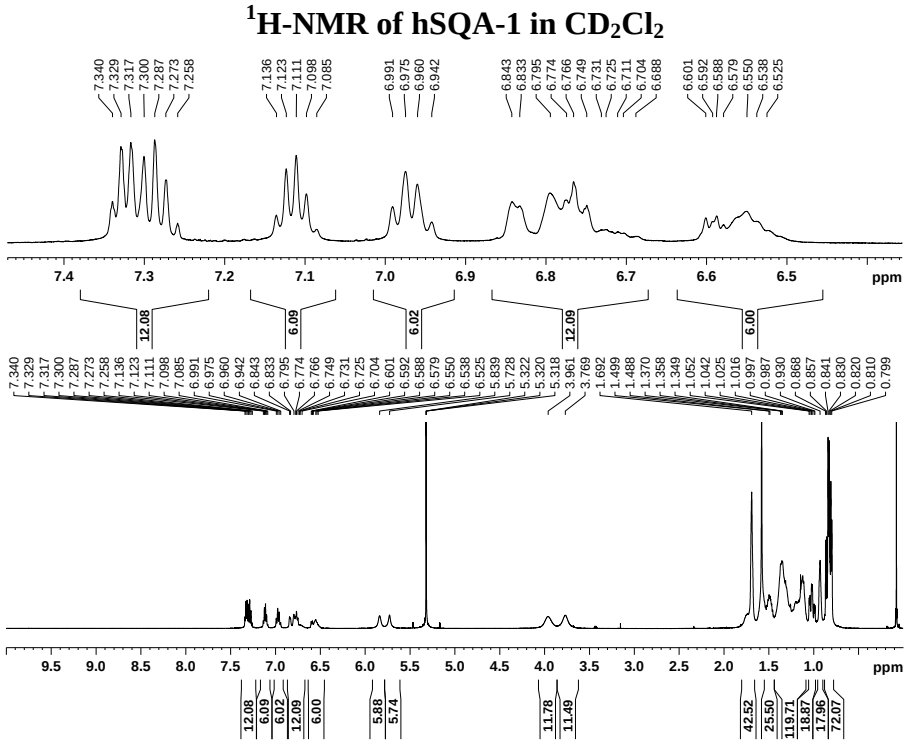

Figure 87: ^{1}H-NMR spectrum of squaraine dye **hSQA-1** in CD_2Cl_2 recorded with 600.1 MHz NMR at 298 K.

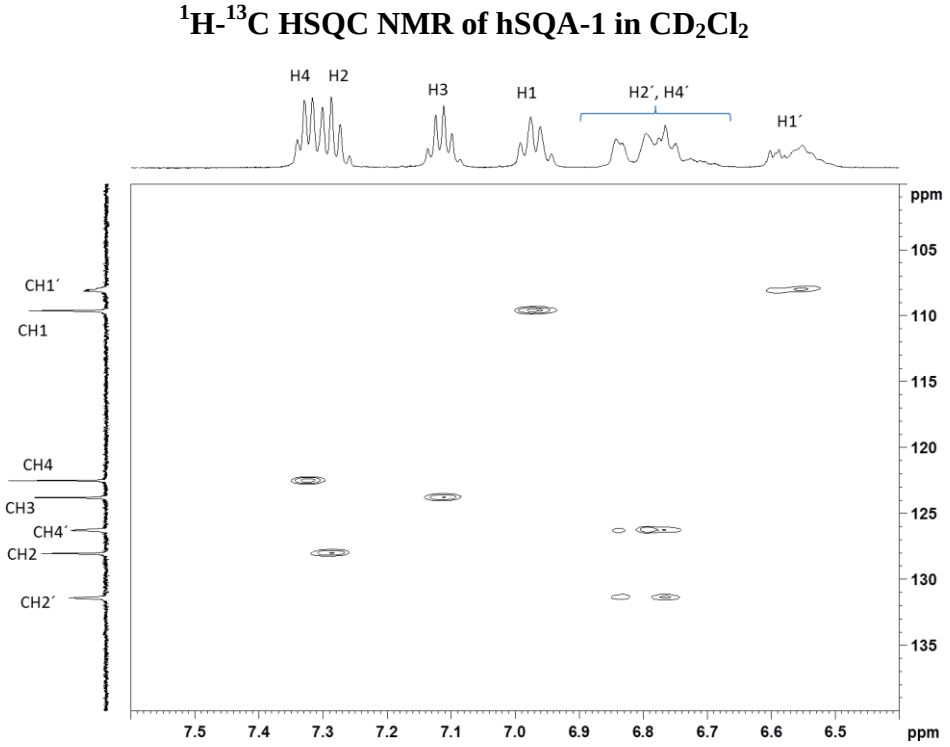

Figure 88: Partial ^{1}H-^{13}C HSQC of the relevant aromatic region of squaraine dye **hSQA-1** in CD_2Cl_2 recorded with 600.1 MHz NMR at 295 K.

^{1}H-^{1}H COSY NMR of hSQA-1 in CD_2Cl_2

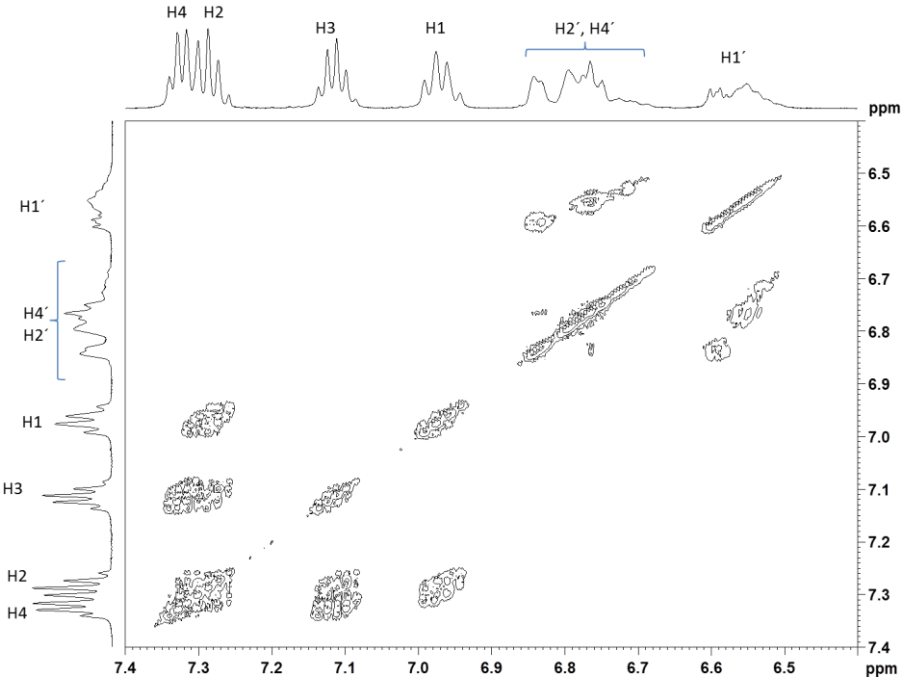

Figure 89 Partial ^{1}H-^{1}H COSY of the relevant aromatic region of squaraine dye **hSQA-1** in CD_2Cl_2 recorded with 600.1 MHz NMR at 295 K.

^{13}C-NMR Spectra of hSQA-1 in CD_2Cl_2 and Acetone-d_6

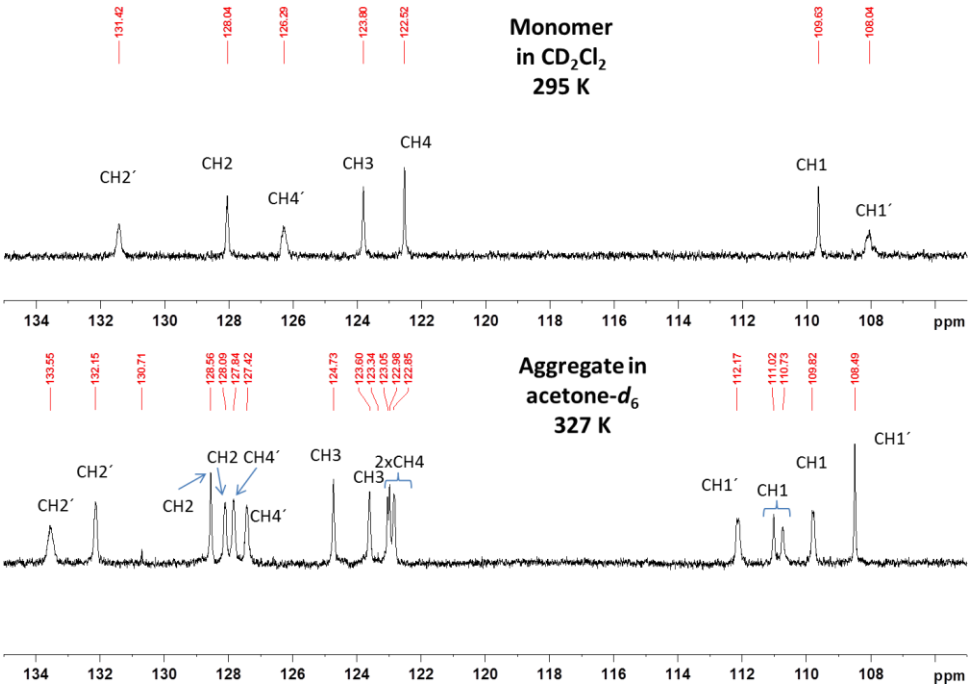

Figure 90: Partial ^{13}C-spectra of the relevant aromatic region of squaraine dye **hSQA-1** in CD_2Cl_2 (295 K) and acetone-d_6 (327 K) recorded with 600.1 MHz NMR.

^{1}H-^{13}C HSQC NMR of hSQA-1 in Acetone-d_6

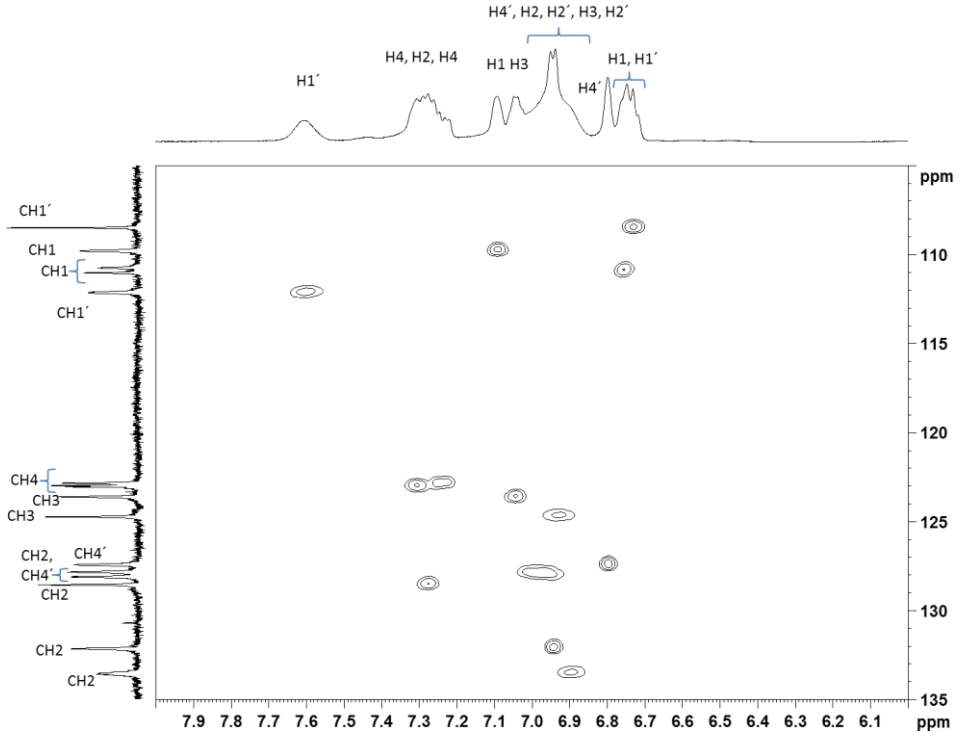

Figure 91: Partial ^{1}H-^{13}C HSQC NMR of the relevant aromatic region of squaraine dye **hSQA-1** in acetone-d_6 recorded with 600.1 MHz NMR at 327 K.

^{1}H-^{1}H COSY NMR of hSQA-1 in Acetone-d_6

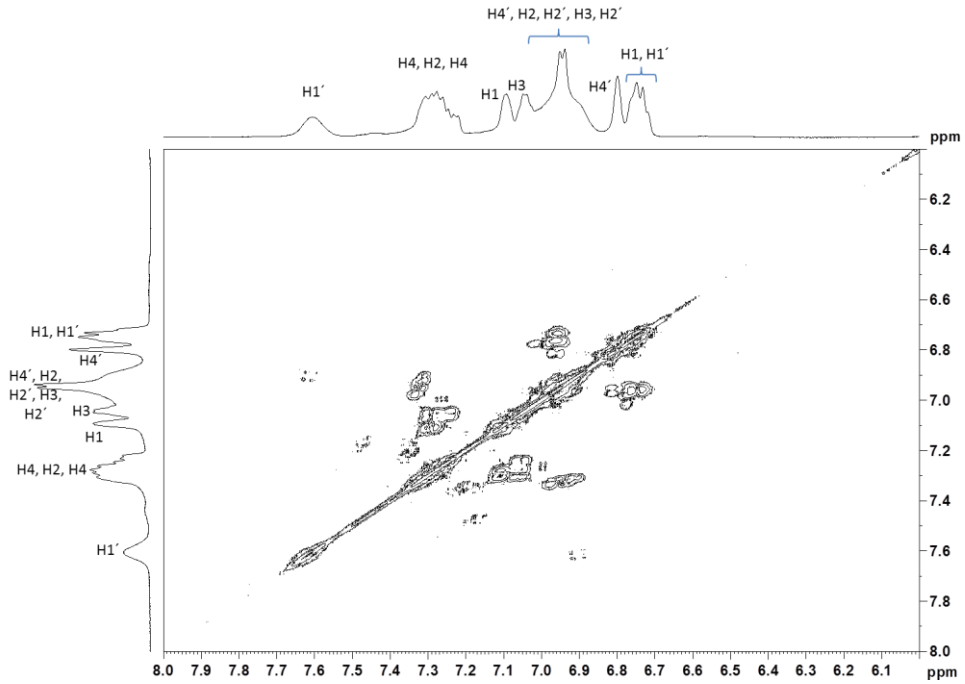

Figure 92: Partial ^{1}H-^{1}H COSY NMR of the relevant aromatic region of squaraine dye **hSQA-1** in acetone-d_6 recorded with 600.1 MHz NMR at 327 K.

9.3 List of Publications

1. *Photoinduced Electron Transfer Dynamics in Triarylamine-Naphthalene Diimide Cascades*, F. Zieschang, M. H. Schreck, A. Schmiedel, M. Holzapfel, J. H. Klein, C. Walter, B. Engels, C. Lambert, *J. Phys. Chem. C* **2014**, *118*, 27698-27714.

2. *Decoupling Charge Transport and Electroluminescence in a High Mobility Polymer Semiconductor*, D. J. Harkin, K. Broch, M. H. Schreck, H. Ceymann, A. Stoy, C.-K. Yong, M. Nikolka, I. McCulloch, N. Stingelin, C. Lambert, H. Sirringhaus, *Adv. Mater.* **2016**, *28*, 6378-6385.

3. *Cooperative Enhancement versus Additivity of Two-Photon-Absorption Cross Sections in Linear and Branched Squaraine Superchromophores*, H. Ceymann, A. Rosspeintner, M. H. Schreck, C. Mützel, A. Stoy, E. Vauthey, C. Lambert, *Phys. Chem. Chem. Phys.* **2016**, *18*, 16404-16413.

4. *Green to Red Electrochromic Fe(II) Metallo-supramolecular Polyelectrolytes Self-Assembled from Fluorescent 2,6-Bis(2-pyridyl)pyrimidine bithiophene*, S. Pai, M. Moos, M. H. Schreck, C. Lambert, D. Kurth, *Inorg. Chem.* **2017**, *56*, 1418-1432.

5. *Exciton Dynamics from Strong to Weak Coupling Limit Illustrated on a Series of Squaraine Dimers*, M. I. S. Röhr, H. Marciniak, J. Hoche, M. H. Schreck, H. Ceymann, R. Mitric, C. Lambert, *J. Phys. Chem. C* **2018**, *122*, 8082-8093.

9.4 Conference Contributions

1. Talk: *Exciton Coupling Effects in Squaraine Oligomers*, M. H. Schreck, H. Ceymann, A. Schmiedel, M. Holzapfel, C. Lambert, "KOPO 2015 Conference", 09/2015, Würzburg, Germany.

2. Talk: *Exciton Coupling Effects in Squaraine Oligomers*, M. H. Schreck, H. Ceymann, A. Schmiedel, M. Holzapfel, C. Lambert, "IUPAC: 26th International Symposium on Photochemistry", 04/2016, Osaka, Japan.

3. Poster: *Synthesis and Spectroscopic Properties of Polymeric Heteroazole Squaraine Dyes*, M. H. Schreck, S. F. Völker, C. Lambert, "IUPAC: 25th International Symposium on Photochemistry", 07/2014, Bordeaux, France.

4. Poster: *Synthesis and Spectroscopic Properties of Polymeric Heteroazole Squaraine Dyes*, M. H. Schreck, S. F. Völker, C. Lambert, "Chem-SyStM: Chemistry Symposium of the GDCh", 12/2014, Würzburg, Germany.

5. Poster: *Excitonic Coupling Effects in Oligomeric- and Polymeric Squaraine Dyes*, M. H. Schreck, C. Lambert, "GRK 1221 Workshop", 03/2015, Würzburg, Germany.

6. Poster: *Controlling the Superstructure in Polymeric Squaraine Dyes*, M. H. Schreck, C. Lambert, "FOR 1809 Workshop", 11/2016, Niederstetten, Germany.

7. Poster: *Controlling the Superstructure in Polymeric Squaraine Dyes*, M. H. Schreck, C. Lambert, "Chem-SyStM: Chemistry Symposium of the GDCh", 12/2016, Würzburg, Germany.

8. Poster: *Controlling the Superstructure in Polymeric Squaraine Dyes*, M. H. Schreck, C. Lambert, "FOR 1809 Workshop", 04/2017, Rückersbach, Germany.